**THÈSE DE DOCTORAT DE**
**L'UNIVERSITÉ PIERRE ET MARIE CURIE**

Spécialité: Neuroscience

École doctorale Cerveau – Cognition – Comportement (ED3C)

présentée par

Quang-Cuong PHAM (Phạm Quang Cường)

pour obtenir le grade de

**DOCTEUR de l'UNIVERSITÉ PIERRE ET MARIE CURIE**

# Étude de trajectoires locomotrices humaines

soutenue le 11 décembre 2009

devant le jury composé de

M. Alain BERTHOZ, directeur de thèse
M. Stefan GLASAUER, rapporteur
M. Yoshihiko NAKAMURA, rapporteur
M. Daniel BENNEQUIN, examinateur
M. Jean-Paul LAUMOND, examinateur
M. Didier ORSAL, examinateur
M. Jean-Jacques SLOTINE, examinateur

---

Université Pierre & Marie Curie - Paris 6
Bureau d'accueil, inscription des doctorants et base de données
Esc G, 2$^{ème}$ étage
15 rue de l'école de médecine
75270-PARIS CEDEX 06

Tél. Secrétariat : 01 42 34 68 35
Fax : 01 42 34 68 40
Tél. pour les étudiants de A à EL : 01 42 34 69 54
Tél. pour les étudiants de EM à MON : 01 42 34 68 41
Tél. pour les étudiants de MOO à Z : 01 42 34 68 51
E-mail : scolarite.doctorat@upmc.fr

# Remerciements

Je souhaite tout d'abord remercier P$^{\text{r}}$ Alain Berthoz d'avoir encadré ma thèse avec beaucoup d'attention, tout en m'accordant une grande liberté de réflexion et d'organisation. Je voudrais également exprimer ma profonde reconnaissance envers M. Halim Hicheur, avec qui j'ai réalisé presque la totalité de ce travail dans une collaboration quasi-symbiotique. Halim, merci de m'avoir initié à la recherche en neuroscience, de m'avoir guidé à travers les subtilités expérimentales et conceptuelles de cette discipline, d'avoir relu et corrigé ce manuscrit… mais aussi pour nos nombreuses discussions footballistiques, neuropolitiques, historiques, philosophiques… (et je ne mentionne pas les plus importantes) !

Je tiens à remercier l'ensemble des collègues qui m'ont aidé durant ma thèse sur le plan scientifique, aussi bien d'un point de vue théorique que pratique. Sans vouloir être exhaustif, je voudrais adresser mes remerciements (dans le désordre) à P$^{\text{rs}}$ Bennequin, Slotine, MM. Laumond, Arechavaleta, Crétual, M$^{\text{lle}}$ Olivier, MM. J. Wiener, S. Wiener, Girard, Tabareau, Colas, M$^{\text{me}}$ Yahia-Chérif, MM. Ouarti, Rossant, Terekhov, Droulez, Vidal, Kadone, P$^{\text{r}}$ Sugar, M$^{\text{me}}$ Bernardin, D$^{\text{r}}$ Belmonti…

Je remercie chaleureusement l'ensemble du personnel technique, administratif et scientifique du LPPA, en particulier (dans le désordre) M$^{\text{mes}}$ Maloumian, Delizy, Romera, M. Francheteau, M$^{\text{me}}$ Blondel, M. Dupraz, M$^{\text{me}}$ Zoundi, MM. Boudjelal, Pabois, Leboucher, Ehrette, Rateau, Zaoui, M$^{\text{me}}$ Leniston… qui accomplissent tous les jours un travail formidable, créant un environnement de travail idéal, dont j'ai largement bénéficié au cours de ma thèse.

Je voudrais exprimer ma gratitude envers ma famille et mes amis, en particulier Trân, de leur précieux soutien durant ces longues années d'études.

Je souhaiterais enfin remercier ma bien-aimée Bích Vân de son encouragement et de sa présence, qui me permet d'ores et déjà d'envisager la vie d'après-thèse avec enchantement.

# Résumé

La locomotion humaine est une activité motrice, sensorielle et cognitive qui fait intervenir de multiples niveaux de contrôle, comme la production de “patterns” rythmiques des membres inférieurs, l’ajustement postural du haut du corps pour la stabilisation ou encore la formation de trajectoires du corps entier dans l’espace. L’objectif principal de cette thèse est de fournir certains éléments contribuant à la de compréhension du dernier aspect.

En analysant les résultats d’une série d’expériences, nous montrons que les trajectoires locomotrices sont *stéréotypées*, c’est-à-dire qu’elles sont semblables à travers différents essais d’un même sujet, à travers différents sujets, mais aussi à travers différentes conditions sensorielles (marcher avec ou sans vision) et motrices (marcher en avant ou en arrière, à vitesse normale ou rapide). Ces observations suggèrent que les trajectoires locomotrices sont planifiées et contrôlées à un haut niveau cognitif et, dans une certaine mesure, indépendamment de leur implémentation sensori-motrice. En analysant plus en détail la *variabilité* de ces trajectories, nous soutenons qu’une combinaison de processus *en boucle ouverte* et *en boucle fermée* préside à la formation de trajectoires locomotrices et nous discutons de la nature précise du contrôle en boucle fermée en question. Enfin, nous développons des modèles déterministes et stochastiques qui permettent de confirmer les résultats expérimentaux, en même temps qu’ils organisent ceux-ci dans le cadre théorique du contrôle optimal.

**Mots-clés** locomotion humaine, trajectoires locomotrices, contrôle moteur, contrôle optimal, modélisation, navigation

# Abstract

Locomotion in humans is a complex motor, sensory and cognitive activity requiring multiple levels of control: from the production of repetitive stepping patterns of the lower limbs, through the adjustments of upper-body segments ensuring dynamic stability, to the formation of whole-body trajectories in space. The main objective of this thesis is to provide some elements of understanding of the latter aspect.

Through a series of experiments, we showed that locomotor trajectories are *stereotyped*, that is, they are similar across repetitions of the same subject, across subjects and also across different sensory (walking with or without vision) and motor (walking forward or backward, at normal or fast speed) conditions. These results suggest that locomotor trajectories are planned and controlled at a high cognitive level and, to some extent, independently of their sensorimotor implementations. Going further, through the analysis of trajectory *variability*, we argued that a combination of *open-loop* and *feedback* processes governs the formation of locomotor trajectories and discussed in detail the nature of the feedback control. Finally, we designed deterministic and stochastic models which helped confirming the experimental findings and organized them within the theoretical framework of optimal control.

**Keywords** human locomotion, locomotor trajectories, motor control, optimal control, models, navigation

# Contents

# List of Figures

# Introduction

Locomotion in humans is a complex motor and cognitive activity requiring multiple levels of control: from the production of repetitive stepping patterns of the lower limbs, through the adjustments of upper-body segments ensuring dynamic stability, to the formation of whole-body trajectories in space. In addition, the multiple sensory signals (visual, vestibular, proprioceptive) are continuously processed and integrated together, allowing the dynamic interaction of the body with the environment.

The main objective of this thesis is to provide some elements of understanding of whole-body trajectories. To get a rough idea, consider the following everyday life situation: a person is standing at some position in a room and has to walk towards and through a distant doorway to get out of that room [Fig. 1(A)]. What trajectory in space does he choose to achieve this objective? If he has to perform this task several times, will the resulting trajectories be similar or not? Following what criteria does he select a particular trajectory among the infinitely many possible trajectories? And more conceptually, what can we learn about the functioning of the Central Nervous System (CNS) from the geometric, kinematic and statistical properties of these trajectories?

To address these questions, we designed experimental protocols that adapt the above task to a laboratory environment, and recorded the trajectories produced by human subjects [see Fig. 1(B) for some representative trajectories]. We then studied in detail the properties of these trajectories to infer the laws governing the formation of whole-body trajectories in humans.

Two considerations accompanied us throughout this study. First, we did not examine whole-body trajectories by themselves, but in relation with other levels of analysis, such as the stepping activity or the steering behavior of the head and the trunk segments. Indeed, these multiple levels are distinguished only from a formal viewpoint, for the sake of analysis. In reality, they are tightly linked to each other and are jointly monitored by the CNS to elaborate the appropriate motor commands. This interconnected nature of the multiple

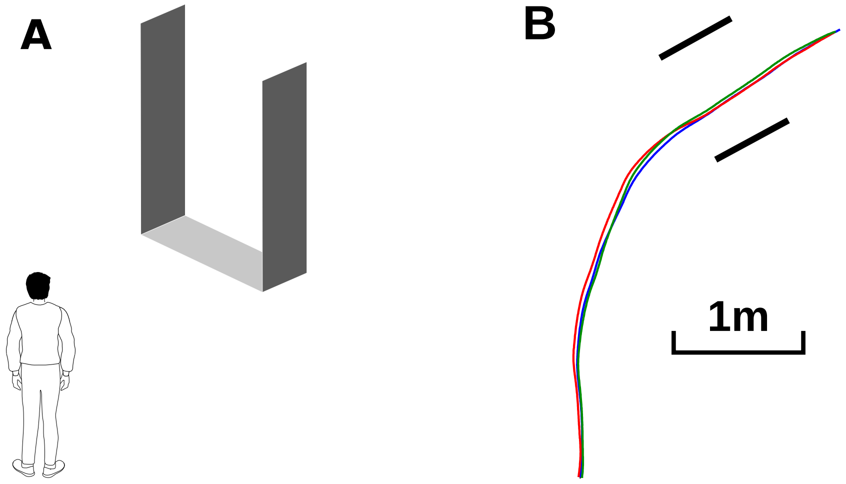

Figure 1: Formation of locomotor trajectories. (**A**) A person is standing at some position in a room and has to walk towards and through a distant doorway to get out of that room. (**B**) Three trajectories of a subject performing this task in a laboratory environment. The thick black bars indicate the panels that made up the doorway. We thank F. Maloumian for designing the body figures used in the illustrations.

control levels thus calls for a dialectical, *integrative* view for the study of locomotion (see Hicheur, 2006).

Second, a large number of our analyses were inspired from the *computational motor control* literature. Computational motor control borrows ideas (such as optimization, feedback loops, internal models, etc.) from classical control theory (a branch of engineering and mathematics) in order to investigate biological movements. This approach has proved successful in explaining many aspects of arm and eye movements. We believe that following this approach can also be fruitful for studying locomotion. Indeed, one of our main working hypotheses was that, as a part of the human repertoire, locomotion should share some control principles with other types of movement (see Berthoz, 2009, chapter 9). This idea may be illustrated by the classical observation that one can write the letter “a” with the finger, the mouth, the knee or even by running on a flat surface. Moreover, these movements of very different biomechanical natures share common geometric and kinematic properties (the “principle of motor equivalence”, see Bernstein, 1967).

Our work includes several novelties with respect to most previous works on locomotion. First, through the experimental paradigm of “walking towards and through a distant doorway”, we were able to study *spontaneously* *generated* trajectories. This contrasts with the usual protocols, where subjects have to walk along *predefined* paths (straight segments, triangles, circles or more complicated figures such as cloverleaves, limacons, etc.). Since the paths contain precious information about the subjects' strategies, it is crucial to use a protocol that do not constrain the paths while still imposes relatively complex trajectories. We note here that this innovating "doorway" paradigm was originally developped by Arechavaleta et al. (2006) to study the nonholonomic coupling of velocity and orientation (see section 3.3).

Second, in resonance with the most recent developments in computational motor control, we not only examined the average behavior, but also the *variability* around this average behavior. Indeed, only few (or none of) previous works on locomotion considered in detail the variability of whole-body trajectories. Here, the analysis of *variability profiles* (how the variability evolves in time) was one of our main tools to investigate the laws governing the formation of locomotor trajectories.

Third, our study combined experimental and modeling approaches. Models can indeed complement experiments by allowing testing *positively formulated* hypotheses. From a conceptual viewpoint, theoretical models that can reproduce experimental observations also strengthen our understanding of human movements. Perhaps, a similar idea was expressed by the great American physicist Richard Feynman when he said

> "What I cannot create, I do not understand."

## Organization of the manuscript

The first part of the manuscript outlines the theoretical context of our study. We first briefly present the recent developments in motor control that inspired some of our analyses (chapter 1). We then review a number of findings in locomotion concerning the stepping activity, the multisensory control of locomotion and the steering behavior (chapter 2). Finally, we discuss previous studies of locomotor trajectories by highlighting their contributions as well as their shortcomings (chapter 3), which our work attempts to address.

In the second part, we present the experimental studies. Chapter 4 first introduces the general methodology and notations. We also briefly discuss in this chapter the main advantages and weaknesses associated with our methodology.

Chapter 5 examines through two experiments how similar or different are locomotor trajectories observed across repetitions, subjects and sensory and motor conditions. In Experiment 1, which implements the "walking towards and through a distant doorway" paradigm, we show that locomotor trajectories are actually *stereotyped*, that is, they are highly similar across repetitions of the same subject and also across subjects. This stereotypy contrasts with a great variability of the feet placements, which suggests that locomotion is planned and controlled at the level of whole-body trajectories. In Experiment 2, we examine the influence of vision (walking with eyes open or closed) and of gait direction (walking forward or backward) on the formation of trajectories. The results obtained from this experiment allow further testing the hypothesis that locomotor trajectories are planned and controlled at a high cognitive level, and to some extent, independently of their sensorimotor implementations.

Chapter 6 studies in more detail the *control* mechanisms involved in the production of locomotor trajectories. For this, we designed three experiments which test respectively the influence of vision (Experiment 3), of speed (Experiment 4) and of the presence of via-points (Experiment 5) on the average trajectories and on the variability profiles. Based on the experimental results, we formulate the hypothesis that a combination of *open-loop* and *feedback* processes governs the formation of locomotor trajectories and discuss in detail the nature of the feedback control.

Chapter 7 reports some preliminary results. Following the aforementioned integrative view, we first explore the relations between the formation of locomotor trajectories and the *steering behavior*. More precisely, based on the analysis of the head and trunk turning profiles recorded in Experiment 2, we assess the inluence of vision and of gait direction on the turning behavior of the head and the trunk. We then examine, through a new Experiment 6, the relations between formation of continuous locomotor trajectories and *navigation*, which we define as a sequence of *discrete* choices (for instance, to navitage from the Arc de Triomphe to the Eiffel tower, one has the choice of going westward by Avenue Kléber or eastward by Avenue d'Iéna). Finally, Experiment 7 explores a new general principle for the control of movements, which postulates that movements should obey geometrical invariances, in particular, the *affine* invariance.

In the third part of the manuscript, we present the modeling studies. Chapter 8 examines some deterministic models of trajectory formation. Our basic assumption is that locomotion is an *optimized* activity. Following the "principle of motor equivalence" mentioned previously, we thus adapted to the context of locomotion *optimal control* models that were initially proposed for hand movements. We show in particular that minimum jerk models accurately predict the average locomotor trajectories recorded in our experiments.

Since the models presented in chapter 8 are deterministic, they cannot help understand the variability patterns highlighted in chapter 6. We thus have to consider in chapter 9 *optimal feedback control* models and assess whether these models can account for the average trajectories *and* the variability profiles experimentally observed.

We conclude with a general discussion of our experimental and modeling findings. We evaluate the possible contributions of our work to the current understanding of human locomotion and of motor control in general. We also discuss some ongoing and future directions of research, which address in particular the clinical and developmental aspects of the ideas defended in this thesis. Finally, we speculate on the possible applications of our findings to the design of humanoid robots.

# Part I

# Theoretical context

This part introduces the concepts and results that form the theoretical basis of the thesis. We review in chapter 1 some of the main results obtained in the field of *computational motor control*. Then, in chapter 2, we discuss some research issues in locomotion, which are important to be conversant with if one is to provide an *integrative* understanding of locomotion. We focus on the aspects that pertain most to our work: the stepping activity, the multisensory control of locomotion and the steering behavior. Finally, in chapter 3, we present previous studies of locomotor trajectories, highlighting their contributions as well as their shortcomings.

We would like to stress that our goal in this part is not to provide a comprehensive review of all the aspects evoked above. Rather, we more modestly aim at equipping the reader with the necessary knowledge to interpret the experimental and modeling results presented later.

# Chapter 1

# Computational motor control

Consider the everyday life task of reaching out to press a button. Achieving this apparently simple objective requires producing an arm movement to bring the hand from its initial position towards another position in space, that of the button. The production of such a movement is however associated with several difficulties: to go from the initial position towards the desired final position, the hand can take an infinite number of different *paths*; given a path, an infinite number of different *trajectories*[1] correspond to that path; given a hand trajectory, an infinite number of different time-varying patterns of the wrist, elbow and shoulder angles can achieve that hand trajectory, etc. (see Fig. 1.1 for a schematic representation of the *redundancy* existing in motor control, from the task level all the way up to the level of the neural commands).

From the above perspective, the "redundancy problem" associated with the production of even simple movements appears to be incredibly complex. Yet, the Central Nervous System (CNS) effortlessly "solves" such problems (and even harder ones, consider for instance the movements of professional violonists or football players) several thousand times a day. Understanding how the CNS achieves this has been the main focus of numerous studies over the past decades. Within this rich literature, we would like to highlight three main developments that form the conceptual basis for our study of locomotor trajectories.

The first such development consisted of identifying *invariants* in the production of arm movements (section 1.1). From the studies of these invariants, it was suggested in particular that the CNS controlled the trajectories of the hand in space, rather than e.g. the joint angles.

---

[1] Throughout this manuscript, a *path* designates a geometric object (devoid of any time parameterization) while a *trajectory* designates a pair: path + a velocity profile along that path.

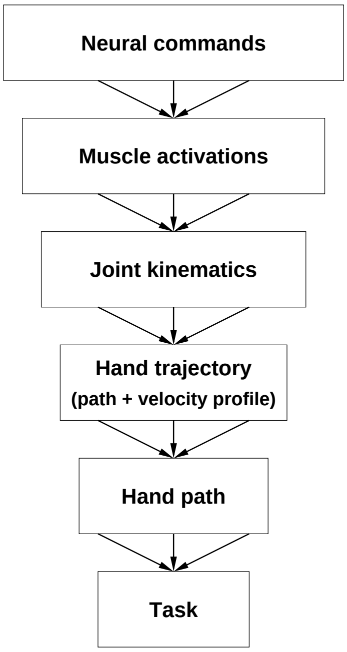

Figure 1.1: Redundancy in the control of arm movements (adapted from Jordan and Wolpert, 1999).

Second, following the “spatial control” view, it was proposed that the hand trajectories in question are *optimal* according to some criteria. Optimal control models were consequently developped in order to identify these criteria (section 1.2).

Third, the focus was more recently put back on the analysis of trajectory *variability*, which is thought to also reflect the control mechanisms at work during the production of a movement. This led to the development of *stochastic* models in order to provide a conceptual understanding of the experimentally observed variability (section 1.3).

## 1.1 Invariants in hand movements

### 1.1.1 Reaching movements

Consider again a reaching task, which is now restricted to the horizontal plane. Despite the infinite number of possible 2D trajectories (paths and velocity profiles) joining two positions in the plane, it was experimentally shown that humans consistently generate approximately straight hand paths and bell-shaped (smooth, single-peaked) velocity profiles (Morasso, 1981,

Fig. 1.2). This is not trivial since the joint angular profiles (in Morasso's experiment: flexion-extension of the elbow and shoulder) which yielded these trajectories were rather complex and displayed no particular regularity (Fig. 1.3, rows 1 and 2). The observation of straight hand paths and bell-shape velocity profiles in 2D reaching was also reported in experiments on monkeys (Georgopoulos et al., 1981, Fig. 1.4).

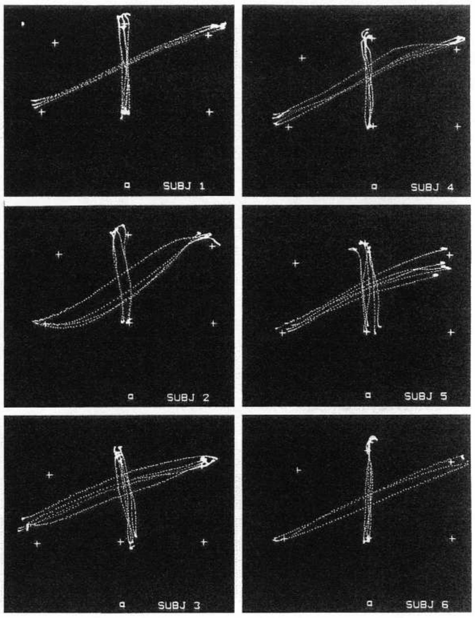

Figure 1.2: Approximately straight hand paths observed in a 2D reaching task in six human subjects (adapted from Morasso, 1981).

There are however some limitations to these findings. For instance, large horizontal arm movements (Uno et al., 1989, Fig. 1.5) and vertical arm movements (Atkeson and Hollerbach, 1985) are slightly curved. The tangential velocity profiles associated with these movements remain nevertheless bell-shaped and symmetrical, irrespective of the load, direction of movements, speed conditions (Atkeson and Hollerbach, 1985, Fig. 1.6).

Taken together, these observations suggested that arm movements are planned and controlled based on the cartesian coordinates of the hand in the extracorporal space, rather than on internal representations of e.g. joint angles (Morasso, 1981; Flash and Hogan, 1985).

This view, termed "*spatial control of arm movements*", is supported by several conceptual considerations. For instance, "*the potential of the 'spatial code' [may] serve as a common language among the different sources of information which subserve coordinated movements (e.g. exteroceptive and*

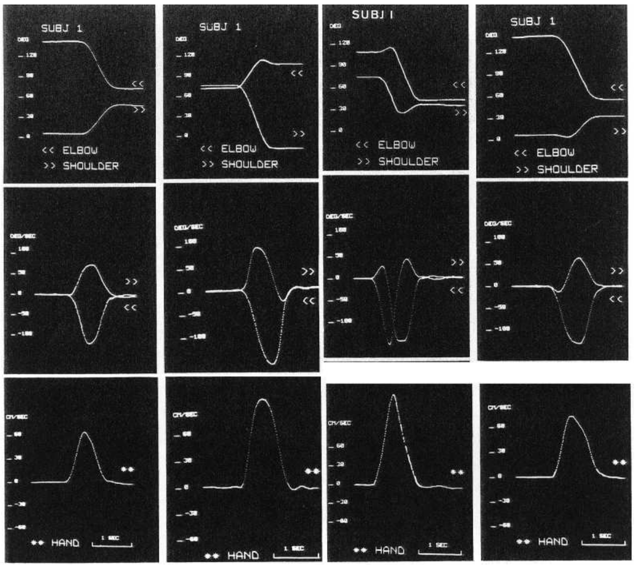

Figure 1.3: Joint angle profiles (row 1), joint angular velocity profiles (row 2) and tangential hand velocity profiles (row 3) recorded in a 2D reaching task in a human subject. Each column corresponds to a different pair of starting position/target position. Note the stereotyped bell-shaped hand velocity profiles across the columns, which contrasts with the variability of the joint behaviors (adapted from Morasso, 1981).

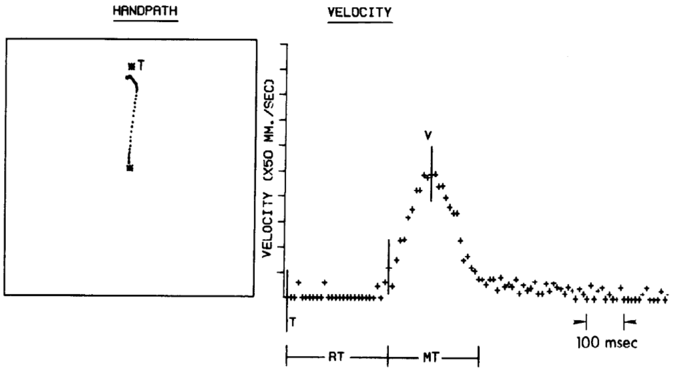

Figure 1.4: Approximately straight hand paths and bell-shaped velocity profiles observed in a 2D reaching task in a rhesus monkey (adapted from Georgopoulos et al., 1981).

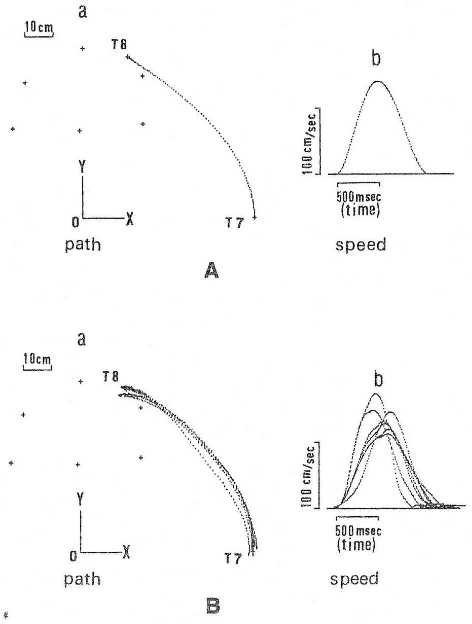

Figure 1.5: Slightly curved hand trajectories and symmetrical bell-shaped velocity profiles observed in large horizontal arm movements (adapted from Uno et al., 1989).

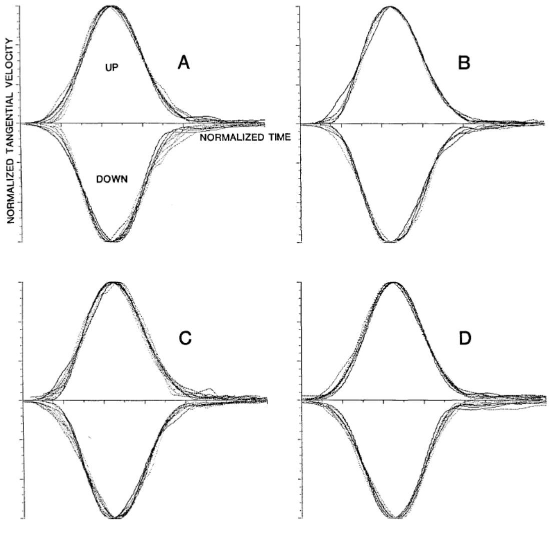

Figure 1.6: Symmetrical bell-shaped velocity profiles in vertical arm movements in different conditions. (**A**) velocity profiles for different speed conditions are superimposed. (**B**) different loads. (**C**) different targets. (**D**) different subjects (adapted from Atkeson and Hollerbach, 1985).

*proprioceptive afferences, motor programs, etc.)*" (Morasso, 1981).

### 1.1.2 Curves drawing

The drawing of *curved* shapes is characterized by another invariant: the hand tends to go slower in the curved portions of the paths and faster in the straight portions. This inverse relationship between velocity and curvature was quantified by the "one-third power law" (Lacquaniti et al., 1983, Fig. 1.7 and 1.8 )

$$v(t) = \gamma r(t)^{1/3} \tag{1.1}$$

where $v$ is the hand velocity, $r$ the radius of curvature and $\gamma$ a constant scaling factor. Equivalently, since $r = 1/\kappa$ where $\kappa$ is the path curvature, the "one-third power law" can also be formulated as

$$a(t) = \gamma \kappa(t)^{2/3} \tag{1.2}$$

where $a$ is the angular velocity. Under this form, the law is thus also known as the "two-thirds power law".

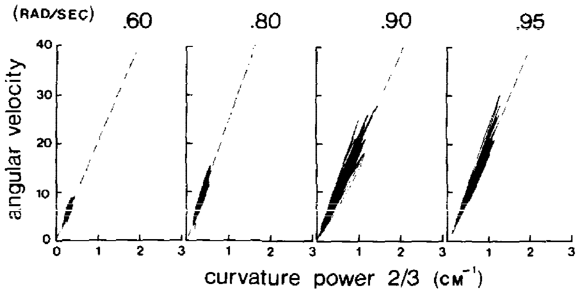

Figure 1.7: The angular velocity as a function of the curvature to the power two-thirds in an ellipses drawing task. Ellipses of different eccentricities (0.6 to 0.95) were considered. One can observe a linear relationship between the two parameters (adapted from Lacquaniti et al., 1983).

This "law" was observed also in perception studies: for instance, a curved movement whose velocity follows the "one-third power law" is perceived by human subjects as having a constant velocity (Viviani and Stucchi, 1992). Also, the "one-third power law" was found to develop during childhood (Viviani and Schneider, 1991).

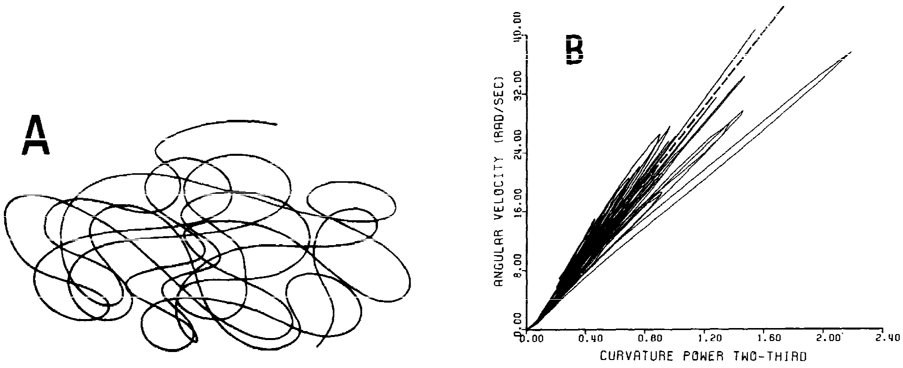

Figure 1.8: A scribbling task. (**A**) geometric paths of the scriblings. (**B**) Angular velocity as a function of the curvature to the power two-thirds. One can observe a piece-wise linear relationship between the two parameters (adapted from Lacquaniti et al., 1983).

### 1.1.3 Geometry considerations

Several ideas were proposed to explain the "one-third power law" mentioned above (see a review in Schaal and Sternad, 2001). In particular, Pollick and Sapiro (1997) remarked that moving along a curve with *constant equi-affine* velocity actually yields the "one-third power law". Indeed, the notion of "velocity" we have been using so far is in fact associated with *euclidian* geometry, which is one among several possible geometries the CNS might use.

A geometry of a space $E$ is associated with a particular group $G$ of transformations of $E$ (see Bennequin et al., 2009, for more details and references). For instance, in the plane, euclidian geometry corresponds to the group of rigid displacements (translations and rotations). Equi-affine geometry corresponds to the larger group of *area-preserving* transformations (translations, rotations but also stretching and shearing) and full affine geometry corresponds to an even larger group, which contains area-preserving transformations *and* dilatations.

One can then define a notion of *length* specific to each particular geometry by demanding that this length be *invariant* under any transformation of the corresponding group. For instance, any curve has the same euclidian length as its image by any translation and rotation. However, a circle does not have the same euclidian perimeter as the ellipse that is obtained from it by *stretching*. By contrast, the equi-affine arc-length $\sigma_1$ defined as

$$\frac{\mathrm{d}\sigma_1}{\mathrm{d}s} = \frac{1}{r^{1/3}}, \tag{1.3}$$

where $r$ is the instantaneous radius of curvature and $s$ is the euclidian arc-length, allows constructing by integration a notion of length that is invariant by any equi-affine transformation.

Given the notion of invariant length, one can then define a notion of velocity that is also invariant, by simply "dividing by d$t$". From Eq. (1.3), one can then see why moving along a curve with constant equi-affine velocity yields the "one-third power law".

More recently, Bennequin et al. (2009) generalized considerably Pollick and Sapiro's idea. According to these authors, a *mixture of several geometries* (euclidian, equi-affine and affine) governs the production of many types of human movements. More precisely, the euclidian velocity $v$ along a curve may be decomposed as

$$v = v_0^{\beta_0} v_1^{\beta_1} v_2^{\beta_2} \tag{1.4}$$

where $v_0$, $v_1$ and $v_2$ denote respectively the expected euclidian velocity under constant affine, equi-affine and euclidian velocities [for instance, we have, from Eq. (1.3), $v_1 \propto v_2/r^{1/3}$], and $\beta_0$, $\beta_1$ and $\beta_2$ are three weighting parameters.

This theory can thus provide a unifying framework to understand different types of movements in terms of their *dominant* geometries. For instance, observing that locomotor trajectories are associated with a large $\beta_2$ and a small $\beta_0$, the authors hypothesized that euclidian geometry is dominant in locomotion. By contrast, the drawing of curves with the hand is more dominated by affine geometry. More conceptually, the authors suggest that the CNS might use several levels of representation of space, each level being organized according to a geometry (or equivalently to a group of transformations or *symmetries*). Then, "*approaching the level of motor execution, fewer and fewer possibilites are allowed, thus reducing the initial larger group of symmetry of all possible movements into smaller groups*". According to this view, the similarities and the differences between the different types of movements (for instance, locomotion and hand movements) would be explained by the way the groups of symmetries are reduced at the different levels of the hierarchy.

## 1.2 Deterministic optimal control models

Optimal control theory provides a pertinent framework to account for the invariants identified in arm movements. Within this framework, the stereotyped hand trajectories may be explained by the hypothesis that the CNS systematically selects the optimal trajectory among all possible trajectories. Besides, optimal control is appealing from a conceptual viewpoint for "*it* *is related to the possibility that the sensorimotor system is the product of processes such as evolution, development, learning or adaptation that continuously act to improve behavioral performance*" (Todorov, 2004).

More precisely, optimal control models postulate that humans select the movement that minimize a certain *cost*, such as efficiency, smoothness, accuracy, duration, etc. Classically, one distinguishes two categories of costs: (i) kinematic costs, which contain only geometrical and time-based quantities of the trajectory, such as position, velocity, acceleration, movement duration, etc. and (ii) kinetic costs, which contain also dynamic quantities such as torques, forces, muscle commands, etc.

### 1.2.1 Kinematic models

Observing that hand trajectories are "*smooth and graceful*", Hogan (1984) proposed a *minimum jerk* model to account for qualitative and quantitative features of single-joint forearm movements. This was motivated by the assumption that minimizing the squared jerk (jerk is mathematically defined as the third-order derivative of the position) may be equivalent to maximizing smoothness. Flash and Hogan (1985) generalized this model to the case of multijoint movements. They showed in particular that the 2D trajectories $(x(t), y(t))$ that minimize the following squared jerk cost:

$$\int_0^1 \left( \left( \frac{\mathrm{d}^3 x}{\mathrm{d}t^3} \right)^2 + \left( \frac{\mathrm{d}^3 y}{\mathrm{d}t^3} \right)^2 \right) \mathrm{d}t \tag{1.5}$$

displayed qualitative and quantitative similarities with experimentally recorded hand trajectories.

More generally, a trajectory is smooth if there are no abrupt variations in time. This implies that higher-order time derivatives of the position have low absolute values. While Hogan (1984) and Flash and Hogan (1985) mostly focused on the squared jerk cost, other costs such as the squared acceleration or the squared snap (snap is the time derivative of jerk) can also be considered. The general nth-order Maximum Square Derivative (MSD) cost is given by:

$$\int_0^1 \left( \left( \frac{\mathrm{d}^n x}{\mathrm{d}t^n} \right)^2 + \left( \frac{\mathrm{d}^n y}{\mathrm{d}t^n} \right)^2 \right) \mathrm{d}t \tag{1.6}$$

The case $n = 1$ corresponds to the minimum velocity cost, $n = 2$ to minimum acceleration, $n = 3$ to minimum jerk and $n = 4$ to minimum snap, etc.

Richardson and Flash (2002) conducted a comparative study in which they examined the capacity of MSD models of different orders to simulate hand trajectories. In particular, they found that 3rd- and 4th- order

MSD models (minimum jerk and minimum snap) usually performed better than those of other orders. In addition to quantitative fit, the trajectories simulated by 3rd- and 4th-order MSD models displayed typical qualitative characteristics of human hand trajectories: smoothness of the trajectory, straight hand paths and bell-shaped velocity profiles in reaching tasks, inverse relationship between velocity and curvature in drawing tasks (see section 1.1.2), etc.

### 1.2.2 Kinetic models

Because of their kinematic nature, the models presented above are independent of the physical environment and of the mechanical system that generate the movements. For instance, the minimum jerk model still predicts straight hand paths even when external forces are applied to the hand. However, Uno et al. (1989) reported that hand trajectories become curved in when external spring-like forces were applied to the hand. They also reported curved trajectories for large 2D movements.

These observations led these researchers to propose a *minimum torque change* model. They modelled the arm system by a 2-joint manipulator and looked for the movements that minimize the following cost

$$\int_0^1 \sum_{i=1}^{2} \left( \frac{\mathrm{d}\tau_i}{\mathrm{d}t} \right)^2 \mathrm{d}t \tag{1.7}$$

where $\tau_i$ is the torque applied at joint $i$. Using this model, they could account for the curvatures existing in perturbed and large arm movements.

However, the observations leading to the development of kinetic models can be modulated. First, curved trajectories observed in presence of external forces were found to become straighter with practice (Shadmehr and Mussa-Ivaldi, 1994, Fig. 1.9).

It can also be argued that the curvature observed in large arm movements result from some "border effects": physical constraints may appear near the physical limits of the system and perturb otherwise straight trajectories.

### 1.2.3 Minimum variance model

The kinematic and kinetic models presented above suffer from the conceptual weakness that they rely on no "principled" explanation. Indeed, besides aesthetic reasons, the advantage of smoothness of movement or low torque change still remains unexplained. Furthermore, how the CNS could estimate

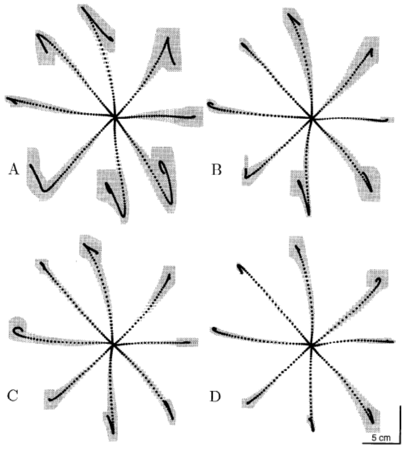

Figure 1.9: Hand reaching trajectories performed in a nonlinear force field. Average trajectories (and the variabilities) computed across the first (**A**), second (**B**), third (**C**) and last (**D**) blocks of 250 trials. One can observe that the trajectories become straighter with practice, implying that hand trajectories are planned according to kinematic objectives (adapted from Shadmehr and Mussa-Ivaldi, 1994).

complex quantities, such as jerk or torque change, and then integrate them over the duration of a trajectory is still the subject of debates.

Harris and Wolpert (1998) proposed a model that relies on the assumption that the motor system is corrupted by noise and that the selected movements are those which minimize the variance of the effector's final position. This model is appealing since the variance expresses in fact the *reaching errors* over multiple trials, and reducing errors is arguably an important goal pursued by the CNS. Besides, reaching errors can also be easily estimated by the CNS, for instance through visual feedbacks. This model could successfully simulate both eye and arm movements. In the case of hand movements, this model produced in particular smooth trajectories, suggesting that smoothness may be a by-product of variance minimization.

However, Harris and Wolpert's version of the minimum variance model imposed a fixed movement duration. A more comprehensive model was developped by Tanaka et al. (2006) in which movement duration was included in the cost. This model could then directly account for the speed-accuracy trade-off (Fitts, 1954).

## 1.3 Stochastic optimal feedback control

The interest sparked off by Harris and Wolpert's study further demonstrated the importance of detailed variability analysis. Indeed, while hand trajectories in reaching tasks are globally stereotyped, there still exists some variability which contains precious information about how the CNS controls movements.

### 1.3.1 Variability of the final position

The analysis of the hand's final position in reaching tasks was first performed to identify the reference frames in which subjects plan their movements. In an experiment where subjects had to point to a remembered 3D target multiple times, McIntyre et al. (1997) found that the variance ellipsoids consistently pointed towards the subject's eyes (see Fig. 1.10). Based on this observation, the authors suggested that humans use a viewer-centered reference frame.

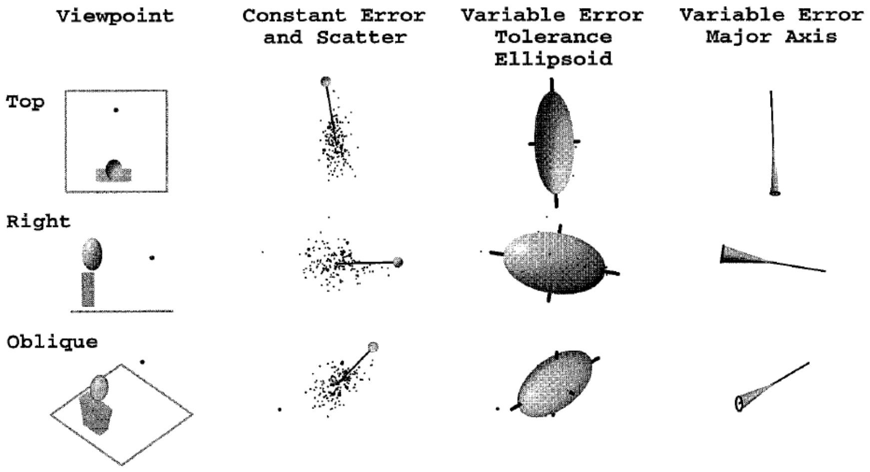

Figure 1.10: Variability patterns of the finger's final position in a 3D reaching experiment (adapted from McIntyre et al., 1997).

Going further, van Beers et al. (2004) distinguish three types of noise that may contribute to movement variability: localization noise, planning noise and execution noise. From this perspective, it can be argued that in experiments such as those in McIntyre et al. (1997) the three types of noise were muddled up by the experimental protocol. By designing a protocol where the contribution of each type of noise could be precisely controlled, van Beers et al. could demonstrate that execution noise (i.e. the noise that affects the motor system during movement execution) contributes "*at least for a large proportion*" of the overall variability of the hand's final position.

### 1.3.2 Trajectory variability and the "desired trajectory" hypothesis

The examination of variability profiles, that is, how the variability evolves in time, can provide further information. In particular, it allows evaluating two competing hypotheses for the online control of movements (Todorov and Jordan, 2002, see Fig. 1.11 for an illustration): (i) the "desired trajectory" (DT) hypothesis, which assumes two separate stages in the production of a movement: a planning stage when a desired optimal trajectory is computed and an execution stage when this desired trajectory is implemented with "trajectory tracking" mechanisms correcting any deviation away from the desired trajectory; (ii) the optimal feedback control (OFC) hypothesis, which states that "*deviations from the average trajectory are corrected only when they interfere with task performance*" (goal-directed corrections, as opposed to DT-directed corrections).

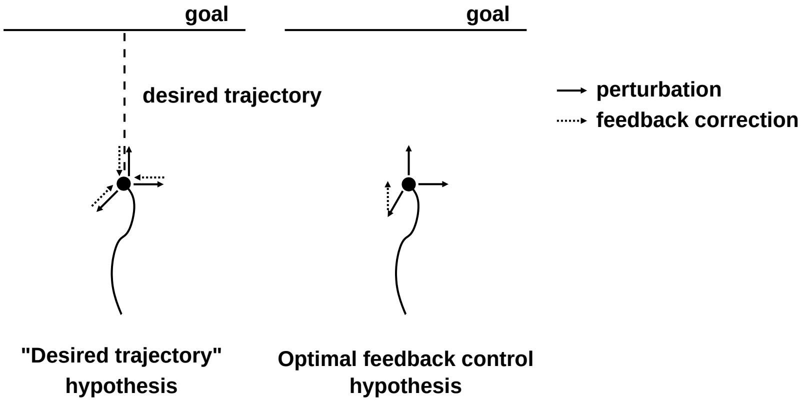

Figure 1.11: The objective is to reach the "goal" line. In the "desired trajectory" hypothesis, any deviation is corrected back to the desired trajectory, while in the optimal feedback control hypothesis, only deviations that interfere with goal achievement are corrected.

Usual optimal control models, including the minimum variance model (Harris and Wolpert, 1998), implicitly assume the DT hypothesis since they predict a single optimal trajectory. Yet tracking the DT is clearly suboptimal, even with respect to the initial criterion (for instance, a trajectory that results from the tracking of a maximum smoothness trajectory may not be smooth).

Todorov and Jordan (2002) proposed several via-point tasks to experimentally test the DT hypothesis. In one task, subjects were asked first to make hand trajectories that must go through 5 given via-points. The experimenter computed the average trajectory across the recorded trajectories. He then placed 20 via-points along this trajectory and asked the subjects to go through these 20 via-points. By construction, the average trajectory of the second task was practically the same as that of the first task. However, the variability profiles were very different (see Fig. 1.12). These observations are incompatible with the basic DT hypothesis, which would predict no difference between the statistics in the two conditions (indeed, the DT is equated to the average trajectory, which is obtained by indeed "averaging out" the trial-to-trial perturbations).

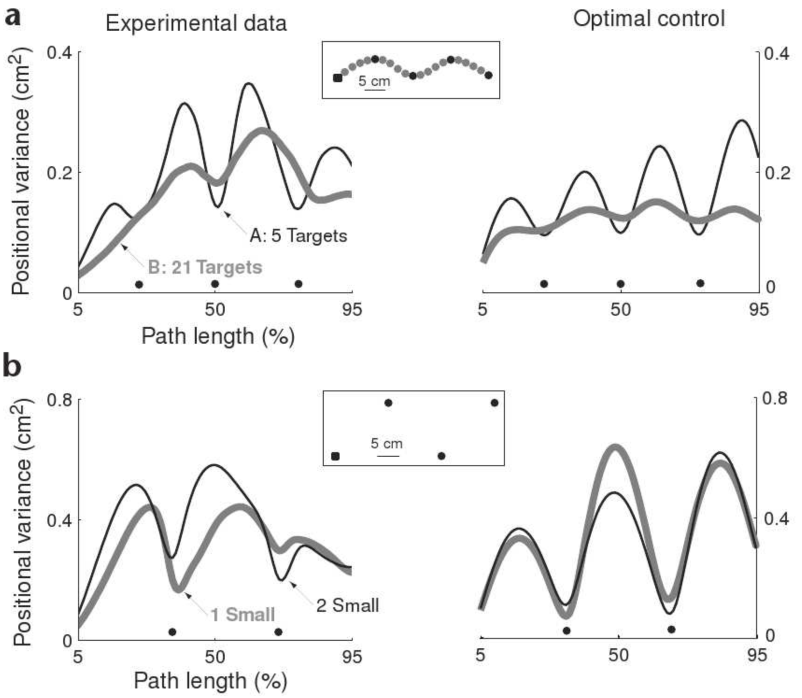

Figure 1.12: Variability profiles in via-points tasks. Dots mark passage through the intermediate targets; the square in each inset marks the starting position. (a) Left: 5 via-points (black targets shown in the inset). Right: 16 more targets (gray) were added. (b) In the "1 small" condition, the first intermediate target was smaller; in the "2 small" condition, the second intermediate target was smaller (adapted from Todorov and Jordan, 2002).

We note nonetheless that these observations cannot rule out a variation of the DT hypothesis which consists of (i) constructing *several* desired sub-trajectories (4 sub-trajectories in the 5 via-point condition – the first trajectory between the starting position and the second via-point, the second trajectory between the second via-point and the third via-point, etc. –, and 19 sub-trajectories in the 20 via-points conditions) and (ii) tracking *sequentially* these sub-trajectories. While unlikely, this variation cannot be theoretically ruled out based solely on the data provided by the experiment (see Pham and Hicheur, 2009).

### 1.3.3 Optimal feedback control models

Instead of tracking a “desired trajectory”, it appears from Todorov and Jordan’s experiments that humans likely use an Optimal Feedback Control (OFC) strategy, correcting only the perturbations that interfere with the task. For instance, in the 5 via-point task, variability was reduced over each via-point while allowed to increase between two via-points.

While OFC schemes have been used in engineering for decades, Hoff and Arbib (1993) implemented one of the first optimal online feedback models in the field of motor control. They designed a feedback version of the minimum jerk model that could deal with perturbations of the target’s position during the movement: roughly, at each time instant $t$, if the target is perturbed, a *new* minimum jerk trajectory is computed and executed, until the next perturbation.

However, Hoff and Arbib’s model lack several features of a full OFC model. First, since in their model only the target was perturbed, the system’s state was supposed to be perfectly known to the controller. However, in reality, the system’s state is also corrupted by noise, and thus can only be known through *estimation* processes. Second, at each time instant $t$ their model calculates a feedback correction towards the perturbed position of the target. However, this is may not always the optimal strategy: an optimal strategy would take into account also the *known statistics of the noise.* For instance, if we know that the noise more likely deviates the target towards the left, then an optimal strategy will correct less the perturbations that deviate the trajectory twoards the left of the target than those that deviate towards the right.

Todorov and Jordan (2002) designed a full optimal feedback controller that includes optimal estimation of the state and takes into account the noise statistics. Using this model, the authors could account for the variability profiles observed in the via-points tasks, but also for numerous other features, including synergy, simplifying rules, discrete coordinations, etc.

# Chapter 2

# Some research issues in locomotion

As mentioned in the Introduction, to fully understand how whole-body trajectories are planned and controlled requires taking into account other levels of control of the locomotor activity. Here, we review some studies devoted to the stepping activity (section 2.1), the multisensory control of locomotion (section 2.2) and the steering behavior (section 2.3). These studies are crucial for our subsequent investigations (see chapters 5, 7 and 6).

## 2.1 Stepping activity

### 2.1.1 Neural structures underlying the generation of the stepping pattern

We have seen in chapter 1 that the planning and control of apparently simple tasks is in fact extremely challenging from a computational viewpoint. The generation of the stepping activity, which mobilizes practically all body muscles, is thus even more complex. In addition, the bipedal nature of human locomotion is associated with a very particular and highly elaborate neural organization which, in large parts, still remains mysterious to neuroscientists.

In some lower vertebrates, such as the lamprey, the forward propulsion of the body, the steering and the maintenance of equilibrium are realized through alternating left-right contractions of the body segments. The contraction patterns are controlled by neural circuits, called Central Pattern Generators (CPGs), which are located in the spinal cord. These CPGs are able to generate a rythmic activity in isolation, that is, in absence of sensory afferences or of supraspinal commands (Grillner, 2003, Fig. 2.1).

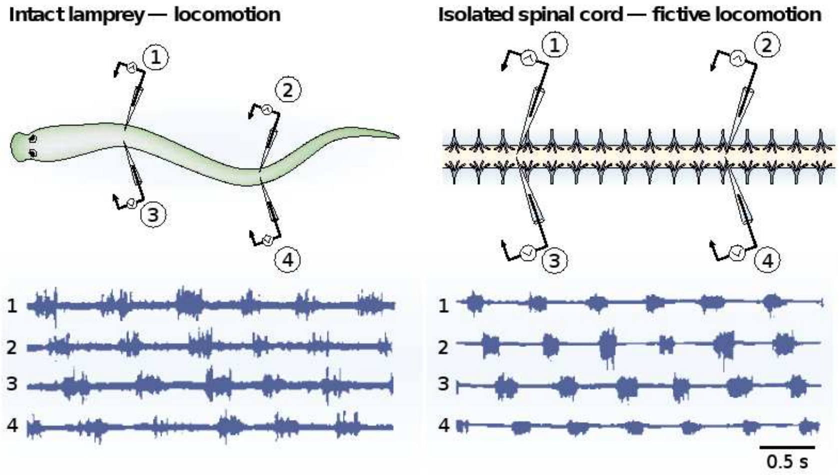

Figure 2.1: Fictive locomotion in the lamprey. The isolated spinal coord can generate a rythmic activity very similar to that observed in the intact animal (adapted from Grillner, 2003).

In quadrupeds, such as the cat, CPGs have also been identified. The existence of such CPGs is associated with the ability of these animals to walk even after a section of the spinal cord: "*Kittens with the spinal cord sectioned several days after birth that are stimulated and trained in a special way can walk on all four limbs. If the lumbosacral division of the spinal cord is isolated in an 8 to 14 day-old kitten, the animal can, in some months, walk on the hindlimbs on the moving treadmill band even when the forlimbs are fixed. [...] Thus, the basic pattern of the stepping movement can be generated by the spinal cord isolated from the brain.*" (Shik and Orlovsky, 1976).

By contrast, it seems that no such localized CGP-like structures exist in humans. In fact, there has been no evidence yet that it is possible to spontaneously generate any locomotor activity in patients with complete spinal cord injury. The neural architecture of human locomotion thus seems to be much more distributed and complex than that of other animals. One may even talk of the "*special nature of human walking and [of] its neural control*" (see for instance Capaday, 2002; Hicheur, 2006).

### 2.1.2 Biomechanical description of the stepping pattern

From a biomechanical viewpoint, the description of the stepping cycle in terms of muscle activity and of joint angles patterns is more complete. The reader is referred to Hicheur (2006) for a clear and comprehensive review of the body of knowledge concerning this aspect. Here, we concentrate on a particular issue that pertains to our study: how the coordination of the legs' segments is re-organized when humans walk backward.

As mentioned previously, the axial gait in the lamprey is essentially based on the alternate contractions of antagonistic myotomes. The backward gait is obtained simply by time-reversing the contraction patterns corresponding to the forward gait (Grillner et al., 1995). In humans however, the simple time-reversal of muscle activity patterns cannot produce backward walking due to "*the multijointed nature of the limbs and [to] the anatomic asymmetry of the body in the anteroposterior direction*" (Grasso et al., 1998b).

Despite these considerations, it appears that the production of backward gait is still supported by the time-reversal of the *limb trajectories* (Fig. 2.2). This simple transformation is however produced by radical and complex changes in the patterns of muscle activity (Thorstensson, 1986). These results are reminiscent of the "spatial control" hypothesis put forward by Morasso (1981) in the context of hand movements (see section 1.1).

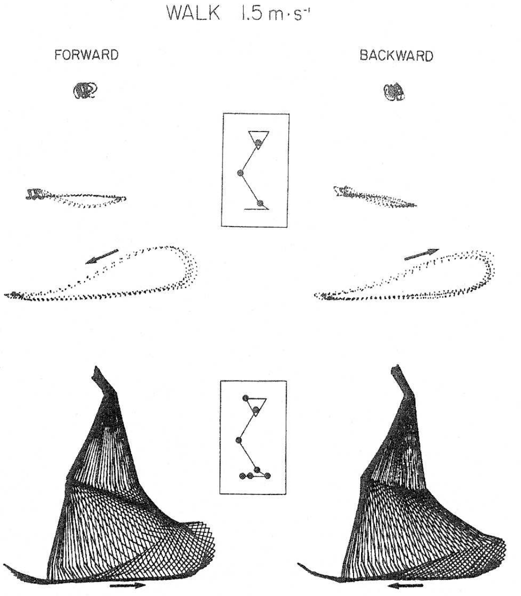

Figure 2.2: Movement trajectories of the left leg during forward and backward walking on a treadmill. Above: superimposed records of the markers on the hip, knee and ankle markers during five consecutive strides. Below: stick figures showing the movements of the whole leg during one stride (adapted from Thorstensson, 1986).

Going deeper in the analysis, Grasso et al. (1998b) showed more precisely that the patterns of *elevation* angles (the angles between the leg segments with the vertical) was conserved after time-reversal. The joint angle patterns (the angles between the leg segments) were also conserved, but to a lesser extent. In any case, in agreement with Thorstensson (1986), the authors found that the muscle activity patterns were completely re-organized to preserve this kinematic symmetry.

## 2.2 Multisensory control of locomotion

As mentioned in the Introduction, multiple sensory signals (visual, vestibular, proprioceptive, cutaneous, etc.) are processed by the CNS during locomotion. Efferent copies of the motor commands are also integrated with the sensory signals, allowing the dynamic and predictive interaction of the body with the environment. The relative contribution of each source of information and the way these sources interact with each other are two important issues in locomotion research.

When normal visual inputs are available, they are sufficient for accurate locomotion and supersede the other sources of information. For instance, Fitzpatrick et al. (1999) and Glasauer et al. (1994) showed that perturbed or abnormal vestibular inputs have practically no effect on locomotion when normal vision is present.

### 2.2.1 Accuracy of nonvisual locomotion

However, there are numerous situations where visual inputs are heavily deteriorated or even completely absent. In these situations, one must use the remaining sources of information to accurately navigate, a method termed *path integration* (Loomis et al., 1999).

Thomson (1983) undertook one of the first investigations of the ability of humans to walk without vision towards a previously seen target. He reported nearly zero *systematic error* for targets placed in front of the subjects, as far as 21m away: that is, the average stopping positions almost coincided with the target's position. Similar results for shorter target distances were reported in posterior studies (see Fig 2.3 for a summary). This accuracy on average was taken as evidence of the veridicality of visual space perception (Loomis et al., 1992).

On the other hand, the *variable error*, that is, the trial-to-trial *variability* of the response, was found to increase with distance (see Loomis et al., 1992).

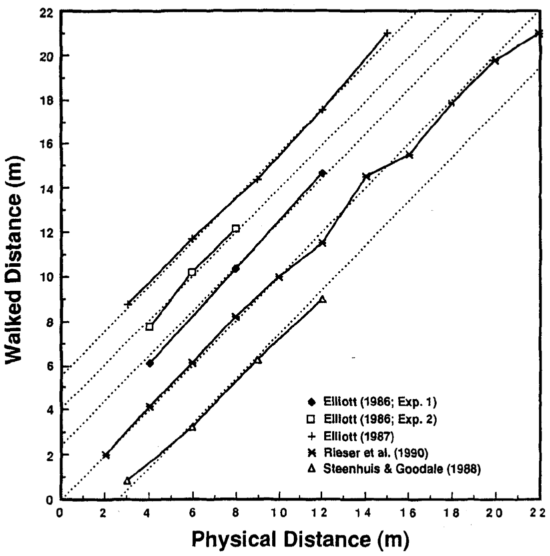

Figure 2.3: Summary of the works investigating linear path integration (adapted from Loomis et al., 1992).

Rieser et al. (1990) showed more precisely that the standard deviation of the actually walked distances is a linear function of the target distance.

The above studies concerned the translatory component of locomotion. It was also shown that humans are able to process continuous or discrete changes in orientation (rotational component) during nonvisual locomotion. For instance, Takei et al. (1996) showed that humans are able to reproduce previously seen circles of radius $\sim$ 1m with reasonable accuracy (see Fig. 2.4). The ability to process *discrete* changes in orientation was also demonstrated in several triangle reproduction experiments (see for instance Glasauer et al., 2002, and Fig. 2.5).

It was shown that nonvisual locomotion performance is enhanced by locomotor experience, and more surprisingly, by mental simulation. Vieilledent et al. (2003) asked subjects to preview an hexagone drawn on the ground. The subjects then underwent a “learning phase” during which they were equipped with blindfolds and noise-delivering headphones. In one group, the subjects had to mentally simulate walking along the hexagon’s sides (without viewing the hexagon). In another group, the subjects were guided nonvisually along the hexagon’s side. In a third group, the subjects sat at rest during the “learning phase”. After the “learning phase”, the subjects were asked to nonvisually reproduce the hexagon by walking. The authors showed that the subjects from the first and the second group performed significantly better than those from the third group. Moreover, the effects of mental simulation

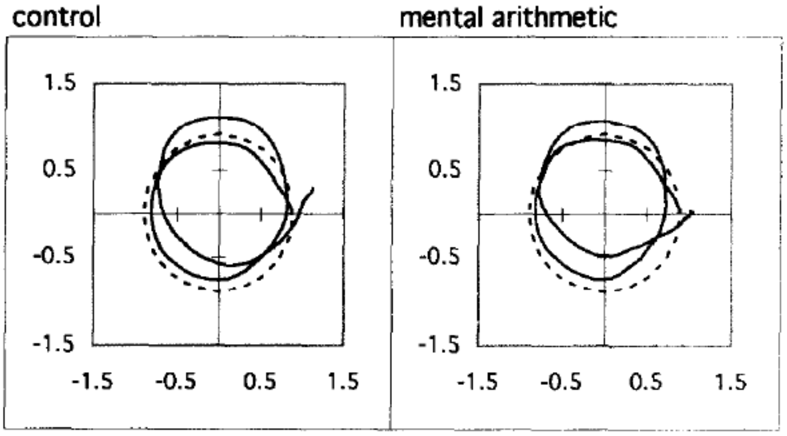

Figure 2.4: Nonvisual reproduction of a previously seen circle in two mental conditions (adapted from Takei et al., 1996).

and physical practice were comparable.

### 2.2.2 The control strategies underlying nonvisual locomotion

Two strategies are usually proposed to account for the task of walking without vision towards a previously seen target. The first strategy consists of planning in advance the movements needed to reach the target and then executing the plan. The second strategy implies an *online* control of locomotion via the retention and the updating of the target's distance or location (Thomson, 1983; Farrell and Thomson, 1999).

To comparatively assess the two strategies, Farrell and Thomson (1999) designed a clever experiment where subjects had to walk with or without vision towards a previously seen target placed at 8 paces, 8 paces minus 40cm or 8 paces plus 40cm in front of them. In each trial, a subject had to start with his right foot and to land on the target with his left foot. By analyzing the variability of lengths of the final steps, the authors showed that the subject *functionally* adjusts the lengths of his final steps, on a trial-to-trial basis, in order to land on the target with the specified foot. This online control behavior was moreover present in both visual and nonvisual conditions. Based on this result, the authors suggested that, during nonvisual locomotion, humans monitor their positions in an online manner, with respect to a memorized target.

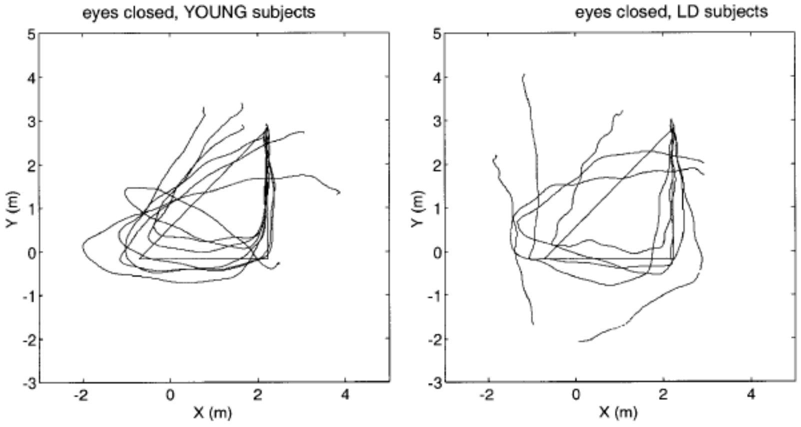

Figure 2.5: Nonvisual reproduction of a previously seen triangles by normal and vestibular subjects (adapted from Glasauer et al., 2002).

### 2.2.3 The role of inertial and substratal information in nonvisual locomotion

The online strategy mentioned above requires in particular to update the target's position (or the distance to the target) during the movement. In absence of vision, this is done by integrating vestibular and proprioceptive signals, as well as efferent copies of motor commands (Loomis et al., 1999). These *idiothetic* sources of information may then be further categorized in two groups: vestibular signals provide *inertial* information, while proprioception and efferent copies provide *substratal* information (Mittelstaedt and Mittelstaedt, 2001).

Glasauer et al. (1994) showed that vestibular patients could walk towards previously seen targets as accurately as normal subjects, which indicate that inertial information is not necessary for the control of linear locomotion. Furthermore, by affecting differentially inertial and substratal signals (e.g. by using treadmills and manipulating step lengths), Mittelstaedt and Mittelstaedt (2001) also showed that substratal information is dominant in nonvisual locomotion.

On contrary, the vestibular system plays a crucial role in tasks where changes in orientation are required (e.g. circle or triangle reproduction tasks, see previously). In such tasks, it was first demonstrated that the linear and rotational components of locomotion are controlled separately (see Berthoz et al., 1999; Hicheur et al., 2005a). While inertial information is not needed for the processing of the linear component, it is essential for the processing of the rotational component. Indeed, in the triangle reproduction task, vestibular patients produced the same distance errors as normal subjects, but significantly larger orientation errors (Glasauer et al., 2002, see Fig. 2.5).

## 2.3 Steering behavior

The changes in the body orientation mentioned previously are achieved through, in particular, continuous and progressive adjustments of the head and trunk directions in the horizontal plane, which are defined as the "steering behavior" (Patla et al., 1999a). The steering behavior constitutes another level of description of goal-oriented locomotion, intermediate between the stepping activity and the formation of whole-body trajectories.

It was observed that changes in the steering behavior significantly affect the formation of locomotor trajectories. For instance, following an unexpected head yaw perturbation, the locomotor trajectory was found to deviate towards the direction of the perturbation (Vallis and Patla, 2004, Fig. 2.6).

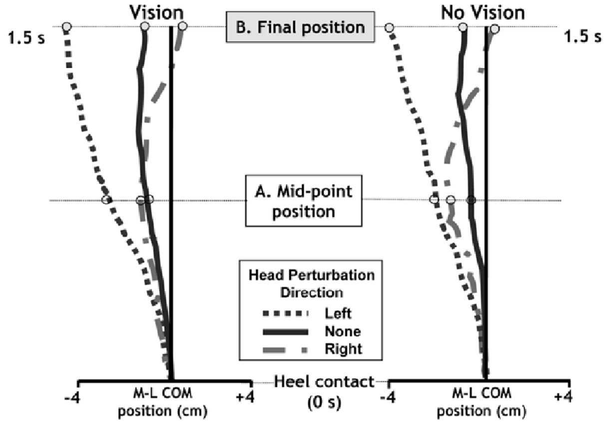

Figure 2.6: Effect of an unexpected head yaw perturbation on the trajectory of the center of mass. A perturbation of the head yaw directed to the left made the trajectory deviate towards the left (dotted lines). When this perturbation was directed to the right, the trajectory deviated towards the right (dashed lines). This effect was present in both visual and nonvisual locomotion (adapted from Vallis and Patla, 2004).

Conversely, the properties of whole-body trajectories determine the head and trunk rotation patterns. For instance, in straight trajectories, the head mostly aligns with the direction of movement (or the heading), but in curved trajectories, the head is oriented towards the *interior* of the curve, thus making a nonzero angle with the heading. This phenomenon is termed "head anticipatory behavior" (Grasso et al., 1996), since the head direction at time $t$ is only reached by the heading at time $t + \Delta t$ (Fig. 2.7). Moreover, it was shown that the larger the curvature, the more the head anticipates (Hicheur et al., 2005b, 2007).

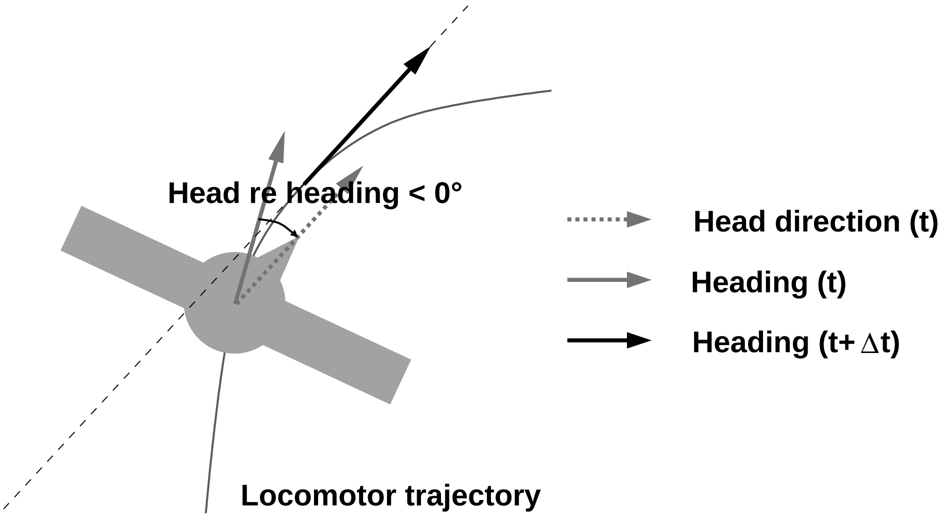

Figure 2.7: When humans walk along a curved trajectory, their heads point towards the interior of the curve, thus anticipating the future direction of movement.

This anticipatory behavior was robustly observed under various conditions: when human subjects walk along circles (Grasso et al., 1996), along shapes with varying curvature (Hicheur et al., 2005b), along a simple turns (Imai et al., 2001; Courtine and Schieppati, 2003; Prévost et al., 2003), without vision or backward (Grasso et al., 1998c). Furthermore, the anticipatory behavior was shown to develop in children between 3 and 8 years old (Grasso et al., 1998a). Table 2.1 summarizes some of the works investigating the anticipatory steering behavior.

Several hypotheses were proposed for the role of head anticipatory behavior. First, it was believed to be a component of an eye-head synergy which aims at *anchoring the gaze* in the future direction of movement (Grasso et al., 1998c), as in car driving (Land and Lee, 1994). However, the fact that this anticipation behavior remains in nonvisual locomotion (Grasso et al., 1996, 1998c; Courtine and Schieppati, 2003) suggests that anchoring gaze is not the only purpose of head anticipation. Rather, since the head contains also auditory and vestibular organs, placing the head in the future direction of movement may provide a stable *reference frame* from which the coordination

| Reference | Free | Goal | BW | NV | Trk | Eye | Pert | Dev |
|---|---|---|---|---|---|---|---|---|
| Grasso et al. (1996) |  |  |  | √ | √ | √ |  |  |
| Grasso et al. (1998a) | √ |  |  | √ | √ |  |  | √ |
| Grasso et al. (1998c) | √ |  | √ | √ |  |  |  |  |
| Patla et al. (1999a) | √ |  |  |  | √ |  |  |  |
| Imai et al. (2001) | √ |  |  |  | √ | √ |  |  |
| Hollands et al. (2001) | √ |  |  |  | √ |  | √ |  |
| Vallis et al. (2001) | √ |  |  |  | √ |  | √ |  |
| Courtine and Schieppati (2003) |  |  |  | √ | √ |  |  |  |
| Prévost et al. (2003) | √ |  |  | √ |  |  |  |  |
| Vallis and Patla (2004) | √ |  |  |  | √ |  | √ |  |
| Hicheur and Berthoz (2005) |  |  |  |  | √ |  |  |  |
| Hicheur et al. (2007) | √ | √ |  |  | √ |  |  |  |
| Pham et al. (2010) | √ | √ | √ | √ | √ |  |  |  |

Table 2.1: Summary of the works investigating the anticipatory steering behavior. Free: this work includes trajectories whose paths were not predefined. Goal: includes relatively complex goal-oriented trajectories. BW: tests backward locomotion. NV: tests nonvisual locomotion. Trk: examines trunk movements. Eye: examines eye movements. Pert: investigates effects of head yaw perturbations. Dev: investigates the effects of development.

of the other body segments can be planned (Hollands et al., 2001; Hicheur et al., 2005b).

# Chapter 3

# Some studies of locomotion at the level of whole-body trajectories

We present in this section three main currents of research that deal with the formation of locomotor trajectories. According to proponents of the *"ecological"* current, locomotor trajectories may result from dynamic interactions of the subject with his environment (section 3.1). Another current of research, which takes inspiration from studies of arm movements, looked for *invariants* in locomotor trajectories, in particular those relating locomotor speed to path curvature (section 3.2). More recently, a robotics-inspired approach put the emphasis on the *nonholonomic* coupling between the subject's orientation and his walking direction (section 3.3).

## 3.1 Ecological approaches

Ecological approaches emphasize the dynamic relations of the subject with his environment. In a task of walking towards a distant target in an environment filled with obstacles (Fajen and Warren, 2003), the targets are viewed as *attractors*, obstacles as *repellers* and the subject as a *dynamical system* evolving in a field of attractors and repellers. Locomotor trajectories can then be viewed as solutions of the dynamical equation: "*the [subject] adopts a particular route through the scene on the basis of local responses to visually specified [targets] and obstacles. The observed route is not determined in advance through explicit planning, but rather emerges in an online manner from the [subject's] interactions with the environment*". Variations of this model (Fajen and Warren, 2007) allow studying the case of moving targets.

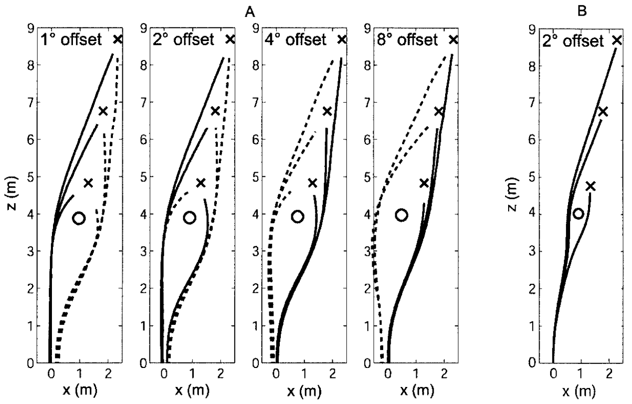

Figure 3.1: (**A**) actual trajectories recorded in a goal-oriented task with obstacle avoidance. The goals were represented by crosses and the target was represented by a circle. Different initial angles were tested. The solid line corresponded to the most frequently taken path. (**B**) trajectories simulated by a dynamical model (adapted from Fajen and Warren, 2003).

The two important features of ecological approaches highlighted by the previous quote are the *online* and *visual* nature of the interactions. Accounting for (i) the ability of humans to reach targets in nonvisual locomotion and (ii) the similarity of visual and nonvisual average trajectories (see our results later in section 5.2) may thus constitute challenging issues for proponents of the ecological approaches.

## 3.2 Invariants of locomotor trajectories

We mentioned previously that the drawing of curved shapes with the hand is characterized by an inverse relationship between velocity and curvature, which was mathematically formalized by the so-called "one-third power law" (see section 1.1). Following the "principle of motor equivalence" evoked in the Introduction, several works have examined whether locomotor trajectories also obey this law. Vieilledent et al. (2001) asked subjects to walk along ellipses drawn on the ground and reported that this law was indeed respected. Hicheur et al. (2005c) argued that ellipses are special cases and that the results reported by Vieilledent et al. were therefore not conclusive. The authors consequently developped an experimental protocol where more complex shapes such as cloverleaves or limacon were tested. They reported that the one-third exponent was not observed for all shapes. Rather, the speed-curvature relationship was quantified by power laws with different exponents $\beta$ which depended on the shapes.

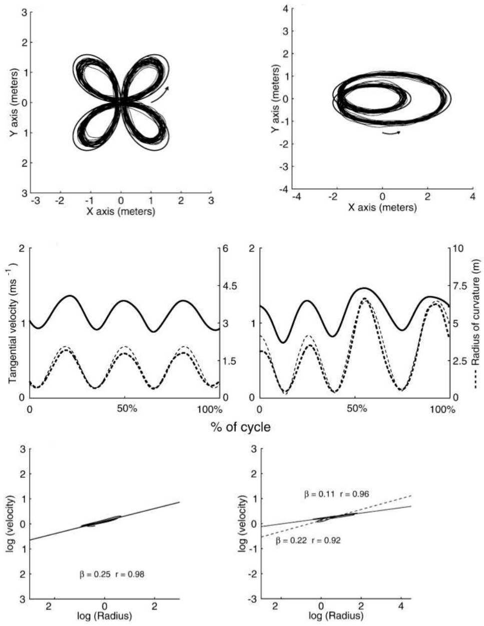

Figure 3.2: Power law in human locomotion. Top: actual geometrical paths recorded for the cloverleaf (left) and the limacon (right). Middle: velocity profiles (plain lines), curvature profiles (dashed lines). Bottom: velocity as a function of curvature (log-log plot) (adapted from Hicheur et al., 2005c).

More recently, Olivier and Cretual (2007) confirmed the result of Hicheur et al. that one-third power law was not verified by locomotor trajectories produced in a turning task. However, they showed that, across multiple trials indexed by $i$, the following relationship was robustly verified

$$v_i(t_i) = \gamma r_i(t_i)^{1/3} \tag{3.1}$$

where $t_i$ is the instant in trial $i$ when the maximum curvature was attained, $r_i(t_i)$ and $v_i(t_i)$ are the radius of curvature and the speed at this instant.

## 3.3 Nonholonomic coupling of orientation and walking direction

A bicycle, a car or a wheeled robot do not move sideways but tangentially to their main axes. This constraint acting on wheeled vehicles is known as a *nonholonomic* constraint (Laumond, 1998). Observing that humans also walks forward and not sideways, Arechavaleta et al. (2006) suggested that this nonholonomic constraint also governs human locomotion. To test this hypothesis, the authors designed the "walking towards and through a distant doorway" protocol mentioned in the Introduction (for a precise description of that protocol, see section 5.2). They then compared the walking direction profile $\theta(t)$ with the head, trunk and pelvis angle profiles ($\phi_H(t)$, $\phi_T(t)$, $\phi_P(t)$ respectively). They found that the trunk orientation best approximated the walking direction after time shift, that is

$$\dot{\phi}_T(t+\epsilon) \simeq \dot{\theta}(t) \tag{3.2}$$

where $\epsilon = 1/6s$ corresponds to the trunk anticipation time (see also our study of head and trunk anticipatory behavior in chapter 7).

Based on this result, Arechavaleta et al. (2008a) suggested that human locomotion can be described by a bicycle-like system

$$\begin{pmatrix} \dot{x}_T \\ \dot{y}_T \\ \dot{\theta} \\ \dot{\phi}_T \end{pmatrix} = \begin{pmatrix} \cos(\theta) \\ \sin(\theta) \\ \tan(\phi_T/L) \\ 0 \end{pmatrix} u_1 + \begin{pmatrix} 0 \\ 0 \\ 0 \\ 1 \end{pmatrix} u_2 \tag{3.3}$$

where $(x_T, y_T)$ is the position of the shoulders' midpoint (taken as reference for the body position, see also the General Methodology, section 4.1.2), $L$ is the length between the front wheel and the back wheel (computed based on the value of the trunk anticipation time $\epsilon$), $u_1$ is the driving speed and $u_2$ is the turning rate. To verify this hypothesis, the authors extracted $u_1$ and $u_2$ from the experimental data (the locomotor tengential speed and the turning speed) and injected the values into the system to calculate $(x_T, y_T)$. They showed that 87% of the 1560 recorded trajectories could be approximated by this model with an error of less than 20cm.

Going a step further, Arechavaleta et al. (2008b) proposed an extended version of this model which includes a third command $u_3$ representing the curvature. They showed that an optimal control scheme minimizing $u_1$, $u_2$ and $u_3$ could reproduce the experimental trajectories (see Arechavaleta et al., 2008b, and Fig. 3.3).

Undoubtedly, the nonholonomic approach has provided important insights for the understanding of goal-oriented locomotion. However, in our opinion, the current versions of the nonholonomic models still display some serious issues. First, while there exists a clear correlation between the heading and the trunk direction, these two variables are by no means identical because of the anticipatory steering behavior (see section 2.3 and our study in section 7.1). The authors did address this issue by adding a constant

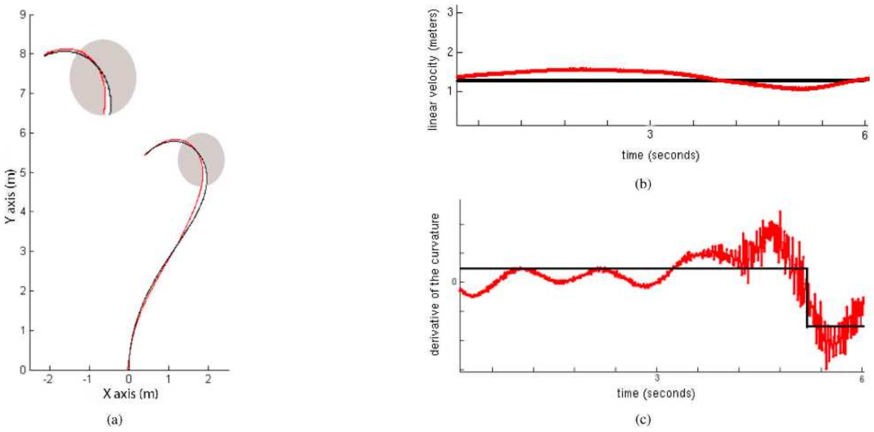

Figure 3.3: A nonholonomic model for trajectories formation. Left: geometric paths (red: actual, black: simulation by the nonholonomic model). Right top: velocity profiles. Right bottom: curvature profiles (adapted from Arechavaleta et al., 2008b).

anticipation time $\epsilon$. However, as shown in our study of section 7.1, the anticipation time is in fact a complex quantity, which changes during the steering and which also depends on the global curvature of the trajectory. How this essential modulation of the nonholonomic constraint affects the trajectories simulated by the model is an important question.

Second, the optimization process of the current nonholonomic model seems to yield a constant velocity profile even for curved trajectories (see e.g. Fig. 3.3), which is not observed in actual movements (for instance, there exists an inverse relationship between velocity and curvature, see section 3.2). The variation of the velocity over the whole movement can be as large as 50% of the average velocity (see e.g. Fig. 3.2), which is by no means negligible.

Third, a common shortcoming of all the models presented in this chapter is their *deterministic* nature. Yet, the variability patterns displayed by locomotor trajectories and by human movements in general are important to study (see section 1.3) but cannot be investigated using deterministic models. This aspect is discussed in detail in chapters 6 and 9.

The models we present in chapters 8 and 9 address some of the issues we have just raised. However, since they do not take into account the nonholonomic constraint, our models lack several important features of human locomotion. We believe that our modeling approach and the nonholonomic view are in fact complementary: combining the two approaches thus represents a promising direction of research.

# Part II

# Experimental study

# Chapter 4

# General methodology and notations

This chapter presents the main methodology and notations used in the locomotion experiments (Experiments 1 to 6). The specific methodology of each particular experiment is detailed in the Methods section of that experiment.

Section 4.1 describes the experimental methods used to record subject's movements (cameras, markers sets, etc.) while section 4.2 presents the main analyses that were performed on the recorded experimental data.

## 4.1 Materials and methods

### 4.1.1 Motion capture system

In order to record subject's whole-body movements and segmental displacements, we used the Vicon® (Oxford Metrics, Oxford, UK) motion capture system (see Fig. 4.1). Several light-reflective markers were attached to the subject. The 3D positions of these markers were recorded at a 120Hz sampling frequency in all experiments, except in Experiment 6, where a 200Hz sampling frequency was used.

In Experiments 1 and 2, the full markers set (39 markers) was used, allowing a full-body motion capture. In the other experiments, more limited sets of markers were used according to need. The following markers were considered in the data analyses

- Head markers: four markers were attached to the subject's head. These markers were used to reconstruct the head orientation in the horizontal plane

Figure 4.1: The laboratory where Experiments 2, 3 and 4 took place. The lab was equipped with Vicon® infrared cameras. A subject with light-reflective markers was walking towards the white cardboard arrow placed on the ground.

- Shoulders markers: Two markers were placed on the subject's left and right acromions. These markers were used to compute the orientation of the trunk. In addition, the subject's position in space was defined by the midpoint of the shoulders markers (see below)

- Feet markers: Two markers were placed on each foot, one on the heel and one between toes 2 and 3 (toe 1 is the big toe). These two markers were used to reconstruct the successive positions of the foot during the locomotor task

### 4.1.2 Definition of the "locomotor trajectory"

To study whole-body trajectories in space, we used, as stated above, the *midpoint of the segment joining the two shoulders markers* (Fig. 4.2). Indeed, because of their particular positions on the body, shoulders markers were the most faithfully reconstructed by the motion capture system. Moreover, the shoulders' markers' midpoint is very easy to compute, in contrast with other possible reference points such as the Center of Mass (CoM), whose localization requires the capture of the full marker set as well as anthropometric data (Olivier and Cretual, 2007).

However the choice of the reference point induce some differences. First,

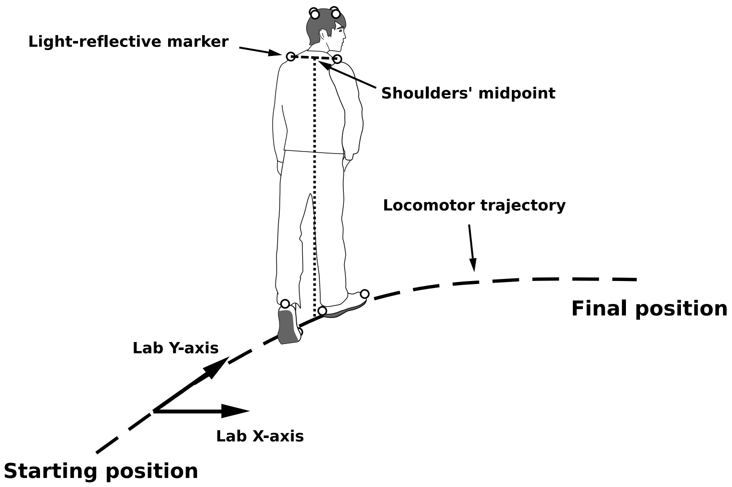

Figure 4.2: Markers set and definition of the locomotor trajectory. The trajectory was defined by projecting the midpoint of the two shoulders' markers on the ground.

since humans tend to lean towards the *interior* of the curve while walking along a curved path, the projection of the shoulders' midpoint on the ground lies *inside* the curved path (Hicheur et al., 2005c). Thus, the curvature computed based on the shoulders' midpoint 2D trajectory is larger than that of the predefined paths. Similarly, since the CoM is localized lower than the shoulders' line, the shoulders' midpoint 2D curvature is often larger than the CoM 2D curvature. However, it should be noted that the differences between the shoulders' midpoint 2D trajectory and the CoM 2D trajectory (less than 10 centimeters) were rather small with respect to the lengths of these trajectories (more than 5 meters in our experiments).

## 4.2 Data analysis

The data collected by the motion capture system was analyzed using computer softwares, mainly the free software GNU Octave. We were interested in the average behavior across repetitions of the same subject or across subjects, as well as the variability around this average behavior. In particular, we performed comparisons of the average behaviors and of the variabilities recorded in different conditions.

### 4.2.1 Filtering and time-rescaling

The data were filtered only when we needed to calculate derivatives (velocity, acceleration, jerk, curvature, etc.) In such cases, a second-order Butterworth filter with cut-off frequency 6.25Hz was applied before the derivation.

To homogenize the trajectories before calculating average and variability values, we first localized the time instants $t_0$ and $t_1$ when the trajectory begins and ends (see the Methods in each experiment for detail). We then time-rescaled the trajectory such that $t_0 = 0$ and $t_1 = 1$.

This procedure, while necessary, presents a serious drawback: it "erases" the movement duration. We were therefore not able to study some important aspects involving movement duration, such as the duration-accuracy trade-off (Fitts, 1954; Tanaka et al., 2006).

### 4.2.2 Statistical analysis of locomotor trajectories

The average trajectory $(x_{\mathrm{av}}(t), y_{\mathrm{av}}(t))_{0 \le t \le 1}$ of a given set of $N$ trajectories $\{(x_i(t), y_i(t))_{0 \le t \le 1}\}_{1 \le i \le N}$ was computed as follows

$$x_{\mathrm{av}}(t) = \frac{1}{N}\sum_{i=1}^{N} x_i(t), \quad y_{\mathrm{av}}(t) = \frac{1}{N}\sum_{i=1}^{N} y_i(t) \tag{4.1}$$

The Trajectory Deviation (TD) [1], which measures the variability of sample trajectories around the average trajectory, was calculated as [see Fig. 4.3(A)]

$$\mathrm{TD}(t) = \sqrt{\frac{1}{N-1}\sum_{i=1}^{N}(x_i(t) - x_{\mathrm{av}}(t))^2 + (y_i(t) - y_{\mathrm{av}}(t))^2}. \tag{4.2}$$

The *variability profile*, which is central in our analyses, was defined as the time-evolution of the Trajectory Deviation $(\mathrm{TD}(t))_{0 \le t \le 1}$.

To quantify the variability of the trajectories over the whole movement, we considered the Average Trajectory Deviation (ATD) and the Maximal Trajectory Deviation (MTD)

$$\mathrm{ATD} = \int_0^1 \mathrm{TD}(t)\mathrm{d}t \tag{4.3}$$

$$\mathrm{MTD} = \max_{0 \le t \le 1} \mathrm{TD}(t) \tag{4.4}$$

---

[1] We used the term "deviation" in reference to the usual 1D "standard deviation".

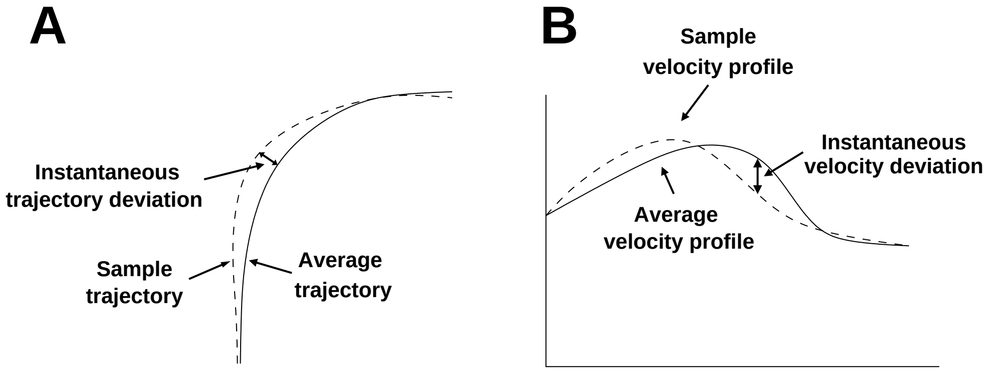

Figure 4.3: Trajectory and velocity deviations

**Variance ellipses** For a graphical examination of trajectory variabilities, we plotted the variance ellipses calculated by principal component analysis. Intuitively, the variance ellipse at time $t$ is centered at $(x_{\mathrm{av}}(t), y_{\mathrm{av}}(t))$ and its orientation and magnitude indicate how the $(x_i(t), y_i(t))$ $(i = 1 \ldots N$ are distributed around $(x_{\mathrm{av}}(t), y_{\mathrm{av}}(t))$. Note that $r_1(t)^2 + r_2(t)^2 = \mathrm{TD}(t)^2$ where $r_1$ and $r_2$ are the lengths of the ellipse's semi-major and semi-minor axes.

### 4.2.3 Statistical analysis of velocity profiles

In order to compare velocity profiles in terms of their variations in time rather than in terms of their absolute variabilities (which are due in part to the variability of the walking tempos in different subjects), we considered the normalized velocity profile, which was defined as

$$v_i(t) = \frac{\sqrt{\dot{x}_i(t)^2 + \dot{y}_i(t)^2}}{\int_0^1 \sqrt{\dot{x}_i(t)^2 + \dot{y}_i(t)^2} \mathrm{d}t} \tag{4.5}$$

The average normalized velocity profile and the instantaneous normalized Velocity Deviation (nVD) were then computed by [see Fig. 4.3(B)]

$$v_{\mathrm{av}}(t) = \frac{1}{N} \sum_{i=1}^{N} v_i(t) \tag{4.6}$$

$$\mathrm{nVD} = \sqrt{\frac{1}{N-1} \sum_{i=1}^{N} (v_i(t) - v_{\mathrm{av}}(t))^2} \tag{4.7}$$

Finally, we defined the Average and Maximal normalized Velocity Deviations (AnVD and MnVD) over the whole movement as

$$\mathrm{AnVD} = \int_0^1 \mathrm{nVD}(t)\mathrm{d}t \tag{4.8}$$

$$\mathrm{MnVD} = \max_{0\leq t\leq 1} \mathrm{nVD}(t) \tag{4.9}$$

### 4.2.4 Comparison of trajectories in different conditions

In order to quantify the similarity of trajectories between two different conditions, say A and B, we considered the Trajectory Separation (TS) defined as

$$\mathrm{TS}_{\mathrm{A/B}}(t) = \sqrt{(x_{\mathrm{A}}(t) - x_{\mathrm{B}}(t))^2 + (y_{\mathrm{A}}(t) - y_{\mathrm{B}}(t))^2} \tag{4.10}$$

We then defined the average and maximal trajectory errors ($\mathrm{ATS}_{\mathrm{A/B}}$ and $\mathrm{MTS}_{\mathrm{A/B}}$) over the whole trajectory as

$$\mathrm{ATS}_{\mathrm{A/B}} = \int_0^1 \mathrm{TS}_{\mathrm{A/B}}(t)\mathrm{d}t \tag{4.11}$$

$$\mathrm{MTS}_{\mathrm{A/B}} = \max_{0\leq t\leq 1} \mathrm{TS}_{\mathrm{A/B}}(t) \tag{4.12}$$

Note that $\mathrm{ATS}_{\mathrm{A/B}}$ and $\mathrm{MTS}_{\mathrm{A/B}}$ take into account the instantaneous errors at all time instants. They are therefore sensitive to differences at both the geometric level and the velocity profile level.

# Chapter 5

# The formation of locomotor trajectories in humans: a stereotyped behavior

## 5.1 Overview

Let's start from the situation evoked at the beginning of the Introduction: a person is standing at some position in a room and has to walk towards and through a distant doorway to get out of that room [Fig. 1(A)]. We remarked in chapter 1 that a similar task for the hand (namely: bring the hand from a given position in space towards another position) involved serious difficulties, in particular, those associated with the *redundancy* problem. Here, we face the same difficulties: an infinite number of locomotor trajectories (paths + velocity profiles) can bring the person from his initial position towards the door's position. A given trajectory can be implemented by an infinite number of sequences of foot positions (FP), which in turn can be generated by an infinite number of possible muscle activation patterns, etc. Moreover, the difficulties associated with the redundancy problems are amplified by the greater complexity of the locomotor activity (at the motor, sensory, cognitive, etc. levels).

In this context, we set out to identify the level at which goal-oriented locomotion is planned and controlled. We considered two possible levels: the step- and the trajectory-level. In a step-level strategy, subjects would plan and execute precise sequences of foot positions leading to the target. On contrary, in a trajectory-level strategy, subjects would plan first a trajectory and then implement such a trajectory by appropriate sequences of foot positions. To comparatively assess the two possibilities, we recorded in

Experiment 1 the whole-body trajectories and the foot positions of subjects performing the "walking towards a distant doorway" task. We assessed the variability of the trajectories across repetitions and subjects, and compared this variability with the variability of the corresponding sequences of FP. Our basic assumption was that, if locomotion is planned and controlled at the step-level, then the sequences of FP would be stereotyped. Otherwise, if the sequences of FP are much more variable than the whole-body trajectories, then a trajectory-level control is more likely.

If locomotion is planned and controlled at the level of whole-body trajectories, it would then be interesting to examine how these trajectories are affected by changes in the sensory and motor conditions. In Experiment 2, we thus asked subjects to perform a task similar to the "walking towards a distant doorway" task in different sensory (walking with or without vision) and motor (walking forward or backward) conditions. The results then allow discussing the hypothesis that locomotor trajectories are planned and controlled at a high cognitive level, and to some extent, independently of their sensorimotor implementations.

Experiment 1 was designed and run by G. Arechavaleta, H. Hicheur, J.-P. Laumond and A. Berthoz in June 2005. The analysis was performed by these authors and Q.-C. Pham and was presented in Hicheur et al. (2007), to which the reader is referred for more details. Experiment 2 was designed and run by Q.-C. Pham and H. Hicheur in February 2007. We thank A.-H. Olivier and A. Cretual for their help with this experiment. The results of this experiment were first reported in Pham et al. (2010), to which the reader is referred for more details.

## 5.2 Experiment 1: stereotypy of locomotor trajectories, variability of foot positions

### 5.2.1 Methods

#### Subjects and materials

Six male subjects participated in this experiment. Each subject generated 120 trajectories (40 spatial targets × 3 repetitions), so that a total of 720 trajectories were recorded.

The targets consisted of a 1m × 1m × 2m door (width, depth and height respectively) placed at various positions and orientations in the laboratory (Fig. 5.1 and Fig. 5.2). Fourteen targets were used: their distances from the starting position ranged between 3m and 6.5m and their orientations with respect to the subject's initial walking direction ranged between $-150°$ to $+150°$.

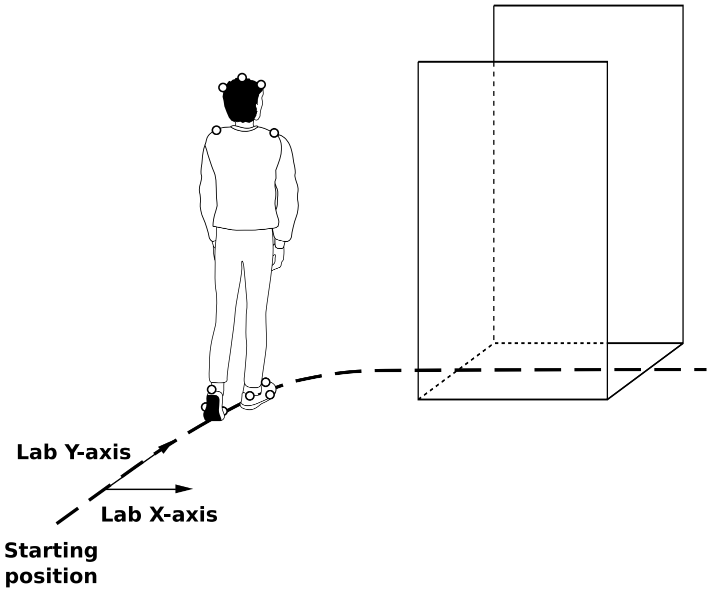

Figure 5.1: In Experiment 1, the targets of consisted of a 1m × 1m × 2m door (width, depth and height respectively) placed at various positions and orientations in the laboratory.

### Protocol

The subject had to start from a fixed position in the laboratory and walk toward and through a distant doorway (Fig. 5.1). To constrain the subject's initial walking direction, we asked him to begin his walk 1m before crossing the start line, orthogonally to the lab's X-axis. He was then completely free to choose his walking speed and no specific restriction was provided regarding the path to follow.

The subject was not asked to stop right after entering the doorway. Typically, the subject walked straight for a few meters (about four steps) after going through the doorway before returning to the starting position. The experimenter stopped recording a few meters after the subject had passed through the door.

### Analysis

**Categorization and computation of the trajectories** The tested trajectories were classified *a priori* into four categories according to the amount

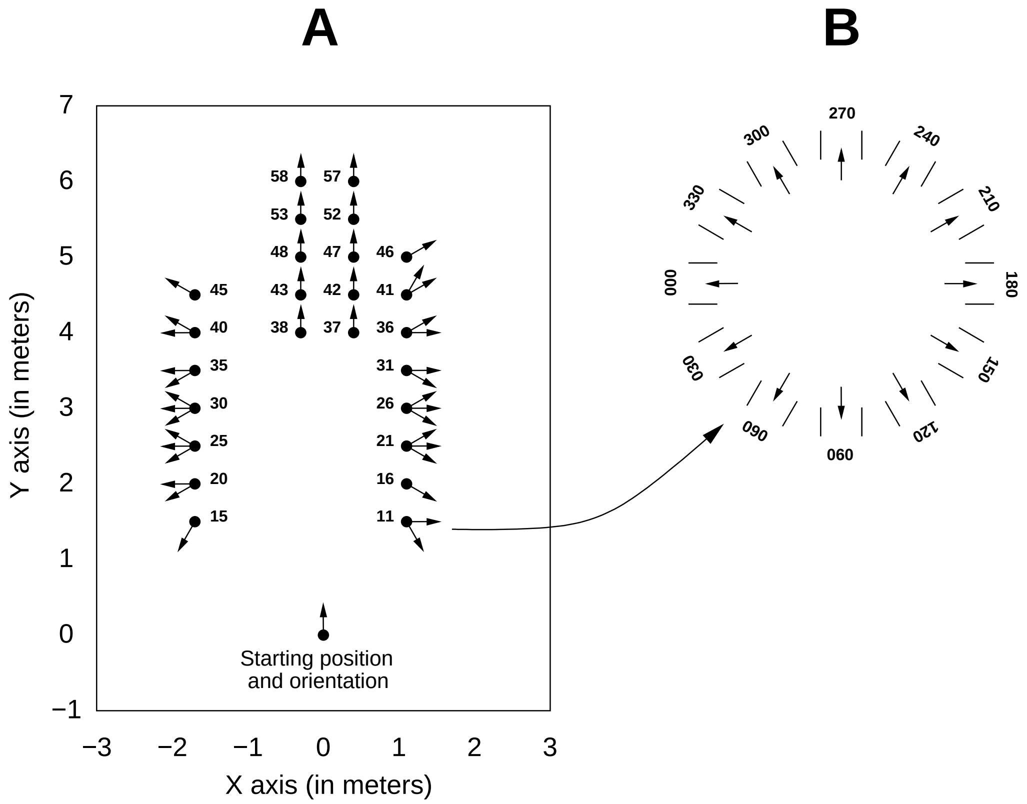

Figure 5.2: Fourty targets were used in Experiment 1. Each target was labelled by two numbers: its position (e.g. 21) and its orientation (e.g. 180).

of trajectory curvature they required: quasi-straight trajectories (ST), trajectories of low (LC), medium (MC) and high (HC) curvature (see Table 5.1). Fig. 5.3 shows four actually recorded trajectories, one per category.

To homogenize the computation of trajectories across subjects and repetitions, we cut out the initial and final parts of the trajectories. For each trial, we thus considered only data between instant $t_0$ when the subject crossed over the X-axis and instant $t_1$ when he reached the middle of the doorway. Finally, the trajectory was time-rescaled so that $t_0 = 0$ and $t_1 = 1$ (see section 4.2.1).

**Variability of trajectories and of velocity profiles** To quantify the variability of whole-body trajectories, we used the measures defined in chapter 4, namely: Trajectory Deviation (TD), Average and Maximal Trajectory Deviation (ATD and MTD), normalized Velocity Deviation (nVD), Average and Maximal normalized Velocity Deviations (AnVD and MnVD). Note that

| HC | MC | LC | ST |
|---|---|---|---|
| 11-120 | 11-180 | 21-210 | 37-270 |
| 15-060 | 20-000 | 25-330 | 38-270 |
| 16-150 | 21-180 | 26-210 | 42-270 |
| 20-030 | 25-000 | 30-330 | 43-270 |
| 21-150 | 26-180 | 36-210 | 47-270 |
| 25-030 | 30-000 | 40-330 | 48-270 |
| 26-150 | 31-180 | 41-210 | 52-270 |
| 30-030 | 35-000 | 41-240 | 53-270 |
| 31-150 | 36-180 | 45-330 | 57-270 |
| 35-030 | 40-000 | 46-210 | 58-270 |

Table 5.1: Categorization of trajectories

all the Deviations were computed in an inter-subject fashion.

**Variability of the sequences of FP** We examined the pattern of FP from the beginning of the task until the subjects reached the goal. To this purpose, we first detected the successive steps performed by subjects before computing the variability of the foot positions $(f^x, f^y)$ across the different repetitions of the same subject. We used heel-strike and toe-off events for defining steps (Hicheur et al., 2006). These events were derived from the time course of heel and toe Z-position profiles and corresponded to the local minima of these two signals. We considered one step as the interval separating two successive heel strikes of the same foot and computed the FP at these particular events.

A first type of inter-subject variability can arise from the anatomical differences between the subjects (as presented before, they had different heights and this resulted in different step lengths). In the present analysis, we did not consider the inter-subject variability in the sequences of FP (which is considerably higher than the intra-subject variability; not presented) but we calculated, for each subject and for a particular target, the variability of the FP across repetitions.

Typically, a subject performed $M$ to $M+1$ steps to reach the goal. In order to compare the sequences of FP across trials, we selected the first $M$ steps and calculated, for each step $i \in [1, M]$, the variability around the average foot position $(f^x_{\mathrm{av}}(i), f^y_{\mathrm{av}}(i))$. More precisely, the Foot Deviation (FD) at step $i$ was given by

$$\mathrm{FD}(i) = \sqrt{\frac{1}{N-1}\sum_{j=1}^{N}(f^x_j(i) - f^x_{\mathrm{av}}(i))^2 + (f^y_j(i) - f^y_{\mathrm{av}}(i))^2} \qquad (5.1)$$

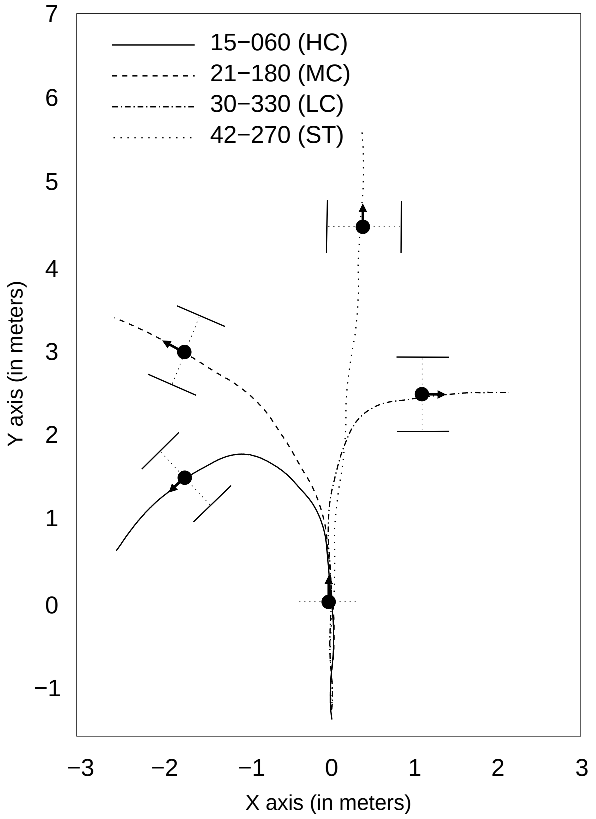

Figure 5.3: Four sample trajectories, one per category.

where $N$ is the number of repetitions executed by the subject for this target (here, $N = 3$), $(f_j^x(i), f_j^y(i))$ the position of the foot at step $i$ in repetition $j$[1].

Next, the Average and Maximal Foot Deviation (AFD and MFD) were given by

$$\text{AFD} = \frac{1}{M}\sum_{i=1}^{M} \text{FD}(i) \tag{5.2}$$

$$\text{MFD} = \max_{1\leq i\leq M} \text{FD}(i) \tag{5.3}$$

This analysis was performed for each subject and we then averaged the AFD and MFD values across subjects (intra-subject analysis).

In order to compare the variability of the sequences of FP with that of whole-body trajectories, we also expressed the former as a percentage of the

---

[1] Note that the corresponding equation in the original manuscript (Eq. (3) in Hicheur et al., 2007) was incorrect. The FD calculations in Hicheur et al. (2007) did however comply with the correct equation given in the current manuscript.

step length. The latter was also expressed, at this stage of the analysis, as a percentage of the trajectory length.

### 5.2.2 Results

For all the 40 trajectories, we observed very similar geometrical forms of the locomotor paths and velocity profiles across repetitions and subjects. This indicates a stereotypy at the level of the spatial and kinematic attributes of the locomotor trajectories. In contrast, we observed much more variability when locomotion was analysed at the level of the sequences of FP in space.

#### Spatial and kinematic stereotypy of the locomotor trajectories

**Trajectories** As illustrated in Fig. 5.4 (for all the tested targets) and in Fig. 5.5(A) (for four typical targets), we observed that the locomotor trajectories produced by the different subjects across different repetitions were very similar.

For a more quantitative assessment, we considered the Average and Maximal Trajectory Deviations (ATD and MTD). As illustrated by Fig. 5.6(A), the average ATD and MTD were lower than 0.10m and 0.17m, respectively.

We observed that the larger the turn amplitude, the greater the Trajectory Deviation [$F(3,531) = 58.15$, $p < 0.01$ for the ATD and $F(3,531) = 66.39$, $p < 0.01$ for the MTD]. However, it was remarkable that, even for the highly curved trajectories, the ATD was $\sim$ 10cm.

**Velocity profiles** At the more detailed level of the velocity profiles, we also observed a strong similarity across subjects and repetitions. This is illustrated in Fig. 5.5(B) for four typical targets, in which were plotted the standard deviations around the average normalized velocity profiles. Fig. 5.6(B) quantitatively confirms this observation: the MnVDs and AnVDs were always lower than 0.1.

#### Variability of the sequences of FP

While all subjects generated stereotyped locomotor trajectories, their behaviour was much more variable when examined at the level of the step. Part of this variability can be related to the anatomical differences between subjects (see Methods).

In the present section, we calculated various parameters of the stepping behaviour within trials of single subjects (intra-subject analysis): this was

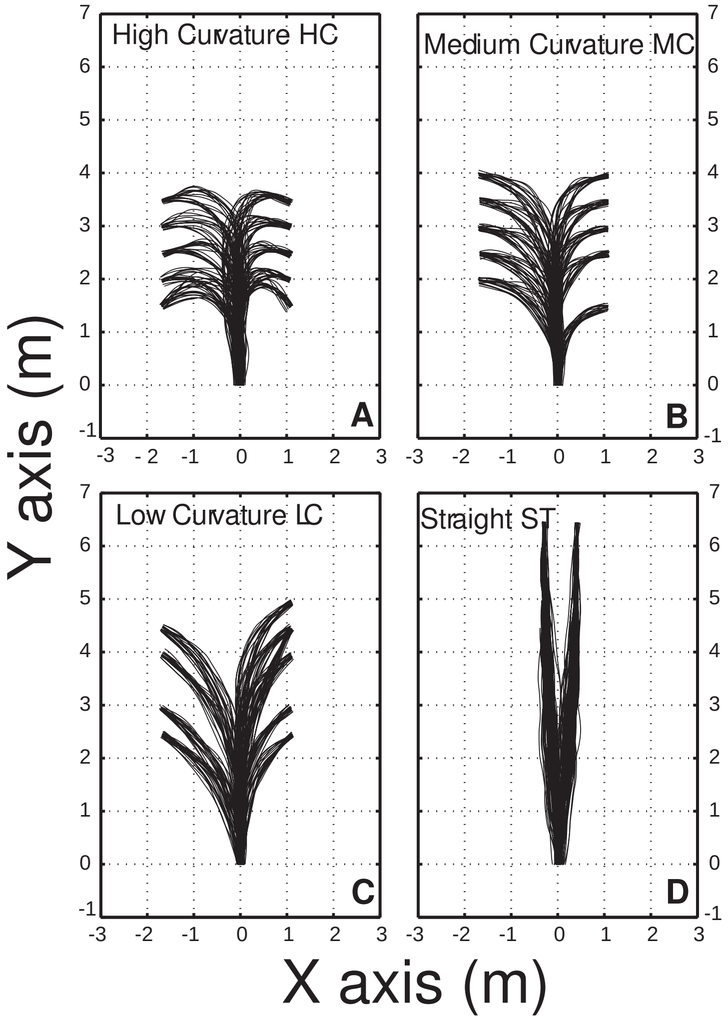

Figure 5.4: **(A-D)** Trajectories for all the tested targets, classified into four categories: high (HC), medium (MC), low (LC) curvatures and quasi-straight (ST). Ten targets were tested for each category. Note that for some positions, two orientations were tested (see Table 5.1 and Fig. 5.2).

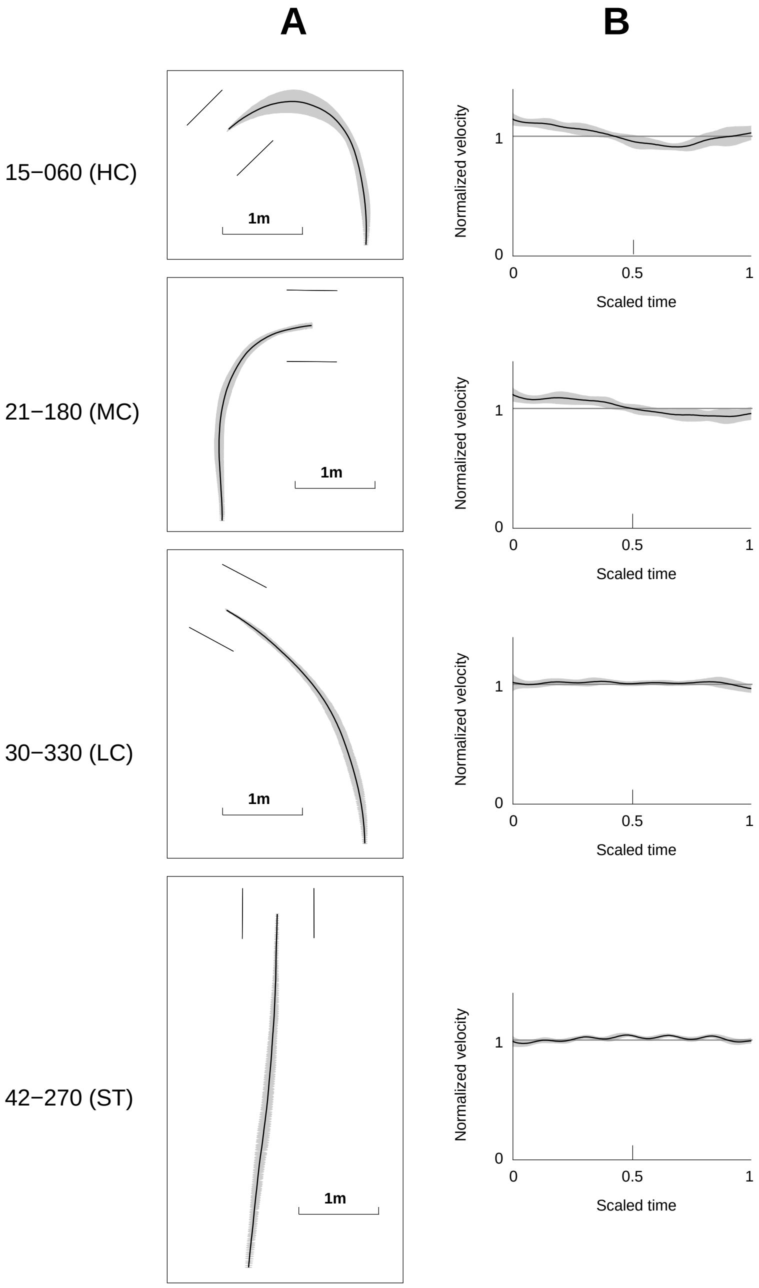

Figure 5.5: **(A)** Typical average trajectories and the corresponding variance ellipses. **(B)** Normalized velocity profiles and the corresponding standard deviations.

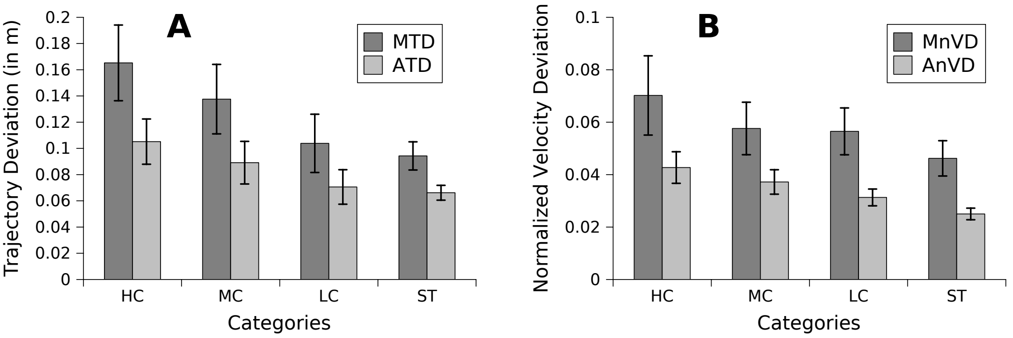

Figure 5.6: **(A)** Average and Maximal Trajectory Deviations (ATD and MTD) averaged across targets of the same category. **(B)** Average and Maximal normalized Velocity Deviations (AnVD and MnVD).

done in order to quantify the spatial dispersion of the FP independently of the inter-subject anatomical differences.

The FP at the step instants are presented for all subjects and for four typical trajectories in Fig. 5.7. One can already see in this figure the contrast between the variability of the sequences of FP and the similarity of the corresponding trajectories.

The different types of spatial dispersion (associated with different subjects) of the FP are illustrated in Fig. 5.8 where we plotted data of single subjects. We observed that the subjects, when performing different trials of the same target, generated a similar trajectory but placed their feet at different positions. The global body trajectory in space remained unaffected because every deviation (from one trial to another) of a given foot towards the right or the left of the X-axis was compensated for by a displacement of the position of the contralateral foot in the opposite direction [this was observed in most of the subjects, see Fig. 5.8(A-D)].

Another source of foot positioning variability across repetitions was that subjects alternated between the left and the right foot for initiating their walk. Even after taking this into account, the FP – independently of whether we considered the left or the right foot – still displayed a large spatial dispersion across repetitions [see Fig. 5.8(B,C)]. The trajectories presented in Fig. 5.8(B) thus combined these two sources of variability. Finally, we observed in a minority of cases that stereotypy in the body trajectories in space was associated with somewhat similar foot positioning across repetitions [see Fig. 5.8(D)].

The quantifications of these observations were presented in Fig. 5.7(C), where the spatial dispersion of the FP across repetitions was plotted for the four categories of trajectories. The spatial dispersion of the FP around the

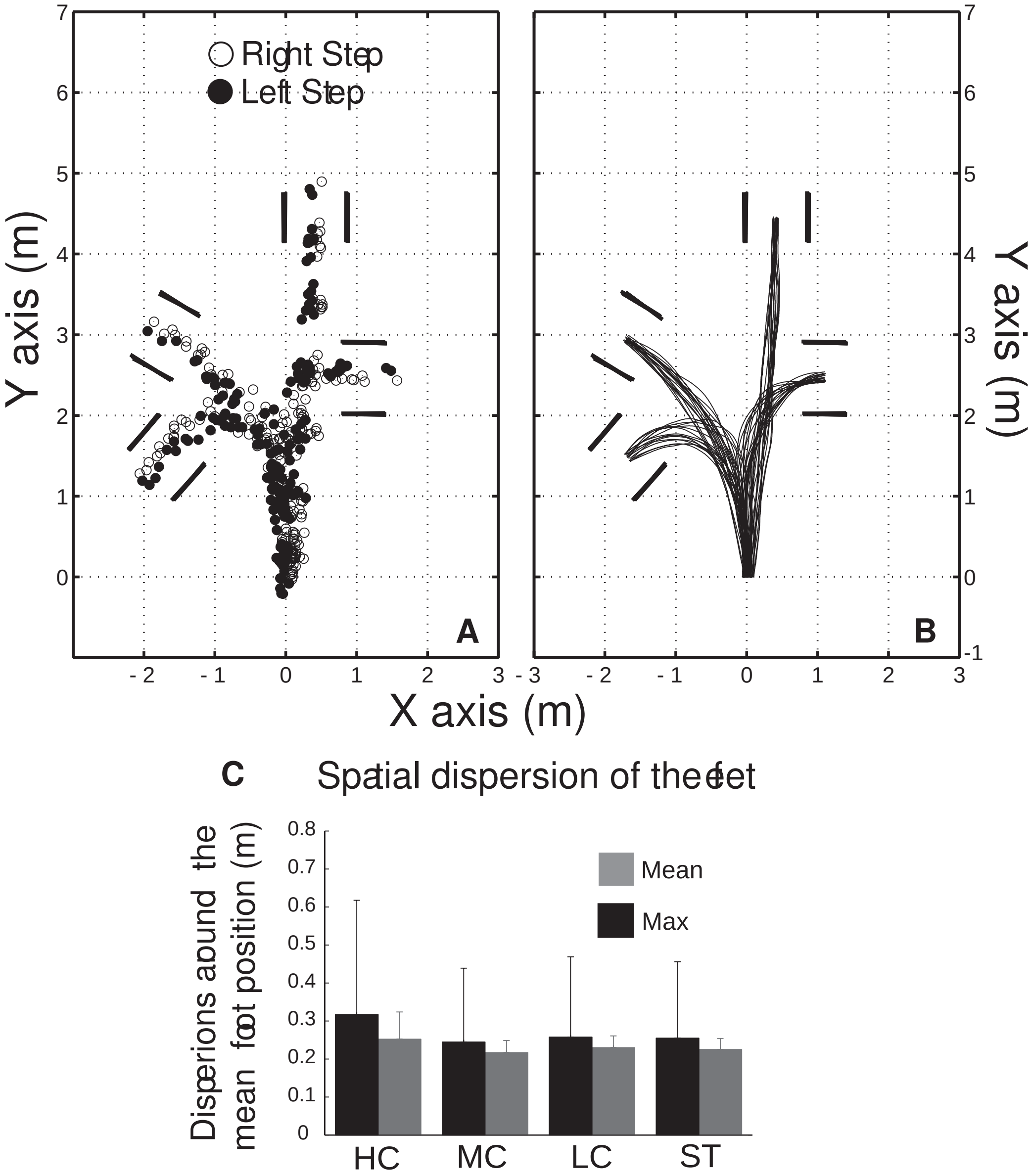

Figure 5.7: (**A**) Sequences of foot positions for four typical targets and for all subjects and trials. (**B**) Corresponding trajectories: note the similarity between the trajectories and the more variable sequences of FP. (**C**) Average and Maximal Foot Deviation (in m) averaged across targets of each category.

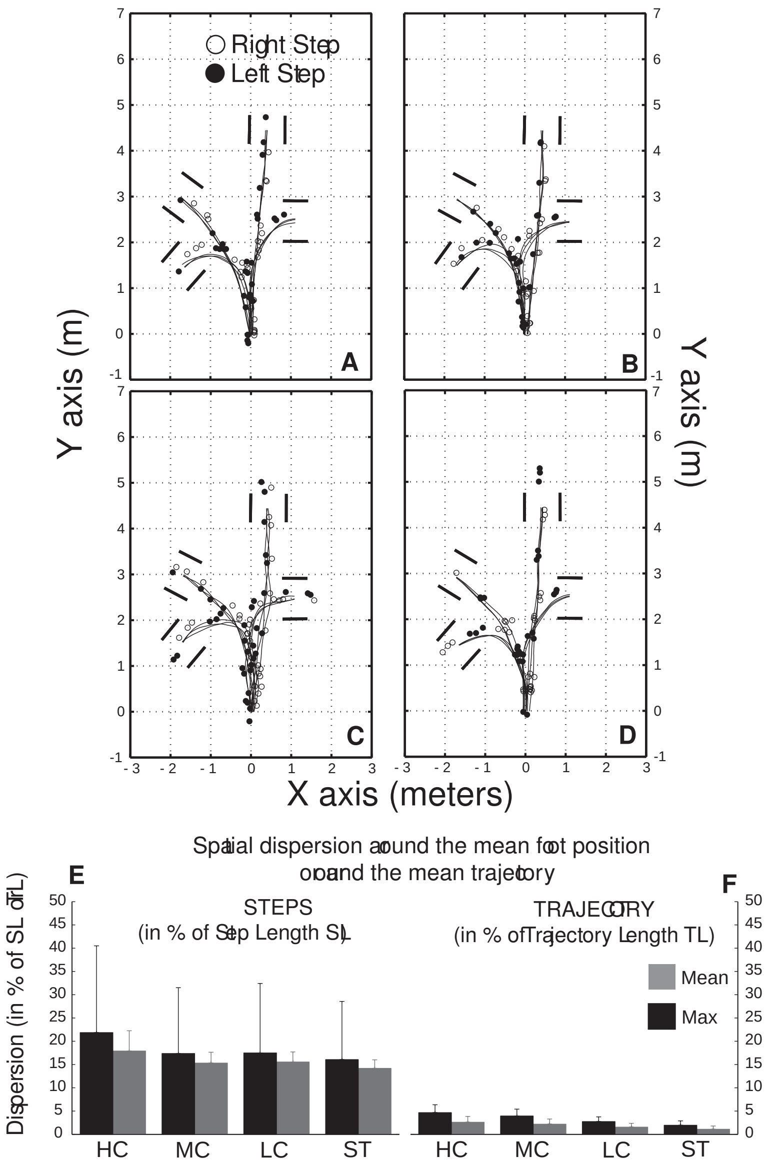

Figure 5.8: (**A**) Foot positions at the step instants (the left and right foot locations are plotted for each of the three consecutive trials) and corresponding trajectories for a particular subject and four typical targets. Note that the number of steps for completing the task may vary from $M$ to $M + 1$ for the same target (see Methods). (**B**-**D**) Same plots for three other subjects. Note the similarity between the trajectories and the greater variability of the FP in space. (**E**) Spatial dispersion of the actual FP around the average FP expressed in percentage of the step length. (**F**) Spatial dispersion of the actual trajectories around the average trajectory expressed in percentage of the trajectory length.

average FP ranged between 0.14m and 0.22m and was not dependent upon the type of trajectory [F(3,492) = 0.93, $p > 0.01$ for the AFD and F(3,492) = 3.34, $p > 0.01$ for the MFD].

These absolute values of FP spatial dispersion obtained at the level of the step (AFD) were twice as high as the corresponding ATD (reported in Fig. 5.6). This greater variability was even more evident when these parameters were expressed either in percentage of the step length (for the AFD) or in percentage of the trajectory length (for the ATD), see Fig. 5.8(E,F). The statistical significance of these differences was particularly strong [F(1,164) = 647.04, $p < 0.01$ for the AFD of the left foot versus the ATD, and F(1,172) = 711.06, $p < 0.01$ for AFD of the right foot versus the ATD]. The same observations hold for the maximal deviation parameters [F(1,164) = 457.03, $p < 0.01$ for MFD of the left foot versus MTD and F(1,172) = 693.89, $p < 0.01$ for the MFD of the right foot versus MTD].

Taken together, these results indicate that for a simple goal-oriented task subjects generated very similar trajectories but using different sequences of FP: this suggests that the locomotor trajectory is unlikely to be constructed as a succession of “foot reachings”.

## 5.3 Experiment 2: influence of vision and gait direction on locomotor trajectories

The stereotypy of whole-body trajectories, which contrasted with a larger variability of the sequences of foot positions reported in the previous study, suggests that goal-oriented locomotion is planned and controlled at the level of whole-body trajectories.

In the present experiment, we investigate the influence of changes in the sensory and motor conditions on these trajectories. More precisely, we asked subjects to do a goal-oriented locomotor task, in four experimental conditions: Visual Forward (VF, color code in figures: red), Nonvisual Forward (NF, magenta), Visual Backward (VB, green), Nonvisual Backward (NB, cyan). We then examined how these different conditions affected the locomotor trajectories produced.

### 5.3.1 Methods

#### Subjects and materials

Fourteen male subjects participated in this experiment. Each subject generated 132 trajectories (4 conditions × 11 targets × 3 repetitions), so that a total of 1848 trajectories were recorded. The targets consisted of a 0.2m × 1.2m cardboard arrow placed on the ground at various positions and orientations in the laboratory (Fig. 5.9 and Fig. 5.10). Nineteen targets were used: their distances from the starting position ranged between 4m and 7.5m and their orientations with respect to the subject's initial travelling direction ranged between −180° and +180°. Three targets were placed straight ahead of the subject ("straight" targets) while the others were placed on the side ("angled" targets) (Fig. 5.10). The three straight targets were used for all subjects. A subgroup of 6 subjects walked towards the 8 targets located on the left, while the remaining 8 subjects walked towards the 8 targets on the right. Thus, each subject was tested on 11 targets.

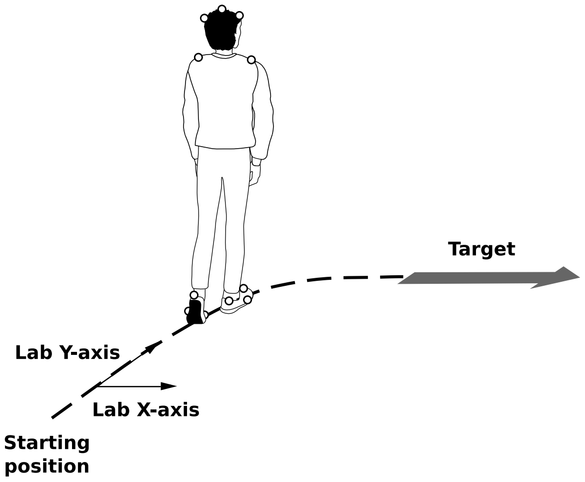

Figure 5.9: In Experiment 2, the targets consisted of a a 0.2m × 1.2m cardboard arrow placed at various positions and orientations in the laboratory.

The choice of the arrow (instead of the door used in Experiment 1) was motivated by the nonvisual trials: in these trials, we needed to remove the target quickly and silently after the observation period (see Protocol).

### Protocol

The subject had to start from a fixed position in the laboratory and to walk towards a distant target indicated by an arrow (Fig. 5.9). As in Experiment 1, we constrained the subject's initial walking direction by asking him to start at position (0,-1m) and to walk the first meter [from (0,-1m) to (0,0)] orthogonally to the X-axis. After crossing the X-axis, no specific restriction relative to the path to follow was provided to the subject. We imposed the

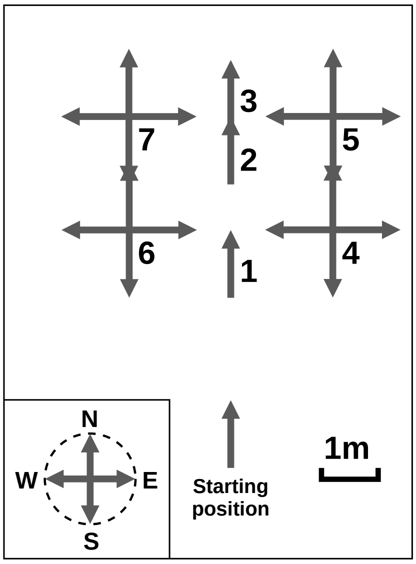

Figure 5.10: Nineteen targets were used in Experiment 2. Each target (e.g. 1N, 4W, 5S, . . . ) was labelled by a number (e.g. 4) indicating its position, and a letter (e.g W) indicating its orientation.

subject's final walking direction by asking the subject to enter the arrow by the shaft and to stop walking above the arrow head.

The subject walked either with eyes open (visual conditions: V) or closed (nonvisual conditions: N). In this experiment, he was asked to walk at his preferred, normal, speed. In the visual conditions (VF, VB), the arrow was visible throughout the whole movement. In the nonvisual conditions (NF, NB), the subject first observed the arrow while standing at the starting position. This observation period typically lasted less than 3 seconds. When the subject was ready, he closed his eyes and attempted to complete the task without vision. The subject was asked to complete the task with the same initial and final constraints as in the VF condition — namely, walk the first meter orthogonally to the X-axis, enter the arrow by the shaft and stop above the arrow head. Right after the observation period, the experimenter removed the arrow in order to avoid any tactile feedback. Once the subject had completely stopped, he was asked to keep his eyes closed while the experimenter took his hand and guided him randomly for a few seconds in the laboratory before stopping at a random position. The subject was then allowed to re-open his eyes and to go back to the starting position. This procedure prevented the subject from visual feedback during both task execution and post-task periods, avoiding in this way any spatial calibration of the room using kinaesthetic cues.

The subject walked either forward (VF, NF) or backward (VB, NB). The subject's head movements were not constrained, such that during VB locomotion, he could turn his head on the side in order to view the arrow.

The trials in the four conditions were executed in the same session and were randomized in order to reduce learning effects associated with a particular condition or target. The subject completed two to three trials before the experiment actually started in order to be familiar with the task and to dispel any fear of hitting the walls during the nonvisual trials (the distance between the most distant target and the wall was $\sim$ 3m).

### Analysis

To quantify the variability of the trajectories in the different conditions, we considered the measures defined in chapter 4, namely: the instantaneous Trajectory Deviation (TD) and the Maximal Trajectory Deviation (MTD) over the whole movement. We noted $\mathrm{TD}_{\mathrm{VF}}$, $\mathrm{TD}_{\mathrm{VB}}$, etc. the TD corresponding to condition VF, VB, etc.

Similarly, to quantify the similarity of the average trajectories in two different conditions, we considered the Trajectory Separation (TS) and the Maximal Trajectory Separation (MTS), e.g.: $\mathrm{TS}_{\mathrm{VF/VB}}$, $\mathrm{MTS}_{\mathrm{VF/NF}}$, etc.

### Targets pooling

As evoked above, six subjects walked towards targets located on their left and eight subjects walked towards targets located on their right (Fig. 5.10). We found no significant effect of the side on the parameters of interest: for instance, the $\mathrm{MTS}_{\mathrm{L/R}}$ (MTS between the average trajectory of the left-trajectories and that of the right-trajectories) was smaller than the $\mathrm{MTD}_{\mathrm{R}}$ (MTD of the right-trajectories) in conditions VF and NF. In the two-way ANOVA test with replications where the factors were the measure ($\mathrm{MTS}_{\mathrm{L/R}}$ vs $\mathrm{MTD}_{\mathrm{R}}$) and the visual condition, the effect of the measure was significant [F(1,40) = 37.4, $p < 0.05$] and there was no significant interaction effect [F(1,40) = 2.82, $p > 0.05$]. Thus, in all subsequent analyses, we flipped the left-trajectories towards the right and pooled them together with their symmetrical counterparts (trajectories of target 4 with those of target 6, trajectories of target 5 with those of targets 7).

### 5.3.2 Results

#### Effects of vision

**Comparison of Visual Forward (VF) and Nonvisual Forward (NF) conditions** For a given target, the average trajectories in the VF condition and in the NF condition were found to be very similar at the path level [Fig. 5.3.2(A1,B1,C1)]. This observation was verified even for targets imposing strongly curved trajectories [e.g. target 5S, Fig. 5.3.2(C1)] or for targets imposing changes in curvature sign [e.g. target 5W, Fig. 5.3.2(B1)].

At the level of velocity profiles, one could also observe similar patterns in the VF and NF conditions [Fig. 5.3.2(A2,B2,C2)]. We noted however that the normalized velocity profiles started at a higher value in the NF than in the VF condition, and that their maximum values were reached also earlier: for e.g. target 5W, the maximum velocity was reached at $t \simeq 0.2$ in NF and $t \simeq 0.4$ in VF [Fig. 5.3.2(B2)].

Quantitatively, the average $\mathrm{MTS}_{\mathrm{VF/NF}}$ across the 11 tested targets was 0.30m [Fig. 5.3.2(D)] in absolute terms, or 5.5% of the VF trajectory length. These values are to be compared with the average $\mathrm{MTD}_{\mathrm{VF}}$, which was 0.31m or 5.7%, and the average $\mathrm{MTD}_{\mathrm{NF}}$, which was 0.74m or 13.4%.

In contrast with the similarity of the average trajectories, the variability profiles were largely dissimilar. In absolute terms, the values of $\mathrm{MTD}_{\mathrm{VF}}$ and $\mathrm{MTD}_{\mathrm{NF}}$ reported above already showed that trajectories were much more stereotyped in the VF than in the NF condition.

In addition, the *shapes* of the variability profiles were very different [Fig. 5.3.2(A3,B3,C3)]. In the VF condition, the variability profiles were bump-shaped: at time $t = 0$, the variability was close to 0, then it increased until $t \simeq 0.5$, and then decreased towards 0 at the end of the movement $t = 1$. By contrast, the variability in the NF condition never decreased towards 0 at $t = 1$. All these remarks will be developped in chapter 6, where we study in more detail the variability profiles and provide some elements to interprete their shapes.

**Comparison of Visual Backward (VB) and Nonvisual Backward (NB) conditions** Here, we also found a large similarity of the average trajectories in the VB and NB conditions, albeit to a lesser extent than previously found in the comparison of the VF and NF conditions. This observation was verified at both the path level [Fig. 5.12(A1,B1,C1) and at the velocity profile level [Fig. 5.12(A2,B2,C2)]. However, the same remark regarding the slight differences in the shapes of the velocity in the VF/NF comparison could also be made for the VB/NB comparison.

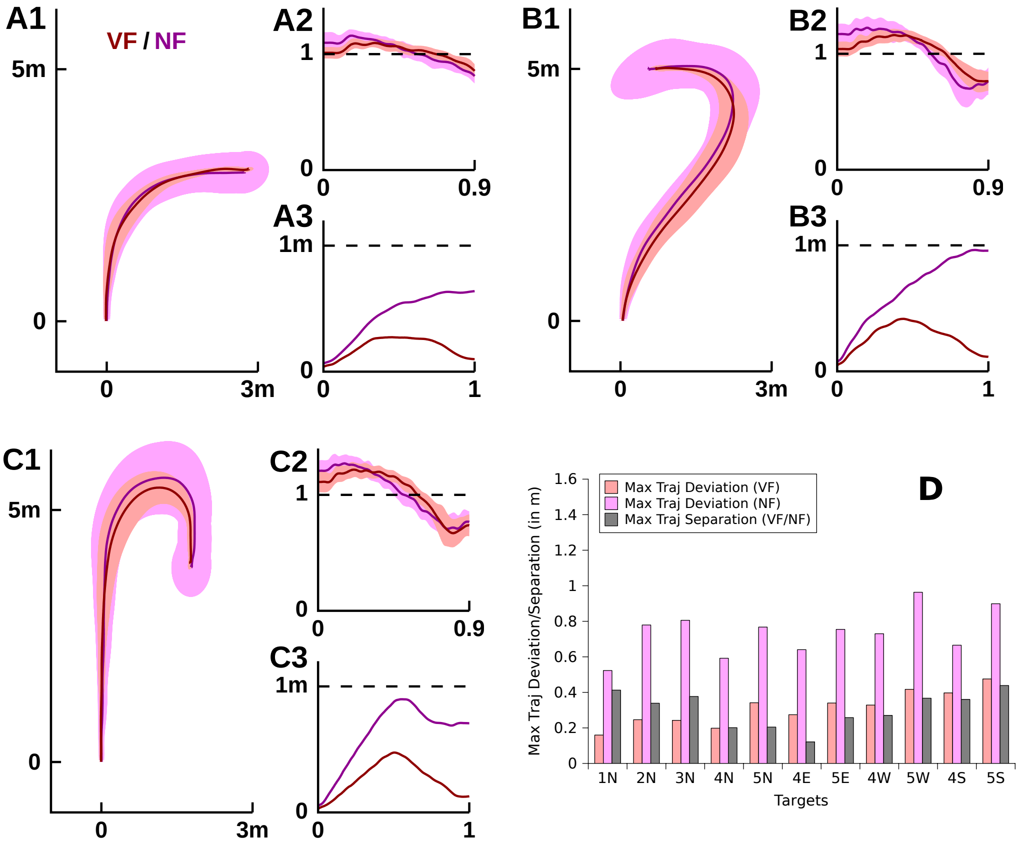

Figure 5.11: Comparison of locomotor trajectories in the Visual Forward (VF: red) and Nonvisual Forward (NF: magenta) conditions. **(A)** Comparison for target 4E. A1: geometric paths of the average trajectories. Variance ellipses around the average trajectory at every time instant (see Methods) are shaded in light colors. A2: average velocity profiles. The velocity profiles were normalized so that their average values over the movement duration equals 1 (see Methods). Standard deviations around the average velocity profiles are shaded in light colors. A3: trajectory variability profiles (TD(t)). **(B)** Same as in A, but for target 5W. **(C)** Same as in A, but for target 5S. **(D)** Maximal Trajectory Deviation/Separation (MTD/MTS) in meters: MTD in the VF condition (light red bars), MTD in the NF condition (light magenta bars), MTS between the average trajectory of VF and NF (grey bars).

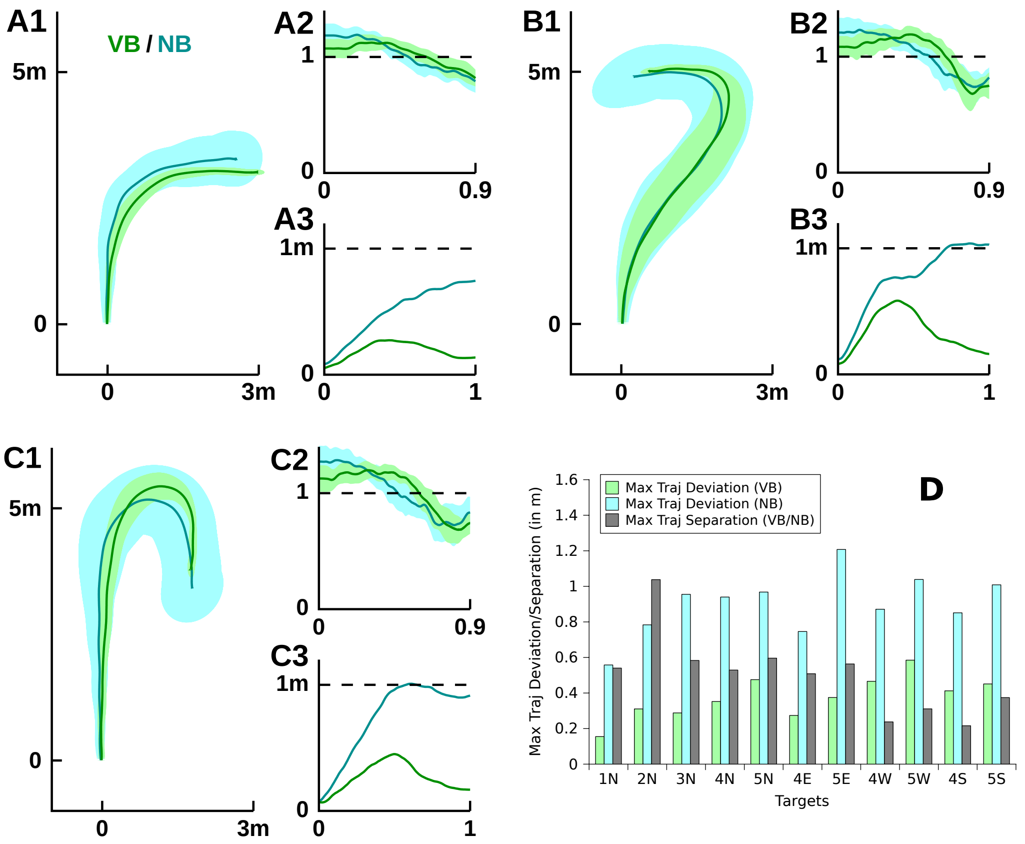

Figure 5.12: Comparison of locomotor trajectories in the Visual Backward (VB: green) and Nonvisual Backward (NB: cyan) conditions. For details, see legends of Fig. 5.3.2.

Quantitatively, the average $\mathrm{MTS}_{\mathrm{VB/NB}}$ across the 11 tested targets was 0.50m [Fig. 5.12(D)] in absolute terms, or 9.2% of the VB trajectory length. These values are to be compared with the average $\mathrm{MTD}_{\mathrm{VB}}$, which was 0.38m or 6.4%, and the $\mathrm{MTD}_{\mathrm{NB}}$, was 0.90m or 15.7%.

Regarding the shapes of the variability profiles, we observed, as in the VF/NF comparison, large differences in terms of both magnitude and shapes between VB and NB conditions [Fig. 5.12(A3,B3,C3)].

### Effects of gait direction

**Comparison of Visual Forward (VF) and Visual Backward (VB) conditions** In targets which imposed no change in curvature sign (all targets except 4W, 4N, 5W, 5N), the average trajectories observed in the VF and VB conditions were very similar at the path level [targets 4E and 5S Fig. 5.13(A1,C1)]. In targets which imposed a change in curvature sign (4W, 4N, 5W, 5N), the VB paths were slightly shifted to the interior of the main curve with respect to the VF paths [targets 5W: Fig. 5.13(B1); also target 4W: not shown]. However, quantitatively, this difference resulted in a MTS smaller than 0.4m [Fig. 5.13(D)]. In terms of the velocity profiles, we found very similar patterns, in every targets [Fig. 5.13(A2,B2,C2)]. This similarity was larger here than in the previous VF/NF and VB/NB comparisons.

Quantitatively, the average $\mathrm{MTS}_{\mathrm{VF/VB}}$ across the 11 tested targets was 0.22m [Fig. 5.12(D)] in absolute terms, or 4.0% of the VF trajectory length. These values are to be compared with the the average $\mathrm{MTD}_{\mathrm{VF}}$, which was 0.31m or 5.7%, and the average $\mathrm{MTD}_{\mathrm{VB}}$, which was 0.38m or 6.4%.

Finally, we noted that the variability profiles were similar in the two conditions, both in terms of magnitudes (average $\mathrm{MTD}_{\mathrm{VF}} = 0.31\mathrm{m}$, average $\mathrm{MTD}_{\mathrm{VB}} = 0.38\mathrm{m}$) and shapes [Fig. 5.13(A3,B3,C3)].

**Comparison of Nonvisual Forward (NF) and Nonvisual Backward (NB) conditions** Here, the similarity of the average trajectories was not as strong as in the previous comparison. Yet it was still remarkable given the difficulty of the task (walking to distant targets defined in both position and orientation without visual feedback). At the path level, the average trajectories had globally the same forms, with some shift between the two conditions [Fig. 5.14(A1,B1,C1)]. In particular, in targets which imposed a change in curvature sign, we observed that, as in the VF/VB comparison, the NB paths were shifted towards the interior of the main curve with respect to the NF paths [target 5W: Fig. 5.14(B1); also target 4W: not shown]. As in the VF/VB comparison, the velocity profiles were very similar in the two compared conditions, in all targets [Fig. 5.14(A2,B2,C2)].

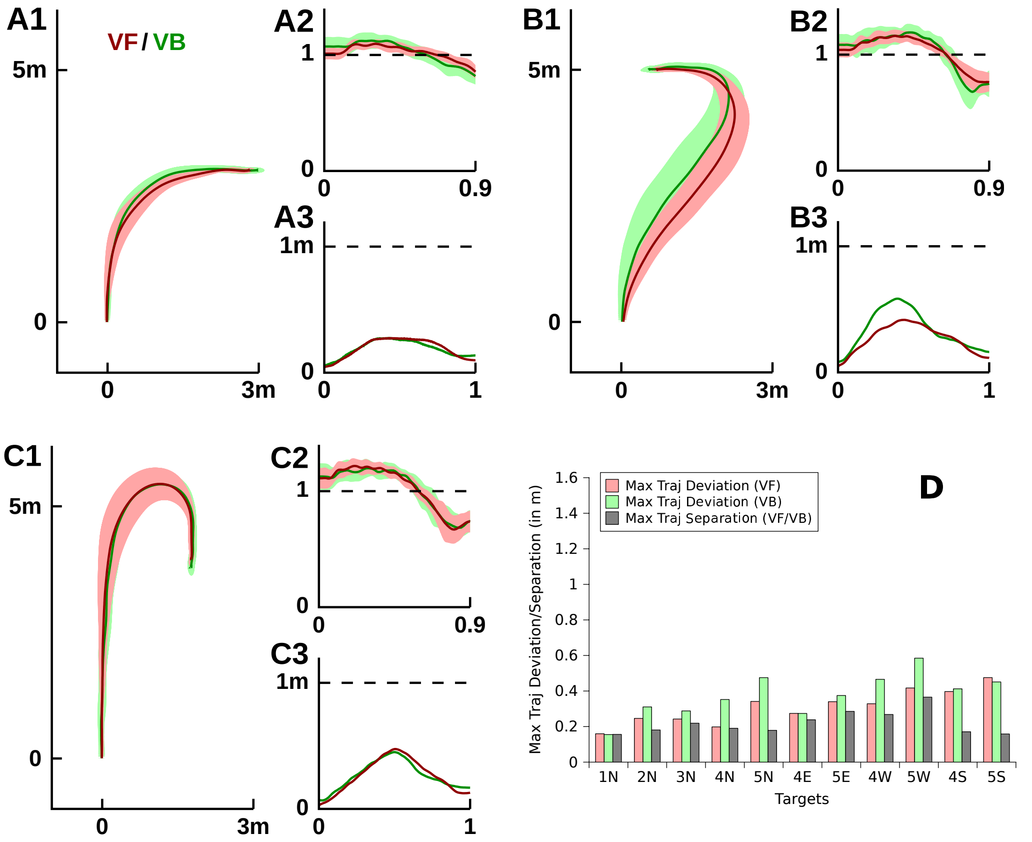

Figure 5.13: Comparison of locomotor trajectories in the Visual Forward (VF: red) and Visual Backward (VB: green) conditions. For details, see legends of Fig. 5.3.2.

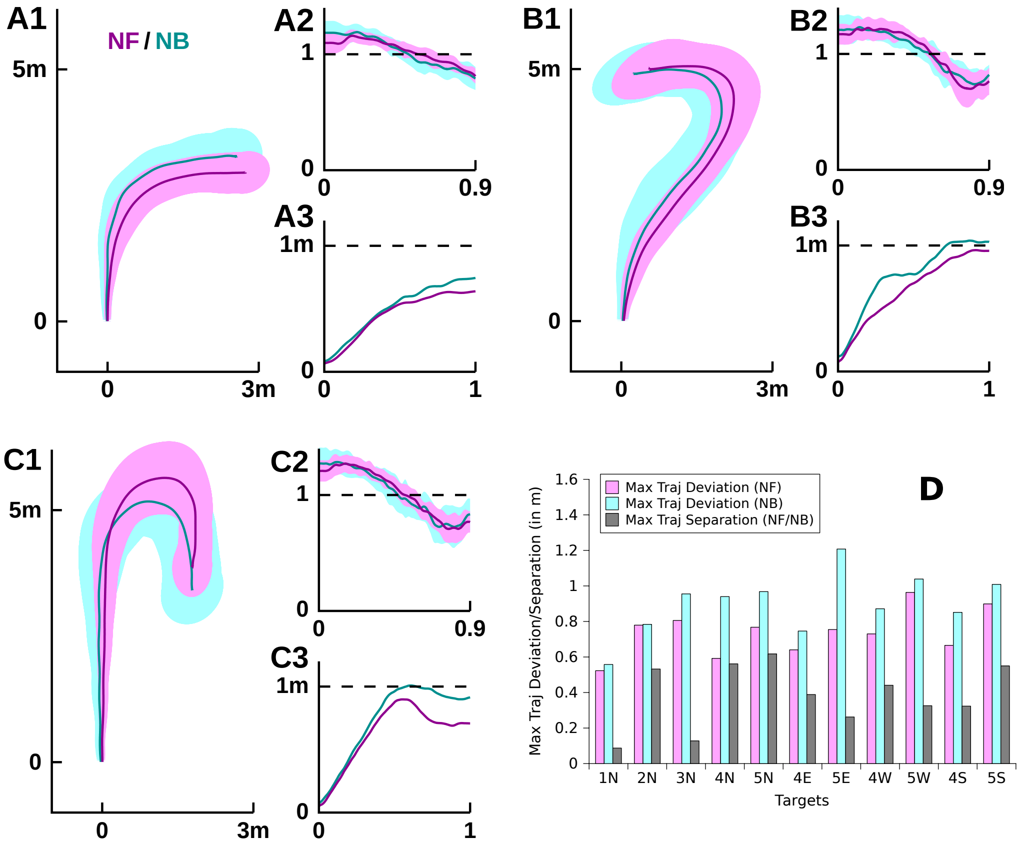

Figure 5.14: Comparison of locomotor trajectories in the Nonvisual Forward (NF: magenta) and Nonvisual Backward (NB: cyan) conditions. For details, see legends of Fig. 5.3.2.

Quantitatively, the average $\mathrm{MTS}_{\mathrm{NF/NB}}$ across the 11 tested targets was 0.38m (Fig. 5.14(D)) in absolute terms, or 6.9% of the NF trajectory length. These values are to be compared with the the average $\mathrm{MTD}_{\mathrm{NF}}$, which was 0.74m or 13.6%, and the average $\mathrm{MTD}_{\mathrm{NB}}$, which was 0.90m or 16.5%.

In terms of the variability profiles, we observed a larger variability in the NB conditions (see the values given above). However the difference between the NF and NB conditions was low as compared to the VF/NF and VB/NB comparisons. In addition, the variability profiles displayed similar shapes [Fig. 5.14(A3,B3,C3)].

**Results summary**

The main findings provided by this experiment can be summarized as follows

- The average trajectories were globally similar across visual and gait direction conditions, at both the path and velocity profile levels
- The variability profiles were globally similar across gait direction conditions
- Vision largely affected the variability profiles, both in terms of magnitude (larger variability in the nonvisual conditions than in the visual conditions) and shape.

At a finer level of analysis, we also reported that

- In targets which imposed a change in curvature sign, the backward (VB, NB) paths were shifted towards the interior of the main curve with respect to the forward (VF, NF) paths
- The normalized velocity profiles were similar across gait conditions, but were slightly different across visual conditions: in the nonvisual conditions (NF, NB), the velocity reached its maximal value earlier than in the visual conditions (VF, VB).

## 5.4 Discussion

### 5.4.1 The spatial control of locomotion

We observed in Experiment 1 that subjects produced stereotyped trajectories, which contrasted with much more variable sequences of foot positions. The variability of the sequences of foot positions may seem contradictory with the observation made by Patla et al. (1999b), who showed that humans precisely control the landing positions of the feet in obstacle-avoidance tasks. However, it should be recalled that our experiment took place in a large, obstacle-free room. We propose that in such environments, goal-oriented locomotion is planned and controlled at the trajectory-level, in a "top-down" fashion (Berthoz, 1997), and not as precise sequences of foot "pointings". This idea is reminiscent of the "spatial control of hand movements" hypothesis put forward by Morasso (see also our review in section 1.1), which postulates that the *central* command is formulated in terms of trajectories of the hand in space and not in terms of joint kinematics or muscle activity.

The second argument in favour of the "top-down" strategy is provided by the comparison of forward and backward locomotion. Indeed, it was shown that these two modes of locomotion involved very different patterns of muscle activity (see Grasso et al., 1998b, and also our review in section 2.1.2). We observed nevertheless that the trajectories produced in forward and backward locomotion were very similar, at the geometric (paths), kinematic (paths + velocity profiles) and statistical (variability profiles) levels. This observation thus further indicates that whole-body trajectories may be planned and controlled at a high cognitive level, and to some extent, independently of their precise implementations (in terms of sequences of foot positions or of patterns of muscle activity).

### 5.4.2 The nature of the control variable(s)

The previous discussion is also related to the conceptual distinction between kinematic and kinetic variables usually presented in the literature. While kinematic variables (e.g. the hand's position, velocity, acceleration, jerk, etc. measured in the laboratory reference frame) describe the movement of the end-effector in the extracorporal space, kinetic variables (e.g. the torques applied at the joints, the muscle activations, etc.) are related to the internal mechanical properties of the motor system (see our review in section 1.2).

In the case of arm movements, the motor apparatus can be realistically modelled by a two-link manipulator controlled by torques applied at the joints (Uno et al., 1989). In this context, the opposition between kinematic control of the end-effector (the hand) and kinetic control of the torques can be readily investigated. For locomotion, given the greater dimensionality of the motor system (at the segmental, muscular, motor commands, etc. levels), it is less easy to formulate a kinetic control hypothesis.

In any case, the two observations discussed in the previous section argue in favor of a kinematic control of goal-oriented locomotion, in terms of whole-body trajectories in extracorporal space. While these observations do not rule out the possibility that the CNS may take into account kinetic variables (such as the forces exerted on the ground or at the legs' joints or the patterns of muscle activations) in the generation of locomotor trajectories, we suggest that these variables are rather used at the motor implementation level. Following this idea, the transformation from kinematic objectives into dynamic strategies may be acquired with learning (see also Winter and Eng, 1995).

### 5.4.3 Visual and nonvisual locomotion may share the same open-loop process

Experiment 2 first showed that, in order to reach a distant target, subjects produced very similar average trajectories in the Visual Foward (VF) and Nonvisual Forward (NF) conditions (see also the comparison of VB and NB average trajectories). If we consider only the final part rather than the entire trajectory, this finding implies that the average final position and final walking direction in condition NF are close to those in condition VF, which in turn correspond to the target's position and orientation since in condition VF, the task's final constraints were well respected. In previous studies of nonvisual locomotion (see our review in section 2.2), it was also reported that, in a task where the subject had to walk without visual feedback to a previously seen target, the average final position of the subject almost coincided with the actual position of the target. This precise average response was interpreted as reflecting the veridicality of the subjects' "visual space perception" (see Loomis et al., 1992). However, in these studies, the targets consisted of spots placed at various distances *in front* of the subject. Using targets defined in both position and orientation and placed at various off-axis positions, our study confirms and generalizes the aforementioned results. It also suggests that the notion of veridicality of visual space perception may not be limited to "straight ahead distances" but may be also valid for the perception of "off-axis distances" and of changes in the body orientation.

But more importantly, not only the average final positions and orientations, but also the entire average trajectories that the subjects had to produce to reach these positions and orientations were similar between conditions VF and NF (and between VB and NB). Since the average trajectory is obtained by indeed "averaging out" all the fluctuations, it reflects the *open-loop* process that governs the subject's movements in absence of perturbations (Todorov and Jordan, 2002). Thus, the similarity of the average trajectories implies that the control mechanisms in visual and nonvisual locomotion share a *common open-loop process*. This idea may have a deep theoretical implication. Indeed, a number of neuroscientists believe that our representation of space is strongly related to our movements (see for instance Berthoz and Petit, 2009), a notion that can be summarized by the following statement of the great French mathematician Henri Poincaré: "*To localize an object in space is to build a representation of the movements one has to make in order to reach it*" (Poincaré, 1902, chapter 4, our translation)[2]. Following this line of thinking, the proposed common open-loop process may represent the physiological basis of the psychological notion of "veridicality of visual space perception".

In a recent article, Fajen and Warren (2003) challenged the very existence of open-loop processes in the control of locomotion. Based on a simulation study where the targets were modeled by attractors, the obstacles by repellers and the subject by a simple second-order dynamical system evolving in a field of attractors and repellers, these authors argued that "*the [subject] adopts a particular route through the scene on the basis of local responses to visually specified [targets] and obstacles. The observed route is not determined in advance through explicit planning, but rather emerges in an online manner from the [subject's] interactions with the environment*". It should also be remarked that these interactions, which are crucial in Fajen and Warren's approach, are fundamentally based on the availability of visual inputs (see also our review in section 3.1). The similarity of the average trajectories in conditions VF and NF reported in the present article suggests, on the contrary, that the formation of locomotor trajectories is not exclusively driven by vision. Rather, we suggest that a combination of open-loop and online control mechanisms underlies the steering of locomotion. The precise nature of the online control mechanisms in question is investigated in chapter 6.

---

[2] However, we disagree with Poincaré when he pushed further into this "subjectivist" position and challenged the very existence of objective reality in Poincaré (1905): "*Non, sans doute, une réalité complètement indépendante de l'esprit qui la conçoit, la voit ou la sent, c'est une impossibilité. Un monde si extérieur que cela, si même il existait, nous serait à jamais inaccessible. Mais ce que nous appelons la réalité objective, c'est, en dernière analyse, ce qui est commun à plusieurs êtres pensants, et pourrait être commun à tous; cette partie commune, nous le verrons, ce ne peut être que l'harmonie exprimée par des lois mathématiques*". A sharp critism of this idealistic viewpoint can be found in Lénine (1908) (see also chapter 2 in Berthoz and Petit, 2009).

# Chapter 6

# The control mechanisms underlying the formation of locomotor trajectories

## 6.1 Overview

We showed in chapter 5 that whole-body trajectories produced in a "walking towards and through a distant doorway" task were highly reproducible across repetitions and subjects. In particular, the variability of the recorded trajectories around the average trajectory was found to be much lower than the variability of the sequences of foot positions in the same task. Moreover, the average trajectory was found to be very similar across different walking conditions (with vision/without vision, walking forward/walking backward). These observations suggested that goal-oriented locomotion is controlled at the level of whole-body trajectories.

In this chapter, we investigate the nature of the *control mechanism* at work during the production of these trajectories. A basic assumption of our study is that, theoretically, this control mechanism may be divided in two parts (Fig. 6.1): (i) an *open-loop process*, which can be executed independently of sensory feedbacks and (ii) a *feedback module*, which can modify the open-loop process based on sensory feedbacks in order to correct the perturbations that may arise during task execution.

Within this framework, we discuss two issues (indicated by the question marks on Fig. 6.1): (i) does online feedback control exist in visual and nonvisual locomotion? and (ii) what is the precise nature of the feedback control scheme?

More specifically, based in particular on the analysis of the variability

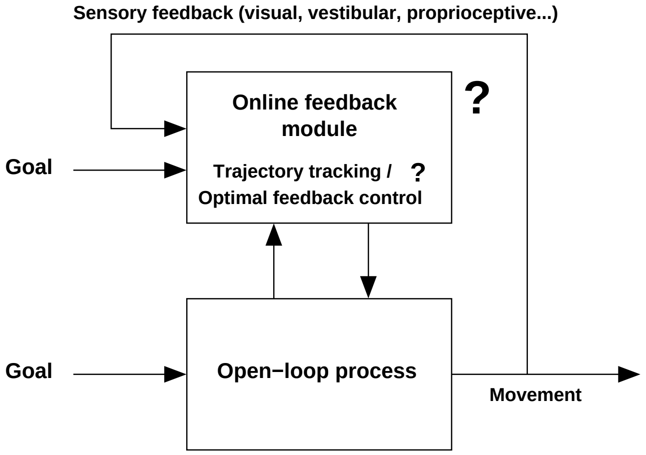

Figure 6.1: Sketch of a general controller, including both an open-loop process and a feedback module. The question marks indicate some of the issues studied in the present chapter: namely, (i) does online feedback control exist in visual and nonvisual locomotion? and (ii) what is the precise nature of the feedback control scheme, trajectory tracking or optimal feedback control?

profiles, we argue that online feedback control is present in both visual and nonvisual locomotion and suggest the relations between the visual and nonvisual control strategies (Experiment 3). We then investigate the precise nature of the online feedback control and discuss two competing hypotheses (Experiment 5):

**(i)** the "desired trajectory" (DT) hypothesis which assumes two separate stages in the production of a movement: a planning stage when a desired optimal trajectory is computed and an execution stage when this DT is implemented with trajectory-tracking mechanisms correcting any deviation away from the DT

**(ii)** the optimal feedback control hypothesis (Todorov and Jordan, 2002) which states that "*deviations from the average trajectory are corrected only when they interfere with task performance*" (goal-directed corrections, as opposed to desired-trajectory-related corrections)

The reader is referred to section 1.3 for a more detailed discussion about "desired trajectory" tracking and optimal feedback control.

Another issue that we also discuss concerns the influence of walking speed on the control of locomotor trajectories (Experiment 4). This is important to understand the nature of execution noise in locomotion.

Experiments 3 and 4 were designed and run by Q.-C. Pham and H. Hicheur in February 2008. We thank A.-H. Olivier and A. Cretual for their help with these experiments. Experiment 5 was designed and run by Q.-C. Pham and H. Hicheur in October 2008. The results of these experiments were first reported in Pham and Hicheur (2009), to which the reader is referred for more details.

## 6.2 Experiment 3: influence of vision on the variability profiles

### 6.2.1 Methods

#### Subjects and Materials

Five male subjects participated in this experiment. Each subject generated 80 trajectories (2 visual conditions × 5 targets × 8 repetitions), so that a total of 400 trajectories were recorded.

As in Experiment 2 (section 5.3), the targets consisted of a 0.2m × 1.2m cardboard arrow placed on the ground at various positions and orientations (Fig. 6.2). Five targets were used: two "straight" targets (targets 1 and 2) and three "angled" targets (targets 3, 4 and 5).

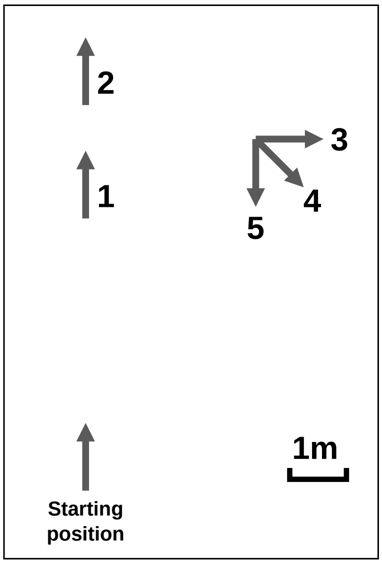

Figure 6.2: Five targets were used in Experiments 3 and 4: two "straight" targets (targets 1 and 2) and three "angled" targets (targets 3, 4 and 5).

### Protocol

Two conditions were tested in this experiment: walking with vision (visual: VI) and without vision (nonvisual: NV). The protocol for each trial was the same as in Experiment 2 (see section 5.3 for details, note that VI corresponds to VF in Experiment 2, while NV corresponds to NF). We increased the number of repetitions per target and per condition to 8 (up from 3 in Experiment 2) in order to study intra-subject variability profiles with better reliability. As usual, the trials were randomized in order to reduce learning effects.

### Analysis

In addition to the usual measures (TD: Trajectory Deviation, TS: Trajectory Separation, MTD: Maximal Trajectory Deviation, MTS: Maximal Trajectory Separation, etc.) defined in chapter 4, we considered here two other quantities: the Steps Number and the Linearity Coefficient.

**Number of steps** In Experiment 1 (section 5.2), we carried out an extensive step-level analysis in order to compare the variability of foot placements with that of whole-body trajectories. Here the purpose of the step-level analysis was solely to assess whether the subjects used a steps-counting strategy in the nonvisual trials. For this, we considered the Z-coordinates of the left and right heel markers as functions of time. The total number of local maxima of these two signals then gave the number of steps (SN, Steps Number) executed by the subject. The trial-to-trial variability of this quantity was given by the Steps Number Deviation (SND) computed as

$$\mathrm{SND} = \sqrt{\frac{1}{N-2}\sum_{i=2}^{N}(\mathrm{SN}_i - \mathrm{SN}_{\mathrm{av}})^2} \tag{6.1}$$

where $N$ is the number of repetitions executed by the subject for this target (here, $N = 8$).

Note that we discarded the first trial in the computation of both the average and the standard deviation of the SNs. Indeed, since the steps-counting strategy consists of (i) count the number steps executed in one visual trial and (ii) reproduce the same number of steps in the corresponding nonvisual trials, the discard was done to include only the nonvisual trials that were preceded by at least one visual trial (and for symmetry, we applied this procedure to visual trials as well).

**Linearity coefficient** To measure how close a variability profile is from a linear profile, we computed its Linearity Coefficient (LC). The LC of a time series $(y_i(t_i), 1 \leq i \leq N)$ quantifies the distance between this time series and its best linear approximation $y = ct$, with $0 \leq \text{LC} \leq 1$ and $\text{LC} = 1$ for a linear profile. First, the optimal coefficient $c$ was computed by

$$c = \frac{\sum_{i=1}^{T} y_i t_i}{\sum_{i=1}^{T} t_i^2} \tag{6.2}$$

Next, the squared approximation error was given by

$$\text{ESS} = \sum_{i=1}^{T} (y_i - ct_i)^2 \tag{6.3}$$

Finally, the Linearity Coefficient was given by

$$\text{LC} = 1 - \text{ESS}/\text{Var}(y) \tag{6.4}$$

### 6.2.2 Direct results

#### Vision affects the variability around the average trajectories

The observation made in section 5.3 that variability was larger in nonvisual locomotion than in visual locomotion was confirmed here on an intra-subject basis (Fig. 6.3). In the two-way ANOVA test where the factors were the visual condition and the target, the main effect of the visual condition on the MTD was found to be significant [F(1,40) = 86.1, $p < 0.05$] , and there was no significant interaction effect [F(4,40) = 0.61, $p > 0.05$].

#### No steps-counting strategy in nonvisual trials

It could be argued that, despite the randomized order of the trials, the subjects may have used a steps-counting strategy (see Methods). Such a strategy would imply a low trial-to-trial variability in the number of steps in condition NV. We observed, on the contrary, that the average SND across targets and subjects was 0.79 in condition NV, which was higher than in condition VI (SND = 0.54), where arguably no steps-counting strategy was used. In the two-way ANOVA test where the factors were the visual condition and the target, the main effect of the visual condition on the SND was found to be significant [F(1,40) = 7.6, $p < 0.05$], and there was no significant interaction effect [F(4,40) = 0.82, $p > 0.05$].

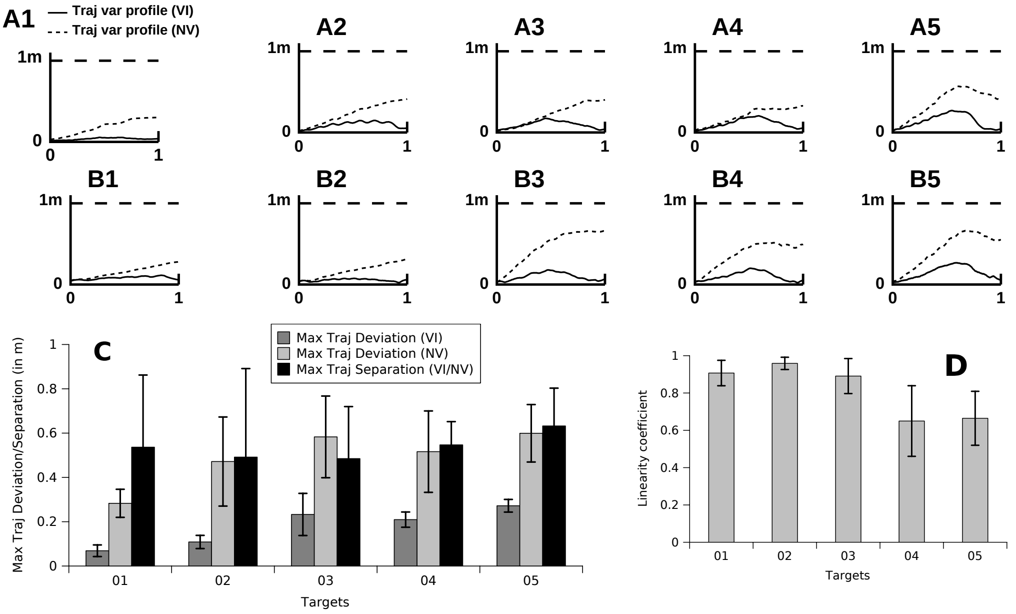

Figure 6.3: Comparison of variability profiles in the Visual (VI: plain lines) and Nonvisual (NV: dashed lines) conditions. **(A)** Variability profiles for subject L.H. A1: target 1, ..., A5: target 5. **(B)** Same as in A, but for subject N.V. **(C)** Average Maximal Trajectory Deviation (MTD) across targets in condition VI (dark gray bars) and in condition NV (light gray bars), average Maximal Trajectory Separation (MTS) across targets between conditions VI and NV (black bars). Here, the MTD and MTS were computed in an intra-subject fashion. First, for each subject, a MTD (or MTS) was computed over the 8 trials corresponding to this subject, then the average values and standard deviations of the MTD (or MTS) of the 5 subjects were plotted. **(D)** Linearity coefficients LC. ($0 \leq \text{LC} \leq 1$ and $\text{LC} = 1$ for a linear function, see Methods).

### The bump-shape of the variability profiles in visual locomotion

We noted that in both conditions VI and NV, the variability was low at the beginning of the movement. This is related to the fact that, for a given target, the subject started all the trials from the same starting position.

In condition VI, the variability was also close to zero at the end of the movement. This is because, when vision was available, the subject could complete all the trials successfully by stopping at the requested final position. Regarding the middle part of the variability profiles, the straight targets and the angled targets yielded different behaviors. For the former, the variability was close to zero during the whole movement [see the plain lines in Fig. 6.3(A1,A2,B1,B2)] while for the latter, the variability was higher around the middle of the movement than around the ends, hence yielding a "bump-shape" variability profile [Fig. 6.3(A3,A4,A5,B3,B4,B5)].

### The special shapes of the variability profiles in nonvisual locomotion

In condition NV, contrary to condition VI, the variability did not decrease towards zero at the end of the movement. For the straight targets (targets 1 and 2), the variability increased approximately linearly with time, so that the variability profiles could be approximated by a straight line [see the dashed lines in Fig. 6.3(A1,A2,B1,B22)]. This was confirmed by the calculation of the average Linearity Coefficients across subjects, which were close to 1 for these targets [Fig. 6.3(D)].

For the most angled targets (targets 4 and 5), the variability profiles were not linear: the average LC across subjects was around 0.65 for these targets. Indeed, the variability profiles corresponding to these targets were clearly composed of two parts: a first part where the variability increased linearly and a second part where the variability remained constant [see the dashed lines in Fig. 6.3(A4,B4)] or even decreased [Fig. 6.3(A5,B5)]. We propose in section 6.2.3 a hypothesis accounting for this remarkable feature.

## 6.2.3 Variability around the average trajectory: combination of two independent components

### A hypothesis on the structure of the variability profiles

We propose to study now in more detail the *structure* of the variability profiles observed in the nonvisual condition. In this experiment, two parameters were varied: the presence or absence of visual feedback and the "complexity" of the target, that is, more specifically, whether the target was "straight" or

| Visual condition/Target | Straight targets | Angled targets |
|---|---|---|
| Visual | 0 + 0 | 0 + Bump |
| Nonvisual | Line + 0 | Line + Bump |

Table 6.1: The "two-sources" hypothesis. In each cell, we indicated the putative contribution of source 1 (vision-dependent, "trajectory-complexity"-independent) + the putative contribution of source 2 (vision-independent, "trajectory-complexity" dependent).

"angled". We make the hypothesis that these two parameters *independently contribute* to the variability profiles.

More precisely, our hypothesis states that the variability recorded for the different targets and visual conditions results from the accumulation of the variabilities produced by two mutually independent sources. The first source is vision-dependent and "trajectory complexity"-independent: that is, independent of whether the target is "straight" or "angled". The second source is "trajectory complexity"-dependent and vision-independent. The psychological and physiological interpretations of these two sources are addressed later (see Discussion, section 6.5).

The variability resulting from source 1 – which is "trajectory complexity"-independent – can be isolated by examining the trials involving only "straight" targets: indeed, for these "easy" trials, the contribution of source 2 – which is "trajectory complexity"-dependent – should be minimal. Now, from the results above, we know that the variability in question is almost zero in the visual condition, and that it increases approximately linearly with time in the nonvisual condition. Similarly, the variability resulting from source 2 – which is vision-independent – can be isolated by examining the trials executed with vision. For the "straight" targets, this variability is almost zero, while for the "angled" targets, this variability describes, as a function of time, the shape of a bump.

### An observation supporting the hypothesis

The proposed "two-sources" hypothesis allows now to make the following nontrivial observation: the special shape of the variability profiles observed in condition NV for the "angled" targets can be decomposed as the sum of a *straight line* (source 1) and of a *bump profile* (source 2): see Table 6.1 for a summary.

To illustrate this, let us denote by $\mathrm{TD}_{\mathrm{VI}}^n$ and $\mathrm{TD}_{\mathrm{NV}}^n$ the variability profiles corresponding to target $n$ in conditions VI and NV respectively. The above observation implies that $\mathrm{TD}_{\mathrm{NV}}^n$ would be similar to the sum of the bump-shaped variability profile observed for the same target in condition VI ($\mathrm{TD}^{n}_{\mathrm{VI}}$), plus a straight-line variability profile (for simplicity, we chose the variability profile corresponding to target 2: $\mathrm{TD}^{2}_{\mathrm{NV}}$).

Fig. 6.4(A) shows the comparison of $\mathrm{TD}^{4}_{\mathrm{NV}}$ with the sum $\mathrm{TD}^{4}_{\mathrm{VI}} + \mathrm{TD}^{2}_{\mathrm{NV}}$ for the five tested subjects. Similarly, Fig. 6.4(B) shows the comparison of $\mathrm{TD}^{5}_{\mathrm{NV}}$ with the sum $\mathrm{TD}^{5}_{\mathrm{VI}} + \mathrm{TD}^{2}_{\mathrm{NV}}$. One can observe in each case a good match between the compared profiles.

However, this observation should not be taken literally. While the proposed hypothesis concerns the noise *sources*, we compared above the *trajectory variabilities*, that is, the *output* of the whole trajectory generation process. In this respect, it should be noted that, whenever the trajectory generation mechanisms contain nonlinearities, the additivity of the two noise sources would not translate into the additivity of the trajectory variability profiles. Following this remark, we did not seek to find the best combination of the two *squared* variability profiles (indeed, the variability profiles were given by the 2D "*standard deviations*" of the trajectories, but for linear systems only *variances* add up). We chose instead to show directly the sum of the variability profiles, as a way to hint how the special shapes of the variability profiles can be obtained from the combination of a line and a bump profile. In order to assess the hypothesis in a more formal way, it is necessary to evaluate the input-output relationship between the incoming noise and the resulting trajectory variability. This is addressed in chapter 9 where we propose a possible implementation of the trajectory generation mechanism.

## 6.3 Experiment 4: influence of speed on the variability profiles

### 6.3.1 Methods

Five male subjects participated in this experiment. Each subject generated 80 trajectories (2 visual conditions × 5 targets × 8 repetitions), so that a total of 400 trajectories were recorded.

The methodology and the protocol used in this experiment were the same as in Experiment 3, except that we varied the speed instruction: subjects were asked to walk either at their preferred speed (Normal speed – NS) or at a higher speed (Fast speed – FS). Vision was available in both speed conditions.

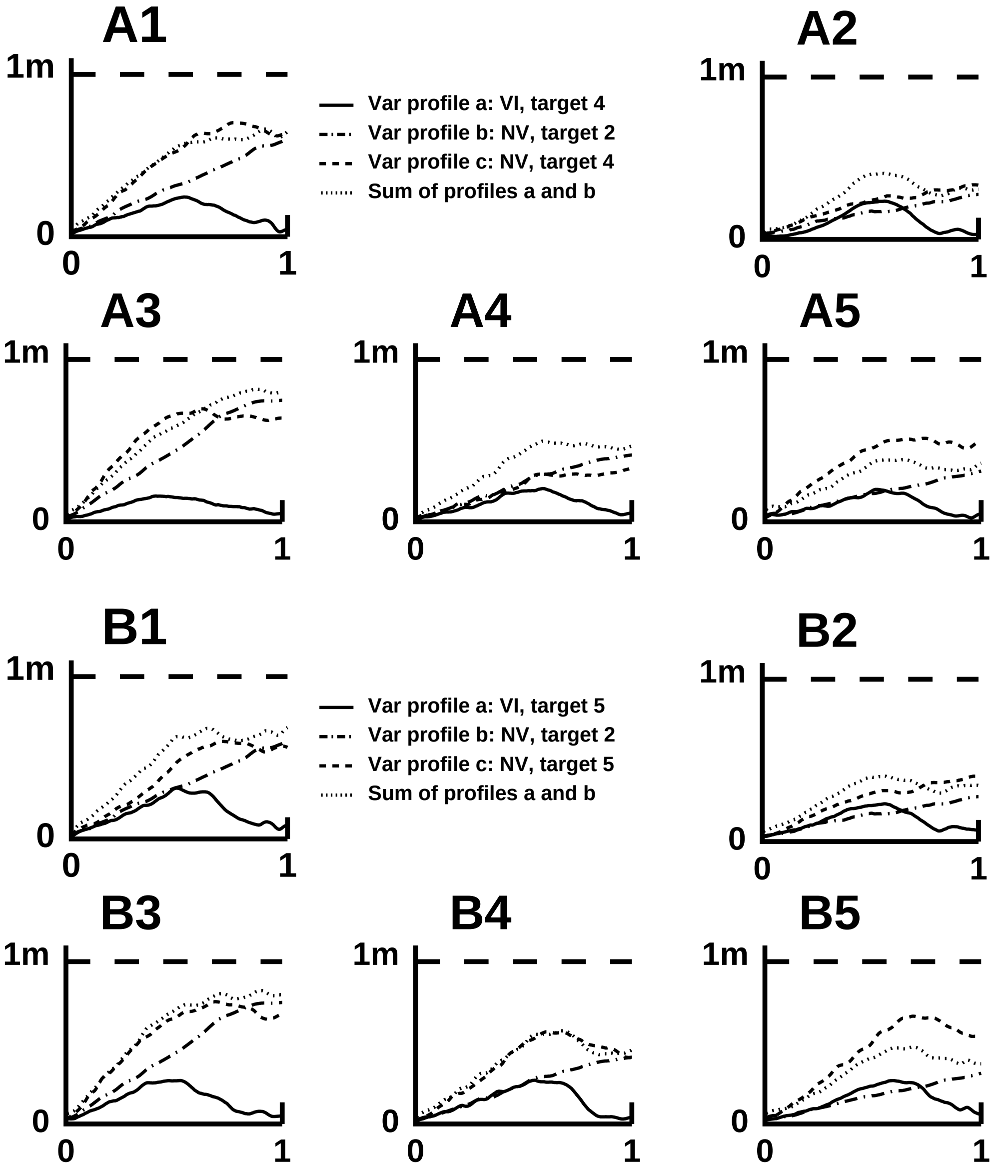

Figure 6.4: Testing the "two-sources" hypothesis. **(A)** Actual and predicted variability profiles for target 4 and subjects A. N. (A1), D. P. (A2), G. N. (A3), L. H. (A4), N. V. (A5). Plain line: variability profile for target 4 in condition VI, Dashed-dotted line: variability profile for target 2 in condition NV. Compare the dashed line (variability profile for target 4 in condition NV) with the dotted line (sum of the plain line and the dashed-dotted line). **(B)** Same legends as in (A), but for target 5.

### 6.3.2 Results

The speed instructions were well respected: subjects did walk faster in the FS condition than in condition NS. The average speed across targets, subjects and trials was 1.34 ± 0.11m.s$^{-1}$ in condition NS and 1.60 ± 0.16m.s$^{-1}$ in condition FS. From condition NS to FS, the subjects increased their speed by up to 30% (the speed increase ranged between 13% and 30%). In the two-way ANOVA test where the factors were the speed condition and the target, the main effect of the speed condition was significant [F(1,40) = 55.1, $p < 0.05$] and there was no significant interaction effect [F(4,40) = 0.09, $p > 0.05$].

The average trajectories were also similar in the two speed conditions [Fig. 6.5(C)]. The average Maximal Trajectory Separation $\mathrm{MTS}_{\mathrm{NS/FS}}$ computed across targets and subjects was 0.18 ± 0.06m while the average $\mathrm{MTD}_{\mathrm{NS}}$ was 0.18 ± 0.08m. In the two-way ANOVA test where the factors were the speed condition and the target, the main effect of speed condition was not significant [F(1,40) = 0.01, $p > 0.05$]. However, the interaction effect was significant [F(4,40) = 5.7, $p < 0.05$]. In other words, the difference between the average trajectories in the two conditions was globally of the same magnitude as the variability within condition NS, but target-wise, there were differences between $\mathrm{MTS}_{\mathrm{NS/FS}}$ and $\mathrm{MTD}_{\mathrm{NS}}$. However, for the most interesting targets (targets 4 and 5), we found that $\mathrm{MTS}_{\mathrm{NS/FS}} < \mathrm{MTD}_{\mathrm{NS}}$ [Fig. 6.5(C)].

The variability profiles measured in the two speed conditions were very similar, in terms of both shape and magnitude (see [Fig. 6.5(A,B) for typical variability profiles]. For the straight targets, the variability was low throughout the movement, and for the angled targets, bump-shaped variability profiles were consistently observed across both speed conditions. Quantitatively, in the two-way ANOVA test where the factors were the speed condition and the target, the main effect of speed condition on the MTDs was not significant [F(1,40) = 0.006, $p > 0.05$], neither was the interaction effect [F(4,40) = 1.2, $p > 0.05$]

## 6.4 Experiment 5: testing the "desired-trajectory" hypothesis

This simple experiment adapts a hand movement experiment from Todorov and Jordan (2002) to the context of locomotion in order to test the "desired-trajectory" hypothesis (see this chapter's Overview and section 1.3).

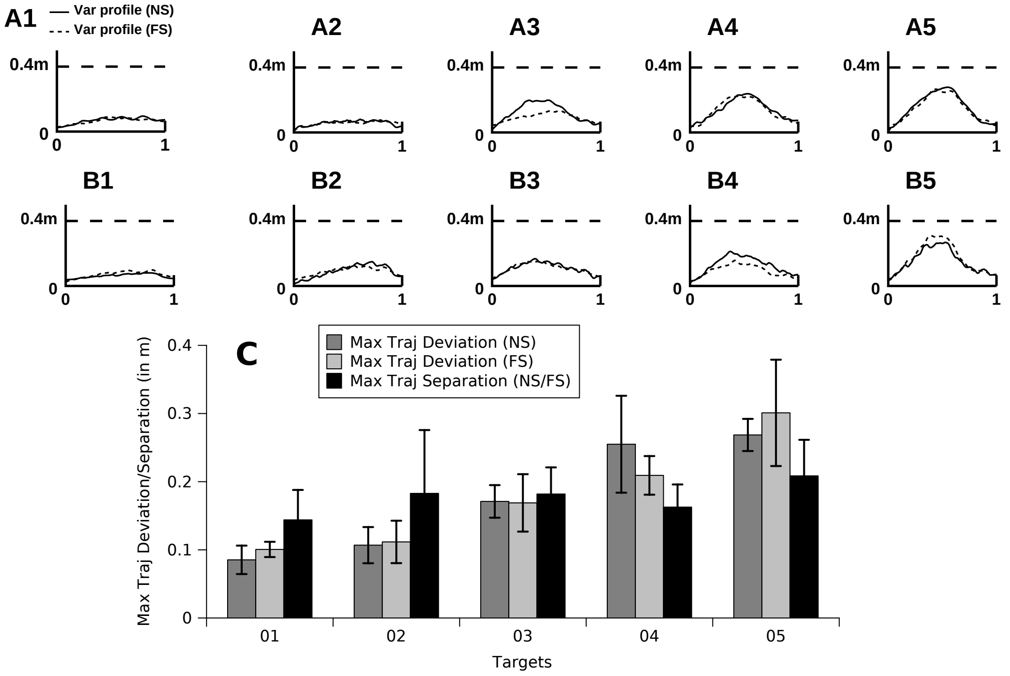

Figure 6.5: Comparison of variability profiles in the Normal speed (NS: plain lines) and Fast speed (FS: dashed lines) conditions. For details, see legends of Fig. 6.3. **(A)** Variability profiles for subject B.B. **(B)** Same as in A, but for subject R.K. **(C)** Average Maximal Trajectory Deviation across targets in condition NS (dark gray bars) and in condition FS (light gray bars), average Maximal Trajectory Separation across targets between conditions NS and FS (black bars).

### 6.4.1 Methods

Five subjects (three males, two females) participated in this experiment. Each subject generated 30 trajectories (3 sessions × 10 repetitions), so that a total of 150 trajectories were recorded.

The experiment was divided in three sessions separated by several hours. In the first session, the task was the same as in Experiments 2, 3 and 4: namely, walking towards a distant arrow. We used only one target, similar to target 5 in Fig. 6.2. The subject performed 10 trials in this session, all with vision and at normal speed. We computed the average trajectory $(x_{\mathrm{av}}(t), y_{\mathrm{av}}(t))_{0\leq t\leq 1}$ across these 10 trials. We denoted respectively by $P_1$, $P_2$ and $P_3$ the spatial positions $(x_{\mathrm{av}}(0.33), y_{\mathrm{av}}(0.33))$, $(x_{\mathrm{av}}(0.5), y_{\mathrm{av}}(0.5))$ and $(x_{\mathrm{av}}(0.67), y_{\mathrm{av}}(0.67))$.

In the second session, we placed a piece of black tape on the ground at position $P_2$. The subject was then asked, as in the first session, to walk towards the distant arrow. In addition, he had now to go through the via-point indicated by the piece of black tape. Again, the subject had to perform 10 repetitions.

The third session was similar to the second session, except that the subject had to go successively through the *three* via-points $P_1$, $P_2$ and $P_3$.

In this experiment, the average trajectories and the variability profiles were computed differently, in a manner similar to that described in the legend of Fig. 5 in Liu and Todorov (2007). This was done in order to better assess the effects of the *spatial* via-points.

### 6.4.2 Results

We noted first that the average trajectories recorded in the three sessions were very similar, as we could expect from the experimental set-up. For instance, the Maximal Trajectory Separation between the average trajectory of session 1 (0-via-point) and that of session 2 (1-via-point) was 0.12 ± 0.07m. Similarly, the MTS between the average trajectory of session 1 (0-via-point) and that of session 3 (3-via-points) was 0.11 ± 0.06m.

Consistently with the previous results, the variability profiles observed in the 0-via-point condition were bump-shaped [Fig. 6.6(A1,B)]. By contrast, the variability profiles in the 1-via-point condition were clearly two-peaked, with a local minimum occurring around $t = 0.5$ [Fig. 6.6(A2,B)]. The variability profiles in the 3-via-points condition displayed smaller variations than in the two previous conditions. In particular, we observed no significant peaks or valleys [Fig. 6.6(A3,B)].

Quantitatively, the MTD in the 1-via-point (0.06 ± 0.02m) and the 3-

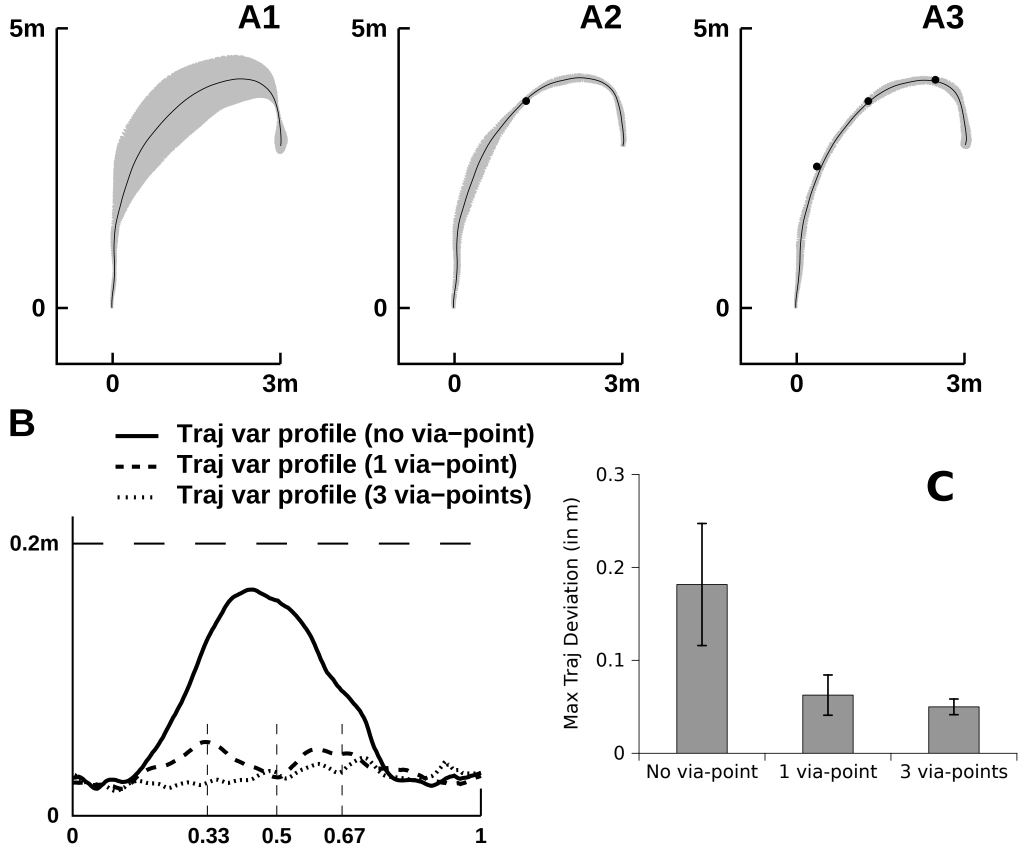

Figure 6.6: Testing the "desired trajectory" hypothesis. **(A)** Average trajectories and variance ellipses around the average trajectories. A1: 0-via-point condition. A2: 1-via-point condition. A3: 3-via-points condition. **(B)** Average variability profiles computed across subjects. Plain line: no via-point; Dashed line: 1 via-point; Dotted line: 3 via-points. We also indicated the time instants $t = 0.33$, $t = 0.5$ and $t = 0.67$ for which the via-points where computed. **(C)** Average Maximal Trajectory Deviation (MTD) across subjects in the three conditions.

via-points (0.05 ± 0.008m) conditions were lower than the MTD in the 0-via-point condition (0.18 ± 0.06m) [Fig. 6.6(C)]. The one-way ANOVA test revealed that the number of via-points (0, 1 or 3) has a significant effect on the MTDs [F(2,12) = 16.3, $p < 0.05$]. Post-hoc Tukey tests revealed that this effect was significant between the 0- and 1-via-point conditions, between the 0- and 3 via-points conditions, but not between the 1- and 3-via-points conditions.

## 6.5 Discussion

### 6.5.1 Origin of the variability and nature of the control mechanisms in the visual condition

We showed in chapter 5 that subjects produced stereotyped trajectories in order to reach a distant target. However, we also noticed some variabilities around the average trajectories. Here, by increasing the number of repetitions per subjects per target and by using more complex experimental paradigms, we could analyze with a greater precision the *intra-subject variability profiles* and get deeper into the understanding of the control mechanisms underlying goal-oriented locomotion.

#### Execution noise in locomotion

Within the theoretical framework of computational motor control, it was proposed that movement variability may arise during three processes: target localization, movement planning and movement execution (Schmidt et al., 1979; van Beers et al., 2004). We assume here that this three-sources distinction also holds for locomotor "reaching". Given this, we argue that the variability profiles observed in the visual conditions of Experiments 3, 4 and 5 mostly resulted from execution noise. Indeed, regarding first the target localization process, the target was clearly visible and remained so during the whole movement. Second, since we conducted an intra-subject analysis, the contribution of planning variability to the overall variability was reduced: indeed, a large part of planning variability arises from differences in subjects' morphologies or personal preferences. Finally, we reason by analogy with hand movements and follow van Beers et al. who demonstrated that, for hand movements, "*in general, execution noise account[ed] for at least a large proportion of movement variability*".

In hand movements, execution noise may arise at different levels (van Beers et al., 2004; Faisal et al., 2008): motor commands (the elaboration and the transmission of the neural signals may be corrupted at any stage of the neural chain, from cortical structures to motoneurons) or muscle contractions (the motor response of a muscle to a given neural signal is inherently variable), etc. Since locomotion involves the production of complex muscle contraction patterns (lower-body muscles for forward propulsion, but also arm and trunk muscles for stability and neck muscles for steering purposes), execution noise can also step in at all these levels. However, since the number of muscles involved in locomotion is much larger than in hand movements, the exact relationship between whole-body trajectory variability and the muscles' execution noises is harder to establish.

As evoked in this chapter's Overview, locomotion involves also a "navigational" aspect in addition to the purely motor aspect. Indeed, locomotion is the only motor activity in which the spatial position and orientation of the body change throughout movement execution. In this respect, special attention should be devoted to the references frames that are used for the perception of movement (Berthoz, 1991): in contrast with the case of hand movements, these reference frames move during the locomotor task. The errors in the updating of the body's position and orientation due to the manipulation of different reference frames may then contribute to the variability of the trajectory during movement execution. To study in detail the specific contribution of the motor and "navigational" levels to execution noise, a differential analysis may be conducted, for example, by comparing the variability observed during navigation in virtual environments with that observed during real-world locomotion.

### Online feedback control of locomotion in the visual condition

To fully explain the variability of locomotor trajectories, one has to understand not only the nature of the noise but also that of the control mechanisms at work, since the form of the variability arises from the interplay between these two elements. A given noise pattern may indeed give rise to different variability profiles depending on the control scheme used by the subject.

More precisely, we have distinguished in the Overview two families of control schemes: purely open-loop control and online feedback control. As already mentioned, in a purely open-loop control scheme, there are no feedback corrections during the performance of the task. Errors can hence only accumulate, leading to monotonically increasing variability (Todorov and Jordan, 2002, see also our modeling results in chapter 9). By contrast, the results of Experiments 3 and 4 showed that, for the "angled" targets, the variability profiles in condition VI always increased at the beginning of the movement but then decreased towards zero at the end of the movement, yielding bump-shaped profiles (see also chapter 9). Taken together, these observations indicate that online feedback control is present in visual locomotion. This is not surprising since in general, purely open-loop control exists only in very fast, balistic movements such as fast arm reaching. Here, since the movements we studied lasted from 3 to 10 seconds, this allows the detection of errors and the implementation of online corrections if necessary.

### On the "desired-trajectory" hypothesis for locomotion

The precise nature of the online feedback control cannot however be determined solely from the variability profiles recorded in Experiments 3 and 4. Indeed, both the "desired-trajectory" (DT) hypothesis and the fully optimal control hypothesis would yield bump-shaped variability profiles in the limited conditions of these experiments. However, the results of Experiment 5 are incompatible with a basic DT control scheme. Indeed, as indicated in the Overview, the DT hypothesis implies that, during a planning stage, a desired optimal trajectory is computed. Empirically, this DT can be equated to the average trajectory computed across a large number of trials. Then, during the execution stage, a "trajectory-tracking" mechanism is used to achieve the DT. In Experiment 5, since the average trajectories were forced by the experimental protocol to be similar in the three conditions (0-, 1- and 3-via-points), the DT hypothesis would predict practically no difference between the statistics of the trajectories produced in these conditions. Thus, the large differences we reported concerning the variability profiles in the three conditions indicated that the DT hypothesis should be rejected.

We note nonetheless that the results of Experiment 5 cannot rule out a variation of the DT hypothesis which consists of (i) constructing several desired sub-trajectories (2 sub-trajectories in the 1-via-point condition – the first trajectory between the starting position and the via-point, the second trajectory between the via-point and the final condition –, and 4 sub-trajectories in the 3-via-points conditions) and (ii) tracking *sequentially* these sub-trajectories. While this variation may seem unlikely (indeed, in post-experiment interviews, the subjects reported that they conceived the trajectory as a whole and not as a sequence of sub-trajectories glued together at the via-points), it cannot be theoretically ruled out. This remark also applies for the original experiments of Fig. 3 in Todorov and Jordan (2002) which inspired our Experiment 5 (see also our review in section 1.3).

A more likely explanation of the results of Experiment 5 involves an optimal feedback control scheme. Within this scheme, online corrections would be made with respect to the task goal [namely, go through the via-points (if present) and reach the targets] and not with respect to any intermediate representation (e.g. a desired trajectory). In the 0-via-point condition, since no other constraints than the goal is specified, random deviations away from the average trajectory are not corrected if they do not interfere with this task, allowing the variability to accumulate around the middle of the trajectory, thus yielding bump-shaped variability profiles. By contrast, when via-points are imposed, corrections would be made to ensure that the trajectory go through these via-points, resulting in low variability around the via-points (see also the discussion about "trajectory redundancy" in Todorov and Jordan (2002). We explore this hypothesis by designing an optimal feedback control model in chapter 9.

### 6.5.2 Online control of locomotor trajectories in nonvisual locomotion

We showed in chapter 5 that, in order to reach a distant target, subjects produced very similar average trajectories in the Visual (VI) and Nonvisual (NV) conditions. Based on this observation, we then suggested that visual and nonvisual locomotion share the same *open-loop* process (see section 5.4.3).

While it is easy to conceive that online feedback control is present in normal visual locomotion, the fact that such a mechanism may also be present when vision is totally excluded during task execution may be more surprising. Yet we observed in Experiment 3 that the nonvisual variability profiles were not always monotonic: for "angled" targets, the variability decreased near the end of the trajectory. The same arguments as previously then implies that online control is also present in nonvisual locomotion.

The idea that online control may be present in nonvisual locomotion was proposed earlier in the literature by Farrell and Thomson (1999). In their experiment, the subject had to walk with or without vision towards a previously seen target placed at 8 paces, 8 paces minus 40cm or 8 paces plus 40cm in front of him. He had to start with his right foot and to land on the target with his left foot. The authors showed that, in both visual conditions, the subject functionally adjusts the lengths of his final steps, on a trial-to-trial basis, in order to land on the target with the specified foot (see also our review in section 2.2).

The precise nature of that online control has however remained unclear. For instance, while Farrell and Thomson rightly remarked that, in the nonvisual condition, "*[the subjects] adjust their step lengths in a way similar to that seen in the visual condition*", they did not provide an interpretation of the nature of the processes common or specific across visual conditions.

Here, the “two-sources” hypothesis (see section 6.2.3), directly addressed the nature of this online control. Indeed, we showed that the variability in the nonvisual condition results from the combination of a vision-dependent component and a “trajectory-complexity”-dependent component.

The first component – whose contribution is zero in condition VI and an increasing linear function of time in condition NV – can be interpreted as resulting from the errors in the subject’s estimation of his state which, in turn, are caused by the absence of visual feedbacks.

The second component – whose contribution is zero for “straight” targets and bump-shaped for “angled” targets – can be interpreted as resulting from the interplay between execution noise and optimal feedback control, as explained previously in the case of visual locomotion. The fact that this component is present also in nonvisual locomotion, under almost the same form, thus suggests that the very control mechanisms that governs visual locomotion underlie nonvisual locomotion as well.

Whether our conclusions about the control mechanisms at work during nonvisual locomotion also hold in adventitiously and congenitally blind subjects remains yet to be investigated. We believe indeed that a better understanding of the control mechanisms governing nonvisual locomotion and navigation can help develop new tools assisting visually impaired individuals in their daily activities.

# Chapter 7

# Some other experimental results

We present in this chapter some preliminary results that concern other aspects of trajectory formation. In section 7.1, we study the relations between the steering behavior (in particular, head and trunk turning profiles) and other levels of locomotor control: the stepping activity and the formation of whole-body trajectories. In section 7.2, we examine the relations between locomotor trajectory formation and navigation through a new experiment (Experiment 6). In particular, we investigate the control principles underlying discrete navigational choices (such as, e.g. choosing one *route* out of several possible routes). Finally, we present Experiment 7 (section 7.3), which provides a direct test for affine invariance in hand trajectories.

The results concerning the steering behavior were first presented in Pham et al. (2010), to which the reader is referred for more details. Experiment 6 was designed and run by Q.-C. Pham, H. Hicheur and J. Wiener in November 2007. Experiment 7 was designed and run by Q.-C. Pham and D. Bennequin in June 2008.

## 7.1 Back to Experiment 2: anticipatory steering behavior

As noted in our review (see section 2.3), most works devoted to the study of the head anticipatory behavior were based on experimental protocols involving straight or predefined paths. These works thus did not allow examining the dynamic relations between the steering behavior and the formation of locomotor trajectories.

Here, we analyze the head and trunk turning profiles based on the data collected in Experiment 2 (see section 5.3 for details about the experimental protocol). Briefly, we asked subjects to walk from a starting position and orientation in space towards a distant target defined also in position and orientation. The subjects had to do so under four conditions: Visual Forward (VF), Nonvisual Forward (NF) Visual Backward (VB) and Nonvisual Backward (NB).

This protocol thus allowed (i) studying the steering behavior in freely-generated locomotor trajectories and (ii) assessing the separate and combined effects of gait reversal (walking backward) and absence of vision on the steering behavior.

### 7.1.1 Methods

#### Definition of head and trunk angles

In section 5.3, we studied whole-body trajectories using the midpoint of the shoulders' markers. Here, our analysis of the steering behavior is based on the data recorded for the head and shoulders markers.The head and trunk orientations in the horizontal plane were computed based on the four head markers and the two shoulders markers respectively (see General Methodology in section 4.1 and Fig. 7.1 below). The trunk direction was given by the orthogonal direction to the shoulders segment defined by the two shoulders markers.

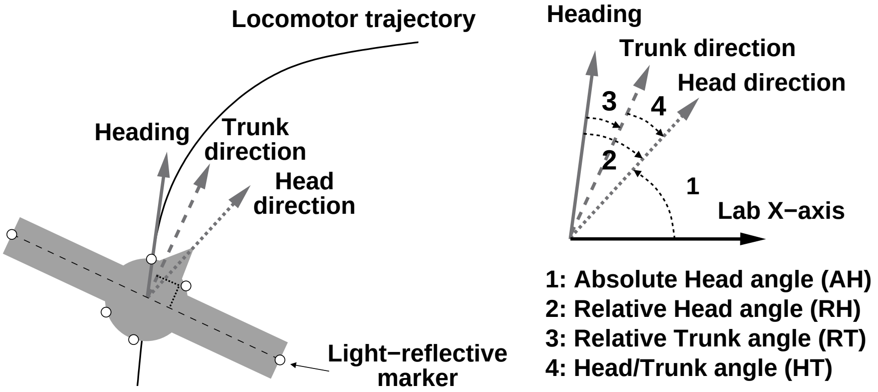

Figure 7.1: Definition of head and trunk angles

As shown in Fig. 7.1, we considered four time-varying angles: the Absolute Head angle (AH, angle between the head direction and the laboratory X-axis), the Relative Head angle (RH, angle between the head direction and the heading), the Relative Trunk angle (RT, angle between the trunk direction and the heading) and the Head/Trunk angle (HT, angle between the head direction and the trunk direction). The "heading" just mentioned is the tangent direction to the trajectory (or the travelling direction, see Imai et al., 2001).

### Stereotypy of the steering behavior

Several statistics were computed to assess the stereotypy of the head turning behavior, in the same way as in the General Methodology (chapter 4) for assessing the stereotypy of whole-body trajectories. First, the average Absolute Head angle profile $(\mathrm{AH}_{\mathrm{av}}(t))_{0\leq t\leq 1}$ was computed as

$$\mathrm{AH}_{\mathrm{av}}(t) = \frac{1}{N}\sum_{i=1}^{N}\mathrm{AH}_i(t) \tag{7.1}$$

where $N$ is the number of trajectories recorded for a given target (here, $N = 14$ subjects $\times$ 3 repetitions $= 42$).

The Absolute Head angle Deviation (AHD), which measures the variability of the AH around the average profile, was then defined by

$$\mathrm{AHD}(t) = \sqrt{\frac{1}{N-1}\sum_{i=1}^{N}(\mathrm{AH}_i(t) - \mathrm{AH}_{\mathrm{av}}(t))^2} \tag{7.2}$$

The Maximum Absolute Head angle Deviation (MAHD) was next given by

$$\mathrm{MAHD} = \max_{0\leq t\leq 1}\mathrm{AHD}(t) \tag{7.3}$$

We defined similarly the RHD (Relative Head angle Deviation), MRHD (Maximum RHD), RTD (Relative Trunk angle Deviation), MRTD (Maximum RTD), HTD (Head/Trunk angle Deviation) and MHTD (Maximum HTD).

### Degree of head and trunk anticipation

When humans walk forward on a straight trajectory, the directions of their head and trunk mostly align with the heading, which corresponds to RH $\simeq$ RT $\simeq$ HT $\simeq 0$ (the residual oscillations induced by the stepping activity are neglected, see Hicheur and Berthoz, 2005). By contrast, when they walk along a curved path, their head and trunk significantly deviate from the heading and are directed towards the *interior* of the curve, thus making nonzero angles with the heading. Furthermore, the larger these angles, the more the head and the trunk *anticipate* with respect to the heading. Thus, to *quantify* the degree of head and trunk anticipation, we computed, for each trial $1 \leq i \leq N$ the Maximum Relative Head angle (MRH), the Maximum Relative Trunk angle (MRT) and the Maximum Head/Trunk angle (MHT) as

$$\mathrm{MRH}_i = \max_{0 \leq t \leq 1} |\mathrm{RH}_i(t)| \tag{7.4}$$

$$\mathrm{MRT}_i = \max_{0 \leq t \leq 1} |\mathrm{RT}_i(t)| \tag{7.5}$$

$$\mathrm{MHT}_i = \max_{0 \leq t \leq 1} |\mathrm{HT}_i(t)| \tag{7.6}$$

These values can then be averaged across subjects and repetitions ($1 \leq i \leq N$) yielding average and standard deviation values. At this point, it should be noted that the SD of the $\mathrm{MRH}_i$ obtained by this calculation should not be confused with the MRHD defined previously.

In the backward conditions (VB and NB), since the "natural" angle between the head (and trunk) direction and the heading is $-180°$ [see Fig. 7.4(A)], the $\mathrm{MRH}_i$ (and the $\mathrm{MRT}_i$) was computed by

$$\mathrm{MRH}_i = \max_{0 \leq t \leq 1} |\mathrm{RH}_i(t) + 180°| \tag{7.7}$$

### Timing of anticipation

In addition to the degree of anticipation, it was also interesting to assess its *timing*, which may provide insights into the temporal coordination of the different segments during steering (Imai et al., 2001). To this purpose, we determined the time instants when the maxima defined in the preceding section were attained. For instance, the Time of Maximum Relative Head angle (TMRH) was defined by

$$\mathrm{TMRH}_i = \mathrm{argmax}_{0 \leq t \leq 1} |\mathrm{RH}_i(t)| \tag{7.8}$$

The Time of Maximum Relative Trunk angle (TMRT) and the Time of Maximum Head/Trunk angle (TMHT) were defined similarly.

Finally, these values could also be averaged across subjects and repetitions ($1 \leq i \leq N$), yielding average and standard deviation values.

## 7.1.2 Results

### Head orientation in space

The examination of the average Absolute Head angle (AH) profiles (Fig. 7.2) revealed large differences between conditions VF, NF and NB on one hand, and condition VB on the other.

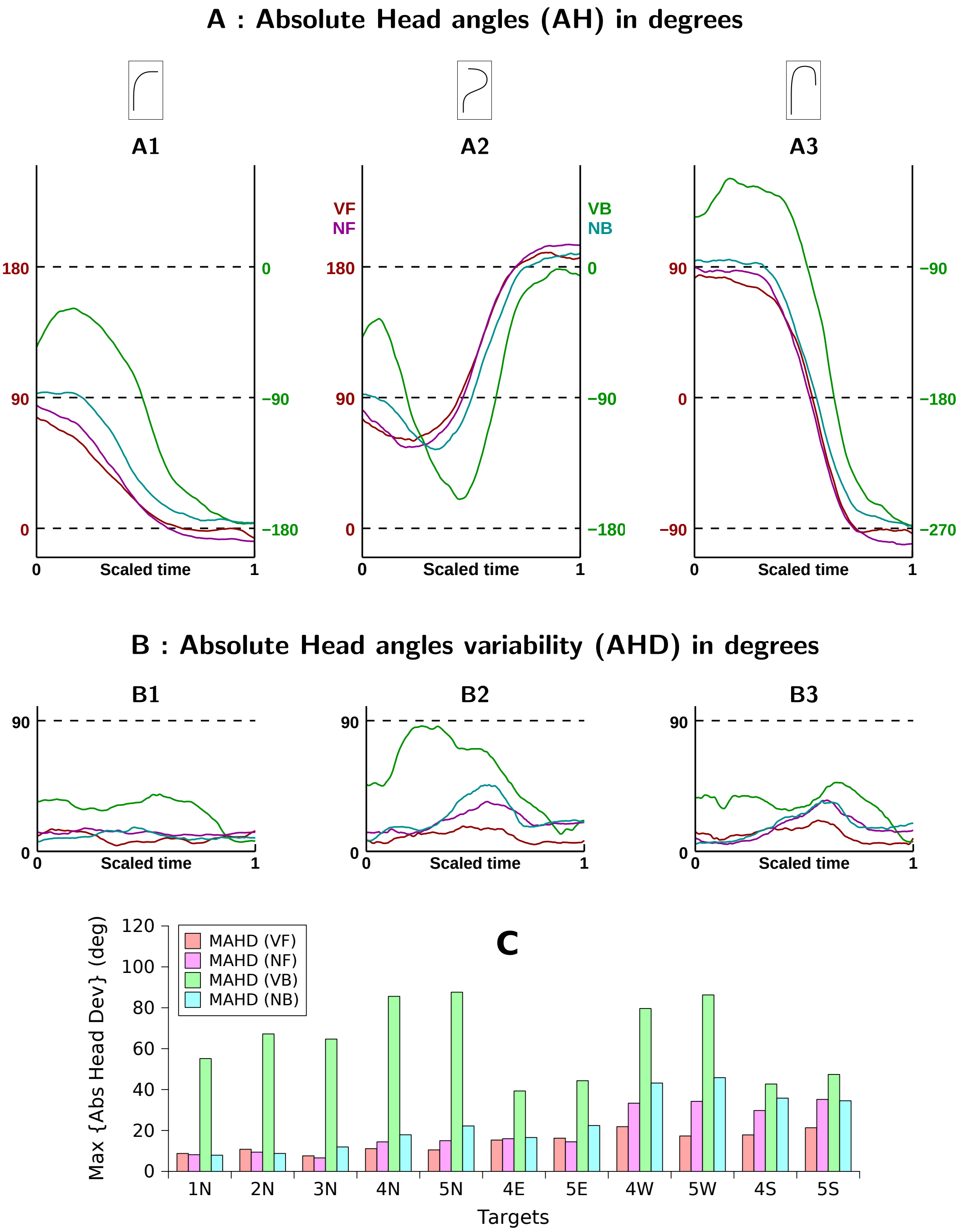

Figure 7.2: Absolute Head (AH) angles in the four tested conditions (VF: red, NF: magenta, VB: green, NB: cyan). (**A**) Average AH profiles. A1: target 4E, A2: target 5W, A3: target 5S. Left scale for the forward conditions (VF, NF) and right scale for the backward conditions (VB, NB). (**B**) AH variability profiles. (**C**) Variability of the AH profiles: Maximal Absolute Head angle Deviation (MAHD) in degrees.

In conditions VF, NF and NB, the head direction at the beginning and the end of a trajectory was aligned with the heading: orthogonal to the X-axis at the beginning ($\mathrm{AH}_{\mathrm{av}}(0) = 90°$ in VF and NF, $\mathrm{AH}_{\mathrm{av}}(0) = -90°$ in NB), and aligned with the arrow's direction at the end of the trajectory ($\mathrm{AH}_{\mathrm{av}}(1) = \text{target\_angle}$ in VF and NF, $\mathrm{AH}_{\mathrm{av}}(1) = -\text{target\_angle}$ in NB). Between $t = 0$ and $t = 1$, the average AH profiles had sigmoid-like shapes – with some differences, however, among the three conditions [red, magenta and cyan lines in Fig. 7.2(A1,A2,A3); this is studied in more detail in the next section].

By contrast, in condition VB, the head direction was not aligned with the heading at the beginning of the trajectory: $\mathrm{AH}_{\mathrm{av}}(0) \simeq -45°$. Indeed, right from the start, subjects turned their head backwards to look at the target "over their shoulders". In addition, between $t = 0$ and $t = 1$, the average AH profiles displayed large variations in time [green lines in Fig. 7.2(A1,A2,A3)], unlike the smooth sigmoid-shape profiles observed in conditions VF, NF and NB.

In term of the variabilities, the AHDs were relatively low in conditions VF, NF and NB and much larger in condition VB [Fig. 7.2(B1,B2,B3)]. Quantitatively, the average MAHDs across targets were respectively 14.4°, 19.7° and 24.3° in conditions VF, NF, NB, while the average MAHD was 63.6° for VB [see also Fig. 7.2(C)].

These observations confirm the results reported in Hicheur et al. (2007) where we demonstrated the stereotypy of the head turning behavior. Moreover, they extend those results to the cases of nonvisual forward and backward locomotion. Together with the similarity of the average AH profiles in the VF, NF and NB conditions, they suggest that the head orientation during nonvisual forward and backward locomotion is controlled following the same strategy as in visual forward locomotion. In the sequel, we analyze in greater details these strategies, with a particular emphasis on the "anticipatory" aspects. Condition VB appeared to be a specific condition where the subjects adopted highly variable steering strategies and as such, VB steering results will not be presented in the next sections.

### Head anticipatory behavior in conditions VF and NF

**Condition VF** The examination of the Relative Head angles (RH) profiles [Fig. 7.3(B1,B2,B3)] revealed a clear anticipatory behavior. In condition VF (red lines), one may distinguish two main parts. In the first part, between $t = 0$ and $t \simeq 0.3$, the RH remained close to zero. Here there was no anticipation: the head remained mostly aligned with the heading. This part corresponded indeed to the straight portion of the trajectory.

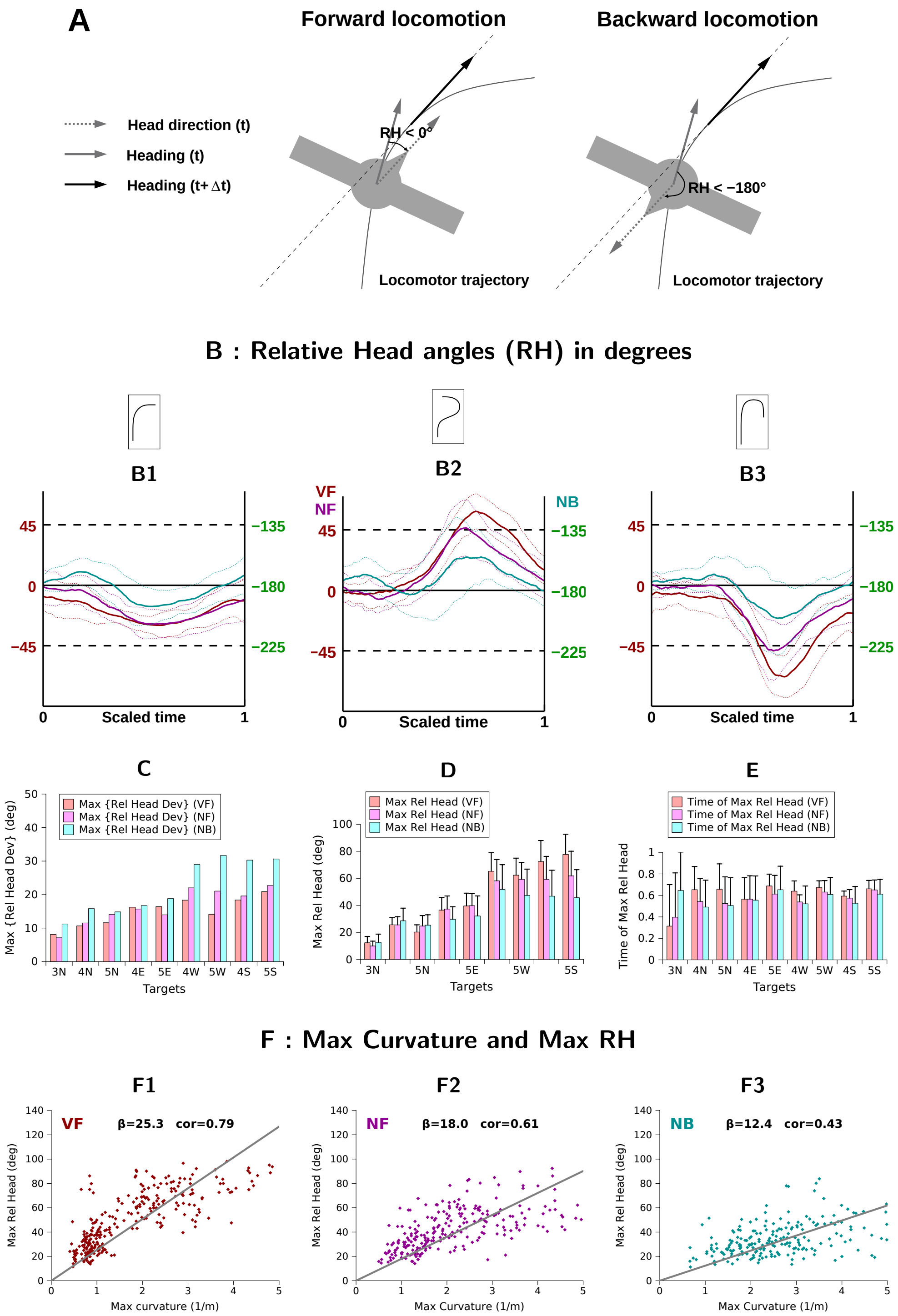

Figure 7.3: Head anticipatory behavior. (**A**) Anticipatory behavior in forward and in backward locomotion. (**B**) Average RH profiles (plain lines) ± SD (dashed lines) for conditions VF (red), NF (magenta) and NB (cyan). B1: target 4E, B2: target 5W, B3: target 5S. (**C**) Variability of the RH profiles: Maximal Relative Head angles Deviation (MRHD). (**D**) Degree of head anticipation: Maximal Relative Head angles (MRH) averaged across subjects and repetitions (and the corresponding SD bars). (**E**) Timing of head anticipation: time when MRH was attained, averaged across subjects and repetitions. (**F**) Regression analysis of the dependence between path curvature and head anticipation. We tested the model (Maximum Relative Head angle) $= \beta \times$(Maximum Curvature) for condition VF (F1), NF (F2) and NB (F3).

In the second part, for targets where the subject had to steer towards the right [targets 4E and 5S: Fig. 7.3(B1,B3)], the RH first decreased to reach its minimal value around $t = 0.6$. Then, it increased again, to get back near 0 at $t = 1$. The RH was thus negative for $0.3 \leq t \leq 1$: the head was oriented towards the interior of the curve. This part corresponded to the curved portion of the trajectory. Similarly, for targets where the subject had to steer towards the left [targets 5W: Fig. 7.3(B2)], the RH first increased and then decreased, yielding also an anticipatory behavior. The average Maximal RH across subjects and repetitions ranged between 12.4° (target 1N) and 77.8° (target 5S).

In agreement with previous studies (Hicheur et al., 2005b, 2007), we noted that the more curved the trajectories, the larger the MRH [Fig. 7.3(D), red bars]. The linear regression analysis performed over the angled trajectories (that is, excluding targets 1N, 2N and 3N) revealed a good correlation between the MRH and the Maximum Curvature (MC) [$\beta = 25.3$, $\mathrm{cor} = 0.79$, see Fig. 7.3(F1)].

**Condition NF** In condition NF, the anticipatory behavior could also be clearly observed. The NF profiles displayed similar shapes as the VF profiles, but with a smaller magnitude [Fig. 7.3(B1,B2,B3), magenta lines].

Quantitatively, the average MRHs ranged between 10.0° (target 3N) and 61.9° (target 5S) in this condition. The MRH values were significantly smaller than in condition VF (ANOVA test). However, similarly to condition VF, the more curved the trajectories, the larger the MRH [Fig. 7.3(D), magenta bars]. The linear regression analysis performed over the angled trajectories confirmed this observation [$\beta = 18.0$, $\mathrm{cor} = 0.61$, see Fig. 7.3(F2)]. Note that $\beta_{\mathrm{NF}} < \beta_{\mathrm{VF}}$ because the MRHs were smaller in NF than in VF while the curvatures were approximately the same in the two conditions due to the similarity of the paths.

Finally, we noted that these anticipatory behaviors were stereotyped across subjects and repetitions: the average Maximum RH Deviation (MRHD) across targets was 14.1° for condition VF and 15.1° for condition NF [Fig. 7.3(C)].

### Head anticipatory behavior in condition NB

Note that, since when walking backward the "natural" angle between the head direction and the heading is $-180°$ (see Methods), the anticipatory behavior in backward conditions happens when the head direction at time $t$ is reached by the *opposite* of the heading only at time $t + \Delta t$ with $\Delta t > 0$. Geometrically, this means that the head is oriented towards the *exterior* of the curve [see Fig. 7.3(A) and also Grasso et al. 1998c]. Numerically, this means RH $< -180°$ for targets where the subject had to steer towards the right (targets 4E and 5S) and RH $> -180°$ for targets where the subject had to steer towards the left (targets 5W).

Given this, we observed a clear anticipatory behavior in condition NB [Fig. 7.3(B1,B2,B3), cyan lines]. The magnitude of the anticipation was smaller than in conditions VF and NF: the average MRHs ranged between 10.8° (target 1N) and 51.9° (target 4W). The dependence of the degree of anticipation on trajectory curvature could also be observed [Fig. 7.3(D), cyan bars]. The linear regression analysis performed over the angled trajectories confirmed this observation [$\beta = 12.4$, cor $= 0.43$, see Fig. 7.3(F3)]. Here, we also noted that $\beta_{\mathrm{NB}} < \beta_{\mathrm{NF}} < \beta_{\mathrm{VF}}$ for the same reason as in the previous section.

### Head/trunk coordination for anticipation

The orientation of the head with respect to the trajectory can be achieved through the combination of trunk/heading and head/trunk rotations. Fig. 7.4(A1,A2,A3) show the Relative Trunk angle (RT) profiles (angle between the trunk direction and the heading). The anticipatory behavior could be clearly observed in the three conditions. Again, the magnitude of the anticipation was the largest in condition VF, followed by condition NF and then NB. We also noted that the magnitude of anticipation was smaller for the trunk than for the head. Indeed the average MRTs were significantly smaller than the MRHs (ANOVA test).

Fig. 7.4(B1,B2,B3) show the Head/Trunk angle (HT) profiles. Again, this angle was larger in VF than in NF than in NB. Globally, we observed indeed that MHT < MRT < MRH (ANOVA test).

Regarding the *timing* of the anticipation, we observed that the maximum of the anticipation occurred earlier for HT than for RT [Fig. 7.4(E) shows the time when RT reached its maximum and Fig. 7.4(F) shows the time when HT reached its maximum]. Thus, in the first part of the curve ($0.3 \le t \le 0.5$), head anticipation was achieved mainly by turning the head with respect to the trunk, and in the second part ($0.5 \le t \le 0.8$) head anticipation was achieved mainly by turning the trunk with respect to the heading [Fig. 7.4(C1,C2,C3)]. In this second part, the head does practically not move with respect to the trunk [HT is close to 0, see Fig. 7.4(B1,B2,B3)].

Regarding now the *distribution* of head anticipation between RT and HT, we observed graphically in Fig. 7.4(C1,C2,C3) that, overall, RT contributed more than HT. This was confirmed by comparing the average values of RT and of HT for $0.3 \le t \le 1$ : the contribution of RT to head anticipation was $\simeq 65\%$ while that of HT was $\simeq 35\%$ in all targets and conditions [Fig. 7.4(D)].

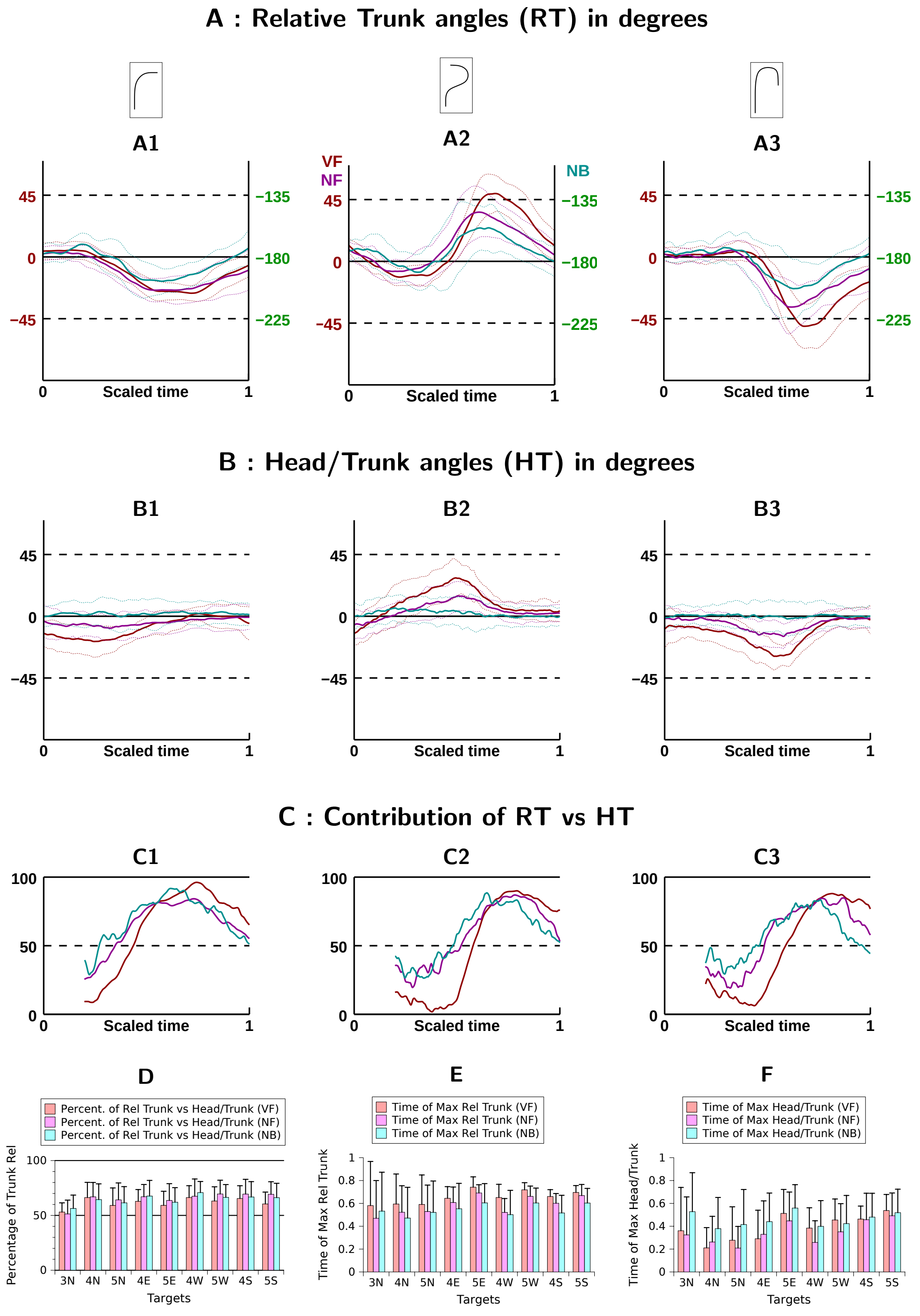

Figure 7.4: Head/Trunk coordination for anticipation in conditions VF (red), NF (magenta) and NB (cyan). (**A**) Average Relative Trunk angle (RT) profiles (plain lines) ± SD (dashed lines). A1: target 4E, A2: target 5W, A3: target 5S. (**B**) Average Head/Trunk angle (HT) profiles (plain lines) ± SD (dashed lines). (**C**) Contribution of Relative Trunk vs contribution of Head/Trunk to head anticipation in time: a value of 100% means that only RH contributes while a value of 0% means that only Head/Trunk contributes. (**D**) Contribution of Relative Trunk vs contribution of Head/Trunk to head anticipation over the whole trajectory. (**E**) Time when Maximum RT was attained, averaged across subjects and repetitions. (**F**) Time when Maximum HT was attained, averaged across subjects and repetitions.

It was remarkable that all the above observations on the head/trunk coordination (timing and distribution) were applicable for the three conditions VF, NF and NB, with only minor differences.

### 7.1.3 Discussion

Two important aspects were brought into light by our results. First, the steering behavior was found to be similar in the three conditions Visual Forward, Nonvisual Forward and Nonvisual Backward. In particular, we demonstrated here for the first time that the head anticipates the future walking direction [Grasso et al. (1998c) have already remarked this phenomenon but their results lacked statistical support]. Second, we described quatitatively and temporally the relative contributions of the head and the trunk in the anticipatory behavior. Assessing the contribution of these findings to the understanding of how humans steer is one of our current objectives.

## 7.2 Experiment 6: formation of trajectories and navigation

As mentioned in the Introduction, we mean by *navigation* a sequence of *discrete* choices, for instance: to navitage from the Arc de Triomphe to the Eiffel tower, one has the choice of going westward by Avenue Kléber or eastward by Avenue d'Iéna. Thus navigation can be viewed as a process that operates at a higher level than the production of trajectories that we have considered so far. We investigate in this section the relations between these two levels.

### 7.2.1 Methods

**Subjects and materials**

Sixteen subjects participated in this experiment. All subjects were right-handed. Each subject generated 80 trajectories (except subject C. M. who did only 48 trials), so that a total of 1248 trajectories were recorded.

The target consisted of either an "arrow" or a "point". The "arrow" was materialized by a 0.2m × 1.2m cardboard arrow placed on the ground. The "point" was materialized by a cardboard disk of radius 0.08m (Fig. 7.5).

In each trial, a subject was instructed to walk through three via-points before reaching the target (see details in Protocol). The via-points were indicated by cardboard disks of radius 0.08m.

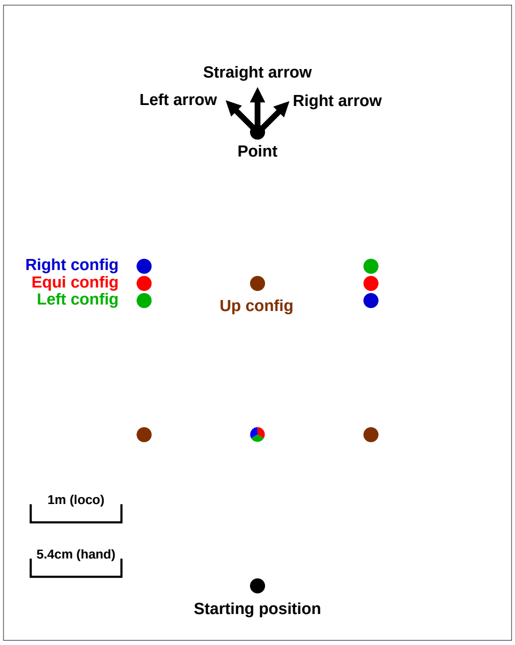

Figure 7.5: Targets and via-points configurations.

Two markers were placed on the subject's left and right shoulders. Their positions were recorded with the infrared camera system described in the General Methodology (chapter 4).

### Protocol

The subject had to start from the starting position $(0, 0)$ and walk through three spatial via-points before reaching the target. The order for visiting the via-points was not imposed.

Four targets were considered: the "left arrow" (LA), the "right arrow" (RA), the "straight arrow" (SA) and the "point" (PT). The point and the arrows' shafts were fixed at position $(0, 5\text{m})$. The straight arrow was aligned with the Y-axis, while the left and right arrows were rotated by respectively $+45°$ and $-45°$ with respect to the Y-axis (Fig. 7.5).

When the target was an arrow, the subject had to enter the arrow by the shaft and stop above the arrow head, as in Experiments 2, 3, 4 and 5 reported in the previous chapters. When the target was the point, the subject had to stop above the point.

As mentioned above, the subjects had to walk through three via-points before reaching the target. We considered four different arrangements of these via-points, referred to as the EQUI, LEFT, RIGHT and UP configurations.

In the EQUI configuration, a proximal, axial via-point was placed at $(0, 1.66\text{m})$, while two distal, off-axis via-points were placed at $(-1.25\text{m}, 3.33\text{m})$ and symmetrically at $(+1.25\text{m}, 3.33\text{m})$.

The LEFT and RIGHT configurations share the proximal via-point with the EQUI configuration, but the Y-coordinates of the distal via-points were slightly modified to introduce some asymmetry. In the LEFT configuration, the *left* via-point was moved *closer* to the X-axis, at position $(-1.25\text{m}, 3.33\text{m} - \delta)$ where $\delta = 0.1\text{m}$. The *right* via-point was, on the other hand, moved *further* from the X-axis, at position $(-1.25\text{m}, 3.33\text{m} + \delta)$. In the RIGHT configuration, the *right* via-point was placed *closer* to the X-axis, at position $(-1.25\text{m}, 3.33\text{m} - \delta)$, while the *left* via-point was placed *further* from the X-axis, at position $(+1.25\text{m}, 3.33\text{m} + \delta)$.

Finally, the UP configuration was the image of the EQUI configuration by the reflection of axis $\Delta$ where $\Delta$ is parallel to the X-axis and passes through the point $(0, 2.5\text{m})$.

Sixteen conditions were obtained by pairing each of the four targets with each of the four configurations. Each condition was tested three times, resulting in 48 trials. These trials were randomized in order to reduce learning effects.

After these 48 trials had been completed, we asked the subject to walk the 16 conditions again, but the order for visiting the via-points was now imposed. Indeed, while there exist up to six possible orders, two particular ones were considered as "most natural" in the EQUI, LEFT and RIGHT configurations. The first order, termed "left-first", consisted of the following sequence: first the proximal via-point, then the left distal via-point and finally the right distal via-point. Similarly, the second one, termed "right-first", consisted of the sequence: proximal, right distal, left distal. Thus, in this second session of the experiment, the subject had to make, for each configuration, one trial following the "left-first" and one following the "right-first" order, resulting in 32 trials. These trials were also randomized.

The first session (of 48 trials), in which the via-points orders were not imposed, was termed "free", while the second session (of 32 trials) was termed "constrained".

### 7.2.2 Results

In the previous chapters, we investigated how subjects chose a trajectory in terms of its geometry and kinematics in order to reach a distant target. This can be considered as a *continuous* choice, since the trajectory in question was chosen among a continuum of possible trajectories joining the starting position and the target. Here, in addition, the subjects had also to make a *discrete* navigational choice, in terms of the sequence in which they visit the via-points.

As mentioned above, for conditions EQUI, LEFT and RIGHT, two particular orders can be considered as the most natural: the “left-first” and “right-first” orders. Fig. 7.6 shows sample trajectories produced by one subject.

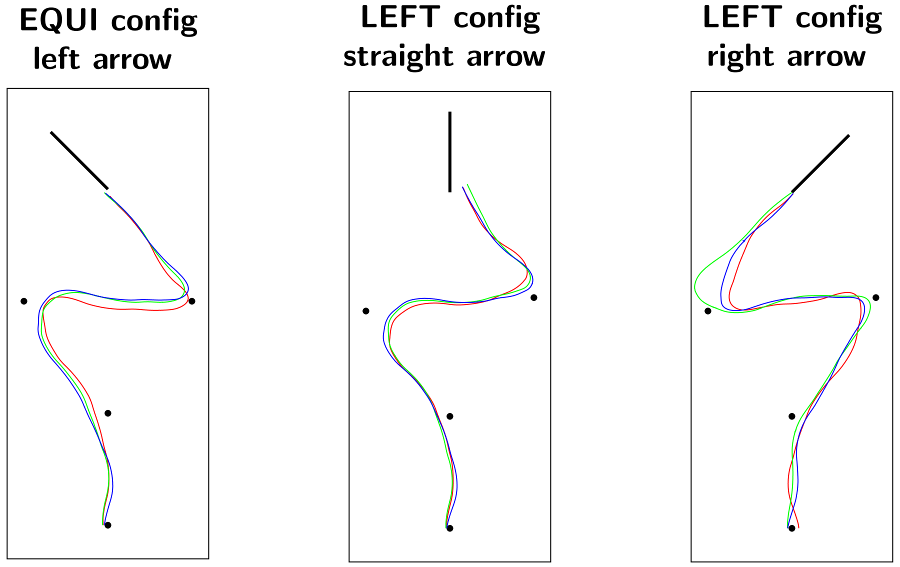

Figure 7.6: Trajectories produced by one typical subject.

In the “EQUI config – left arrow” trials, where the via-points were in a symmetrical disposition, the subject chose to go first to the left via-point in order to reach the arrow after the last via-point with a “natural” walking direction. We say here that his choice was motivated by the arrow’s orientation.

In the “LEFT config – straight arrow” trials, since now the arrow was symmetrical, the choice of the subject was determined by the via-points configuration. The choice made by the subject was indeed associated with a shorter trajectory length (comparison with the constrained trials).

In the “LEFT config – right arrow” trials, the via-points configuration and the arrow yielded contradictory indications. We observed that in this case, the choice of the subject was determined by the arrow: he indeed chose a longer route (comparison with the constrained trials) in order to arrive at the arrow with a natural “walking” diretion.

Fig. 7.7 shows the statistics computed across all subjects and repetitions. Our previous remarks concerning one particular subject were confirmed on a larger scale.

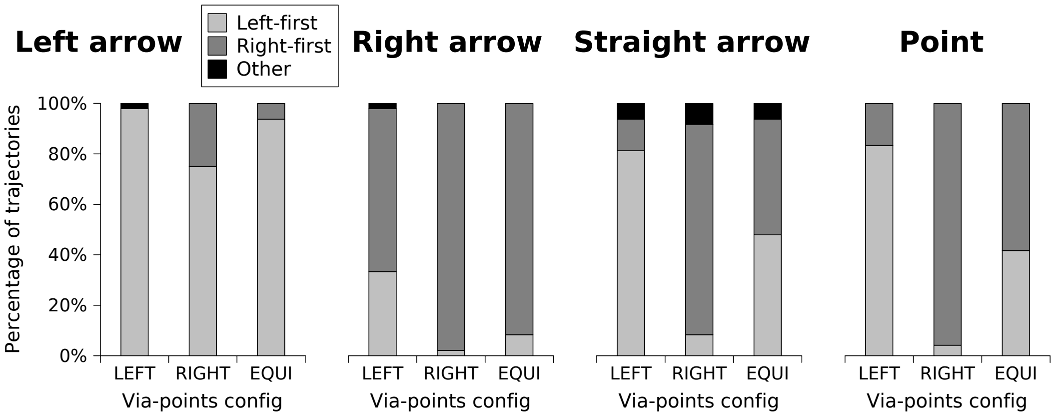

Figure 7.7: Categorization of the trajectories.

### 7.2.3 Discussion

The prelimary results showed that minimizing trajectory length was not the only objective underlying nagivational choices. Indeed, when this objective was contradictory with another one (associated here with the final walking direction), the subjects were often urged to take longer routes. Discerning the precise criteria (trajectory length, smoothness, amount of body turns, etc.), based on the data provided by this Experiment 6, is one of our current projects.

## 7.3 Experiment 7: a direct test for affine invariance in hand movements

As mentioned in our review (see section 1.1.3), geometry-based theories have been recently proposed to explain some invariants observed in human movements. In particular, Bennequin et al. (2009) argued that a mixture of several geometries (euclidian, equi-affine and affine) may govern the production of locomotor and hand trajectories.

In the case of hand movements, the authors assumed *a priori* that the hand velocity $v$ can be decomposed as

$$v = v_0^{\beta_0} v_1^{\beta_1} v_2^{\beta_2} \tag{7.9}$$

where $v_0$, $v_1$ and $v_2$ denote respectively the expected euclidian velocity under constant affine, equi-affine and euclidian velocities, and $\beta_0$, $\beta_1$ and $\beta_2$ are three weighting parameters. They then looked for the triplet ($\beta_0$,$\beta_1$,$\beta_2$) that yields the best fit to the experimental data. Observing that $\beta_2$ was smaller than $\beta_0$ and $\beta_1$ in the optimal triplet, the authors then concluded that equi-affine and affine geometries are dominant in the planning and control of hand trajectories.

However, such a reasoning may constitute a case of "circular theorizing" [see Engelbrecht (2001), we note however that Bennequin et al. (2009) did provide other direct tests supporting their theory]. In order to address this issue, we propose in this section a *direct* test for affine invariance, which does not assume the *a priori* decomposition of Eq. (7.9). More precisely, we test whether the prediction that "*when curve segments are similar under transformations belonging to the [affine] group, the parameterizations of these segments will also be similar*" (Bennequin et al., 2009) holds true.

### 7.3.1 Methods

#### Subjects, materials, protocol

Four subjects, one male and three females, participated in this experiment. All subjects were right-handed.

A white A3 (29.7cm × 42.0cm) sheet of paper was placed horizontally on a table. In each trial, a subject sat in front of the table and had to make scribblings on the sheet's surface with his right index (same protocole as shown in Fig. 2 on page 157, except that the computer screen was replaced by a sheet of paper). A marker was attached to the tip of his index. The position of this marker was recorded with the infrared camera system described in the General Methodology (chapter 4). The subject was asked to make continuous movements with his index while respecting the following three constraints: stay within the sheet, fill the sheet equally, avoid abrupt movements and cusps (see a typical scribbling in Fig. 7.8).

Each trial consisted of 30 seconds of scribbling. The subject made three trials (separated by $\sim$ 1 minute) at his preferred speed. He was then asked to make three other trials, at a faster speed. A total of 4 subjects × 6 trials = 24 trajectories were thus recorded in this experiment.

#### Analysis

**Hausdorff distance and $\mathcal{L}_2$ distance** We consider two distance measures in this study: the Hausdorff distance and the $\mathcal{L}_2$ distance. The Hausdorff distance between two *ensembles* $X$ and $Y$ is given by

$$d_{\mathrm{H}}(X,Y) = \max\{\sup_{x\in X}\inf_{y\in Y}\|x-y\|,\ \sup_{y\in Y}\inf_{x\in X}\|x-y\|\}. \tag{7.10}$$

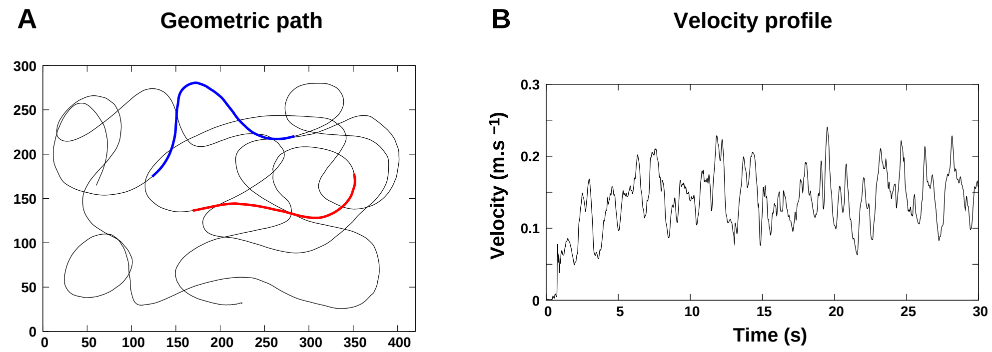

Figure 7.8: A typical normal speed trial. (**A**) The geometric path of the trajectory. Two random sub-trajectories are highlighted in blue and red. (**B**) The velocity profile of the entire trajectory.

When applied to two trajectories, the Hausdorff distance thus quantifies the proximity of the two *geometric paths*, irrespective of the parameterizations (or equivalently, of the velocity profiles).

The $\mathcal{L}_2$ distance between two trajectories $\Gamma_1$ and $\Gamma_2$ is given by

$$d_{\mathcal{L}_2}(\Gamma_1, \Gamma_2) = \sqrt{\int_0^1 \|\Gamma_1(t) - \Gamma_2(t)\|^2 \mathrm{d}t}. \tag{7.11}$$

This distance thus takes into account the geometric paths but also the parameterizations of the trajectories.

**Sub-trajectories** From each recorded trajectory, we extracted 40 random sub-trajectories. The duration of each sub-trajectory was selected uniformly randomly in the interval $(0.4\text{s}, 1\text{s})$. The starting time of each sub-trajectory was also selected randomly from a uniform distribution [see Fig. 7.8(A), which depicts two random sub-trajectories extracted from a given trajectory].

Given a sub-trajectory $\Gamma_i = (\mathbf{p}_i(t))_{t\in[0,T_i]}$ indexed by $i$ , we note $\Lambda_i$ its geometric path, $(\mathbf{v}_i(t))_{t\in[0,T_i]}$ its time-varying velocity vector and $L_i$ its length.

Out of the 780 possible pairs of sub-trajectories of each trial, we extracted 450 random pairs. Thus, the database for each speed condition consisted of $5400 = 450 \times 12$ pairs of sub-trajectories.

**Optimal affine transformation** Given two sub-trajectories $\Gamma_1$ and $\Gamma_2$, we looked first for an affine transformation $f_a$ which minimizes the Hausdorff distance between the geometric path of $f_a(\Gamma_1)$ and that of $\Gamma_2$ [see Fig. 7.9(A) for an example]. This was done by numerically optimizing the six coefficients that define any affine transformation (four corresponding to the linear map and two corresponding to the translation).

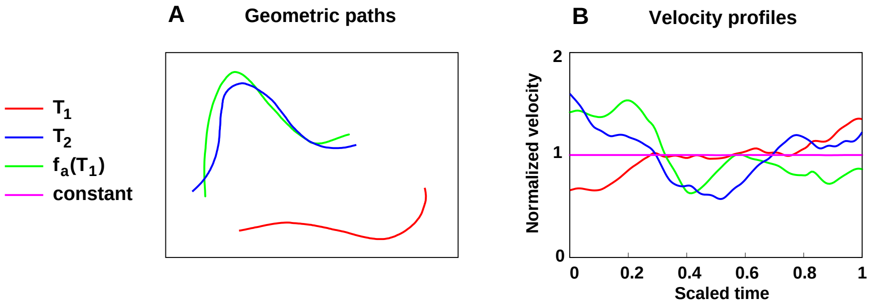

Figure 7.9: An optimal affine transformation between two sub-trajectories. (**A**) Geometric paths of the sub-trajectories $\Gamma_1$ (red), $\Gamma_2$ (blue) and of the image of $\Gamma_1$ by the optimal affine transformation $[f_a(\Gamma_1)$, green$]$. (**B**) Normalized velocity profiles of $\Gamma_1$ (red), $\Gamma_2$ (blue) and $f_a(\Gamma_1)$ (green). The constant normalized velocity profile is depicted in magenta.

**Affine, euclidian and constant parameterizations** Since $f_a$ is optimal with respect to the Hausdorff distance, we know that the geometric path $\Lambda$ of $f_a(\Gamma_1)$ is "close" to $\Lambda_2$. To compare the *temporal* structures, we needed to endow $\Lambda$ with a parameterization. We considered three possible parameterizations of $\Lambda$, which could be also formulated in the form of velocity profiles.

The first velocity profile, denoted $v_a$, is simply that of $f_a(\Gamma_1)$, i.e.

$$\forall t \in [0, T_1] \quad v_a(t) = \|\mathbf{v}_a(t)\| = \left\| \frac{\mathrm{d}f_a(\mathbf{p}_1)}{\mathrm{d}t} \right\| = \|\mathbf{J}_{f_a}\mathbf{v}_1(t)\| = \|\mathbf{A}_a\mathbf{v}_1(t)\|, \tag{7.12}$$

where $\mathbf{J}_f$ denotes the Jacobian matrix of a mapping $f$ and $\mathbf{A}_a$ denotes the linear mapping associated with the affine transformation $f_a$. If hand trajectories are perfectly *affine-invariant* and that $\Lambda$ perfectly matches $\Lambda_2$, then we will have $T_1 = T_2$ and $v_a = v_2$ for all $t \in [0, T_1]$. For this reason, we call $v_a$ the *affine* velocity profile of $\Lambda$.

The second velocity profile, denoted $v_e$, is obtained by "transporting" the velocity profile of $\Gamma_1$ onto $\Lambda$, i.e.

$$\forall t \in [0, T_1] \quad v_e(t) = \frac{L}{L_1} v_1(t), \tag{7.13}$$

where $L$ is the length of $\Lambda$ (the rescaling was done to ensure that we have $\int_0^{T_1} v_e(t)\mathrm{d}t = L$). If hand trajectories are perfectly *euclidian-invariant* and that $\Lambda$ perfectly matches $\Lambda_2$, then we will have $T_1 = \frac{L_1}{L_2}T_2$ and $v_e = \frac{L_2}{L_1}v_2$ for all $t \in [0, T_1]$. For this reason, we call $v_e$ the *euclidian* velocity profile of $\Lambda$.

Finally, we consider the *constant* velocity profile $v_c$, which is defined by

$$\forall t \in [0, T_1] \quad v_c(t) = \frac{L}{T_1}. \tag{7.14}$$

To compare velocity profiles defined for different durations, we needed to normalize them as described in section 4.2.3 of the General Methodology. After normalization, we could compute the $\mathcal{L}_2$ distance between two normalized profiles by

$$d_{\mathcal{L}_2}(v_1, v_2) = \sqrt{\int_0^1 (v_1(t) - v_2(t))^2 \mathrm{d}t}. \tag{7.15}$$

Note that this distance is different from the Average normalized Velocity profile Separation (AnVS defined in section 4.2.3), which corresponds in fact to the $\mathcal{L}_1$ distance.

### 7.3.2 Results

#### Testing affine invariance

We first tested directly the prediction mentioned in the beginning of this section: "*when curve segments are similar under transformations belonging to the [affine] group, the parameterizations of these segments will also be similar*". More precisely, we compared the $\mathcal{L}_2$ distance between the normalized velocity profile of $\Gamma_2$ and respectively the normalized affine, euclidian and constant velocity profiles defined previously.

In Fig. 7.9(B), one can see qualitatively that the affine velocity profile (green line) was more similar to the velocity profile of $\Gamma_2$ (blue line) than the initial velocity profile of $\Gamma_1$ (red line). The quantitative results are plotted in Fig. 7.10. One can observe a clear positive correlation between $d_{\mathrm{H}}(\Lambda, \Lambda_2)$ and $d_{\mathcal{L}_2}(v_a, v_2)$. This positive correlation was not trivial since, by contrast, there was practically no correlation in the cases of $v_c$ and $v_e$.

#### Comparing different parameterizations

However, il could be argued that the positive correlation observed previously resulted solely from the fact that $v_a$ yielded bad results for large Hausdorff distances. We thus concentrate here on pairs of sub-trajectories with low Hausdorff distances (that is, whose paths were affinely similar). In addition,

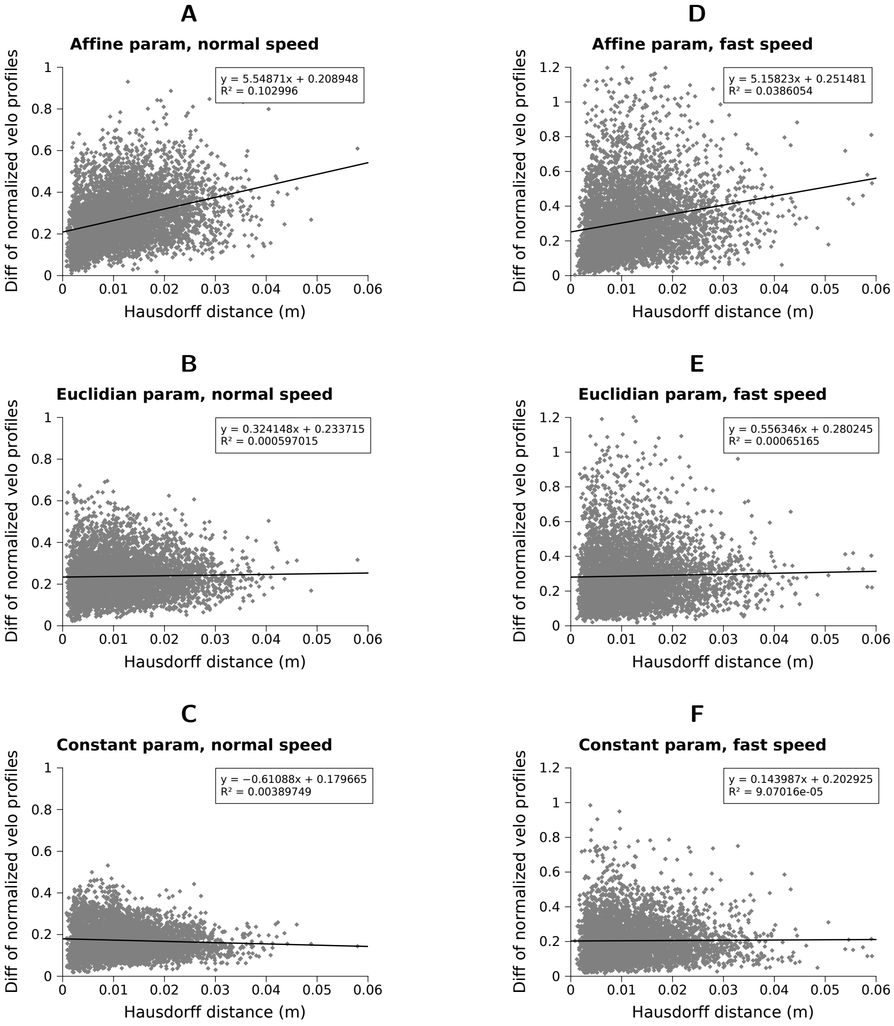

Figure 7.10: Correlations between spatial similarity and parameterization similarity. Each pair of sub-trajectories was represented by a dot whose X-coordinate was the Hausdorff distance between the two trajectories of the pair and whose Y-coordinate was the distance between the two velocity profiles. (**A,B,C**) affine, euclidian and constant velocity profiles, normal speed. (**D,E,F**) affine, euclidian and constant velocity profiles, fast speed.

| Hausdorff dist (%) | Normal Speed | Fast Speed |
|---|---|---|
| $1.00 \leq d < 1.25$ | 44 | 8 |
| $1.25 \leq d < 1.50$ | 78 | 22 |
| $1.50 \leq d < 1.75$ | 143 | 57 |
| $1.75 \leq d < 2.00$ | 193 | 78 |
| $2.00 \leq d < 2.25$ | 174 | 135 |
| $2.25 \leq d < 2.50$ | 160 | 152 |
| $2.50 \leq d < 2.75$ | 125 | 174 |
| $2.75 \leq d < 3.00$ | 112 | 209 |
| $3.00 \leq d < 3.25$ | 143 | 230 |
| $3.25 \leq d < 3.50$ | 143 | 270 |
| $3.50 \leq d < 3.75$ | 172 | 226 |
| $3.75 \leq d < 4.00$ | 152 | 231 |
| $4.00 \leq d < 4.25$ | 158 | 222 |
| $4.25 \leq d < 4.50$ | 157 | 186 |
| $4.50 \leq d < 4.75$ | 172 | 206 |
| $4.75 \leq d < 5.00$ | 172 | 201 |

Table 7.1: Number of pairs in each bin in the two speed conditions.

to avoid artifacts caused by the normalization of the velocities, we examined directly the distance between trajectories, that is, the $\mathcal{L}_2$ distance between $\Gamma_1$ and $\Lambda$, where the latter was endowed respectively with $v_a$, $v_e$ and $v_c$.

We first categorized the pairs of sub-trajectories into bins according to their Hausdorff distances expressed in percentage of the length of $\Gamma_2$. The size of each bin is given in Table 7.1. For each bin, we computed the average and the SD of the $\mathcal{L}_2$ distances across the pairs in the bin.

The results are plotted in Fig. 7.11. One can clearly see that, in both speed conditions, the affine parameterization yielded better results than the euclidian and the constant ones for low Hausdorff distances (up to $d_{\mathrm{H}} \simeq 2.5\%$ of $L_2$ in the normal speed condition and up to $d_{\mathrm{H}} \simeq 2\%$ of $L_2$).

### 7.3.3 Discussion

We demonstrated that there exists a positive correlation between (i) the affine similarity the geometric paths of two sub-trajectories and (ii) the similarity of their parameterizations. By contrast, when the parameterization of one of the two sub-trajectories was defined according to euclidian geometry or replaced by a constant parameterization then this correlation disappeared. These observations constitute direct evidence for the existence of affine invariance in movement timing.

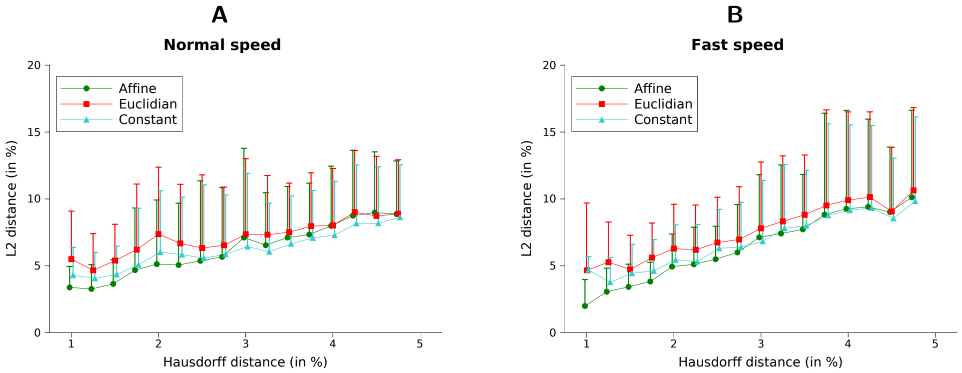

Figure 7.11: Comparison of different parameterizations. Average and SD of the $\mathcal{L}_2$ distance between $\Gamma_2$ and $\Lambda$ endowed with respectively the affine (green), euclidian (red) and constant (cyan) velocity profiles. (**A**) normal speed. (**B**) fast speed.

The existence of affine invariance in movement timing was further supported when we showed that, for sub-trajectories whose geometric paths were affinely similar, the velocity profile of one sub-trajectory was similar to the affine "image" of the profile of the other sub-trajectory. This similarity was stronger than in the case of the euclidian "image" or in the case of a constant velocity profile.

Since affine and euclidian invariance cannot make any valid prediction when the sub-trajectories are largely affinely dissimilar, the constant velocity profiles, which yield "safe" parameterizations, produced better comparison results for large Hausdorff distances.

Because of time constraints, we could not consider equi-affine parameterizations at the current stage of the analysis. This will be done in the very near future.

Finally, we note that this experiment can be easily adapted to the case of "locomotor scribblings". This will provide a direct test for the existence of affine geometry in the planning and control of locomotor trajectories. Following Bennequin et al. (2009), we make the prediction that euclidian geometry is more present in locomotion than in hand movements.

# Part III

# Modeling study

# Chapter 8

# Deterministic models of trajectories formation

## 8.1 Overview

The previous chapters have equipped us with some important knowledge about the planning and control of locomotion. First, whole-body trajectories in goal-oriented tasks are stereotyped, implying a trajectory-level control of locomotion (see section 5.2). Second, the average trajectories produced in different sensory and motor conditions are highly similar, indicating that the formation of these trajectories is, to some extent, independent of their sensorimotor implementation (see section 5.3). Third, a detailed analysis of variability profiles suggested that the formation of trajectories in visual and nonvisual locomotion is supported by similar open-loop and online feedback processes (see chapter 6).

The purpose of this and the following chapter is to provide a theoretical framework that can account for the above findings. Taking once again inspiration from the computational motor control literature (see our review in section 1.2), we make the hypothesis that the formation of locomotor trajectories is an *optimized* process. In particular, from the observation that locomotor trajectories are generally smooth, we investigate here whether maximum smoothness models can simulate experimentally recorded trajectories.

The comparative study of the Minimum Squared Derivative models was conducted by Q.-C. Pham, H. Hicheur, G. Arechavaleta, J.-P. Laumond and A. Berthoz, and published in Pham et al. (2007). The modified minimum jerk model was designed by Q.-C. Pham and H. Hicheur and presented in Pham and Hicheur (2009). For more details, the reader is referred to the original articles.

## 8.2 Comparison of Minimum Squared Derivative (MSD) models

Qualitatively, a trajectory is smooth if there are no abrupt variations in time. This implies that higher-order time derivatives of the position have low absolute values. While earlier studies (Hogan, 1984; Flash and Hogan, 1985) mostly focused on the squared jerk cost, other costs such as the squared acceleration or the squared snap (snap is the time derivative of jerk) can also be considered. More generally, the nth-order MSD cost is given by:

$$\int_0^1 \left( \left( \frac{\mathrm{d}^n x}{\mathrm{d}t^n} \right)^2 + \left( \frac{\mathrm{d}^n y}{\mathrm{d}t^n} \right)^2 \right) \mathrm{d}t \tag{8.1}$$

The case $n = 1$ corresponds to the minimum velocity cost, $n = 2$ to minimum acceleration, $n = 3$ to minimum jerk and $n = 4$ to minimum snap.

Richardson and Flash (2002) conducted a comparative study where they examined the abilities of MSD models of different orders to simulate hand trajectories. In particular, they found that third- and fourth-order MSD models (minimum jerk and minimum snap) usually performed better than those of other orders. In addition to quantitative fit, the trajectories simulated by the third- and fourth-order MSD models displayed typical qualitative characteristics of human hand trajectories: smoothness of the trajectory, straight hand paths and bell-shaped velocity profiles in reaching tasks (see section 1.1), inverse relationship between velocity and curvature in drawing tasks (the so-called “one-third power law”, see our review in section 1.1.2), etc.

At the trajectory level, human locomotion seems to share some of these qualitative features. Indeed, one can observe that human locomotor trajectories are generally smooth. Straight paths are also generated for reaching a spatial goal in an environment free of obstacles, provided that the initial body orientation is compatible with such a path. Finally, humans tend to decelerate in the curved parts and accelerate in the straighter parts of a trajectory. This last observation was confirmed by a recent comparative study (Hicheur et al., 2005c) where the authors quantitatively examined the relationship between velocity and curvature in locomotor tasks where subjects had to walk along complex shapes. While the one-third exponent was not observed for these shapes, the inverse variations of velocity and curvature could be reproduced by multiple power laws whose exponents depended on the shapes (see our review in section 3.2). This variability of the exponents suggested that the power laws relating the velocity to curvature in human locomotion could be by-products of more general principles, for instance the optimality principles just mentioned.

Taken together, these observations raise the possibility that MSD principles underlie the generation of human locomotion trajectories. If verified, this would suggest that the same set of principles account for different types of movements (hand movements and locomotor movements in our case) and would provide interesting theoretical insights into the understanding of the functional organization of the motor system in general. In order to test this hypothesis, we compared the trajectories recorded in Experiment 1 (see section 5.2) with the optimal trajectories simulated by four MSD models.

### 8.2.1 Methods

#### Description of the model

As mentioned above, MSD principles have proved to be particularly relevant for modeling hand movements. In order to test how such smoothness-based principles can simulate locomotor trajectories, we constructed mathematically MSD trajectories as follows.

For a given target, we first extracted a set of 12 parameters (initial and final positions, velocities and accelerations for the $x$ and $y$ components) from the experimental data (Experiment 1, section 5.2)

$$x_0 = \frac{1}{N}\sum_{i=1}^{N} x_i(0), \quad v_0^x = \frac{1}{N}\sum_{i=1}^{N} \dot{x}_i(0), \quad a_0^x = \frac{1}{N}\sum_{i=1}^{N} \ddot{x}_i(0) \tag{8.2}$$

and similarly for $x_1$, $v_1^x$, $a_1^x$, $y_0$, $v_0^y$, $a_0^y$, $y_1$, $v_1^y$, $a_1^y$ ($N$ corresponds to the number of trajectories recorded for this target).

Some of these 12 parameters were task-related and thus were not related to any spontaneous strategy. Indeed, according to the experimental protocol, the initial and final positions ($x_0$, $y_0$, $x_1$, $y_1$) corresponded, respectively, to the origin of the laboratory's reference frame and to the centre of the door. Similarly, the initial walking direction was imposed to be parallel to the Y-axis while the final walking direction was constrained by the orientation of the door. As subjects were carefully monitored during the session, the extracted values of these parameters were very close to the imposed ones: over the 709 trajectories, the average distance (± SD) between the actual and the imposed initial positions was 3.0 ± 2.5cm, the average distance between the actual and the imposed final positions was 3.2 ± 2.2cm, the average absolute difference between the actual and the imposed initial orientations was 9.6 ± 7.9° and the average absolute difference between the actual and the imposed final orientations was 5.9 ± 4.4°. Thus, our choice to extract these values from the data rather than to compute them a priori from the task was only motivated by convenience.

In contrast, initial and final accelerations ($a_0^x$, $a_0^y$, $a_1^x$, $a_1^y$) and initial and final speeds (the norms of the velocity vectors) were not imposed by the task and thus contained information about the subjects' movement strategies or their personal preferences. Considering these parameters as free parameters in the optimization procedure yielded close-to-zero values, which was not consistent with the observations. On the other hand, estimating them by an independent method would be complicated and not relevant with respect to our objectives (see Discussion for more details on the issue of putting experimental values into the models).

On the computational level, as our objective consisted of simulating the whole trajectory kinematics (path and velocity profile), these values actually contained relatively little information. In contrast, the original two-thirds power law (Lacquaniti et al., 1983), the modified two-thirds power law (Viviani and Schneider, 1991) or the constrained minimum jerk model (Todorov and Jordan, 1998) aimed at simulating only the velocity profile. Moreover, these models required as inputs the entire recorded path in conjunction with either the end-point velocities and accelerations (for the constrained minimum jerk model) or the entire velocity profile (for the modified two-thirds power law). However, it should be recognized that some of the trajectories studied in the references cited above were more complex than ours.

It should also be noted that the movement duration was implicitly extracted in the time-rescaling procedure (see also General Methodology, chapter 4).

Next, we derived the planar trajectory $(x(t), y(t))$ that minimizes the cost given in equation 2 and verifies the following 12 boundary conditions

$$\begin{array}{l} x(0)=x_0,\ x(1)=x_1,\ \dot{x}(0)=v_0^x,\ \dot{x}(1)=v_1^x,\ \ddot{x}(0)=a_0^x,\ \ddot{x}(1)=a_1^x \\ y(0)=y_0,\ y(1)=y_1,\ \dot{y}(0)=v_0^y,\ \dot{y}(1)=v_1^y,\ \ddot{y}(0)=a_0^y,\ \ddot{y}(1)=a_1^y \end{array} \tag{8.3}$$

In usual MSD approaches, the number of boundary conditions depends on the order of the derivative that is minimized. For instance, the minimum velocity, minimum acceleration, minimum jerk and minimum snap models require, respectively, 4, 8, 12 and 16 boundary conditions. However, these choices are arbitrary and are not motivated by any theoretical consideration (see Harris, 2004; Harris and Harwood, 2005, for a detailed discussion of the issue of boundary conditions in models of biological movements). They introduce furthermore a bias in favour of the higher-order MSDs. In our comparative approach, we chose to use the *same* set of boundary conditions given by Eq. (8.3) in all four models in order not to favour any particular model. The mathematical details for the derivation of the MSD trajectories are given in Box 1.

**Box 1 (Computation of MSD trajectories)**

As the MSD cost functional [Eq. (8.1)] and the boundary conditions [Eq. (8.3)] are uncoupled in $x$ and in $y$, it is sufficient to find optimal functions separately for $x$ and $y$ (Flash and Hogan, 1985). The problem thus consists of finding a function $x$ defined on [0,1] that minimizes the functional

$$\int_0^1 \left(\frac{\mathrm{d}^n x}{\mathrm{d}t^n}\right)^2 \mathrm{d}t \tag{8.4}$$

and verifies the boundary conditions

$$x(0) = x_0,\ x(1) = x_1,\ \dot{x}(0) = v_0^x,\ \dot{x}(1) = v_1^x,\ \ddot{x}(0) = a_0^x,\ \ddot{x}(1) = a_1^x \tag{8.5}$$

**Minimum jerk trajectories** For MSD of orders $n \geq 3$, it turns out that the optimum function $x$ is a polynomial of degree $2n - 1$ in the variable $t$ (see Flash and Hogan, 1985, for a proof of this result). For instance, when $n = 3$ (minimum jerk), $x$ is a 5th-degree polynomial:

$$x(t) = a_5 t^5 + a_4 t^4 + a_3 t^4 + a_2 t^2 + a_1 t + a_0 \tag{8.6}$$

The six boundary conditions then yield a 6th-order linear system that in turn uniquely determines the six coefficients $a_0,\dots,a_5$.

**Minimum snap trajectories** For $n = 4$, $x$ is a $7^{\text{th}}$-degree polynomial, which corresponds to eight unknown coefficients, say $a_0,\dots,a_7$. Using the six boundary conditions, we can express $a_0,\dots,a_5$ as affine functions of $a_6$ and $a_7$. Replacing next $a_4$ and $a_5$ by their expressions in terms of $a_6$ and $a_7$ in the cost functional

$$\int_0^1 \left(\frac{\mathrm{d}^4 x}{\mathrm{d}t^4}\right)^2 \mathrm{d}t = \int_0^1 (840 a_7 t^3 + 360 a_6 t^2 + 120 a_5 t + 24 a_4)^2 \mathrm{d}t \tag{8.7}$$

yields a second-order polynomial in the variables $a_6$ and $a_7$. Standard minimization techniques of multivariate polynomials then allow us to obtain algebraic expressions of $a_6$, $a_7$ and then $a_0,\dots,a_5$.

**Minimum velocity and minimum acceleration trajectories in restricted solutions spaces** If $n \leq 2$, the problem is ill-posed (Harris and Harwood, 2005) in the sense that no optimal trajectory exists. However, if we restrict the solution space to the set of polynomials of degree less than or equal to $d$ (where $d$ is an integer $\geq 6$), then we can find a unique optimal trajectory $x_d$. As $d$ grows, the cost associated with $x_d$ decreases (because the solution space is larger). However, when $d \to \infty$, $x_d$ converges to a trajectory that no longer verifies the boundary conditions.

As minimum jerk and minimum snap principles yield polynomials of degrees less than or equal to 7, we set $d = 7$ in order to make unbiased comparisons of the four models.

In the case $n = 2$ (minimum acceleration), the problem thus consists of finding the optimal function $x$ in the form

$$x(t) = a_7t^7 + a_6t^6 + a_5t^5 + a_4t^4 + a_3t^4 + a_2t^2 + a_1t + a_0 \tag{8.8}$$

that verifies the boundary conditions of Eq. (8.5) and minimizes the cost

$$\int_0^1 \left(\frac{\mathrm{d}^2x}{\mathrm{d}t^2}\right)^2 \mathrm{d}t = \int_0^1 (42a_7t^5 + 30a_6t^4 + 20a_5t^3 + 12a_4t^2 + 6a_3t + 2a_2)^2 \mathrm{d}t \tag{8.9}$$

The same procedure as in the minimum snap case can be applied to find the optimal coefficients $a_0$,...,$a_7$.

The case $n = 1$ (minimum velocity) can be treated similarly.

### Analysis of the models' performances

To evaluate the models' performance, we compared the trajectories simulated by the models with actual trajectories recorded in Experiment 1 (see section 5.2). As in section 5.2, the trajectories were classified into four categories according to their curvature: quasi-straight trajectories (ST), trajectories of low (LC), medium (MC) and high (HC) curvature.

The comparisons were quantified by the following measures: Average and Maximal Trajectory Error (ATE and MTE), Average and Maximal normalized Velocity Error (AnVE and MnVE). Each measure was indexed by the subscripts "v" (velocity), "a" (acceleration), "j" (jerk) and "s" (snap) indicating the MSD model corresponding to that measure.

**Trajectory error** At the level of the trajectory, we computed, for each target, the instantaneous Trajectory Error ($\mathrm{TE_M}$) of the simulated trajectory $(x_\mathrm{M}(t), y_\mathrm{M}(t))$ (where M is the model in question) with respect to the average trajectory $(x_\mathrm{av}(t), y_\mathrm{av}(t))$ as

$$\mathrm{TE_M}(t) = \sqrt{(x_\mathrm{M}(t) - x_\mathrm{av}(t))^2 + (y_\mathrm{M}(t) - y_\mathrm{av}(t))^2} \tag{8.10}$$

We then defined the Average and Maximal Trajectory Errors ($\mathrm{ATE_M}$ and $\mathrm{MTE_M}$) over the whole trajectory as

$$\mathrm{ATE_M} = \int_0^1 \mathrm{TE_M}(t)\mathrm{d}t \tag{8.11}$$

$$\mathrm{MTE_M} = \max_{0\leq t\leq 1} \mathrm{TE_M}(t) \tag{8.12}$$

Note that $\mathrm{ATE_M}$ and $\mathrm{MTE_M}$ take into account the instantaneous errors at all time instants. They are therefore sensitive to dissimilarities at both the geometric path level and at the velocity profile level.

**Velocity profile error** If the actual and simulated trajectories have similar geometric paths, it makes sense to compare their velocity profiles. We computed the normalized velocity profile of the simulated trajectory $(x_\mathrm{M}(t), y_\mathrm{M}(t))$ as

$$v_\mathrm{M}(t) = \frac{\sqrt{\dot{x}_\mathrm{M}(t)^2 + \dot{y}_\mathrm{M}(t)^2}}{\int_0^1 \sqrt{\dot{x}_\mathrm{M}(t)^2 + \dot{y}_\mathrm{M}(t)^2}\mathrm{d}t} \tag{8.13}$$

The Average and Maximal normalized Velocity Errors ($\mathrm{AnVE_M}$ and $\mathrm{MnVE_M}$) over the whole trajectory could then be defined as

$$\mathrm{AnVE_M} = \int_0^1 |v_\mathrm{M}(t) - v_\mathrm{av}(t)|\mathrm{d}t \tag{8.14}$$

$$\mathrm{MnVE_M} = \max_{0\leq t\leq 1} |v_\mathrm{M}(t) - v_\mathrm{av}(t)| \tag{8.15}$$

## 8.2.2 Results

### Minimum velocity model

The simulations of the minimum velocity model for four representative targets (one target per category) are shown in Fig. 8.1. The geometric paths simulated by this model tended to be the straightest possible. Thus, the simulations were accurate for the targets of category ST. By contrast, for the targets that required some amount of curvature (HC, MC and LC), the simulated paths were strongly bent towards the interior of the curve, resulting in large inaccuracies around the middle of the trajectories.

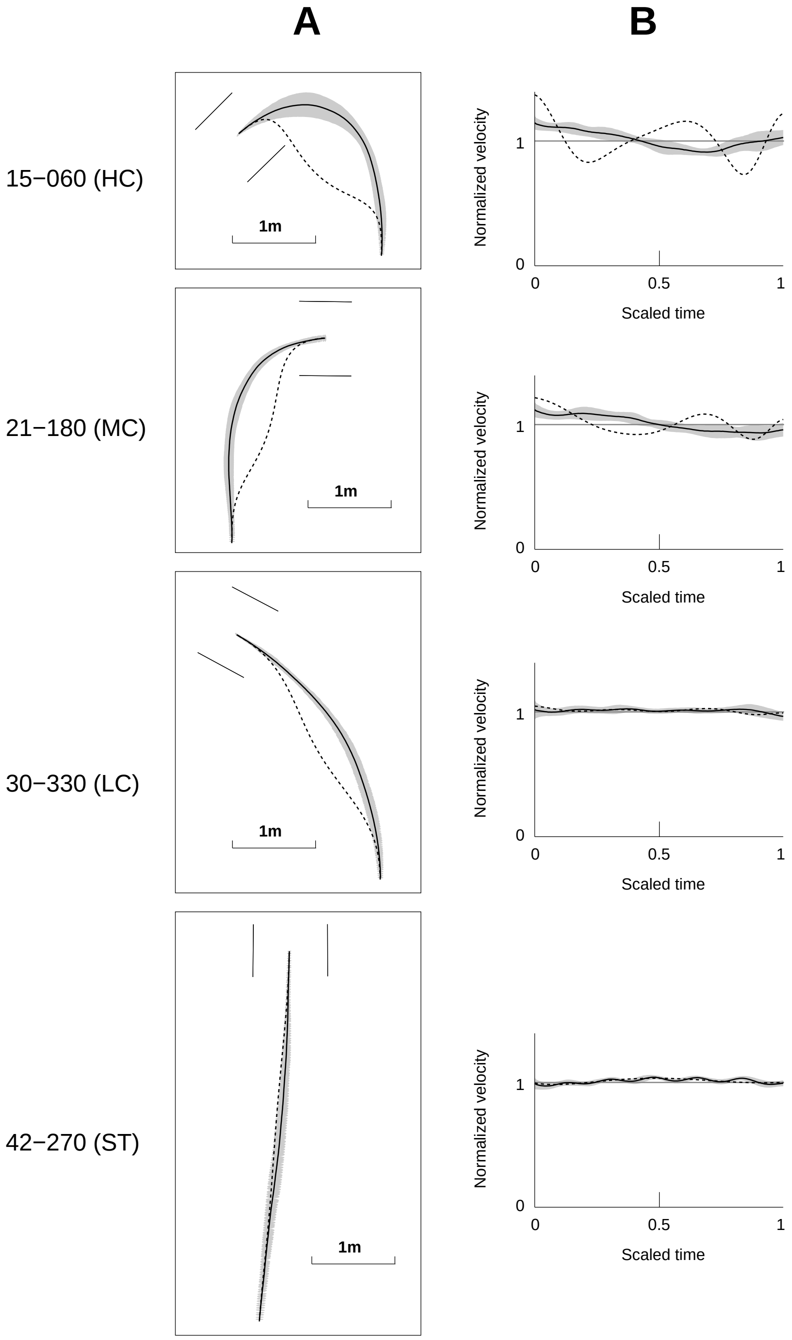

Figure 8.1: Simulations of the minimum velocity model for four representative trajectories. **(A)** Geometric paths of the average (solid lines) and the simulated (dashed lines) trajectories. The variance ellipses (in grey) are also plotted in order to show the spatial variability around the average trajectory at every time instant (see Materials and methods). **(B)** Normalized velocity profiles of the average (solid lines) and of the simulated (dashed lines) trajectory. The standard deviation around the average velocity profile is shaded in grey. The dark grey horizontal line shows the mean value (in time) of the normalized velocity profiles.

### Minimum acceleration model

The simulations of the minimum acceleration model are presented in Fig. 8.2. Qualitatively, for categories HC, MC and LC, the geometric paths simulated by this model were much more accurate than those simulated by the minimum velocity model. However, the simulated paths were still not satisfactory for categories HC and MC, which included the most curved trajectories. Indeed, as in the minimum velocity model, the simulated paths for these categories tended to be straighter than the actual paths. More specifically, in the regions of relatively high curvatures, the simulated paths fell outside the grey area of the variance ellipses, implying that their distances to the average paths were greater than the experimental variability in these regions.

The comparison of the velocity profiles only makes sense when the geometric paths are similar, i.e. in the case of category ST for the minimum velocity model and in the case of categories LC and ST for the minimum acceleration model. In these cases, the average velocity profiles were almost constant in time, which was well reproduced by both models.

### Minimum jerk and minimum snap models

The simulations of these models are presented in Fig. 8.3 and 8.4, respectively. The trajectories simulated by the two models were very similar for the four representative targets. In contrast with the two previous models, the geometric paths simulated by these two models for the HC and MC trajectories were smoothly curved and bear impressive resemblance with the average recorded trajectories. In particular, the simulated paths always lay inside the grey area of the variance ellipses, implying that the distances between the simulated and the average paths were smaller than the experimental variability at every time instant.

At the level of the velocity profiles, we noted that the average velocity profiles were approximately constant in time for categories LC and ST (the only minor variations were due to the step-level oscillations). This was well reproduced by both models. For categories HC and MC, in the average velocity profile, the velocity decreased and became minimal around $t = 0.7$ (where $t$ is time scaled from 0 to 1) before increasing again. This variation of the velocity was related to the variation of curvature in the corresponding geometric paths. The inverse relationship in human locomotion was experimentally observed by Vieilledent et al. (2001) and by Hicheur et al. (2005c) (see our review in section 3.2). The simulated velocity profiles successfully captured this behavior, although with some slight overshoots. For instance, for the representative target of category HC, the velocity profile of the mini-

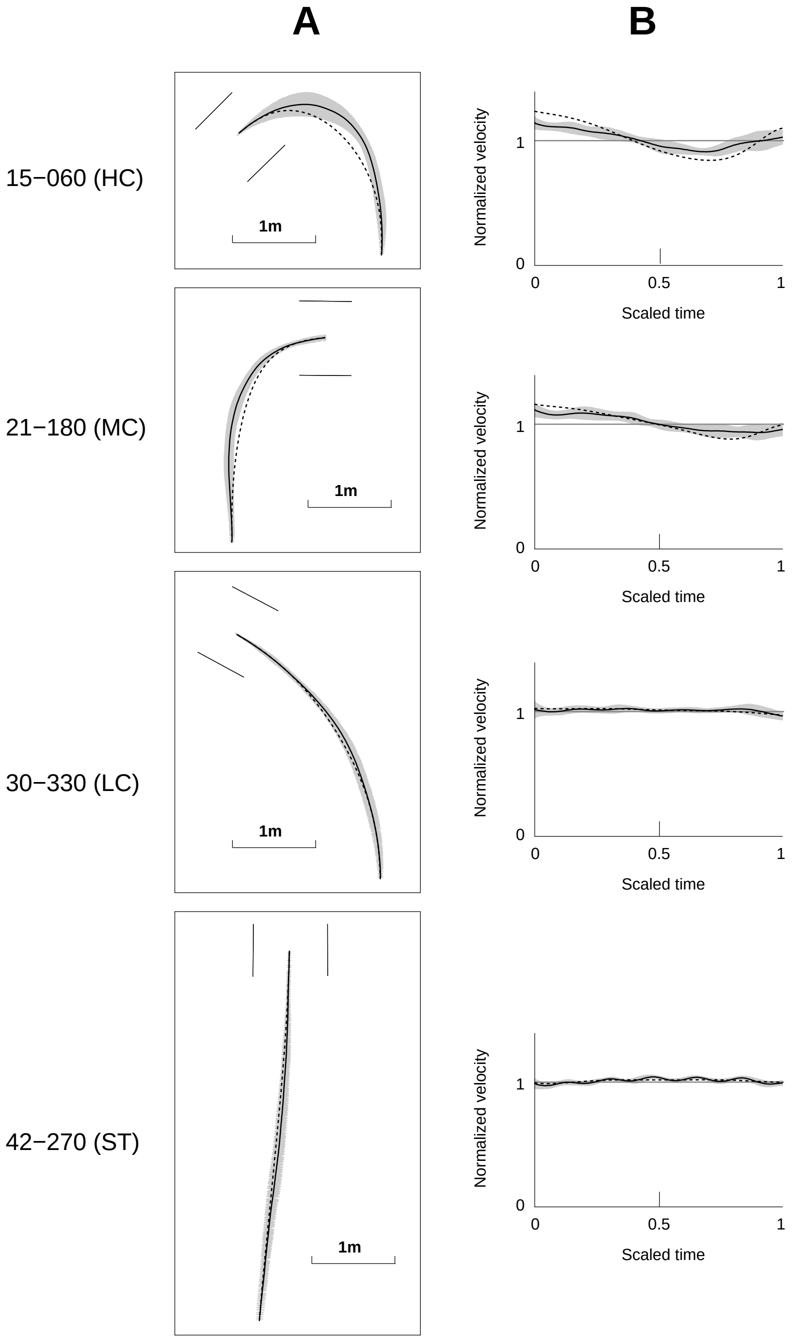

Figure 8.2: Simulations of the minimum acceleration model for four representative trajectories. For details, see legend of Fig. 8.1.

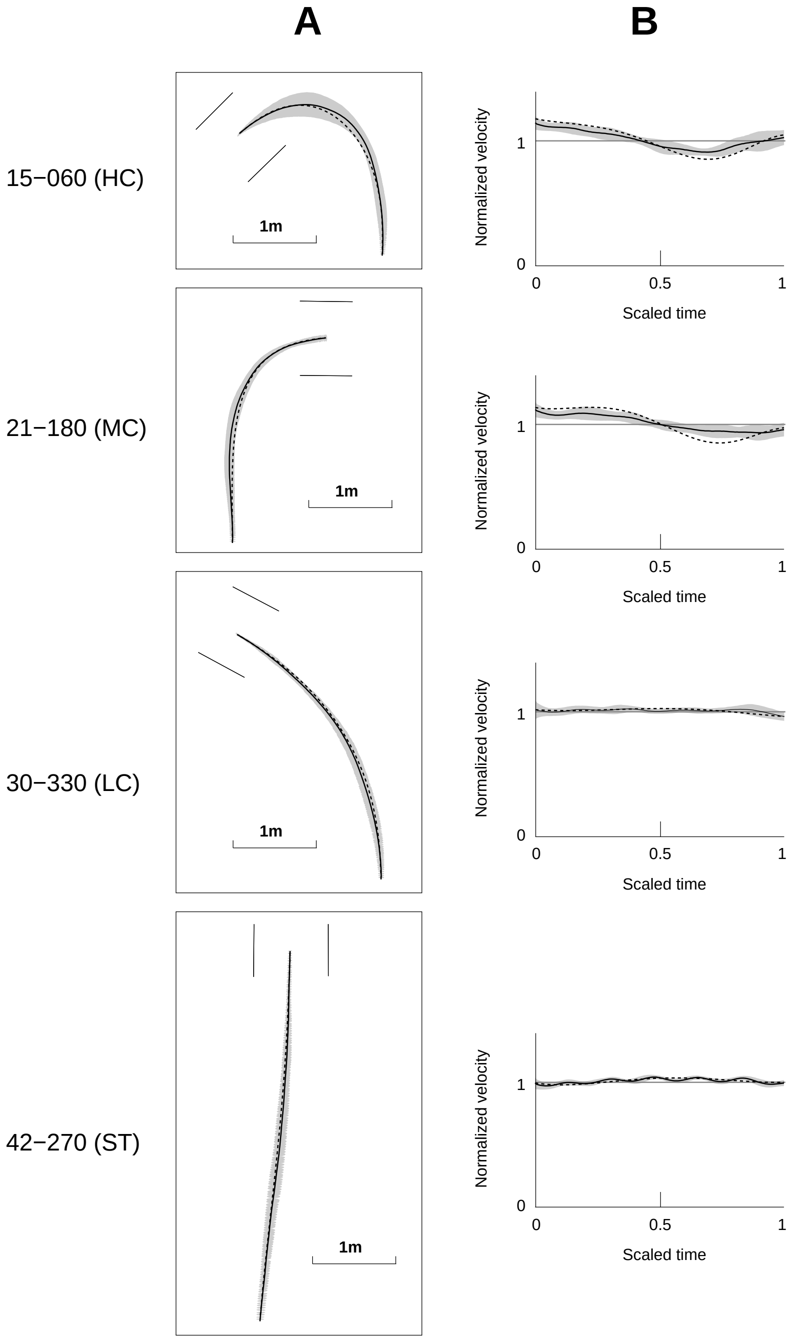

Figure 8.3: Simulations of the minimum jerk model for four representative trajectories. For details, see legend of Fig. 8.1.

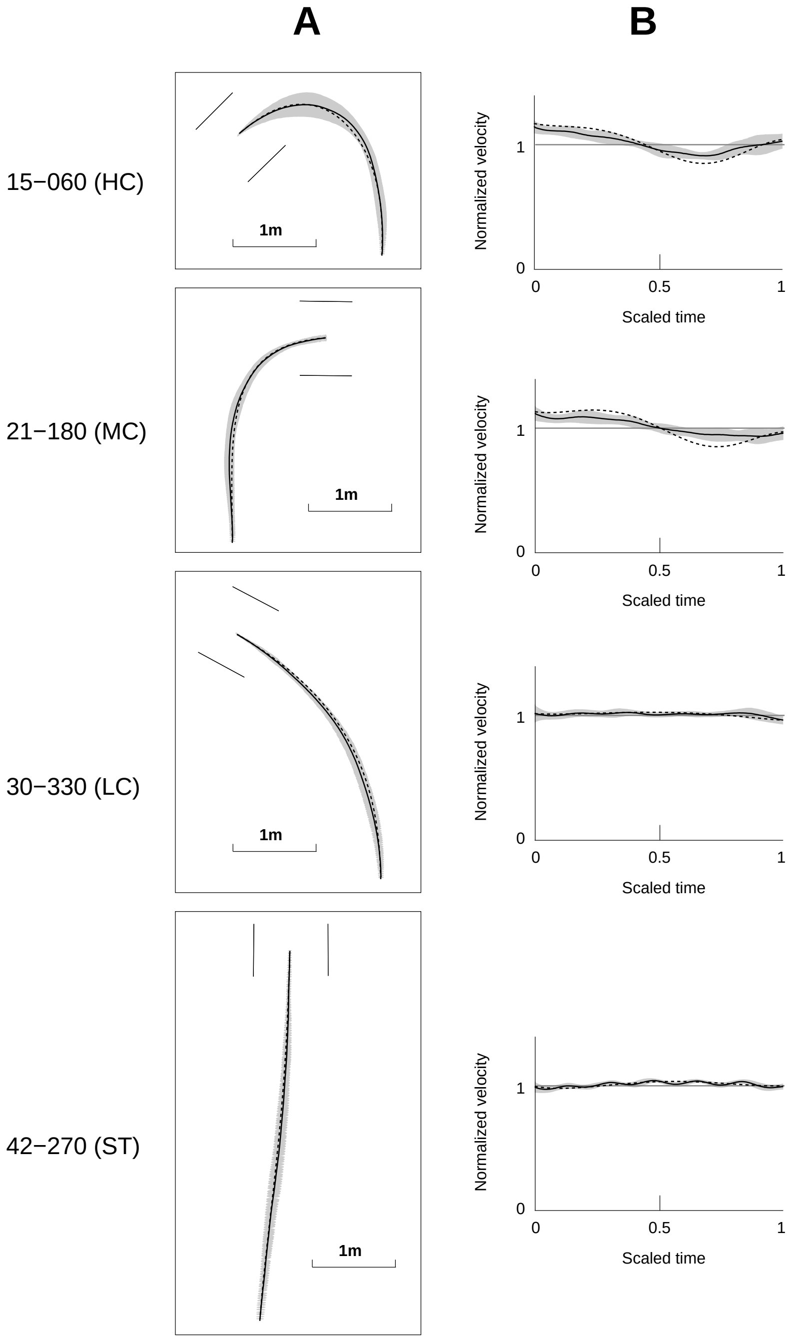

Figure 8.4: Simulations of the minimum snap model for four representative trajectories. For details, see legend of Fig. 8.1.

mum jerk trajectory had almost the same global behavior as the average one: both decreased and became minimal around $t = 0.7$ before increasing again. However the variations in the simulated profile were slightly larger than the variations in the average profile (this phenomenon is further discussed in section 8.3).

### Quantitative examination

**Trajectory errors** The average and maximal trajectory errors as defined in Methods are presented in Fig. 8.5. As noted above, the minimum velocity model (dark grey bars) produced acceptable simulations only for straight trajectories (category ST). As soon as the targets imposed some amount of trajectory curvature (categories LC, MC and HC), the minimum velocity trajectories differed completely from the actual trajectories.

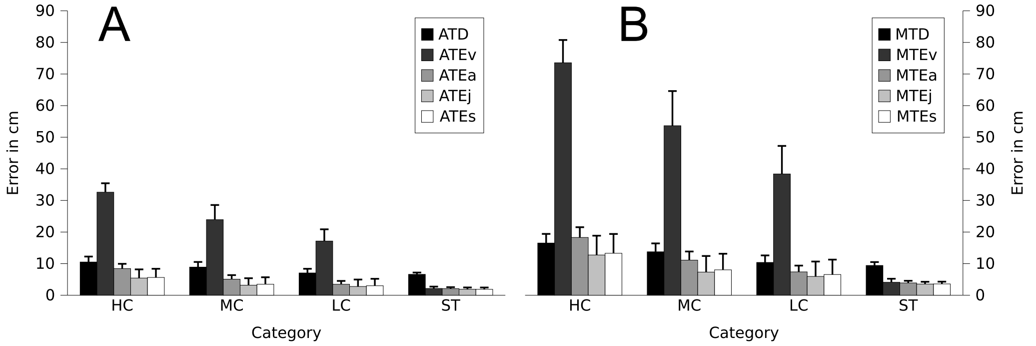

Figure 8.5: **(A)** Average and **(B)** maximal trajectory errors (ATE and MTE; the suffixes v, a, s, j refer, respectively, to velocity, acceleration, jerk and snap) in centimetres: dark grey bars for minimum velocity, medium grey bars for minimum acceleration, light grey bars for minimum jerk and white bars for minimum snap, averaged over targets corresponding to the same category. For comparison, the average and maximal trajectory deviations (ATD and MTD) are also plotted (black bars).

The minimum acceleration model (medium grey bars) performed somewhat better, but for categories HC and MC it was still not satisfactory. For example, the average maximal simulation error over the 20 targets belonging to these categories, $\mathrm{MTE}_{\mathrm{a}}^{\mathrm{HC+MC}}$ (0.147m) was of the same amplitude as the corresponding experimental variability (black bars) $\mathrm{MTD}^{\mathrm{HC+MC}}$ (0.151m).

By contrast, minimum jerk (light grey bars) and minimum snap (white bars) models provided strikingly good simulations. In fact, as noted above, the simulations of minimum jerk and minimum snap models were mostly similar. As a matter of fact, the largest difference between the two models was observed for target 31-150 (category HC), where the maximal distance between the two simulated trajectories was 0.036m. Over the 20 targets of categories HC and MC, the average (± SD) maximal distance between minimum jerk and minimum snap trajectories was only 0.021m (± 0.006m).

Even in the case of the highly curved trajectories of category HC, the distance between the average trajectory and the minimum jerk trajectory was $< 0.13$m over the whole trajectory ($\mathrm{MTE}_\mathrm{j}^\mathrm{HC} = 0.127$m). As the average trajectory length for this category was 3.7m, this corresponded to a maximal error of only 3.4%. Moreover, the simulation errors of the minimum jerk and minimum snap models were smaller than the experimental variability. For categories HC and MC, $\mathrm{MTE}_\mathrm{j}^\mathrm{HC+MC}$ (0.103m) was much smaller than $\mathrm{MTD}^\mathrm{HC+MC}$ (0.151m). This result is related to our previous qualitative observation that the paths simulated by these models always lay inside the variance ellipses.

Next, we compared statistically the experimental variability with the respective performances of minimum acceleration, minimum jerk and minimum snap models over the 20 targets belonging to categories HC and MC (we observed that the three models yielded similar performance for the straight and close-to-straight trajectories ST and LC). We recall that, on average, $\mathrm{MTD}^\mathrm{HC+MC} = 0.151$m; $\mathrm{MTE}_\mathrm{a}^\mathrm{HC+MC} = 0.147$m; $\mathrm{MTE}_\mathrm{j}^\mathrm{HC+MC} = 0.103$m and $\mathrm{MTE}_\mathrm{s}^\mathrm{HC+MC} = 0.107$m. The one-way ANOVA test with replications revealed a significant difference among the four means [F(3,76)=5.73, $p < 0.05$]. The post-hoc Tukey test revealed that there was no significant difference between MTD and $\mathrm{MTE}_\mathrm{a}$, or between $\mathrm{MTE}_\mathrm{j}$ and $\mathrm{MTE}_\mathrm{s}$. By contrast, there was a significant difference between MTD and $\mathrm{MTE}_\mathrm{j}$, or between $\mathrm{MTE}_\mathrm{a}$ and $\mathrm{MTE}_\mathrm{j}$.

The superiority of minimum jerk and minimum snap models over minimum acceleration and minimum velocity models can be explained as follows. Minimizing the mean squared velocity cost is almost equivalent to finding the shortest path, i.e. the straightest path in euclidean geometry, that satisfies the boundary conditions. This prevents the minimum velocity model from simulating accurate trajectories as soon as the targets required some amount of curvature. As for the minimum acceleration model, the mean squared acceleration cost penalises, by definition, large variations in time of the velocity vector. This is not consistent with the experimental observation of significant variations in the velocity vector (in particular, the variations in the *orientation* of this vector) around the regions of high curvature in MC and HC trajectories. By contrast, minimum jerk and minimum snap allow more flexibility for the variations in the velocity vector and are thus more capable of generating smoothly curved trajectories.

**Velocity profile errors** The average and maximal normalized velocity errors as defined in Methods are presented in Fig. 8.6. These errors in terms of the velocity profiles followed the same tendency as those in terms of trajectory kinematics: in all categories, the velocity profiles of minimum jerk (light grey bars) and minimum snap (white bars) trajectories differed very slightly from the average velocity profiles. Even for category HC, the AnVE was only 6% (of the average actual velocity) while the MnVE over the trajectory was < 12%. In absolute terms, these errors were close to the experimental variability (black bars).

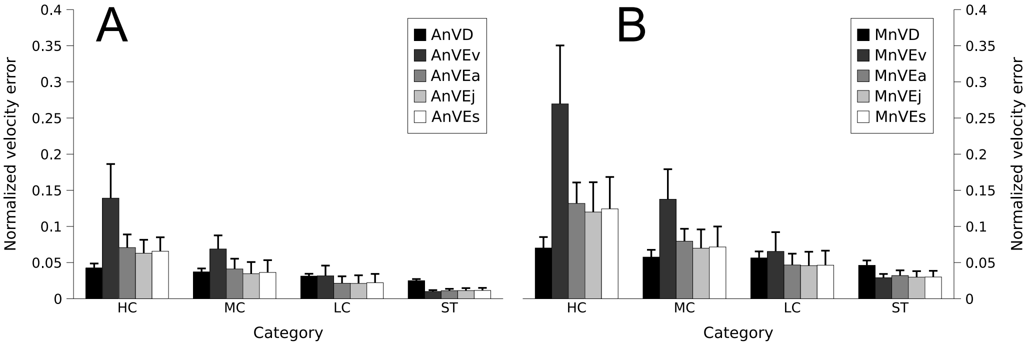

Figure 8.6: **(A)** Average and **(B)** maximal normalized velocity errors (AnVE and MnVE; the suffixes v, a, s, j refer, respectively, to velocity, acceleration, jerk and snap): dark grey bars for minimum velocity, medium-grey bars for minimum acceleration, light-grey bars for minimum jerk and white bars for minimum snap, averaged over targets corresponding to the same category. For comparison, the average and maximal normalized velocity deviations (AnTD and MnTD) are also plotted (black bars). In the process of computing the above quantities, all velocity profiles were normalized so that their average values over the movement duration equals 1 (see Materials and methods).

## 8.3 Modified minimum-jerk model

### 8.3.1 Methods

In the previous section, we presented a minimum jerk model that could reproduce with great accuracy locomotor trajectories of moderate curvature. However, we noticed that the velocity profiles of the simulated trajectories displayed slightly larger variations than that experimentally observed. Moreover, it is likely that this phenomenon becomes even worse for trajectories with larger curvature, making the original minimum jerk model unsuitable for simulating the heavily curved trajectories recorded in Experiment 2 (see section 5.3). Here we propose a modified version of this model to tackle this issue.

### Description of the model

We added an extra term that penalizes large variations of the velocity. The influence of this term was weighted by a constant $\mu$ that we set to a unique value in all the simulations for genericity. We thus looked for the trajectory $(x(t), (t))_{0 \le t \le 1}$ that minimizes

$$\int_0^1 \left( \dddot{x}^2 + \dddot{y}^2 + \mu \left( \frac{d}{\mathrm{d}t} \sqrt{\dot{x}^2 + \dot{y}^2} \right)^2 \right) \mathrm{d}t \tag{8.16}$$

subject to the constraints of Eq. (8.3) where the 12 boundary conditions $(x_0,\ v_x^0,\ a_x^0, \ldots)$ were set to the respective average experimental values as in Eq. (8.2). We found approximated solutions by numerically solving this optimization problem in the subspace of polynomials of degrees $\le 7$ (see Box 1 for more details).

### Analysis of the model' performance

We compared the trajectories simulated by the model with that recorded in Experiment 2 (see section 5.3). For clarity, we classified the targets in two groups: group I contained the straight and moderately angled targets (1N, 2N, 3N, 4N, 5N, 4E, 5E) and group II contained the highly angled target (4W, 5W, 4S, 5S).

As in the previous section, the comparisons were quantified by the ATE, MTE, AnVE and MnVE (see section 8.2.1). These measures are indexed by “j” (jerk) for the original minimum jerk model and by “m” (modified) for the modified model.

## 8.3.2 Results

For the straight and moderately angled targets of group I, the original and the modified minimum jerk models yielded accurate simulations, in terms of both trajectory path [Fig. 8.7(A1)] and velocity profile [Fig. 8.7(A2)]. The average $\mathrm{MTE_j}$ across the targets of group I was 0.11m, and the average $\mathrm{MTE_m}$ was 0.14m, while the average MTD was 0.26m [Fig. 8.7(D)]. The difference between the three means was significant [F(2,18) = 10.2, $p <$

0.05]. A post-hoc Tukey test revealed that the difference between MTD and $\mathrm{MTE_j}$ and the difference between MTD and $\mathrm{MTE_m}$ were significant, while the difference between $\mathrm{MTE_j}$ and $\mathrm{MTE_m}$ was not. The last result can be explained by the fact that, since the magnitude of the variations in the velocity profiles simulated by the original model were not too large, the addition of the extra term in the objective function did not affect the simulated trajectories [Fig. 8.7(A1,A2)].

By contrast, for the highly angled targets of group II, the velocity profiles simulated by the original minimum jerk model showed large fluctuations [Fig. 8.7(B2,C2)]. This resulted in a larger dissimilarity between the simulated and the experimentally recorded trajectories, in terms of both velocity profiles and geometric paths [Fig. 8.7(B1,(C1)]. Quantitatively, the average $\mathrm{MTE_j}$ across the targets of group II was 0.54m, the average $\mathrm{MTE_m}$ was 0.29m, while the average MTD was 0.40m [Fig. 8.7(D)]. The difference between the three means was significant [F(2,18) = 10.2, $p < 0.05$]. A post-hoc Tukey test revealed that the difference between $\mathrm{MTE_j}$ and $\mathrm{MTE_m}$ was significant, meaning that the modified minimum jerk did significantly better than the original model. Indeed, the addition of the extra term effectively reduced the variations of the speed, so that the velocity profiles simulated by the modified model very closely resembled the experimentally observed ones [Fig. 8.7(B2,C2)]. In terms of geometric paths, the modified model also "bent" the minimum jerk paths towards the observed paths, although no "instruction" about the path was specified in the modified model.

## 8.4 Discussion

### 8.4.1 Predictive power of the models

As pointed out by Todorov and Jordan (2002), the predictive power of a model is not only measured by how well it fits the experimental data. At least two other characteristics must be taken into account. The first characteristic is the quantity of information that needs to be extracted from the experimental data. Obviously, the less information extracted from the data, the greater the challenge for the model. In order to simulate the velocity profiles of curved hand movements, the constrained minimum jerk model requires, as inputs, the entire movement path and the initial and final velocities (Todorov and Jordan, 1998). Viviani and Flash (1995) used experimental values of the velocity and acceleration at several via-points in order to simulate the velocity profiles in curves drawing tasks. By contrast, our models, which simulate both the paths and the velocity profiles, required to extract

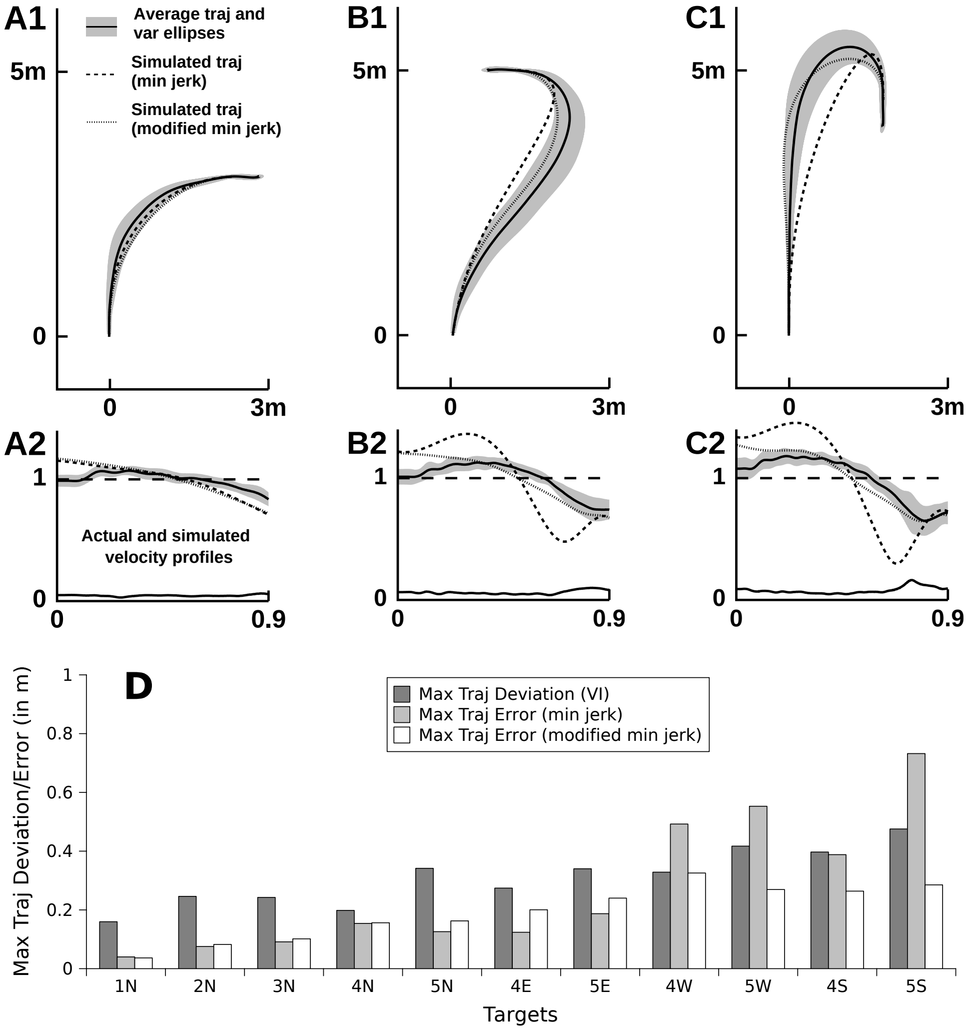

Figure 8.7: Modeling results for the Modified Minimum Jerk model. **(A)** modeling results for target 4E. A1: geometric path of the average trajectory (plain line) and variance ellipses around the average trajectory (gray area), geometric path of the trajectory simulated by the original minimum jerk model (dashed line) and by the modified minimum jerk model (dotted line). A2: average velocity profile (plain line), velocity profile simulated by the original minimum jerk model (dashed line) and by the modified minimum jerk model (dotted line). **(B)** Same as (A), but for target 5W. **(C)** Same as (A), but for target 5S. **(D)** Maximal Trajectory Deviation/Error (MTD/MTE) in meters: MTD in the VI condition (dark gray bars), MTE for the original minimum jerk model (light gray bars), MTE for the modified minimum jerk model (white bars).

only a small number of parameters, namely: the initial and final speeds and accelerations, and the movement duration (see the descriptions of the models).

The second characteristic for estimating the predictive power of a model is the presence and the number of free parameters that must be "tuned" in order to fit the data. For instance, Viviani and Schneider (1991) proposed a modified power law for modeling the velocity profile of curved hand movements

$$v(t) = \gamma(\kappa(t) + \epsilon)^{\beta} \tag{8.17}$$

In this model, the velocity gain factor $\gamma$ and the exponent $\beta$ needed to be tuned in order to fit the actual velocity profile. By contrast, the original MSD models did not contain any such free parameters. The modified minimum jerk model contained one free parameter $\mu$. However, the value of this parameter was chosen once for all, contrary to Viviani and Schneider's model, where multiple values of $\gamma$ and $\beta$ were considered.

### 8.4.2 Common strategies may govern the formation of hand and whole-body trajectories

Hand and whole-body movements differ greatly in their spatial and temporal scales: for instance, hand trajectories are usually tens of centimetres long while travelled distances during locomotor tasks are usually more than 10 times longer. This difference in magnitude is associated with a difference in the nature and the number of muscles involved in the production of the movement: while hand movements activate mostly the arm muscles, locomotor activity mobilizes practically all of the body muscles (lower limbs muscles for body propulsion, upper body muscles for trunk stabilization, neck muscles for steering, etc.).

However, some recent studies suggested that the generation of hand and whole-body movements share common strategies. For instance, Papaxanthis et al. (2003) reported that vertical whole-body and arm movements executed in the sagittal plane share kinematic similarities. The authors then suggested that the central nervous system (CNS) uses similar motor plans for the performance of arm and whole-body movements in the sagittal plane. The comparison of the velocity-curvature relations in human locomotion and in hand movements has also been conducted, using the same (up to a scaling factor) predefined curved paths in the two types of movements (Hicheur et al., 2005c, see also our review in section 3.2). At the computational level, Harris and Wolpert (1998) tested the assumption that the CNS learns a new movement by minimizing the variance of the final effector position for both hand and eye movements.

In this context, our observation that the minimum jerk and minimum snap models best simulate locomotor trajectories should be related to the case of hand movements, where very similar results were reported (Flash and Hogan, 1985; Richardson and Flash, 2002, see also our review in section 1.2). For instance, in the task of periodic drawing of closed shapes, Richardson and Flash showed that MSD models of order $n \geq 3$ provided more accurate predictions than MSD models of lower orders.

From a theoretical viewpoint, our finding that the same models could account for both hand and whole-body movements further supports the "motor equivalence principle" evoked in the Introduction, which hypothesized that common mechanisms are implemented by the motor system in the generation of various types of movements. More specifically, this hypothesis can be related to the theory put forward by Bernstein (1967), according to whom there may exist, at the higher levels of the motor system, kinematic representations of movements that are independent of the nature (in our case, the arm or the whole locomotor system) of the actual effector.

However, it should be noted that, contrary to the case of hand movements where the laboratory (allocentric) reference frame (RF) and the body (egocentric) RF are equivalent, here the body RF moves and turns with respect to the laboratory RF when the subject is moving. In this context, the quantities used in our models (the position of the subject and its derivatives) are only interesting when computed in the laboratory RF since, in his body RF, the subject's position is constant in time. From a theoretical viewpoint, while egocentric and allocentric strategies for spatial navigation and spatial memory are usually debated in the literature (see Berthoz and Viaud-Delmon, 1999), the question of what RF(s) are actually used for the planning and control of goal-oriented locomotion has received little attention. Here, our results suggest that whole-body trajectories are optimized in the laboratory RF.

Finally, we would like to bring the reader's attention to the issues raised by Engelbrecht (2001) regarding the danger of circular theorizing when using optimization principles in motor control. We believe that our approach avoids some of these issues and intend to discuss this in detail in a future contribution.

# Chapter 9

# Optimal feedback control models

## 9.1 Overview

The models presented in the previous chapter were sucessful in reproducing the *average* trajectories for a large variety of targets, formalizing thereby the observation that locomotor trajectories are smooth and strengthening the hypothesis that locomotion and arm movements share common control objectives. However, being in essence deterministic, these models are of no help for our understanding of trajectory *variability.* Yet, the analysis of the variability profiles in chapter 6 provided a large amount of information about the nature of the control mechanisms at work during locomotion. There is therefore a need for a *stochastic* models that can help integrate these findings about trajectory variability into a theoretical framework, while allowing testing *positively formulated* control mechanisms.

In particular, we propose that the online control of whole-body trajectories in visual and nonvisual locomotion (see sections 6.5.1 and 6.5.2) may be based on *optimal feedback control* (see our review in section 1.3). To test this idea, we designed a simplified optimal feedback control model and compared the simulations of this model (and those of alternative models) with the experimentally recorded trajectories. This model also allows formally testing whether the combination of the two sources (vision-independent and "trajectory-complexity"-independent, see section 6.2.3) could give rise to the special shape of the varibility profiles observed in Experiment 3 (see section 6.2).

The different models of this chapter were designed by Q.-C. Pham and H. Hicheur and presented in Pham and Hicheur (2009). For more details, the reader is referred to the original article.

## 9.2 Visual condition (VI)

### 9.2.1 Description of the model

The model given by Algorithm 1 implements a simplified optimal feedback control scheme (Hoff and Arbib, 1993; Todorov and Jordan, 2002). Following the experimental results of chapter 6, this model relied on an open-loop process which is complemented by an online feedback module (see Fig.6.1 and Fig. 9.1 for illustrations). The open-loop process was based on the maximum-smoothness principle (see chapter 8) while the feedback module was based on the optimal feedback control principle.

**Algorithm 1** (see Fig. 9.1 for illustration)

**1.** Discretize the movement into $n$ steps ($10 \leq n \leq 20$ depending on the target)

**2.** At each step $i$, compute first a Minimum Modified Jerk trajectory between the current state $s(i)$ (position, velocity, acceleration at time $i$) and the final state. This is the "initially planned trajectory"

**3.** Add a random perturbation to $s'(i+1)$, the state of the "initially planned trajectory" at step $i{+}1$. This yields the actual state $s(i{+}1)$

**4.** Interpolate a smooth trajectory between $s(i)$ and $s(i+1)$ (for simplicity, we used a MJ trajectory since it is the lowest-order polynomial trajectory $T$ that satisfy $T(0) = s(i)$ and $T(1) = s(i{+}1)$ see Box 1). This yields the actual sub-trajectory between $i$ and $i+1$

**5.** Repeat from step 2

This model is a not a fully optimal feedback control model in the sense of Todorov and Jordan (2002) because in the step where we computed the $(i+1)^{\text{th}}$ optimal sub-trajectory (step 2 of Algorithm 1), we minimized the deterministic cost instead of the "cost-to-go" (which also takes into account the statistics of the noise, see Todorov and Jordan, 2002). However, this model preserves the main idea of optimal feedback control, namely, that the

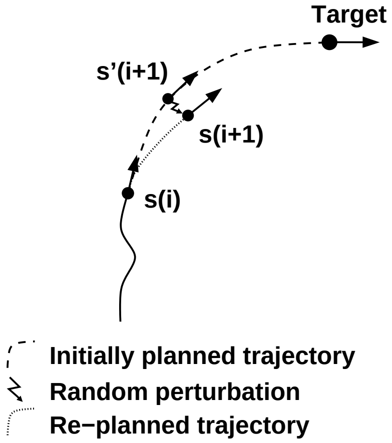

Figure 9.1: Description of the models (condition VI). Illustration for the simplified optimal feedback control of Algorithm 1.

sub-trajectories are recomputed at every step optimally with respect to the final target and not with respect to any intermediate representation of the task (such as a "desired trajectory").

The initial and final velocities and accelerations in Algorithm 1 were set to the average experimental values, as in the deterministic models (see chapter 8). To reproduce the small baseline variability present at the beginning and at the end of the movement, the initial and final positions were chosen from a 2D Gaussian distribution with standard deviation ($\sigma^x_{\text{baseline}} = 0.027$m; $\sigma^y_{\text{baseline}} = 0.027$m) and centered around the actual starting position and the actual target's position.

Regarding the perturbations added at step 3 of the Algorithm, Harris and Wolpert (1998) argued that the amount of execution noise (see Discussion) is likely an increasing function of the "motor commands". However, since we did not model directly the whole locomotor apparatus but only its outcome – the locomotor trajectory – it is unclear how execution noise may be "converted" into trajectory perturbations. Here, in the context of locomotion, a series of observations suggests that the magnitude of the trajectory perturbations caused by execution noise is likely determined by the instantaneous trajectory curvature and not by, for instance, velocity or acceleration. First, trajectory variability was higher for the angled targets, which impose curved trajectories, than for the straight targets (Experiment 3, section 6.2). This rules out velocity as a determining factor, because velocity was usually lower for curved trajectories. Second, the variability profiles were the same in the Normal (NS) and Fast Speed (FS) conditions (Experiment 4, section 6.3) although kinematic quantities, such as velocity or acceleration, were larger in the FS condition than in the NS condition. By contrast, the observed geometric paths (hence the curvature distributions) were the same in the two conditions.

Thus, we set the magnitude of the trajectories perturbations to be an increasing affine function (van Beers et al., 2004) of the absolute value of the curvature (in a different context, the absolute value of the curvature was used in a model of locomotor trajectories formation, see Arechavaleta et al., 2008b, and also section 3.3). The total trajectory perturbation is then the sum of a constant perturbation and a signal-dependent perturbation that scales linearly with the absolute value of the curvature

$$\sigma^x_{\text{exec}} = \sigma^y_{\text{exec}} = \sigma_{\text{const}} + |\kappa(t)|\sigma_{\text{sd}} \tag{9.1}$$

where $\sigma_{\text{const}}$=0.03m and $\sigma_{\text{sd}}$=0.14m$^2$ for all targets.

Finally, it should be noted that our method of adding noise directly to the states (and not to the commands) constitutes a simplification. A more rigorous version of our model would require reformulating the MMJ optimization into a dynamical model, as Hoff and Arbib (1993) did for the original MJ optimization. However, in our case, the addition of the $\gamma$ term in the MMJ made such a reformulation much more difficult.

### 9.2.2 Results

In condition VI, the sample trajectories simulated by the optimal feedback control model [Fig. 9.2(B)] were globally similar to trajectories observed in one typical subject [Fig. 9.2(A)]. The variability profiles generated by the model also reproduced the typical features of actual variability profiles, namely: low and approximately constant profile for the straight targets [target 2: Fig. 9.2(C)] and bump-shaped profile for the angled target [target 5: Fig. 9.2(D)].

## 9.3 Nonvisual condition (NV)

### 9.3.1 Description of the model

To understand the variability patterns observed in condition NV, we evaluate two competing control schemes: a purely open-loop control scheme and an online feedback control scheme in presence of uncertainties on the position of the target.

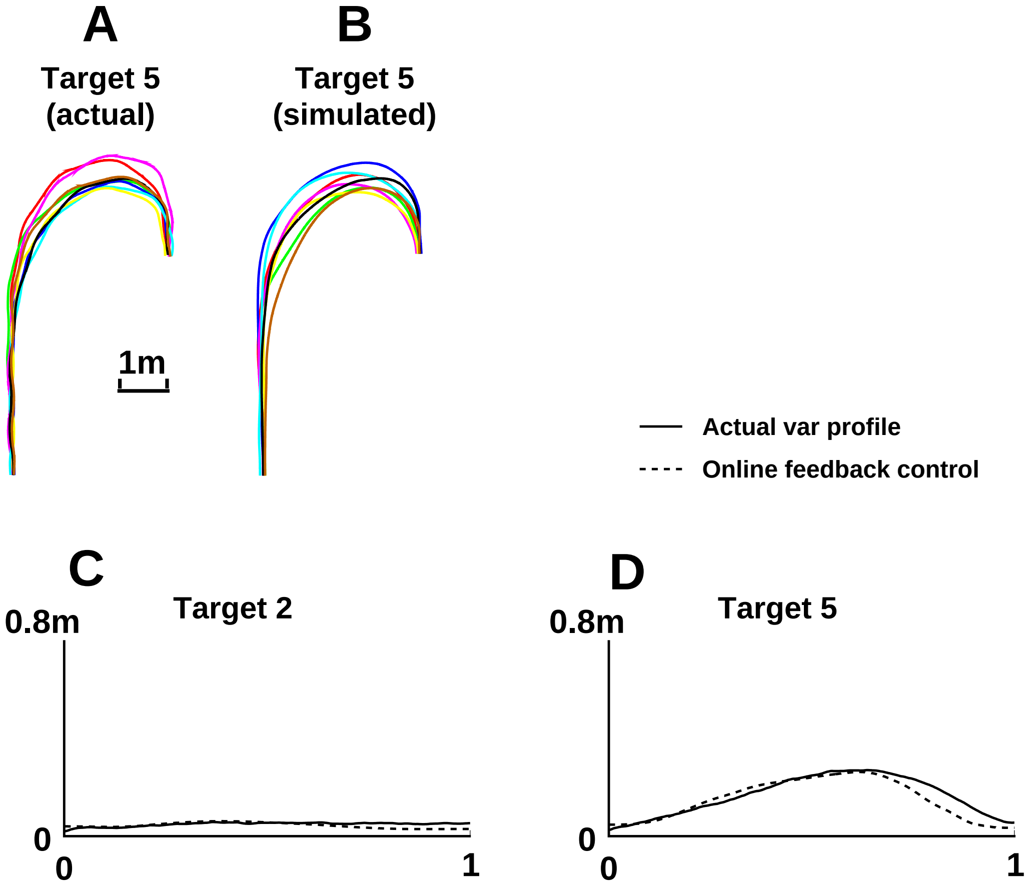

Figure 9.2: Modeling results for the stochastic models, visual (VI) condition. (**A**) eight actual trajectories of subject N. V. for target 5. (**B**) eight sample trajectories simulated by the stochastic model for target 5. (**C**) Variability profiles for target 2. Plain line: average variability profile across subjects. Dashed line: variability profile computed over 20 simulated trajectories. (**D**) same as in C, but for target 5.

**Purely open-loop control (Models OL)** We modeled three possible purely open-loop control schemes, which are specified in terms of the time series of velocity, acceleration or jerk, as follows.

We computed first the Minimum Modified Jerk (MMJ) trajectory between the initial and final states as defined in the deterministic model (see section 8.3). We then computed, by successive differentiations, three 2D time series $(v^x(i), v^y(i))$, $(a^x(i), a^y(i))$ and $(j^x(i), j^y(i))$, representing respectively the velocity, acceleration and jerk corresponding to this MMJ trajectory. In model $\mathrm{OL_v}$, we added Gaussian random perturbations with standard deviation $\sigma_v(i)$ to $v^x(i)$ and $v^y(i)$ $(i = 1 \dots N)$ to obtain a random time series $(\tilde{v}^x(i), \tilde{v}^y(i))$. Note that $\sigma_v(i)$ was also an affine function of the instantaneous trajectory absolute curvature (the coefficients were the same as above, but appropriately rescaled to match the experimental final variability). The time series $(\tilde{v}^x(i), \tilde{v}^y(i))$ was finally integrated with respect to time to yield a random trajectory.

In model $\mathrm{OL_a}$ (respectively $\mathrm{OL_j}$), instead of adding the perturbation to the velocity vectors, we added Gaussian random perturbations with standard deviation $\sigma_a(i)$ [resp. $\sigma_j(i)$] to the acceleration (respectively jerk) vectors. Then these random vectors were integrated twice (respectively three times) to yield a random trajectory.

**Online feedback control (Model OF)** This model was based on the simplified optimal feedback control model used for condition VI (Algorithm 1). Remark first that, in the VI model, the subject's state $s(i)$ (position, velocity, acceleration) was assumed to be perfectly known to the subject at every time step. To model the absence of vision in condition NV, we introduced perturbations in the subject's estimation of his state. For simplicity, we assumed that these perturbations yielded errors in terms of subject's estimated orientation and distance to target [the reduction of the state to the pair (distance, orientation) is rather classical in studies of nonvisual locomotion, see for instance Loomis et al. (1993); Glasauer et al. (2002) and also section 2.2]. Remark now that, from a computational viewpoint, these errors can be rendered, in our model, by perturbing directly the target's orientation and position in space [however, in relation with the discussion on egocentric and allocentric strategies for navigation Burgess et al. (2002), it should be noted that the physiological mechanisms underlying the errors in the estimation of self's state and of the target's state may completely differ].

To make this clear, consider for instance that the subject makes an error $\epsilon$ in the estimation of his orientation. This is equivalent to assume that he actually makes no error in the estimation of his orientation, but that the subjects' estimation of the "external world" is rotated by an angle $-\epsilon$ around the subject. Since the "external world" in our model comprised only the target, this corresponds to the following perturbations of the target: (i) a rotation centered on the subject and of angle $-\epsilon$ of the target's position and (ii) a shift of $-\epsilon$ of the target's angle [see Fig. 9.3(B)]. Similarly, an error $\delta$ in the subject's estimation of his distance to the target corresponds to a translation of the "external world" by $-\delta$ along the subject-target axis.

More specifically, we modified Algorithm 1 by adding, between step 4 and step 5, the following step "4b"

**Algorithm 2 (Modification of Algorithm 1 for condition NV)**
[see Fig. 9.3(A), 9.3(B) for illustration]

```
4b. (i) Draw a random distance $\delta$ from a Gaussian distribution of
        mean 0 and of standard deviation $\sigma_\delta$ ($\sigma_\delta = 0.03$m in the simulations).
        Shift the target's position by $-\delta$ along the subject-target axis
    (ii) Draw a random angle $\epsilon$ from a Gaussian distribution of mean 0
        and of standard deviation $\sigma_\epsilon$ ($\sigma_\epsilon = 1.8°$ in the simulations).
        Rotate the target's position by $-\epsilon$ around the subject. Shift
        the required final velocity $(v_1^x, v_1^y)$ and acceleration $(a_1^x,\ a_1^y)$
        angle by $-\epsilon$
```

There exist several other possibilities to model the absence of vision. One can for instance add an extra 2D-Gaussian perturbation to the target's position at each time step in order to simulate the spatial memory decay. One can set $\sigma_\delta$ and $\sigma_\epsilon$ as functions of the execution noise intensity. The estimation process can also be more complex, for instance, combining optimally vestibular and proprioceptive measurements with internal simulations (see the state estimation literature for hand movements reviewed in e.g. Jordan and Wolpert, 1999). However, we chose to follow the simple approach above in this first modeling study. It will be necessary in future works to design new experiments and refine this part of the model in order to study in detail the effects and the interactions of spatial memory decay and of the different sensory signals (e.g. visual, vestibular and proprioceptive) on the variability of nonvisual trajectories.

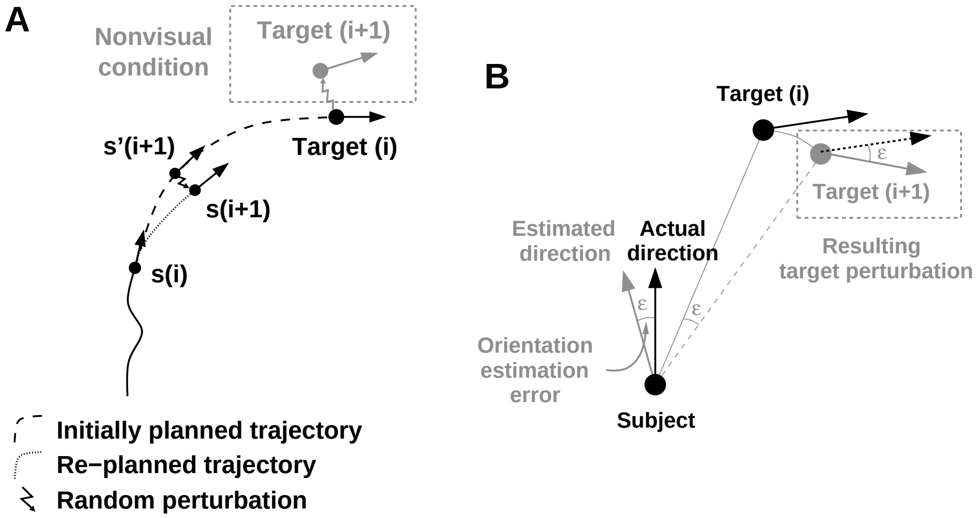

Figure 9.3: Description of the models (condition NV). (**A**) Illustration for Algorithm 2. (**B**) Effect of an error in the subject's estimation of his orientation in space.

### 9.3.2 Results

In condition NV, the sample trajectories simulated by model OF [Fig. 9.4(B)] were globally similar to trajectories observed in one typical subject [Fig. 9.4(A)]. Regarding the variability profiles, for the straight targets, the sample variability profile produced by model OF (online feedback control) has the form of a sigmoid, but which was very close to a straight line [dashed line, Fig. 9.4(C)]. For the angled targets, the sample variability profile produced by model OF increased approximately linearly until $t = 0.8$ and then slightly decreased [dashed line, Fig. 9.4(D)].

By contrast, this non-monotonicity, which is a characteristic feature of actual variability profiles (see the results of Experiment 3), could not be reproduced by none of the purely open-loop models. Indeed, in all of these models, the variability profiles were always increasing [dashed-triply-dotted, dashed-dotted and dotted lines, Fig. 9.4(D)].

## 9.4 Discussion

We made in chapter 6 several remarks about how the properties of the variability profiles may reflect the control mechanisms underlying locomotion. First, we argued that purely open-loop control would lead to monotonically increasing variability profiles, since, in absence of feedback corrections, errors

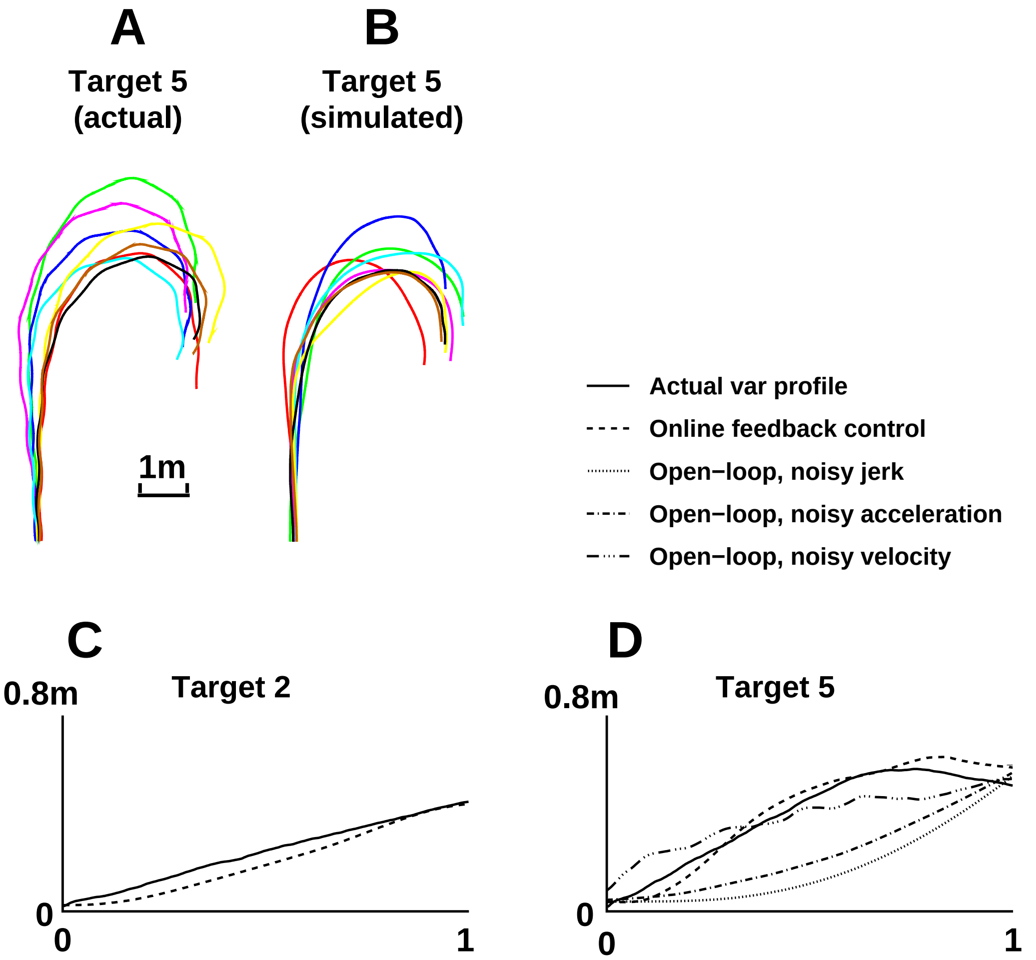

Figure 9.4: Modeling results for the stochastic models, nonvisual (NV) condition. (**A**) eight actual trajectories of subject N. V. for target 5. (**B**) eight sample trajectories simulated by the stochastic model for target 5. (**C**) Variability profiles for target 2. Plain line: average variability profile across subjects. Dashed line: variability profile computed over 20 simulated trajectories. (**D**) Variability profiles for target 5. Plain line: average variability profile across subjects. Dashed line: variability profile computed over 20 sample trajectories (model OF). Dashed-triply-dotted line: model $\mathrm{OL}_\mathrm{v}$ (open-loop control, noisy velocity). Dashed-dotted line: model $\mathrm{OL}_\mathrm{a}$ (open-loop, noisy acceleration). Dotted line: model $\mathrm{OL}_\mathrm{j}$ (open-loop, noisy jerk).

can only accumulate. This remark was confirmed by the modeling study: the purely open-loop models ($\mathrm{OL_v}$, $\mathrm{OL_a}$, $\mathrm{OL_j}$) indeed produced monotonically increasing variability profiles.

Second, remarking that the special shape of the variability profile observed in condition NV could be decomposed as the sum of a straight line and a bump, we formulated the hypothesis that two sources of noise independently contribute to the variability of locomotor trajectories (the "two-sources" hypothesis, see section 6.2.3). Here, model OF also contained two main sources of noise (we do not discuss the small baseline noise whose contribution was negligible). The first source is associated with the interplay between execution noise and feedback corrections (see Algorithm 1). This source, in isolation, produced bump-shape variability profiles. The second source is associated with the state estimation errors (see Algorithm 2). This source, in isolation, produced straight profiles. By showing that the combination of these two sources could give rise to a non-monotonic shape similar to that observed in section 6.2.3, we confirmed, in a direct way, the "two-sources" hypothesis.

Third, from the results of the via-points experiment (section 6.4), we concluded that the online control of locomotion is unlikely based on the tracking of some "desired trajectory". Here, by designing an optimal feedback control model that could simulate accurately the statistical properties of actual trajectories, we show positively that optimal feedback control may underlie the control of both visual and nonvisual locomotion.

# General discussion

# Summary of the results and discussion

Consider again the situation evoked at the beginning of this thesis: a person is standing at some position in a room and has to walk towards and through a distant doorway to get out of that room [Fig. 1(A)]. We raised a number of questions concerning this task, for instance: what trajectory in space does the person choose to achieve this objective? if he has to perform this task several times, will the resulting trajectories be similar or not? following what criteria does he select a particular trajectory among the infinitely many possible trajectories? etc. We summarize in the present chapter some of the answers provided by our experimental and modeling studies. We would like also to discuss, from a broader perspective, the contribution of our results to the understanding of human locomotion in particular and of motor control in general.

## Summary of the main results

We showed in chapter 5 that locomotor trajectories produced to reach a distant target defined in position and orientation (the doorway) were highly similar across repetitions and across subjects. This stereotypy contrasted with a large variability of the sequences of foot positions. This led us to suggest that, in a large, obstacle-free environment, goal-oriented locomotion is planned and controlled globally at the level of whole-body trajectories in space, rather than as sequences of foot positions or patterns of muscle activity. We then showed that the whole-body trajectories in question were, on average, unaffected by changes in the sensory and motor conditions. The average trajectories produced to reach a distant target were indeed found to be highly similar across sensory (walking with or without visual feedback) and motor (walking forward or backward) conditions. These observations further supported the hypothesis that locomotor trajectories are planned and controlled at the higher levels of the Central Nervous System (CNS), and *to some extent*, independently of their sensori-motor implementation.

Although globally stereotyped, the trajectories we recorded still displayed some variability, which we next examined. Based on the analysis and the comparison of variability profiles in the visual and nonvisual conditions, we showed that a combination of open-loop and feedback processes underlie the planning and control of locomotor trajectories. In particular, assuming this architecture, the similarity of the average trajectories in visual and nonvisual locomotion would reflect the identity of the open-loop processes in these two conditions. Finally, we showed that the online feedback processes may be based on optimal feedback control schemes, rather than on the tracking of some "desired-trajectories".

The nature of the open-loop and the feedback processes was then further investigated though a modeling study. We showed in particular that parsimonious maximum smoothness models accurately accounted for the average trajectories recorded in a large variety of targets. We then formalized the control architecture mentioned previously by designing a stochastic model whose open-loop module was based on the maximum smoothness principle and whose feedback module was based on optimal feedback control. These models could simulate with great accuracy both the average trajectories and the variability patterns experimentally observed in visual and nonvisual locomotion. This result provided a positive and *constructive* support for the control architecture hypothesized based on the experimental observations.

## Contribution of our work to the understanding of locomotion and of motor control

While the study of locomotion at the level of whole-body trajectories has already been undertaken in a number of previous works (see our review in chapter 3), we believe that the results just summarized provide the first *systematic* account of how locomotor trajectories are planned and controlled in humans.

Indeed, as noted in the Introduction, most previous works on locomotor trajectories considered either straight-ahead walking or predefined paths and thus could not address how humans plan and control *complex* trajectories in a free environment. Arechavaleta et al. (2006) did study spontaneously generated trajectories (these authors are indeed credited with the invention of the "walking towards and through a distant doorway" paradigm) but they were interested primarily in verifying the nonholonomic constraint (see our review in section 3.3) and neglected to assess whether the locomotor trajectories are stereotyped in the first place.

Yet, the demonstration of the stereotypy of locomotor trajectories allowed identifying these trajectories as a possible “controlled variable” monitored by the central nervous system. This step furthermore constituted the prerequisite for the subsequent experimental (effects of sensory and motor conditions, control strategies) as well as modeling (maximum smoothness, optimal feedback control) studies.

Correlatively, another important and innovative aspect of our study was the detailed analysis of variability profiles. Indeed, while the analysis of the variability along the average trajectory has been performed in some studies of hand movements (see our review in section 1.3.2), only *discrete* variability analyses have been considered so far in locomotion (e.g. variability of the final position in locomotor “reaching” or variability of the intermediate positions in triangle completion or polygon walking tasks, see our review in section 2.2). Perhaps, the most advanced use of variability analysis was made by Farrell and Thomson (1999) who calculated the variability of the lengths of the final steps in a locomotor “reaching” task. By doing so, as mentioned in our review (see section 2.2.2), the authors could provide some insights into the control strategies underlying nonvisual locomotion.

Here, systematizing and extending Farrell and Thomson’s approach were crucial in identifying the precise nature of the control mechanisms at work during goal-oriented visual and nonvisual locomotion. More generally, we believe that most studies of locomotion or navigation will benefit from a systematic analysis of the time-varying variability patterns.

Taken together, our results provide the conceptual basis for future studies of locomotion at the level of trajectories. Such studies may include external perturbations or manipulate sensory signals (for instance using wedge prisms, virtual reality or vestibular stimulations, etc.) in order to carry forward our understanding of human goal-oriented locomotion.

## Relations with computational motor control

Computational motor control has undergone several conceptual developments over the past decades: from the identification of movements invariants, through the conception of (deterministic) optimal control models, to the formulation of stochastic control schemes motivated by the analysis of movement variability (see our review in chapter 1). As evident from the summary of the results, our approach of locomotion has greatly benefited from these conceptual developments.

Conversely, what insights can our results provide for the understanding of motor control in general? As noted in the Discussion of chapter 8, the productions of hand and locomotor movements greatly differ in their spatial and temporal scales, as well as in the nature and the number of the underlying physiological apparatuses (the arm in hand movements and the entire body in locomotion). In this context, the fact that several properties (such as the spatial control, the smoothness of the trajectories or the optimality of the feedback control mechanisms) are shared by the two types of movements may have important conceptual consequences.

First, if a property, or "law", is verified in many types of movements then this increases the *genericity* of the law, which can then be regarded as a "general organizing principle". For instance, the idea that the motor system, in general, operates like an optimal feedback controller is further strengthened by our results.

Second, as also noted in the Discussion of chapter 8, the fact that hand and locomotor movements share so many important properties further supports Bernstein's "motor equivalence principle". More precisely, also according to Bernstein (1967), at the higher levels of the motor system, hand movements and locomotion may share common "kinematic representations" (this notion is also related to the "spatial control" put forward by Morasso, 1981). Going further, we speculate that these "kinematic representations" are not the only neural functions common to the two types of movements. We propose that the other shared properties – smoothness of the trajectories and optimal feedback control – may also originate from common neural functions and from the common neural *structures* that subserve these functions. Indeed, a number of neurophysiological studies have identified precise neural structures that may subserve specific "computational" functions (see in particular the review of "computational neuroanatomy" by Shadmehr and Krakauer, 2008). For instance, the parietal cortex may serve as a state estimator, the basal ganglia may be involved in optimal control while the primary and the premotor cortices may act as feedback controllers. In this context, can we speculate that the smoothness of hand and locomotor trajectories results from similar optimization processes that take place in the basal ganglia, or that goal-directed optimal feedbacks of hand and locomotor trajectories are underlied by similar mechanisms in the primary and premotor motor cortices? Addressing these questions requires new neurophysiological data from both clinical (as in Shadmehr and Krakauer, 2008) and neuroimaging studies (starting perhaps with imaginary locomotion).

# Some current and future directions of research

We conclude by presenting some current and future directions of research.

## Direct comparison of locomotor and hand trajectories

While the hand/locomotion comparative view presented previously may seem appealing, we have noted a number of differences between hand and locomotor trajectories. For instance, as evoked in our review (see section 3.2), the "one-third power law", which robustly applies for hand drawing of curves, is not verified by locomotor trajectories. Correlatively, we also mentioned in the Discussion of the "affine experiment" (section 7.3) the prediction of Bennequin et al. (2009) that euclidian rather than full-affine geometry may be dominant in locomotion.

Here, we propose to *directly* assess the similarity of hand and locomotor trajectories. For this, we adapted Experiment 6 (see section 7.2) to the context of hand movements. We designed a protocol almost identical to that of Experiment 6, with the only difference that all distances were scaled down by a factor of 18.5 (see Fig. 7.5). Instead of walking through the via-points towards the final target, we asked the same subjects of Experiment 6 to make hand movements (see Fig. 2). This experiment was designed and run by Q.-C. Pham, H. Hicheur and J. Wiener in November 2007. We thank Y. Dupraz for his help in manufacturing the experimental materials.

Some preliminary results are shown in Fig. 3. We believe that a qualitative and comparative comparison of the hand trajectories recorded in this experiment with the locomotor trajectories recorded in Experiment 6 will give further insights into the relations between the mechanisms governing the production the two types of movements.

Figure 2: Protocol for the hand movement experiment. A subject sat in front of a table with the tip of his index lying on the plastic pane that covered the computer screen. He was asked to produce hand trajectories while making as few body movements as possible (the furthest target was well within the reaching range of the subjects so that, in practice, the subjects used only their arms while the rest of their bodies remained still). At the beginning of each trial, the subject put the tip of his index on the disk representing the starting position. The computer screen displayed the via-points and the target. The subject was then asked to guide his index through the via-points and reach the target while always keeping the tip of his index on the plastic pane. He was asked to monitor only the tip of his index, and not to care about e.g. the orientation of the finger. A light-reflective marker was attached to the tip of the index. The position of this marker was recorded with the infrared camera system described in the General Methodology (chapter 4).

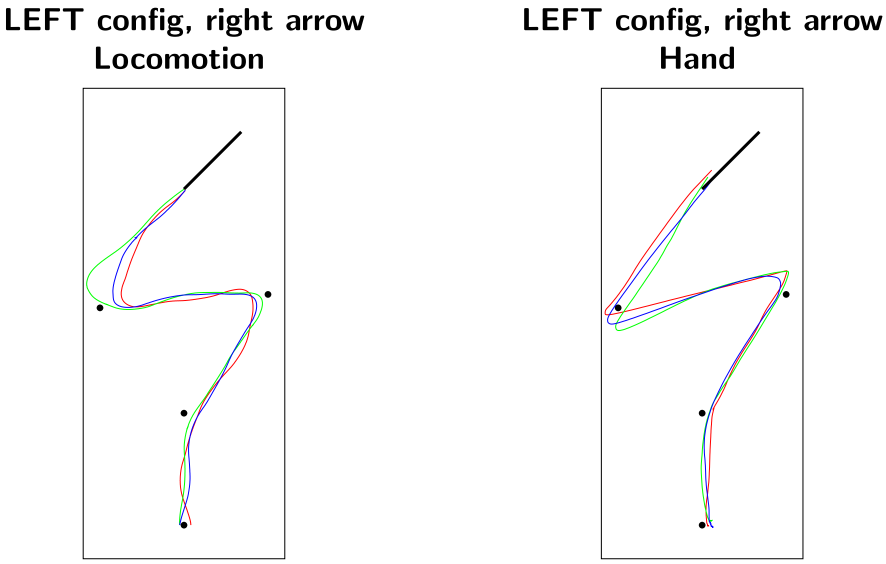

Figure 3: Some preliminary results of the hand/locomotion comparison. One can observe a global similarity of the hand and the locomotor trajectories. However hand trajectories seem to be more “acute” than locomotor ones.

# Clinical and developmental aspects

All our experiments up to now have involved healthy adult subjects. Following our previous reflections on clinical studies, it would be interesting to assess how the stereotypy or the optimality of the locomotor behavior are affected in patients with motor or cognitive deficits. As argued previously, this would provide further insights into the neural structures underlying the planning and control of locomotor trajectories. Conversely, in a medical perspective, our results on the stereotypy and the smoothness of trajectories may also help design new tests for detecting and evaluating locomotor disorders.

Studying how and when these features are acquired in children is another promising extension of our study. Indeed, such a developmental approach has provided precious insights into the origin and the nature of several “laws” underlying human movements [see for instance the developmental study of the “one-third power law” in Viviani and Schneider (1991) or of the steering behavior in Grasso et al. (1998a)].

In fact, we are currently involved in a study headed by D$^{\text{r}}$ V. Belmonti (Department of Developmental Neuroscience, University of Pisa, Italy), which involves children from 5 to 12 years old, some of whom are affected by spastic bilateral cerebral palsy (in particular, spastic diplegia). This neurological disorder is associated with motor, and sometimes, mental troubles of varying degrees.

In the pilot experiment, the subjects (one diplegic subject aged 6 and three normal subjects aged 6 to 12) were asked to walk out of a corridor towards one of three spatial targets (Fig. 4). This protocol was very similar to those of our Experiments 1 to 5 (see chapters 5) and 6. The target was illuminated either at the beginning of the trial (LighPre) or just as the subject got out of the corridor (LightPost). In addition, the experimenter either walked behind the subject (Touch) or let the subject walk alone (NoTouch). Clinical experiments have indeed shown that some of these children can improve their locomotion if lightly touched or even just followed by an adult. This finding seems to point to perceptual and cognitive factors affecting motor performance in cerebral palsy, which represents a supplementary motivation for our approach.

Figure 4: A diplegic subject executing the goal-oriented locomotor task (condition LightPre/NoTouch). Photo courtesy of D$^{r}$ V. Belmonti, University of Pisa, Italy.

Fig. 5 shows the trajectories of a 6 years old diplegic subject and of three normal subjects, aged 6 to 12 in the four conditions (LightPre/Touch, LightPre/NoTouch, LightPost/Touch, LightPost/NoTouch).

One can observe from these preliminary results that the trajectories of the diplegic subject were somewhat jerkier than those of the normal subject at the same age. In addition, the smoothness of the trajectory also seemed to increase with age.

We are now proceeding to run the full experiment, which will involve more subjects and test more repetitions per subject. This will allow us

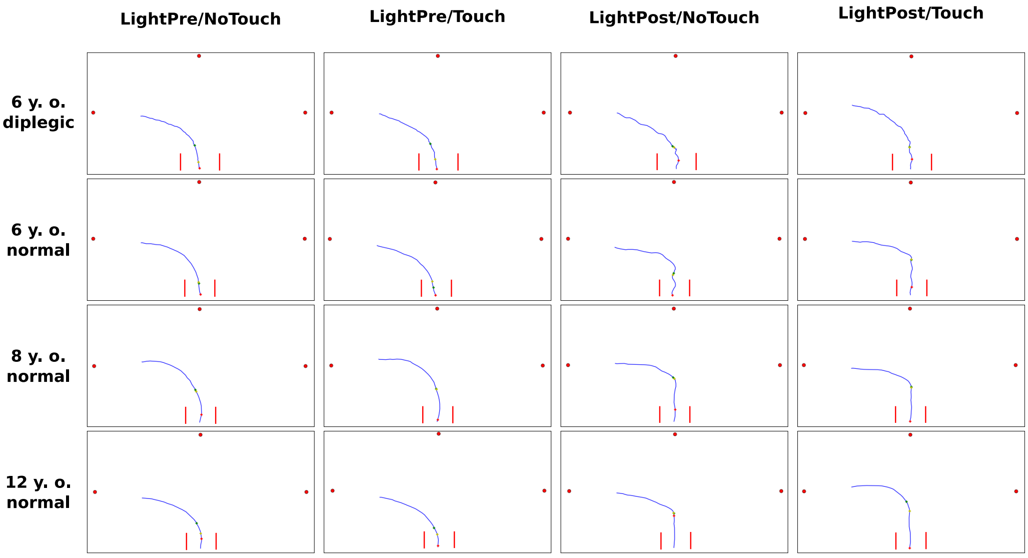

Figure 5: Trajectories of diplegic and normal children aged 6 to 12 in a goal-oriented task. The subjects had to walk out of the corridor (indicated by the parallel lines) towards one of the three targets (indicated by small disks). Plots courtesy of D$^{r}$ V. Belmonti, University of Pisa, Italy.

examining whether the previous preliminary observations are confirmed on a larger scale. We shall also be able to study the intra-subject variability profiles with better reliability.

# Robotics applications

Research in motor control has greatly benefited from ideas originally developped in mechanical engineering or robotics. In fact, the field of "computational motor control" can be considered as the application of control theory to biological systems. In particular, many concepts used in the present work, such as redundancy, optimal control, open-loop and feedbacks processes, etc. are direct translations of the respective control theory notions. Regarding more precisely human locomotion, the recent developments of humanoid robotics have provided physiologists with some new and exciting ideas: for instance, the efficiency of *passive-dynamics* walking robots suggests the importance of passive-dynamics in human locomotion (see a review by Collins et al., 2005, and Fig. 6).

Conversely, roboticists have recently begun to take inspiration from biological systems to build efficient and adaptive robots. To stay within the field of locomotion, one can mention the salamander-like robot constructed

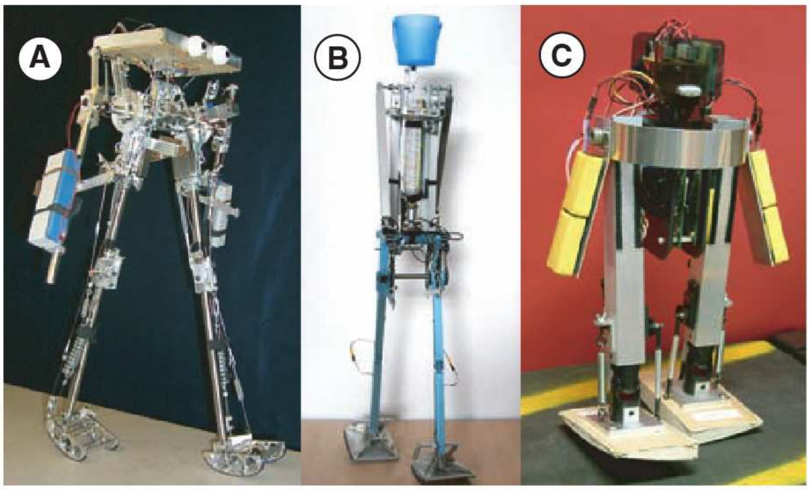

Figure 6: Three passive-dynamics bipedal robots (adapted from Collins et al., 2005).

by Ijspeert et al. (2007), who used coupled Central Pattern Generators (see our review of CPGs in section 2.1.1) to generate highly adaptive swimming and walking patterns (Fig. 7). Regarding more precisely bipedal locomotion, one can mention for example Manoonpong et al. (2007), who took inspiration from the neural architecture controlling human locomotion in the design of a bipedal robot (Fig. 8). In this context, are our results on the trajectory-level, “top-down” control of locomotion (chapter 5), on the optimal control of locomotor trajectories (chapters 8 and 9) or on the steering behavior (section 7.1) of any help in the conception of walking humanoid robots? Addressing this question is the focus of our future investigations.

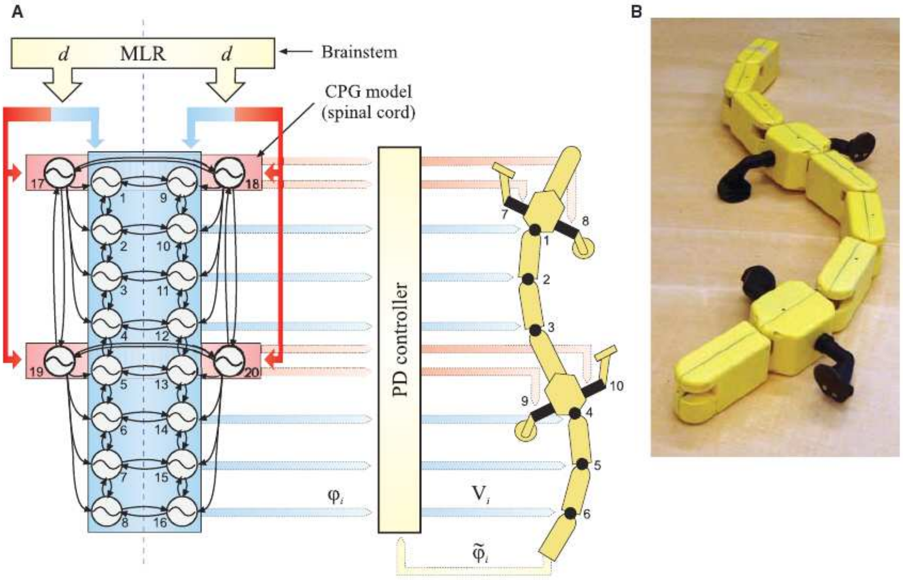

Figure 7: A CPG-based salamander-like robot. (**A**) the control architecture based on coupled CPGs. (**B**) photo of the robot (adapted from Ijspeert et al., 2007).

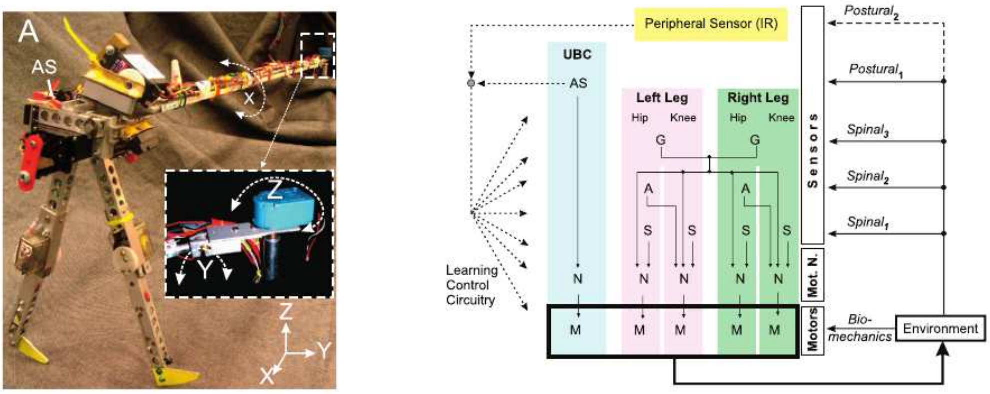

Figure 8: A bipedal robot with a human-inspired control architecture (adapted from Manoonpong et al., 2007).

# Bibliography

Arechavaleta, G., Laumond, J.-P., Hicheur, H., and Berthoz, A. (2006). The non-holonomic nature of human locomotion: a modeling study. In *Proceedings of the IEEE/RAS-EMBS International Conference on Biomedical Robots and Biomechatronics*.

Arechavaleta, G., Laumond, J.-P., Hicheur, H., and Berthoz, A. (2008a). On the nonholonomic nature of human locomotion. *Autonomous Robots*, 25(1):25–35.

Arechavaleta, G., Laumond, J.-P., Hicheur, H., and Berthoz, A. (2008b). An optimality principle governing human walking. *IEEE Transactions on Robotics*, 24(1):5–14.

Atkeson, C. G. and Hollerbach, J. M. (1985). Kinematic features of unrestrained vertical arm movements. *J Neurosci*, 5(9):2318–30.

Bennequin, D., Fuchs, R., Berthoz, A., and Flash, T. (2009). Movement timing and invariance arise from several geometries. *PLoS Comput Biol*, 5(7):e1000426.

Bernstein, N. (1967). *The Coordination and Regulation of Movements.* Pergamon Press, Oxford.

Berthoz, A. (1991). Reference frames for the perception and control of movement. In Paillard, J., editor, *Brain & Space.* Oxford University Press.

Berthoz, A. (1997). *Le sens du mouvement.* Odile Jacob, Paris.

Berthoz, A. (2009). *La simplexité.* Odile Jacob, Paris.

Berthoz, A., Amorim, M.-A., Glasauer, S., Grasso, R., Takei, Y., and Viaud-Delmon, I. (1999). Dissociation between distance and direction during locomotor navigation. In Golledge, R. G., editor, *Wayfinding behavior: cognitive mapping and other spatial processes.* John Hopkins University Press.

Berthoz, A. and Petit, J.-L. (2009). *Phénoménologie et physiologie de l'action*. Odile Jacob, Paris.

Berthoz, A. and Viaud-Delmon, I. (1999). Multisensory integration in spatial orientation. *Curr Opin Neurobiol*, 9(6):708–12.

Burgess, N., Maguire, E. A., and O'Keefe, J. (2002). The human hippocampus and spatial and episodic memory. *Neuron*, 35(4):625–41.

Capaday, C. (2002). The special nature of human walking and its neural control. *Trends Neurosci*, 25(7):370–6.

Collins, S., Ruina, A., Tedrake, R., and Wisse, M. (2005). Efficient bipedal robots based on passive-dynamic walkers. *Science*, 307(5712):1082–5.

Courtine, G. and Schieppati, M. (2003). Human walking along a curved path. I. Body trajectory, segment orientation and the effect of vision. *Eur J Neurosci*, 18(1):177–90.

Engelbrecht, S. (2001). Minimum principles in motor control. *J Math Psychol*, 45(3):497–542.

Faisal, A. A., Selen, L. P. J., and Wolpert, D. M. (2008). Noise in the nervous system. *Nat Rev Neurosci*, 9(4):292–303.

Fajen, B. R. and Warren, W. H. (2003). Behavioral dynamics of steering, obstacle avoidance, and route selection. *J Exp Psychol Hum Percept Perform*, 29(2):343–62.

Fajen, B. R. and Warren, W. H. (2007). Behavioral dynamics of intercepting a moving target. *Exp Brain Res*, 180(2):303–19.

Farrell, M. and Thomson, J. (1999). On-line updating of spatial information druing locomotion without vision. *J Mot Behav*, 31(1):39–53.

Fitts, P. M. (1954). The information capacity of the human motor system in controlling the amplitude of movement. *J Exp Psychol*, 47(6):381–91.

Fitzpatrick, R. C., Wardman, D. L., and Taylor, J. L. (1999). Effects of galvanic vestibular stimulation during human walking. *J Physiol*, 517 ( Pt 3):931–9.

Flash, T. and Hogan, N. (1985). The coordination of arm movements: an experimentally confirmed mathematical model. *J Neurosci*, 5(7):1688–703.

Georgopoulos, A. P., Kalaska, J. F., and Massey, J. T. (1981). Spatial trajectories and reaction times of aimed movements: effects of practice, uncertainty, and change in target location. *J Neurophysiol*, 46(4):725–43.

Glasauer, S., Amorim, M.-A., Viaud-Delmon, I., and Berthoz, A. (2002). Differential effects of labyrinthine dysfunction on distance and direction during blindfolded walking of a triangular path. *Exp Brain Res*, 145(4):489–97.

Glasauer, S., Amorim, M. A., Vitte, E., and Berthoz, A. (1994). Goal-directed linear locomotion in normal and labyrinthine-defective subjects. *Exp Brain Res*, 98(2):323–35.

Grasso, R., Assaiante, C., Prévost, P., and Berthoz, A. (1998a). Development of anticipatory orienting strategies during locomotor tasks in children. *Neurosci Biobehav Rev*, 22(4):533–9.

Grasso, R., Bianchi, L., and Lacquaniti, F. (1998b). Motor patterns for human gait: backward versus forward locomotion. *J Neurophysiol*, 80(4):1868–85.

Grasso, R., Glasauer, S., Takei, Y., and Berthoz, A. (1996). The predictive brain: anticipatory control of head direction for the steering of locomotion. *Neuroreport*, 7(6):1170–4.

Grasso, R., Prévost, P., Ivanenko, Y. P., and Berthoz, A. (1998c). Eye-head coordination for the steering of locomotion in humans: an anticipatory synergy. *Neurosci Lett*, 253(2):115–8.

Grillner, S. (2003). The motor infrastructure: from ion channels to neuronal networks. *Nat Rev Neurosci*, 4(7):573–86.

Grillner, S., Deliagina, T., Ekeberg O, el Manira, A., Hill, R. H., Lansner, A., Orlovsky, G. N., and Wallén, P. (1995). Neural networks that coordinate locomotion and body orientation in lamprey. *Trends Neurosci*, 18(6):270–9.

Harris, C. M. (2004). Exploring smoothness and discontinuities in human motor behaviour with Fourier analysis. *Math Biosci*, 188:99–116.

Harris, C. M. and Harwood, M. R. (2005). Boundary conditions in human movement. In *Proceedings of the IASTED International Conference on Biomedical Engineering*. Acta Press.

Harris, C. M. and Wolpert, D. M. (1998). Signal-dependent noise determines motor planning. *Nature*, 394(6695):780–4.

Hicheur, H. (2006). *Contrôle et guidage de la locomotion humaine*. PhD thesis, Université Pierre et Marie Curie - Paris VI.

Hicheur, H. and Berthoz, A. (2005). How do humans turn? Head and body movements for the steering of locomotion. In *Fifth IEEE-RAS International Conference on Humanoid Robots*.

Hicheur, H., Glasauer, S., Vieilledent, S., and Berthoz, A. (2005a). Head direction control during active locomotion in humans. In *Head Direction Cells and the Neural Mechanisms of Spatial Orientation*, pages 383–408. MIT Press, Cambridge, MA.

Hicheur, H., Pham, Q.-C., Arechavaleta, G., Laumond, J.-P., and Berthoz, A. (2007). The formation of trajectories during goal-oriented locomotion in humans. I. A stereotyped behaviour. *Eur J Neurosci*, 26(8):2376–90.

Hicheur, H., Terekhov, A. V., and Berthoz, A. (2006). Intersegmental coordination during human locomotion: does planar covariation of elevation angles reflect central constraints? *J Neurophysiol*, 96(3):1406–19.

Hicheur, H., Vieilledent, S., and Berthoz, A. (2005b). Head motion in humans alternating between straight and curved walking path: combination of stabilizing and anticipatory orienting mechanisms. *Neurosci Lett*, 383(1-2):87–92.

Hicheur, H., Vieilledent, S., Richardson, M. J. E., Flash, T., and Berthoz, A. (2005c). Velocity and curvature in human locomotion along complex curved paths: a comparison with hand movements. *Exp Brain Res*, 162(2):145–54.

Hoff, B. and Arbib, M. (1993). Models of trajectory formation and temporal interaction of reach and grasp. *J Mot Behav*, 25(3):175–192.

Hogan, N. (1984). An organizing principle for a class of voluntary movements. *J Neurosci*, 4(11):2745–54.

Hollands, M. A., Sorensen, K. L., and Patla, A. E. (2001). Effects of head immobilization on the coordination and control of head and body reorientation and translation during steering. *Exp Brain Res*, 140(2):223–33.

Ijspeert, A. J., Crespi, A., Ryczko, D., and Cabelguen, J.-M. (2007). From swimming to walking with a salamander robot driven by a spinal cord model. *Science*, 315(5817):1416–20.

Imai, T., Moore, S. T., Raphan, T., and Cohen, B. (2001). Interaction of the body, head, and eyes during walking and turning. *Exp Brain Res*, 136(1):1–18.

Jordan, M. I. and Wolpert, D. M. (1999). Computational motor control. In *The Cognitive Neurosciences*, pages 601–620. MIT Press, Cambridge (MA).

Lacquaniti, F., Terzuolo, C., and Viviani, P. (1983). The law relating the kinematic and figural aspects of drawing movements. *Acta Psychol (Amst)*, 54(1-3):115–30.

Land, M. and Lee, D. (1994). Where we look when we steer. *Nature*, 369:742–744.

Laumond, J.-P. (1998). *Robot Motion Planning and Control.* Springer-Verlag, New York.

Lénine, V. I. (1908). *Matérialisme et empiriocriticisme.* Éditions sociales (French translation, 1948), Paris.

Liu, D. and Todorov, E. (2007). Evidence for the flexible sensorimotor strategies predicted by optimal feedback control. *J Neurosci*, 27(35):9354–68.

Loomis, J. M., Da Silva, J. A., Fujita, N., and Fukusima, S. S. (1992). Visual space perception and visually directed action. *J Exp Psychol Hum Percept Perform*, 18(4):906–21.

Loomis, J. M., Klatzky, R. L., Golledge, R. G., Cicinelli, J. G., Pellegrino, J. W., and Fry, P. A. (1993). Nonvisual navigation by blind and sighted: assessment of path integration ability. *J Exp Psychol Gen*, 122(1):73–91.

Loomis, J. M., Klatzky, R. L., Golledge, R. G., and Philbeck, J. W. (1999). Human navigation by path integration. In *Wayfinding behavior: cognitive mapping and other spatial processes.* John Hopkins University Press.

Manoonpong, P., Geng, T., Kulvicius, T., Porr, B., and Wörgötter, F. (2007). Adaptive, fast walking in a biped robot under neuronal control and learning. *PLoS Comput Biol*, 3(7):e134.

McIntyre, J., Stratta, F., and Lacquaniti, F. (1997). Viewer-centered frame of reference for pointing to memorized targets in three-dimensional space. *J Neurophysiol*, 78(3):1601–18.

Mittelstaedt, M. L. and Mittelstaedt, H. (2001). Idiothetic navigation in humans: estimation of path length. *Exp Brain Res*, 139(3):318–32.

Morasso, P. (1981). Spatial control of arm movements. *Exp Brain Res*, 42(2):223–7.

Olivier, A.-H. and Cretual, A. (2007). Velocity/curvature relations along a single turn in human locomotion. *Neurosci Lett*, 412(2):148–53.

Papaxanthis, C., Dubost, V., and Pozzo, T. (2003). Similar planning strategies for whole-body and arm movements performed in the sagittal plane. *Neuroscience*, 117(4):779–83.

Patla, A. E., Adkin, A., and Ballard, T. (1999a). Online steering: coordination and control of body center of mass, head and body reorientation. *Exp Brain Res*, 129(4):629–34.

Patla, A. E., Prentice, S. D., Rietdyk, S., Allard, F., and Martin, C. (1999b). What guides the selection of alternate foot placement during locomotion in humans. *Exp Brain Res*, 128(4):441–50.

Pham, Q.-C., Berthoz, A., and Hicheur, H. (2010). The influence of vision and gait direction on the formation of locomotor trajectories and the anticipatory steering behaviors. *Submitted to Exp Brain Res.*

Pham, Q.-C. and Hicheur, H. (2009). On the open-loop and feedback processes that underlie the formation of trajectories during visual and nonvisual locomotion in humans. *J Neurophysiol*, 102(5):2800–15.

Pham, Q.-C., Hicheur, H., Arechavaleta, G., Laumond, J.-P., and Berthoz, A. (2007). The formation of trajectories during goal-oriented locomotion in humans. II. A maximum smoothness model. *Eur J Neurosci*, 26(8):2391–403.

Poincaré, H. (1902). *La science et l'hypothèse.* Flammarion, Paris.

Poincaré, H. (1905). *La valeur de la science.* Flammarion, Paris.

Pollick, F. E. and Sapiro, G. (1997). Constant affine velocity predicts the 1/3 power law of planar motion perception and generation. *Vision Res*, 37(3):347–53.

Prévost, P., Ivanenko, Y., Grasso, R., and Berthoz, A. (2003). Spatial invariance in anticipatory orienting behaviour during human navigation. *Neurosci Lett*, 339(3):243–7.

Richardson, M. J. E. and Flash, T. (2002). Comparing smooth arm movements with the two-thirds power law and the related segmented-control hypothesis. *J Neurosci*, 22(18):8201–11.

Rieser, J. J., Ashmead, D. H., Talor, C. R., and Youngquist, G. A. (1990). Visual perception and the guidance of locomotion without vision to previously seen targets. *Perception*, 19(5):675–89.

Schaal, S. and Sternad, D. (2001). Origins and violations of the 2/3 power law in rhythmic three-dimensional arm movements. *Exp Brain Res*, 136(1):60–72.

Schmidt, R. A., Zelaznik, H., Hawkins, B., Frank, J. S., and Quinn, J. J. T. (1979). Motor-output variability: a theory for the accuracy of rapid motor acts. *Psychol Rev*, 47(5):415–51.

Shadmehr, R. and Krakauer, J. W. (2008). A computational neuroanatomy for motor control. *Exp Brain Res*, 185(3):359–81.

Shadmehr, R. and Mussa-Ivaldi, F. A. (1994). Adaptive representation of dynamics during learning of a motor task. *J Neurosci*, 14(5 Pt 2):3208–24.

Shik, M. L. and Orlovsky, G. N. (1976). Neurophysiology of locomotor automatism. *Physiol Rev*, 56(3):465–501.

Takei, Y., Grasso, R., and Berthoz, A. (1996). Quantitative analysis of human walking trajectory on a circular path in darkness. *Brain Res Bull*, 40(5-6):491–5; discussion 495–6.

Tanaka, H., Krakauer, J. W., and Qian, N. (2006). An optimization principle for determining movement duration. *J Neurophysiol*, 95(6):3875–86.

Thomson, J. A. (1983). Is continuous visual monitoring necessary in visually guided locomotion? *J Exp Psychol Hum Percept Perform*, 9(3):427–43.

Thorstensson, A. (1986). How is the normal locomotor program modified to produce backward walking? *Exp Brain Res*, 61(3):664–8.

Todorov, E. (2004). Optimality principles in sensorimotor control. *Nat Neurosci*, 7(9):907–15.

Todorov, E. and Jordan, M. I. (1998). Smoothness maximization along a predefined path accurately predicts the speed profiles of complex arm movements. *J Neurophysiol*, 80(2):696–714.

Todorov, E. and Jordan, M. I. (2002). Optimal feedback control as a theory of motor coordination. *Nat Neurosci*, 5(11):1226–35.

Uno, Y., Kawato, M., and Suzuki, R. (1989). Formation and control of optimal trajectory in human multijoint arm movement. minimum torque-change model. *Biol Cybern*, 61(2):89–101.

Vallis, L. A. and Patla, A. E. (2004). Expected and unexpected head yaw movements result in different modifications of gait and whole body coordination strategies. *Exp Brain Res*, 157(1):94–110.

Vallis, L. A., Patla, A. E., and Adkin, A. L. (2001). Control of steering in the presence of unexpected head yaw movements. influence on sequencing of subtasks. *Exp Brain Res*, 138(1):128–34.

van Beers, R. J., Haggard, P., and Wolpert, D. M. (2004). The role of execution noise in movement variability. *J Neurophysiol*, 91(2):1050–63.

Vieilledent, S., Kerlirzin, Y., Dalbera, S., and Berthoz, A. (2001). Relationship between velocity and curvature of a human locomotor trajectory. *Neurosci Lett*, 305(1):65–9.

Vieilledent, S., Kosslyn, S. M., Berthoz, A., and Giraudo, M. D. (2003). Does mental simulation of following a path improve navigation performance without vision? *Brain Res Cogn Brain Res*, 16(2):238–49.

Viviani, P. and Flash, T. (1995). Minimum-jerk, two-thirds power law, and isochrony: converging approaches to movement planning. *J Exp Psychol Hum Percept Perform*, 21(1):32–53.

Viviani, P. and Schneider, R. (1991). A developmental study of the relationship between geometry and kinematics in drawing movements. *J Exp Psychol Hum Percept Perform*, 17(1):198–218.

Viviani, P. and Stucchi, N. (1992). Biological movements look uniform: evidence of motor-perceptual interactions. *J Exp Psychol Hum Percept Perform*, 18(3):603–23.

Winter, D. A. and Eng, P. (1995). Kinetics: our window into the goals and strategies of the central nervous system. *Behav Brain Res*, 67(2):111–20.

# Appendix:
# Original manuscripts

This Appendix reproduces the articles written during my thesis. Part A contains the “human locomotion” articles whose contents have been presented in the previous chapters. Part B contains the “contraction theory” articles that I have worked on during my thesis, as part of another project.

# Contents

# Appendix A

# Human locomotion articles

## A.1 The Formation of Trajectories during Goal-Oriented Locomotion in Humans. I. A Stereotyped Behavior.

By H. Hicheur, Q.-C. Pham, G. Arechavaleta, J.-P. Laumond and A. Berthoz. Published in *European Journal of Neuroscience*, vol. 26, pp. 2376-2390, 2007.

*European Journal of Neuroscience, Vol. 26, pp. 2376–2390, 2007* doi:10.1111/j.1460-9568.2007.05836.x

# The formation of trajectories during goal-oriented locomotion in humans. I. A stereotyped behaviour

Halim Hicheur,[1] Quang-Cuong Pham,[1] Gustavo Arechavaleta,[2] Jean-Paul Laumond[2] and Alain Berthoz[1]
[1]Laboratoire de Physiologie de la Perception et de l'Action, Collège de France CNRS UMR7152, 11 place Marcelin Berthelot, 75005 Paris, France
[2]LAAS-CNRS, 7 avenue du Colonel Roche, 31077 Toulouse, France, LPPA, Collège de France-CNRS, 11 place Marcelin Berthelot 75005 Paris, France

*Keywords*: control strategy, human locomotion, planning, step, stereotypy, trajectory

## Abstract

Human locomotion was investigated in a goal-oriented task where subjects had to walk to and through a doorway starting from a fixed position and orientation in space. The door was located at different positions and orientations in space, resulting in a total of 40 targets. While no specific constraint was provided to subjects in terms of the path they were to follow or the expected walking speeds, all of them generated very similar trajectories in terms of both path geometry and velocity profiles. These results are reminiscent of the stereotyped properties of the hand trajectories observed in arm reaching movements in studies over the last 20 years. This observation supports the hypothesis that common constraining mechanisms govern the generation of segmental and whole-body trajectories. In contrast, we observed that the subjects placed their feet at different spatial positions across repetitions, making unlikely the hypothesis that goal-oriented locomotion is planned as a succession of steps. Rather, our results suggest that common planning and/or control strategies underlie the formation of the whole locomotor trajectory during a spatially oriented task.

## Introduction

When moving from a point A to point B in space, a great variety of trajectories can be taken. Even for a single (successful) trajectory, a theoretically infinite number of motor behaviours can be implemented by the motor system (a notion known as 'motor redundancy'). As the generation of a single motor behaviour is associated with several levels of description, the elaboration of the motor command appears to be a particularly complex problem. Indeed, a great number of kinematic patterns (the velocity profiles of the segments involved in the task, for instance), dynamic patterns (the patterns of forces required to move these segments), myoelectric patterns (the muscular activation patterns producing these forces) or neuronal discharge pattern (the motor units innervating the muscles) may be combined for the generation of the successful motor behaviour (see Wolpert, 1997, for a review). In the case of multijoint movements, the problem becomes even more complex as the high dimensionality of the system results in an increased motor redundancy.

In contrast with this theoretical complexity, it has been experimentally observed that the arm reaching movements exhibit several motor invariants which are systematically reproduced by different subjects across repetitions. In this type of task, hand trajectories have been found to be highly stereotyped and particularly smooth. They are also marked by bell-shaped velocity profiles (for review see Bullock & Grossberg, 1988) and by a specific relation between path curvature and hand velocity, known as the two-thirds power law (Lacquaniti *et al*., 1983). The observation that hand trajectories exhibit many invariants in different motor tasks (in contrast with much more variable joint angular profiles) led Morasso (1981) to propose that the central command underlying arm pointing movements is formulated in terms of hand trajectories in space. The kinematic nature of the control of arm movements was then associated with the notion of end-point movement control. However, the distinction between the different kinematic coordinates in which the CNS may encode (for instance) the direction of movement is still an open question (Soechting & Flanders, 1994).

The existence of such robust invariant features of motor execution was proposed as being the product of general principles governing movement execution. Among these principles, the optimal nature of motor control in biological systems was emphasized and minimizing cost functions were systematically used in computational approaches of movement learning and control (Todorov, 2004). These aspects are detailed in the companion paper.

In contrast with the numerous behavioural and computational studies devoted to the understanding of the trajectories in arm movements in humans, the generation and the control of whole-body displacements in space has received little attention. However, in addition to its purely sensorimotor component, locomotion also must be understood and analysed as a spatially oriented activity requiring navigational guidance. It immediately follows that characterizing locomotion at the level of trajectory is of crucial interest. Recent studies have assessed the vestibular contribution to the control of direction and distance during human locomotion (Glasauer *et al*., 2002), multisensory contributions to the control of walking along a straight trajectory (Kennedy *et al*., 2003) and the nature of the visual strategies governing the steering of

---

*Correspondence*: Dr Halim Hicheur, as above.
E-mail: halim.hicheur@college-de-france.fr

*Received 01 March 2007, revised 16 August 2007, accepted 20 August 2007*

locomotion (Warren *et al*., 2001; Wilkie & Wann, 2006). Recently, we examined the principles underlying the control of locomotor trajectories by testing the hypothesis that common principles govern the generation of hand and whole-body trajectories (Hicheur *et al*., 2005b). In tasks where subjects had to walk along different types of curved paths, we observed a strong correlation between path curvature and walking velocity reminiscent of the power law observed for hand movements (Lacquaniti *et al*., 1983), but with significant deviations from the two-thirds exponent. We discussed the functional significance of our results by taking into account both the central and peripheral mechanisms that might account for the close relationships between path geometry and trajectory kinematics observed during human locomotion. It should be noted that these observations were restricted to a steering task where subjects had to walk along predefined paths.

Here, we investigated the generation of whole-body trajectories in a simple goal-oriented task. We wanted to examine whether the locomotor behaviour, analysed at the level of the step and at the level of the trajectory, exhibit motor invariants as observed in arm reaching movements. As locomotion is a motor activity mobilizing all the body segments, the locomotor systems are of a higher dimensionality and the redundancy of the motor solutions allowing the displacement of the whole body towards the spatial target is theoretically greater than that of arm movements. Nevertheless, a first reason explaining why such different movements (arm movements and locomotion) might share common principles was suggested by Georgopoulos & Grillner (1989). These authors proposed an analogy between hand reaching tasks and accurate foot placement during locomotion: in order to perform the visuomotor coordination in these two contexts, the same neural structures seem to be involved in the accurate positioning of the limb. The generation of the limb trajectory would thus be realised according to common mechanisms. In the case of goal-oriented locomotion, and following this suggestion, it is possible to hypothesize that the trajectory of the whole body could be built as a sequence of foot 'pointings' on the ground.

The purpose of the current study was to describe the spatial and temporal features of the locomotor trajectories. In particular, we tested the hypothesis that, as for hand movements, the body trajectories in space exhibit geometric and kinematic stereotypy while various motor strategies can be implemented for reaching the desired goal. To do this, we designed a goal-oriented locomotor task similar to a 'walking towards and through a distant doorway' situation. Subjects had to start from a fixed position and orientation in space and to walk throughout a door located at different positions and orientations in space.

This first manuscript presents numerous quantitative analyses showing that human locomotor trajectories are generated according to common spatial or temporal criteria. In the companion paper (Pham *et al*. 2007), we propose a computational approach for modelling the principles underlying the generation of locomotor trajectories.

## Materials and methods

### *Subjects: experimental setup*

Six healthy male subjects volunteered for participation in the experiments. Each of them generated 120 trajectories corresponding to 40 spatial targets × 3 trials so that a total of 720 trajectories (6 subjects × 120 trials) were recorded for the experiment (parts of the recorded data were used for a study presented at the IEEE BioRobotics conference, Pisa, Italy, 2006; see Arechavaleta *et al*., 2006). Subjects gave their informed consent prior to their inclusion in the study. Experiments conformed to the Code of Ethics of the Declaration of Helsinki. The mean age, height and weight of the subjects were, respectively, 26.00 ± 2.76 years, 1.80 ± 0.07 m and 72.8 ± 6.15 kg. Three-dimensional positions of light-reflective markers were recorded using an optoelectronic Vicon V8 motion-capture system wired to 24 cameras at a 120-Hz sampling frequency. Subjects were equipped with 39 markers of which 10 were directly used for the analysis. Three reflective markers were fixed on a helmet (∼ 200 g). The helmet was donned so that the midpoint between the two first markers was aligned with the head yaw rotation (naso-occipital) axis. Thus the line which indicates the head orientation passed through these two markers (Head Forward F and Backward B). To assess the body displacement in space we used the midpoint between left and right shoulder markers, which were located on left and right acromions, respectively (see Hicheur *et al*., 2005b). Two markers were located on the pelvis (left and right anterior superior iliac spines) and two markers were located on each foot: they were placed at the top of the foot (subjects were allowed to wear shoes) between toes 2 and 3 (1 is the big toe), and on the heel at the same height as toe marker. These markers were used for detecting the step events (explained below). We defined head, trunk, pelvis and trajectory reference frames as illustrated in Fig. 1A. Forty targets were used for the experiment: the target consisted of a doorway which was placed at a specific $(x,y)$ position in the motion-capture space with an orientation $\alpha$ (Fig. 1B and E). Four markers were rigidly fixed to the target and were recorded during the whole duration of all trials. This allowed us to verify that the position and the orientation of the door (for a given condition) were the same for all subjects.

### *Protocol*

The aim of this protocol was to study the locomotor trajectories generated by different subjects and to test whether these trajectories display properties similar to those reported for hand reaching movements.

Subjects had to start from a fixed position in the laboratory and walk toward and through the doorway (Fig. 1A). To verify that all subjects began the task in the same conditions we asked them to begin their walk 1 m before crossing the start line and with a body initial orientation which had to be approximately orthogonal to the $X$-axis of the laboratory. They were then completely free to choose their walking speed and no specific restriction was placed on them regarding the path to follow. They were not asked to stop walking after entering the doorway because this instruction could have biased their behaviour a few steps before reaching the door. Rather, they were left free either to directly come back to the starting position or to walk in the laboratory for several seconds before coming back to the starting position. Typically, subjects walked straight for a few metres (about four steps) after passing through the doorway before returning to the starting position. The experimenter stopped recording the movement of the subject a few metres after he passed through the door. The angular displacement of the body in space induced by the different orientations of the doorway (see Table 1) ranged between −150 and +150°. As subjects were carefully monitored during the session, the average distance (±SD, across all the recorded trajectories) between the actual and the imposed initial positions was 3.0 ± 2.5 cm, the average distance between the actual and the imposed final positions was 3.2 ± 2.2 cm, the average absolute difference between the actual and the imposed initial orientations was 9.6 ± 7.9° and the average absolute difference between the actual and the imposed final orientations was 5.9 ± 4.4°.

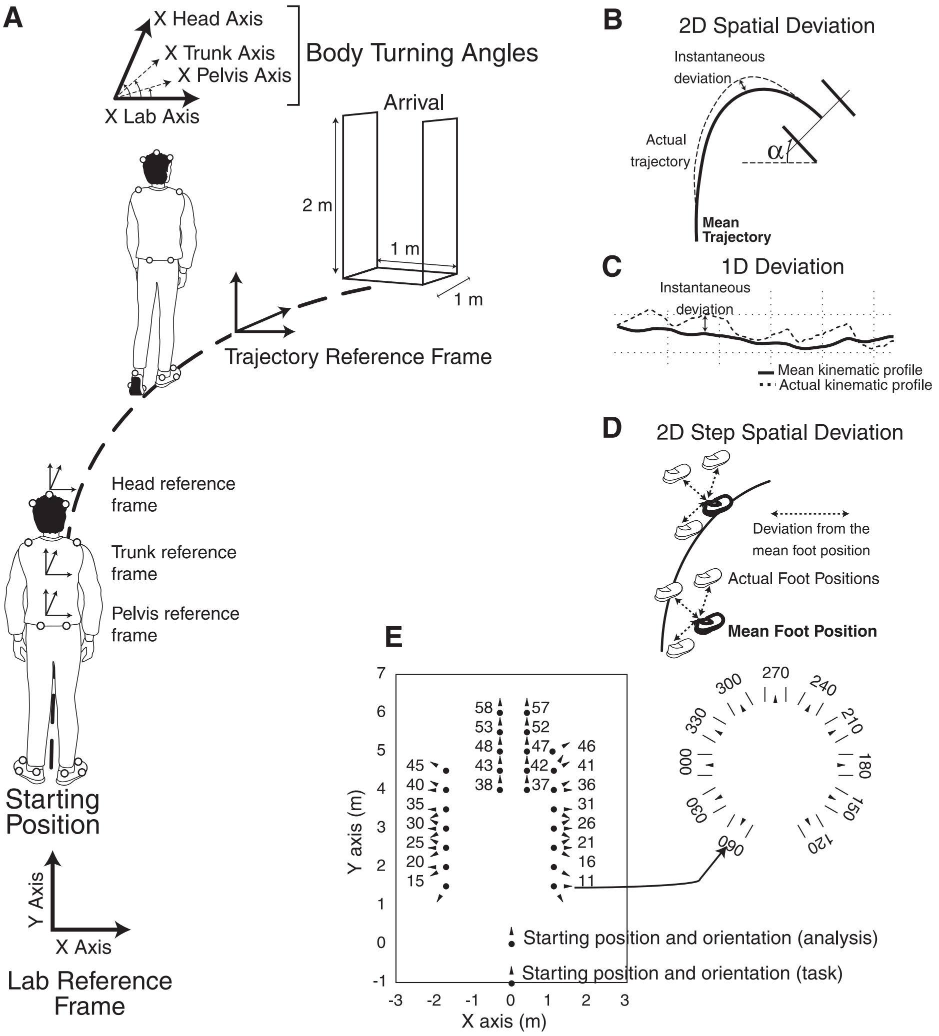

FIG. 1. (A) Experimental protocol: subjects had to start from a fixed position in the laboratory and to walk through a distant doorway. The position and the orientation α of the door were the two manipulated parameters and 40 combinations, position and orientation, were tested. (B) The spatial deviation of the actual trajectory from the mean trajectory was measured as the distance integrated over time between the mean (across subjects and trials) and the actual trajectories. (C) The variability of the velocity or turning profiles (kinematic profile) was measured as the deviation between the actual kinematic profile and the mean kinematic profile (across subjects and trials). (D) For different repetitions of a given condition, the spatial dispersion of the foot positions around the mean foot position was measured. (E) Spatial disposition of the 40 tested targets (see also Table 1). Each target position is represented by a small black disk. The possible target orientations for each target position are indicated by arrows.

### *Analysis*

In this study, we wanted to understand whether whole-body trajectories are organised according to common spatial or temporal criteria across different subjects during goal-oriented locomotion. We therefore focused on two levels of description of the locomotor behaviour. Firstly, we examined the geometric and kinematic properties of the locomotor trajectories in order to characterize the spatial control of the whole-body movement. This approach can be associated with the notion of end-point trajectory control. Secondly, we studied in detail the succession of locomotor cycles. This approach tests whether locomotion is planned as a succession of discrete cycles from which emerges the global trajectory.

### *Categorization and computation of the trajectories*

The tested trajectories were classified into four categories according to the amount of body turn they required: quasi-straight trajectories (ST), and trajectories of low (LC), medium (MC) and high (HC) curvature (see Table 1).

The total distances travelled by subjects ranged between 4.50 ± 0.25 m (across subjects and trials) for the nearest target and 9.38 ± 2.54 m for the furthest target. However, in order to compare the different trajectories with precise criteria, the final calculation of the travelled distance was performed between the instant $t_0$ where subjects crossed over the $X$-axis and the instant $t_1$ where they entered the doorway, according to the task requirements (the final position was calculated at the instant where the body crossed over the middle of the door). This method yielded values of trajectory length between 2.03 ± 0.08 and 6.46 ± 0.01 m (across subjects and trials). The individual values (across subjects and trials, for each tested target), in terms of trajectory length, duration and average walking speed, are presented for the 40 targets according to each category in Table 1.

After this procedure, and for each target, the trajectories were time-resampled so that for all subjects and trials of the same target,

TABLE 1. Mean values across six subjects and three trials, in terms of turn amplitude, travelled distance, duration and walking speed for each particular target and for each target category

| Trajectory groups | Target position* | Target orientation* | Turn (°) | Distance (m) | Duration (s) | Speed (m/s) |
|---|---|---|---|---|---|---|
| HC | 11 | 120 | −150 | 2.90 ± 0.18 | 2.66 ± 0.29 | 1.09 ± 0.06 |
| HC | 15 | 060 | 150 | 3.17 ± 0.29 | 2.71 ± 0.39 | 1.18 ± 0.07 |
| HC | 16 | 150 | −120 | 2.98 ± 0.16 | 2.65 ± 0.27 | 1.13 ± 0.07 |
| HC | 20 | 030 | 120 | 3.28 ± 0.25 | 2.68 ± 0.40 | 1.23 ± 0.09 |
| HC | 21 | 150 | −120 | 3.47 ± 0.14 | 2.96 ± 0.28 | 1.18 ± 0.08 |
| HC | 25 | 030 | 120 | 3.77 ± 0.20 | 3.01 ± 0.33 | 1.26 ± 0.08 |
| HC | 26 | 150 | −120 | 4.02 ± 0.19 | 3.32 ± 0.29 | 1.21 ± 0.07 |
| HC | 30 | 030 | 120 | 4.23 ± 0.24 | 3.38 ± 0.43 | 1.27 ± 0.10 |
| HC | 31 | 150 | −120 | 4.52 ± 0.15 | 3.68 ± 0.31 | 1.24 ± 0.08 |
| HC | 35 | 030 | 120 | 4.76 ± 0.21 | 3.67 ± 0.34 | 1.30 ± 0.08 |
| Mean HC | | | | 3.71 ± 0.65 | 3.07 ± 0.41 | 1.21 ± 0.07 |
| MC | 11 | 180 | −90 | 2.03 ± 0.08 | 1.68 ± 0.19 | 1.21 ± 0.10 |
| MC | 20 | 000 | 90 | 2.97 ± 0.13 | 2.31 ± 0.26 | 1.29 ± 0.09 |
| MC | 21 | 180 | −90 | 3.11 ± 0.09 | 2.51 ± 0.26 | 1.25 ± 0.10 |
| MC | 25 | 000 | 90 | 3.40 ± 0.14 | 2.59 ± 0.27 | 1.32 ± 0.09 |
| MC | 26 | 180 | −90 | 3.60 ± 0.11 | 2.86 ± 0.25 | 1.26 ± 0.09 |
| MC | 30 | 000 | 90 | 3.89 ± 0.15 | 3.01 ± 0.30 | 1.30 ± 0.08 |
| MC | 31 | 180 | −90 | 4.10 ± 0.12 | 3.18 ± 0.29 | 1.30 ± 0.10 |
| MC | 35 | 000 | 90 | 4.39 ± 0.15 | 3.31 ± 0.34 | 1.34 ± 0.10 |
| MC | 36 | 180 | −90 | 4.60 ± 0.10 | 3.57 ± 0.30 | 1.30 ± 0.09 |
| MC | 40 | 000 | 90 | 4.87 ± 0.14 | 3.65 ± 0.30 | 1.34 ± 0.08 |
| Mean MC | | | | 3.70 ± 0.86 | 2.87 ± 0.61 | 1.29 ± 0.04 |
| LC | 21 | 210 | −60 | 2.81 ± 0.07 | 2.09 ± 0.22 | 1.36 ± 0.10 |
| LC | 25 | 330 | 60 | 3.10 ± 0.07 | 2.25 ± 0.13 | 1.38 ± 0.06 |
| LC | 26 | 210 | −60 | 3.31 ± 0.04 | 2.43 ± 0.18 | 1.37 ± 0.09 |
| LC | 30 | 330 | 60 | 3.58 ± 0.07 | 2.58 ± 0.20 | 1.39 ± 0.09 |
| LC | 36 | 210 | −60 | 4.33 ± 0.08 | 3.25 ± 0.31 | 1.34 ± 0.11 |
| LC | 40 | 330 | 60 | 4.55 ± 0.06 | 3.37 ± 0.27 | 1.36 ± 0.09 |
| LC | 41 | 210 | −60 | 4.84 ± 0.08 | 3.62 ± 0.23 | 1.34 ± 0.07 |
| LC | 41 | 240 | −30 | 4.66 ± 0.03 | 3.26 ± 0.24 | 1.44 ± 0.11 |
| LC | 45 | 330 | 60 | 5.06 ± 0.08 | 3.71 ± 0.32 | 1.37 ± 0.11 |
| LC | 46 | 210 | −60 | 5.36 ± 0.10 | 3.97 ± 0.33 | 1.36 ± 0.10 |
| Mean LC | | | | 4.16 ± 0.89 | 3.05 ± 0.66 | 1.37 ± 0.03 |
| ST | 37 | 270 | 0 | 3.97 ± 0.01 | 2.66 ± 0.16 | 1.50 ± 0.08 |
| ST | 38 | 270 | 0 | 3.96 ± 0.01 | 2.65 ± 0.12 | 1.50 ± 0.07 |
| ST | 42 | 270 | 0 | 4.47 ± 0.01 | 2.99 ± 0.24 | 1.50 ± 0.12 |
| ST | 43 | 270 | 0 | 4.47 ± 0.01 | 3.05 ± 0.21 | 1.47 ± 0.09 |
| ST | 47 | 270 | 0 | 4.98 ± 0.01 | 3.42 ± 0.20 | 1.46 ± 0.08 |
| ST | 48 | 270 | 0 | 4.98 ± 0.01 | 3.44 ± 0.26 | 1.45 ± 0.11 |
| ST | 52 | 270 | 0 | 5.97 ± 0.01 | 4.18 ± 0.15 | 1.43 ± 0.05 |
| ST | 53 | 270 | 0 | 5.98 ± 0.01 | 4.14 ± 0.25 | 1.45 ± 0.09 |
| ST | 57 | 270 | 0 | 6.45 ± 0.01 | 4.38 ± 0.25 | 1.48 ± 0.09 |
| ST | 58 | 270 | 0 | 6.46 ± 0.01 | 4.31 ± 0.22 | 1.50 ± 0.08 |
| Mean ST | | | | 5.17 ± 0.97 | 3.52 ± 0.68 | 1.47 ± 0.03 |

Mean values are ±SD. *See Fig. 1E for details of position and orientation). HC, high curvature; MC, medium curvature; LC, low curvature; ST, quasi-straight trajectory.

$t_0 = 0$ and $t_1 = 1$. This was done in order to compare the actual trajectories to the mean trajectory. The number of frames ($N_f$) of the re-sampled trajectories was chosen individually for each target across trials, as the $N_f$ contained in the trial (trajectory) with the shortest duration. Thus, all the trajectories recorded for a single target had the same $N_f$. A Matlab routine (Mathworks V6.5®) was then implemented in order to re-sample the individual trajectories according to this parameter: this routine consists of a linear interpolation of the new (re-sampled) trajectory using $N_f$ as the number of frames contained in this re-sampled trajectory.

After the 40 trajectories were sorted in the four categories, all the quantitative parameters (see below) were computed separately for each target. A mean value for each of these parameters was then calculated for each group of trajectories across the 10 targets (× 6 subjects × 3 trials) ranked in each category.

### *Spatial variability of the trajectories*

In order to examine the similarity in the time courses and forms of the trajectories produced by the different subjects, we computed the mean trajectory (across subjects and trials) and calculated, for each trajectory toward a given target, the deviation from the mean trajectory; this gave an index of the spatial variability in the trajectories (see Fig. 1C).

The averaged trajectory ($x_{av}(t)$,$y_{av}(t)$) was calculated as follows:

$$\left( x_{\text{av}}(t) = \frac{1}{N_f}\sum_{i=1}^{N_f} x_i(t), \quad y_{\text{av}}(t) = \frac{1}{N_f}\sum_{i=1}^{N_f} y_i(t) \right) \tag{1}$$

where $N_f$ is the number of frames contained in the re-scaled trajectory.

The trajectory deviation (TD) was computed as the sum of the instantaneous distances between the averaged ($x_{av}(t)$,$y_{av}(t)$) and the actual ($x_i(t)$,$y_i(t)$) trajectory, and was calculated as follows:

$$\mathrm{TD} = \sqrt{\frac{1}{N_f}\sum_{i=1}^{N_f}\left((x_i(t) - x_{\mathrm{av}}(t))^2 + (y_i(t) - y_{\mathrm{av}}(t))^2\right)} \qquad (2)$$

The averaged and maximal deviations between the actual trajectories and the mean trajectory are denoted ATD and MTD, respectively. This procedure was repeated for each of the 40 tested targets.

### Spatial variability of the foot placements

We examined the pattern of foot positions from the beginning of the task until the subjects reached the goal. To this purpose, we first detected the successive steps performed by subjects before computing the variability in the foot locations ($(x_f(t), y_f(t))$) across the different repetitions of the same subject. We used heel-strike and toe-off events for defining steps (Hicheur *et al.*, 2006). These events were derived from the time course of heel and toe $Z$-position profiles and correspond to the local minima of these two signals. We considered one step as the interval separating two successive heel strikes of the same foot and computed the foot positions at these particular events.

A first type of intersubject variability was observed at the level of the foot placements during the task because of the anatomical differences between the subjects (as presented before, they had different heights and this resulted in different step lengths). In the present analysis, we did not consider the intersubject differences (which considerably increased the magnitude of the variability; not presented) in the foot placement but we calculated, for each subject and for a particular target, the variability of the foot positions across the different repetitions. This was done in order to compare the pattern of the successive positions of the feet across trials. Typically, a subject performed M to M + 1 steps to reach the goal. In order to compare the spatial position of the feet across trials, we selected the first M steps and calculated, for each step, the dispersion around the mean foot position. This was quantified in exactly the same way as described for the parameters previously presented. However, the measure here was discrete because we did not integrate the variability continuously throughout the trajectory but rather measured it at the different step instants (see Fig. 1B). In order to compare this spatial variability in the foot positioning with that of the whole-body trajectory, we also expressed the spatial dispersion of the foot as a percentage of the step length. The spatial deviation from the mean trajectory presented above was also expressed, at this stage of the analysis, as a percentage of the trajectory length.

The foot position variability computed at the step instants is given by the parameter FD where:

$$FD = \sqrt{\frac{1}{M}\sum_{j=1}^{M}\left(\left(x_{\mathrm{feet}_j}(t) - x_{\mathrm{av.feet}}(t)\right)^2 + \left(y_{\mathrm{feet}_j}(t) - y_{\mathrm{av.feet}}(t)\right)^2\right)} \qquad (3)$$

where $M$ is the number of steps produced by a subject in order to reach the target, and where ($x_{\mathrm{feetj}}(t)$,($y_{\mathrm{feetj}}(t)$) and ($x_{\mathrm{av.feetj}}(t)$,$y_{\mathrm{av.feetj}}(t)$) are the actual and mean foot positions, respectively. We computed, as for the previous parameters, the averaged and the maximal dispersion of the foot (left and right) around the mean foot position (AFD and MFD, respectively). This analysis was performed for each subject and we then averaged this value across subjects.

### Kinematic variability: velocity profiles and turning behaviour

In addition to the spatial variability of the locomotor behaviour analysed both at the trajectory and step level, we performed a quantitative examination of the velocity and turning profiles variability throughout the trajectory, across subjects and trials.

#### *Velocity profiles*

The instantaneous tangential velocity of the body was computed according to the formula $v(t) = \sqrt{\dot{x}(t)^2 + \dot{y}(t)^2}$ . In order to measure the variability of the velocity profile among the different subjects and trials, we computed the mean velocity profile $v_{\mathrm{av}}(t)$ and calculated the deviation from the mean velocity profile VD and its associated averaged and maximal deviations (AVD and MVD, respectively), following the same procedure as the one used in equations 1 and 2. However, here the deviation accounts for a one-dimensional variability (Fig. 1C).

#### *Turning behaviour: head, trunk and pelvis rotation in space*

Also of interest was the variability of body rotation in space among subjects and trials. The calculation of the parameter $\theta(t)$ corresponds to the angle formed by the shoulder segment and the laboratory $X$-axis: it provides a measure of the time course of the body turning behaviour in a space-fixed reference frame. We computed the parameters BD (body deviation) and the parameters ABD (average BD) and MBD (maximal BD) in order to examine the extent to which subjects produced similar turning behaviours. We performed the same measurements for the head and pelvis rotation profiles and this basically resulted in similar qualitative observations. Thus, the measure of variability is provided for the trunk rotation profile only (Fig. 7E).

### Anticipatory head behaviour

During human locomotion when the body turns along a curved path, the head angle anticipates the instantaneous walking direction. In the present study, we quantified the variability of this head anticipatory behaviour across subjects and for the different targets. This was done in order to address the motor implementation of the trajectory (e.g. how the head drives the steering behaviour). Indeed, it was found that this anticipatory head behaviour remains in the blindfolded condition (Grasso *et al.*, 1996; Prevost *et al.*, 2002; see also Hicheur *et al.*, 2005a for a review) and that spatial, rather than temporal, cues drive the anticipatory head motion. In this last study, it was observed that subjects initiated 90° turns at a constant distance from the point of maximum curvature rather than at a constant time. Here, we performed a similar analysis but testing turns of different amplitudes (see Table 1) in order to examine whether this observation holds across the different tested targets. We calculated, for all the recorded trajectories (and 40 associated targets), the time and the distance before the turn initiation. The turn initiation was measured as the instant where the head maximally deviates from the walking direction provided by the tangent to the trajectory. We then computed the time $\tau$ and the distance $d$ at which this instant occurred. These parameters referred to the instant and position where the target was reached and are expressed as percentages of trajectory length or total movement duration. The amplitude of the maximal head deviation was also calculated for all trajectories.

### Statistical analysis

We performed repeated-measurements ANOVA and $t$-tests with the Statistica 5.1 software package (Statsoft ®) in order to compare the variability calculated across the four categories of trajectories. The mean and maximal deviations from the averaged trajectory were compared in order to quantify the effect of the trajectory's curvature magnitude on the variability of the behaviour. The level of significance of the tests was set at $P < 0.01$. A second set of tests was devoted to comparing the spatial variability expressed either as percentages of the trajectory length or as percentages of the step length (see previous section). The variability parameters were computed for the 720 recorded trajectories (however, because we lost foot markers in a few trials, the real number of trajectories included in the different statistical tests was 713) and a total of 4385 steps were analysed (2161 left steps and 2224 right steps).

While the trajectories were categorized according to the turn amplitude (see Table 1), we performed a second series of statistical tests in which we analysed the effects of the path length and the door orientation (and its required turn amplitude) as well the interaction between these two variables (path length × turn amplitude) for all the tested targets, irrespective of the categories presented in Table 1 (the targets being defined in terms of position and orientation). To this purpose, we performed a multiple regression analysis for the three independent variables mentioned above (path length, turn amplitude and interaction term) across the 713 recorded trajectories. This was done in order to detect potential significant effects of these independent variables on a particular dependent variable (e.g. the mean walking speed, the mean deviation from the average trajectory, the mean deviation from the mean foot position, the mean deviation from the average velocity profile, and the maximal head deviation and its spatial and temporal occurrences; see above).

## Results

For all the 40 trajectories we observed very similar geometrical forms of the locomotor paths and velocity and body rotation profiles across the different repetitions and subjects. This indicates stereotypy at the level of the spatial, kinematic and 'behavioural' attributes of the locomotor trajectories. In contrast, we observed much more variability when the locomotion was analysed at the level of the foot positions in space.

### Spatial stereotypy of the locomotor trajectories

As illustrated in Fig. 2 (for all the tested targets) and in Fig. 3A (for four typical targets), we observed that the locomotor trajectories produced by the different subjects across different repetitions were very similar. We measured the spatial stereotypy as the ATD and MTD. As illustrated in the histograms presented in Fig. 3B, the ATD and MTD were < 10 and 17 cm, respectively. We observed that the larger the turn amplitude, the greater the deviation from the mean trajectory ($F_{3,531} = 58.15$, $P < 0.01$ for the ATD and $F_{3,531} = 66.39$, $P < 0.01$ for the MTD). However, it is remarkable that even for the highly curved trajectories the ATD was ~10 cm. The results from the multiple regression analysis, performed for all the tested orientations, confirmed the previous result observed at the level of the different categories of trajectories. Indeed, the turn amplitude was found to significantly affect the ATD ($F_{1,711} = 136.71$, $P < 0.01$). The path length was not found to significantly affect this parameter ($F_{1,711} = 1.20$, $P > 0.01$) but an interaction between the path length and door orientation was observed ($F_{1,711} = 185.86$, $P < 0.01$).

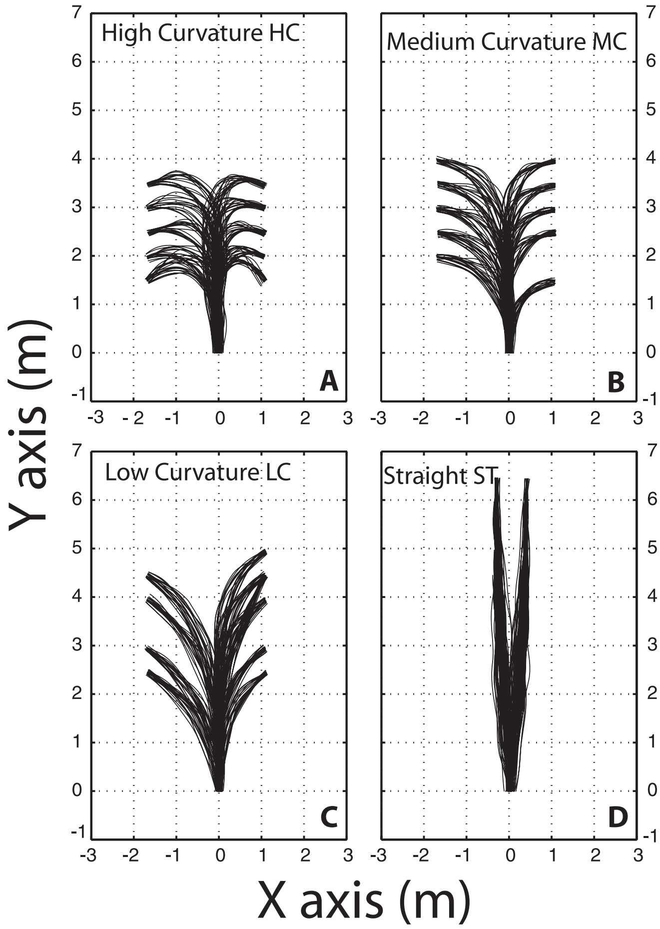

Fig. 2. (A–D) Trajectories for all the tested targets, classified into four categories: high (HC), medium (MC) and low (LC) curvatures and quasi-straight (ST) trajectory groups. Ten targets were tested for each category. Note that for a single target position, two orientations might have been tested (see Table 1 and Fig. 1D for the target positions for which two orientations were tested).

### Spatial variability of the foot placement

While all subjects generated stereotyped locomotor trajectories, their behaviour was much more variable when examined at the level of the step. Part of this variability can be related to the anatomical differences between subjects (see Materials and methods).

In the present section, we calculated various parameters of the stepping behaviour within trials of a single subject (intrasubject analysis): this was done in order to quantify the spatial dispersion of the foot positions independently of the anatomical intersubject differences.

The foot positions at the step instants are presented for all subjects and for four typical trajectories in Fig. 4A. This figure shows the contrast between the foot placements and the corresponding trajectories plotted on the right side of the same figure. The different types of spatial dispersion of the feet are illustrated in Fig. 5A. In most of the configurations accounting for this variability we observed that subjects, when performing different trials of the same target, generated a similar trajectory but located their feet at different positions. The global body trajectory in space remained unaffected because every deviation (from one trial to another) of a given foot towards the right or the left of the $X$-axis was compensated for by a displacement of the

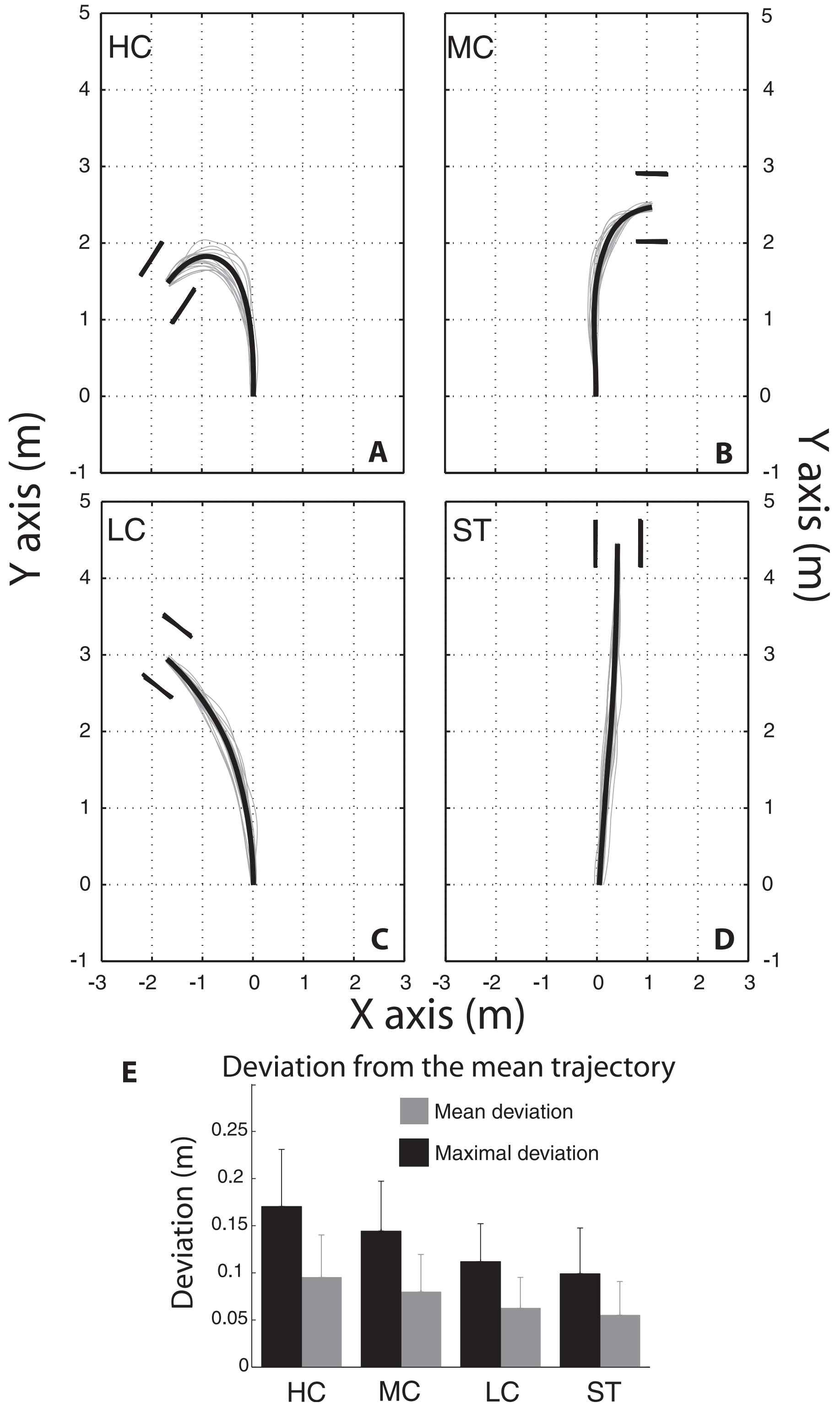

FIG. 3. (A–D) Actual (grey) and mean (black) trajectories computed for four typical targets. (E) Mean and maximal deviations from the mean trajectory calculated for each target category.

position of the contralateral foot in the opposite direction (this was observed in most of the subjects; see Fig. 5A–D).

Another source of foot positioning variability across repetitions is due to the fact that subjects alternated between the left and the right foot for initiating their walk. Even after taking this into account, the foot positions (independently of whether we considered the left or the right foot) still exhibited some spatial dispersion across successive paths (see Fig. 5B and C). The trajectories presented in Fig. 5B thus combine these two sources of variability (e.g. anatomical differences and alternating right–left foot). Finally, we observed in a minority of

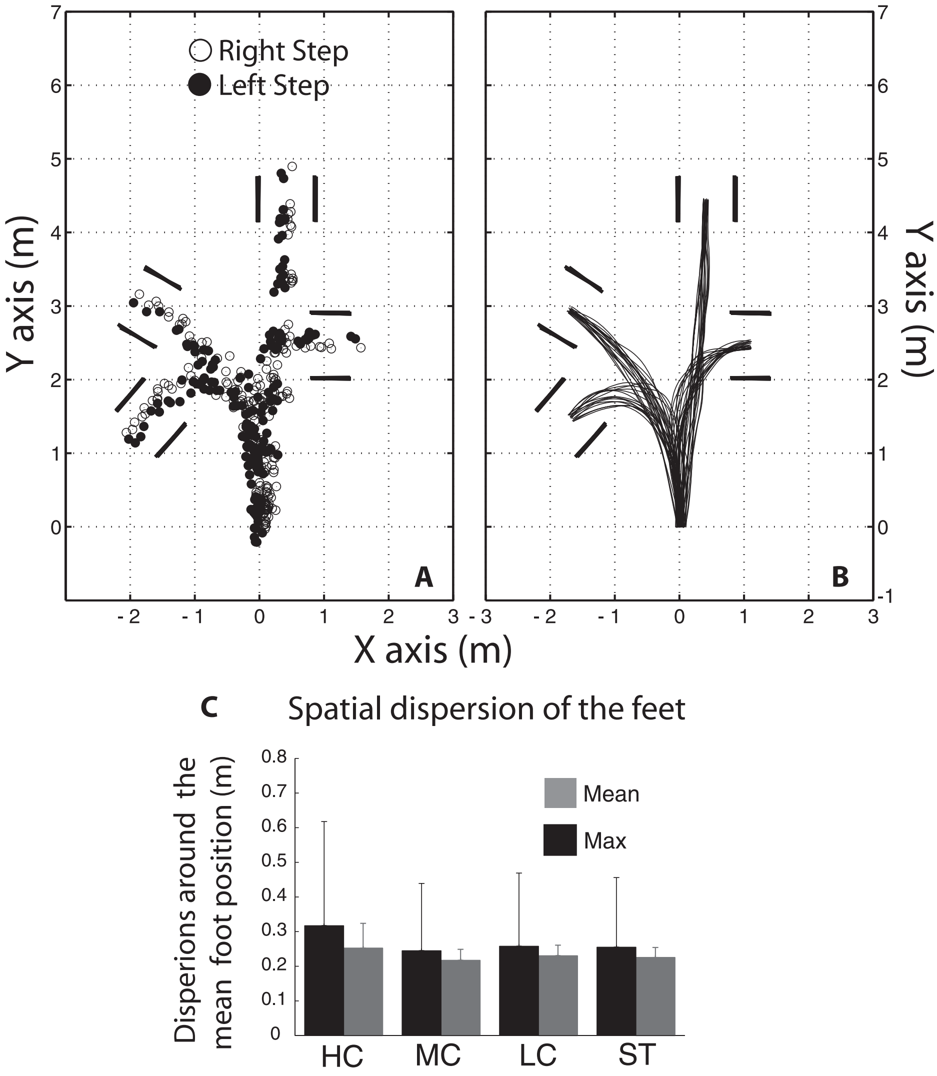

FIG. 4. (A) Foot location for four typical targets (same ones as in Fig. 3) for all subjects and trials and (B) corresponding trajectories: note the similarity between the trajectories and the more variable foot placements. (C) Mean and maximal spatial dispersion (in m) of the foot positions calculated for each target category.

cases that stereotypy in the body trajectories in space was associated with somewhat similar foot positioning across successive paths (see Fig. 5D).

The quantification of these observations is presented in Fig. 4C, in which the spatial dispersion of the foot positions across repetitions is plotted for the four categories of trajectories. The spatial dispersion of the feet around the mean foot positions was not dependent upon the type of trajectory ($F_{3,492} = 0.93$, $P > 0.01$ for the ATD and $F_{3,492} = 3.34$, $P > 0.01$ for the MTD) and ranged between 14 and 22 cm. The results from the multiple regression analysis, performed for all the tested orientations, confirmed that the variability in the foot placements was not dependent on the turn amplitude or on the path length. Indeed, the turn amplitude was not found to significantly affect the deviation from the mean trajectory ($F_{1,702} = 0.96$, $P > 0.01$; note that 10 trials were not analysed because of lost foot markers; see Materials and methods). The path length was also not found to significantly affect this parameter ($F_{1,702} = 0.10$, $P > 0.01$) and no interaction between the path length and door orientation was observed ($F_{1,702} = 0.76$, $P > 0.01$).

These absolute values of foot spatial dispersion obtained at the level of the step were twice as high as the ATD with respect to the mean trajectory presented in Fig. 3. This greater variability is even more evident if these parameters are expressed either as percentages of the step length or as percentages of the trajectory length (see histograms in Fig. 5E and F). The statistical significance of these differences is particularly strong ($F_{1,164} = 647.04$, $P < 0.01$ for the left foot dispersion around the mean left foot position compared with the spatial deviation around the mean trajectory, and $F_{1,172} = 711.06$, $P < 0.01$ for the right foot spatial dispersion compared to the deviation from the mean trajectory). The same observations hold for the maximal deviation parameters ($F_{1,164} = 457.03$, $P < 0.01$ for the left foot spatial dispersion compared to the deviation from the mean trajectory and $F_{1,172} = 693.89$, $P < 0.01$ for the same comparison performed with the right foot).

Taken together, these results show that for a simple goal-oriented task subjects generated very similar trajectories but using different foot placements: this indicates that the locomotor trajectory is unlikely to be constructed as a succession of 'foot reaching'. In the subsequent sections, we tested whether the motor implementation of the trajectory (in terms of either how subjects modulated their walking speed or how they changed their body orientation along the trajectory) presented stereotyped features across subjects.

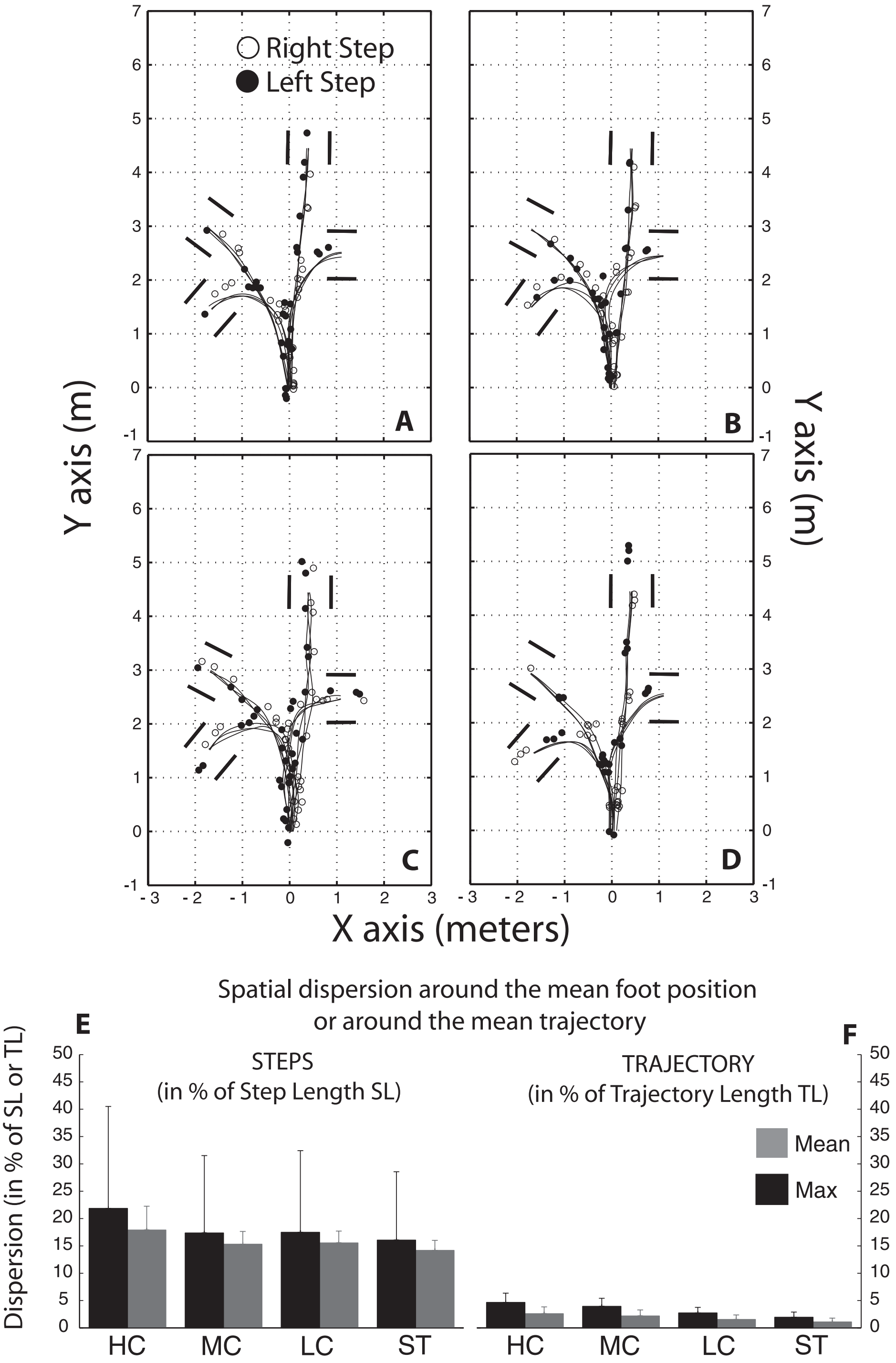

FIG. 5. (A) Foot locations at the step instants (the left and right foot locations are plotted for each of the three consecutive trials) and corresponding trajectories for a particular subject and four typical targets. Note that the number of steps for completing the task may vary from M to M + 1 for the same target (see Materials and methods). (B–D) Same plots for three other subjects. Note the similarity between the trajectories and the greater variability of the foot locations in space. (E) Spatial dispersion of the actual foot locations around the mean foot positions expressed as percentages of the step length. (F) Spatial dispersion of the actual trajectories around the mean trajectory expressed as percentages of the trajectory length.

## *Kinematic stereotypy*

### *Velocity profiles*

In addition to the spatial proximity of the locomotor trajectories (which corresponds to the static component of the trajectory, that is, the locomotor path), we observed that the velocity profiles were very similar across subjects and repetitions. This is illustrated in Fig. 6A–D, in which are plotted the velocity profiles produced by the different subjects for the four categories of trajectories. The histograms quantifying the proximity between these profiles are presented in the bottom of the same figure (Fig. 6E). In contrast with what was observed for the spatial attribute of the trajectory, VD (the mean deviation from the average velocity profile; ~0.10 m⁄ s) was not affected by the length or the amount of body turn induced by the

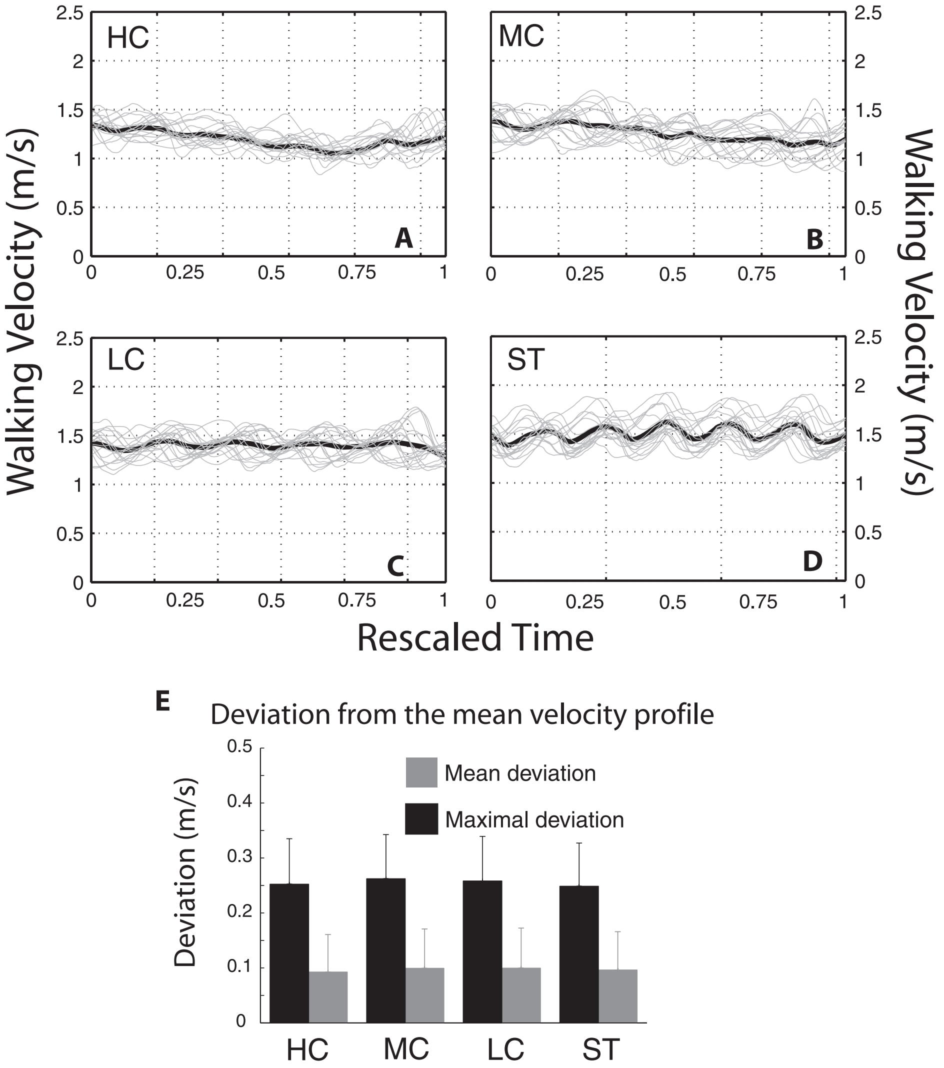

FIG. 6. (A–D) Actual (grey) and mean (black) walking velocity profiles computed for four typical targets (same ones as in Fig. 3) (E) Mean and maximal deviations around the mean velocity profile calculated for each target category.

trajectories ($F_{3,531} = 2.33$, $P > 0.01$ for the mean deviation from the mean velocity profile and $F_{3,531} = 1.50$, $P > 0.01$ for the maximal deviation). The multiple regression analysis failed to reveal any interaction effect (turn amplitude × path length) on the prediction of the MVD ($F_{1,711} = 4.72$, $P > 0.01$). VD significantly varied according to the turn amplitude ($F_{1,711} = 6.81$, $P < 0.01$) but was not significantly affected by the path length ($F_{1,711} = 1.24$, $P > 0.01$). However, this analysis revealed that the mean walking speed as well as the minimum of walking speed significantly ($P < 0.01$) varied with both the turn amplitude and the path length (the interaction effect turn amplitude × path length was also significant; $P < 0.01$).

### *Turning behaviour: head, trunk and pelvis rotation in space*

Although subjects generated similar velocity profiles, the time course of their turning behaviour could have been different throughout the trajectory execution. However, as depicted in Fig. 7A–D, the subjects generated very similar turning behaviours as quantified by the continuous reorientation of the body in space (head, trunk and pelvis angles with respect to the *X*-axis of the laboratory reference frame). We observed that the variability of the body rotation in space (calculated from the trunk segment; see Materials and methods) was < 6° on average and < 15° at most (Fig. 7E).

A statistically significant difference was observed between the four categories of trajectories ($F_{3,531} = 107.87$, $P < 0.01$ for ATD and $F_{3,531} = 116.57$, $P < 0.01$ for MTD): the more curved the trajectory the greater the deviations from the mean body rotation profile (however, only a 6° difference from the mean body rotation profile was observed for the most curved trajectory on average). This profile is similar to the one observed for ATD; although these deviations were small at the absolute level, they can be explained as follows. The amplitude of the turn induced by the curved trajectories was of a decreasing magnitude and reached its minimum for the near-to-straight walking. By normalizing the deviation with respect to a fixed value corresponding to the amplitude of the turn induced by the target orientation (this amplitude was calculated as the angle between the door and the *Y*-axis of the laboratory), the pattern of an increasing variability with an increasing curvature of the trajectory can be replaced by a deviation from the mean body rotation profile which is comparable across the four categories of targets. This possible explanation also holds for the deviation from the actual trajectory. However, we prefer to report absolute rather than relative measurements because this

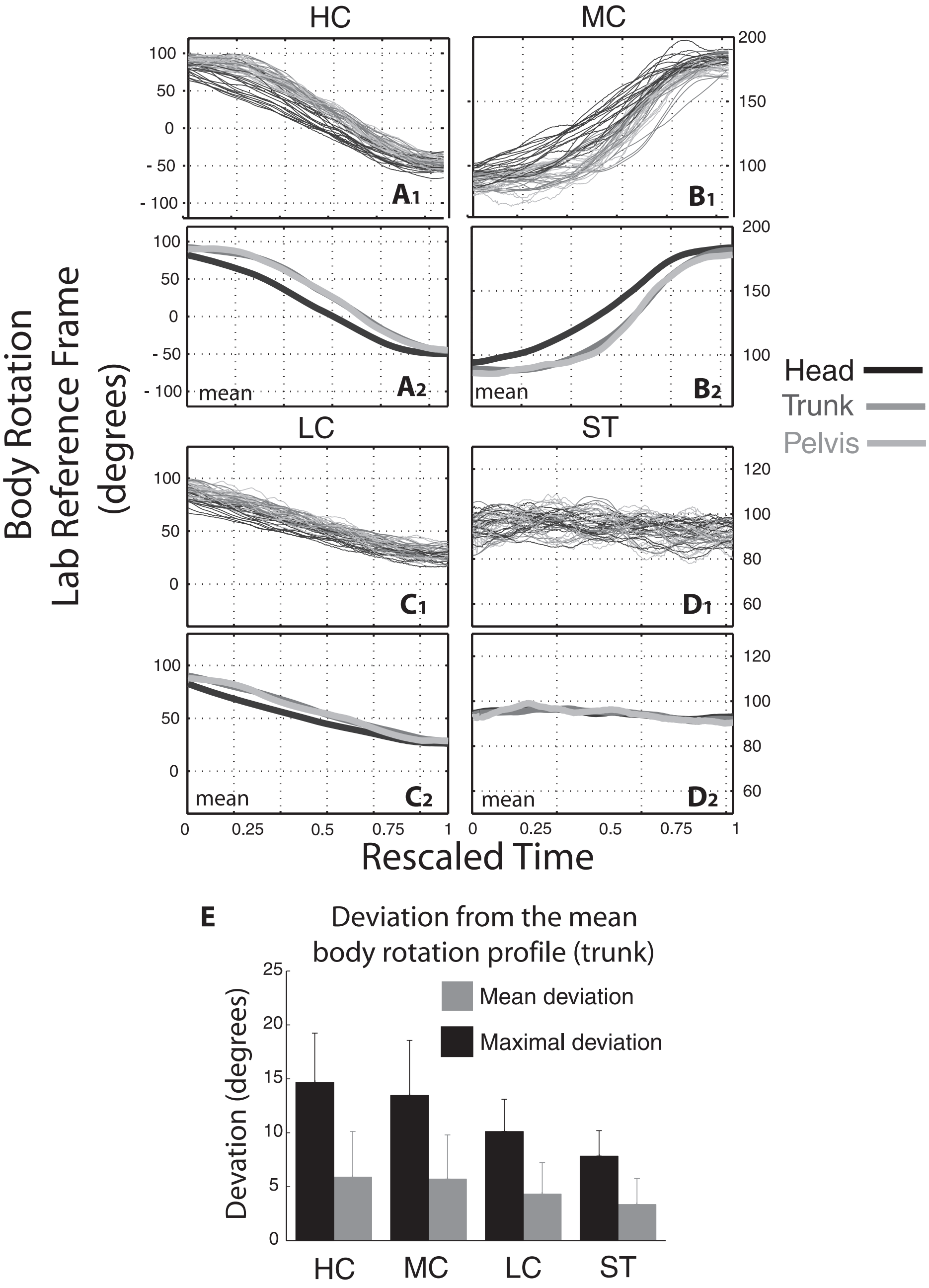

FIG. 7. Actual (A$_1$, B$_1$, C$_1$ and D$_1$) and mean (A$_2$, B$_2$, C$_2$ and D$_2$) body rotation profiles (head, trunk and pelvis rotations in the horizontal plane of the laboratory reference frame) computed for four typical targets (same ones as in Fig. 3) (C) Mean and maximal deviations around the body rotation profile calculated for each target category.

describes the way the magnitude of curvature affects the variability of the locomotor behaviour.

In any case, and for all the trajectories, the very small magnitude of variability in the computed spatial and kinematic profiles provides evidence for a stereotyped behaviour during a goal-oriented locomotor task in humans.

### *Anticipatory head behaviour: time and distance before turn initiation*

In agreement with previous observations we observed that, for the trajectories analysed here, the head direction anticipated the actual walking direction. This was observable both when computing the head deviation in the trajectory reference frame (Fig. 8A–D) and when computing the head, trunk and pelvis orientation profiles in the laboratory reference frame (Fig. 7A–D). In the second case, the head orientation was systematically in advance of the trunk and pelvis orientation (in the case of left turns, this is illustrated by the fact that the curve corresponding to the head orientation is ahead of those of the trunk and pelvis, and vice versa), confirming that the head drives the steering of the locomotion.

The amplitude of the maximal head angular deviation is presented in Fig. 8B. In the case of straight-ahead walking, the maximal head deviation reached ~ 10°, which corresponds to the natural oscillations induced by step alternation. The maximal head deviation (from 23 to

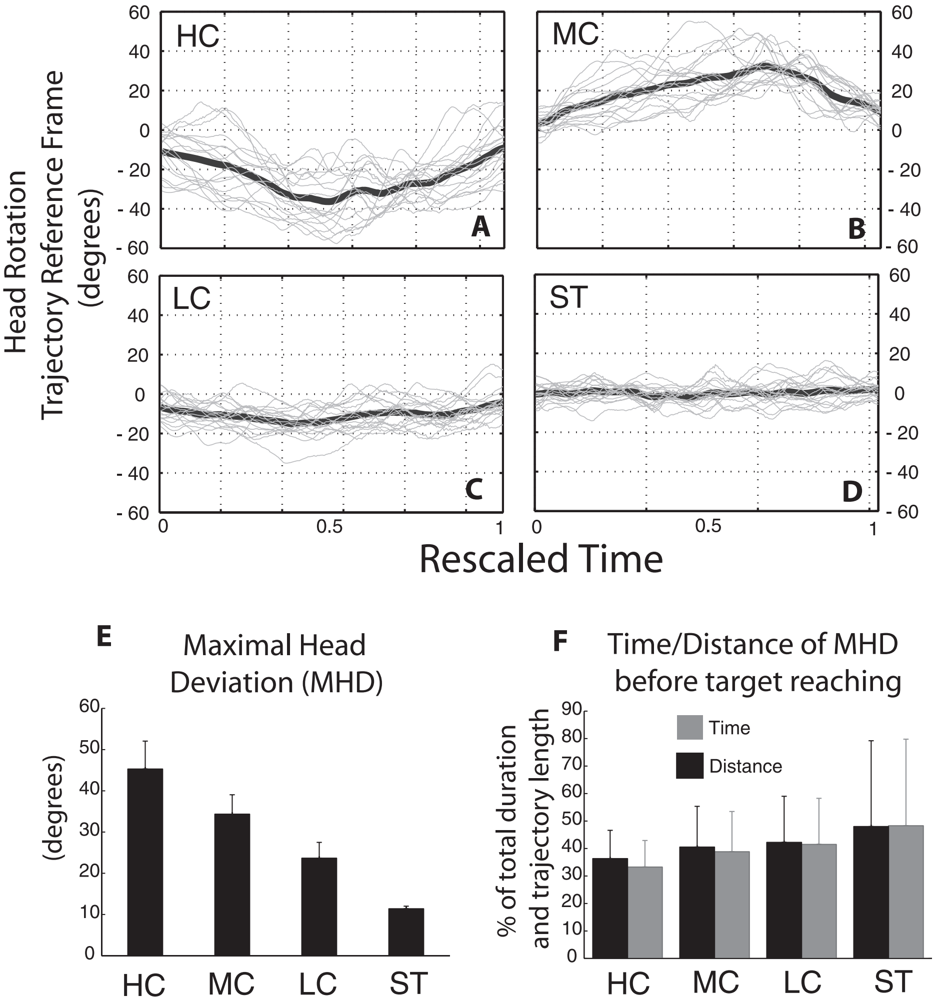

FIG. 8. (A–D) Actual (grey) and mean (black) head rotation profiles (trajectory reference frame) computed for four typical targets (same ones as in Fig. 3) (E) Turn initiation: magnitude of the maximal head deviation MHD calculated for each target category. (F) Time and distance from the target (as percentages of the total duration and as percentages of the trajectory length, respectively) at which the head maximally deviates (note the greater variability with the decreasing curvature).

45°) was greater for the more curved trajectories ($F_{3,531} = 2158.6$, $P < 0.01$). The multiple regression analysis revealed a statistically significant interaction effect (turn amplitude × path length) on the prediction of the maximal head deviation (MHD; $F_{1,711} = 1008.27$, $P < 0.01$). A statistically significant difference was also observed when individually comparing the different path lengths ($F_{1,711} = 154.75$, $P < 0.01$) and the different door orientations ($F_{1,711} = 1421.06$, $P < 0.01$) for all the recorded trajectories.

The instant and the distance at which the maximum of head deviation occurred also inform about the spatial and temporal sequencing of the steering (re-orientations in space) of the whole body. These parameters are expressed either as percentages of the total movement duration or as percentages of the trajectory length (Fig. 8B). The greater variability in these parameters was obtained for the near-to-straight trajectories; this illustrates the fact that no systematic anticipatory behaviour of the head was observed for this condition. In contrast, we observed that the maximum head deviation ranged from ~42 (for the least curved trajectory) to ~36% (for the most curved trajectory) of the trajectory length and movement duration.

Interestingly, the variability in these measurements was also a function of the type of trajectory: the more curved the trajectory the less the variability (and the more systematic the behaviour). We were not able to distinguish whether subjects initiated their turn at a specific spatial position rather than at a specific instant before the target. Nevertheless, we observed that, on average, the head maximal rotation always occurred before completing the first half of movement. Furthermore, our results show that the turn-amplitude parameter dictated the time and the distance (before the target was reached) at which the head maximally anticipated ($F_{3,531} = 72.415$, $P < 0.01$ when comparing this maximal head deviation between the different groups of trajectories). The multiple regression analysis revealed a statistically significant interaction effect (turn amplitude × path length) on the prediction of the spatial occurrence of the MHD only ($F_{1,711} = 12.53$, $P < 0.01$). This was associated with a statistically significant effect of the turn amplitude ($F_{1,711} = 7.30$, $P < 0.01$) but no significant effect of the path length was observed ($F_{1,711} = 4.09$, $P > 0.01$; note that $P = 0.04$). A different result was observed at the level of the temporal occurrence of the MHD: the effects of both the turn amplitude ($F_{1,711} = 1.97$, $P > 0.01$) and of the interaction term (path length × turn amplitude; $F_{1,711} = 5.16$, $P > 0.01$; note that $P = 0.02$) were not significant. In contrast, the path length was found to significantly affect the temporal occurrence of the MHD ($F_{1,711} = 7.72$, $P = 0.01$). Taken together, the results of these statistical comparisons showed that the turn initiation (as quantified by the MHD) was a function of both the turn amplitude and the path length. Furthermore, the path length seemed to mainly affect the instant where the turn was initiated while the turn amplitude tended to preferentially affect the distance from the target at which the turn was initiated.

## Discussion

When a subject is asked to go through a distant doorway (starting from a known position and body orientation in space), he has several possibilities for planning and executing the movement or the sequence of movements allowing him to reach this goal. At least two strategies can be used: one consists of placing his feet at specific positions on the ground, implementing step-by-step a trajectory of the whole body. Alternatively, the subject can plan the whole trajectory and implement different movements allowing him to follow this trajectory. While these two possibilities are not exclusive and might be combined in some way (for instance in the presence of an unexpected obstacle) we observed that, in a simple goal-oriented task, on repeated trials subjects reproduced very similar trajectories, albeit using much more variable spatial foot positioning (this greater variability was evident from both the intersubjects and intrasubject analysis). The observation of a stereotypy of the locomotor trajectories is particularly striking because locomotion mobilizes all body segments. This results, at a theoretical level, in a greater dimensionality of the motor system and the corresponding number of motor solutions (redundancy) compared to the motor apparatus involved in the generation of arm movements.

Indeed, we observed that for reaching the same target the subjects did not position their feet at the same positions in space. In contrast, the paths they followed were very similar in terms of both spatial and kinematic variability.

### *The spatial control of locomotion: path stereotypy and step variability*

We believe that these observations are the first reported for human locomotion and are partly reminiscent of the results published more than 20 years ago regarding hand reaching movements (e.g. Morasso, 1981). However, locomotion is a special case because it supposes the integration of two levels of understanding and description of the movement. The first is related to the stepping level and is not necessarily coincident with the second one, which is related to the task for which it is necessary to consider the locomotor trajectory as a whole. While our results show that it is unlikely that locomotor trajectories are constructed as succession of ‘foot pointings’ we observed, in agreement with the concept of dimensionality and redundancy evoked in the Introduction, that various combinations of foot placement (originating from different leg movements) are performed by subjects in order to reach the target. However, it should be noted that in avoidance tasks where the foot placement was constrained it was shown that minimal displacement of the foot from its normal landing spot was validated as an important factor for selecting alternate foot placement (Patla *et al.*, 1999). In contrast, in our simpler and less constrained environment the kinematic invariance observed at the level of the trajectory might be taken as evidence for a spatial control of locomotion where the spatial accuracy of the body displacement in the environment is explicitly specified in the motor planning and execution. While this statement raises the question of which control variable can be used at this stage, we demonstrate here that the control of the trajectory is expressed in terms of space-related displacement of the body rather than foot-related displacement. In a similar vein, based on the observation that a significantly greater variability was observed in the joint angular displacements than in the hand trajectories (for different tasks), Morasso (1981) proposed the hypothesis that the central command is formulated in terms of trajectories of the hand in space. In our case, the different combinations of foot displacements may also be associated with different motor strategies allowing the steering of the body along the planned trajectory of the body in space.

### *Stereotypy in the steering behaviour: a top-down scheme for the control of locomotion*

It must be emphasized that the stereotypy of the locomotor behaviour reported in this study not only concerns the spatial aspect (the geometry of the locomotor path) but also characterizes the temporal component of the locomotor trajectory. Indeed, the velocity profiles as well as the body turning profiles were also very similar across subjects throughout the trajectory. This means that not only did the subjects follow similar paths but they also regulated their steering behaviour along the trajectory in a similar manner. This is not contradictory with the observation of the variable foot positioning because the motor behaviour here is considered at the trajectory level. However, as revealed by the multiple regression analysis, the individual and combined effects of the door orientation (and its required turn amplitude) and of the door position (and its associated path length) on the spatial variability of the trajectories and on the velocity profiles should be noted here. While the variability of these parameters is $< 20$cm for the MTD and $< 0.10$ m/s for the MVD for all the tested targets, the observation of an increasing variability with the turn amplitude and the path length may restrict our observations (of stereotyped trajectories and velocity profiles) to a particular size of the locomotor space. Further experiments might help in testing how stereotyped would be trajectories generated in larger environments.

For straight trajectories, the velocity was nearly constant while it decreased with the increasing magnitude of the turn. An interesting observation here is that the velocity variations were very similar across subjects: subjects could have abruptly decelerated their walking velocity when negotiating the turn or they could have reduced their velocity early before entering the turn, then maintaining a constant low velocity during the turn. However, they all decreased their velocity continuously and progressively, resulting in smooth locomotor trajectories (this aspect is studied at the theoretical level in the companion paper).

The analysis of the steering behaviour confirmed the initiatory role of the head for the steering behaviour: a top-down temporal sequencing of the body reorientation, beginning first with the head then followed by the trunk and the pelvis, was observed. While this organization could not be observed for the nearly straight trajectories, the anticipatory deviation of the head towards the future walking direction was found to be a function of the magnitude of the turn; the greater the turn, the larger the head deviation and the later (and the closer to the target) occurred the maximum of head deviation. However, for this last parameter we were not able to distinguish between the spatial and/or temporal cues that drive the head deviation but we did observe that there was a combined effect of the turn amplitude and the path length on the spatial and temporal occurrences of the maximal head deviation. As mentioned earlier, it is unlikely that the formation of the whole-body trajectories would emerge from a planning strategy based on the foot positioning, given the variability of the latter parameter. Thus, the body displacement in space might be expressed, at the planning level, either by the head or the trunk movement in space.

As the head contains both the vestibular and visual systems, and is linked to the remaining parts of the body by the neck which contains proprioceptive sensors, the head movement in space might be a critical variable for the steering of locomotion. This has been formalized by Imai *et al*. (2001) as the gravito-inertial acceleration (GIA) vector and it corresponds to the sum of linear accelerations acting on the head. These authors showed that orienting mechanisms direct the eyes, head and trunk movements to tilts of the GIA in space during curved walking. In addition to these orienting mechanisms, the stabilization of gaze through vestibulo-ocular and vestibulocollic reflexes (resulting in a stabilization of the visual scene) might facilitate the smooth changes in the body reorientations in space (as observable in Fig. 7A–C) from the turning profiles where continuous, rather than abrupt, direction changes characterize the steering behaviour).

Independently of the availability of sensory information, spatial memory abilities might also significantly contribute to the control of the locomotor trajectories. Here, we restricted our experimental protocol to the simplest goal-oriented task and we did not manipulate either sensory information or spatial memory, so it would be interesting to further examine their contribution to the stereotyped behaviour of subjects in a future study where perturbations might be applied to the displacement of the subjects. Taken together, all these observations confirm that the head serves as a mobile reference frame for the spatial control of the whole-body displacement in space (see Pozzo *et al*., 1990 and Hicheur *et al*., 2005a for a review).

### *Common principles may govern the formation of both hand and locomotor trajectories*

Locomotion, which involves all the body limbs, is part of the basic motor repertoire of humans. However, the dimensionality of the locomotor system is higher than that of the motor system responsible for the hand movement, making it difficult to define the conceptual link between the system that controls the hand movement and that which controls the whole-body movement.

Recently, however, Papaxanthis *et al*. (2003) showed, by studying upward and backward movements performed in the sagittal plane, that similar planning strategies for whole-body and arm movements might be implemented by human subjects. While they discussed their observations with respect to how gravitoinertial forces are integrated in the elaboration of the motor command for hand and whole-body movements, here we would like to discuss possible similarities in the spatial control of hand and whole-body movements. Indeed, we studied a spatially oriented locomotor task and suggested an analogy with hand reaching tasks. For hand movements, the possibility that the control of movement is realised according to the end-effector coordinates in space was proposed both in experimental observations and theoretical studies (see Introduction). For instance, it was proposed that the CNS learns reaching movements by minimizing the variance of the final end-effector position (Harris & Wolpert, 1998). At first glance, it would be inappropriate to speculate that locomotion is controlled on the basis of a final position of the body in space; indeed, because locomotion is most often performed in temporal and spatial scales greater than those of hand movements, the formation of the locomotor trajectory could well be planned in a piecewise manner.

This possibility of segmenting the planning of the locomotor trajectories in a sequential manner has also been proposed by Viviani & Cenzato (1985) for hand drawing movements. The authors based this interpretation on the observation that one parameter in the velocity–curvature relationships (the so-called one-third power law), the velocity gain factor, was modulated at particular points separating geometrically distinct parts of the trajectory. We recently observed such modulation when studying human locomotion along predefined complex trajectories (Hicheur *et al*., 2005b), suggesting that the control strategy or a number of the control parameters of the body displacement in space are tuned according to some spatial criterion which still remains to be identified. In our study, the possibility that a segmentation process is present might be associated with the observation that subjects first walked along a straight line before initiating a turn in order to reach the goal. However, for a given target we were unable to detect whether the subjects initiated their turn at a specific (invariant) distance or time before reaching the target, so the hypothesis of a segmented control of locomotion cannot be supported using these parameters. It should be noted that, even for hand movements, this hypothesis has been considerably challenged recently (Richardson & Flash, 2002).

In our opinion, the main reason that could explain the analogy between the planning of either hand or whole-body trajectories is that, during motor learning, the CNS plans and regulates the movement by choosing optimal solutions. This possibility, which has been amply tested in many experimental situations and theoretically formalized for arm reaching movements (see Todorov, 2004 for a recent review), may be studied in a systematic way in animal and human locomotion (the topic of the companion paper).

## Acknowledgements

This study was partly supported by a CNES (Centre National d'Etudes Spatiales) grant and by a Human Frontiers grant n° R6P0054/2004. The authors are grateful to Dr S. I. Wiener for suggestions in the text and France Maloumian for help with Fig. 1. The authors are grateful to two anonymous reviewers for their fruitful suggestions and to S. Dalbera for technical assistance during the experiments.

## Abbreviations

ABD, average BD; ATD, averaged TD; AVD, averaged VD; BD, body deviation; FD, foot position variability; HC, high curvature trajectories; LC, low curvature trajectories; M, number of steps to reach the goal; MBD, maximal BD; MC, medium curvature trajectories; MHD, maximal head deviation; MTD, maximal TD; MVD, maximal VD; $N_f$, number of frames; ST, quasi-straight trajectories; TD, trajectory deviation; VD, deviation from the mean velocity profile.

## References

Arechavaleta, G., Laumond, J.-P., Hicheur, H. & Berthoz, A. (2006) The non-hotonomic nature of human locomotion: a modeling study. *Proceeding of the IEEE/RAS-EMBS International Conference on Biomedical Robots and Biomechatronics*, pp. 158–163.

Bullock, D. & Grossberg, S. (1988) Neural dynamics of planned arm movements: emergent invariants and speed-accuracy properties during trajectory formation. *Psychol. Rev.*, **95**, 49–90.

Georgopoulos, A.P. & Grillner, S. (1989) Visuomotor coordination in reaching and locomotion. *Science*, **245**, 1209–12010.

Glasauer, S., Amorim, M.A., Viaud-Delmon, I. & Berthoz, A. (2002) Differential effects of labyrinthine dysfunction on distance and direction during blindfolded walking on a triangular path. *Exp. Brain Res.*, **145**, 489–497.

Grasso, R., Glasauer, S., Takei, Y. & Berthoz, A. (1996) The predictive brain: anticipatory control of head direction for the steering of locomotion. *Neuroreport*, **7**, 1170–1174.

Harris, C.M. & Wolpert, D.M. (1998) Signal-dependent noise determines motor planning. *Nature*, **394**, 780–784.

Hicheur, H., Glasauer, S., Vieilledent, S. & Berthoz, A. (2005a) Head direction control during active locomotion in humans. In Wiener, S.I. & Taube, J.S. (eds), *Head Direction Cells and the Neural Mechanisms of Spatial Orientation.* MIT Press, Cambridge, MA, pp. 383–408.

Hicheur, H., Terekhov, A.V. & Berthoz, A. (2006) Intersegmental coordination during human locomotion: does planar covariation of elevation angles reflect central constraints? *J. Neurophysiol.*, **96**, 1406–1419.

Hicheur, H., Vieilledent, S., Richardson, M.J.E., Flash, T. & Berthoz, A. (2005b) Velocity and curvature in human locomotion along complex curved paths: a comparison with hand movements. *Exp. Brain Res.*, **162**, 145–154.

Imai, T., Moore, S.T., Raphan, T. & Cohen, B. (2001) Interaction of body, head, and eyes during walking and turning. *Exp. Brain Res.*, **136**, 1–18.

Kennedy, P.M., Carlsen, A.N., Inglis, J.T., Chow, R., Franks, I.M. & Chua, R. (2003) Relative contributions of visual and vestibular information on the trajectory of human gait. *Exp. Brain Res.*, **153**, 113–117.

Lacquaniti, F., Terzuolo, C. & Viviani, P. (1983) The law relating the kinematic and figural aspects of drawing movements. *Acta Psychol.*, **54**, 115–130.

Morasso, P. (1981) Spatial control of arm movements. *Exp. Brain Res.*, **42**, 223–227.

Papaxanthis, C., Dubost, V. & Pozzo, T. (2003) Similar planning strategies for whole body and arm movements performed in the sagittal plane. *Neuroscience*, **117**, 779–783.

Patla, A.E., Prentice, S.D., Rietdyk, S., Allard, F. & Martin, C. (1999) What guides the selection of alternate foot placement during locomotion in humans. *Exp. Brain Res.*, **128**, 441–450.

Pham, Q.-C., Hicheur, H., Arechavaleta, G., Laumond, J.-P. & Berthoz, A. (2007) The formation of trajectories during goal-orientated locomotion in humans. II. A maximum smoothness model. *Eur. J. Neurosci.*, **26**, 2390–2402.

Pozzo, T., Berthoz, A. & Lefort, L. (1990) Head stabilization during various locomotor tasks in humans. I. Normal subjects. *Exp. Brain Res.*, **82**, 97–106.

Prevost, P., Ivanenko, Y., Grasso, R. & Berthoz, A. (2002) Spatial invariance in anticipatory orienting behaviour during human navigation. *Neurosci. Lett.*, **339**, 243–247.

Richardson, M.J. & Flash, T. (2002) Comparing smooth arm movements with the two-thirds power law and the related segmented-control hypothesis. *J. Neurosci.*, **22**, 8201–8211.

Soechting, J.F. & Flanders, M. (1994) Moving in three-dimensional space: frames of reference, vectors and coordinate systems. *Annu. Rev. Neurosci.*, **15**, 167–191.

Todorov, E. (2004) Optimality principles in sensorimotor control. *Nat. Neurosci.*, **7**, 907–915.

Viviani, P. & Cenzato, M. (1985) Segmentation and coupling in complex movements. *J. Exp. Psychol. Hum. Percep. Perf.*, **11**, 828–845.

Warren, W.H., Kay, B.A., Zosh, W.D., Duchon, A.P. & Sahuc, S. (2001) Optic flow is used to control human walking. *Nat. Neurosci.*, **4**, 213–216.

Wilkie, R.M. & Wann, J.P. (2006) Judgments of path, not heading, guide locomotion. *J. Exp. Psychol. Hum. Percept. Perform.*, **32**, 88–96.

Wolpert, D.M. (1997) Computational approaches to motor control. *Trends Cogn. Sci.*, **1**, 207–216.

## A.2 The Formation of Trajectories during Goal-Oriented Locomotion in Humans. II. A Maximum Smoothness Model

By Q.-C. Pham, H. Hicheur, G. Arechavaleta, J.-P. Laumond and A. Berthoz.
Published in *European Journal of Neuroscience*, vol. 26, pp. 2391-2403, 2007.

European Journal of Neuroscience, Vol. 26, pp. 2391–2403, 2007 doi:10.1111/j.1460-9568.2007.05835.x

# The formation of trajectories during goal-oriented locomotion in humans. II. A maximum smoothness model

Quang-Cuong Pham,[1] Halim Hicheur,[1] Gustavo Arechavaleta,[2] Jean-Paul Laumond[2] and Alain Berthoz[1]
[1]Laboratoire de Physiologie de la Perception et de l'Action, Collège de France, CNRS UMR7152, 11 place Marcelin Berthelot, 75005 Paris, France
[2]LAAS-CNRS, 7 avenue du Colonel Roche, 31077 Toulouse, France, LPPA, Collège de France-CNRS, 11, place Marcelin Berthelot, 75005 Paris

*Keywords*: human locomotion, maximum smoothness, minimum jerk, optimization principles, trajectory

## Abstract

Despite the theoretically infinite number of possible trajectories a human may take to reach a distant doorway, we observed that locomotor trajectories corresponding to this task were actually stereotyped, both at the geometric and the kinematic levels. In this paper, we propose a computational model for the formation of human locomotor trajectories. Our model is adapted from smoothness maximization models that have been studied in the context of hand trajectory generation. The trajectories predicted by our model are very similar to the experimentally recorded ones. We discuss the theoretical implications of this result in the context of movement planning and control in humans. In particular, this result supports the hypothesis that common principles, such as smoothness maximization, may govern the generation of very different types of movements (in this case, hand movements and whole-body movements).

## Introduction

The existence of invariant properties of biological motion has been reported in many experimental studies, in particular those related to arm movements in animals and humans (Jordan & Wolpert, 1999). For instance, in the case of reaching and drawing experiments, stereotyped behaviours in terms of velocity profiles and smoothness of the hand trajectories in space are reported in the literature (Morasso, 1981; Atkeson & Hollerbach, 1985). This stereotypy is particularly striking in light of the theoretically infinite number of motor solutions to reach a spatial target. The existence of such motor invariants and stereotypy were proposed to be the by-product of control laws characteristic of biological systems. As a consequence, computational approaches have been developed over the past 20 years in order to formulate the principles underlying the motor control.

In the companion paper (Hicheur *et al*., 2007), we demonstrated for the first time that locomotor trajectories produced by humans in a simple goal-oriented task were also highly stereotyped. We also observed that this stereotypy of whole-body trajectories contrasted with a much greater variability in the feet placement. This observation indicates that goal-oriented locomotion should be considered not only at the level of the steps but also at the level of the whole trajectory. It is then necessary to develop a computational approach to provide some elements of understanding of the mechanisms underlying the generation of locomotor trajectories.

### Optimal control approaches

This paper addresses this problem within the framework of optimization theory. The optimal nature of locomotor behaviour was first investigated from a biomechanical viewpoint at the level of the step formation. For instance, it has been shown that humans choose walking or running so as to minimize the metabolic energy cost at their current speed, as measured by their consumption of oxygen (Alexander, 1989).

Optimization theory is an appealing framework as it is related to the possibility that the sensorimotor system is the product of processes such as evolution, development, learning or adaptation that continuously act to improve behavioural performance (Todorov, 2004). In practice, optimality principles have been successful in modelling a great variety of biological movements.

For instance, observing that skilled movements are generally smooth and graceful, Hogan (1984) proposed a minimum jerk principle to predict qualitative and quantitative features of single-joint forearm movements. This is motivated by the assumption that minimizing the squared jerk (jerk is mathematically defined as the third-order derivative of the position) may be equivalent to maximizing smoothness. Flash & Hogan (1985) generalized this model to the case of multijoint motion. They showed in particular that planar trajectories $(x(t),y(t))$ that minimize the following squared jerk cost:

$$\int_0^1 \left( \left(\frac{\mathrm{d}^3x}{\mathrm{d}t^3}\right)^2 + \left(\frac{\mathrm{d}^3y}{\mathrm{d}t^3}\right)^2 \right) \mathrm{d}t \qquad (1)$$

displayed qualitative and quantitative similarities with experimentally recorded hand trajectories.

---

*Correspondence*: Quang-Cuong Pham, [1]Laboratoire de Physiologie de la Perception et de l'Action, as above.
E-mail: cuong.pham@normalesup.org

*Received 01 March 2007, revised 16 August 2007, accepted 20 August 2007*

In the above approach, the optimal trajectory is determined only by the kinematics of the hand and is thus independent of the physical system that generates the movement. Alternatively, Uno *et al.* (1989) proposed a minimum torque change model that takes into account dynamic properties of the arm. They modelled the arm as a two-joint manipulator controlled by torques applied at the joints, and showed that the trajectories that minimize the total squared time derivatives of the torques displayed some features of actual hand trajectories.

Recently, a number of studies have emphasized the importance of biological noise present in the motor system at many levels, ranging from the neural commands to the muscular apparatus. These studies presented computational approaches that involve a stochastic component and were successful in predicting several properties of human movements (see for instance the minimum variance model of Harris & Wolpert, 1998, or the optimal stochastic feedback control framework of Todorov & Jordan, 2002).

### *Minimum squared derivative (MSD) principles*

Qualitatively, a trajectory is smooth if there are no abrupt variations in time. This implies that higher-order time derivatives of the position have low absolute values. While earlier studies (Hogan, 1984; Flash & Hogan, 1985) mostly focused on the squared jerk cost (see above), other costs such as the squared acceleration or the squared snap (snap is the time derivative of jerk) can also be considered. More generally, the $n^{\text{th}}$-order MSD cost is given by:

$$\int_0^1 \left( \left( \frac{\mathrm{d}^n x}{\mathrm{d}t^n} \right)^2 + \left( \frac{\mathrm{d}^n y}{\mathrm{d}t^n} \right)^2 \right) \mathrm{d}t \qquad (2)$$

The case $n = 1$ corresponds to the minimum velocity cost, $n = 2$ to minimum acceleration, $n = 3$ to minimum jerk and $n = 4$ to minimum snap, etc.

Richardson & Flash (2002) conducted a comparative study in which they examined the capacities of MSD principles of different orders to predict hand trajectories. In particular, they found that 3rd- and 4th-order MSD principles (minimum jerk and minimum snap) usually performed better than those of other orders. In addition to quantitative fit, the trajectories predicted by 3rd- and 4th-order MSD principles displayed typical qualitative characteristics of human hand trajectories: smoothness of the trajectory, straight hand paths and bell-shaped velocity profiles in reaching tasks, inverse relationship between velocity and curvature in drawing tasks (the so-called two-thirds power law: Lacquaniti *et al.*, 1983), etc.

At the trajectory level, human locomotion seems to share some of these qualitative features. Indeed, one can observe that human locomotor trajectories are generally smooth. Straight paths are also generated for reaching a spatial goal in an environment free of obstacles, provided that the initial body orientation is compatible with such a path. Finally, humans tend to decelerate in the curved parts and accelerate in the straighter parts of a trajectory. This last observation was confirmed by a recent comparative study (Hicheur *et al.*, 2005) where the authors quantitatively examined the relationship between velocity and curvature in locomotor tasks where subjects had to walk along complex shapes. While the two-thirds exponent was not observed for these shapes (as opposed to the case of hand movements: Viviani & Flash, 1995), the inverse variations of velocity and curvature could be reproduced by multiple power laws whose exponents depended on the shape. This variability of the exponents suggested that the power laws relating the velocity to curvature in human locomotion could be by-products of more general principles, for instance the optimality principles mentioned above.

Taken together, these observations raise the possibility that MSD principles underlie the generation of human locomotion trajectories. If verified, this would suggest that the same set of principles account for different types of movements (hand movements and locomotor movements in our case) and would provide interesting theoretical insights into the understanding of the functional organization of the motor system in general. In order to test this hypothesis, we designed an experiment in which subjects had to produce a wide variety of locomotor trajectories. We then compared the experimentally recorded trajectories with the optimal trajectories predicted by four smoothness maximization models derived from the MSD approach.

## Materials and methods

### *Experimental data*

The experimental protocol is presented in detail in the companion paper. Subjects gave their informed consent prior to their inclusion in the study. Experiments conformed to the Code of Ethics of the Declaration of Helsinki. Briefly, we designed a goal-oriented locomotor task similar to a 'walking through a distant doorway' situation in order to observe the formation of relatively complex locomotor trajectories. We asked the subjects to walk along the laboratory-based *Y*-axis for about one meter before reaching the actual initial position (the origin (0,0) of the laboratory's reference frame), so that their walking direction was approximately orthogonal to the *X*-axis when they reached the point (0,0). They then had to walk towards and through a distant doorway (also designated below as 'the target') located at various positions and with various orientations (see Fig. 1). The doorway was $\sim 1$ m wide, so that the subjects had no difficulty going through it at normal walking speeds. Between the point (0,0) and the target, no specific instructions were provided to the subjects relative to the path to follow. The subjects were also free to choose their walking speed over the whole trajectory.

In order to facilitate the analysis, we classified the 40 tested targets in four categories according to the different turning magnitudes induced by the door orientations. The four categories were: HC (high curvature), MC (medium curvature), LC (low curvature) and ST (straight; see Fig. 2 for an illustration of four typical trajectories recorded in one subject). The experimental database used for our study was composed of 709 trajectories (we had to eliminate 11 faulty trials out of the $40 \text{ targets} \times 6 \text{ subjects} \times 3 \text{ trials} = 720$ trials). The analysis was performed on the time interval separating the instant $t_0$ when subjects crossed the *X*-axis and the instant $t_1$ when they reached the centre of the door, according to the task requirements (see Fig. 2). The trajectory was then time-rescaled so that $t_0 = 0$ and $t_1 = 1$.

### *Modelling approach*

As mentioned in the introduction, MSD principles have proved to be particularly relevant for modelling hand movements. In order to test how such smoothness-based principles can predict locomotor trajectories, we constructed mathematically MSD trajectories as follows.

For a given target, we first extracted a set of 12 parameters (initial and final positions, velocities and accelerations for the $x$ and $y$ components) from the experimental data:

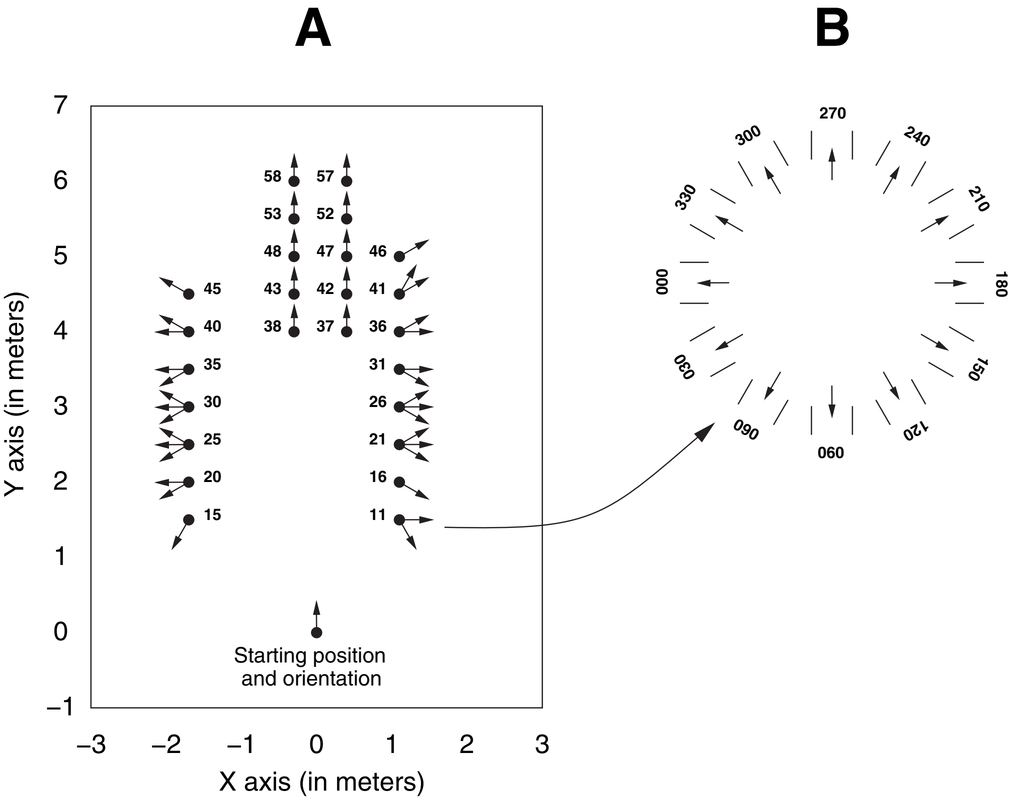

FIG. 1. (A) Spatial disposition of the 40 tested targets. Each target position is represented by a small black disk. The possible target orientations for each target position are indicated by arrows. (B) The 12 target orientations, ranging from 0 to 330°.

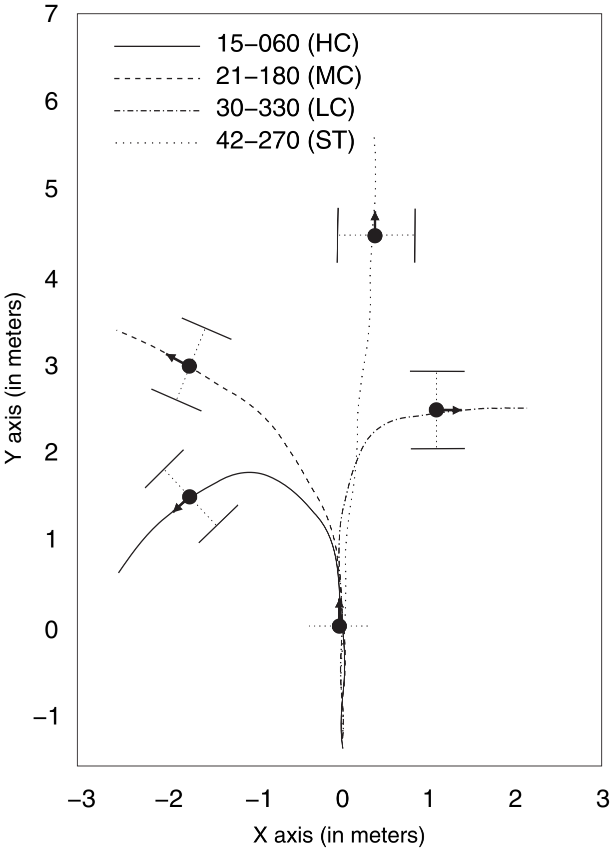

FIG. 2. Four actually recorded trajectories, one trajectory per category.

$$x_0 = \frac{1}{N}\sum_{1}^{N} x_i(0) \quad v_0^x = \frac{1}{N}\sum_{1}^{N} \dot{x}_i(0) \quad a_0^x = \frac{1}{N}\sum_{1}^{N} \ddot{x}_i(0) \tag{3}$$

and similarly for $x_1, v_1^x, a_1^x, y_0, v_0^y, a_0^y, y_1, v_1^y, a_1^y$($N$ corresponds to the number of trajectories recorded for this target).

Some of these 12 parameters were task-related and thus were not related to any spontaneous strategy. Indeed, according to the experimental protocol, the initial and final positions ($x_0$, $y_0$, $x_1$, $y_1$) corresponded, respectively, to the origin of the laboratory's reference frame and to the centre of the door. Similarly, the initial movement direction was imposed as parallel to the $Y$-axis while the final movement direction was constrained by the orientation of the door. As subjects were carefully monitored during the session, the extracted values of these parameters were very close to the imposed ones: over the 709 trajectories, the average distance (± SD) between the actual and the imposed initial positions was 3.0 ± 2.5 cm, the average distance between the actual and the imposed final positions was 3.2 ± 2.2 cm, the average absolute difference between the actual and the imposed initial orientations was 9.6 ± 7.9° and the average absolute difference between the actual and the imposed final orientations was 5.9 ± 4.4°. Thus, our choice to extract these values from the data rather than to compute them *a priori* from the task was only motivated by convenience.

In contrast, initial and final accelerations ($a_0^x, a_0^y, a_1^x, a_1^y$) and initial and final speeds (the norms of the velocity vectors) were not imposed by the task and thus contained information about the subjects' movement strategies or their personal preferences. Considering these parameters as free parameters in the optimization procedure yielded close-to-zero values, which was not consistent with the observations. On the other hand, estimating them by an independent method would be complicated and not relevant with respect to our objectives (see Discussion for more details on the issue of putting experimental values into the models).

At a computational level, as our objective consisted of predicting the whole trajectory kinematics (path and velocity profile), these values actually contained relatively little information. In contrast, the original two-thirds power law (Lacquaniti *et al.*, 1983), the modified two-thirds power law (Viviani & Schneider, 1991) or the constrained minimum jerk model (Todorov & Jordan, 1998) aimed at predicting only the velocity profile. Moreover, these models required as inputs the entire recorded path in conjunction with either the end-point velocities and accelerations (for the constrained minimum jerk model) or the entire velocity profile (for the modified two-thirds power law). However, it should be recognized that some of the trajectories studied in the references cited above were rather more complex than ours.

It should also be noted that the movement duration was implicitly extracted in the time-rescaling procedure.

Next, we derived the planar trajectory ($x(t)$,$y(t)$) that minimizes the cost given in equation 2 and verifies the following 12 boundary conditions:

$$\begin{aligned} x(0)=x_0, x(1)=x_1, \dot{x}(0)=v_0^x, \dot{x}(1)=v_1^x, \ddot{x}(0)=a_0^x, \ddot{x}(1)=a_1^x \\ y(0)=y_0, y(1)=y_1, \dot{y}(0)=v_0^y, \dot{y}(1)=v_1^y, \ddot{y}(0)=a_0^y, \ddot{y}(1)=a_1^y \end{aligned} \tag{4}$$

In usual MSD approaches, the number of boundary conditions depends on the order of the derivative that is minimized. For instance, the minimum velocity, minimum acceleration, minimum jerk and minimum snap models require, respectively, 4, 8, 12 and 16 boundary conditions. However, these choices are arbitrary and are not motivated by any theoretical consideration (see Harris, 2004 and Harris & Harwood, 2005 for a detailed discussion of the issue of boundary conditions in models of biological movements). They introduce furthermore a bias in favour of the higher-order MSDs. In our comparative approach, we chose to use the same set of boundary conditions given by equation 4 in all four models in order not to favour any particular model. The mathematical details for the derivation of the MSD trajectories are given in the Appendix.

### *Performance of the models*

We performed a series of quantitative comparisons between the actual and the predicted trajectories either at the global level of the trajectory or at the more detailed level of the velocity profile.

In the companion paper, similar comparisons were conducted in order to assess the stereotyped behaviour of actual trajectories corresponding to a single task. For this, the average trajectory was compared to actual trajectories, resulting in several measurements [e.g. average and maximal trajectory deviations (ATD and MTD) and average and maximal velocity deviations (AVD and MVD)].

Here, we were interested in the predictive capacities of our models. We thus compared the average trajectory corresponding to a given task to the trajectories predicted by our models for the same task. This was reasonable as actual trajectories were stereotyped and, consequently, very similar to the average trajectory.

### *Trajectory prediction*

In order to quantify the prediction error at the level of the trajectory, we computed, for each target, the instantaneous trajectory error ($\mathrm{TE_c}$) of the predicted trajectory ($x_\mathrm{c}(t)$,$y_\mathrm{c}(t)$) (replace ‘c’ with ‘v’ for minimum velocity, ‘a’ for minimum acceleration, ‘j’ for minimum jerk and ‘s’ for minimum snap) with respect to the average (av) trajectory ($x_\mathrm{av}(t)$,$y_\mathrm{av}(t)$) as:

$$\mathrm{TE_c}(t)=\sqrt{(x_\mathrm{c}(t)-x_\mathrm{av}(t))^2+(y_\mathrm{c}(t)-y_\mathrm{av}(t))^2} \tag{5}$$

We then defined the average and maximal trajectory errors ($\mathrm{ATE_c}$ and $\mathrm{MTE_c}$) over the whole trajectory:

$$\mathrm{ATE_c}=\int_0^1 \mathrm{TE_c}(t)\mathrm{d}t \tag{6}$$

$$\mathrm{MTE_c}=\max_{0\le t\le 1}\mathrm{TE_c}(t) \tag{7}$$

Note that $\mathrm{ATE_c}$ and $\mathrm{MTE_c}$ take into account the instantaneous errors at all time instants. They are therefore sensitive to dissimilarities at both the geometric level and at the velocity profile level.

For each category X (X = HC, MC, LC, ST), the average $\mathrm{ATE_c}$ and $\mathrm{MTE_c}$ over all targets belonging to this category were denoted, respectively, $ATE_c^X$ and $MTE_c^X$.

For a graphical examination of the models’ performances, we also plotted in Figs 3–6 the variance ellipses calculated by principal component analysis. Intuitively, the variance ellipse at time $t$ is centred at ($x_\mathrm{av}(t)$,$y_\mathrm{av}(t)$) and its orientation and magnitude indicate how the ($x_\mathrm{i}(t)$,$\mathrm{y_i}(t)$) ($i$ = 1…$N$, where $N$ corresponds to the number of trajectories recorded for this target) are distributed around ($x_\mathrm{av}(t)$, $\mathrm{y_{av}}(t)$). Note that $r_1(t)^2 + r_2(t)^2 = \mathrm{TD}(t)^2$ where $r_1$ and $r_2$ are the lengths of the ellipse’s semi major and semi minor axes and TD is the trajectory deviation defined in the companion paper.

### *Velocity profile prediction*

In contrast to the companion paper, the goal here is to compare the velocity profiles in terms of their variations in time rather than in terms of their absolute variabilities (which are due in part to the variability of the walking tempos in different subjects; these have been measured in the companion paper).

For a given trajectory ($x_\mathrm{i}(t)$,$y_\mathrm{i}(t)$), we thus considered the normalized velocity profile defined as:

$$v_i(t)=\frac{\sqrt{\dot{x}_i(t)^2+\dot{y}_i(t)^2}}{\int_0^1\sqrt{\dot{x}_i(u)^2+\dot{y}_i(u)^2\mathrm{d}u}} \tag{8}$$

The average normalized velocity profile and the instantaneous normalized velocity deviation (nVD) were then defined as:

$$v_\mathrm{av}(t)=\frac{1}{N}\sum_1^N v_i(t) \tag{9}$$

$$\mathrm{nVD}(t)=\sqrt{\frac{1}{N-1}\sum_1^N(v_i(t)-v_{av}(t))^2} \tag{10}$$

Finally, we defined the Average and Maximal normalized Velocity Deviations (AnVD and MnVD) over the trajectory as:

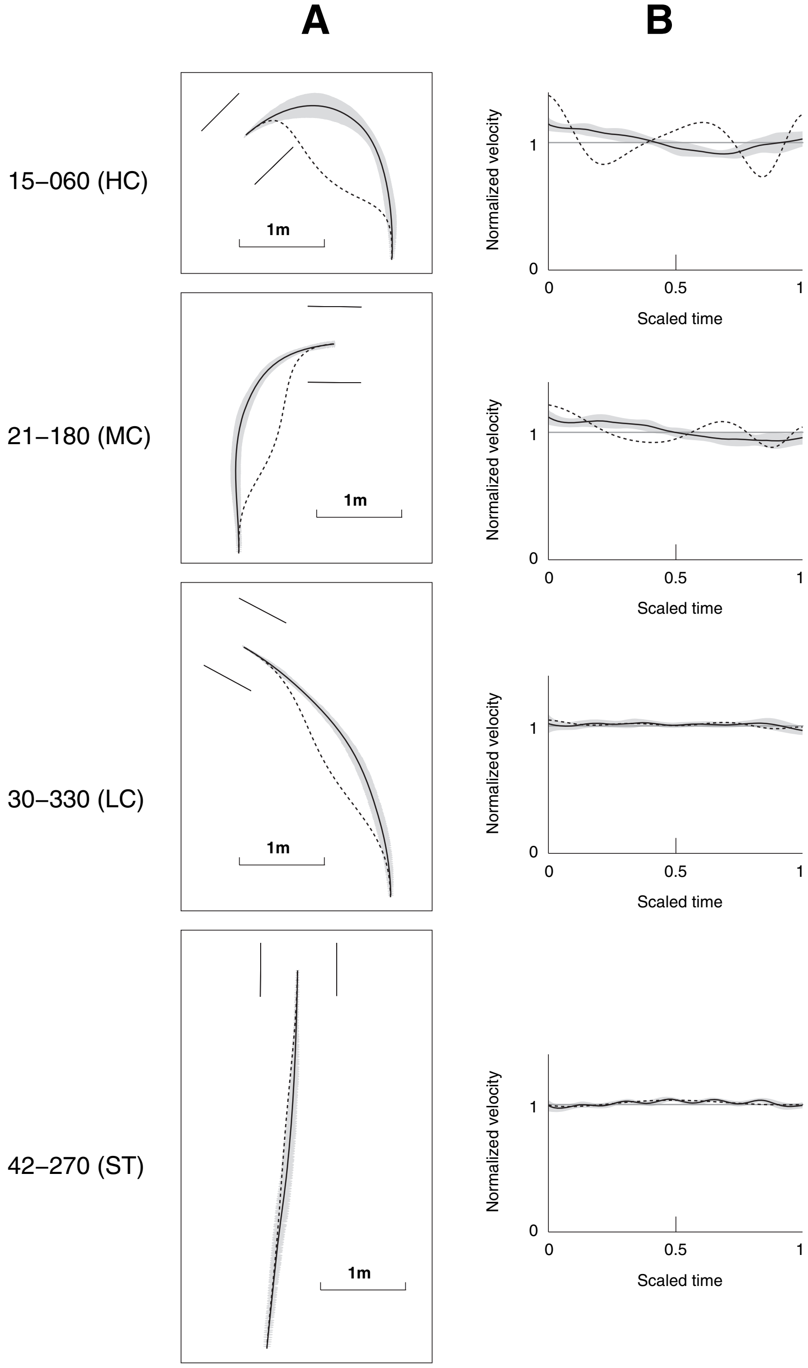

FIG. 3. Prediction of the minimum velocity model for four representative trajectories. (A) Geometric paths of the average (solid lines) and the predicted (dashed lines) trajectories. The variance ellipses (in grey) are also plotted in order to show the spatial variability around the average trajectory at every time instant (see Materials and methods). (B) Normalized velocity profiles of the average (solid lines) and of the predicted (dashed lines) trajectory. The standard deviation around the average velocity profile is shaded in grey. The dark grey horizontal line shows the mean value (in time) of the normalized velocity profiles.

$$\mathrm{AnVD} = \int_0^1 \mathrm{nVD}(t)\mathrm{d}t \tag{11}$$

$$\mathrm{MnVD} = \max_{0\leq t\leq 1} \mathrm{nVD}(t) \tag{12}$$

Next, we computed the normalized velocity profile of the predicted trajectory ($x_c(t)$,$y_c(t)$) as:

$$v_c(t) = \frac{\sqrt{\dot{x}_c(t)^2 + \dot{y}_c(t)^2}}{\int_0^1 \sqrt{\dot{x}_c(u)^2 + \dot{y}_c(u)^2}\mathrm{d}u} \tag{13}$$

Finally, average and maximal normalized velocity errors ($\mathrm{AnVE_c}$ and $\mathrm{MnVE_c}$) over the whole trajectory were computed as:

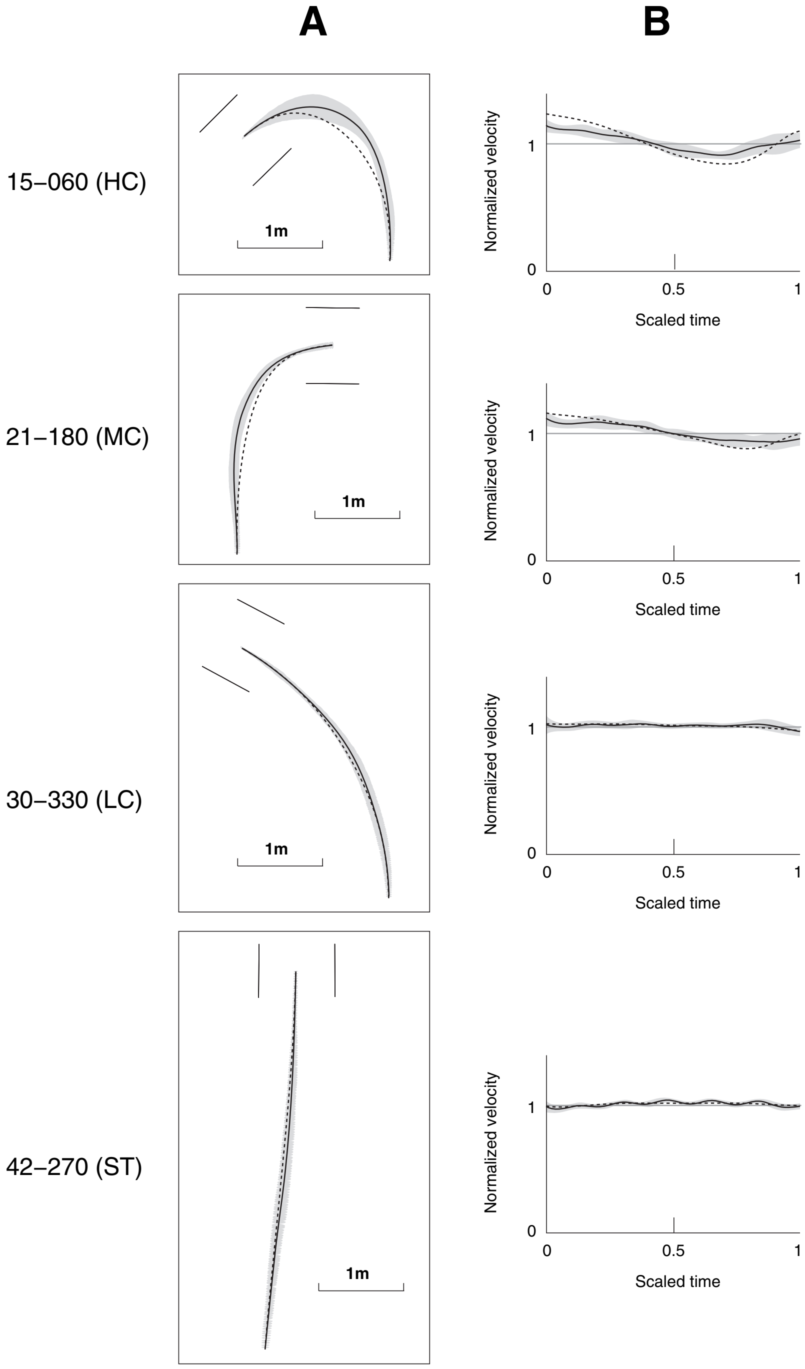

FIG. 4. Prediction of the minimum acceleration model for four representative trajectories. For details, see legend of Fig. 3.

$$\mathrm{AnVE_c} = \int_0^1 |v_c(t) - v_{av}(t)|\mathrm{d}t \qquad (14)$$

$$\mathrm{MnVE_c} = \max_{0 \le t \le 1} |v_c(t) - v_{av}(t)| \qquad (15)$$

For each category X (X = HC, MC, LC, ST), the average $\mathrm{AnVE_c}$ and $\mathrm{MnVE_c}$ over all targets belonging this category were denoted, respectively, $\mathrm{AnVE_c^X}$and $\mathrm{MnVE_c^X}$

### *Statistical analysis*

We performed repeated-measurements ANOVA with the Statistica 5.1 software package (Statsoft ®) in order to compare statistically the performance of the models. More specifically, given two models, we compared their maximum trajectory errors in order to assess whether one model was significantly better than the other. We also tested whether the maximum trajectory errors of a model were significantly smaller or greater than the corresponding maximum trajectory deviations (the experimental variabilities).

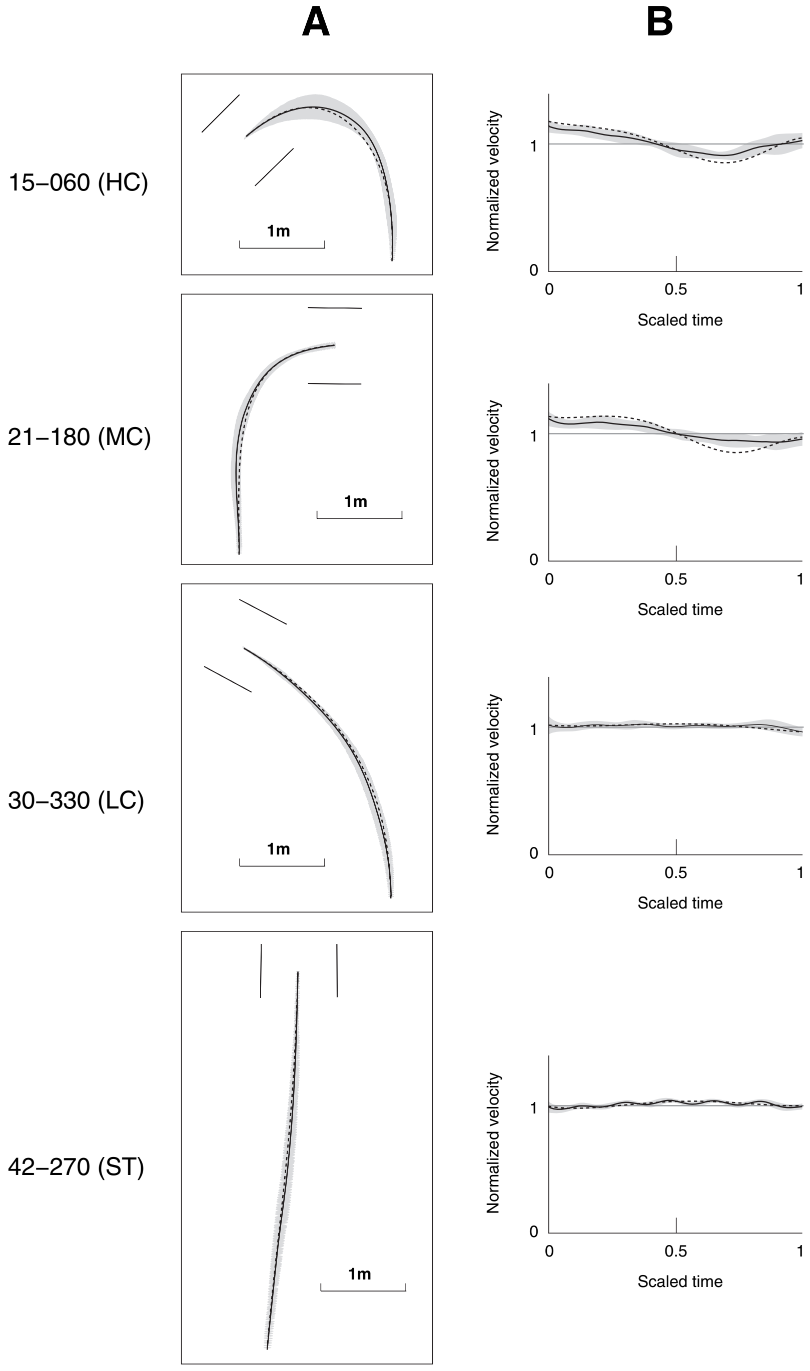

FIG. 5. Prediction of the minimum jerk model for four representative trajectories. For details, see legend of Fig. 3.

## Results

### *Qualitative examination*

*Minimum velocity model*

In Fig. 3, we plotted the predictions of the minimum velocity model for four representative targets, one for each category. We observed that the geometric paths predicted by this model tended to be the straightest possible. Thus, the predicted paths for the targets of category ST were accurate. However, for the targets that required some amount of curvature (HC, MC and LC), the predicted paths were strongly bent towards the interior of the curve, resulting in a big inaccuracy around the middle of the path.

*Minimum acceleration model*

Predictions of the minimum acceleration model are presented in Fig. 4. Qualitatively, for categories HC, MC and LC, the geometric paths predicted by this model were much more accurate than those predicted by the minimum velocity model. However, the predictions were still not satisfactory for categories HC and MC, which included the most curved trajectories. Indeed, as in the minimum velocity model, the predicted paths for these categories tended to be straighter than the actual paths. More specifically, in the regions of relatively high curvatures, the predicted paths fell outside the grey area of the variance ellipses, implying that their distances to the average paths were greater than the experimental variability in these regions.

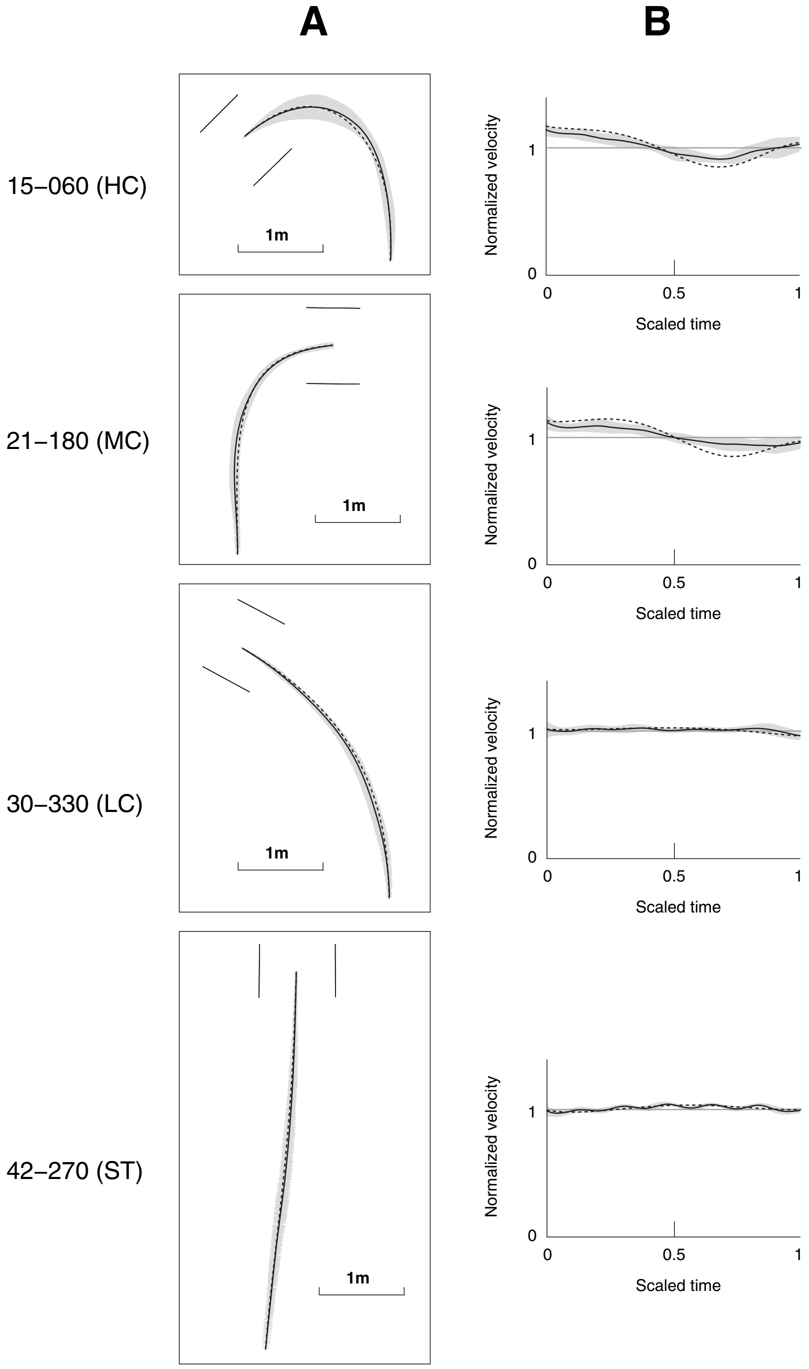

FIG. 6. Prediction of the minimum snap model for four representative trajectories. For details, see legend of Fig. 3.

The comparison of the velocity profiles only makes sense when the geometric paths are similar, i.e. in the case of category ST for the minimum velocity model and in the case of categories LC and ST for the minimum acceleration model. In these cases, the average velocity profiles were almost constant in time, which was well reproduced by both models.

### *Minimum jerk and minimum snap models*

The predictions of these models are presented in Figs 5 and 6, respectively. We first observed that the trajectories predicted by the two models were very similar for the four representative targets. In contrast to the two previous models, the geometric paths predicted by these two models for the HC and MC trajectories are smoothly curved and bear impressive resemblance with the average ones. As an illustration, the predicted paths always lay inside the grey area of the variance ellipses, implying that the distance between the predicted and the average paths was smaller than the experimental variability at every time instant.

At the level of the velocity profiles, we noted that the average velocity profiles were approximately constant in time for categories LC and ST (the only minor variations were due to the step-level oscillations). This was well reproduced by both models. For categories HC and MC, in the average velocity profile, the velocity decreased and became minimal around $t = 0.7$ (where $t$ is time scaled from 0 to 1) before increasing again. This variation of the velocity was related to the variation of curvature in the corresponding geometric paths. The inverse relationship in human locomotion has been experimentally observed by Vieilledent *et al.* (2001) and by Hicheur *et al.* (2005). The predicted velocity profiles successfully captured this behaviour, although with some slight overshoot. For instance, for category HC the velocity profile of the minimum jerk trajectory had almost the same global behaviour as the average one: both decreased and became minimal around $t = 0.7$ before increasing again. However the variations in the predicted profile were slightly larger than the variations in the average profile.

## Quantitative examination

We next proceed to a more precise, quantitative comparison between average and predicted trajectories.

### *Trajectory errors*

The average and maximal trajectory errors as defined in Methods are plotted in Fig. 7. As noted above, the minimum velocity model (dark grey bars) produced acceptable predictions only in the case of straight trajectories (category ST). As soon as the targets imposed some amount of trajectory curvature (categories LC, MC and HC), the minimum velocity trajectories differed completely from the actual trajectories.

The minimum acceleration principle (medium grey bars) performed somewhat better but for categories HC and MC it was still not satisfactory. For example, the average maximal prediction error over the 20 targets belonging to these categories, $\mathrm{MTE}_a^{HC+MC}$(14.7 cm), was not significantly different ($F_{1,19} = 0.27$, $P > 0.01$) from the corresponding experimental variability (black bars) $\mathrm{MTD}^{HC+MC}$ (15.1 cm).

In contrast, minimum jerk (light grey bars) and minimum snap (white bars) principles provided strikingly good predictions. In fact, as noted above, the predictions of minimum jerk and minimum snap models were mostly similar. As a matter of fact, the largest difference between the two models was observed for target 31–150 (category HC), where the maximal distance between the two predicted trajectories was 3.6 cm. Over the 20 targets of categories HC and MC, the average (± SD) maximal distance between minimum jerk and minimum snap trajectories was only 2.1 cm (± 0.6 cm).

Even in the case of the highly curved trajectories of category HC, the distance between the average trajectory and the minimum jerk trajectory was < 13 cm over the whole trajectory ($\mathrm{MTE}_j^{HC} = 12.7$ cm). As the average trajectory length for this category was 3.7 m, this corresponds to a maximal error of only 3.4%. Moreover, the prediction errors of the minimum jerk and minimum snap models were smaller than the experimental variability. For categories HC and MC, $\mathrm{MTE}_j^{HC+MC}$(10.3 cm) was significantly smaller ($F_{1,19} = 20.7$, $P < 0.01$) than $\mathrm{MTD}^{HC+MC}$ (15.1 cm). This result is related to our previous qualitative observation that the paths predicted by these models always lay inside the variance ellipses.

Next, the respective performances of minimum acceleration, minimum jerk and minimum snap models were compared over the 20 targets belonging to categories HC and MC (we observed that the three models yielded similar performance for the straight and close-to-straight trajectories ST and LC). The average maximal prediction error over these targets were $\mathrm{MTE}_a^{HC+MC}$,14.7 cm; $\mathrm{MTE}_j^{HC+MC}$,10.3 cm; and $\mathrm{MTE}_s^{HC+MC}$,10.7 cm. The difference between the minimum acceleration and minimum jerk average MTEs was statistically significant ($F_{1,19} = 29.10$, $P < 0.01$). The difference between the minimum jerk and minimum snap average MTEs was also significant, albeit to a lesser extent ($F_{1,19} = 9.80$, $P < 0.01$).

The superiority of minimum jerk and minimum snap models over minimum acceleration and minimum velocity models can be explained as follows. Minimizing the mean squared velocity cost is almost equivalent to finding the shortest path, i.e. the straightest path in Euclidean geometry, that satisfies the boundary conditions. This prevents the minimum velocity model from predicting accurate trajectories as soon as the targets required some amount of curvature. As for the minimum acceleration model, the mean squared acceleration cost penalises, by definition, large variations in time of the velocity vector. This is not consistent with the experimental observation of significant variations in the velocity vector (in particular, the variations in the orientation of this vector) around the regions of high curvature in MC and HC trajectories. In contrast, minimum jerk and minimum snap allow more flexibility for the variations in the velocity vector and are thus more capable of generating smoothly curved trajectories.

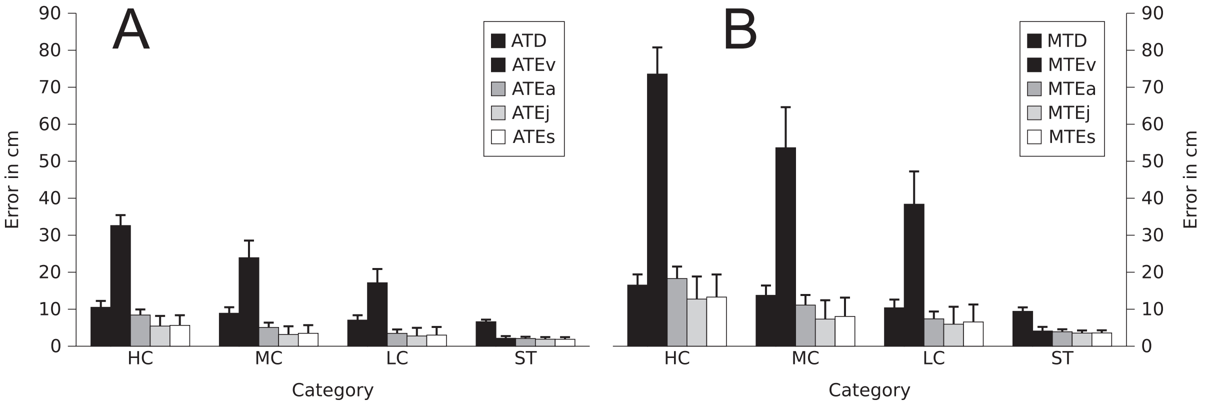

FIG. 7. (A) Average and (B) maximal trajectory errors (ATE and MTE; the suffixes v, a, s, j refer, respectively, to velocity, acceleration, jerk and snap) in centimetres: dark grey bars for minimum velocity, medium grey bars for minimum acceleration, light grey bars for minimum jerk and white bars for minimum snap, averaged over targets corresponding to the same category. For comparison, the average and maximal trajectory deviations (ATD and MTD) are also plotted (black bars).

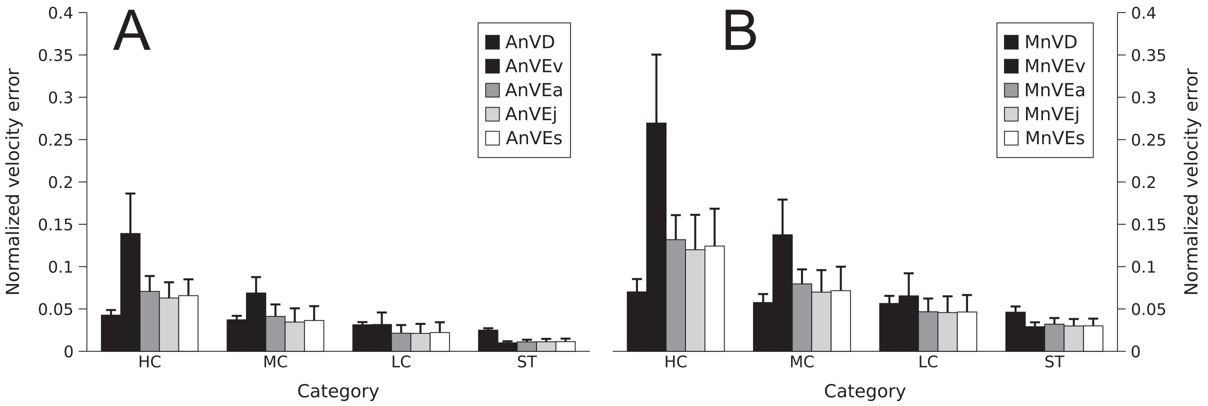

FIG. 8. (A) Average and (B) maximal normalized velocity errors (AnVE and MnVE; the suffixes v, a, s, j refer, respectively, to velocity, acceleration, jerk and snap): dark grey bars for minimum velocity, medium-grey bars for minimum acceleration, light-grey bars for minimum jerk and white bars for minimum snap, averaged over targets corresponding to the same category. For comparison, the average and maximal normalized velocity deviations (AnTD and MnTD) are also plotted (black bars). In the process of computing the above quantities, all velocity profiles were normalized so that their average values over the movement duration equals 1 (see Materials and methods).

### *Velocity profile errors*

The average and maximal normalized velocity errors as defined in Materials and Methods are plotted in Fig. 8. These errors in terms of the velocity profile followed the same tendency as those in terms of trajectory kinematics: in all categories, the velocity profiles of minimum jerk (light grey bars) and minimum snap (white bars) trajectories deviated very slightly from the average velocity profiles. Even for category HC, the average normalized velocity error was only 6% (of the average actual velocity) while the maximal normalized velocity error over the trajectory was < 12%. In absolute terms, these errors were close to the same order of magnitude as the experimental variability (black bars).

## Discussion

Despite the great number of possible trajectories to reach a distant doorway, humans exhibit stereotyped behaviour in terms of both path geometry and trajectory kinematics (see companion paper). This suggests that some underlying principles may govern the formation of whole-body trajectories in space. In the present study, we developed a comparative approach in which we tested four optimization models already studied in the literature in the context of hand trajectory generation (Richardson & Flash, 2002). To assess their validity, we applied these models to a wide range of locomotor tasks involving trajectories of various lengths and curvatures. Through qualitative and quantitative examinations, we established that two out of the four models, namely the minimum jerk and the minimum snap models, provided predictions remarkably close to actual trajectories, at both the geometric and the kinematic levels.

### *Predictive power of the models*

As pointed out by Todorov & Jordan (2002), the predictive power of a model is not only measured by how well it fits the experimental data. At least two other characteristics must be taken into account. The first characteristic is the quantity of information that needs to be extracted from the experimental data. Obviously, the less information extracted from the data, the greater the challenge for the model. In order to predict the velocity profiles of curved hand movements, the constrained minimum jerk model requires, as inputs, the entire movement path and the initial and final velocities (Todorov & Jordan, 2002). Viviani & Flash (1995) used experimental values of the velocity and acceleration at several via-points in order to predict the velocity profiles in curves drawing tasks. In contrast, our models (which predict both the path and the velocity profile) were required to extract only a small number of parameters, namely the initial and final speeds and accelerations, and the movement duration (see Materials and methods). The last parameter was extracted in the time-rescaling procedure, which normalizes the durations of actual and simulated trajectories. This procedure is pervasive in the literature (Flash & Hogan, 1985; Uno *et al*., 1989; Harris & Wolpert, 1998; Todorov & Jordan, 1998; Richardson & Flash, 2002) but, in light of our current discussion, it also reduces the predictive power of the model. Recently, Tanaka *et al*. (2006) proposed a variation of the minimum variance model (Harris & Wolpert, 1998) that was able to determine the movement duration from a first principles approach. The authors considered the movement duration as a parameter to be optimized, and performed the subsequent optimization under the constraint that the movement achieves a predetermined level of accuracy. Within our experimental protocol, the determination of the movement duration and, more generally, the issue of speed–accuracy tradeoff in human locomotion could not be satisfactorily investigated; testing different walking speeds and varying the constraints on the spatial accuracy (e.g. varying the size of the doorway) will help in addressing these questions in future studies.

The second characteristic for estimating the predictive power of a model is the presence and the number of free parameters that must be tuned in order to fit the data. For instance, Viviani & Schneider (1991) proposed a modified power law for modelling the velocity profile of curved hand movements:

$$v(t) = \gamma(\kappa(t) + \varepsilon)^{\beta} \tag{16}$$

In this model, the velocity gain factor $\gamma$ and the exponent $\beta$ needed to be tuned in order to fit the actual velocity profile. In contrast, our models did not contain any such free parameters.

### *Accuracy demands and smoothness of the trajectories*

Also related to the above discussion on the speed–accuracy tradeoff is the relationship between the task's accuracy demands and the smoothness of the resulting trajectories. Sosnik *et al*. (2006) have reported that stringent accuracy demands resulted not only in an increased movement duration but also in a decreased movement smoothness. In our experiments, the doorway was large enough (see Materials and methods) that it allowed subjects to get through without any difficulties at normal walking speeds, resulting in smooth trajectories, as we observed. Again, varying e.g. the size of the doorway in future experiments will help in further exploring the relationship between the accuracy demands and the smoothness of the resulting locomotor trajectories.

### *The role of online control in the implementation of locomotor trajectories*

Although trajectories corresponding to a given task were highly stereotyped, there still existed a small trial-to-trial variability, ranging between 10 and 15 cm for the straight and highly curved trajectories, respectively (see the companion paper). This variability could be related to morphological differences between the subjects and to the noise present in the human sensory and motor systems (Harris & Wolpert, 1998).

Remarkably, the variability was smaller at the beginning and the end of the trajectory and larger in between (see for instance the HC trajectory in Fig. 3A). If the movement was executed in open-loop (i.e. in a purely feedforward manner), the variability would increase throughout the movement. Thus, the observed variability pattern indicates that an online feedback control process is at work during the implementation of the optimal trajectory (presumably according to a minimum jerk or minimum snap criterion, as suggested by our results). The nature of such a control process is, however, less clear. In the case of hand movements, a number of hypotheses have been proposed, including trajectory-tracking mechanisms through servo control (McIntyre & Bizzi, 1993) or optimal feedback control schemes (Todorov & Jordan, 2002). Within this context, increasing the complexity of the goal-oriented task (for instance using a multiple via-points task, as in Todorov & Jordan, 2002), applying external perturbations during the movement execution or testing specifically the contribution of sensory information (for instance by manipulating the visual inputs with prism glasses, as in Rushton *et al*., 1998) will help in unveiling the nature of the online control process at work during the implementation of locomotor trajectories.

### *Common strategies may govern the formation of hand and whole-body trajectories*

As evoked in the companion paper, recent studies suggest that the generation of hand and whole-body movements share common strategies. For instance, Papaxanthis *et al*. (2003) have recently observed that vertical whole-body and arm movements executed in the sagittal plane share kinematic similarities. The authors then suggested that the central nervous system (CNS) uses similar motor plans for the performance of arm and whole-body movements in the sagittal plane. The comparison of the velocity–curvature relations in human locomotion and in hand movements has also been conducted, using the same (up to a scaling factor) predefined curved paths in both types of movements (Hicheur *et al*., 2005). At the computational level, Harris & Wolpert (1998) tested the assumption that the CNS learns a new movement by minimizing the variance of the final effector position for both hand and eye movements.

In this context, our observation that the minimum jerk and minimum snap models best predict locomotor trajectories should be related to the case of hand movements, where very similar results have been reported (Flash & Hogan, 1985; Richardson & Flash, 2002). For instance, in the task of periodic drawing of closed shapes, Richardson & Flash (2002) showed that MSD models of order $n > 2$ provided more accurate predictions than MSD models of lower orders.

However, hand and whole-body movements differ greatly in their spatial and temporal scales: for instance, hand trajectories are usually tens of centimetres long while travelled distances during locomotor tasks are usually $>10\times$ longer. This difference in magnitude is associated with a difference in the nature and the number of muscles involved in the production of the movement: while hand movements activate mostly the arm muscles, locomotor activity mobilizes most of the body muscles (lower limbs muscles for body propulsion, upper body muscles for trunk stabilization, neck muscles for steering, etc.). Thus, the fact that the same models could account for both hand and whole-body movements is a striking observation and strongly supports the hypothesis that common mechanisms (in our case, maximizing movement smoothness) are implemented by the motor system in the generation of various types of movements. More specifically, this hypothesis could be related to a theory put forward by Bernstein (1967), according to which there exist, at the higher levels of the motor system, kinematic representations of movements that are independent of the nature (in our case, the arm or the whole locomotor system) of the actual effector.

### *The nature of the control variable(s)*

The last remark is associated with the conceptual distinction between kinematic and dynamic variables usually presented in the literature (Jordan & Wolpert, 1999). While kinematic variables (e.g. the hand's position, velocity, acceleration, jerk, etc. measured in the laboratory reference frame) describe the movement of the end-effector in the extracorporeal space, dynamic variables (e.g. the torques applied at the joints, the muscle activations, etc.) are related to the internal mechanical properties of the motor system.

In the case of arm movements, the motor apparatus can be realistically modelled by a two-link manipulator controlled by torques applied at the joints (Uno *et al*., 1989). In this context, the opposition between kinematic control of the end-effector (the hand) and dynamic control of the torques can be readily investigated. For locomotion, however, given the greater dimensionality of the motor system (at the segmental, muscular, etc. levels), there is a theoretically greater complexity of the motor control problem. Thus, the issue of identifying precisely which variables are being controlled could not be satisfactorily addressed in this study; testing other locomotor tasks and using different kinds of perturbations will help in further exploring the mechanisms underlying the generation of locomotor trajectories. Nevertheless, two series of observations argue in favour of a kinematic control of goal-oriented locomotion. First, we provided evidence in the companion paper that locomotor trajectories are stereotyped, in particular at the kinematic level. In the present study, we were able to accurately predict locomotor trajectories with kinematic-based models. While this does not rule out the possibility that the CNS may take into account dynamic variables in the generation of locomotor trajectories, we suggest that dynamic variables are rather used at the motor implementation level. Following this idea, the transformation from kinematic objectives into dynamic strategies may be acquired with learning (see also Winter & Eng, 1995).

Finally, it should be noted that, contrary to the case of hand movements where the laboratory (allocentric) reference frame (RF) and the body (egocentric) RF are equivalent, here the body RF moves and turns with respect to the laboratory RF when the subject is moving. In this context, the kinematic quantities used in our models (the position of the subject and its derivatives) are only interesting when computed in the laboratory RF as, in his body RF, the subject's position is constant in time. From a theoretical viewpoint, while egocentric and allocentric strategies for spatial navigation and spatial memory are usually debated in the literature (see Berthoz & Viaud-Delmon, 1999), the question of which RF(s) are actually used for the planning and control of goal-oriented locomotion has received little attention. Here, our results suggest that whole-body trajectories are optimized in the laboratory RF. However, further refinements of our experiments and models will also have to consider the possibility of egocentric components in the mechanisms underlying the formation of whole-body trajectories.

### *An integrative approach for the study of human locomotion*

While our approach focused on the global, trajectory-level, descriptions, some fine-grained properties of the locomotor activity can be captured only if the step-level parameters are taken into account. For instance, the variations of the tangential velocity during the step cycle must be included in our models in order to account for the small oscillations observed in the velocity profiles (see for example the average velocity profile corresponding to target 42–270 in Fig. 3B).

Recently, Arechavaleta *et al*. (2006) proposed a robotics-inspired approach that emphasized the nonholonomic nature of human locomotion. For a wheeled vehicle (e.g. a bicycle, a car, a car with trailers, etc.), the kinematic constraint that forces the vehicle to move in the direction of its main axis is known as being nonholonomic (Laumond, 1998). This constraint dramatically reduces the possible movements of the vehicle and, as a result, it strongly affects the nature of the vehicle's optimal trajectories. For instance, as a wheeled vehicle cannot move sideways, the quickest way to parallel park is not associated with a straight path (as it would be in the usual geometry) but consists rather of a series of complicated manoeuvres. In the context of human locomotion, this constraint was interpreted as forcing the subject to move in the direction of his 'axis', which was defined as the orthogonal direction to the shoulders' segment. This constraint was partly verified experimentally (see Arechavaleta *et al*., 2006 for more details). However, in the models presented here, we did not take into account the body orientation and the related nonholonomic constraint. Nevertheless, our models could predict the trajectories with great accuracy, which suggests that, for the range of turning amplitudes tested in our experiments, the body orientation may not be a determining factor in the generation of locomotor trajectories. For more demanding tasks (involving for instance very narrow turns), it is likely that constraints on the body orientation such as the nonholonomic one exert a positive effect on the whole-body trajectories. Both experimental and theoretical issues regarding the integration of such elements into our models are the subject of ongoing research.

## Acknowledgements

This study was supported by Human Frontiers grant n° R6P0054/2004. We thank Professor D. Bennequin and Dr S. I. Wiener for helpful comments. We are also grateful to two anonymous reviewers whose suggestions have greatly improved the manuscript.

## Abbreviations

AnVD, average normalized velocity deviation; AnVE$_c$, average maximal normalized velocity error; ATD, average trajectory deviation; ATE$_c$, average trajectory error; AVD, average velocity deviation; HC, high curvature; LC, low curvature; MC, medium curvature; MnVD, maximal normalized velocity deviation; MnVE$_c$, maximal normalized velocity error; MSD, minimum squared derivative; MTD, maximal trajectory deviation; MTE$_c$, maximal trajectory error; MVD, maximal velocity deviation; nVD, normalized velocity deviation; ST, straight; TE$_c$, instantaneous trajectory error. Subscripts; a, minimum acceleration; av, average; c, (subscript) standing for v, a, j or s; j, minimum jerk; s, minimum snap; v, minimum velocity.

## References

Alexander, R.M. (1989) Optimization and gaits in the locomotion of vertebrates. *Physiol. Rev.*, **69**, 1199–1227.

Arechavaleta, G., Laumond, J.P., Hicheur, H. & Berthoz, A. (2006) The non holonomic nature of human locomotion: a modeling study. *Proceedings of the IEEE/RAS-EMBS International Conference on Biomedical Robots and Biomechatronics*. Feb. 2006, Pisa, Italy, pp. 158–163

Atkeson, C.G. & Hollerbach, J.M. (1985) Kinematic features of unrestrained vertical arm movements. *J. Neurosci.*, **5**, 2318–2330.

Bernstein, N. (1967) *The Coordination and Regulation of Movements*. Pergamon Press, Oxford.

Berthoz, A. & Viaud-Delmon, I. (1999) Multisensory integration in spatial orientation. *Curr. Opin. Neurobiol.*, **9**, 708–712.

Flash, T. & Hogan, N. (1985) The coordination of arm movements: An experimentally confirmed mathematical model. *J. Neurosci.*, **5**, 1688–1703.

Harris, C.M. (2004) Exploring smoothness and discontinuities in human motor behavior with Fourier analysis. *Math. Biosci.*, **188**, 99–116.

Harris, C.M. & Harwood, M.R. (2005) Boundary conditions in human movement. *Proceedings of the IASTED International Conference on Biomedical Engineering.* Feb. 2005, Innsbruck, Austria. Acta Press, Calgary, Canada. pp. 629–640.

Harris, C.M. & Wolpert, D.M. (1998) Signal-dependent noise determines motor planning. *Nature*, **394**, 780–784.

Hicheur, H., Vieilledent, S., Richardson, M.J.E., Flash, T. & Berthoz, A. (2005) Velocity and curvature in human locomotion along complex curved paths: a comparison with hand movements. *Exp. Brain Res.*, **162**, 145–154.

Hicheur, H., Pham, Q.-C., Arechavaleta, G., Laumond, J.-P. & Berthoz, A. (2007) The formation of trajectories during goal-oriented locomotion in humans: I. A stereotyped behaviour. *Eur. J. Neurosci.*, **26**, 2376–2389.

Hogan, N. (1984) An organizing principle for a class or voluntary movements. *J. Neurosci.*, **4**, 2745–2754.

Jordan, M.I. & Wolpert, D.M. (1999) Computational motor control. In: Gazzaniga, M. (Ed.), *The Cognitive Neurosciences.* MIT Press, Cambridge (MA), pp. 601–620.

Lacquaniti, F., Terzuolo, C. & Viviani, P. (1983) The law relating the kinematic and figural aspects of drawing movements. *Acta Psychol.*, **54**, 115–130.

Laumond, J.P. (1998) *Robot Motion Planning and Control.* Springer Verlag, New York.

McIntyre, J. & Bizzi, E. (1993) Servo hypotheses for the biological control of movement. *J. Mot. Behav.*, **25**, 193–202.

Morasso, P. (1981) Spatial control of arm movements. *Exp. Brain Res.*, **42**, 223–227.

Papaxanthis, C., Dubost, V. & Pozzo, T. (2003) Similar planning strategies for whole-body and arm movements performed in the sagittal plane. *Neuroscience*, **117**, 779–783.

Richardson, M.J. & Flash, T. (2002) Comparing smooth arm movements with the two-thirds power law and the related segmented-control hypothesis. *J. Neurosci.*, **22**, 8201–8211.

Rushton, S.K., Harris, J.M., Lloyd, M.R. & Wann, J.P. (1998) Guidance of locomotion on foot uses perceived target location rather than optic flow. *Curr. Biol.*, **8**, 1191–1194.

Sosnik, R., Flash, T., Hauptmann, B. & Karni, A. (2006) The acquisition and implementation of the smoothness maximization motion strategy is dependent on spatial accuracy demands. *Exp. Brain Res.*, **176**, 311–331.

Tanaka, H., Krakauer, J.W. & Qian, N. (2006) An optimization principle for determining movement duration. *J. Neurophysiol.*, **95**, 3875–3886.

Todorov, E. (2004) Optimality principles in sensorimotor control. *Nat. Neurosci.*, **7**, 907–915.

Todorov, E. & Jordan, M.I. (1998) Smoothness maximization along a predefined path accurately predicts the speed profiles of complex arm movements. *J. Neurophysiol.*, **80**, 696–714.

Todorov, E. & Jordan, M.I. (2002) Optimal feedback control as a theory of motor coordination. *Nat. Neurosci.*, **5**, 1226–1235.

Uno, Y., Kawato, M. & Suzuki, R. (1989) Formation and control of optimal trajectory in human multijoint arm movement. *Biol. Cyber.*, **61**, 89–101.

Vieilledent, S., Kerlirzin, Y., Dalbera, S. & Berthoz, A. (2001) Relationship between velocity and curvature of a locomotor trajectory in human. *Neurosci. Lett.*, **305**, 65–69.

Viviani, P. & Flash, T. (1995) Minimum jerk, two-thirds power law, and isochrony: converging approaches to movement planning. *J. Exp. Psychol. Hum. Percep. Perf.*, **21**, 32–53.

Viviani, P. & Schneider, R. (1991) A developmental study of the relationship between geometry and kinematics in drawing movements. *J. Exp. Child Psychol.*, **17**, 198–218.

Winter, D.A. & Eng, P. (1995) Kinetics: our window into the goals and strategies of the central nervous system. *Behav. Brain Res.*, **67**, 111–120.

## Appendix

As the MSD cost functional (2) and the boundary conditions (4) are uncoupled in $x$ and in $y$, it is sufficient to find optimal functions separately for $x$ and $y$ (Flash & Hogan, 1985). The problem thus consists of finding a function $x$ defined on [0,1] that minimizes the functional

$$\int_0^1 \left(\frac{d^n x}{dt^n}\right)^2 dt \tag{17}$$

and verifies the boundary conditions

$$x(0) = x_0, x(1) = x_1, \dot{x}(0) = v_0^x, \dot{x}(1) = v_1^x, \ddot{x}(0) = a_0^x, \ddot{x}(1) = a_1^x \tag{18}$$

### *Minimum jerk trajectories*

For MSD of orders $n \geq 3$, it turns out that the optimum function x is a polynomial of degree $2n - 1$ in the variable $t$ (see Flash & Hogan, 1985 for a proof of this result). For instance, when $n = 3$ (minimum jerk), $x$ is a 5th-degree polynomial:

$$x(t) = a_5 t^5 + a_4 t^4 + a_3 t^3 + a_2 t^2 + a_1 t + a_0 \tag{19}$$

The six boundary conditions then yield a 6th-order linear system that in turn uniquely determines the six coefficients $a_0, \ldots a_5$.

### *Minimum snap trajectories*

For $n = 4$, $x$ is a 7th-degree polynomial, which corresponds to eight unknown coefficients, say $a_0, \ldots a_7$. Using the six boundary conditions, we can express $a_0, \ldots a_5$ as affine functions of $a_6$ and $a_7$. Replacing next $a_4$ and $a_5$ by their expressions in terms of $a_6$ and $a_7$ in the cost functional

$$\int_0^1 \left(\frac{d^4 x}{dt^4}\right)^2 dt = \int_0^1 (840 a_7 t^3 + 360 a_6 t^2 + 120 a_5 t + 24 a_4)^2 dt \tag{20}$$

yields a second-order polynomial in the variables $a_6$ and $a_7$. Standard minimization techniques of multivariate polynomials then allow us to obtain algebraic expressions of $a_6$, $a_7$ and then $a_0, \ldots a_5$.

### *Minimum velocity and minimum acceleration trajectories in restricted solutions space*

If $n \leq 2$, the problem is ill-posed (Harris & Harwood, 2005) in the sense that no optimal trajectory exists. However, if we restrict the solution space to the set of polynomials of degree less than or equal to $d$ (where $d$ is an integer $\geq 6$), then we can find a unique optimal trajectory $x_d$. As $d$ grows, the cost associated with $x_d$ decreases (because the solution space is larger). However, when $d \to \infty$, $x_d$ converges to a trajectory that no longer verifies the boundary conditions.

As minimum jerk and minimum snap principles yield polynomials of degrees less than or equal to 7, we set $d = 7$ in order to make unbiased comparisons of the four models.

In the case $n = 2$ (minimum acceleration), the problem thus consists of finding the optimal function $x$ in the form

$$x(t) = a_7 t^7 + a_6 t^6 + a_5 t^5 + a_4 t^4 + a_3 t^3 + a_2 t^2 + a_1 t + a_0 \tag{21}$$

that verifies the boundary conditions (18) and minimizes the cost

$$\int_0^1 \left(\frac{d^2 x}{dt^2}\right)^2 dt = \int_0^1 (42 a_7 t^5 + 30 a_6 t^4 + 20 a_5 t^3 + 12 a_4 t^2 + 6 a_3 t + 2 a_2)^2 dt \tag{22}$$

The same procedure as in the minimum snap case can be applied to find the optimal coefficients $a_0, \ldots a_7$.

The case $n = 1$ (minimum velocity) can be treated similarly.

## A.3 On the Open-loop and Feedback Processes that Underly the Formation of Trajectories during Visual and Nonvisual Locomotion in Humans

By Q.-C. Pham and H. Hicheur. Published in *Journal of Neurophysiology*, vol. 102, pp. 2800-2815, 2009.

*J Neurophysiol* 102: 2800–2815, 2009.
First published September 9, 2009; doi:10.1152/jn.00284.2009.

# On the Open-Loop and Feedback Processes That Underlie the Formation of Trajectories During Visual and Nonvisual Locomotion in Humans

**Quang-Cuong Pham**[1] **and Halim Hicheur**[1,2]
[1]*Laboratoire de Physiologie de la Perception et de l'Action, Collège de France-Centre National de la Recherche Scientifique, Unité Mixte de Recherche 7152, Paris, France; and* [2]*Hertie Institute for Clinical Brain Research, Department of Cognitive Neurology, University Clinic Tuebingen, Germany*

Submitted 31 March 2009; accepted in final form 3 September 2009

**Pham QC, Hicheur H.** On the open-loop and feedback processes that underlie the formation of trajectories during visual and nonvisual locomotion in humans. *J Neurophysiol* 102: 2800–2815, 2009. First published September 9, 2009; doi:10.1152/jn.00284.2009. We investigated the nature of the control mechanisms at work during goal-oriented locomotion. In particular, we tested the effects of vision, locomotor speed, and the presence of via points on the geometric and kinematic properties of locomotor trajectories. We first observed that the average trajectories recorded in visual and nonvisual locomotion were highly comparable, suggesting the existence of vision-independent processes underlying the formation of locomotor trajectories. Then by analyzing and comparing the variability around the average trajectories across different experimental conditions, we were able to demonstrate the existence of on-line feedback control in both visual and nonvisual locomotion and to clarify the relations between visual and nonvisual control strategies. Based on these insights, we designed a model in which maximum-smoothness and optimal feedback control principles account, respectively, for the open-loop and feedback processes. Taken together, the experimental and modeling findings provide a novel understanding of the nature of the motor, sensory, and "navigational" processes underlying goal-oriented locomotion.

## INTRODUCTION

The study of human locomotion includes different levels of analysis from the neuronal discharges governing the muscular activity (see Capaday 2002 for a review) to the mechanical forces exerted on the ground, allowing the propulsion of the body. While the understanding the locomotor behavior per se greatly benefited from such analyses, only few studies were devoted to clarify the relations between the mechanical, sensorimotor aspects of locomotion and its "navigational," cognitive components (see Hicheur et al. 2005a for a review). Yet it is critical to provide an integrative view of locomotion, associating our knowledge of the mechanical, sensorimotor, and navigational components of locomotion within a unifying framework: indeed, these different components are necessarily taken into account by the central nervous system (CNS) for the production of the locomotor commands.

It is well known in the field of motor control that the same shape can be implemented by various effectors (the "principle of motor equivalence") (see Bernstein 1967). For example, one can draw the letter A with the finger, the hand, or even by running on a flat surface. Following this idea, we have previously tested the hypothesis that the control of locomotor trajectories obey the same laws as those originally formulated for hand movements, such as the 2/3 power law relating the path curvature to the tangential velocity of the body (Hicheur et al. 2005b; see also Olivier and Crétual 2007; Vieilledent et al. 2001). While this hypothesis could be partially supported, more general principles accounting for the formation of whole-body trajectories remained to be investigated in particular those based on the optimal nature of motor control.

We have thus recently undertaken the study of *goal-oriented* locomotion in a task involving walking toward and through a distant doorway (Arechavaleta et al. 2006; Hicheur et al. 2007). While neither the paths nor the walking speeds were constrained, we observed that humans generated *stereotyped* trajectories at both the geometric (the paths) and kinematic (the velocity and turning profiles) levels, which contrasted with a large variability of feet placements (Hicheur et al. 2007). This indicated that locomotion is not controlled as a mere *sequence of steps*: rather higher-level cognitive strategies govern the formation of *whole-body trajectories*. While providing an integrative view on human locomotion by addressing both its step- and trajectory-related aspects, this approach also brought about a new understanding of locomotion that takes advantage of the recent theoretical advances in *computational motor control* (for reviews, see Jordan and Wolpert 1999; Todorov 2004). A further step in this direction was made when, based on the observation that locomotor trajectories were particularly smooth, we reported that a maximum-smoothness model, originally formulated for hand movements (Flash and Hogan 1985), could also predict locomotor trajectories with great accuracy (Pham et al. 2007).

Our ambition in the present article is to further develop this integrative and computational approach to provide a deeper understanding of the *control mechanisms* at work during the production of locomotor trajectories in a goal-oriented task. For instance, the maximum smoothness model, which is deterministic, could not explain the *variability* around the average trajectories. Yet the analysis of movement variability is crucial for the understanding of human movements. In the particular case of locomotion, Winter and Eng (1995) showed, by studying the variability of the knee and hip angles, that the "controlled variable" is rather the *sum* of these two angles than any of them taken separately (in other words, a synergetic control of the joint angles). More recently, the optimal feedback control theory, which specifically relies on the analysis of movement variability, was proposed as a general theory of human movements (Todorov and Jordan 2002).

---

Address for reprint requests and other correspondence: Q.-C. Pham, Laboratoire de Physiologie de la Perception et de l'Action, Collège de France Centre National de la Recherche Scientifique Unité Mixte de Recherche 7152, 11 Place Marcelin Berthelot, 75005 Paris, France (E-mail: cuong.pham@normalesup.org).

In the present article, we therefore not only study the average locomotor trajectories but also the *variability profiles* (how variability evolves in time). To discover the fine structure of these variability profiles, we adopted a *differential approach*, where variability profiles in different experimental conditions were compared. In particular, we varied the visual condition (walking with eyes open or closed), the speed condition (walking at normal or fast speed), and the presence of via points along the locomotor path. Yet the comparison of the variability in two different conditions can only be fruitful if this variability is structured around the same average behavior. We thus conducted a first experiment where we tested, for a large range of spatial targets, whether the average trajectories in visual and nonvisual locomotion were similar or not. In the subsequent experiments, we used a more restricted number of spatial targets but a larger number of repetitions per target to examine and compare with better confidence the variability profiles.

A basic assumption of our study is that, theoretically, the control mechanism governing the formation of locomotor trajectories may be divided in two parts (Fig. 1): an *open-loop process*, which can be executed independently of sensory feedbacks, and a *feedback module*, which can modify the open-loop process based on sensory feedbacks to correct the random perturbations that may occur during task execution. Based on the experimental results, we argue that on-line feedback control is present in *both* visual and nonvisual locomotion and suggest the relations between the visual and nonvisual control strategies. We then investigate the precise nature of the on-line feedback control and discuss two competing hypotheses: the "desired trajectory" hypothesis, which assumes two separate stages in the production of a movement: a planning stage when a desired optimal trajectory is computed and an execution stage when this desired trajectory is implemented with "trajectory tracking" mechanisms correcting any deviation away from the desired trajectory; and the optimal feedback control hypothesis (Todorov and Jordan 2002), which states that "deviations from the average trajectory are corrected only when they interfere with task performance" (*goal-directed* corrections, as opposed to desired-trajectory-related corrections).

To test these hypotheses in a direct way, we also consider several *models* of trajectory formation relying on either purely open-loop or optimal feedback control. By analyzing and comparing the models' predictions with experimental data (in terms of both average trajectories and variability profiles), we provide evidence that locomotor trajectories, even in the absence of vision, are controlled in an optimal way.

## EXPERIMENTAL METHODS

Four experiments were conducted involving a total of 22 healthy subjects. Subjects gave their informed consent prior to their inclusion in the study. The experiments conformed to the Code of Ethics of the Declaration of Helsinki. In *experiment 1,* we studied the effect of vision on the average trajectories and on the *magnitude* of the variability around the average trajectory. *Experiment 2* was designed to more specifically examine the *time course* of the variability (variability profile) in the visual (VI) and nonvisual (NV) conditions. *Experiment 3* addressed the influence of speed and *experiment 4* aimed at assessing the desired trajectory hypothesis in the context of locomotion.

### *Materials*

A number of light-reflective markers were attached to the subject: 42 in *experiments 1–3* (allowing full-body movement capture), and 2 in *experiment 4* (the 2 shoulder markers). The three-dimensional (3D) positions of these markers were recorded at a 120-Hz sampling frequency using an optoelectronic Vicon V8 motion-capture system wired to 12 cameras. To study whole-body trajectories in space, we used the midpoint between the left and right shoulder markers that were located on the left and right acromions, respectively (see Hicheur et al. 2007). In *experiment 2,* we used in addition the left and right heel markers to compute the number of steps.

In all trials, the target was indicated by a cardboard arrow of dimension 1.20 × 0.25 m (length and width, respectively). The arrow was placed at a specific $(x,y)$ position in the motion capture space with an orientation $\alpha$ (Fig. 2, *A–C*).

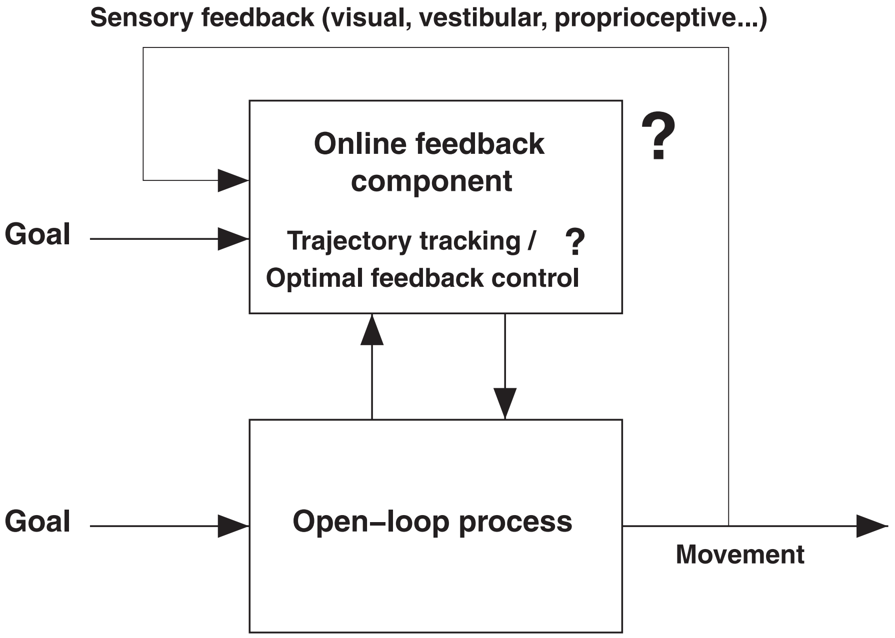

FIG. 1. Sketch of a general controller, including an open-loop process and a feedback module. The question marks indicate some of the issues investigated in the present article: namely, does on-line feedback control exist in visual and nonvisual locomotion and what is the precise nature of the feedback control scheme, trajectory tracking or optimal feedback control?

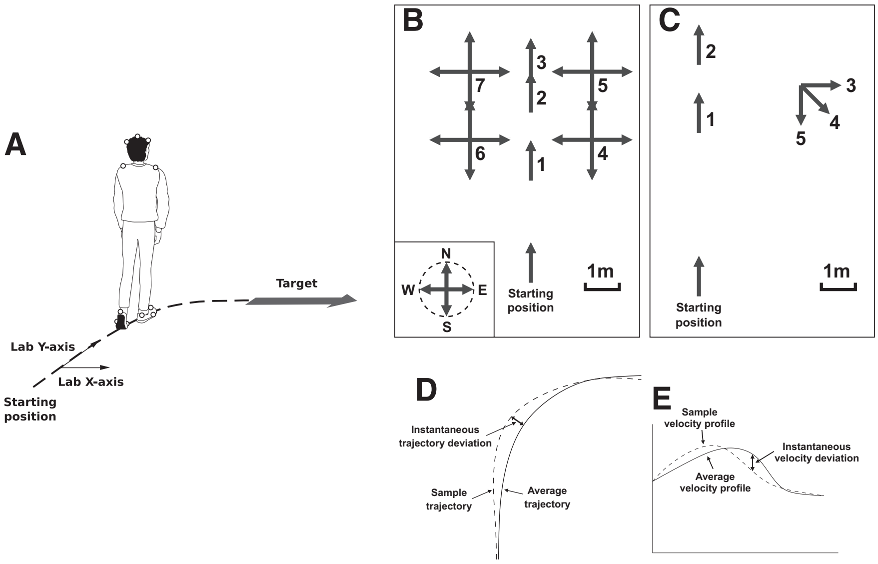

FIG. 2. *A*: experimental protocol: the subject had to start from a fixed position in the laboratory and walk toward a distant arrow placed on the ground. He had to enter the arrow by the shaft and stop above the arrow head. *B*: spatial layout of the 19 targets in *experiment 1*: each target was referred to by a number (1–7) indicating its position and by a letter (N: north, S: south, E: east, W: west) indicating its orientation. *C*: spatial layout of the 5 targets in *experiment 2. D*: the instantaneous trajectory deviation [TD($t$)] measures the variability of actual trajectories around the average trajectory (*Eq. 1*). *E*: the instantaneous velocity deviation [VD($t$)] measures the variability of actual velocity profiles around the average velocity profile (*Eq. 5*).

*Experiments 1–3* took place in a laboratory of dimensions ~10 × 10 × 5 m (length, width, and height, respectively). *Experiment 4* was carried out in a smaller laboratory (~6 × 8 × 4 m).

## *Experiment 1*

Fourteen male subjects participated in this experiment. The mean age, height, and weight of the subjects were, respectively, 24.6 ± 3.2 yr, 1.80 ± 0.04 (SD) m, and 73.3 ± 5.7 kg.

In each trial, the subject had to start from a fixed position in the laboratory and to walk toward a distant target indicated by an arrow (Fig. 2*A*). We constrained the subject's initial walking direction by asking him to start at position (0,−1 m) and to walk the first meter [from (0,−1 m) to (0,0)] orthogonally to the $x$ axis (Fig. 2, *A–C*). After crossing the $x$ axis, no specific restriction relative to the path to follow was provided to the subject. We imposed the subject's final walking direction by asking the subject to enter the arrow by the shaft and to stop walking above the arrowhead.

The subject walked either with eyes open (VI) or closed (NV). In this experiment, he was asked to walk at his preferred normal speed. In condition VI, the arrow was visible throughout the whole movement. In condition NV, the subject first observed the arrow while standing at the starting position. This observation period typically lasted <3 s. When the subject was ready, he closed his eyes and attempted to complete the task without vision. The subject was asked to complete the task with the same initial and final constraints as in condition VI—namely, walk the first meter orthogonally to the $x$ axis, enter the arrow by the shaft, and stop above the arrowhead. Right after the observation period, the experimenter removed the arrow to avoid tactile feedbacks. Once the subject had completely stopped, he was asked to keep his eyes closed while the experimenter took his hand and guided him randomly for a few seconds in the laboratory before stopping at a random position. The subject was then allowed to re-open his eyes and to go back to the starting position. This procedure prevented the subject from acquiring visual feedbacks during both task and posttask periods (avoiding in this way spatial calibrations of the room using kinesthetic cues). The trials were randomized to avoid learning effects for a particular condition or target. The subject completed two to three trials before the experiment actually started to be familiar with the task and to dispel any fear of hitting the walls during the nonvisual trials (the distance between the most distant target and the wall was ~3 m).

The angular displacement of the body in space induced by the different orientations of the arrow ranged between −180 and 180° (Fig. 2*B*). Three targets were placed straight ahead of the subject (straight targets), while the others were placed on the side (angled targets).

The three straight targets were used for all subjects. A subgroup of six subjects walked toward the angled targets located on the left, while the remaining eight subjects walked toward the angled targets on the right. Thus each subject generated 66 trajectories corresponding to 11 spatial targets (3 straight + 8 angled) × two conditions (VI and NV) × 3 trials so that a total of 924 trajectories (14 subjects × 66 trials) were recorded for this experiment.

## *Experiment 2*

The methodology used in this experiment was the same as in *experiment 1* except that here we examined specifically the time course of the variability profiles in conditions VI and NV. We increased the number of repetitions to eight per condition and target. This allowed us to study *intrasubject* variability profiles with a greater reliability.

This experiment was realized in the same laboratory as *experiment 1.* We tested five male subjects, four of whom had already participated in *experiment 1,* which took place 12 mo before. The mean age, height, and weight of the subjects were, respectively, 29.2 ± 4.2 yr, 1.80 ± 0.06 m, and 68.8 ± 5.1 kg.

We reduced the number of targets to five: two straight targets and three angled targets (Fig. 2*C*). Thus each subject executed 80 trials (2 visual conditions × 5 targets × 8 repetitions). As in *experiment 1,* the trials were randomized to reduce learning effects. A total of 400 trajectories (5 subjects × 80 trials) were recorded.

## *Experiment 3*

The methodology and the protocol used in this experiment were the same as in *experiment 2* except that we varied the speed instruction: subjects were asked to walk either at their preferred speed (normal speed, NS) or at a higher speed (fast speed, FS). Vision was available in both speed conditions.

We tested five male subjects in this experiment, three of whom had already participated in *experiment 1,* which took place 12 mo before. The mean age, height, and weight of the subjects were, respectively, equal to 25.8 ± 3.6 yr, 1.80 ± 0.02 m, and 75.9 ± 3.7 kg. As in *experiment 2,* a total of 400 trajectories (5 subjects × 2 speed conditions × 5 targets × 8 repetitions) were recorded.

### *Experiment 4*

This simple experiment adapted a hand movement experiment from (Todorov and Jordan 2002) to the context of locomotion to test the "desired trajectory" hypothesis (see INTRODUCTION).

The experiment was divided in three sessions separated by several hours. In the first session, the task was the same as in the previous experiments, namely, walking toward a distant arrow. We used only one target, similar to target 5 in Fig. 2*C*. The subject performed 10 trials in this session all with vision and at normal speed. We then computed the average trajectory $[x_{av}(t), y_{av}(t)]$, $0 \leq t \leq 1$ across these 10 trials. We denoted, respectively, by $P_1$, $P_2$, and $P_3$ the spatial positions $[x_{av}(0.33), y_{av}(0.33)]$, $[x_{av}(0.5), y_{av}(0.5)]$, and $[x_{av}(0.67), y_{av}(0.67)]$.

In the second session, we placed a piece of black tape on the ground at position $P_2$. The subject was then asked, as in the first session, to walk toward the distant arrow. In addition, he had now to go through the via point indicated by the piece of black tape. Again the subject had to perform 10 repetitions. The third session was similar in all aspects to the second session except that the subject had to go successively through the *three* via points, $P_1$–$P_3$.

We tested five subjects, three males and two females. None had participated in the previous experiments. The mean age, height, and weight of the subjects were, respectively, equal to 30.2 ± 3.8 yr, 1.74 ± 0.08 m, and 68.0 ± 11.9 kg. A total of 150 trajectories (5 subjects × 3 sessions × 10 repetitions) were recorded.

### *Data analysis*

All the data analyses below were performed with the free software GNU Octave unless otherwise stated.

### *Computation of the trajectories*

The beginning ($t = 0$) of each trajectory was set to the time instant when the subject crossed the $x$ axis. To have the same criterion for the VI and NV conditions, the end of each trajectory ($t = 1$) was set to the time instant when the subject's speed became <0.06 m/s (this value was <5% of the average nominal walking speed). We chose this strictly positive threshold because even when the subject had completely stopped, the speed of their shoulders' midpoint was not exactly zero due to the small residual movements of the upper body.

When a derivative of the position (velocity, acceleration, etc.) was needed, a second-order Butterworth filter with cut-off frequency 6.25 Hz was applied before the derivation.

### *Average trajectories, variability profiles, velocity profiles*

For a given target, the average trajectory $[x_{av}(t), y_{av}(t)]$ was defined by

$$x_{av}(t) = \frac{1}{N}\sum_{i=1}^{N} x_i(t);\ y_{av} = \frac{1}{N}\sum_{i=1}^{N} y_i(t) \tag{1}$$

where $N$ corresponds to the number of trajectories recorded for this target ($n = 42$ for the intersubject analysis of *experiment 1; n* = 8, 8, and 10, respectively, for the intrasubject analyses of *experiments 2–4*).

To measure the variability of actual trajectories around the average trajectory, we defined the instantaneous trajectory deviation (TD) at time $t$ as (see Fig. 2*E* for illustration)

$$\mathrm{TD}(t) = \sqrt{\frac{1}{N-1}\sum_{i=1}^{N}[x_i(t) - x_{av}(t)]^2 + [y_i(t) - y_{av}(t)]^2} \tag{2}$$

We then defined the maximum trajectory deviation (MTD) by

$$\mathrm{MTD}(t) = \max_{0 \leq t \leq 1} \mathrm{TD}(t) \tag{3}$$

Variance ellipses were calculated by principal component analysis: the variance ellipse at time $t$ is centered at $[x_{av}(t), y_{av}(t)]$ and its orientation and size indicate how the $[x_i(t), y_i(t)]$ ($i = 1, \ldots, N$) are distributed around $[x_{av}(t), y_{av}(t)]$. Note that $r_1(t)^2 + r_2(t)^2 = \mathrm{TD}(t)^2$ where $r_1$ and $r_2$ are the lengths of the ellipse's semi major and semi minor axes (Pham et al. 2007).

The variability profiles and the variance ellipses of *experiment*t 4 were computed differently, in a manner similar to that described in the legend of Fig. 5 in Liu and Todorov (2007). This was done to better assess the effects of the *spatial* via points.

If a set of trajectories have similar geometric paths, it makes sense to study also the variability of their velocity profiles. For this, we defined the normalized velocity profile $v_i$ and the average normalized velocity profile $v_{av}$ as follows

$$v_i = \frac{\sqrt{\dot{x}_i^2 + \dot{y}_i^2}}{\displaystyle\int_0^1 \sqrt{\dot{x}_i^2 + \dot{y}_i^2}\mathrm{d}t};\ v_{av} = \frac{1}{N}\sum_{i=1}^{N} v_i \tag{4}$$

Next, the instantaneous velocity deviation (VD) can be defined by

$$\mathrm{VD}(t) = \sqrt{\frac{1}{N-1}\sum_{i=1}^{N}[v_i(t) - v_{av}(t)]^2} \tag{5}$$

Note that because the velocity profiles were normalized, $v_i$ and VD have no units.

### *Comparison of trajectories in two conditions*

For comparing the average trajectories recorded in two different conditions, say A and B, we defined, for each target, the instantaneous trajectory separation (TS) by

$$\mathrm{TS}_{A/B}(t) = \sqrt{[x_A(t) - x_B(t)]^2 + [y_A(t) - y_B(t)]^2} \tag{6}$$

where $(x_A, y_A)$ and $(x_B, y_B)$ denote the average trajectories respectively in condition A and in condition B.

We then defined the maximum trajectory separation (MTS) by

$$\mathrm{MTS}_{A/B}(t) = \max_{0 \leq t \leq 1} \mathrm{TS}_{A/B}(t) \tag{7}$$

### *Targets pooling in experiment 1*

In *experiment 1,* six subjects walked toward targets located on their left and eight subjects walked toward targets located on their right (see Fig. 2*B*). We found no significant effect of the side on the parameters of interest: for instance, the $\mathrm{MTS}_{L/R}$ (MTS between the average trajectory of the left trajectories and that of the right trajectories) was smaller than the $\mathrm{MTD}_R$ (MTD of the right trajectories) in both conditions VI and NV. In the two-way ANOVA test with replications where the factors were the measure ($\mathrm{MTS}_{L/R}$ vs. $\mathrm{MTD}_R$) and the visual condition, the effect of the measure was significant [$F(1,40) = 37.4$, $P < 0.05$], and there was no significant interaction effect [$F(1,40) = 2.82$, $P > 0.05$]. Thus for all the following analyses, we flipped the left trajectories toward the right and pooled them together with their symmetrical trajectories (trajectories of target 4 with those of target 6, trajectories of target 5 with those of targets 7).

### *Step-level analysis in experiment 2*

In Hicheur et al. (2007), we carried out an extensive step-level analysis to compare the variability of feet placements with that of whole-body trajectories. Here the purpose of the step-level analysis was solely to assess whether the subjects used a *steps-counting* strategy in the nonvisual trials, which may consist of count the number steps executed in one visual trial and reproduce the same number of steps in the corresponding nonvisual trials.

For this, we considered the $z$ coordinates of the left and right heel markers as functions of time. The total number of local maxima of these two signals then gave the number of steps (SN, steps number) executed by the subject. The trial-to-trial variability of this quantity was given by the steps number deviation (SND)

$$\mathrm{SND} = \sqrt{\frac{1}{N-2}\sum_{i=2}^{N}(\mathrm{SN}_i - \mathrm{SN}_{\mathrm{av}})^2} \tag{8}$$

where $N$ is the number of repetitions ($n = 8$ here). Note that we discarded the first trial in the computation of both the average and the SD of the SNs. The discard was done to include only the nonvisual trials that were preceded by at least one visual trial (this is required by the steps-counting strategy, see preceding text). For symmetry, we discarded also the first visual trial.

## Linearity coefficient

To measure how close a variability profile is from a linear profile, we defined a linearity coefficient (LC). The LC of a time series [$y_i(t_i)$, $1 \le i \le N$] quantifies the distance between this time series and its best linear approximation $y = ct$, with $0 \le \mathrm{LC} \le 1$ and LC = 1 for a linear profile. First, the optimal coefficient $c$ was computed by

$$c = \left(\sum_{i=1}^{T} y_i t_i\right) \Big/ \left(\left(\sum_{i=1}^{T} t_i^2\right)\right) \tag{9}$$

Next, the squared approximation error was given by

$$\mathrm{ESS} = \sum_{i=1}^{T}(y_i - ct_i)^2 \tag{10}$$

Finally, the LC was given by

$$\mathrm{LC} = 1 - \mathrm{ESS}/\mathrm{Var}(y) \tag{11}$$

## Statistical tests

Student's $t$-test and ANOVA tests were performed with Gnumeric (GNOME Foundation, Cambridge, MA) while Tukey tests were performed with Matlab (The MathWorks, Natick, MA). The level of significance of the tests was set to $P < 0.05$.

In *experiment 1,* paired $t$-test were performed to compare the MTDs in conditions VI and NV or the MTD in condition VI with the $\mathrm{MTS}_{\mathrm{VI/NV}}$. In both cases, the values to be compared were paired with respect to the target (df = 10).

In *experiment 2,* we used two-way ANOVA tests with replications (or 2-way repeated-measures ANOVA) to assess the effect of the visual condition on the MTDs and on the SNDs. The first factor of the test was the visual condition (df = 1), and the second factor was the target (df = 4).

Two-way ANOVA tests with replications were used to assess the effect of the speed instruction on the actually measured average speeds or the MTDs. The first factor of the test was the speed condition (df = 1), and the second factor was the target (df = 4). We also compared the MTD in condition NS with the $\mathrm{MTS}_{\mathrm{NS/FS}}$ using a similar two-way ANOVA test.

In *experiment 4,* we used a one-way ANOVA test with replications to assess the effect of the via-point condition (no, 1, or 3 via points) on the MTDs. If a significant effect was found, we performed post hoc Tukey tests to assess the effect of the via-points within each pair of conditions.

# EXPERIMENTAL STUDY

## Results

VISION DOES NOT AFFECT THE AVERAGE TRAJECTORIES (*EXPERIMENT 1*). Average trajectories in the VI and NV conditions were similar both at the geometric level (the paths) and the kinematic level (the velocity profiles): see Fig. 3, *A, 1* and *2, B, 1* and *2,* and *C, 1* and *2.* Specifically, the NV trajectories displayed all the typical features observed in the VI trajectories: straight paths for straight targets, smoothly curved paths for angled targets, inverse relationship between velocity and curvature. The similarity was particularly striking even for the most angled targets such as 4W, 5W, 4S, and 5S.

More quantitatively, the average $\mathrm{MTS}_{\mathrm{VI/NV}}$ across targets was 0.30 ± 0.10 m (or 5.7 ± 2.9% of trajectory length). There was no statistically significant difference between the $\mathrm{MTS}_{\mathrm{VI/NV}}$ and the $\mathrm{MTD}_{\mathrm{VI}}$, which was 0.31 ± 0.10 m (paired 2-tailed $t$-test, df = 10, $t = -0.18$, $P > 0.05$). In other words, the difference between the average trajectories in the two conditions was of the same magnitude as the variability within condition VI.

VISION AFFECTS THE VARIABILITY AROUND THE AVERAGE TRAJECTORIES (*EXPERIMENTS 1* AND *2*). *Intersubject variability (experiment 1).* While the average trajectories in the VI and NV conditions were similar, the absence of visual feedbacks yielded large differences in terms of the variability profiles. In *experiment 1,* the average $\mathrm{MTD}_{\mathrm{NV}}$ across targets was equal to 0.74 ± 0.13 m, which was significantly larger than the $\mathrm{MTD}_{\mathrm{VI}}$ (paired 1-tailed $t$-test, df = 10, $t = 16.0$, $P < 0.05$). Moreover, the shapes of the intersubject variability profiles differed greatly between the two conditions (this is further discussed later).

*Intrasubject variability (*experiment 2*).* The preceding observation that the intersubject variability was larger in nonvisual locomotion than in visual locomotion was confirmed in *experiment 2* on an intrasubject basis (Fig. 4*C*). In the two-way ANOVA test where the factors were the visual condition and the target, the main effect of the visual condition on the MTD was found to be significant [$F(1,40) = 86.1$, $P < 0.05$], and there was no significant interaction effect [$F(4,40) = 0.61$, $P > 0.05$].

We noted, however, that the difference between the average trajectories of conditions VI and NV in *experiment 2* was larger than the corresponding values reported in *experiment 1*: here the average $\mathrm{MTS}_{\mathrm{VI/NV}}$ across targets and subjects was 0.54 ± 0.25 m (Fig. 4*C*), whereas the average $\mathrm{MTS}_{\mathrm{VI/NV}}$ across targets was 0.30 ± 0.10 m in *experiment 1.* This difference could be explained by the fact that in *experiment 2,* the average trajectories were computed across 8 trials (intrasubject average), whereas in *experiment 1,* these were computed across 42 trials (intersubject average). Had we grouped together the five subjects of *experiment 2* (thus averaging across 40 trials), this would yield a value of 0.35 ± 0.12 m for $\mathrm{MTS}_{\mathrm{VI/NV}}$, a value comparable to that of *experiment 1* given in the preceding text.

NO STEPS-COUNTING STRATEGY IN NONVISUAL TRIALS (*EXPERIMENT 2*). It could be argued that despite the randomized order of the trials, the subjects may have used a steps-counting strategy (see METHODS). Such a strategy would imply a low trial-to-trial variability in the number of steps in condition NV. We observed, on the contrary, that the average SND across targets and subjects was 0.79 in condition NV, which was higher than in condition VI (SND = 0.54), where arguably no

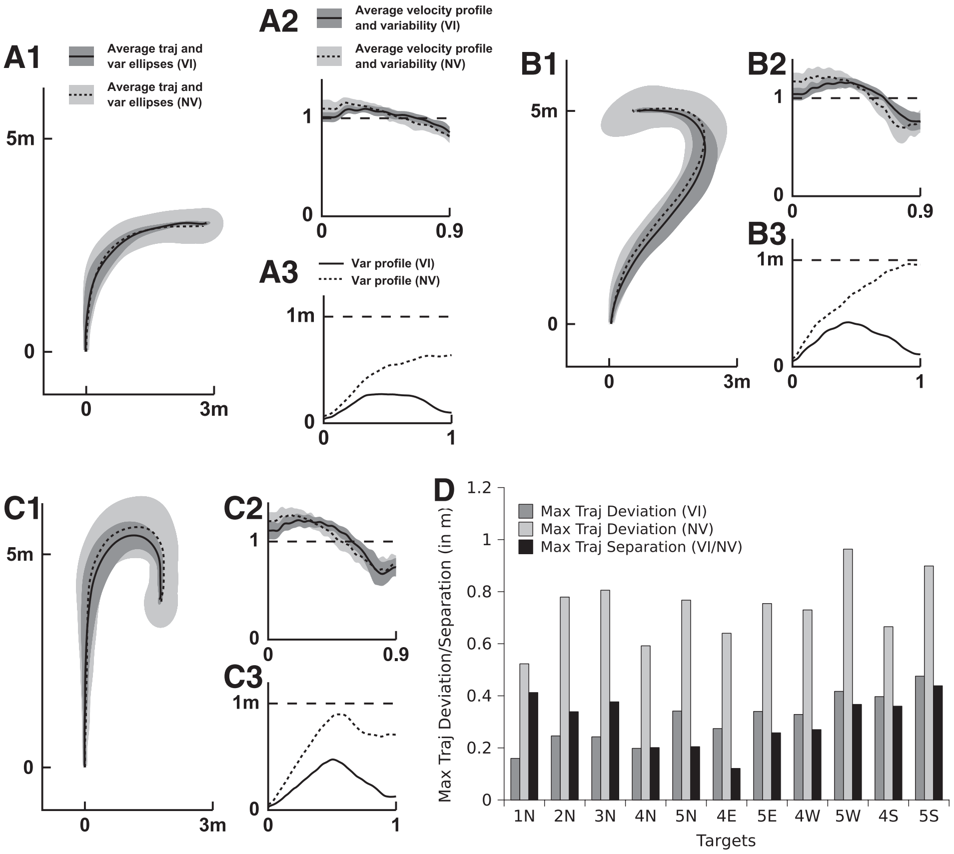

FIG. 3. *Experiment 1*: comparison of locomotor trajectories in the visual (VI: plain lines) and nonvisual (NV: dashed lines) conditions. *A*: comparison for target 4E. *A1*: geometric paths of the average trajectories. Variance ellipses around the average trajectory at every time instant (see METHODS) are shaded in dark gray (VI) and light gray (NV). *A2*: average velocity profiles. The velocity profiles were normalized so that their average values over the movement duration equals 1 (see METHODS). SDs around the average velocity profiles are shaded in dark gray (VI) and light gray (NV). *A3*: variability profiles [TD(*t*)]. *B*: same as in *A* but for target 5W. *C*: same as in *A* but for target 5S. *D*: maximal trajectory deviation/separation (MTD/MTS) in meters: MTD in condition VI (dark gray bars), MTD in condition NV (light gray bars), MTS between the average trajectory of VI and NV (black bars).

steps-counting strategy was used. In the two-way ANOVA test where the factors were the visual condition and the target, the main effect of the visual condition on the SND was found to be significant [$F(1,40) = 7.6$, $P < 0.05$], and there was no significant interaction effect [$F(4,40) = 0.82$, $P > 0.05$].

BUMP-SHAPE OF THE VARIABILITY PROFILES IN VISUAL LOCOMOTION (*EXPERIMENT 2*). We noted that in both conditions VI and NV, the variability was low at the beginning of the movement. This is related to the fact that for given a target, the subject started all the trials from the same starting position.

In condition VI, the variability was also close to zero at the end of the movement. This is because when vision was available, the subject could complete all the trials successfully by stopping at the requested final position. Regarding the middle part of the variability profiles, one may distinguish between the straight targets and the angled targets. For the former, the variability was close to zero during the whole movement (see the plain lines in Fig.

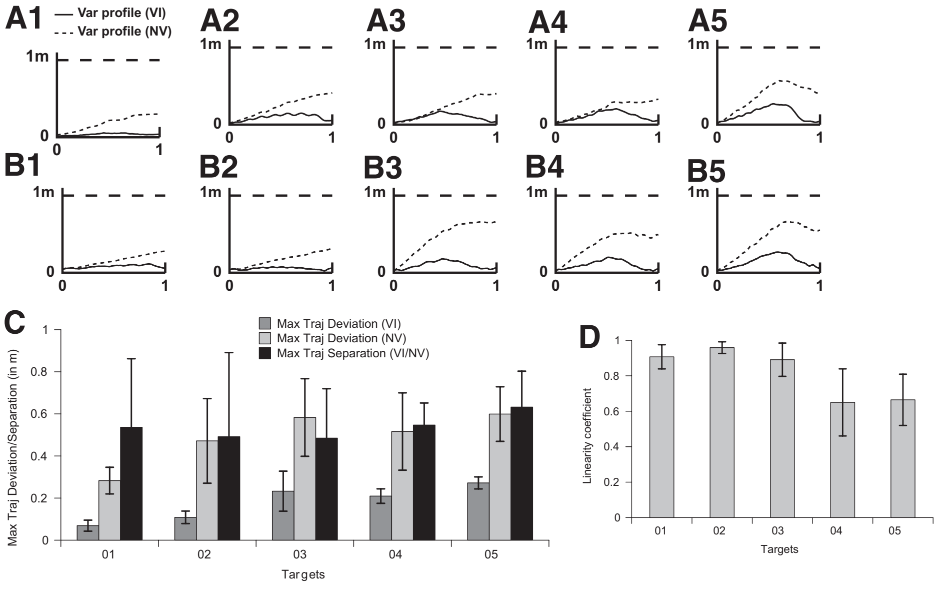

FIG. 4. *Experiment* 2: comparison of variability profiles in the VI (plain lines) and NV (dashed lines) conditions. *A*: variability profiles for *subject LH*. *A1*: target 1 . *A5*: target 5. *B*: same as in *A* but for *subject NV*. *C*: average MTD across targets in condition VI (dark gray bars) and in condition NV (light gray bars), average MTS across targets between conditions VI and NV (black bars). Here the MTD and MTS were computed in an intrasubject fashion. First, for each subject, a MTD (or MTS) was computed over the 8 trials corresponding to this subject, then the average values and SDs of the MTD (or MTS) across the 5 subjects were plotted. *D*: linearity coefficients LC ($0 \leq LC \leq 1$ and LC = 1 for a linear function, see METHODS).

4, *A, 1* and *2,* and *B, 1* and *2*), whereas for the latter, the variability was higher around the middle of the movement than around the ends, yielding a *"bump-shape" variability profile* (*A, 3–5,* and *B, 3–5*).

SPECIAL SHAPES OF THE VARIABILITY PROFILES IN NONVISUAL LOCOMOTION (*EXPERIMENT 2*). In condition NV, the variability did not decrease toward zero at the end of the movement as in condition VI. For the straight targets (targets 1 and 2), the variability increased approximately linearly with time so that the variability profiles could be approximated by a straight line (Fig. 4, *A, 1* and *2,* and *B, 1* and *2,* dashed lines). This was confirmed by the calculation of the average LC across subjects, which were close to 1 for these targets (Fig. 4*D*).

For the most angled targets (targets 4 and 5), the variability profiles were not linear: the average LC across subjects was ~0.65 for these targets. Indeed the variability profiles corresponding to these targets were clearly composed of two parts: a first part where the variability increased linearly and a second part where the variability remained constant (see the dashed lines in Fig. 4, *A4* and *B4*) or even decreased (*A5* and *B5*). We propose in *Variability around the average trajectory* a hypothesis accounting for this interesting property.

WALKING SPEED AFFECTS NEITHER THE AVERAGE TRAJECTORIES NOR THE VARIABILITY PROFILES (*EXPERIMENT 3*). The speed instruction was well respected: subjects did walk faster in condition FS than in condition NS. The average speed across targets, subjects and trials was 1.34 ± 0.11 m/s in condition NS and 1.60 ± 0.16 m/s in condition FS. From condition NS to FS, the subjects increased their speed by between 13 and 30%. In the two-way ANOVA test where the factors were the speed condition and the target, the main effect of the speed condition was significant [$F(1,40) = 55.1$, $P < 0.05$], and there was no significant interaction effect [$F(4,40) = 0.09$, $P > 0.05$].

The average trajectories were also similar in the two speed conditions (Fig. 5*C*). The average $\mathrm{MTS}_{\mathrm{NS/FS}}$ computed across targets and subjects was 0.18 ± 0.06 m, whereas the average $\mathrm{MTD}_{\mathrm{NS}}$ was 0.18 ± 0.08 m. In the two-way ANOVA test where the factors were the speed condition and the target, the main effect of the speed condition was not significant [$F(1,40) = 0.01$, $P > 0.05$]. However, the interaction effect was significant [$F(4,40) = 5.7$, $P < 0.05$]. In other words, the difference between the average trajectories in the two conditions was globally of the same magnitude as the variability within condition NS, but target-wise, there were differences between $\mathrm{MTS}_{\mathrm{NS/FS}}$ and $\mathrm{MTD}_{\mathrm{NS}}$. However, for the most interesting targets (targets 4 and 5), we found that $\mathrm{MTS}_{\mathrm{NS/FS}} < \mathrm{MTD}_{\mathrm{NS}}$ (Fig. 5*C*).

The variability profiles measured in the two speed conditions were very similar, in terms of both shape and magnitude (see Fig. 5, *A* and *B,* for typical variability profiles). For the straight targets, the variability was low throughout the movement, and for the angled targets, bump-shaped variability profiles were consistently observed in both speed conditions. In the two-way ANOVA test where the factors were the speed condition and the target, the main effect of speed condition on the MTDs was not significant [$F(1,40) = 0.006$, $P > 0.05$], neither was the interaction effect [$F(4,40) = 1.2$, $P > 0.05$].

PRESENCE OF VIA-POINTS AFFECTS THE VARIABILITY PROFILES (*EXPERIMENT 4*). We noted first that the average trajectories recorded in the three sessions were very similar, as we could expect from the experimental setup. For instance, the MTS between the average trajectory of session 1 (no-via-point) and that of session 2 (1-via-point) was 0.12 ± 0.07 m. Similarly, the MTS between the average trajectory of session 1 (no-via-point) and that of session 3 (3-via-points) was 0.11 ± 0.06 m.

Consistently with the previous results, the variability profiles observed in the no-via-point condition were bump-shaped (Fig. 6, *A1* and *B*). By contrast, the variability profiles in the 1-via-point condition were clearly two-peaked with a local minimum occurring around $t = 0.5$ (Fig. 6, *A2* and *B*). The variability profiles in the 3-via-points condition displayed smaller variations than in the two previous conditions. In particular, we observed no significant peaks or valleys (Fig. 6*A3* and *B*).

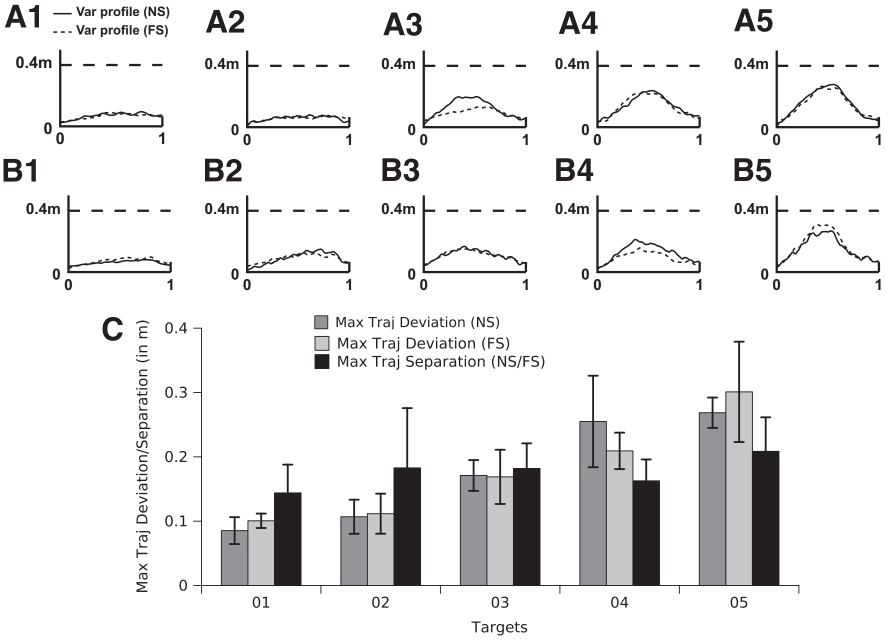

FIG. 5. *Experiment* 3: comparison of variability profiles in the normal speed (NS: plain lines) and fast speed (FS: dashed lines) conditions. For details, see legend of Fig. 4. *A*: variability profiles for *subject B. B*: same as in *A* but for *subject RK. C*: average MTD across targets in condition NS (dark gray bars) and in condition FS (light gray bars), average MTS across targets between conditions NS and FS (black bars).

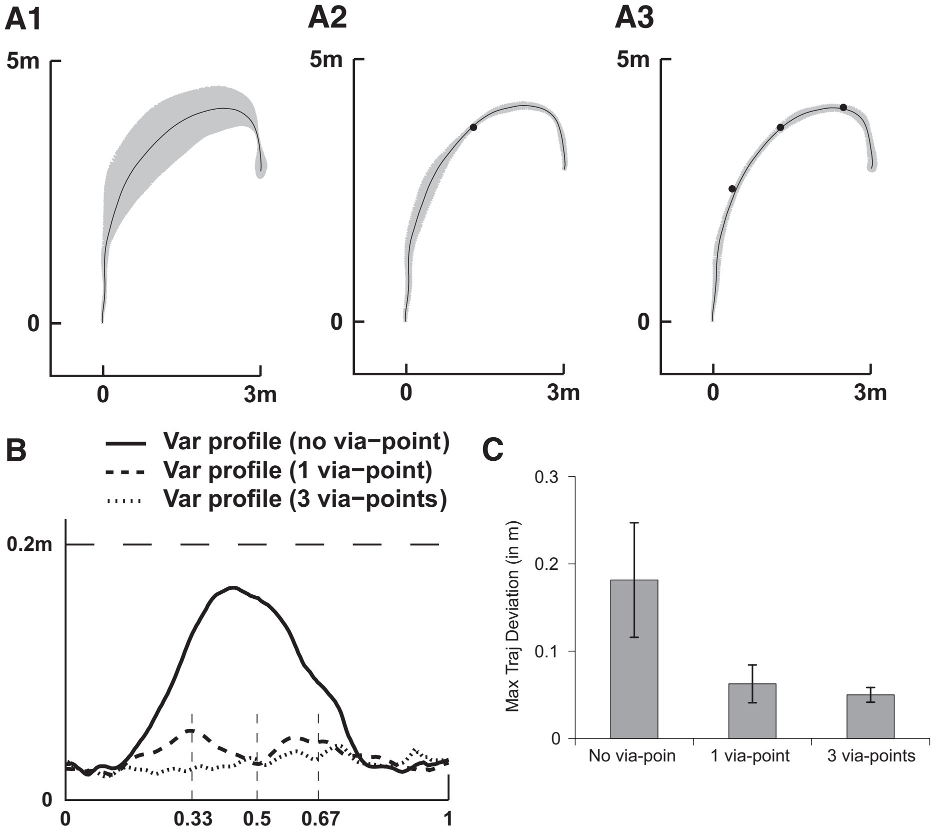

FIG. 6. *Experiment 4*: testing the desired-trajectory hypothesis. *A*: average trajectories and variance ellipses around the average trajectories. *A1*: no-via-point condition. *A2*: 1-via-point condition. *A3*: 3-via-points condition. *B*: average variability profiles computed across subjects. —, no via point; - - -, 1 via point; · · ·, 3 via points. We also indicated the time instants $t = 0.33$, $t = 0.5$, and $t = 0.67$ for which the via points where computed. *C*: average MTD across subjects in the 3 conditions.

Quantitatively, the MTD in the 1-via-point (0.06 ± 0.02 m) and the 3-via-points (0.05 ± 0.008 m) conditions were lower than the MTD in the no-via-point condition (0.18 ± 0.06 m). The one-way ANOVA test revealed that the number of via points (0, 1, or 3) has a significant effect on the MTDs [$F(2,12) = 16.3$, $P < 0.05$]. The post hoc Tukey tests revealed that this effect was significant between the 0- and 1-via-point conditions and between the 0- and 3 via-points conditions but not between the 1- and 3-via-points conditions.

### *Variability around the average trajectory: combination of two independent components*

HYPOTHESIS ON THE STRUCTURE OF THE VARIABILITY PROFILES. We propose to study now in more detail the *structure* of the variability profiles observed in the nonvisual condition, based on the results of *experiment 2*. In this experiment, two parameters were varied: the presence or absence of visual feedbacks and the "complexity" of the target; that is, specifically, whether the target was "straight" or "angled." We make the hypothesis that these two parameters *independently contribute* to the variability profiles.

More precisely, our hypothesis states that the variability recorded for the different targets and visual conditions results from the combination of the variabilities produced by two mutually independent sources. The first source is vision-dependent and "trajectory complexity"-independent: that is, independent of whether the target is straight or angled. The second source is trajectory complexity-dependent and vision-independent. The psychological and physiological interpretations of these two sources are addressed in the DISCUSSION.

The variability resulting from source 1—which is trajectory complexity-independent—can be isolated by examining the trials involving only straight targets: indeed, for these "easy" trials, the contribution of source 2—which is trajectory complexity-dependent—should be minimal. Now from the results of *experiment 2,* we know that the variability in question is almost zero in the visual condition and that it increases approximately linearly with time in the nonvisual condition. Similarly, the variability resulting from source 2—which is vision-independent—can be isolated by examining the trials executed with vision. For the straight targets, this variability is almost zero, whereas for the angled targets, this variability describes, as a function of time, the shape of a bump (see RESULTS of *experiment 2* in the preceding text).

OBSERVATION SUPPORTING THE HYPOTHESIS. The proposed "two-sources" hypothesis allows now to make the following nontrivial observation: the special shape of the variability profiles observed in condition NV for the angled targets can be decomposed as the sum of a *straight line* (source 1) and of a *bump profile* (source 2): see Table 1 for a summary.

TABLE 1. *The two-sources hypothesis*

| Visual Condition/Target | Straight Targets | Angled Targets |
|---|---|---|
| Visual | 0 + 0 | 0 + Bump |
| Nonvisual | Line + 0 | Line + Bump |

In each cell, we indicate the putative contribution of source 1 (vision-dependent, "trajectory-complexity″-independent) + the putative contribution of source 2 (vision-independent, "trajectory-complexity" dependent).

To illustrate this, let us denote by $TD^{n}_{VI}$ and $TD^{n}_{NV}$ the variability profiles corresponding to target *n* in condition VI and condition NV, respectively. The preceding observation implies that $TD^{n}_{NV}$ would be similar to the sum of the *bump-shaped variability profile* observed for the same target in condition VI ($TD^{n}_{VI}$), plus a *straight-line variability profile* (for simplicity, we chose the variability profile corresponding to target 2: $TD^{2}_{NV}$).

Figure 7A shows the comparison of $TD^{4}_{NV}$ with the sum $TD^{4}_{VI} + TD^{2}_{NV}$ for the five tested subjects of *experiment 2*. Similarly, Fig. 7*B* shows the comparison of $TD^{5}_{NV}$ with the sum $TD^{5}_{VI} + TD^{2}_{NV}$. One can observe in each case a good match between the compared profiles.

However, this observation should not be taken literally. While the proposed hypothesis concerns the noise *sources*, we compared above the *trajectory variabilities*, that is, the *output* of the whole trajectory generation process. In this respect, it should be noted that, whenever the trajectory generation mechanisms contain nonlinearities, the additivity of the two noise sources would not translate into the additivity of the trajectory variability profiles. Following this remark, we did not seek to find the best combination of the two *squared* variability profiles (indeed, the variability profiles were given by the 2D SDs of the trajectories, but for linear systems only *variances* add up). We chose instead to show directly the sum of the variability profiles as a way to hint how the special shapes of the variability profiles observed in *experiment 2* can be obtained from the combination of a line and a bump profile. To assess the hypothesis in a more formal way, it is necessary to evaluate the input-output relationship between the incoming noise and the resulting trajectory variability. This is addressed in the modeling study where we propose a possible *implementation* of the trajectory generation mechanism.

## MODELING STUDY

While integrating the previous experimental findings within a unifying framework, the following modeling study also allows testing *positively formulated* control mechanisms. In particular, we propose that the on-line control of whole-body trajectories in visual *and* nonvisual locomotion may be based on optimal feedback control. To test this idea, we designed a simplified optimal feedback control model and compared the predictions of this model (and those of alternative models) with

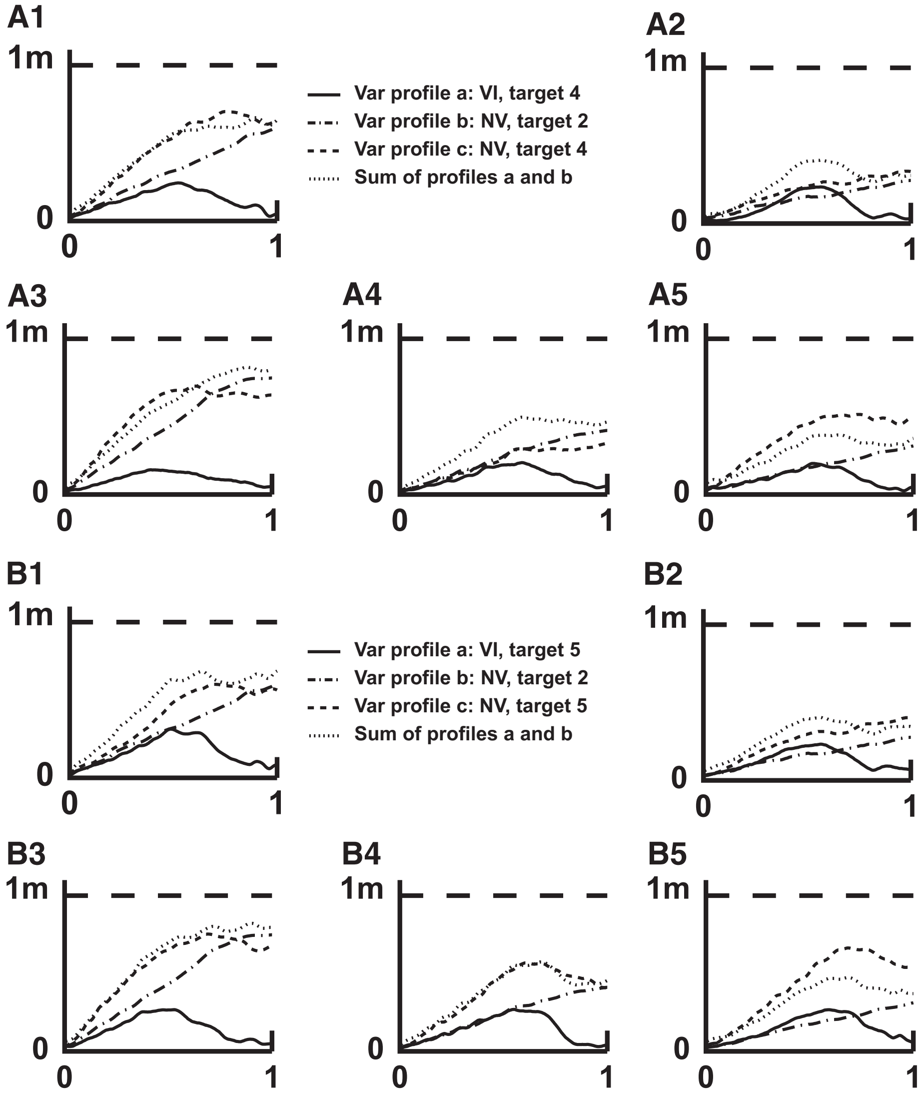

FIG. 7. Testing the 2-sources hypothesis. *A*: variability profiles for target 4 and *subjects AN* (*A1*), *DP* (*A2*), *GN* (*A3*), *LH* (*A4*), and *NV* (*A5*). —, variability profile for target 4 in condition VI; -·-, variability profile for target 2 in condition NV. Compare - - - (variability profile for target 4 in condition NV) with ··· (sum of the — and the -·-). *B*: same legend as in *A* but for target 5.

the experimentally recorded trajectories. Furthermore, as stated previously, the model allows formally testing whether the combination of the two sources (vision-independent and trajectory-complexity-independent) could give rise to the special shape of the variability profiles observed in *experiment 2.*

We first describe a modified version of the minimum jerk model on which our optimal feedback control model is based.

### *Deterministic modified minimum jerk (MMJ) model*

DESCRIPTION *OF THE MODEL.* In (Pham et al. 2007), we presented a minimum jerk model (Flash and Hogan 1985) that could reproduce with great accuracy locomotor trajectories of moderate curvature. However, we noticed that the original minimum jerk model predicted velocity profiles that displayed slightly larger variations than those experimentally observed. For this reason, the simple minimum jerk model failed to predict trajectories recorded in the present experiments, which were highly curved.

To overcome this, we added an extra term that penalizes large variations of the velocity. The influence of this term is weighted by a constant $\gamma$ that we set to a unique value ($\gamma = 1{,}000$) in all the simulations for genericity. Thus we looked for the trajectory $[x(t), y(t)]$, $0 \leq t \leq 1$ that minimizes

$$\int_0^1 \dddot{x}^2 + \dddot{y}^2 + y\left(\frac{d}{dt}\sqrt{\dot{x}^2 + \dot{y}^2}\right)^2 dt \qquad (12)$$

subject to the constraints

$$\begin{aligned} &x(0) = x_0;\ \dot{x}(0) = v_0^x;\ \ddot{x}(0) = a_0^x;\ x(1) = x_1;\ \dot{x}(1) = v_1^x;\ \ddot{x}(1) = a_1^x \\ &y(0) = y_0;\ \dot{y}(0) = v_0^y;\ \ddot{y}(0) = a_0^y;\ y(1) = y_1;\ \dot{y}(1) = v_1^y;\ \ddot{y}(1) = a_1^y \end{aligned} \qquad (13)$$

where the 12 boundary conditions ($x_0$, ${v^x}_0$, ${a^x}_0$, . . .) were set to the respective average experimental values. We found approximated solutions by numerically solving this optimization problem in the subspace of polynomials of degrees $\leq 7$ (see Pham et al. 2007 for more details).

### *Performance of the model*

To assess the quality of the model's prediction, we defined the instantaneous trajectory error (TE) of model M ($M = j$ for the original minimum jerk model and $M = m$ for the modified minimum jerk model) by

$$\mathrm{TE_M}(t) = \sqrt{[x_\mathrm{M}(t) - x_\mathrm{av}(t)]^2 + [y_\mathrm{M}(t) - y_\mathrm{av}(t)]^2} \qquad (14)$$

where $[x_\mathrm{av}(t), y_\mathrm{av}(t)]$ is the experimentally recorded average trajectory and $([x_\mathrm{M}(t), y_\mathrm{M}(t)]$ is the trajectory predicted by the model. The maximal trajectory error (MTE) was defined by

$$\mathrm{MTE_M} = \max_{0 \leq t \leq 1} \mathrm{TE_M}(t) \qquad (15)$$

We compared, for the targets of *experiment 1,* the average trajectories measured in condition VI with the predicted trajectories. For clarity, we divided the targets into two groups: group I containing straight and moderately angled targets (1N, 2N, 3N, 4N, 5N, 4E, 5E) and group II containing highly angled targets (4W, 5W, 4S, 5S). One-way ANOVA tests with replications were then performed to compare the MTD of the trajectories recorded in condition VI with the MTE of the models (3 levels: MTD, $\mathrm{MTE_j}$, $\mathrm{MTE_m}$). If a significant effect was found, we performed post hoc Tukey tests to compare between each pair.

### *Result: the modified minimum jerk can accurately predict the average trajectories for a wide range of targets*

For the straight and moderately angled targets (group I: targets 1N, 2N, 3N, 4N, 5N, 4E, 5E), the original and the modified minimum jerk models yielded accurate predictions, in terms of both trajectory path (Fig. 8*A1*) and velocity profile (*A2*). The average $\mathrm{MTE_j}$ across the targets of group I was 0.11 m, and the average $\mathrm{MTE_m}$ was $<$0.14 m, while the average MTD was 0.26 m. The difference among the three means was significant [$F(2{,}18) = 10.2$, $P < 0.05$]. The post hoc Tukey tests revealed that the difference between MTD and $\mathrm{MTE_j}$ and the difference between MTD and $\mathrm{MTE_m}$ were significant, whereas the difference between $\mathrm{MTE_j}$ and $\mathrm{MTE_m}$ was not. The last result can be explained by the fact that, because the magnitude of the variations in the velocity profiles predicted by the original model were not too large, the addition of the extra term in the objective function did not affect the predicted trajectories (Fig. 8*A, 1* and *2*).

By contrast, for the highly angled targets (group II: targets 4W, 5W, 4S, 5S, see Fig. 8, *B2* and *C2*), the velocity profiles predicted by the original minimum jerk model showed very large fluctuations. This resulted in a larger dissimilarity between the predicted and the experimentally recorded trajectories, in terms of both velocity profile (Fig. 8, *B2* and *C2*) and trajectory path (*B1* and *C1*). Quantitatively, the average $\mathrm{MTE_j}$ across the targets of group II was 0.54 m, the average $\mathrm{MTE_m}$ was 0.29 m, whereas the average MTD was 0.40 m. The difference among the three means was significant [$F(2{,}9) = 7.7$, $P < 0.05$]. The post hoc Tukey tests revealed that the difference between $\mathrm{MTE_j}$ and $\mathrm{MTE_m}$ was significant, meaning that the modified minimum jerk does significantly better than the original model. Indeed the addition of the extra term effectively reduced the variations of the speed, so that the velocity profiles predicted by the modified model very closely resembled the experimentally observed ones (Fig. 8, *B2* and *C2*). In terms of trajectory paths, the modified model also "bent" the minimum jerk paths toward the experimentally observed paths, although no "instruction" about the path was specified in this model.

### *Stochastic models*

VISUAL (VI) CONDITION. The model given by algorithm 1 implements a *simplified optimal feedback control* scheme (Hoff and Arbib 1993; Todorov and Jordan 2002). Following the experimental results, this model relies on an open-loop process that is complemented by an on-line feedback module (see Figs. 1 and 9*A* for illustrations). The open-loop process is based on the maximum-smoothness principle (see preceding text), whereas the feedback module is based on the optimal feedback control principle.

### *Algorithm 1 (see Fig. 9A for illustration)*

*1)* Discretize the movement into $n$ steps ($10 \leq n \leq 20$ depending on the target).

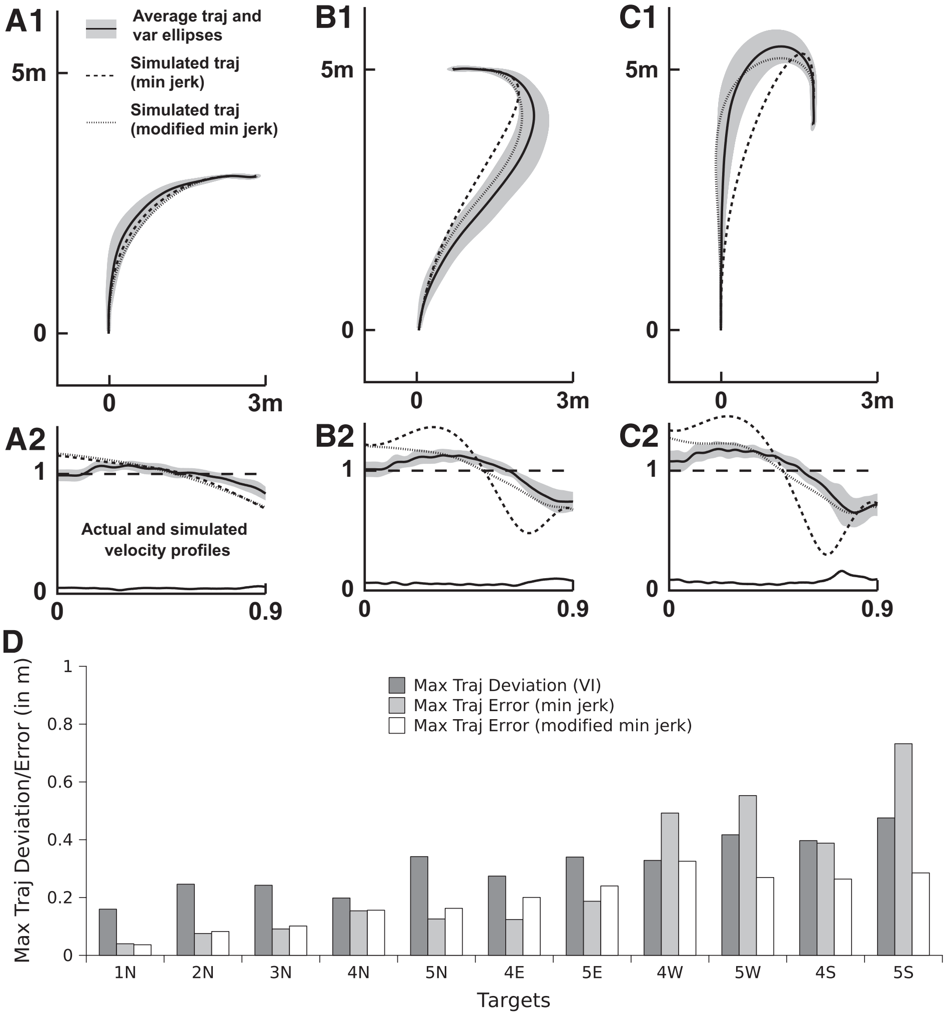

FIG. 8. Modeling results for the deterministic modified minimum jerk model. *A*: modeling results for target 4E. *A1*: geometric path of the average trajectory (plain line) and variance ellipses around the average trajectory (gray area), geometric path of the trajectory predicted by the original minimum jerk model (dashed line) and by the modified minimum jerk model (dotted line). *A2*: average normalized velocity profile (plain line), normalized velocity profiles predicted by the original minimum jerk model (dashed line) and by the modified minimum jerk model (dotted line). The normalization was done so that the mean normalized velocity over the whole trajectory equals 1 (see METHODS and also Pham et al. 2007). (*B*) Same as in *A* but for target 5W. *C*: same as in *A* but for target 5S. *D*: MTD in condition VI (dark gray bars), maximal trajectory error (MTE) for the original minimum jerk model (light gray bars), MTE for the modified minimum jerk model (white bars).

*2)* At each step *i*, compute first a MMJ trajectory between the current state $s(i)$ (position, velocity, acceleration at time step *i*) and the final state. This is the initially planned trajectory.

*3)* Add a random perturbation to $s'(i + 1)$, the state of the initially planned trajectory at step $i + 1$. This yields the actual state $s(i + 1)$.

*4)* Interpolate a smooth trajectory between $s(i)$ and $s(i + 1)$ (for simplicity, we used a MJ trajectory because it is the lowest-order polynomial trajectory $T$ that satisfy $T(0) = s(i)$ and $T(1) = s(i + 1)$: see APPENDIX in Pham et al. 2007 and references therein). This yields the actual sub-trajectory between *i* and $i + 1$.

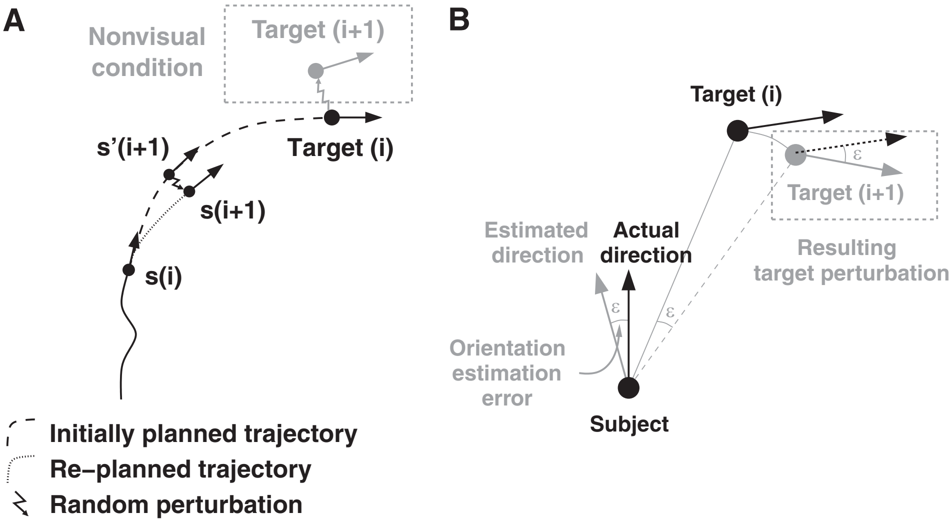

FIG. 9. Illustration for the simplified optimal feedback control models. *A*: illustration for algorithm 1 and for its modified version (NV condition). *B*: effect of an error in the subject's estimation of his orientation in space.

*5)* Repeat from step 2.

We note that this model is a not a fully optimal feedback control model in the sense of Todorov and Jordan (2002) because in the step where we computed the $(i + 1)^{\text{th}}$ optimal subtrajectory (step 2 of algorithm 1), we minimized the deterministic cost instead of the "cost-to-go" (which also takes into account the statistics of the noise) (see Todorov and Jordan 2002). However, this model preserves the main idea of optimal feedback control, namely, that the subtrajectories are recomputed at every step optimally with respect to the final target and not with respect to any intermediate representation of the task (such as a "desired trajectory").

The initial and final velocities and accelerations in algorithm 1 were set to the average experimental values as in the deterministic model. To reproduce the small baseline variability present at the beginning and at the end of the movement, the initial and final positions were chosen from a 2D Gaussian distribution with SD ($\sigma^x_{\text{baseline}} = 0.027$ m; $\sigma\sigma^y_{\text{baseline}} = 0.027$ m) and centered around the actual starting position and the actual target's position.

Regarding the perturbations added at step 3 of the algorithm, Harris and Wolpert (1998) argued that the amount of execution noise (see DISCUSSION) is likely an increasing function of the "motor commands." However, because we did not model directly the whole locomotor apparatus but only its outcome (the locomotor trajectory), it is unclear how execution noise may be "converted" into trajectory perturbations. Here, in the context of locomotion, a series of observations suggest that the magnitude of the trajectory perturbations caused by execution noise is likely determined by the instantaneous trajectory curvature and not by, for instance, velocity or acceleration. First, trajectory variability was higher for the angled targets, which impose curved trajectories, than for the straight targets (*experiments 1* and *2*). This rules out velocity as a determining factor, because velocity was usually lower for curved trajectories. Second, the variability profiles were the same in the NS and FS conditions (*experiment 3*) although the kinematic quantities, such as velocity or acceleration, were larger in condition FS than in condition NS. By contrast, the observed geometric paths (hence the curvature distributions) were the same in the two conditions.

We thus set the magnitude of the trajectories perturbations to be an increasing affine function (van Beers et al. 2004) of the absolute value of the curvature (in a different context, the absolute value of the curvature was used in a model of locomotor trajectories formation) (see Arechavaleta et al. 2008). The total trajectory perturbation is then the sum of a constant perturbation and a signal-dependent perturbation that scales linearly with the absolute value of the curvature

$$\sigma^x_{\text{exec}}(t) = \sigma^y_{\text{exec}}(t) = \sigma_{\text{const}} + |\kappa(t)|\sigma_{\text{sd}} \qquad (16)$$

where $\sigma_{\text{const}} = 0.03$ m and $\sigma_{\text{sd}} = 0.14$ m$^2$ for all targets.

Finally, it should be noted that our method of adding noise directly to the states (and not to the commands) constitutes a simplification. A more rigorous version of our model would require reformulating the MMJ optimization into a dynamical model, as Hoff and Arbib (1993) did for the original MJ optimization. However, in our case, the addition of the $\gamma$ term in the MMJ made such a reformulation much more difficult.

NV CONDITION. To understand the variability patterns observed in condition NV, we evaluate two competing control schemes: a purely open-loop control scheme and an on-line feedback control scheme with state estimation errors.

*Purely open-loop control (models OL).* Here we model three possible purely open-loop control schemes, which are specified in terms of the time series of velocity, acceleration, or jerk.

We computed first the deterministic MMJ trajectory between the initial and final states (see preceding text). We then computed, by successive differentiations, three 2D time series $[v_x(i),v_y(i)]$, $[a_x(i),a_y(i)]$, and $[j_x(i),j_y(i)]$, representing respectively the velocity, acceleration and jerk profiles corresponding to this MMJ trajectory.

In model OL$_{\text{v}}$, we added Gaussian random perturbations with SD $\sigma_{\text{v}}(i)$ to $v_x(i)$ and $v_y(i)$ ($i = 1,\ldots, N$) to obtain a random time series $[v^*_x(i),v^*_y\ (i)]$. Note that $\sigma_{\text{v}}$(i) was also an affine function of the instantaneous trajectory absolute curvature (the coefficients were the same as in the preceding text, but appropriately rescaled to match the experimental variability at $t = 1$). The time series $[v^*_x(i),v^*_y\ (i)]$ was finally integrated with respect to time to yield a random trajectory.

In models OL$_{\text{a}}$ (respectively, OL$_{\text{j}}$), instead of adding the perturbation to the velocity vectors, we added Gaussian random perturbations with SD $\sigma_{\text{a}}(i)$ [respectively, $\sigma_{\text{j}}(i)$] to the acceleration (respectively, jerk) vectors. These random vectors were then integrated twice (respectively, 3 times) to yield a random trajectory.

*On-line feedback control (model OF).* This model was based on the simplified optimal feedback control model used for condition VI (algorithm 1). Remark first that in the VI model, the subject's state $s(i)$ (position, velocity, acceleration) was assumed to be perfectly known to the subject at every time step. To model the absence of vision in condition NV, we introduced perturbations in the subject's estimation of his state. For simplicity, we assumed that these perturbations yielded errors in terms of subject's estimated orientation and distance to target [the reduction of the state to the pair (distance, orientation) is rather classical in studies of nonvisual locomotion] (see for instance Glasauer et al. 2002; Loomis et al. 1993). Remark now that from a *computational* viewpoint, these errors can be rendered, in our model, by perturbing directly the target's orientation and position in space [however, in relation with the discussion on egocentric and allocentric strategies for navigation (Burgess et al. 2002), it should be noted that the *physiological* mechanisms underlying the errors in the estimation of self's state and of the target's state may completely differ].

To make this clear, consider for instance that the subject makes an error $\varepsilon$ in the estimation of his orientation. This is equivalent to assume that he actually makes *no error* in the estimation of his orientation but that the subjects' estimation of the "external world" is rotated by an angle $-\varepsilon$ around the subject. Because the external world in our model comprised only the target, this corresponds to the following perturbations of the target: a rotation centered on the subject and of angle $-\varepsilon$ of the target's position and a shift of $-\varepsilon$ of the target's angle (see Fig. 9*B*). Similarly, an error $\delta$ in the subject's estimation of his distance to the target corresponds to a translation of the external world by -δ along the subject-target axis.

More specifically, we modified algorithm 1 by adding, between steps 4 and 5, the following step "4b".

*Modification of Algorithm 1 for condition NV (see Fig. 9,* A *and* B, *for illustration)*

*1)* Draw a random distance δ from a Gaussian distribution of mean 0 and of SD $\sigma_\delta$ ($\sigma_\delta = 0.03$ m in the simulations). Shift the target's position by -δ along the subject-target axis.

*2)* Draw a random angle $\varepsilon$ from a Gaussian distribution of mean 0 and of SD $\sigma_\varepsilon$ ($\sigma_\varepsilon = 1.8^\circ$ in the simulations). Rotate the target's position by -$\varepsilon$ around the subject. Shift the required final velocity ($v_1^x$, $v_1^y$) and acceleration ($a_1^x$, $a_1^y$) angle by -$\varepsilon$.

There exist several other possibilities to model the absence of vision. One can for instance add an extra 2D-Gaussian perturbation to the target's position at each time step to simulate the spatial memory decay. One can set $\sigma_\delta$ and $\sigma_\varepsilon$ as functions of the execution noise intensity. The estimation process can also be more complex, for instance, combining optimally vestibular and proprioceptive measurements with internal predictions (see the state estimation literature for hand movements reviewed in e.g., Jordan and Wolpert 1999). However, we chose to follow the simple approach above in this first modeling study. It will be necessary in future works to design new experiments and refine this part of the model to study in detail the effects and the interactions of spatial memory decay and of the different sensory signals (e.g., visual, vestibular and proprioceptive) on the variability of nonvisual trajectories.

*Result: plausibility of optimal feedback control*

In condition VI, the sample trajectories predicted by the optimal feedback control model were globally similar to the trajectories observed in one typical subject (Fig. 10*A*). The variability profiles produced by the model also reproduced the typical features of actual variability profiles, namely: low and approximately constant profile for the straight targets (target 2: Fig. 10*B1*) and bump-shaped profile for the angled targets (target 5: *B2*).

In condition NV, the sample trajectories predicted by model OF (on-line feedback control) were also globally similar to the trajectories observed in one typical subject (Fig. 10*C*). Regarding the variability profiles, for the straight targets, the sample variability profile produced by model OF has the form of a straight sigmoid, which was very close to a straight line (dashed line, Fig. 10*D1*). For the angled targets, the sample variability profile produced by model OF increased approximately linearly until $t = 0.8$ and then slightly decreased (dashed line, Fig. 10*D2*).

By contrast, this nonmonotonicity, which is a characteristic property of actual variability profiles (see the results of *experiment 2*), could not be reproduced by none of the OL (purely open-loop) Models. Indeed in all of these models, the variability profiles were always increasing (OL$_\text{v}$: dashed-triply-dotted, OL$_\text{a}$: dashed-dotted, OL$_\text{j}$: dotted lines, Fig. 10*D2*).

## DISCUSSION

### *Visual and nonvisual locomotion share the same open-loop process*

Our experimental observations first showed that to reach a distant target, subjects produced very similar average trajectories in the VI and NV conditions. If we consider only the *final part* rather than the entire trajectory, this finding implies that the average final position and final walking direction in condition NV are close to those in condition VI, which in turn correspond to the target's position and orientation because in condition VI, the task's final constraints were well respected. In earlier studies of nonvisual locomotion (see for instance Loomis et al. 1992; Thomson 1983), it was also reported that in a task where the subject had to walk without visual feedbacks to a previously seen targets, the average final position of

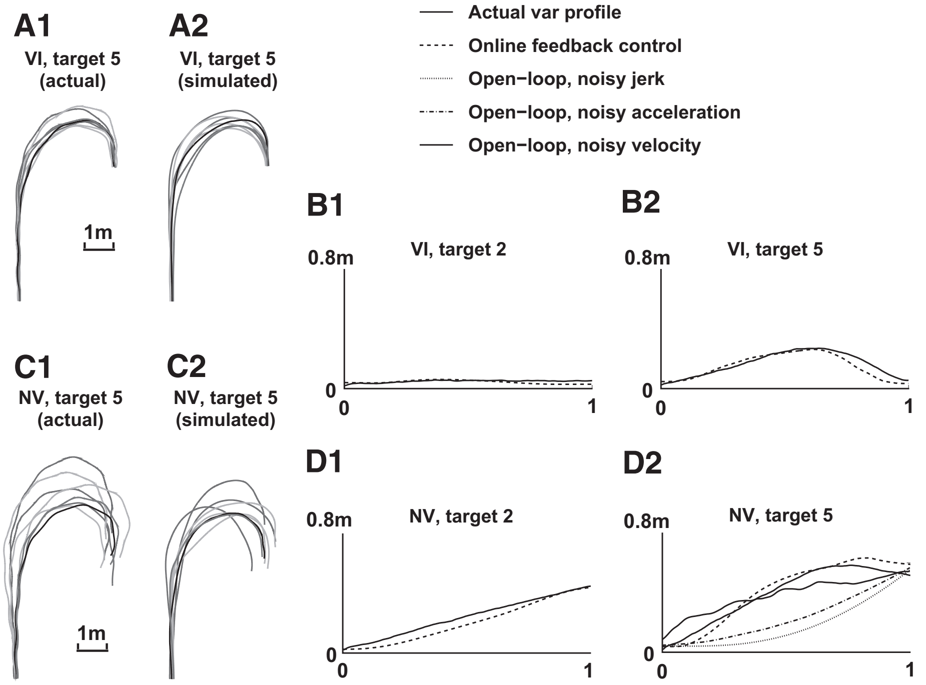

FIG. 10. Modeling results for the stochastic models. *A*: trajectories in the VI condition. *A1*: 8 actual trajectories of *subject NV* for target 5. *A2*: 8 sample trajectories simulated by the stochastic model for target 5. *B*: variability profiles in condition VI. *B1*: variability profiles for target 2. —: average variability profile across subjects. - - -: variability profile computed over 20 simulated trajectories. *B2*: same as in *B1* but for target 5. *C*: trajectories in the NV condition. *C1*: 8 actual trajectories of *subject NV* for target 5. *C2*: 8 sample trajectories simulated by model OF (stochastic MMJ + state estimation error) for target 5. *D*: variability profiles in condition NV. *D1*: variability profiles for target 2. —: average variability profile across subjects. - - -: variability profile computed over 20 sample trajectories (model OF). *D2*: variability profiles for target 5. —: average variability profile across subjects. - - -: variability profile computed over 20 sample trajectories (model OF). -···-: model OL$_\text{v}$ (open-loop control, noisy velocity). -···-. Model OL$_\text{a}$ (open-loop, noisy acceleration). ···: model OL$_\text{j}$ (open-loop, noisy jerk).

the subject almost coincides with the actual position of the target. This precise average response was interpreted as reflecting the veridicality of the subjects' visual space perception (see Loomis et al. 1992). However, in these studies, the targets consisted of spots placed at various distances *in front* of the subject. Using targets defined in both position and orientation and placed at various off-axis positions, our study confirms and generalizes the earlier results mentioned in the preceding text. It also suggests that the notion of visual space perception veridicality may not be limited to straight-ahead distances but may be also valid for the perception of off-axis distances and of changes in the body orientation.

But more importantly, not only the average final positions and orientations were similar in the VI and NV conditions, but also the *entire average trajectories* that the subjects had to produce to reach these positions and orientations. Because the average trajectory is obtained by indeed "averaging out" all the fluctuations, it reflects the open-loop process that governs the subject's movements in absence of perturbations (Todorov and Jordan 2002). Thus the similarity of the average trajectories implies that the control mechanisms in visual and nonvisual locomotion share a common *open-loop process*. This idea may have a deep theoretical implication. Indeed a number of neuroscientists believe that our representation of the space is strongly related to our movements (see for instance Berthoz and Petit 2006), a notion that can be summarized by the following statement of the great French mathematician Henri Poincaré: "To localize an object in space is to build a representation of the movements one has to make to reach it" (Poincaré 1902; chapter 4). Following this line of thinking, the proposed common open-loop process may represent the physiological basis of the psychological notion of veridicality of visual space perception.

In a recent article, Fajen and Warren (2003) challenged the very existence of an open-loop process in the control of locomotion. Based on a simulation study where the targets were modeled by attractors, the obstacles by repellers and the subject by a simple second-order dynamical system evolving in a field of attractors and repellers, these authors argued that "the [subject] adopts a particular route through the scene on the basis of local responses to visually specified [targets] and obstacles. The observed route is not determined in advance through explicit planning, but rather emerges in an on-line manner from the [subject's] interactions with the environment." It should also be remarked that these interactions, which are crucial in Fajen and Warren's approach, are fundamentally based on the availability of visual inputs. In opposition to this view, the similarity of the average trajectories in the VI and NV condition reported in the present article suggests that the formation of locomotor trajectories is not exclusively driven by vision. Rather as formalized in our experimentally-confirmed model, a combination of *open-loop* and *on-line* control mechanisms underlies goal-oriented locomotion.

In the present study, we did not address the physiology underlying the on-line control mechanisms. For instance, in condition VI, how optic-flow-based (Warren et al. 2001) or gaze-direction-based (Rushton et al. 1998) information is combined and processed in the on-line feedback module could not be answered in our study. Similarly, in condition NV, the specific contributions of vestibular and proprioceptive feedback and of efference copy/corollary discharge could not be discriminated here; this may be done through clinical studies, involving for instance patients with vestibular disorders (Glasauer et al. 2002).

### *Origin of the variability and nature of the control mechanisms in visual locomotion*

EXECUTION NOISE IN LOCOMOTION. In contrast with the similarity of the average trajectories, we reported large differences in terms of variability profiles in conditions VI and NV. Before addressing this aspect, we first discuss in more detail the origin and nature of the variability in visual locomotion.

Within the theoretical framework of computational motor control as it has been developed for hand reaching movements, it was proposed that movement variability may arise during three processes: target localization, movement planning, and movement execution (Schmidt et al. 1979; van Beers et al. 2004). We assume here that this three-sources distinction also holds for "locomotor reaching." Given this, we argue that the variability profiles observed in the visual conditions of *experiments 2–4* mostly resulted from execution noise. Indeed regarding first the target localization process, the target was clearly visible and remained so during the whole movement. Second, because we conducted an *intrasubject* analysis, the contribution of planning variability to the overall variability was reduced: indeed, a large part of planning variability arises from differences in subjects' morphologies or personal preferences. Finally, we reason by analogy with hand movements and follow van Beers and colleagues (2004) who demonstrated that—for hand movements—"in general, execution noise account for at least a large proportion of movement variability."

In hand movements, execution noise may arise at different levels (Faisal et al. 2008; van Beers et al. 2004): motor commands (the elaboration and the transmission of the neural signals may be corrupted at any stage of the neural chain, from cortical structures to motoneurons), muscle contractions (the motor response of a muscle to a given neural signal is inherently variable), etc. Because locomotion involves the production of muscle contraction patterns (lower-body muscles for forward propulsion, but also arm and trunk muscles for stability and neck muscles for steering), execution noise can also step in at all these levels. However, because the number of muscles involved in locomotion is much larger than in hand movements, the exact relationship between whole-body trajectory variability and the muscles' execution noises is harder to establish.

As evoked in the INTRODUCTION, locomotion involves also a "navigational" aspect in addition to the purely motor aspect. Indeed, locomotion is the only motor activity in which the spatial position and orientation (in conditions other than straight-ahead locomotion) of the body and of the sensory systems change throughout movement execution. In this respect, special attention should be devoted to the references frames that are used for the perception of movement (Berthoz 1991): in contrast with the case of hand movements, these reference frames move during the locomotor task. For instance, the manipulation of changing points of view over time may introduce errors in the recovering of the heading from retinal flow. In any case, the errors in the updating of the body's position and orientation may in turn contribute to the variability of the trajectory during movement execution. Other cognitive processes, such as the fixation of various objects in the environment (see for instance Turano et al. 2001), may also introduce perturbations at this level. To study in detail the specific contribution of the motor and "navigational" levels to execution noise, a differential analysis may be conducted, for example, by comparing the variability observed during navigation in virtual environments with that observed during real-world locomotion.

ON-LINE FEEDBACK CONTROL OF LOCOMOTION IN VISUAL LOCOMOTION. To fully explain the variability of locomotor trajectories, one has to understand not only the nature of the *noise* but also that of the *control mechanisms* at work for the form of the variability arises from the interplay between these two elements. A given noise pattern may indeed give rise to different variability profiles depending on the control scheme used by the subject.

More precisely, we have distinguished in the INTRODUCTION two families of control schemes: purely open-loop control and on-line feedback control. As already mentioned, in a purely open-loop control scheme, there are no feedback corrections during task execution. The errors can hence only *accumulate*, leading to monotonically increasing variability (see also Todorov and Jordan 2002). This observation was confirmed by the modeling study: the purely open-loop models all produced monotonically increasing variability profiles. By contrast, the results of *experiments 1–3* showed that, for the "angled" targets, the variability profiles in condition VI always increased at the beginning of the movement but then decreased toward zero at the end of the movement, yielding bump-shaped profiles. From a computational perspective, these variability profiles were well reproduced by the on-line feedback model corresponding to condition VI. Taken together, these observations indicate that on-line feedback control is present in visual locomotion. This is not surprising because in general, purely open-loop control exists only in very fast, ballistic movements such as fast hand reaching. Here, since the movements we studied lasted from 3 to 10 s, this allowed the detection of the errors and the implementation of on-line corrections if necessary.

ON THE "DESIRED TRAJECTORY" HYPOTHESIS FOR LOCOMOTION. The precise nature of the on-line feedback control cannot however be determined solely from the variability profiles recorded in *experiments 1–3.* Indeed both the "desired trajectory" hypothesis and the fully optimal control hypothesis can yield bump-shaped variability profiles in the limited conditions of these experiments. However, the results of *experiment 4* are incompatible with a basic desired trajectory control scheme. Indeed as indicated in the INTRODUCTION, the desired trajectory hypothesis implies that during the planning stage, a desired optimal trajectory is computed. Empirically, this desired trajectory can be assimilated to the average trajectory computed across a large number of trials. Then during the execution stage, a trajectory tracking mechanism is used to achieve the desired trajectory. In *experiment 4,* because the average trajectories were forced by the experimental protocol to be very similar in the three conditions (0, 1, and 3 via points), the desired trajectory hypothesis would predict practically no difference between the statistics of the trajectories performed in these conditions. Thus the large differences we reported regarding the variability profiles in the three conditions indicated that the desired trajectory hypothesis should be rejected.

We note nonetheless that the results of *experiment 4* cannot rule out a variation of the desired trajectory hypothesis, which consists of *1*) constructing *several* desired subtrajectories (2 subtrajectories in the 1-via-point condition —the 1st trajectory between the starting position and the via point, the 2nd trajectory between the via point and the final position—and 4 subtrajectories in the 3-via-points conditions) and *2*) tracking *sequentially* these subtrajectories. While this variation may seem unlikely (indeed, in postexperiment interviews, the subjects reported that they conceived the trajectory as a whole and not as a sequence of subtrajectories glued together at the via points), it cannot be theoretically ruled out. This remark also applies for the original experiment of Fig. 3 in (Todorov and Jordan 2002) which inspired our *experiment 4.*

A more likely explanation for the results of *experiment 4* involves an optimal feedback control scheme. Within this scheme, on-line corrections would be made with respect to the task goal [namely, go through the via points (if present) and reach the targets] and not with respect to any intermediate representation (e.g., a desired trajectory). In the no-via-point condition, because no other constraints than the goal was specified, random deviations away from the average trajectory were not corrected if they did not interfere with this task, allowing variability to accumulate around the middle of the trajectory, thus yielding bump-shaped variability profiles. By contrast, when via-points were imposed, the corrections were made to ensure that the trajectory go through these via-points, resulting in low variability around the via-points (see also the discussion about trajectory redundancy in Todorov and Jordan 2002).

### *On-line control of locomotor trajectories in nonvisual locomotion*

While it is easy to conceive that on-line feedback control is present in normal visual locomotion, the fact that such a mechanism may also be present when vision is totally excluded during task execution may be more surprising. Yet we observed in *experiment 2* that the nonvisual variability profiles were not always monotonic: for "angled" targets, the variability decreased near the end of the trajectory. The same arguments as previously then imply that on-line control is also present in nonvisual locomotion.

The idea that on-line control may be present in nonvisual locomotion had been proposed earlier in the literature. For instance, in Farrell and Thomson's (1999) experiment, the subject had to walk with or without vision toward a previously seen target placed at eight paces, eight paces minus 40 cm, or eight paces plus 40 cm in front of him. He had to start with his right foot and to land on the target with his left foot. The authors showed that in both conditions, the subject *functionally* adjusts the lengths of his final steps, *on a trial-to-trial basis*, to land on the target with the specified foot.

The precise nature of that on-line control has however remained unclear. For instance, while Farrell and Thomson rightly remarked that, in the nonvisual condition, "[the subjects] adjust their step lengths in a way similar to that seen in the visual condition," they did not provide an interpretation of the nature of the processes common or specific in visual and nonvisual locomotion.

Here, the two-sources hypothesis (see *Variability around the average trajectories*), directly addressed the nature of this on-line control. Indeed we showed that the variability in the nonvisual condition results from the combination of a vision-dependent component and a trajectory-complexity-dependent component.

The first component—the contribution of which is zero in condition VI and an increasing linear function of time in condition NV—can be interpreted as resulting from the errors in the subject's estimation of his state, which, in turn, are caused by the absence of visual feedbacks. This was confirmed by the modeling study, where the perturbation of the subject's state estimation at each step could reproduce the variability profiles experimentally observed in condition NV.

The second component—the contribution of which is zero for "straight" targets and bump-shaped for "angled" targets—can be interpreted as resulting from the interplay between execution noise and optimal feedback control, as explained previously in the case of visual locomotion. The fact that this component is present also in nonvisual locomotion, under almost the same form (see also the modeling study), thus suggests that the very control mechanisms that governs visual locomotion underlie nonvisual locomotion as well.

Whether our conclusions about the control mechanisms at work during nonvisual locomotion also hold in adventitiously and congenitally blind subjects remains yet to be investigated. We believe indeed that a better understanding of the control mechanisms governing nonvisual locomotion and navigation can help develop new tools assisting visually impaired individuals in their daily activities.

## ACKNOWLEDGMENTS

We are deeply grateful to A. H. Olivier and A. Crétual for help with the experiments and to A. Berthoz for thoughtful comments on an earlier version of the manuscript.

## GRANTS

This work was supported in part by the Agence Nationale de la Recherche PsiRob Locanthrope project. H. Hicheur was supported in part by the Alexander von Humboldt foundation.

## REFERENCES

**Amorim MA, Glasauer S, Corpinot K, Berthoz A.** Updating an object's orientation and location during nonvisual navigation: a comparison between two processing modes. *Percept Psychophys* 59: 404–18, 1997.

**Arechavaleta G, Laumond JP, Hicheur H, Berthoz A.** The non-holonomic nature of human locomotion: a modeling study. In: *Proceedings of the IEEE/RAS-EMBS International Conference on Biomedical Robots and Biomechatronics.* Pisa, Italy, 2006.

**Arechavaleta G, Laumond JP, Hicheur H, Berthoz A.** An optimality principle governing human walking. *IEEE Trans Robot* 24: 5–14, 2008.

**Bernstein N.** *The Coordination and Regulation of Movements.* Oxford, UK: Pergamon, 1967.

**Berthoz A.** Reference frames for the perception and control of movement. In: *Brain and Space,* edited by J. Paillard. New York: Oxford Univ. Press, 1991.

**Berthoz A, Petit JL.** *Phénoménologie et physiologie de l'action.* Paris: Odile Jacob, 2006.

**Burgess N, Maguire EA, O'Keefe J.** The human hippocampus and spatial and episodic memory. *Neuron* 35: 625–641, 2002.

**Capaday C.** The special nature of human walking and its neural control. *Trends Neurosci* 25: 370–376, 2002.

**Faisal AA, Selen LP, Wolpert DM.** Noise in the nervous system. *Nat Rev Neurosci* 9: 292–303, 2008.

**Fajen BR, Warren WH.** Behavioral dynamics of steering, obstacle avoidance, and route selection. *J Exp Psycho Hum Percept Perform* 29: 343–362, 2003.

**Farrell MJ, Thomson JA.** On-line updating of spatial information during locomotion without vision. *J Mot Behav* 31: 39–53, 1999.

**Flash T, Hogan N.** The coordination of arm movements: an experimentally confirmed mathematical model. *J Neurosci* 5: 1688–1703, 1985.

**Glasauer S, Amorim MA, Viaud-Delmon I, Berthoz A.** Differential effects of labyrinthine dysfunction on distance and direction during blindfolded walking of a triangular path. *Exp Brain Res* 145: 489–497, 2002.

**Harris CM, Wolpert DM.** Signal-dependent noise determines motor planning. *Nature* 394: 780–784, 1998.

**Hicheur H, Glasauer S, Vieilledent S, Berthoz A.** Head direction control during active locomotion in humans. In: *Head Direction Cells and the Neural Mechanisms of Spatial Orientation*, edited by Wiener SI, Taube JS. Cambridge, MA: MIT Press, 2005a, p. 383–408.

**Hicheur H, Pham QC, Arechavaleta G, Laumond JP, Berthoz A.** The formation of trajectories during goal-oriented locomotion in humans. I. A stereotyped behavior. *Eur J Neurosci* 26: 2376–2390, 2007.

**Hicheur H, Vieilledent S, Richardson MJ, Flash T, Berthoz A.** Velocity and curvature in human locomotion along complex curved paths: a comparison with hand movements. *Exp Brain Res* 162: 145–154, 2005b.

**Hoff B, Arbib MA.** Models of trajectory formation and temporal interaction of reach and grasp. *J Mot Behav* 25: 175–192, 1993.

**Jordan MI, Wolpert DM.** Computational motor control. In: *The Cognitive Neurosciences.* Cambridge, MA: The MIT Press, 1999.

**Liu D, Todorov E.** Evidence for the flexible sensorimotor strategies predicted by optimal feedback control. *J Neurosci* 27: 9354–9368, 2007.

**Loomis JM, Da Silva JA, Fujita N, Fukusima SS.** Visual space perception and visually directed action. *J Exp Psychol Hum Percept Perform* 18: 906–921, 1992.

**Loomis JM, Klatzky RL, Golledge RG, Cicinelli JG, Pellegrino JW, Fry PA.** Nonvisual navigation by blind and sighted: assessment of path integration ability. *J Exp Psychol Gen* 122: 73–91, 1993.

**Olivier AH, Crétual A.** Velocity/curvature relations along a single turn in human locomotion. *Neurosci Lett* 412: 148–153, 2007.

**Pham QC, Hicheur H, Arechavaleta G, Laumond JP, Berthoz A.** The formation of trajectories during goal-oriented locomotion in humans. II. A maximum smoothness model. *Eur J Neurosci* 26: 2391–2403, 2007.

**Philbeck JW, Loomis JM, Beall AC.** Visually perceived location is an invariant in the control of action. *Percept Psychophys* 59: 601–612, 1997.

**Poincaré H.** *La Science et l'Hypothèse.* Paris: Flammarion, 1902.

**Rushton SK, Harris JM, Lloyd MR, Wann JP.** Guidance of locomotion on foot uses perceived target location rather than optic flow. *Curr Biol* 8: 1191–1194, 1998.

**Schmidt RA, Zelaznik H, Hawkins B, Frank JS, Quinn JT Jr.** Motor-output variability: a theory for the accuracy of rapid motor acts. *Psychol Rev* 47: 415–451, 1979.

**Thomson JA.** Is continuous visual monitoring necessary in visually guided locomotion? *J Exp Psychol Hum Percept Perform* 9: 427–443, 1983.

**Todorov E.** Optimality principles in sensorimotor control. *Nat Neurosci* 7: 907–915, 2004.

**Todorov E, Jordan MI.** Optimal feedback control as a theory of motor coordination. *Nat Neurosci* 5: 1226–135, 2002.

**Turano KA, Geruschat DR, Baker FH, Stahl JW, Shapiro MD.** Direction of gaze while walking a simple route: persons with normal vision and persons with retinitis pigmentosa. *Optom Vis Sci* 78: 667–675, 2001.

**van Beers RJ, Haggard P, Wolpert DM.** The role of execution noise in movement variability. *J Neurophysiol* 91: 1050–1063, 2004.

**Vieilledent S, Kerlirzin Y, Dalbera S, Berthoz A.** Relationship between velocity and curvature of a human locomotor trajectory. *Neurosci Lett* 305: 65–69, 2001.

**Warren WH Jr, Kay BA, Zosh WD, Duchon AP, Sahuc S.** Optic flow is used to control human walking. *Nat Neurosci* 4: 213–216, 2001.

**Winter DA, Eng P.** Kinetics: our window into the goals and strategies of the central nervous system. *Behav Brain Res* 67: 111–120, 1995.

## A.4 The Influence of Vision and Gait Direction on the Formation of Locomotor Trajectories and on the Anticipatory Steering Behavior

By Q.-C. Pham, A. Berthoz and H. Hicheur. In preparation, to be submitted to *Experimental Brain Research*.

# The influence of vision and gait direction on the formation of locomotor trajectories and on the anticipatory steering behavior

**Quang-Cuong Pham[1], Alain Berthoz[1], Halim Hicheur[1,2]**

[1] Laboratoire de Physiologie de la Perception et de l'Action, Collège de France CNRS UMR 7152, 11 place Marcelin Berthelot, 75005 Paris, France

[2, present address] Hertie Institute for Clinical Brain Research, Department of Cognitive Neurology, University Clinic Tuebingen, Germany

*Correspondence*: cuong.pham@normalesup.org

## Abstract

We study the influence of vision (walking with or without vision) and of gait direction (walking forward or backward) on the formation of whole-body trajectories in a goal-oriented task. In a free environment, subjects had to walk from a given position and orientation towards a distant arrow that indicated their final position and orientation. We found that the average trajectories were mostly similar in the different conditions, which suggests that locomotor trajectories are generated at a high cognitive level, and to some extent, independently of the detailed sensorimotor implementations. We also studied how the head and the trunk turning behaviors are affected by changes in the sensory and motor conditions.

Keywords : human locomotion, trajectories, vision, backward, anticipation, steering

## Introduction

Locomotion in humans is a complex motor and cognitive activity requiring multiple levels of control: from the production of repetitive stepping patterns of the lower limbs, through the adjustments of upper-body segments ensuring dynamic stability, to the formation of whole-body trajectories in space. These different levels are integrated together by the Central Nervous System (CNS) for the production and the regulation of the locomotor commands, allowing navigating safely in a particular environment. In this respect, a comprehensive understanding of locomotion requires investigating the *relations* between these different levels. Here, we set out to address the following question: how does a change in the conditions of production of the stepping patterns or a change in the visual conditions affect the formation of whole-body trajectories and the steering behavior?

### Influence of gait direction and vision on the properties of locomotor trajectories

#### *Influence of gait direction*

We recently showed, in a simple goal-oriented task where human subjects had to walk towards and throughout a doorway, that locomotor trajectories were stereotyped, which contrasted with a significantly greater variability in the feet placements (Hicheur et al 2007). This suggested that goal-oriented locomotion is planned and controlled at the level of whole-body trajectories rather than at the level of the steps. However, how dramatic changes in the walking conditions, such as the reversal of gait direction (walking backward), affects the formation of trajectories remains unknown. At the step-level, despite the complete reorganization of the muscular activation patterns that backward walking implies, the *lower limbs kinematics* were shown to be practically invariant up to time reversal (Thortensson 1986, Grasso et al 1998b). Whether this invariance also holds at the level of whole-body trajectories is one of the questions addressed by the present study. If so the hypothesis that locomotor trajectories are planned and controlled at a “supra-motor” level would be further supported.

#### *Influence of vision*

The crucial influence of vision on the formation locomotor trajectories has been investigated by visually-perturbed and nonvisual experimental protocols. Using prisms and virtual environments, researchers studied whether the perceived location of the target (Rushton et al 1998), optic flow (Lappe et al 1999) or a combination thereof (Warren et al 2001) underlie locomotion towards a distant target when (normal or altered) visual feedbacks are available.

When no visual feedbacks are available, it was reported that subjects were still able to walk towards a previously seen distant target placed up to ~ 10 meters in front of them (Thomson 1983, see Loomis et al 1992 for a review). Similarly, the processing of discrete (triangle completion experiments: Loomis et al 1993) or continuous (circular locomotion experiments: Takei et al 1997) changes in *orientation* was shown to be faithfully implemented in nonvisual locomotion. More recently, we demonstrated that, to reach a distant target defined in both position and orientation, subjects produced similar *average* trajectories in visual and nonvisual locomotion (see Fig. 1 and Pham and Hicheur 2009). This led us to suggest that a common *open-loop,* vision-independent process governs the formation of locomotor trajectories. Going a step further, by examining the *variability* around the average trajectories, we showed that similar *online* control mechanisms, likely based on optimal feedback control principles (Todorov and Jordan 2002), underlie visual and nonvisual locomotion (Pham and Hicheur, 2009).

Here, our goal was to investigate the combined effects of vision and gait direction on the formation of locomotor trajectories. As mentioned above, this allows assessing the general hypothesis that these trajectories are generated, to a great extent, independently of their detailed sensori-motor implementations (this notion has already been proposed and verified in hand movements, see e.g. Morasso 1981, Atkeson and Hollerbach 1985).

### Anticipatory steering behavior

The goal-oriented tasks considered in our experiments require bringing the body from a given orientation in space towards another orientation. This change in the body orientation is achieved through continuous and progressive adjustments of the head and trunk orientations throughout movement execution: this is defined as the "steering behavior" (Patla et al 1999a). The steering behavior constitutes another level of description of goal-oriented locomotion, intermediate between the stepping activity and the whole-body trajectory in space.

Changes in the steering behavior significantly affect the formation of locomotor trajectories: for instance, expected and unexpected head yaw movements were shown to affect whole-body trajectories (Vallis and Patla 2004). Conversely, the properties of the trajectories determine head and trunk rotation patterns. For instance, in straight trajectories, the head mostly aligns with the instantaneous direction of movement (heading), but in curved trajectories, the head is oriented towards the *interior* of the curve, thus making a nonzero angle with the heading (this phenonenon is termed "head anticipatory behavior", see Grasso et al 1996, and for a review, Hicheur et al 2005a). Moreover, it was shown that the larger the trajectory curvature, the more the head anticipates (Hicheur et al 2005b, Hicheur et al 2007).

Functionally, the head anticipatory behavior (and more generally, the gaze anticipatory behavior, see Grasso et al 1998a) may play a fundamental role in the challenging biomechanical task of changing walking direction: placing the head (or directing gaze) in the future direction of walking may help provide a reference frame from which the other parts of the body will be organized (Grasso et al 1996, Hollands et al 2001). Indeed, changes in walking direction were found to be initiated by the head, which is followed by trunk and legs' reorientations (Imai et al 2001). The anticipatory behavior remains in absence of vision (Grasso et al 1996, Courtine and Schieppati 2003) and develops in children from 3 years old (Grasso et al 1998a). It should be noted that in all the cited studies, the subjects were instructed to walk along predefined paths or along previously seen predefined paths (nonvisual condition). Whether head anticipation patterns are produced as functions of the *predefined* paths or, to some extent, do they contribute to *define* the *actual* paths could not thus be answered by theses studies.

Here, no constraint relative the path to follow was imposed to the subjects. We also studied in detail the steering behavior during backward locomotion (preliminary observations were reported by Grasso and colleagues (1998c)). Moreover, we examined not only the *degree* of head anticipation but also the *temporal* coordination between the head and trunk rotations. This allows assessing the role of each particular component of the anticipatory behavior (head anticipation, trunk anticipation, head/trunk coordination) in the different sensory and motor conditions.

### Experimental setting

In order to understand the combined and separate effects of gait direction and of vision i) on the locomotor trajectories and ii) on the steering behavior, we designed an experimental protocol where subjects had to walk forward or backward, with or without vision. The comparison of the locomotor trajectories and of the steering behavior across these different conditions allowed us to test the hypothesis that locomotor trajectories are generated at a high cognitive level, and to some extent, independently of the detailed sensori-motor implementations. It also allowed us to describe the inter-relations between the locomotor trajectories and the anticipatory steering behavior in the different sensory and motor conditions.

## Methods

In this study, we wanted to study the effects of vision (walking with (V) or without (N) vision) and of gait direction (walking forward (F) or backward (B)) on locomotor trajectories and on the steering behavior. We used a 2x2 design, implying four experimental conditions: walking with vision forward (VF), with vision backward (VB), without vision forward (NF) and without vision backward (NB). Part of the data involving the VF and NF conditions was presented in a previous paper (Pham and Hicheur 2009).

### Experimental methods

#### *Subjects and materials*

Fourteen healthy male subjects volunteered for participation in the experiment. Subjects gave their informed consent prior to their inclusion in the study. Experiments conformed to the Code of Ethics of the Declaration of Helsinki. The mean age, height and weight of the subjects were respectively equal to 24.6 ± 3.2 years, 1.80 ± 0.04m and 73.3 ± 5.7kg.

Fourty-two light-reflective markers were attached to the subjects, allowing full-body movement capture. The 3D positions of the markers were recorded using an optoelectronic Vicon V8 motion capture system wired to 12 cameras at a 120Hz sampling frequency. To study whole-body trajectories in space, we used the midpoint between left and right shoulder markers which were located on left and right acromions, respectively (see Hicheur et al 2007). These markers were also used to compute the trunk direction (Fig. 2C). The four markers attached to the subjects' heads were used to compute the head direction (Fig. 2C).

In each trial, the target was indicated by a cardboard arrow of dimension 1.20m x 0.25m. The arrow was placed at a specific $(x,y)$ position in the motion capture space with an orientation alpha (Fig. 2B). The angular displacement of the body in space induced by the different orientations of the arrow ranged between -180° to 180°. Three targets were placed directly in front of the subject (straight targets) while the others were placed on the side (angled targets), thus imposing curved trajectories. The three straight targets were used for all subjects. A subgroup of 6 subjects walked towards the angled targets located on the left, while the remaining 8 subjects walked towards the angled targets on the right. Thus, each subject generated 132 trajectories corresponding to 11 spatial targets (3 straight + 8 angled) x 4 conditions x 3 trials, so that a total of 1848 trajectories (14 subjects x 132 trials) were recorded for this experiment.

Incomplete or erroneous trajectories were discarded, resulting in 1608 trajectories being actually processed.

The dimensions of the laboratory where the experiments took place were approximately 10m x 10m x 5m (length, width and height respectively).

#### *Protocol*

In each trial, the subject had to start from a fixed position in the laboratory and to walk towards a distant target indicated by the arrow. We constrained the subject's initial travelling direction (or the heading, see Imai et al 2001) by asking him to start at position (0,-1m) and to walk the first meter (from (0,-1m) to (0,0)) orthogonally to the X-axis (Fig. 2A, 2B). We imposed the subject's final travelling direction by asking the subject to enter the arrow by the shaft and to stop walking above the arrow head. The initial and final constraints were devoted to ensure that subjects performed the experiment in the same conditions. No specific restriction relative to the path to follow was provided to the subject in between the initial and final positions.

The subject walked at his preferred, self-selected speed either with eyes open (visual conditions: VF, VB) or closed (nonvisual conditions: NF, NB). In the visual conditions, the arrow was visible throughout the whole movement. In the nonvisual conditions, the subject first observed the arrow while standing at the starting position. When the subject was ready, he closed his eyes and attempted to complete the task – walk the first meter orthogonally to the X-axis, enter the arrow by the shaft and stop above the arrow head – without vision. The experimenter removed the arrow right after the observation period (which typically lasted less than 3 seconds) in order to avoid any tactile feedbacks (which might have occurred if the subject would have touched the arrow with his feet). Once the subject had completely stopped, he was asked to keep his eyes closed. The experimenter then took the subject's hand and guided him randomly for a few seconds in the laboratory before stopping at a random position. The subject was then allowed to re-open his eyes and to go back to the starting position. This procedure prevented subject from post-execution spatial calibrations using kinaesthetic cues.

The trials were randomized in order to avoid learning effects for a particular condition or target. The subject completed two to three trials before the experiment actually started in order to be familiar with the task and to dispel any fear of hitting the walls during the nonvisual trials (the distance between the most distant target and the wall was ~ 3m).

### Analysis of locomotor trajectories

All the data analyses below were performed with the free software GNU Octave, unless otherwise stated. Some of the analyses were described in (Pham et Hicheur 2009), to which the reader is referred for more details.

#### *Computation of the trajectories*

The beginning ($t = 0$) of each trajectory was set to the time instant when the subject crossed the X-axis. In order to have the same criterion for the visual and nonvisual conditions, the end of each trajectory ($t = 1$) was set to the time instant when the subject's speed became smaller than $0.06\text{m.s}^{-1}$ (this value was smaller than 5% of the average nominal walking speed). We chose this strictly positive threshold because even when the subject had completely stopped, the speed of their shoulders' midpoint was not exactly zero due to the small residual movements of the upper-body.

When a derivative of the position (velocity, acceleration,...) was needed, a second-order Butterworth filter with cut-off frequency 6.25Hz was applied before the derivation.

#### *Average trajectories, variability profiles, velocity profiles*

For a given target, the average trajectory ($x_{\text{av}}(t)$, $y_{\text{av}}(t)$) was defined as

$$x_{\text{av}}(t)=\frac{1}{N}\sum_{i=1}^{N} x_i(t)\ ;\ y_{\text{av}}=\frac{1}{N}\sum_{i=1}^{N} y_i(t) \tag{1}$$

where N corresponds to the number of trajectories recorded for a given target and condition ($N = 14$ subjects x 3 trials = 42 when no trial is discarded for this target and condition).

To measure the variability of actual trajectories around the average trajectory, we defined the instantaneous Trajectory Deviation (TD) at time $t$ as (see Fig. 2C for illustration)

$$\text{TD}(t)=\sqrt{\frac{1}{N-1}\sum_{i=1}^{N}(x_i(t)-x_{\text{av}}(t))^2+(y_i(t)-y_{\text{av}}(t))^2} \tag{2}$$

We then defined the Maximum Trajectory Deviation (MTD) as

$$\text{MTD}(t)=\max_{0\leqslant t\leqslant 1} \text{TD}(t) \tag{3}$$

Variance ellipses were calculated by Principal Component Analysis: the variance ellipse at time $t$ is centred at ($x_{\text{av}}(t)$, $y_{\text{av}}(t)$) and its orientation and size indicate how the ($x_i(t)$, $y_i(t)$) ($i = 1 \ldots N$) are distributed around ($x_{\text{av}}(t)$, $y_{\text{av}}(t)$).

The normalized velocity profile $v_{\text{i}}$ and the average normalized velocity profile $v_{\text{av}}$ were defined as

$$v_i = \frac{\sqrt{\dot{x}_i^2 + \dot{y}_i^2}}{\int_0^1 \sqrt{\dot{x}_i^2 + \dot{y}_i^2}\, dt} \; ; \; v_{\text{av}} = \frac{1}{N} \sum_{i=1}^{N} v_i \tag{4}$$

The instantaneous Velocity Deviation (VD) were next defined as (Fig. 2C)

$$\text{VD}(t) = \sqrt{\frac{1}{N-1} \sum_{i=1}^{N} (v_i(t) - v_{\text{av}}(t))^2} \tag{5}$$

Note that, since the velocity profiles were normalized, $v_i$ and VD have no units.

*Comparison of trajectories in two conditions*

For comparing the average trajectories recorded in two different conditions, say A and B, we defined, for each target, the instantaneous Trajectory Separation (TS) as

$$\text{TS}_{\text{A/B}}(t) = \sqrt{(x_{\text{A}}(t) - x_{\text{B}}(t))^2 + (y_{\text{A}}(t) - y_{\text{B}}(t))^2} \tag{6}$$

where $(x_{\text{A}}, y_{\text{A}})$ and $(x_{\text{B}}, y_{\text{B}})$ denote the average trajectories respectively in condition A and in condition B.

We then defined the Maximum Trajectory Separation (MTS) as

$$\text{MTS}_{\text{A/B}}(t) = \max_{0 \leqslant t \leqslant 1} \text{TS}_{\text{A/B}}(t) \tag{7}$$

*Targets pooling*

In Experiment 1, six subjects walked towards targets located on their left and eight subjects walked towards targets located on their right (see Fig. 2B). We found no significant effect of the side on the parameters of interest: for instance, the $\text{MTS}_{\text{L/R}}$ (MTS between the average trajectory of the left-trajectories and that of the right-trajectories) was smaller than the $\text{MTD}_{\text{R}}$ (MTD of the right-trajectories) in both VI and NV conditions. In the two-way ANOVA test with replications where the factors were the measure ($\text{MTS}_{\text{L/R}}$ vs $\text{MTD}_{\text{R}}$) and the visual condition, the effect of the measure was significant ($F = 37.4$, $p < 0.05$) and there was no significant interaction effect ($F = 2.82$, $p > 0.05$). Thus, for all the following analyses, we flipped the left-trajectories towards the right and pooled them together with their symmetrical trajectories (trajectories of target 4 with those of target 6, trajectories of target 5 with those of targets 7.

### Analysis of the steering behavior: head and trunk absolute and relative orientations

*Definition of head and trunk angles*

The head and trunk orientations in the horizontal plane were computed based on the four head markers and the two shoulders markers respectively (Fig. 2D). The trunk direction was given by the orthogonal direction to the shoulders segment defined by the two shoulders markers.

We considered four time-varying angles: the Absolute Head angle (AH, angle between the head direction and the laboratory X-axis), the Relative Head angle (RH, angle between the head direction and the heading, which is defined as the tangent direction to the trajectory, see Imai et al 2001), the Relative Trunk angle (RT, angle between the trunk direction and the heading) and the Head/Trunk angle (HT, angle between the head direction and the trunk direction) (Fig. 2D).

*Stereotypy of head and trunk steering behavior*

Several statistics were computed to assess the stereotypy of the head turning behavior, as previously done for assessing the stereotypy of whole-body trajectories.

First, the average Absolute Head angle was computed as

$$\mathrm{AH}_{\mathrm{av}}(t)=\frac{1}{N}\sum_{i=1}^{N}\mathrm{AH}_i(t) \tag{8}$$

where $N$ is the number of trajectories recorded for a given target (here, $N$ = 14 subjects x 3 repetitions = 42).

The Absolute Head angle Deviation (AHD), which measures the variability of the AH around the average profile, was then defined by

$$\mathrm{AHD}(t)=\sqrt{\frac{1}{N-1}\sum_{i=1}^{N}(\mathrm{AH}_i(t)-\mathrm{AH}_{\mathrm{av}}(t))^2} \tag{9}$$

The Maximum Absolute Head angle Deviation (MAHD) was next given by

$$\mathrm{MAHD}(t)=\max_{0\leqslant t\leqslant 1}\mathrm{AHD}(t) \tag{10}$$

We defined similarly the RHD (Relative Head angle Deviation), MRHD (Maximum RHD), RTD (Relative Trunk angle Deviation), MRTD (Maximum RTD), HTD (Head/Trunk angle Deviation) and MHTD (Maximum HTD). All these parameters quantified the extent to which the head and trunk angular movements were similar across repetitions and subjects.

*Degree of anticipation*

When humans walk forward along a straight path, the directions of their head and trunk mostly align with the heading, which corresponds to RH ~ 0, RT ~ 0, HT ~ 0 (the residual oscillations induced by the stepping activity are neglected, see Hicheur and Berthoz 2005). By contrast, when they walk along a curved path, their head and trunk significantly deviate from the heading and are oriented towards the *interior* of the curve, thus making nonzero angles with the heading. Furthermore, the larger these angles, the more the head and the trunk *anticipate* with respect to the heading. Thus, to *quantify* the degree of head and trunk anticipation, we computed, for each trajectory $1 \le i \le N$ the Maximum Relative Head angle (MRH) as

$$\mathrm{MRH}_i=\max_{0\leqslant t\leqslant 1}\left|\mathrm{RH}_i(t)\right| \tag{11}$$

and similarly for the Maximum Relative Trunk angle (MRT) and the Maximum Head/Trunk angle (MHT).

These values were then averaged across subjects and repetitions ($1 \le i \le N$), yielding average and standard deviation values. At this point, it should be noted that the SD of the $\mathrm{MRH}_i$ obtained by this calculation should not be confused with the MRHD defined above.

In the backward conditions (VB and NB), since the “natural” angle between the head (and trunk) direction and the heading is -180° (see Fig. 7A), the $\mathrm{MRH}_i$ (and the $\mathrm{MTH}_i$) was computed by

$$\mathrm{MRH}_i=\max_{0\leqslant t\leqslant 1}\left|\mathrm{RH}_i(t)+180\right| \tag{12}$$

*Timing of anticipation*

In addition to the degree of anticipation, it was also interesting to assess its *timing*, which yields insights into the temporal coordination of the different segments (Imai et al 2001). For this, we determined the time instants when the maxima defined in the above paragraph were attained. For instance, the Time of Maximum Relative Head angle (TMRH) was defined by

$$\mathrm{TMRH}_i = \arg\max_{0 \leqslant t \leqslant 1} \left| \mathrm{RH}_i(t) \right| \tag{13}$$

The Time of Maximum Relative Trunk angle (TMRT) and the Time of Maximum Head/Trunk angle (TMHT) were defined similarly.

Finally, these values could also be averaged across subjects and repetitions ($1 \le i \le N$), yielding average and standard deviation values.

### Statistical tests

Student t-tests and ANOVA tests were performed with Gnumeric (GNOME Foundation, Cambridge, MA, USA) while Tukey tests were performed with Matlab® (The MathWorks Inc., Natick, MA, USA). The level of significance of the tests was set to $p < 0.05$.

We used a linear regression analysis to study the relations between head anticipation and trajectory curvature. More precisely, for each trajectory $i$, we computed the Maximum Curvature ($MC_i$) of the trajectory and we performed the regression analysis of $MRH_i$ = beta $MC_i$, which yielded the optimal slope beta and the coefficient of determination $r^2$.

## Results

### Locomotor trajectories

#### *Effects of vision*

*Comparison of Visual Forward (VF) and Nonvisual Forward (NF) conditions*: The results of this comparison were reported in (Pham and Hicheur, 2009), see in particular Fig. 3 in that reference and also Fig. 1 of the present article. Briefly, we showed that the average trajectories in conditions VF and NF were similar both at the geometric level (the paths) and at the kinematic level (the velocity profiles). However, the absence of visual feedback yielded large differences in terms of the variability profiles. In particular, $MTD_{NF}$ was shown to be significantly larger than $MTD_{VF}$. Moreover, the shapes of the variability profiles were qualitatively different: while in condition VF, the variability decreased towards 0 at the end of the movement, yielding bump-shape profiles, it decreased in some targets, but never reached 0 in condition NF.

*Comparison of Visual Backward (VB) and Nonvisual Backward (NB) conditions*: Here, we also found a large similarity of the average trajectories in the VB and NB conditions, albeit to a lesser extent than previously found in the comparison of the VF and NF conditions. This observation was verified at both the path level (Fig. 3A1, 3B1, 3C1) and atthe velocity profile level (Fig. 3A2, 3B2, 3C2). However, the same remark regarding the slight differences in the shapes of the velocity profiles in the VF/NF comparison could also be made for the VB/NB comparison.

Quantitatively, the average Maximal Trajectory Seperation $MTS_{VB/NB}$ across the 11 tested targets was 0.50m (Fig. 3D) in absolute terms, or 9.2% of the VB Trajectory Length (TL). These values are to be compared with the average Maximum Trajectory Deviation within condition VB $MTD_{VB}$, which was 0.38m or 6.4% of the VB TL, and the $MTD_{NB}$, which was 0.90m or 15.7% of the NB TL. Regarding the shapes of the variability profiles, we observed, as in the VF/NF comparison, large differences in terms of both magnitude and shapes between VB and NB conditions (Fig. 3A3, 3B3, 3C3)

#### *Effects of gait direction*

*Comparison of Visual Forward (VF) and Visual Backward (VB) conditions*: In targets which imposed no change in curvature sign (or equivalently whose paths did not contain an inflection point, i.e. all targets except 4W, 4N, 5W, 5N), the average trajectories observed in the VF and VB conditions were very similar at the path level (targets 4E and 5S, Fig. 4A1, 4C1). In targets which imposed a change in curvature sign (4W, 4N, 5W, 5N), the VB paths were slightly shifted to the interior of the main curve with respect to the VF paths (targets 5W: Fig. 4B1; also target 4W: not shown). However quantitatively, this difference resulted in a $MTS_{VF/VB}$ smaller than 0.4m (Fig. 4D). In terms of the velocity profiles, we found very similar patterns, in every targets (Fig. 4A2, 4B2, 4C2). This similarity was larger here than in the previous VF/NF and VB/NB comparisons.

Quantitatively, the average $MTS_{VF/VB}$ across the 11 tested targets was 0.22m (Fig. 4D) in absolute terms, or 4.0% of the VF TL. These values are to be compared with the average $MTD_{VF}$, which was 0.31m or 5.7% of the VF TL, and the average $MTD_{VB}$, which was 0.38m or 6.4% of the VB TL.

Finally, we noted that the variability profiles were similar in the two conditions, both in terms of magnitudes (average $MTD_{VF} = 0.31$m, average $MTD_{VB} = 0.38$m) and shapes (Fig. 4A3, 4B3, 4C3)

*Comparison of Nonvisual Forward (NF) and Nonvisual Backward (NB) conditions*: Here the similarity of the average trajectories was not as strong as in the previous comparison. Yet it was still remarkable given the difficulty of the task (walking to distant targets defined in both position and orientation without visual feedback). At the path level, the average trajectories globally displayed the same forms, with some shift between the two conditions (Fig. 5A1, 5B1, 5C1). In particular, in targets which imposed achange in curvature sign, we observed that, as in the VF/VB comparison, the NB paths were shifted towards the interior of the main curve with respect to the NF paths (target 5W: Fig. 5B; also target 4W: not shown). As in the VF/VB comparison, the velocity profiles were very similar in the two compared conditions, in all targets (Fig. 5A2, 5B2, 5C2).

Quantitatively, the average $MTS_{NF/NB}$ across the 11 tested targets was 0.38m (Fig. 5D) in absolute terms, or 6.9% of the NF trajectory length. These values are to be compared with the average $MTD_{NF}$, which was 0.74m or 13.6% of the NF TL, and the average $MTD_{NB}$, which was 0.90m or 16.5% of the NB TL.

In terms of the variability profiles, we observed a larger variability in condition NB (see the values given above). However the difference between conditions NF and NB was low as compared to the VF/NF and VB/NB comparisons. In addition, the variability profiles displayed similar shapes (Fig. 5A3, 5B3, 5C3).

Taken together, these results show that the average trajectories were highly similar across gait directions and vision conditions (the variability across conditions was comparable – and inferior for most of the cases – to the variability within a single condition). The variability profiles were found to differ across the visual conditions but not across gait directions.

### Steering behavior: head and trunk turning profiles

#### *Absolute head orientation*

The examination of the average Absolute Head angle (AH) profiles (Fig. 6) revealed large differences between conditions VF, NF and NB on one hand, and condition VB on the other.

In conditions VF, NF and NB, the head direction at the beginning and the end of a trajectory was aligned with the heading: orthogonal to the X-axis at the beginning ($AH_{av}(0) = 90°$ in VF and NF, $AH_{av}(0) = -90°$ in NB), and aligned with the arrow's direction at the end of the trajectory ($AH_{av}(1)$ = target_angle in VF and NF, $AH_{av}(1)$ = –target_angle in NB). Between $t = 0$ and $t = 1$, the average AH profiles approximately followed sigmoid-shape profiles – with some differences, however, among the three conditions (red, magenta and cyan lines in Fig. 6A1, 6A2, 6A3; this is studied in more detail in the next section).

By contrast, in condition VB, the head direction was not aligned with the heading at the beginning of the trajectory: $AH_{av}(0) \sim 45°$. Indeed, right from the start, subjects turned their head backwards to look at the target “over their shoulders”. In addition, between $t = 0$ and $t = 1$, the average AH profiles displayed large variations in time (green lines in Fig. 6A1, 6A2, 6A3), unlike the smooth sigmoid-shape profiles observed in conditions VF, NF and NB.

In term of variability, the AH Deviations (AHD) were relatively low in the VF, NF, and NB conditions and much larger in condition VB (Fig. 6B1, 6B2, 6B3). Quantitatively, the average MAHDs across targets were respectively 14.4°, 19.7° and 24.3° in conditions VF, NF, NB, while the average MAHD was 63.6° for VB (see also Fig. 6C). These observations confirmed the results reported in (Hicheur et al 2007) where we demonstrated the stereotypy of the head turning behavior in condition VF. Moreover, they extended those results to the cases of nonvisual forward and backward locomotion. The similarity of the average AH profiles in the VF, NF and NB conditions suggest that the head orientations during nonvisual forward and backward locomotion are controlled following similar strategies as in visual forward locomotion. In the sequel, we analyze in greater details these strategies, with a particular emphasis on the “anticipation” aspects. The VB appeared to be a specific condition where subjects adopted highly variable steering strategies and as such, VB steering results will not be presented in the next parts of the Results.

#### *Head anticipatory behavior in conditions VF and NF*

*Condition VF*: The examination of the Relative Head angles (RH) profiles (Fig. 7B1, 7B2, 7B3) revealed a clear anticipation behavior. In the VF condition (red lines), one may distinguish two main parts. In the first part, between $t = 0$ and $t \sim 0.3$, the RH remained close to zero. Here there was no anticipation: the head remained mostly aligned with the heading. This part corresponded indeed to the straight portion of the trajectory.

In the second part, for targets where the subject had to steer towards the right (targets 4E and 5S: Fig. 7B1, 7B3), the RH first decreased to reach its minimal value around $t = 0.6$. Then, it increased again, to get back near 0 at $t = 1$. The RH was thus negative for $0.3 \leq t \leq 1$: the head was oriented towards the *interior* of the curve. This part corresponded to the curved portion of the trajectory. Similarly, for targets where the subject had to steer towards the left (targets 5W: Fig. 7B2), the RH first increased and then decreased, yielding also an anticipatory behavior. The average Maximal RH across subjects and repetitions ranged between 12.4° (target 1N) and 77.8° (target 5S).

In agreement with previous studies (Hicheur et al 2005b, Hicheur et al 2007), we noted that the more curved the trajectories, the larger the MRH (Fig. 7D, red bars). The linear regression analysis (see Methods) performed over the angled trajectories (that is, excluding targets 1N, 2N and 3N) revealed a good correlation between the MRH and the Maximum Curvature (MC) (beta = 25.3, corr = 0.79, see Fig. 7F1).

*Condition NF*: In condition NF, the anticipation behavior could also be clearly observed. The NF profiles displayed similar shapes as the VF profiles, but with a smaller magnitude (Fig. 7B1, 7B2, 7B3, magenta lines).

Quantitatively, the average MRHs ranged between 10.0° (target 3N) and 61.9° (target 5S) in this condition. The MRH values were significantly smaller than in condition VF. However, similarly to condition VF, the more curved the trajectories, the larger the MRH (Fig. 7D, magenta bars). The linear regression analysis performed over the angled trajectories confirmed this observation (beta = 18.0, $r^2 = 0.61$, see Fig. 7F2). Note that $beta_{NF} < beta_{VF}$ because the MRHs were smaller in NF than in VF while the curvatures were approximately the same in the two conditions due to the similarity of the paths (see above).

Finally, we noted that these anticipation behavior were stereotyped across subjects and repetitions: the average Maximum RH Deviation (MRHD) across targets was 14.1° for condition VF and 15.1° for condition NF (Fig. 7C).

### *Head anticipatory behavior in condition NB*

Note that, since when walking backward the “natural” angle between the head direction and the heading is -180° (see Methods), anticipation behavior in backward conditions are defined by the formula: the head direction at time $t$ is reached by the *opposite* of the heading at time $t$ + Delta $t$ where Delta $t > 0$. Geometrically, this means that the head is oriented towards the *exterior* of the curve (see Fig. 7A and also Grasso et al 1998c). Numerically, this means RH < -180° for targets where the subject had to steer towards the right (targets 4E and 5S) and RH > -180° for targets where the subject had to steer towards the left (targets 5W).

Given these clarifications, we observed a clear anticipation behavior in condition NB (Fig. 7B1, 7B2, 7B3, cyan lines). The magnitude of the anticipation was smaller than in conditions VF and NF: the average MRHs ranged between 10.8° (target 1N) and 51.9° (target 4W). The dependence of the degree of anticipation on trajectory curvature could also be observed (Fig. 7D, cyan bars). The linear regression analysis performed over the angled trajectories confirmed this observation (beta = 12.4, $r^2 = 0.43$, see Fig. 7F3). Here, we also noted that $beta_{NB} < beta_{NF} < beta_{VF}$ for the same reason as above.

### *Head/trunk coordination for anticipation*

The orientation of the head with respect to the trajectory is achieved through the combination of trunk/heading and head/trunk rotations. Fig. 8A1, 8A2, 8A3 show the Relative Trunk angle (RT) profiles (angle between the trunk direction and the heading). The anticipation behavior could be clearly observed in the three conditions. Again, the magnitude of the anticipation was the largest in condition VF, followed by condition NF and then NB. We also noted that the magnitude of anticipation was smaller for the trunk than for the head. Indeed the average MRTs were significantly smaller than the MRHs.

Fig. 8B1, 8B2, 8B3 show the Head/Trunk angle (HT) profiles. Again, this angle was larger in VF than in NF than in NB. Globally, we observed that MHT < MRT < MRH.

Regarding the *timing* of the anticipation, we observed that the maximum of the anticipation occurred earlier for HT than for RT (Fig. 8E shows the time when RT reached its maximum and Fig. 8F shows the time when HT reached its maximum). Thus, in the first part of the curve ($0.3 \leq t \leq 0.5$), the head anticipation was achieved mainly by turning the head with respect to the trunk, and in the second part ($0.5 \leq t \leq 0.8$) head anticipation was achieved mainly by turning the trunk with respect to the heading (Fig. 8C1, 8C2, 8C3). In this second part (figures 8B1, 8B2 and 8B3), the head does practically not move with respect to the trunk

(HT is close to 0).

Regarding now the *distribution* of head anticipation between RT and HT, we observed graphically in Fig. 8C1, 8C2, 8C3 that overall RT contributed more than HT. This was confirmed by comparing the average value of RT and of HT for $0.3 \leq t \leq 1$ : the contribution of RT to head anticipation was ~ 65% while that of HT was ~ 35% in all targets and conditions (Fig. 8D).

It was remarkable that all the above observations on the head/trunk coordination (timing and distribution) applied for the three conditions VF, NF and NB, with only minor differences.

## Discussion

In this study, we experimentally examined the properties of locomotor trajectories performed under different visual (walking with or without vision) or motor (walking forward or backward) conditions. The results are summarized in Table 1.

### Vision independence of the average behavior

The ability of humans to perform basic locomotor tasks in absence of vision has been abundantly documented in the literature. Concerning the processing of *linear* distance, Thomson (1983) showed that, when subjects are asked to walk blindfolded towards previously seen targets placed between 3m and 21m ahead, the constant error (corresponding to our CEP(1), see Methods) was almost 0 for each distance. This result was confirmed in many subsequent studies (see Loomis et al 1992 for a review). Glasauer and colleagues (2002) showed that subjects could reproduce a previously observed triangular path (a isosceles right triangle with two 3m segments), indicating their ability to also process *angular* displacements. Finally, the ability to monitor *continuous* changes in the heading was also demonstrated by Takei and colleagues (1997) for circular paths reproduced without vision.

Here, we demonstrated that subjects accomplished with reasonable success the task of walking blindfolded towards a distant target specified in both position and orientation. They were thus able to combine and utilize the basic abilities mentionned above in a complex task where the paths are not predefined.

We showed that the average trajectories in the Vi and Bl conditions were very similar. This similarity of the average behavior possibly reflects a common strategy governing the formation of trajectories in the two conditions. In other words, in the Bl condition, subjects try to follow the same strategy as in the Vi condition, resulting in similar average trajectories. However, due to the lack of visual feedback, this strategy could not be accomplished perfectly in each trial, resulting in a large trajectory variability. Here, “strategy” should be understood in the broad sense, and should not be reduced for instance to a precomputed motor plan (Thomson 1983) or a “desired trajectory”. A “strategy” in our sense could for example consist of maximizing the smoothness of the trajectory, which was indeed the view taken in the modelling part of the present article.

Together with the motor-independence of the average trajectory discussed above, the results of this section strongly suggest that locomotor trajectories are generated at a cognitive level, independently of both the detailed motor and sensory implementations. In the long term, we believe that further studies combining the examination of motor and sensory processes with navigational abilities will bring new knowledge about the pathology of locomotion and its rehabilitation.

### Motor independence of locomotor trajectory formation

As discussed in (Grasso et al 1998b), the anatomy of the lower body is highly asymmetrical about the frontal plane, both in terms of the bone and the muscle structures. Thus, locomotor movements in opposite directions (Fw and Bw) are produced by very different muscular activation patterns. However, despite these differences, the *trajectories* of the leg segments were found to be surprisingly similar (up to time reversal) in Fw and Bw walking (Thorstensson 1986; Grasso et al 1998b).

During goal-oriented locomotion in free space (as opposed to treadmill walking), further important differences between Fw and Bw walking can be noticed regarding the coordination of upper-body segments. We focus here on the movements of the head, which is critical for locomotion since the head contains both the visual and the vestibular organs. In forward locomotion, the movements of the head display a number of characteristic and well-documented features, such as vertical and horizontal stability (Pozzo et al 1990), anticipation of the future direction of movement by the head (Grasso et al 1996). In backward locomotion, we observed a severe reorganization in the control of the head-neck system: subjects turned their head backwards with respect to the heading (in an anticipatory synergy and to visualize the target and monitor their trajectory). Such a reorganization also deeply influenced the structure of the sensory inputs: for instance, the limited range of yaw movements induces a shift between the visual direction and the heading, which in turn affects both the incoming optic flow and the perceived direction of the target with respect to the body (Rushton et al 1998; Warren et al 2001).

Despite these important differences, we observed that, on average, trajectories in the Fw and Bw conditions were very similar. In some sense, these results can be viewed as generalizations of (Thorstensson 1986; Grasso et al 1998b) to the scale of whole-body trajectories. They also suggest, along with our previous results concerning the foot placement (Hicheur et al 2007; see also Introduction), that the CNS plans and controls goal-oriented locomotion at the level of whole body trajectories in space, and this is done, to some extent, independently of the detailed particular motor implementation of the steering behavior. Then, a detailed motor strategy (in terms of foot placements, muscular activations, intersegmental coordination,...) is produced to actually *implement* these trajectories. We would like to emphasize here that assuming such central planning and control of trajectories is not equivalent to the "desired trajectory" hypothesis: this point will be discussed later.

We noted however some limitations to our experimental findings. For targets 4W and 5W which impose inflection points in the trajectories, the differences between the average trajectories in the Fw and Bw conditions were higher than for the other targets (see Results). Since the existence of inflection points may dramatically increase the complexity of the task, bio-mechanical differences may play a greater role in shaping the trajectories. In the same vein, we noted that, in highly constrained tasks (such as avoidance tasks: Patla et al 1999b), the foot placement may become stereotyped and precisely monitored by the CNS, which contrasts with the highly variable foot placement patterns observed in free-environment experiments (Hicheur et al 2007). Finally, while the shapes of the variability profiles were very similar in the two conditions, the magnitude of the variability was higher in the Bw condition. This may be related to the fact that Bw walking is less natural, more difficult, hence more variable than Fw walking.

**Acknowledgments**

This work was supported in part by the ANR PsiRob Locanthrope project. H.H. was supported in part by the Alexander von Humboldt foundation. We are deeply grateful to A. H. Olivier and A. Cretual for their help with the experiments and to F. Maloumian for her help with the illustrations of Fig. 2.

## References

**Atkeson CG, Hollerbach JM.** Kinematic features of unrestrained vertical arm movements. *J Neurosci.* 1985 Sep;5(9):2318-30.

**Courtine G, Schieppati M.** Human walking along a curved path. I. Body trajectory, segment orientation and the effect of vision. *Eur J Neurosci.* 2003 Jul;18(1):177-90.

Gibson JJ. Perception of the Visual World. Houghton Mifflin, Boston, 1950.

**Glasauer S, Amorim MA, Viaud-Delmon I, Berthoz A.** Differential effects of labyrinthine dysfunction on distance and direction during blindfolded walking of a triangular path. *Exp Brain Res.* 2002 Aug;145(4):489-97.

**Grasso R, Glasauer S, Takei Y, Berthoz A.** The predictive brain: anticipatory control of head direction for the steering of locomotion. *Neuroreport.* 1996 Apr 26;7(6):1170-4.

**Grasso R, Assaiante C, Prévost P, Berthoz A.** Development of anticipatory orienting strategies during locomotor tasks in children. *Neurosci Biobehav Rev.* 1998a Jul;22(4):533-9.

**Grasso R, Bianchi L, Lacquaniti F.** Motor patterns for human gait: backward versus forward locomotion. *J Neurophysiol.* 1998b Oct;80(4):1868-85.

**Grasso R, Prévost P, Ivanenko YP, Berthoz A.** Eye-head coordination for the steering of locomotion in humans: an anticipatory synergy. *Neurosci Lett.* 1998c Sep 4;253(2):115-8.

**Hicheur H, Berthoz A.** How do humans turn? Head and body movements for the steering of locomotion. In *Fifth IEEE-RAS International Conference on Humanoid Robots*, 2005.

**Hicheur H, Glasauer S, Vieilledent S, Berthoz A.** Head Direction Control during Active Locomotion in Humans. In: *Head Direction Cells and the Neural Mechanisms of Spatial Orientation*, edited by S. I. Wiener and J. S. Taube, MA: MIT Press, 2005a, p. 383-408.

**Hicheur H, Vieilledent S, Berthoz A.** Head motion in humans alternating between straight and curved walking path: combination of stabilizing and anticipatory orienting mechanisms. *Neurosci Lett.* 2005b Jul 22-29;383(1-2):87-92.

**Hicheur H, Pham QC, Arechavaleta G, Laumond JP, Berthoz A.** The formation of trajectories during goal-oriented locomotion in humans. I. A stereotyped behaviour. *Eur J Neurosci.* 2007 Oct;26(8):2376-90.

**Kennedy PM, Carlsen AN, Inglis JT, Chow R, Franks IM, Chua R.** Relative contributions of visual and vestibular information on the trajectory of human gait. *Exp Brain Res.* 2003 Nov;153(1):113-7.

**Lappe M, Bremmer F, van den Berg AV.** Perception of self-motion from visual flow. *Trends Cogn Sci.* 1999 Sep;3(9):329-336.

**Loomis JM, Da Silva JA, Fujita N, Fukusima SS.** Visual space perception and visually directed action. *J Exp Psychol Hum Percept Perform.* 1992 Nov;18(4):906-21.

**Loomis JM, Klatzky RL, Golledge RG, Cicinelli JG, Pellegrino JW, Fry PA.** Nonvisual navigation by blind and sighted: assessment of path integration ability. *J Exp Psychol Gen.* 1993 Mar;122(1):73-91.

**Morasso P.** Spatial control of arm movements. *Exp Brain Res.* 1981;42(2):223-7.

**Pham QC, Hicheur H.** On the open-loop and feedback processes that underlie the formation of trajectories during visual and nonvisual locomotion in humans. To be published in *J Neurophysiol*.

**Pham QC, Hicheur H, Arechavaleta G, Laumond JP, Berthoz A.** The formation of trajectories during goal-oriented locomotion in humans. II. A maximum smoothness model. *Eur J Neurosci.* 2007 Oct;26(8):2391-403.

**Patla AE, Adkin A, Ballard T.** Online steering: coordination and control of body center of mass, head and body reorientation. *Exp Brain Res*. 1999a Dec;129(4):629-34.

**Patla AE, Prentice SD, Rietdyk S, Allard F, Martin C.** What guides the selection of alternate foot placement during locomotion in humans. *Exp Brain Res.* 1999b Oct;128(4):441-50.

**Pozzo T, Berthoz A, Lefort L.** Head stabilization during various locomotor tasks in humans. I. Normal subjects. *Exp Brain Res.* 1990;82(1):97-106.

**Rossignol S, Dubuc R, Gossard JP.** Dynamic sensorimotor interactions in locomotion. *Physiol Rev*. 2006 Jan;86(1):89-154.

**Rushton SK, Harris JM, Lloyd MR, Wann JP.** Guidance of locomotion on foot uses perceived target location rather than optic flow. *Curr Biol.* 1998 Oct 22;8(21):1191-4.

**Takei Y, Grasso R, Amorim MA, Berthoz A.** Circular trajectory formation during blind locomotion: a test for path integration and motor memory. *Exp Brain Res.* 1997 Jun;115(2):361-8.

**Thomson JA.** Is continuous visual monitoring necessary in visually guided locomotion? *J Exp Psychol Hum Percept Perform.* 1983 Jun;9(3):427-43.

**Thorstensson A.** How is the normal locomotor program modified to produce backward walking? *Exp Brain Res.* 1986;61(3):664-8.

**Todorov E, Jordan MI.** Optimal feedback control as a theory of motor coordination. *Nat Neurosci.* 2002 Nov;5(11):1226-35.

**Vallis LA, Patla AE.** Expected and unexpected head yaw movements result in different modifications of gait and whole body coordination strategies. *Exp Brain Res.* 2004 Jul;157(1):94-110.

**Vieilledent S, Kerlirzin Y, Dalbera S, Berthoz A.** Relationship between velocity and curvature of a human locomotor trajectory. *Neurosci Lett.* 2001 Jun 1;305(1):65-9.

**Warren WH Jr, Kay BA, Zosh WD, Duchon AP, Sahuc S.** Optic flow is used to control human walking. *Nat Neurosci.* 2001 Feb;4(2):213-6.

## Tables

### Table 1

|  | Whole-body trajectories |  | Steering behaviour |  |  |  |  |
|---|---|---|---|---|---|---|---|
|  | Ave traj | Var prof | Ave prof | Var prof | Timing | Distrib RT/HT | Anticip / Curv |
| Effect of vision | 0 | ++ | x | x | 0 | 0 | x |
| Effect of gait dir | x | 0 | x (NF/NB)<br>++ (VF/VB) | x (NF/NB)<br>++ (VF/VB) | 0 (NF/NB)<br>n.a. (VF/VB) | 0 (NF/NB)<br>n.a. (VF/VB) | x (NF/NB)<br>n.a. (VF/VB) |

## Tables' legends

### Table 1

Summary of the results. 0 : no or practically no effect, x : small effect, ++ : large effect, n.a. : not available.

## Figures' legends

### Figure 1

Comparison of locomotor trajectories in the Visual Forward (VF: red) and Nonvisual Forward (NF: magenta) conditions for target 4S (see Protocol). (**A**) Geometric paths of the average trajectories and variance ellipses (see Methods). (**B**) Average velocity profiles and the corresponding variabilities. (**C**) Variability profiles.

### Figure 2

(**A**) Experimental protocol: subjects had to start from a fixed position in the laboratory and walk towards a distant arrow placed on the ground. Subjects had to enter the arrow by the shaft, and stop above the arrow head. (**B**) Spatial disposition of the 19 targets: each target was referred to by a number (1-7) indicating the position and by a letter (N (north), S (south), E (east), W (west)) indicating the orientation. (**C**) Instantaneous trajectory deviation (TD(*t*)) and instantaneous velocity deviation (VD(*t*)), which measure respectively the variability of actual trajectories around the average trajectory and the variability of actual velocity profiles around the average velocity profile. (**D**) Definition of the head and trunk angles.

### Figure 3

Comparison of locomotor trajectories in the Visual Backward (VB: green) and Nonvisual Backward (NB: cyan) conditions. (**A**) Comparisons for target 4E. A1: geometric paths of the average trajectories. We also plotted the variance ellipses around the average trajectory at every time instant (see Methods) in light green and light cyan. A2: average velocity profiles. The velocity profiles were normalized so that their average values over the movement duration equals 1 (see Methods). Standard deviations around the average velocity profiles are in light green and light cyan. A3: trajectory variability profiles (TD(*t*)). (**B**) Same as in A, but for target 5W. (**C**) Same as in A, but for target 5S. (**D**) Maximal Trajectory Deviation/Separation (MTD/MTS) in meters: MTD in condition VB (green bars), MTD in condition NB (cyan bars), MTS between the average trajectory of VB and NB (grey bars).

### Figure 4

Comparison of locomotor trajectories in the Visual Forward (VF: red) and Visual Backward (VB: green) conditions. For details, see legend of Fig. 3.

### Figure 5

Comparison of locomotor trajectories in the Nonvisual Forward (NF: magenta) and Nonvisual Backward (NB: cyan) conditions. For details, see legend of Fig. 3.

### Figure 6

Absolute Head (AH) angles in the four tested conditions (VF: red, NF: magenta, VB: green, NB: cyan). (**A**) Average AH profiles. A1: target 4E, A2: target 5W, A3: target 5S. Left scale for the forward conditions (VF, NF) and right scale for the backward conditions (VB, NB). (**B**) AH variability profiles. (**C**) Variability of the AH profiles: Maximal Absolute Head angle Deviation (MAHD) in degrees.

### Figure 7

Head anticipatory behavior. (**A**) Anticipatory behavior in forward and in backward locomotion. (**B**) Average RH profiles (plain lines) ± SD (dashed lines) for conditions VF (red), NF (magenta) and NB (cyan). B1: target 4E, B2: target 5W, B3: target 5S. (**C**) Variability of the RH profiles: Maximal Relative Head angles Deviation (MRHD). (**D**) Degree of head anticipation: Maximal Relative Head angles (MRH) averaged across subjects and repetitions (and the corresponding SD bars). (**E**) Timing of head anticipation: time when MRH was attained, averaged across subjects and repetitions. (**F**) Regression analysis of the dependence between path curvature and head anticipation. We tested the model Maximum Relative Head angle = beta Maximum Curvature for condition VF (F1), NF (F2) and NB (F3).

**Figure 8**

Head/Trunk coordination for anticipation in conditions VF (red), NF (magenta) and NB (cyan). (**A**) Average Relative Trunk angle (RT) profiles (plain lines) ± SD (dashed lines). A1: target 4E, A2: target 5W, A3: target 5S. (**B**) Average Head/Trunk angle (HT) profiles (plain lines) ± SD (dashed lines). (**C**) Contribution of Relative Trunk vs contribution of Head/Trunk to head anticipation in time: a value of 100% means that only RH contributes while a value of 0% means that only Head/Trunk contributes. (**D**) Contribution of Relative Trunk vs contribution of Head/Trunk to head anticipation over the whole trajectory. (**E**) Time when Maximum RT was attained, averaged across subjects and repetitions. (**F**) Time when Maximum HT was attained, averaged across subjects and repetitions.

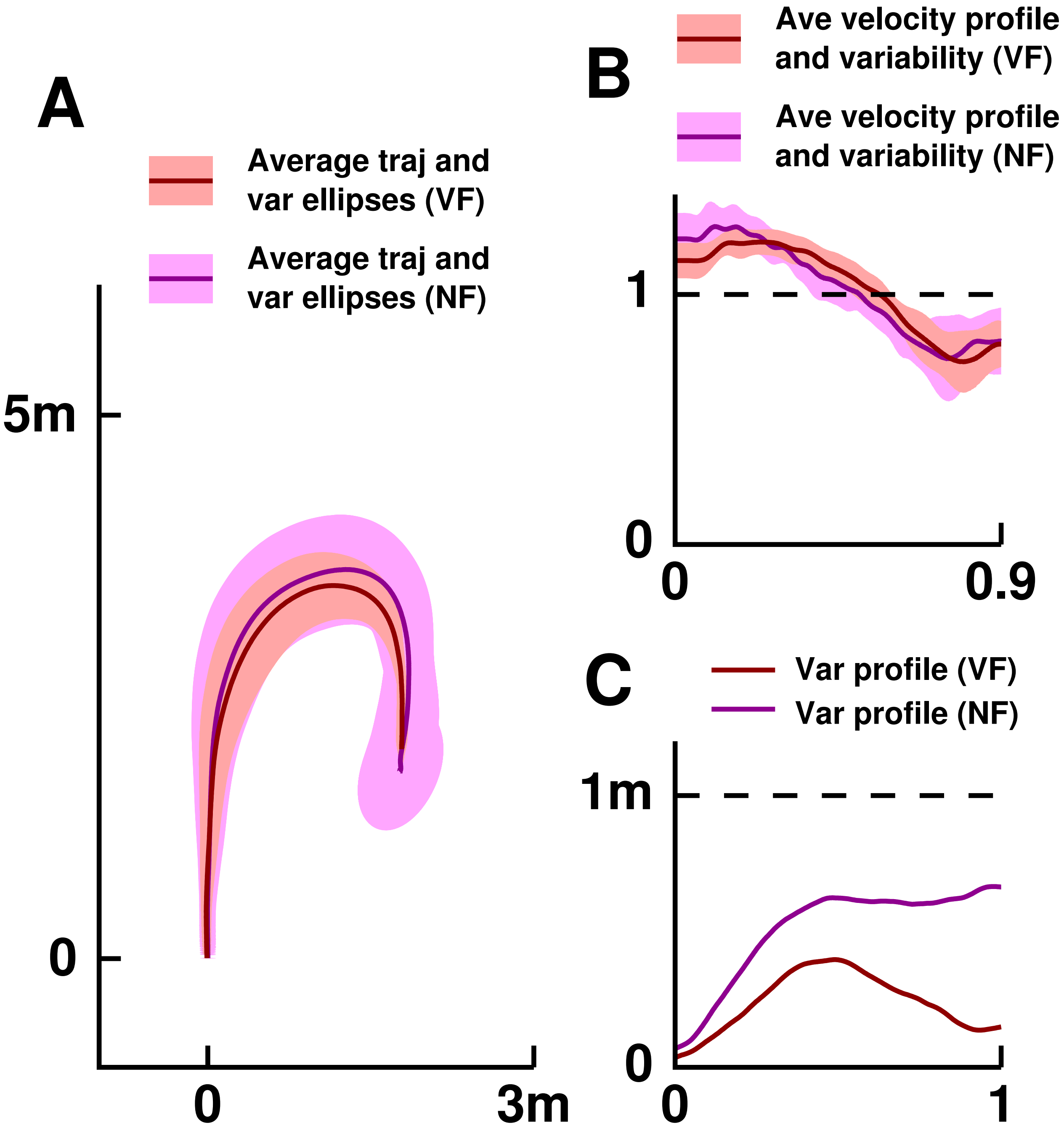
A
Average traj and var ellipses (VF)
Average traj and var ellipses (NF)
5m
0
0
3m
B
Ave velocity profile and variability (VF)
Ave velocity profile and variability (NF)
1
0
0
0.9
C
Var profile (VF)
Var profile (NF)
1m
0
0
1

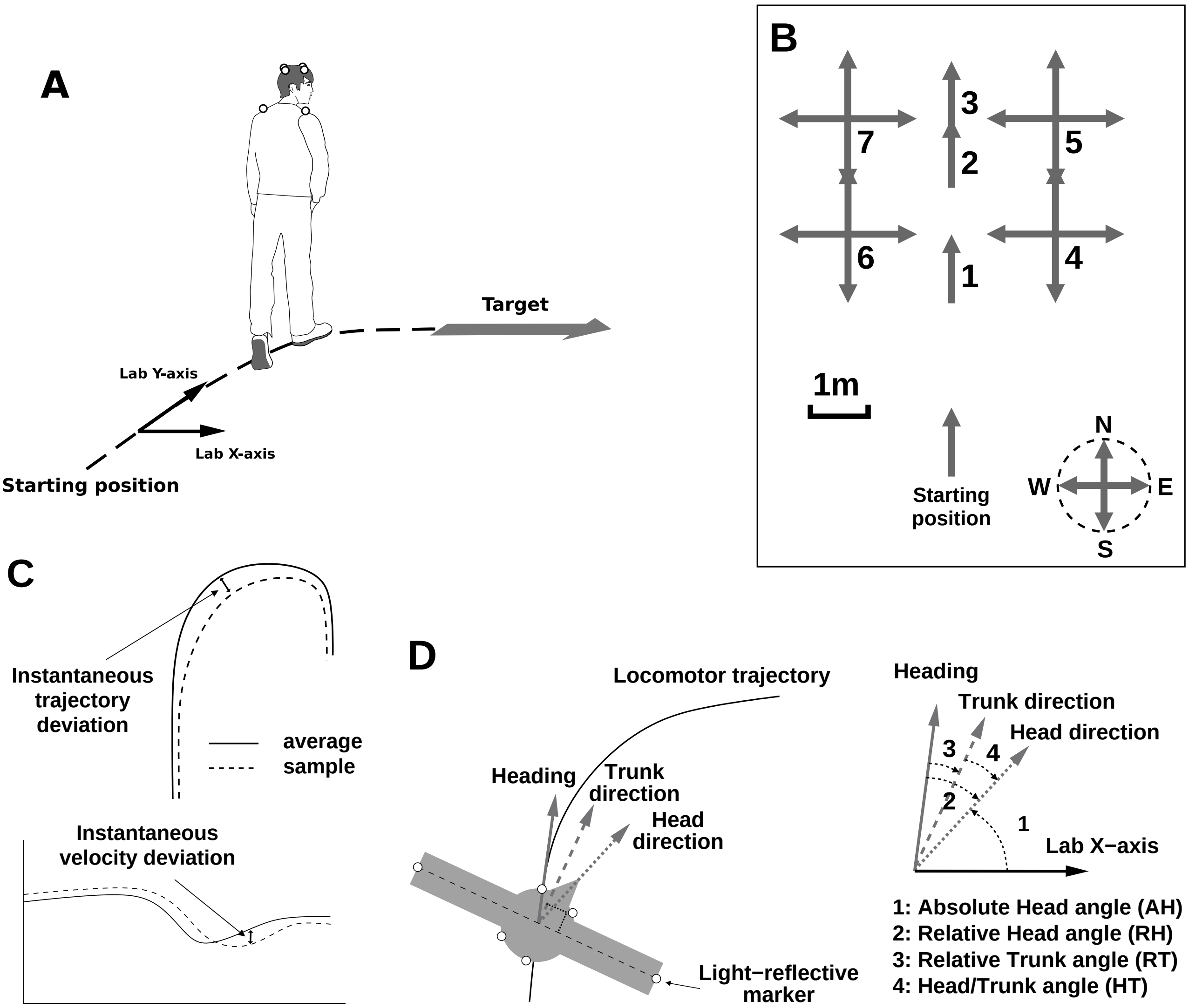
A
Target
Lab Y-axis
Lab X-axis
Starting position
B
3
7
2
5
6
1
4
1m
N
W
E
S
Starting position
C
Instantaneous trajectory deviation
average
sample
Instantaneous velocity deviation
D
Locomotor trajectory
Heading
Trunk direction
Head direction
Light−reflective marker
Heading
Trunk direction
Head direction
3
4
2
1
Lab X−axis
1: Absolute Head angle (AH)
2: Relative Head angle (RH)
3: Relative Trunk angle (RT)
4: Head/Trunk angle (HT)

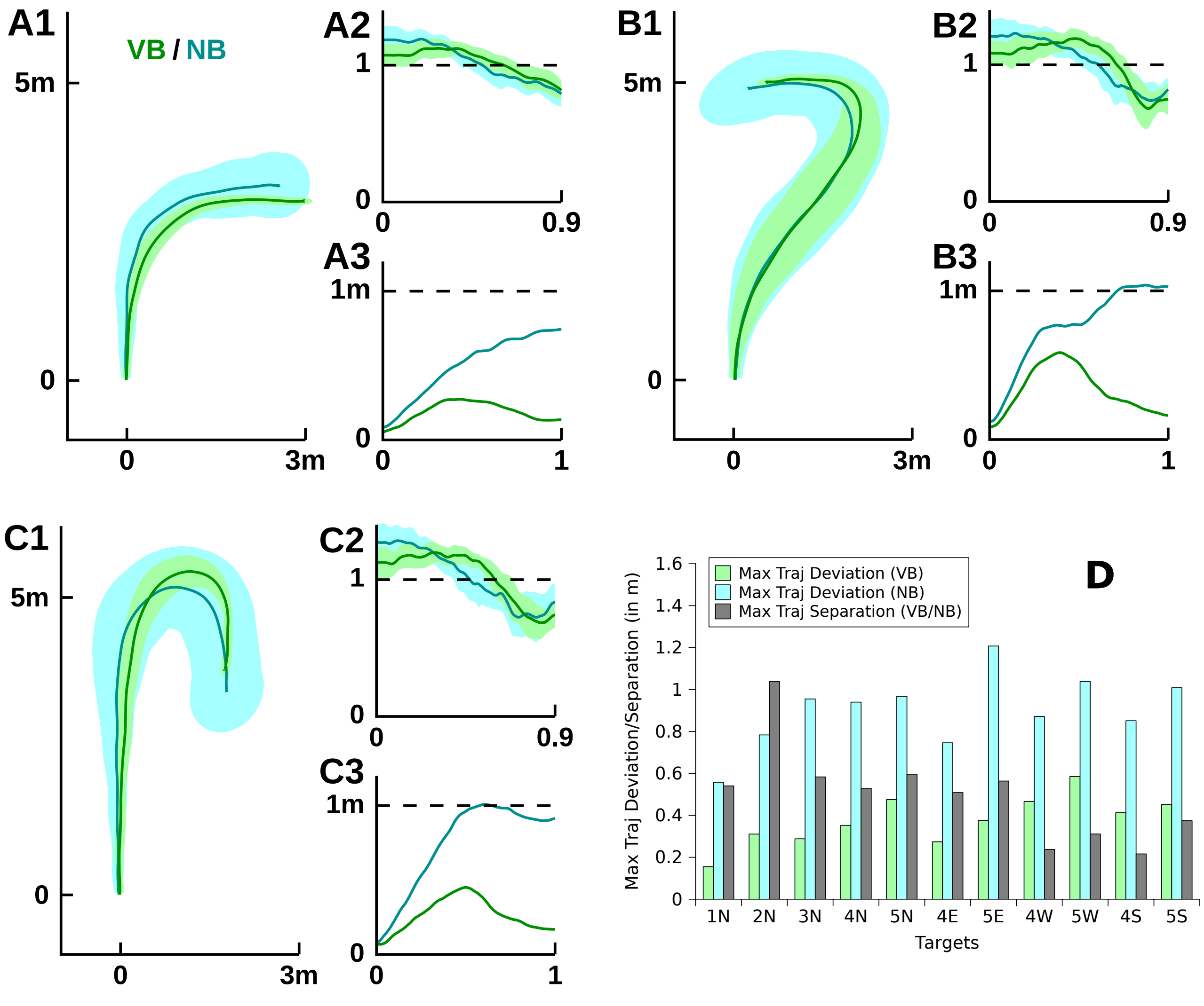
A1
VB / NB
5m
0
0
3m
A2
1
0
0
0.9
A3
1m
0
0
1
B1
5m
0
0
3m
B2
1
0
0
0.9
B3
1m
0
0
1
C1
5m
0
0
3m
C2
1
0
0
0.9
C3
1m
0
0
1
D
Max Traj Deviation (VB)
Max Traj Deviation (NB)
Max Traj Separation (VB/NB)
Max Traj Deviation/Separation (in m)
1.6
1.4
1.2
1
0.8
0.6
0.4
0.2
0
1N
2N
3N
4N
5N
4E
5E
4W
5W
4S
5S
Targets

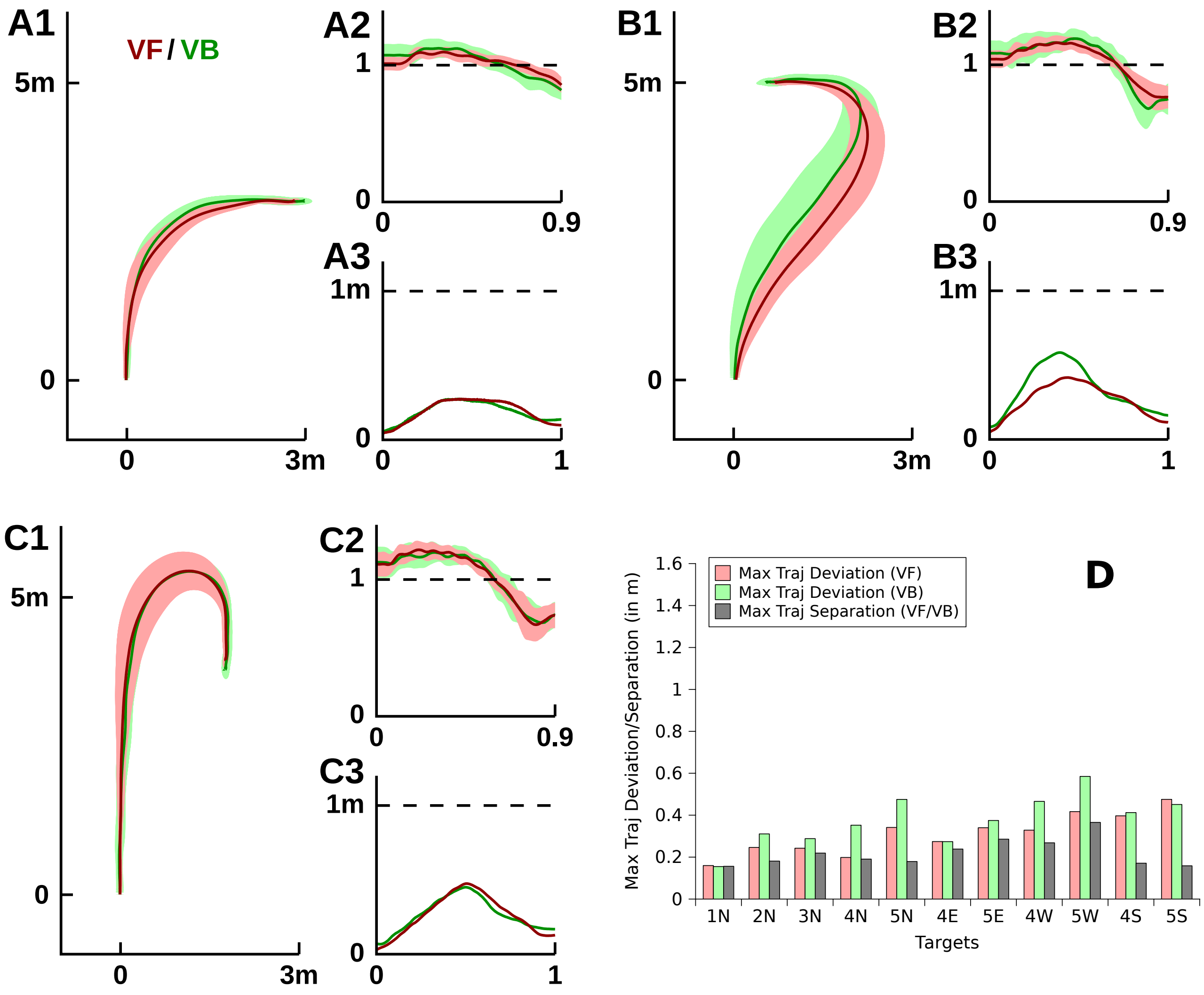
A1
VF / VB
5m
0
0
3m
A2
1
0
0
0.9
A3
1m
0
0
1
B1
5m
0
0
3m
B2
1
0
0
0.9
B3
1m
0
0
1
C1
5m
0
0
3m
C2
1
0
0
0.9
C3
1m
0
0
1
D
Max Traj Deviation (VF)
Max Traj Deviation (VB)
Max Traj Separation (VF/VB)
Max Traj Deviation/Separation (in m)
1.6
1.4
1.2
1
0.8
0.6
0.4
0.2
0
1N
2N
3N
4N
5N
4E
5E
4W
5W
4S
5S
Targets

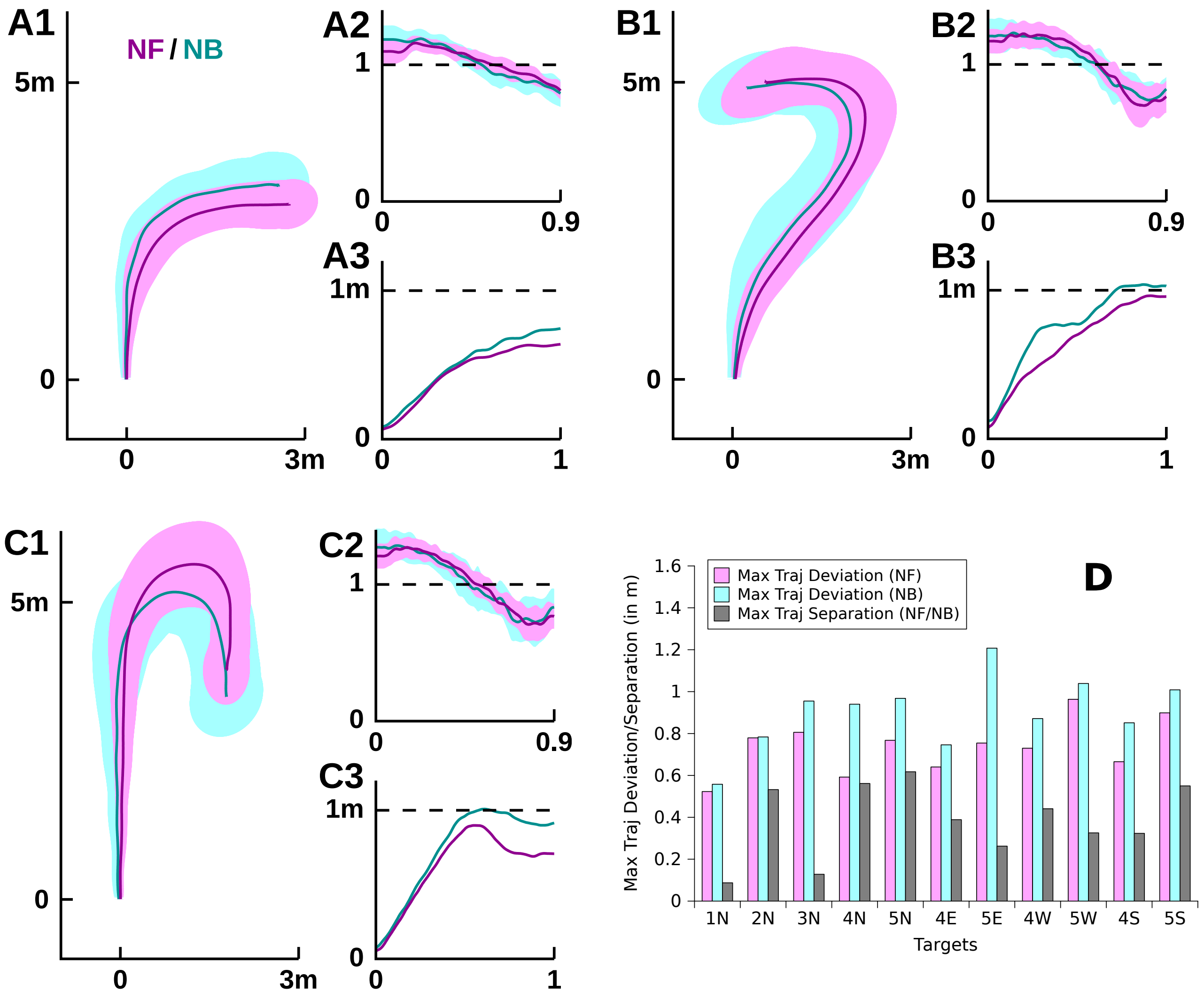
A1
NF / NB
5m
0
0
3m
A2
1
0
0
0.9
A3
1m
0
0
1
B1
5m
0
0
3m
B2
1
0
0
0.9
B3
1m
0
0
1
C1
5m
0
0
3m
C2
1
0
0
0.9
C3
1m
0
0
1
D
Max Traj Deviation (NF)
Max Traj Deviation (NB)
Max Traj Separation (NF/NB)
Max Traj Deviation/Separation (in m)
1.6
1.4
1.2
1
0.8
0.6
0.4
0.2
0
1N
2N
3N
4N
5N
4E
5E
4W
5W
4S
5S
Targets

A : Absolute Head angles (AH) in degrees

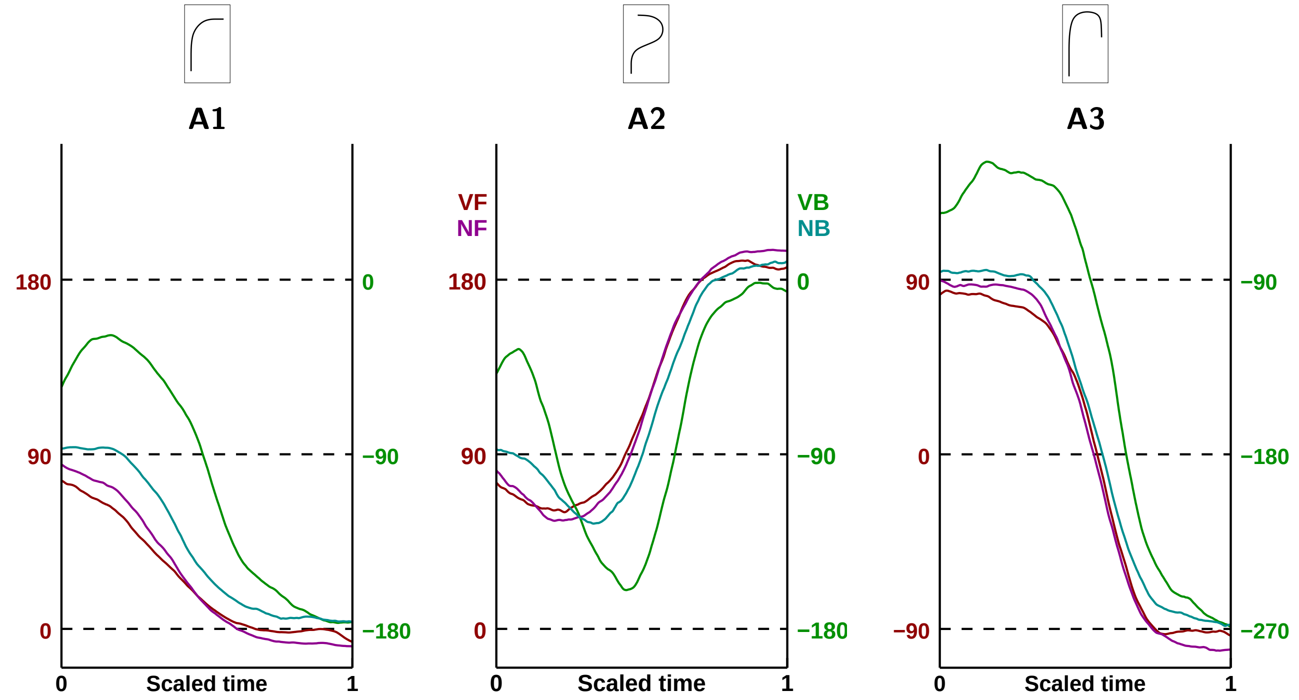

B : Absolute Head angles variability (AHD) in degrees

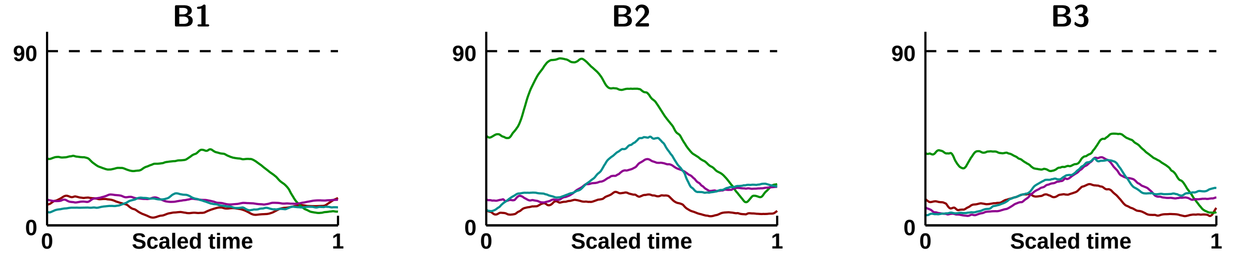

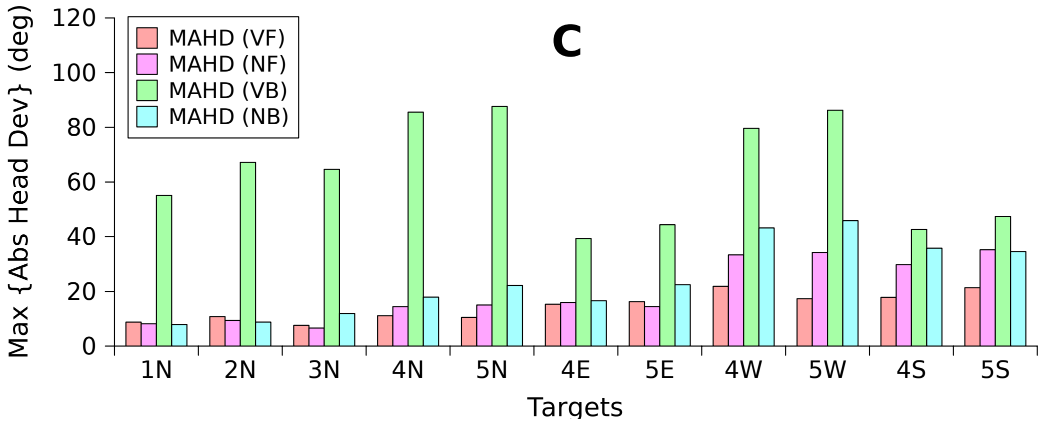

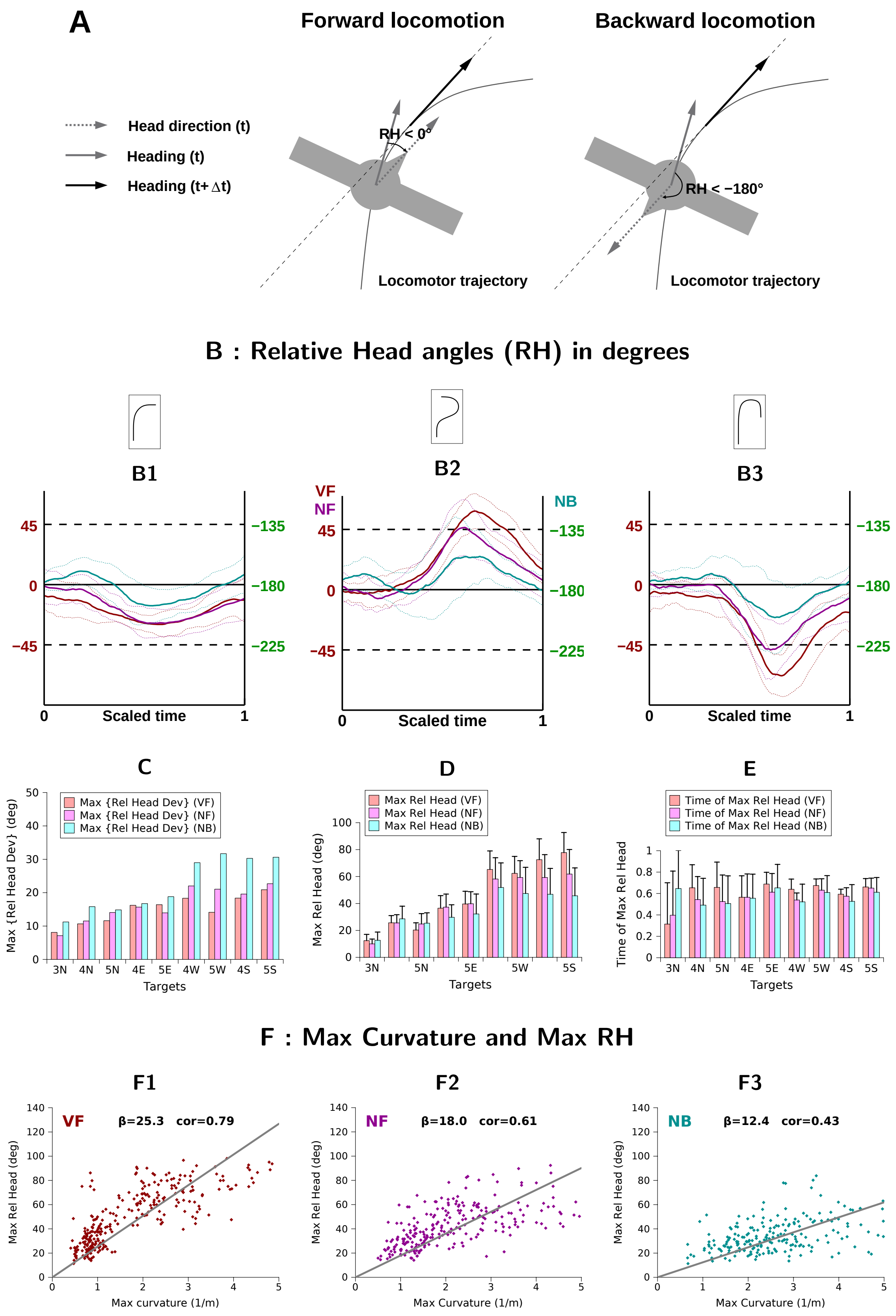
A
Forward locomotion
Backward locomotion
Head direction (t)
Heading (t)
Heading (t+Δt)
RH < 0°
RH < −180°
Locomotor trajectory
Locomotor trajectory
B : Relative Head angles (RH) in degrees
B1
B2
B3
VF
NF
NB
45
0
−45
−135
−180
−225
0
Scaled time
1
C
Max {Rel Head Dev} (VF)
Max {Rel Head Dev} (NF)
Max {Rel Head Dev} (NB)
Max {Rel Head Dev} (deg)
0
10
20
30
40
50
3N
4N
5N
4E
5E
4W
5W
4S
5S
Targets
D
Max Rel Head (VF)
Max Rel Head (NF)
Max Rel Head (NB)
Max Rel Head (deg)
0
20
40
60
80
100
3N
5N
5E
5W
5S
Targets
E
Time of Max Rel Head (VF)
Time of Max Rel Head (NF)
Time of Max Rel Head (NB)
Time of Max Rel Head
0
0.2
0.4
0.6
0.8
1
3N
4N
5N
4E
5E
4W
5W
4S
5S
Targets
F : Max Curvature and Max RH
F1
F2
F3
VF
β=25.3 cor=0.79
NF
β=18.0 cor=0.61
NB
β=12.4 cor=0.43
Max Rel Head (deg)
0
20
40
60
80
100
120
140
0
1
2
3
4
5
Max curvature (1/m)
Max Curvature (1/m)
Max Curvature (1/m)

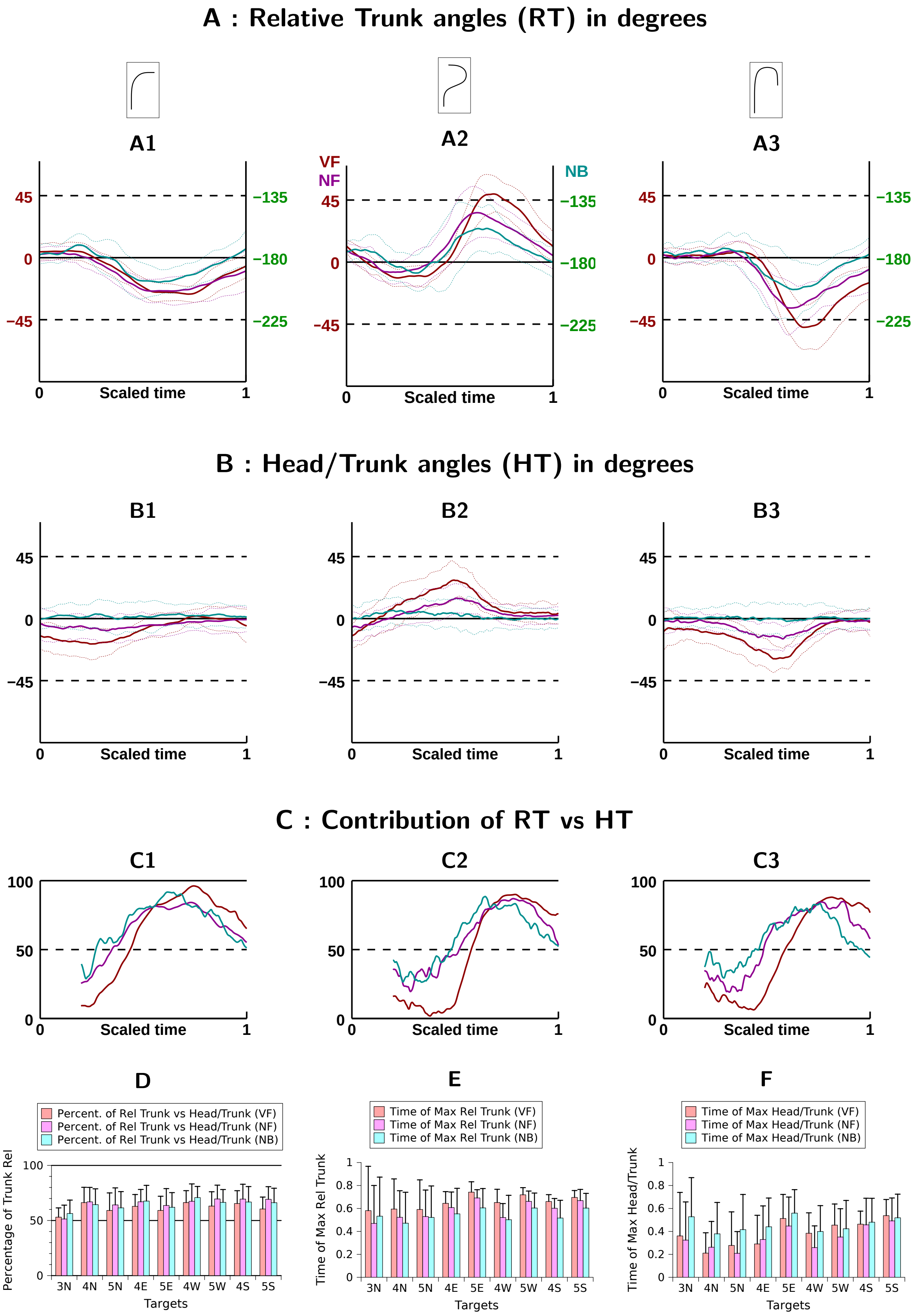
A : Relative Trunk angles (RT) in degrees
A1
A2
A3
VF
NF
NB
45
0
−45
−135
−180
−225
Scaled time
0
1
B : Head/Trunk angles (HT) in degrees
B1
B2
B3
45
0
−45
Scaled time
C : Contribution of RT vs HT
C1
C2
C3
100
50
0
Scaled time
D
Percent. of Rel Trunk vs Head/Trunk (VF)
Percent. of Rel Trunk vs Head/Trunk (NF)
Percent. of Rel Trunk vs Head/Trunk (NB)
Percentage of Trunk Rel
100
50
0
E
Time of Max Rel Trunk (VF)
Time of Max Rel Trunk (NF)
Time of Max Rel Trunk (NB)
Time of Max Rel Trunk
F
Time of Max Head/Trunk (VF)
Time of Max Head/Trunk (NF)
Time of Max Head/Trunk (NB)
Time of Max Head/Trunk
1
0.8
0.6
0.4
0.2
0
3N
4N
5N
4E
5E
4W
5W
4S
5S
Targets

# Appendix B

# Contraction theory articles

## B.1 Where Neuroscience and Dynamic System Theory Meet Autonomous Robotics: a Contracting Basal Ganglia Model for Action Selection

By B. Girard, N. Tabareau, Q.-C. Pham, A. Berthoz and J.-J. Slotine. Published in *Neural Networks*, vol. 21, pp. 628-641, 2008.

Neural Networks 21 (2008) 628–641

Contents lists available at ScienceDirect

Neural Networks

journal homepage: www.elsevier.com/locate/neunet

2008 Special Issue

# Where neuroscience and dynamic system theory meet autonomous robotics: A contracting basal ganglia model for action selection

B. Girard [a,*], N. Tabareau [a], Q.C. Pham [a], A. Berthoz [a], J.-J. Slotine [b]

[a] *Laboratoire de Physiologie de la Perception et de l'Action, UMR7152, CNRS - Collège de France, 11 place Marcelin Berthelot, 75231 Paris Cedex 05, France*
[b] *Nonlinear Systems Laboratory, Massachusetts Institute of Technology, Cambridge, MA 02139, USA*

ARTICLE INFO

*Article history:*
Received 15 March 2007
Received in revised form
7 March 2008
Accepted 7 March 2008

*Keywords:*
Action selection
Basal ganglia
Computational model
Autonomous robotics
Contraction analysis

ABSTRACT

Action selection, the problem of choosing what to do next, is central to any autonomous agent architecture. We use here a multi-disciplinary approach at the convergence of neuroscience, dynamical system theory and autonomous robotics, in order to propose an efficient action selection mechanism based on a new model of the basal ganglia. We first describe new developments of contraction theory regarding locally projected dynamical systems. We exploit these results to design a stable computational model of the cortico-baso-thalamo-cortical loops. Based on recent anatomical data, we include usually neglected neural projections, which participate in performing accurate selection. Finally, the efficiency of this model as an autonomous robot action selection mechanism is assessed in a standard survival task. The model exhibits valuable dithering avoidance and energy-saving properties, when compared with a simple if-then-else decision rule.

## 1. Introduction

Action selection is the problem of motor resource allocation an autonomous agent is faced with, when attempting to achieve its long-term objectives. These may vary from survival and reproduction to delivering letters to researchers' offices, depending on the nature of the considered agent (animal, robot, etc.). Action selection is a topic of interest in various disciplines, including ethology, artificial intelligence, psychology, neuroscience, autonomous robotics, etc. We address here the question of action selection for an autonomous robot, using a computational model of brain regions involved in action selection, namely the cortico-baso-thalamo-cortical loops. In order to avoid unwanted dynamical behaviors resulting from a highly recurrent network, we use contraction analysis (Lohmiller & Slotine, 1998) to obtain a rigorous proof of its stability. The efficiency of this action selection mechanism (ASM) is assessed using a standard minimal survival task in a robotic simulation.

The basal ganglia are a set of interconnected subcortical nuclei common to all vertebrates and involved in numerous processes, from motor functions to cognitive ones (Middleton & Strick, 1994; Mink, 1996). Their role is interpreted as a generic selection circuit, and they have been proposed to form the neural substrate of action selection (Krotopov & Etlinger, 1999; Mink, 1996; Redgrave, Prescott, & Gurney, 1999). The basal ganglia are included in cortico-baso-thalamo-cortical loops (Fig. 1), five main loops have been identified in primates (Alexander, Crutcher, & DeLong, 1990; Alexander, DeLong, & Strick, 1986; Kimura & Graybiel, 1995): one motor, one oculomotor, two prefrontal and one limbic loop. Within each of these loops, the basal ganglia circuitry is organized in interacting channels, among which selection occurs. Depending on the considered loop, this selection may concern, for example, the target of an upcoming saccadic movement, the target of a reaching movement or the piece of information to be stored in working memory. The output nuclei of the basal ganglia are inhibitory and tonically active, and thus maintain their targets under sustained inhibition. Selection occurs *via* disinhibition (Chevalier & Deniau, 1990): the removal of the inhibition exerted by one channel on its specific target circuit allows the activation of that circuit. When considering action selection, the basal ganglia channels are thought to be associated to competing action primitives. Given sensory and motivational inputs, the basal ganglia are thus supposed to arbitrate among these actions and to allow the activation of the winner by disinhibiting the corresponding motor circuits.

The considered network contains a large number of closed loops, from the large cortico-baso-thalamo-cortical loop, to small loops formed by the interconnections between nuclei within the basal ganglia and between the thalamus and the cortex. A system with such a structure may exhibit varied dynamical behaviors, some of which should be avoided by an ASM, like reaching a standstill state which does not depend anymore on the

---

[*] Corresponding author. Tel.: +33 1 44 27 13 91; fax: +33 1 44 27 13 82.
*E-mail address:* benoit.girard@college-de-france.fr (B. Girard).

0893-6080/$ – see front matter © 2008 Elsevier Ltd. All rights reserved.
doi:10.1016/j.neunet.2008.03.009

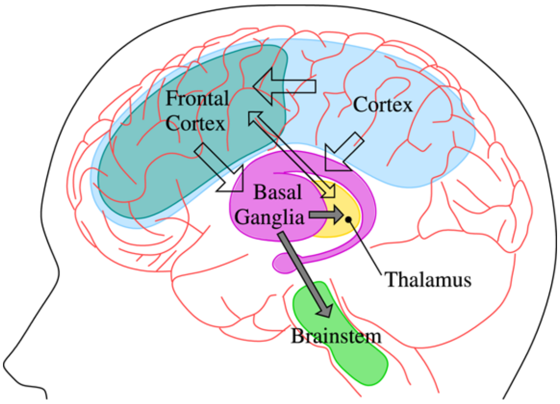

**Fig. 1.** Cortico-baso-thalamo-cortical loops. The basal ganglia receive inputs from the whole cortex, but establish loops with the frontal areas only. Shaded arrows: inhibitory projections.

external input. This motivates the use of a theoretical framework to study the dynamics of basal ganglia models. We propose to use contraction analysis (Lohmiller & Slotine, 1998) in order to guide the design of a new model of the basal ganglia whose stability can be formally established. Contraction analysis is a theoretical tool used to study the dynamic behavior of nonlinear systems. Contraction properties are preserved through a number of particular combinations, which is useful for a modular design of models.

Numerous computational models of the BG have been proposed in order to investigate the details of the operation of the basal ganglia disinhibition process (see Gillies & Arbruthnott, 2000; Gurney, Prescott, Wickens, & Redgrave, 2004, for recent reviews). Among these, the model proposed by Gurney, Prescott, and Redgrave (2001a, 2001b) (henceforth the GPR model) has been successfully tested as an action selection mechanism for autonomous agents (Girard, Cuzin, Guillot, Gurney, & Prescott, 2003; Girard, Filliat, Meyer, Berthoz, & Guillot, 2005; Montes-Gonzalez, Prescott, Gurney, Humphries, & Redgrave, 2000; Prescott, Montes-Gonzalez, Gurney, Humphries, & Redgrave, 2006). In particular, it was shown to be able to solve a minimal survival task, and, compared with a simpler winner-takes-all mechanism, displayed dithering avoidance and energy-saving capabilities.

We present here an action selection mechanism based on a contracting computational model of the basal ganglia (or CBG). In order to adapt the contraction theory to the analysis of rate-coding artificial neural networks, we first extend it to locally projected dynamical systems (Section 2). Using the resulting neuron model and contraction constraints on the model's parameters, we build a computational model of the basal ganglia including usually neglected neural connections (Section 3). We then check the selection properties of the disembodied model and compare them to those of the GPR, so as to emphasize the consequences of using contraction analysis (Section 4). We finally test its efficiency in a survival task similar to the one used to evaluate the GPR (Girard et al., 2003), and emphasize its dithering avoidance and energy-saving properties by comparing it to a simple if-then-else decision rule (Section 5).

Preliminary versions of the basal ganglia computational model were presented in Girard, Tabareau, Berthoz, and Slotine (2006) and Girard, Tabareau, Slotine, and Berthoz (2005).

## 2. Nonlinear contraction analysis for rate-coding neural networks

Basically, a nonlinear time-varying dynamic system is said to be *contracting* if initial conditions or temporary disturbances are forgotten exponentially fast, that is, if any perturbed trajectory returns to its nominal behavior with an exponential convergence rate. Contraction is an extension of the well-known *stability* analysis for linear systems. It has the desirable feature of being preserved through hierarchical and particular feedback combinations. Thus, as we will see below, contraction analysis is an appropriate tool to study stability properties of rate-coding neural networks.

In addition, when a system is contracting, it is sufficient to find a particular bounded trajectory to be sure that the system will eventually tend to this trajectory. Thus contraction theory is a convenient way to analyze the dynamic behavior of a system without linearized approximations.

### 2.1. Contraction theory

We summarize the differential formulation of contraction analysis presented in Lohmiller and Slotine (1998). Contraction analysis is a way to prove the exponential stability of a nonlinear system by studying the properties of its Jacobian. Consider an $n$-dimensional time-varying system of the form:

$$\dot{\mathbf{x}}(t) = \mathbf{f}(\mathbf{x}(t), t) \tag{1}$$

where $\mathbf{x} \in \mathbb{R}^n$ and $t \in \mathbb{R}_+$ and $\mathbf{f}$ is a $n \times 1$ nonlinear vector function which is assumed in the remainder of this paper to be real and smooth, in the sense that all required derivatives exist and are continuous. This equation may also represent the closed-loop dynamics of a neural network model of a brain structure. We recall below the main result of contraction analysis (see Lohmiller and Slotine (1998), for a proof and more details).

**Theorem 1.** *Consider the continuous-time system (1). If there exists a uniformly positive definite metric*

$$\mathbf{M}(\mathbf{x}, t) = \mathbf{\Theta}(\mathbf{x}, t)^{\mathrm{T}}\mathbf{\Theta}(\mathbf{x}, t)$$

*such that the generalized Jacobian*

$$\mathbf{F} = (\dot{\mathbf{\Theta}} + \mathbf{\Theta}\mathbf{J})\mathbf{\Theta}^{-1}$$

*is uniformly negative definite, then all system trajectories converge exponentially to a single trajectory with convergence rate $|\lambda_{\max}|$, where $\lambda_{\max}$ is the largest eigenvalue of the symmetric part of* $\mathbf{F}$.

The symmetric part of a matrix $\mathbf{A}$ is $\mathbf{A}_s = 1/2(\mathbf{A} + \mathbf{A}^{\mathrm{T}})$. A matrix $\mathbf{A}(\mathbf{x}, t)$ is uniformly positive definite if there exists $\beta > 0$ such that

$$\forall \mathbf{x}, t \quad \lambda_{\min}(\mathbf{A}(\mathbf{x}, t)) \geq \beta.$$

### 2.2. Neural networks and locally projected dynamical systems

Networks of leaky integrators are widely used to model the behavior of neuronal assemblies (Dayan & Abbott, 2001). A leaky-integrator network is usually described by the following set of equations

$$\tau_i \dot{x}_i = -x_i(t) + \sum_{j \neq i} K_{ji} x_j(t) + I(t)$$

where $x(t)$ is the synaptic current of a neuron, $\tau_i$ its time constant, $K_{ji}$ the synaptic projection weight from neuron $j$ to neuron $i$ and $I(t)$ the input coming from an external source. Next, $x(t)$ is converted into a non-negative firing rate $y(t)$ using a transfer function, for instance

$$y(t) = \max(x(t), 0) = [x(t)]_+.$$

Another way to enforce non-negativity of the firing rate is to use through *locally projected dynamical systems* (lPDS in short). These systems were introduced in Dupuis and Nagurney (1993) and further analyzed in Zhang and Nagurney (1995). Related ideas can be found in the standard parameter projection method in adaptive control (Ioannou & Sun, 1996; Slotine & Coetsee, 1986). A lPDS is given by

$$\dot{\mathbf{x}} = \mathbf{\Pi}_{\mathbf{\Omega}}(\mathbf{x}, \mathbf{f}(\mathbf{x}, t)) \tag{2}$$

where $\mathbf{\Omega}$ is a convex subset of the state space and $\mathbf{\Pi}_{\mathbf{\Omega}}$ is the vector-projection operator on $\mathbf{\Omega}$ given by

$$\mathbf{\Pi}_{\mathbf{\Omega}}(\mathbf{x}, \mathbf{v}) = \lim_{h \to 0^+} \frac{\mathbf{P}_{\mathbf{\Omega}}(\mathbf{x} + h\mathbf{v}) - \mathbf{x}}{h}.$$

In the above equation, $\mathbf{P}_{\mathbf{\Omega}}$ denotes the point-projection operator on the convex $\mathbf{\Omega}$ defined as

$$\mathbf{P}_{\mathbf{\Omega}}(\mathbf{x}) = \underset{\mathbf{y} \in \mathbf{\Omega}}{\operatorname{argmin}} \|\mathbf{x} - \mathbf{y}\|.$$

Intuitively, if $\mathbf{x}$ is in the interior of $\mathbf{\Omega}$ then $\mathbf{\Pi}_{\mathbf{\Omega}}(\mathbf{x}, \mathbf{v}) = \mathbf{v}$. If $\mathbf{x}$ is on the boundary of $\mathbf{\Omega}$, then $\mathbf{\Pi}_{\mathbf{\Omega}}(\mathbf{x}, \mathbf{v})$ is the maximal component of $\mathbf{v}$ that allows the system to remain within $\mathbf{\Omega}$. In particular, it is easy to see that any trajectory starting in $\mathbf{\Omega}$ remains in $\mathbf{\Omega}$.

Note that Eq. (2) does not define a classical ordinary differential equation since its right-hand side can be discontinuous due to the projection operator. However, under some conditions on $\mathbf{f}$ and $\mathbf{\Omega}$ (similar to the Cauchy–Lipschitz conditions for classical ordinary differential equations, see Dupuis and Nagurney (1993) and Filippov (1988) for more details), existence, uniqueness and some qualitative properties can be established for the solutions of (2). For our purpose, we recall here that any solution $\mathbf{x}$ of (2) is continuous and right differentiable for all $t$. In the remainder of this article, we make the additional assumption that the set of time instants when $\mathbf{x}(t)$ is not differentiable has measure zero.

Within the above framework, the dynamics of a neural network can now be given in the matrix form as

$$\dot{\mathbf{x}} = \mathbf{\Pi}_{\mathbb{H}_n}(\mathbf{x}, \mathbf{W}\mathbf{x} + \mathbf{I}(t)) \tag{3}$$

where $\mathbf{x}(t) = (x_1(t), \dots, x_n(t))^{\mathrm{T}}$ is the states of the neurons, $\mathbf{W}$ is the $n \times n$ matrix whose diagonal elements represent the leaking rate of the neurons and whose non-diagonal elements represent the synaptic projection weight, $\mathbf{I}(t)$ is the vector of external inputs. Finally, $\mathbb{H}_n$ is a *regular n-cube* defined as follows

**Definition 1.** A *regular n-cube* $\mathbb{H}_n$ is a subset of $\mathbb{R}^n$ defined by

$$\mathbb{H}_n = \{(x_1, \dots, x_n)^{\mathrm{T}} \in \mathbb{R}^n : \forall i,\ m_i \le x_i \le M_i\}$$

where $m_1, \dots, m_n, M_1, \dots, M_n \in \mathbb{R}$.

Intuitively, a regular $n$-cube is an $n$-cube whose edges are parallel to the axes.

In practice, networks of leaky integrators described by lPDS as above and their classical counterparts with transfer functions show very similar behavior. However, the stability properties of lPDS networks can be rigorously established through contraction theory (see the next section), which makes them interesting from a theoretical viewpoint.

### 2.3. Contraction analysis of locally projected dynamical system on regular n-cubes

Contraction analysis for systems subject to convex constraints has already been discussed in Lohmiller and Slotine (2000). However, in that work, the projection applied to constrain the system in the convex region depends on the metric which makes the original system contracting. Thus, we cannot use this result here since our projection operator must not depend on the neural network

Since the contraction condition is local, a lPDS can only be contracting if the original, un-projected, system is contracting within $\mathbf{\Omega}$. The converse implication is not true in general, because the projection operator can deeply modify the system's behavior along the boundary of $\mathbf{\Omega}$. We now introduce some definitions in order to be able to state this converse implication in some particular cases.

**Definition 2.** Let $\mathbf{x} \in \delta\mathbf{\Omega}$ where $\delta\mathbf{\Omega}$ denotes the boundary of $\mathbf{\Omega}$. The set of *inward normals* to $\mathbf{\Omega}$ at $\mathbf{x}$ is defined as

$$N_{\mathbf{\Omega}}(\mathbf{x}) = \{\mathbf{n} : \forall \mathbf{y} \in \mathbf{\Omega}, \mathbf{n}^{\mathrm{T}}(\mathbf{x} - \mathbf{y}) \le 0\}.$$

If $\mathbf{x} \in \mathbf{\Omega} - \delta\mathbf{\Omega}$ then we set $N_{\mathbf{\Omega}}(\mathbf{x}) = \{\mathbf{0}\}$.

**Definition 3.** A metric $\mathbf{M}$ is said to be *compatible* with a convex set $\mathbf{\Omega}$ if there exists a coordinate transform $\mathbf{\Theta}$ such that $\mathbf{\Theta}^{\mathrm{T}}\mathbf{\Theta} = \mathbf{M}$ and

$$\forall \mathbf{x} \in \delta\mathbf{\Omega}, \forall \mathbf{n} \in N_{\mathbf{\Omega}}(\mathbf{x}), \quad \mathbf{\Theta}\mathbf{n} \in N_{\mathbf{\Theta}\mathbf{\Omega}}(\mathbf{\Theta}\mathbf{x}).$$

In this case, we say that $\mathbf{\Theta}$ is a square root of $\mathbf{M}$ which is *compatible* with $\mathbf{\Omega}$.

We can give a simple sufficient condition for a metric to be compatible with a regular $n$-cube.

**Proposition 1.** *Any diagonal positive definite metric* $\mathbf{M}$ *is compatible with any regular n-cube* $\mathbb{H}_n$.

**Proof.** Let $\mathbf{x} = (x_1, \dots, x_n)^{\mathrm{T}} \in \delta\mathbb{H}_n$. An inward normal $\mathbf{n} = (n_1, \dots, n_n)^{\mathrm{T}}$ to $\mathbb{H}_n$ at $\mathbf{x}$ is characterized by

$$\begin{cases} n_i \ge 0 & \text{if } x_i = m_i \\ n_i \le 0 & \text{if } x_i = M_i \\ n_i = 0 & \text{if } m_i < x_i < M_i. \end{cases}$$

Since $\mathbf{M}$ is diagonal and positive definite, one has $\mathbf{M} = \operatorname{diag}(d_1^2, \dots, d_n^2)$ with $d_i > 0$. Consider the coordinate transform $\mathbf{\Theta} = \operatorname{diag}(d_1, \dots, d_n)$. Clearly, $\mathbf{\Theta}^{\mathrm{T}}\mathbf{\Theta} = \mathbf{M}$ and $\mathbf{\Theta}\mathbb{H}_n$ is a regular $n$-cube with minimal values $d_1m_1, \dots, d_nm_n$ and maximal values $d_1M_1, \dots, d_nM_n$. It follows from the characterization above that $\mathbf{\Theta}\mathbf{n} = (d_1n_1, \dots, d_nn_n)^{\mathrm{T}} \in N_{\mathbf{\Theta}\mathbb{H}_n}(\mathbf{\Theta}\mathbf{x})$. □

We also need another elementary result.

**Lemma 1.** *Let* $\mathbf{x} \in \mathbf{\Omega}$ *and* $\mathbf{v} \in \mathbb{R}^n$. *There exists* $\mathbf{n}(\mathbf{x}, \mathbf{v}) \in N_{\mathbf{\Omega}}(\mathbf{x})$ *such that*

$$\mathbf{\Pi}_{\mathbf{\Omega}}(\mathbf{x}, \mathbf{v}) = \mathbf{v} + \mathbf{n}(\mathbf{x}, \mathbf{v}).$$

**Proof.** Let $\mathbf{y} \in \mathbf{\Omega}$. We need to show that $A_{\mathbf{y}} = (\mathbf{\Pi}_{\mathbf{\Omega}}(\mathbf{x}, \mathbf{v}) - \mathbf{v})^{\mathrm{T}}(\mathbf{x} - \mathbf{y}) \le 0$. By the definition of $\mathbf{\Pi}_{\mathbf{\Omega}}$, one has

$$A_{\mathbf{y}} = \lim_{h \to 0^+} \frac{1}{h}(\mathbf{P}_{\mathbf{\Omega}}(\mathbf{x} + h\mathbf{v}) - (\mathbf{x} + h\mathbf{v}))^{\mathrm{T}}(\mathbf{x} - \mathbf{y}).$$

Next, introduce the terms $\mathbf{P}_{\mathbf{\Omega}}(\mathbf{x} + h\mathbf{v})$ and $h\mathbf{v}$ into $(\mathbf{x} - \mathbf{y})$

$$\begin{aligned} A_{\mathbf{y}} = \lim_{h \to 0^+} \frac{1}{h}[&(\mathbf{P}_{\mathbf{\Omega}}(\mathbf{x} + h\mathbf{v}) - (\mathbf{x} + h\mathbf{v}))^{\mathrm{T}}(\mathbf{P}_{\mathbf{\Omega}}(\mathbf{x} + h\mathbf{v}) - \mathbf{y}) \\ &+ (\mathbf{P}_{\mathbf{\Omega}}(\mathbf{x} + h\mathbf{v}) - (\mathbf{x} + h\mathbf{v}))^{\mathrm{T}}(\mathbf{x} + h\mathbf{v} - \mathbf{P}_{\mathbf{\Omega}}(\mathbf{x} + h\mathbf{v})) \\ &+ (\mathbf{P}_{\mathbf{\Omega}}(\mathbf{x} + h\mathbf{v}) - (\mathbf{x} + h\mathbf{v}))^{\mathrm{T}}(-h\mathbf{v})]. \end{aligned}$$

The first term in the above equation is non-positive by the property of the point-projection operator. The second term is the negative of a distance and thus is also non-positive. As for the third term, observe that

$$\lim_{h \to 0^+} (\mathbf{P}_{\mathbf{\Omega}}(\mathbf{x} + h\mathbf{v}) - (\mathbf{x} + h\mathbf{v}))^{\mathrm{T}}\mathbf{v} = (\mathbf{P}_{\mathbf{\Omega}}(\mathbf{x}) - \mathbf{x})^{\mathrm{T}}\mathbf{v} = 0$$

since $\mathbf{x} \in \mathbf{\Omega}$. □

We can now state the following theorem

**Theorem 2.** *Let* $\dot{\mathbf{x}} = \mathbf{f}(\mathbf{x}, t)$ *be a dynamical system which is contracting in a constant metric* $\mathbf{M}$ *compatible with a convex set* $\boldsymbol{\Omega}$*. Then the lPDS* $\dot{\mathbf{x}} = \boldsymbol{\Pi}_{\boldsymbol{\Omega}}(\mathbf{x}, \mathbf{f}(\mathbf{x}, t))$ *is also contracting in the same metric and with the same contraction rate.*

**Proof.** Let $\boldsymbol{\Theta}$ be a square root of $\mathbf{M}$ compatible with $\boldsymbol{\Omega}$. Consider $\mathbf{z} = \boldsymbol{\Theta}\mathbf{x}$. By Lemma 1, the system $\mathbf{z}$ is described by

$$\dot{\mathbf{z}} = \boldsymbol{\Theta}\boldsymbol{\Pi}_{\boldsymbol{\Omega}}(\mathbf{x}, \mathbf{f}(\mathbf{x})) = \mathbf{F}(\mathbf{z}) + \boldsymbol{\Theta}\mathbf{n}(\mathbf{x}, \mathbf{f}(\mathbf{x})) \tag{4}$$

where $\mathbf{F}(\mathbf{z}) = \boldsymbol{\Theta}\mathbf{f}(\boldsymbol{\Theta}^{-1}\mathbf{z})$.

Consider two particular trajectories of (4) $\mathbf{z}_1$ and $\mathbf{z}_2$. Denote by $\varDelta$ the squared distance between $\mathbf{z}_1$ and $\mathbf{z}_2$

$$\varDelta(t) = \|\mathbf{z}_1(t) - \mathbf{z}_2(t)\|^2 = (\mathbf{z}_1(t) - \mathbf{z}_2(t))^{\mathrm{T}}(\mathbf{z}_1(t) - \mathbf{z}_2(t)).$$

When $\varDelta$ is differentiable, we have

$$\begin{aligned}\frac{\mathrm{d}}{\mathrm{d}t}\varDelta &= 2(\mathbf{z}_1 - \mathbf{z}_2)^{\mathrm{T}}(\dot{\mathbf{z}}_1 - \dot{\mathbf{z}}_2)\\ &= 2(\mathbf{z}_1 - \mathbf{z}_2)^{\mathrm{T}}(\mathbf{F}(\mathbf{z}_1) + \boldsymbol{\Theta}\mathbf{n}(\mathbf{x}_1, \mathbf{f}(\mathbf{x}_1)) - (\mathbf{F}(\mathbf{z}_2)\\ &\quad + \boldsymbol{\Theta}\mathbf{n}(\mathbf{x}_2, \mathbf{f}(\mathbf{x}_2)))).\end{aligned}$$

Since the metric is compatible with $\boldsymbol{\Omega}$, $\boldsymbol{\Theta}\mathbf{n}(\mathbf{x}_i, \mathbf{f}(\mathbf{x}_i)) \in N_{\boldsymbol{\Theta}\boldsymbol{\Omega}}(\mathbf{z}_i)$ for $i = 1, 2$. Next, by the definition of inward normals, we have $(\mathbf{z}_1 - \mathbf{z}_2)^{\mathrm{T}}\boldsymbol{\Theta}\mathbf{n}(\mathbf{x}_1, \mathbf{f}(\mathbf{x}_1)) \leq 0$ and $-(\mathbf{z}_1 - \mathbf{z}_2)^{\mathrm{T}}\boldsymbol{\Theta}\mathbf{n}(\mathbf{x}_2, \mathbf{f}(\mathbf{x}_2)) \leq 0$, from which we deduce

$$\begin{aligned}\frac{\mathrm{d}}{\mathrm{d}t}\varDelta &\leq 2(\mathbf{z}_1 - \mathbf{z}_2)^{\mathrm{T}}(\mathbf{F}(\mathbf{z}_1) - \mathbf{F}(\mathbf{z}_2))\\ &\leq -2\lambda\varDelta(t)\end{aligned}$$

where $\lambda > 0$ is the contraction rate of $\mathbf{f}$ in the metric $\mathbf{M}$.

Since the set of time instants when $\varDelta(t)$ is not differentiable has measure zero (see Section 2.2), one has

$$\forall t \geq 0, \quad \varDelta(t) = \int_0^t \left(\frac{\mathrm{d}}{\mathrm{d}t}\varDelta\right)\mathrm{d}t \leq -2\lambda\int_0^t \varDelta(s)\mathrm{d}s$$

which yields by Grönwall's lemma

$$\forall t \geq 0, \quad \varDelta(t) \leq \varDelta(0)\mathrm{e}^{-2\lambda t}$$

i.e.

$$\forall t \geq 0, \quad \|\mathbf{z}_1(t) - \mathbf{z}_2(t)\| \leq \|\mathbf{z}_1(0) - \mathbf{z}_2(0)\|\mathrm{e}^{-\lambda t}. \quad \square$$

### 2.4. Combination of contracting systems

One of our motivations for using contraction theory is that contraction properties are preserved under suitable combinations (Lohmiller & Slotine, 1998). This allows both stable aggregation of contracting systems, and variation or optimization of individual subsystems while preserving overall functionality (Slotine & Lohmiller, 2001). We present here three standard combinations of contracting systems which preserve both contraction of the system and diagonality of the metric. Then, constructing our neural network as a lPDS using only those three combinations will give rise to a contracting system in a diagonal metric.

#### 2.4.1. Negative feedback combination

Consider two coupled systems

$$\begin{aligned}\dot{\mathbf{x}}_1 &= \mathbf{f}_1(\mathbf{x}_1, \mathbf{x}_2, t)\\ \dot{\mathbf{x}}_2 &= \mathbf{f}_2(\mathbf{x}_1, \mathbf{x}_2, t).\end{aligned}$$

Assume that system $i$ $(i = 1, 2)$ is contracting with respect to $\mathbf{M}_i = \boldsymbol{\Theta}_i^{\mathrm{T}}\boldsymbol{\Theta}_i$, with rate $\lambda_i$. Assume furthermore that the two systems are connected by *negative feedback* (Tabareau & Slotine, 2006). More precisely, the Jacobian matrices of the couplings verify

$$\boldsymbol{\Theta}_1\mathbf{J}_{12}\boldsymbol{\Theta}_2^{-1} = -k\boldsymbol{\Theta}_2\mathbf{J}_{21}^{\mathrm{T}}\boldsymbol{\Theta}_1^{-1}$$

with $k$ a positive constant. Hence, the Jacobian matrix of the unperturbed global system is given by

$$\mathbf{J} = \begin{pmatrix}\mathbf{J}_1 & -k\boldsymbol{\Theta}_1^{-1}\boldsymbol{\Theta}_2\mathbf{J}_{21}^{\mathrm{T}}\boldsymbol{\Theta}_1^{-1}\boldsymbol{\Theta}_2\\ \mathbf{J}_{21} & \mathbf{J}_2\end{pmatrix}.$$

Consider the coordinate transform

$$\boldsymbol{\Theta} = \begin{pmatrix}\boldsymbol{\Theta}_1 & \mathbf{0}\\ \mathbf{0} & \sqrt{k}\boldsymbol{\Theta}_2\end{pmatrix}$$

associated with the metric $\mathbf{M} = \boldsymbol{\Theta}^{\mathrm{T}}\boldsymbol{\Theta} > \mathbf{0}$. After some calculations, one has

$$\begin{aligned}\left(\boldsymbol{\Theta}\mathbf{J}\boldsymbol{\Theta}^{-1}\right)_s &= \begin{pmatrix}\left(\boldsymbol{\Theta}_1\mathbf{J}_1\boldsymbol{\Theta}_1^{-1}\right)_s & \mathbf{0}\\ \mathbf{0} & \left(\boldsymbol{\Theta}_2\mathbf{J}_2\boldsymbol{\Theta}_2^{-1}\right)_s\end{pmatrix}\\ &\leq \max(-\lambda_1, -\lambda_2)\mathbf{I}.\end{aligned} \tag{5}$$

The augmented system is thus contracting with respect to the metric $\mathbf{M}$, with rate $\min(\lambda_1, \lambda_2)$.

#### 2.4.2. Hierarchical combination

We first recall a standard result in matrix analysis (Horn & Johnson, 1985). Let $\mathbf{A}$ be symmetric matrix in the form

$$\mathbf{A} = \begin{pmatrix}\mathbf{A}_1 & \mathbf{A}_{21}^{\mathrm{T}}\\ \mathbf{A}_{21} & \mathbf{A}_2\end{pmatrix}.$$

Assume that $\mathbf{A}_1$ and $\mathbf{A}_2$ are positive definite. Then $\mathbf{A}$ is positive definite if

$$\sigma^2(\mathbf{A}_{21}) < \lambda_{\min}(\mathbf{A}_1)\lambda_{\min}(\mathbf{A}_2)$$

where $\sigma(\mathbf{A}_{21})$ denotes the largest singular value of $\mathbf{A}_{21}$. In this case, the smallest eigenvalue of $\mathbf{A}$ satisfies

$$\begin{aligned}\lambda_{\min}(\mathbf{A}) \geq{}& \frac{\lambda_{\min}(\mathbf{A}_1) + \lambda_{\min}(\mathbf{A}_2)}{2}\\ &- \sqrt{\left(\frac{\lambda_{\min}(\mathbf{A}_1) - \lambda_{\min}(\mathbf{A}_2)}{2}\right)^2 + \sigma^2(\mathbf{A}_{21})}.\end{aligned}$$

Consider now the same set-up as in Section 2.4.1, except that the connection is now *hierarchical* and upper bounded. More precisely, the Jacobians of the couplings verify

$$\mathbf{J}_{12} = \mathbf{0}, \quad \sigma^2(\boldsymbol{\Theta}_2\mathbf{J}_{21}\boldsymbol{\Theta}_1^{-1}) \leq K.$$

Hence, the Jacobian matrix of the augmented system is given by

$$\mathbf{J} = \begin{pmatrix}\mathbf{J}_1 & \mathbf{0}\\ \mathbf{J}_{21} & \mathbf{J}_2\end{pmatrix}.$$

Consider the coordinate transform

$$\boldsymbol{\Theta}_\epsilon = \begin{pmatrix}\boldsymbol{\Theta}_1 & \mathbf{0}\\ \mathbf{0} & \epsilon\boldsymbol{\Theta}_2\end{pmatrix}$$

associated with the metric $\mathbf{M}_\epsilon = \boldsymbol{\Theta}_\epsilon^{\mathrm{T}}\boldsymbol{\Theta}_\epsilon > \mathbf{0}$. After some calculations, one has

$$\left(\boldsymbol{\Theta}\mathbf{J}\boldsymbol{\Theta}^{-1}\right)_s = \begin{pmatrix}\left(\boldsymbol{\Theta}_1\mathbf{J}_1\boldsymbol{\Theta}_1^{-1}\right)_s & \frac{1}{2}\epsilon(\boldsymbol{\Theta}_2\mathbf{J}_{21}\boldsymbol{\Theta}_1^{-1})^{\mathrm{T}}\\ \frac{1}{2}\epsilon\boldsymbol{\Theta}_2\mathbf{J}_{21}\boldsymbol{\Theta}_1^{-1} & \left(\boldsymbol{\Theta}_2\mathbf{J}_2\boldsymbol{\Theta}_2^{-1}\right)_s\end{pmatrix}.$$

Set now $\epsilon = \sqrt{\frac{2\lambda_1\lambda_2}{K}}$. The augmented system is then contracting with respect to the metric $\mathbf{M}_\epsilon$, with rate $\lambda$ verifying

$$\lambda \geq \frac{1}{2}\left(\lambda_1 + \lambda_2 - \sqrt{\lambda_1^2 + \lambda_2^2}\right).$$

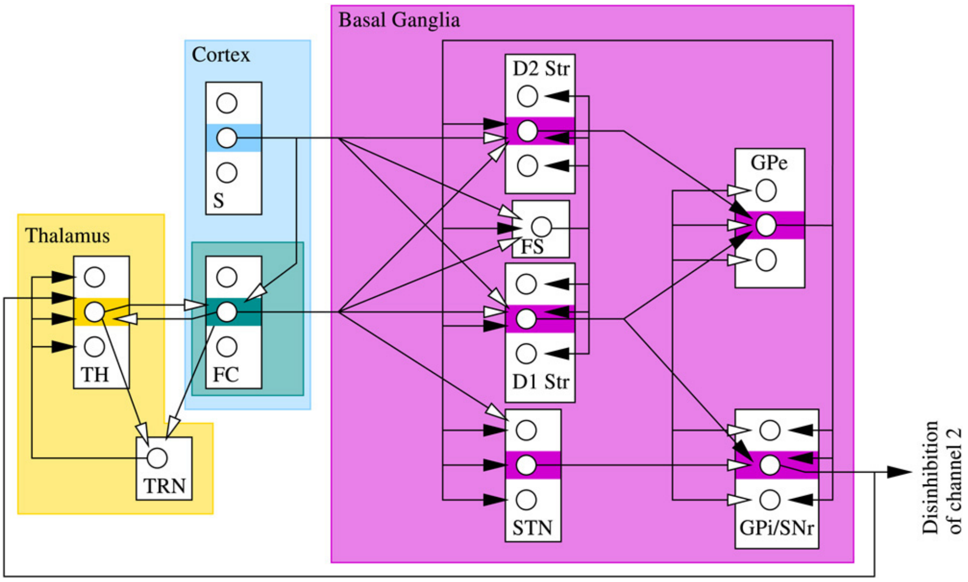

**Fig. 2.** Basal ganglia model. Nuclei are represented by boxes, each circle in these nuclei represents an artificial rate-coding neuron. In this diagram, three channels are competing for selection, represented by the three neurons in each nucleus. The second channel is represented by colored shading. For clarity, the projections from the second channel neurons only are represented, they are identical for the other channels. White arrowheads represent excitations and black arrowheads, inhibitions. D1 and D2: neurons of the striatum with two respective types of dopamine receptors; STN: subthalamic nucleus; GPe: external segment of the globus pallidus; GPi/SNr: internal segment of the globus pallidus and substantia nigra pars reticulata.

### 2.4.3. Small gains

In this section, we require no specific assumption on the form of the couplings

$$\mathbf{J} = \begin{pmatrix} \mathbf{J}_1 & \mathbf{J}_{12} \\ \mathbf{J}_{21} & \mathbf{J}_2 \end{pmatrix}.$$

As for negative feedback, consider the coordinate transform

$$\mathbf{\Theta}_k = \begin{pmatrix} \mathbf{\Theta}_1 & \mathbf{0} \\ \mathbf{0} & \sqrt{k}\mathbf{\Theta}_2 \end{pmatrix} \quad k > 0$$

associated with the metric $\mathbf{M}_k = \mathbf{\Theta}_k^{\mathrm{T}}\mathbf{\Theta}_k > \mathbf{0}$. After some calculations, one has

$$\left(\mathbf{\Theta}_k\mathbf{J}\mathbf{\Theta}_k^{-1}\right)_s = \begin{pmatrix} \left(\mathbf{\Theta}_1\mathbf{J}_1\mathbf{\Theta}_1^{-1}\right)_s & \mathbf{A}_k^{\mathrm{T}} \\ \mathbf{A}_k & \left(\mathbf{\Theta}_2\mathbf{J}_2\mathbf{\Theta}_2^{-1}\right)_s \end{pmatrix}$$

where $\mathbf{A}_k = \frac{1}{2}\left(\sqrt{k}\mathbf{\Theta}_2\mathbf{J}_{21}\mathbf{\Theta}_1^{-1} + \frac{1}{\sqrt{k}}\left(\mathbf{\Theta}_1\mathbf{J}_{12}\mathbf{\Theta}_2^{-1}\right)^{\mathrm{T}}\right)$. Following the result stated at the beginning of Section 2.4.2, if

$$\min_k \sigma^2(\mathbf{A}_k) < \lambda_1\lambda_2$$

then the augmented system is contracting with respect to the metric $\mathbf{M}_k$ for some $k$, with rate $\lambda$ verifying

$$\lambda \geq \frac{\lambda_1 + \lambda_2}{2} - \sqrt{\left(\frac{\lambda_1 - \lambda_2}{2}\right)^2 + \min_k \sigma^2(\mathbf{A}_k)}.$$

## 3. Model description

Rather than using standard leaky-integrator rate-coding neurons, we use the very similar local projected dynamical system model defined by Eq. (3), where each component of the state vector $\mathbf{x}$ is an artificial rate-coding neuron representing the discharge rate of populations of real neurons. Each competing BG channel in each nucleus is represented by one such neuron, and the corresponding thalamic nucleus and cortical areas are also subdivided into identical channels (Fig. 2). The convergence of cortical sensory inputs on the striatum channels is encoded, for simplicity, by a vector of saliences (one salience per channel). Each salience represents the propensity of its corresponding channel to be selected. Each behavior in competition is associated to a specific channel and can be executed if and only if its level of inhibition decreases below a the inhibition level at rest $y_{\mathrm{Rest}}^{\mathrm{GPi}}$ (ie. the SNr/GPi output when the salience vector is null).

The main difference of our architecture with the recent GPR proposal (Gurney et al., 2001a) is the nuclei targeted by the external part of the globus pallidus (GPe) and the nature of these projections. In our model, the GPe projects to the subthalamic nucleus (STN), the internal part of the globus pallidus (GPi) and the substantia nigra pars reticulata (SNr), as well as to the striatum, as documented in Bevan, Booth, Eaton, and Bolam (1998), Kita, Tokuno, and Nambu (1999) and Staines, Atmadja, and Fibiger (1981). Moreover, the striatal terminals target the dendritic trees, while pallidal, nigral and subthalamic terminals form perineuronal nets around the soma of the targeted neurons (Sato, Lavallee, Lévesque, & Parent, 2000). This specific organization allows GPe neurons to influence large sets of neurons in GPi, SNr and STN (Parent et al., 2000), thus the sum of the activity of all GPe channels influences the activity of STN and GPi/SNr neurons (Eqs. (9) and (11)), while there is a simple channel-to-channel projection to the striatum Eqs. (6) and (7).

The striatum is one of the two input nuclei of the BG. It is mainly composed of GABAergic (inhibitory) medium spiny neurons (MSN). As in the GPR model, we distinguish among them, those with D1 and D2 dopamine receptors and modulate the input generated in the dendritic tree by the dopamine level $\gamma$, which here encompasses salience, frontal cortex feedback and GPe projections.

Using the formulation of Eq. (3), the $i$th neurons ($i \in [1, N]$, with $N$ the number of channels) of the D1 and D2 subparts of the striatum are defined as follows

$$(\mathbf{Wx} + \mathbf{I}(t))_{\mathrm{D1}_i} = \frac{1}{\tau}\left((1+\gamma)(w_{\mathrm{FC}}^{\mathrm{D1}}x_i^{\mathrm{FC}} - w_{\mathrm{GPe}}^{\mathrm{D1}}x_i^{\mathrm{GPe}} + w_S^{\mathrm{D1}}S_i(t)) - w_{\mathrm{FS}}^{\mathrm{D1}}x^{\mathrm{FS}} + I_{\mathrm{D1}}\right) \quad (6)$$

$$(\mathbf{Wx} + \mathbf{I}(t))_{\mathrm{D2}_i} = \frac{1}{\tau}\left((1-\gamma)(w_{\mathrm{FC}}^{\mathrm{D2}}x_i^{\mathrm{FC}} - w_{\mathrm{GPe}}^{\mathrm{D2}}x_i^{\mathrm{GPe}} + w_S^{\mathrm{D2}}S_i(t)) - w_{\mathrm{FS}}^{\mathrm{D2}}x^{\mathrm{FS}} + I_{\mathrm{D2}}\right) \quad (7)$$

**Table 1**
Parameters of the simulations

| | | | | | | | | | |
|---|---|---|---|---|---|---|---|---|---|
| $N$ | 6 | $\tau$ | 40 ms | $\tau_{\mathrm{STN}}$ | 5 ms | $\tau_{\mathrm{FS}}$ | 5 ms | $\tau_{\mathrm{FC}}$ | 80 ms |
| $\tau_{\mathrm{TH}}$ | 5 ms | $\tau_{\mathrm{TRN}}$ | 5 ms | $\gamma$ | 0.2 | $w^{\mathrm{D2}}_{\mathrm{GPe}}$ | 1 | $w^{\mathrm{GPe}}_{\mathrm{D2}}$ | 0.4 |
| $w^{\mathrm{D1}}_{\mathrm{GPe}}$ | 1 | $w^{\mathrm{GPe}}_{\mathrm{D1}}$ | 0.4 | $w^{\mathrm{FS}}_{\mathrm{GPe}}$ | 0.05 | $w^{\mathrm{D1}}_{\mathrm{FS}}$ | 0.5 | $w^{\mathrm{D2}}_{\mathrm{FS}}$ | 0.5 |
| $w^{\mathrm{GPe}}_{\mathrm{STN}}$ | 0.7 | $w^{\mathrm{STN}}_{\mathrm{GPe}}$ | 0.45 | $w^{\mathrm{GPi}}_{\mathrm{GPe}}$ | 0.08 | $w^{\mathrm{GPi}}_{\mathrm{STN}}$ | 0.7 | $w^{\mathrm{GPi}}_{\mathrm{D1}}$ | 0.4 |
| $w^{\mathrm{TH}}_{\mathrm{TRN}}$ | 0.35 | $w^{\mathrm{TRN}}_{\mathrm{TH}}$ | 0.35 | $w^{\mathrm{TH}}_{\mathrm{FC}}$ | 0.6 | $w^{\mathrm{FC}}_{\mathrm{TH}}$ | 0.6 | $w^{\mathrm{TRN}}_{\mathrm{FC}}$ | 0.35 |
| $w^{\mathrm{TH}}_{\mathrm{GPi}}$ | 0.18 | $w^{\mathrm{STN}}_{\mathrm{FC}}$ | 0.58 | $w^{\mathrm{D1}}_{\mathrm{FC}}$ | 0.1 | $w^{\mathrm{D2}}_{\mathrm{FC}}$ | 0.1 | $w^{\mathrm{FS}}_{\mathrm{FC}}$ | 0.01 |
| $I_{\mathrm{D1}}$ | −0.1 | $I_{\mathrm{D2}}$ | −0.1 | $I_{\mathrm{STN}}$ | 0.5 | $I_{\mathrm{GPi}}$ | 0.1 | $I_{\mathrm{GPe}}$ | 0.1 |

where $S(t)$ is the salience input vector, and where the negative constant inputs $I_{\mathrm{D1}}$ and $I_{\mathrm{D2}}$, which keep the neurons silent when the inputs are not strong enough, model the up-state/down-state property of the MSNs.

The striatum also contains a small proportion of phenotypically diverse interneurons (Tepper & Bolam, 2004). We include here the fast spiking GABAergic interneurons (FS), that we model roughly as a single population exerting feedforward inhibition on the MSN (Tepper, Koós, & Wilson, 2004), and modulated by GPe feedback (Bevan et al., 1998)

$$(\mathbf{Wx}+\mathbf{I}(t))_{\mathrm{FS}} = \frac{1}{\tau_{\mathrm{FS}}} \sum_{j=1}^{N} \left( w^{\mathrm{FS}}_{\mathrm{FC}} x^{\mathrm{FC}}_j - w^{\mathrm{FS}}_{\mathrm{GPe}} x^{\mathrm{GPe}}_j + w^{\mathrm{FS}}_{S} S_j(t) \right). \tag{8}$$

The subthalamic nucleus (STN) is the second input of the basal ganglia and also receives diffuse projections from the GPe, as explained above. Its glutamatergic neurons have an excitatory effect and project to the GPe and GPi. The resulting input of the STN neuron is given by

$$(\mathbf{Wx}+\mathbf{I}(t))_{\mathrm{STN}_i} = \frac{1}{\tau_{\mathrm{STN}}} \left( w^{\mathrm{STN}}_{\mathrm{FC}} x^{\mathrm{FC}}_i - w^{\mathrm{STN}}_{\mathrm{GPe}} \sum_{j=1}^{N} x^{\mathrm{GPe}}_j + I_{\mathrm{STN}} \right) \tag{9}$$

where the constant positive input $I_{\mathrm{STN}}$ models the tonic activity of the STN.

The GPe is an inhibitory nucleus, it receives channel-to-channel afferents from the whole striatum (Wu, Richard, & Parent, 2000), and a diffuse excitation from the STN

$$(\mathbf{Wx}+\mathbf{I}(t))_{\mathrm{GPe}_i} = \frac{1}{\tau} \left( -w^{\mathrm{GPe}}_{\mathrm{D1}} x^{\mathrm{D1}}_i - w^{\mathrm{GPe}}_{\mathrm{D2}} x^{\mathrm{D2}}_i + w^{\mathrm{GPe}}_{\mathrm{STN}} \sum_{j=1}^{N} x^{\mathrm{STN}}_j + I_{\mathrm{GPe}} \right) \tag{10}$$

where the constant positive input $I_{\mathrm{GPe}}$ models the tonic activity of the GPe.

The GPi and SNr are the inhibitory output nuclei of the BG, which keep their targets under inhibition unless a channel is selected. They receive channel-to-channel projections from the D1 striatum and diffuse projections from the STN and the GPe

$$(\mathbf{Wx}+\mathbf{I}(t))_{\mathrm{GPi}_i} = \frac{1}{\tau} \left( -w^{\mathrm{GPi}}_{\mathrm{D1}} x^{\mathrm{D1}}_i + w^{\mathrm{GPi}}_{\mathrm{STN}} \sum_{j=1}^{N} x^{\mathrm{STN}}_i - w^{\mathrm{GPi}}_{\mathrm{GPe}} \sum_{j=1}^{N} x^{\mathrm{GPe}}_j + I_{\mathrm{GPi}} \right) \tag{11}$$

where the constant positive input $I_{\mathrm{GPi}}$ models the tonic activity of the GPi/SNr.

Finally, the thalamus (TH) forms an excitatory loop with the frontal cortex (FC), these two modules representing different thalamus nuclei and cortical areas, depending on the cortico-baso-thalamo-cortical loop considered. The thalamus is moreover under a global regulatory inhibition of the thalamic reticular nucleus (TRN, represented by a single population of neurons) and a channel-specific selective inhibition from the basal ganglia

$$(\mathbf{Wx}+\mathbf{I}(t))_{\mathrm{TH}_i} = \frac{1}{\tau_{\mathrm{TH}}} \left( w^{\mathrm{TH}}_{\mathrm{FC}} x^{\mathrm{FC}}_i - w^{\mathrm{TH}}_{TRN} x^{TRN} - w^{\mathrm{TH}}_{\mathrm{GPi}} x^{\mathrm{GPi}}_i \right) \tag{12}$$

$$(\mathbf{Wx}+\mathbf{I}(t))_{FC_i} = \frac{1}{\tau_{\mathrm{FC}}} \left( w^{\mathrm{FC}}_{S} S_i + w^{\mathrm{FC}}_{\mathrm{TH}} x^{\mathrm{TH}}_i \right) \tag{13}$$

$$(\mathbf{Wx}+\mathbf{I}(t))_{TRN} = \frac{1}{\tau_{TRN}} \left( \sum_i w^{TRN}_{\mathrm{FC}} x^{\mathrm{FC}}_i + w^{TRN}_{\mathrm{TH}} x^{\mathrm{TH}}_i \right). \tag{14}$$

This model keeps the basic off-center on-surround selecting structure, duplicated in the D1-STN-GPi/SNr and D2-STN-GPe subcircuits, of the GPR. However, the channel-specific feedback from the GPe to the Striatum helps in sharpening the selection by favoring the channel with the highest salience in D1 and D2. Moreover, the global GPe inhibition on the GPi/SNr synergetically interacts with the STN excitation in order to limit the amplitude of variation of the inhibition of the unselected channels. The inhibitory projections of the BG onto the thalamo-cortical excitatory loop limits the amplification of the unselected channels and thus favors a selective amplification of the winning channels. In such an architecture, the frontal cortex preserves the information from all channels but amplifies selectively the winning channel, in a sort of attention "spotlight" process, while the subcortical target circuits of the BG are under very selective inhibition, ensuring that motor commands do not interfere.

## 4. Disembodied model results

We first analyze the contraction of the contracting basal ganglia model (CBG) and its selection properties in simple disembodied tests before evaluating it as an ASM in a simulated robot.

Similarly to the simulations made by Gurney et al. (2001b), we used a 6-channel model. The parameters of the model were hand-tuned in order to obtain a selective system and respecting the local contraction constraints defined below, their values are summarized in Table 1. The simulation was programmed in C++, using the simple Euler approximation for integration, with a time step of 1 ms.

### 4.1. Contraction analysis of the model

According to the theory developed in Section 2.3, our model is contracting if the non-projected dynamics (which are linear) are contracting in a diagonal metric. To find this metric, we will use the three combinations presented in Section 2.4 that preserve diagonality.

Remark that each separated nucleus is trivially contracting in the identity metric because there is no lateral connection. The contracting rate of each nucleus is $\frac{1}{\tau}$, where $\tau$ is the common time constant of the $N$ neurons of the nucleus. Thus, the metric $\mathbf{M}_{BG}$ of the basal ganglia is constituted of the blocks $\kappa_{\mathrm{GPe}}\mathbf{I}$, $\kappa_{\mathrm{STN}}\mathbf{I}$, $\kappa_{\mathrm{D1}}\mathbf{I}$, $\kappa_{\mathrm{D2}}\mathbf{I}$, $\kappa_{\mathrm{FS}}1$ and $\kappa_{\mathrm{GPi}}\mathbf{I}$. Similarly, the thalamic metric $\mathbf{M}_{\mathrm{TH}}$ is constituted of the blocks $\kappa_{\mathrm{FC}}\mathbf{I}$, $\kappa_{\mathrm{TH}}1$ and $\kappa_{TRN}\mathbf{I}$. The resulting metric for the whole system $\mathbf{M}_{\mathrm{CBG}}$ combines $\mathbf{M}_{BG}$ and $\mathbf{M}_{\mathrm{TH}}$ in the following way

$$\mathbf{M}_{\mathrm{CBG}} = \begin{pmatrix} \mathbf{M}_{BG} & 0 \\ 0 & \alpha\mathbf{M}_{\mathrm{TH}} \end{pmatrix}.$$

### 4.1.1. Analysis of the basal ganglia

- $\kappa_{\mathrm{GPe}} = 1$.
  We can set $\kappa_{\mathrm{GPe}}$ to any value as there is no combination at this stage. The current contracting rate is $\frac{1}{\tau}$.
- $\kappa_{\mathrm{STN}} = w_{\mathrm{STN}}^{\mathrm{GPe}}/w_{\mathrm{GPe}}^{\mathrm{STN}}$.
  We use negative feedback. The contracting rate remains unchanged
- $\begin{cases} \kappa_{\mathrm{D1}} = w_{\mathrm{D1}}^{\mathrm{GPe}}/((1+\gamma)w_{\mathrm{GPe}}^{\mathrm{D1}}) \\ \kappa_{\mathrm{D2}} = w_{\mathrm{D2}}^{\mathrm{GPe}}/((1-\gamma)w_{\mathrm{GPe}}^{\mathrm{D2}}). \end{cases}$
  We use small gains to show that the system constituted by the STN, GPe, striatum D1 and D2 is contracting when
  $$\left((1+\gamma)w_{\mathrm{D1}}^{\mathrm{GPe}}w_{\mathrm{GPe}}^{\mathrm{D1}}\right)^2 + \left((1-\gamma)w_{\mathrm{D2}}^{\mathrm{GPe}}w_{\mathrm{GPe}}^{\mathrm{D2}}\right)^2 < 1 \tag{15}$$
  with a contracting rate
  $$\frac{1}{\tau}\left(1 - \sqrt{((1+\gamma)w_{\mathrm{D1}}^{\mathrm{GPe}}w_{\mathrm{GPe}}^{\mathrm{D1}})^2 + ((1-\gamma)w_{\mathrm{D2}}^{\mathrm{GPe}}w_{\mathrm{GPe}}^{\mathrm{D2}})^2}\right).$$
- $\kappa_{\mathrm{FS}} = w_{\mathrm{FS}}^{\mathrm{D1}}/w_{\mathrm{GPe}}^{\mathrm{FS}}$.
  Again by use of small gains.
- $\kappa_{\mathrm{GPi}} = 1/(\tau\sigma(\mathbf{G}))^2$

where $\sigma(\mathbf{G})$ is the largest singular value of the matrix of projections on GPi and $\tau$ is the slowest time constant of neurons in the basal ganglia. This constant is set by using hierarchical combination.

Thus we can guarantee the contraction of the basal ganglia as soon as condition (15) is satisfied.

### 4.1.2. Analysis of the thalamus

- $\kappa_{\mathrm{TH}} = 1$.
  We can set $\kappa_{\mathrm{TH}}$ to any value as there is no combination at this stage. The current contracting rate is $\frac{1}{\tau_{\mathrm{TH}}}$.
- $\kappa_{\mathrm{GPe}} = w_{TRN}^{\mathrm{TH}}/w_{\mathrm{TH}}^{TRN}$.
  We use negative feedback. The contracting rate remains unchanged
- $\kappa_{\mathrm{FC}} = \sqrt{w_{\mathrm{FC}}^{\mathrm{TH}\,2} + Nw_{\mathrm{FC}}^{TRN\,2}}/w_{\mathrm{TH}}^{\mathrm{FC}}$.
  We use small gains to show that the thalamo-cortical module is contracting when
  $$w_{\mathrm{TH}}^{\mathrm{FC}}\left(w_{\mathrm{FC}}^{\mathrm{TH}} + \sqrt{w_{\mathrm{FC}}^{\mathrm{TH}\,2} + Nw_{\mathrm{FC}}^{TRN\,2}}\right) < 1. \tag{16}$$
  Remark that this condition depends on *N*. This would not have been the case if we had modeled the *TRN* by *N* channels instead of 1.

Thus we can guarantee the contraction of the thalamus as soon as condition (16) is satisfied.

It remains to examine the large loop between the thalamus and the basal ganglia involving projections of the GPi and the FC. Again, we use small gains to set $\alpha$.

$$\alpha = \sqrt{\frac{\tau_{FCtx}\kappa_{\mathrm{GPi}}\;(w_{\mathrm{FC}}^{\mathrm{STN}\,2} + w_{\mathrm{FC}}^{\mathrm{D1}\,2} + w_{\mathrm{FC}}^{\mathrm{D2}\,2} + nw_{\mathrm{FC}}^{\mathrm{FS}\,2})}{\tau_{\mathrm{TH}}\kappa_{\mathrm{FC}}\;w_{\mathrm{GPi}}^{\mathrm{TH}\;2}}}.$$

**Proposition 2.** *Let* $\mathbf{M}_{\mathrm{CBG}} = \mathbf{\Theta}_{\mathrm{CBG}}^{\mathrm{T}}\mathbf{\Theta}_{\mathrm{CBG}}$ *be the diagonal metric defined above. By Theorem 2, if the generalized Jacobian* $\mathbf{\Theta}_{\mathrm{CBG}}\mathbf{W}\mathbf{\Theta}_{\mathrm{CBG}}^{-1}$ *is negative definite, the dynamical system* $\dot{\mathbf{x}} = \mathbf{\Pi}_{\mathbb{H}_n}(\mathbf{x}, \mathbf{W}\mathbf{x} + \mathbf{I}(t))$ *describing the cortico-baso-thalamo-cortical loop model is contracting with a rate* $|\lambda_{\max}|$*, where* $\lambda_{\max}$ *is the largest eigenvalue of* $\mathbf{\Theta}_{\mathrm{CBG}}\mathbf{W}\mathbf{\Theta}_{\mathrm{CBG}}^{-1}$.

**Table 2**
Value of the constants defining the metric $M_{\mathrm{CBG}}$ for the set of parameters of our simulation

| $\kappa_{\mathrm{GPe}}$ | $\kappa_{\mathrm{STN}}$ | $\kappa_{\mathrm{D1}}$ | $\kappa_{\mathrm{D2}}$ | $\kappa_{\mathrm{FS}}$ | $\kappa_{\mathrm{GPi}}$ | $\kappa_{\mathrm{TH}}$ | $\kappa_{\mathrm{TRN}}$ | $\kappa_{FCtx}$ | $\alpha$ |
|---|---|---|---|---|---|---|---|---|---|
| 1 | 0.441 | 0.577 | 0.707 | 1 | 0.104 | 1 | 1 | 5.282 | 0.253 |

At this stage, we have provided an algebraic definition of the metric $\mathbf{M}_{\mathrm{CBG}}$. Unfortunately, the complexity of the induced generalized Jacobian prevents us from giving a global algebraic condition on the projection weights for the generalized Jacobian to be negative definite. This is not of major incidence as we can compute numerically, for any instance of the weights, the eigenvalues of the symmetric part of the generalized Jacobian and check that they are all negative.

Table 2 gives the numerical value of the constants defining the metric $M_{\mathrm{CBG}}$ for the set of parameters of our simulation (see Table 1). Using the free software *Octave*, we compute in that case the eigenvalues of the generalized Jacobian and obtain that our model is contracting with contracting rate of 2.20.

Notice that computing the maximum real part of the eigenvalue of the non-projected dynamics (which are linear) gives an upper bound of the contracting rate. For the set of parameters of our simulation, this upper bound is 2.59. It is remarkable that being forced to use diagonal metrics in our proof (which discards a huge set of metrics) has not decreased much the contracting rate.

### 4.2. Basic selection test

We first reproduced the selection test of Gurney et al. (2001b) with our model and with the GPR model version presented in Prescott et al. (2006). In this test, a specific sequence of five different salience vectors (represented by the dashed lines in Fig. 3) is submitted to a 6-channel version of the BG model, in order to show the basic selection properties of the system. Here, we submitted each vector to the system during 2 s before switching to the next one in the sequence.

During the CBG simulation (Fig. 3, top row), with the first vector of null saliences, the system stabilizes in a state where all channels are equally inhibited ($x_i^{\mathrm{GPi}} = 0.095$). Then, the first channel receives a 0.4 input salience which results in a clear disinhibition of this channel ($x_1^{\mathrm{GPi}} = 0.014$) and increased inhibition of the others. When the second channel salience is set to 0.6, it becomes perfectly selected ($x_2^{\mathrm{GPi}} = 0$) while the first one is rapidly inhibited to a level identical to the one of the four last channels. During the fourth step, the salience of the first channel is increased to 0.6, channels 1 and 2 are therefore simultaneously selected ($x_1^{\mathrm{GPi}} = x_2^{\mathrm{GPi}} = 0.03$). Finally, during the last step of the test, channel 1 has its salience reduced to 0.4, and it is then rapidly inhibited, while channel 2 returns to perfect selection ($x_2^{\mathrm{GPi}} = 0$). The CBG thus passes this test in a satisfactory manner: the channels with the highest saliences are always selected while the others are inhibited.

The GPR simulation (Fig. 3, bottom row) is qualitatively quite similar, excepted during the fourth step of the sequence (emphasized with an asterisk): while the salience of channel 1 increases from 0.4 up to 0.6 (the same salience as that of channel 2), channel 2 remains selected and channel 1 is fully inhibited (its level of inhibition is higher than the inhibition at rest). The inputs in channels 1 and 2 being exactly the same, this difference in their selection state is clearly caused by the initial conditions of the system (i.e. the fact that channel 2 was selected before). This example of a dependence on the initial conditions clearly shows that the GPR model is not contracting.

Indeed, as we have seen in Section 2.3, a rate-coding neural network is contracting only if its non-projected dynamics are contracting in a diagonal metric. But a linear system is stable if and

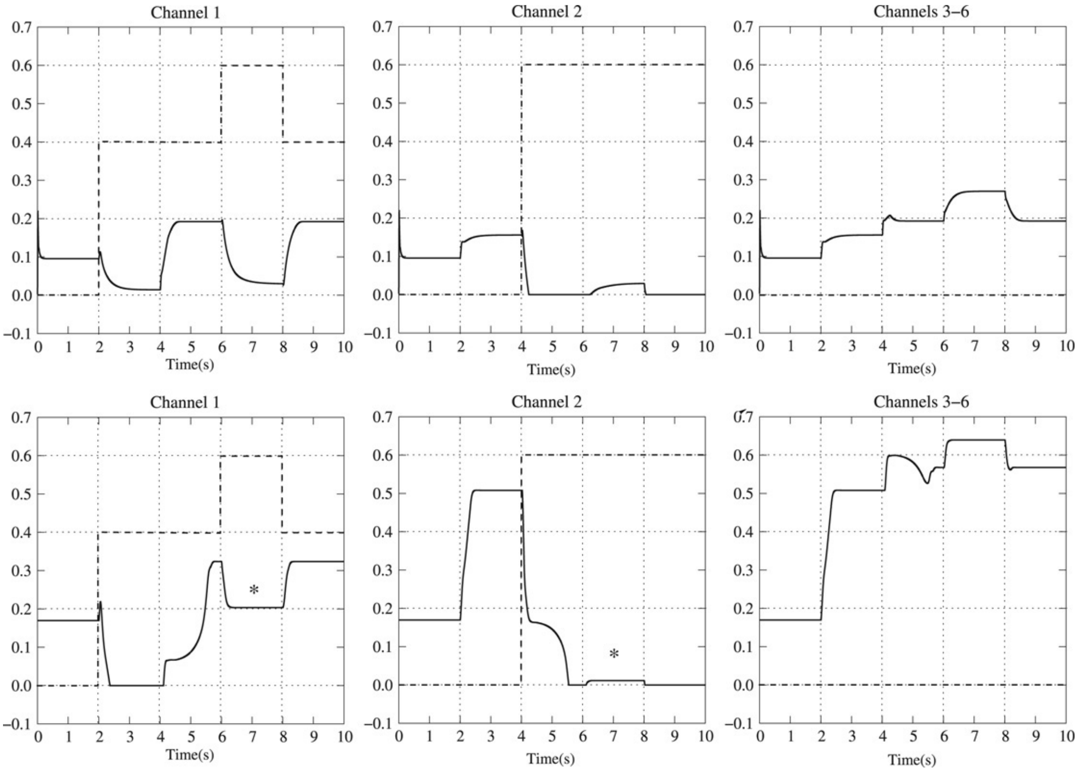

**Fig. 3.** Variation of the GPi/SNr inhibitory output during the Gurney et al. (2001b) test applied to (top) the CBG and (bottom) the GPR. Dashed lines represent the input salience of the channel and solid lines represent the output of the channel. Note that during the fourth step (6 s $< t <$ 8 s), channels 1 and 2 are selected by the CBG, while the GPR selects channel 2 only (asterisk).

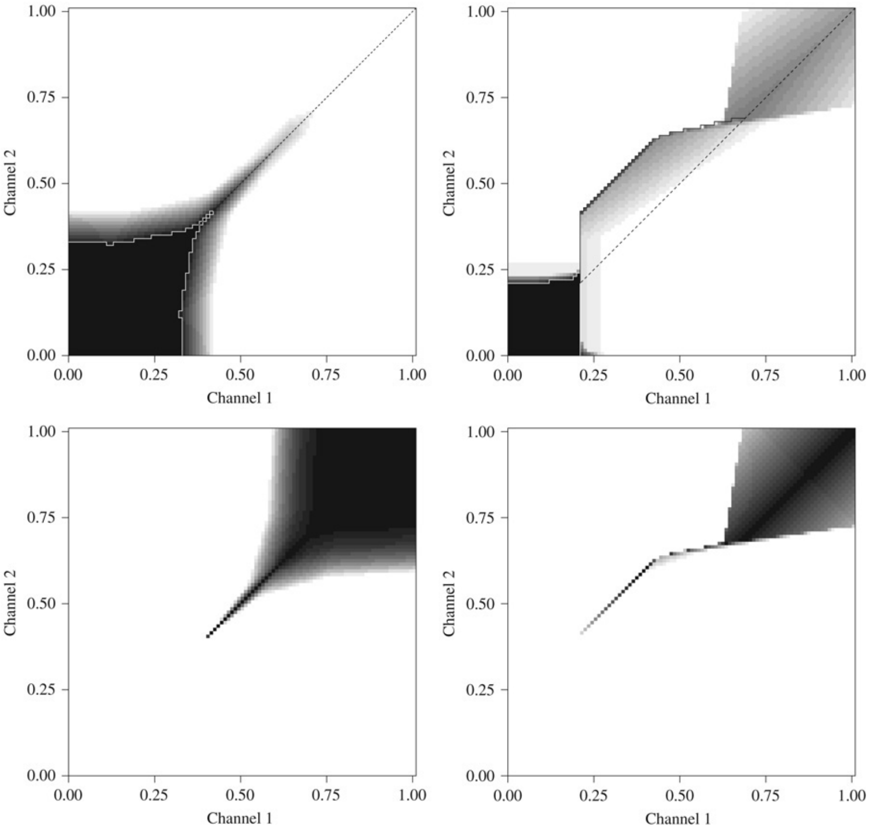

**Fig. 4.** Efficiency (top) and distortion (bottom) in the winning channel for a systematic salience-space search for the CBG (left) and the GPR (right). Top: black to white gradient represents increasing efficiency (from 0 to 1); bottom: black to white gradient represents decreasing distortion (from 1 to 0), maximal distortion corresponding to simultaneous selection of both channels is thus in black. White line: limit beyond which no selection occurs; dashed black line: diagonal representing equal saliences. For the GPR efficiency (top right), note the hysteresis area between the dashed and the full black lines. See the text for further explanations.

only if all its eigenvalues have a negative real part. Computing the eigenvalues of the linear part of the GPR reveals that $N-1$ of them have a positive real part (namely 10.387). We can thus conclude that the GPR is not contracting.

### 4.3. Systematic salience search test

This first result is however not surprising, as revealed by the systematic salience search experiment performed in Prescott et al. (2006), and that we also reproduced with both the GPR and the CBG. In this experiment, the first two channels of the ASM are put in competition in the following manner: the first channel salience is increased from 0 to 1 in steps of 0.01, and for each of these steps, the salience of the second channel is also gradually increased from 0 to 1 in steps of 0.01. The system is run to convergence between all step increases. The internal state of the model is not reset between each channel 2 salience increase, but only for channel 1 steps. This means that the test evaluates the selection response of the system with one channel salience fixed while the other one gradually increases.

In order to evaluate the response of the ASM to this experiment, four numerical values are computed. First, the efficiencies of the selection of channels 1 and 2, equivalent to the percentage of disinhibition, are computed as follows:

$$e_i = [1 - y_i^{\text{GPi}} / y_{\text{Rest}}^{\text{GPi}}]_+ \tag{17}$$

with $i$ the index of the channel, $y_i^{\text{GPi}}$ the output of the $i$th GPi neuron and $y_{\text{Rest}}^{\text{GPi}}$ the output inhibition of all channels when all saliences are null. The absolute efficiency of the selection is defined as the efficiency of the winning channel:

$$e_w = \max_i e_i. \tag{18}$$

Finally, the distortion of the selection, which is null when only the winning channel is disinhibited and increasing with the disinhibition of its competitors, is defined by:

$$d_w = 2 \frac{\sum_i e_i - e_w}{\sum_i e_i}. \tag{19}$$

The results of the experiment are summarized by the $e_w$ and $d_w$ graphs (Fig. 4), where the value of each of these variables is represented with regard to the corresponding channel 1 (abscissa) and channel 2 (ordinate) saliences. First observe that the GPR results we obtain with 6 channels are very similar to those presented in Prescott et al. (2006) for a 5-channel GPR. Concerning $e_w$ (top row), whereas, for the CBG, the selection switches from channel 1 to channel 2 as soon as the salience of channel 2 is larger than the salience of channel 1 (when it crosses the diagonal in dashed black), for the GPR, this switch is delayed until much higher values are reached (when it crosses the black line). As previously noted, this hysteresis effect is a direct consequence of the non-contraction of the GPR.

Note that when high saliences are in competition, the GPR tends to partially select both channels ($e_w < 1$ and $d_w > 0$), while the CBG fully disinhibits both channels ($e_w = 1$ and $d_w$ close to 1). Which behavior is preferable for an ASM is not decided.

Is the GPR's strong dependence on initial conditions a good feature for an ASM? Prescott et al. (2006) argue that it allows behavioral persistence, and that in their experiment, the robot takes advantage of it to avoid dithering between actions. We do not claim that there is a definitive answer to the question. Nevertheless, in the next section, we describe the evaluation of the CBG in a minimal survival task in which the robot also avoids dithering, despite its contracting ASM. This shows that this dependence on initial conditions is not necessary from the point of view of dithering avoidance.

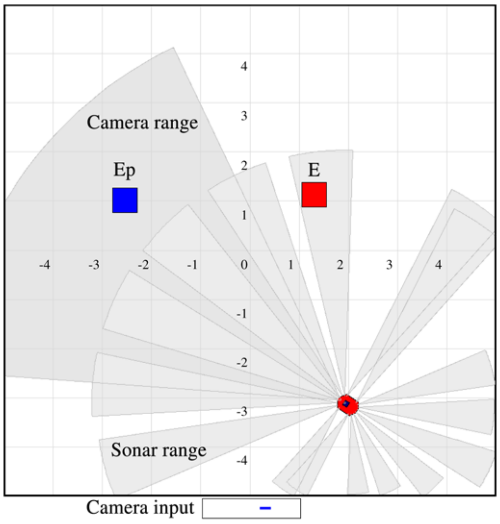

**Fig. 5.** Experimental set-up. Blue square: Potential Energy resource; red square: Energy resource. The light gray surfaces represent the field of view of the sonars, and the darker one the field of view of the camera. The corresponding camera image is represented at the bottom.

## 5. Minimal survival task

### 5.1. Materials and methods

The suitability of the model for action selection in an autonomous robot has been tested in simulation with the same minimal survival task previously used to evaluate the GPR model (Girard et al., 2003). In order to emphasize its properties, and in particular those resulting from the selective feedback loop, its performance was compared to a simple if-then-else decision rule (ITE, fully described in Appendix A).

In such a task, the robot has to go back and forth between locations containing two different kind of resources, in order to keep its energy level above 0. The robot has two internal variables, namely *Energy* and *Potential Energy*, taking values between 0 and 1, and an artificial metabolism, which couples them as follows:

- The Energy ($E$) is continuously decreasing, with a constant consumption rate (0.01 Energy unit per second). When it reaches 0, the robot has run out of energy and the ongoing trial is interrupted. To prevent this, the robot has to regularly acquire Energy by activating the *ReloadOnE* action on an Energy resource. Note that ReloadOnE only *transforms* Potential Energy into Energy (0.2 units of $E_p$ are transformed into 0.2 units of $E$ each second), thus Potential Energy has to be also reloaded.
- The Potential Energy ($E_p$) is a sort of Energy storage, it can be acquired by activating the *ReloadOnEp* action on a Potential Energy resource, and is consumed in the transformation process only.

In this version of the task, the experiments are run in simulation using the Player/Stage robot interface and robot simulator (Gerkey, Vaughan, & Howard, 2003). The simulated robot is a 40 × 50 cm wheeled robot with differential steering, similar to the Activ-Media Pioneer 2DX (Fig. 5), equipped with a ring of 16 sonars and a camera. The sonar sensors have a maximum range of 5 m and a view angle of 15°, the camera has a resolution of 200 × 40 pixels and a view angle of 60° and uses a color-blob-finding vision device to track the position of red and blue objects. The experiment takes place in a 10 × 10 m arena, containing one Energy and one Potential Energy resource (Fig. 5). These resources are represented by colored 50 × 50 cm objects (respectively red and blue), and do not constitute obstacles (as if they were suspended above the arena). They are randomly positioned in the arena for each trial, with the constraint that their center is at least 1 m away from the walls.

The robot has to select from among seven possible actions:

- ReloadOnE (ROE) and ReloadOnEp ($\mathrm{ROE}_p$) affect the robot's survival as previously described. These actions are effective if the robot is facing the corresponding resource and is close enough (45° of the camera field of view is occupied by the resource).
- Wander ($W$) activates random accelerations, decelerations and turning movements.
- Rest ($R$) stops the robot, which is a disadvantage as the robot has to continuously explore the arena to find resources, but Rest also halves the rate of Energy consumption (0.005 unit per s), which promotes long survival. Consequently, it should be activated when there is no risk (i.e. when both internal variables reach high levels) in order to minimize the Potential Energy extracted from the environment to survive.
- AvoidObstacle ($AO$) uses data from the 6 front sonars and the 2 central rear sonars in order to avoid collisions with walls.
- ApproachE ($AE$) and ApproachEp ($AE_p$) use the color-blob-finder in order to orient and displace the robot towards the corresponding resource if it is visible.

The action selection mechanisms base their decisions on the following variables:

- $E$, $E_p$,$(1-E)$ and $(1-E_p)$, which provide the amount (or lack of) Energy and Potential Energy,
- *seeEBlob* and *seeEpBlob*, which are set to 1 if a red (resp. blue) object is in the camera input, and to 0 otherwise,
- *onEBlob* and *onEpBlob*, which are set to 1 if a red (resp. blue) object is larger than 150 pixels (i.e. close enough to allow the use of the corresponding resource), and to 0 otherwise,
- *SFR* and *SFL* are the values of the front-right and front-left sonar sensors, measured in meters, taking values between 0 and 5.

For the CBG, the detailed salience computation using these variables is given in Appendix B.

The action selection mechanisms receive new sensory data every 100 ms, and must then provide an action selection for the next 100 ms. Concerning the ITE, it is simply done by executing the decision rule once with the latest data. Concerning the CBG, the selection is made using the output inhibition resulting from the computation of 100 simulation steps of 1ms, using the latest sensory data. A given action is then considered selected if the inhibition of the corresponding channel is below the inhibition at rest $y^{\mathrm{GPi}}_{\mathrm{Rest}}$ (as defined previously). In the case of multiple channel disinhibition, the following action combination rules have been defined:

- Rest is effective if and only if it is the only disinhibited action,
- ReloadOnE and ReloadOnEp are effective if and only if the robot does not move,
- The other movement-generating actions can be co-activated. In that case, the efficiency of selection (as defined by Eq. (17)) is used to weight the contributions of each action to the final motor command.

The comparison between the CBG and the ITE is made according to the following protocol: 20 random resource positions are drawn and, for each model, 20 trials are run using the same set of positions. The robot begins the experiment with a full battery ($E = 1$) and no Potential Energy storage ($E_p = 0$), this allows a maximal survival duration of 1 min 40 s if no reloading action occurs. Unless the robot runs out of energy ($E = 0$), the trial is stopped after 15 min.

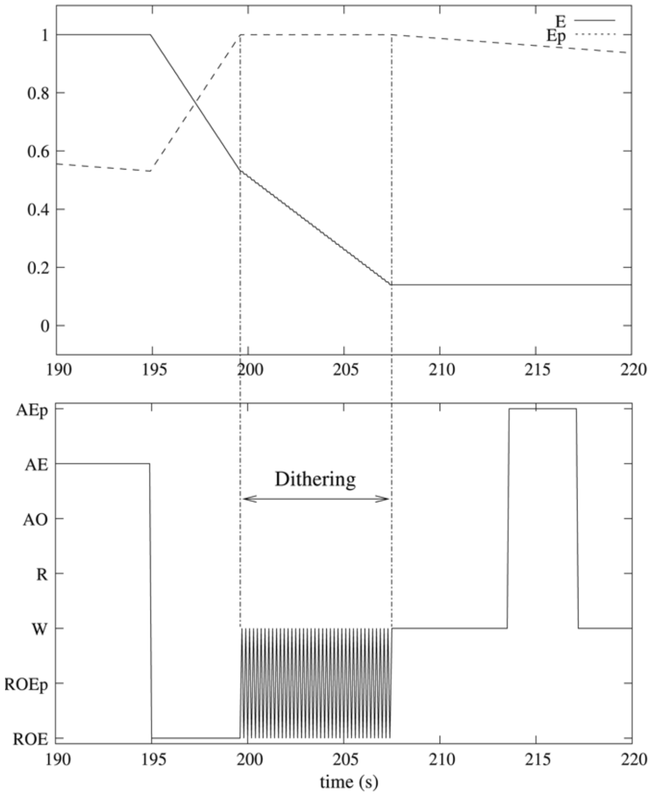

**Fig. 6.** Typical dithering of the ITE between the ReloadOnEnergy and Wander actions. Top: levels of Energy (dashed line) and Potential Energy (full line); bottom: selected action. Note how during the dithering period, more than 0.3 units of $E_p$ are wasted in about 7 s, while they should have allowed 30 s of survival.

### 5.2. Results

The first result is that the CBG and the ITE algorithm have similar survival performance. They are both able to survive the trial in a majority of cases, but can be subject to premature Energy shortage. This is expected, because their ability to find resources is limited by the camera range and field of view, as well as by the random exploration action. The average survival duration is 687 s ($\sigma = 244$) for the CBG and 737 s ($\sigma = 218$) for the ITE, and the two-tailed Kolmogorov–Smirnov test confirms that the two sets of survival durations are not drawn from significantly different distributions ($D_{KS} = 0.2, p = 0.771$). From an action selection point of view, the comparison of the two mechanisms is thus fair: despite the fact that they were tuned independently, they both achieve similar survival performance.

Nevertheless, *a clear behavioral difference between the two mechanisms was observed*, which has significant repercussions on their ability to store Potential Energy and on the Potential Energy extracted from the environment. Indeed, while the CBG may use its feedback loops in order to persist in action execution, the ITE was deliberately deprived of any memory. This was done in order to investigate the effects of this persistence property. The ITE exhibits behavioral dithering in a critical and frequent situation: when the robot fully reloads its Energy, it activates the Wander action, but after 100 ms of Wander execution, some Energy has been consumed and the robot has not moved much. In most cases, it is still on the Energy resource, and if it still has spare $E_p$, ReloadOnE is activated again. This repeats until there is no $E_p$ left or until, in a sequence of small movements, the robot has left the resource (see Fig. 6). This dithering generates a strong energy dissipation: 100 ms of Wander consumes 0.001 units of Energy, and during the following 100 ms, ReloadOnEnergy consumes 0.02 units of $E_p$ while $E$, being bounded by 1, increases by 0.001 only.

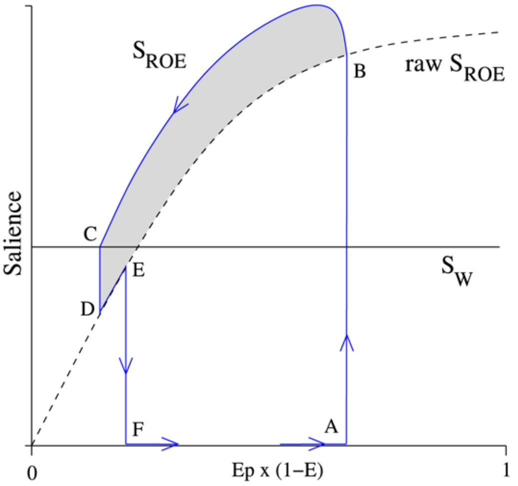

**Fig. 7.** Hysteresis in the variation of the salience of ReloadOnEnergy for the CBG. Black dashed line: variation of $S_{\text{ROE}}$ with regard to ($E_p \times (1 - E)$), with *onEBlob* = 1 and without the persistence term (raw $S_{\text{ROE}}$); blue line: variation of $S_{\text{ROE}}$; shaded area: $S_{\text{ROE}}$ increase resulting from the frontal cortex feedback; black line: salience of Wander ($S_W$). Explanations are given in the text.

On the contrary, in the same situation, the CBG takes advantage of a hysteresis effect caused by the positive feedback from the frontal cortex to the basal ganglia to avoid dithering.

Indeed, the salience of ROE is defined by: $S_{\text{ROE}} = 950 \times f(4 \times onEBlob \times E_p \times (1 - E)) + 0.6 \times x^{\text{FC}}_{\text{ROE}}$ (where $f$ is a sigmoid transfer function, see Appendix B). Consequently, when the robot has a lack of Energy and reaches an Energy resource, *onEBlob* jumps from 0 to 1 and $S_{\text{ROE}}$ also jumps from 0 (Fig. 7, point A) to a level depending on the current $E$ and $E_p$ internal states (Fig. 7, point B) situated on the raw $S_{\text{ROE}}$ curve (Fig. 7, dashed line). In the case depicted in Fig. 7, $S_{\text{ROE}}$ is then much higher than $S_W$, and ROE is thus selected. As a consequence, the corresponding thalamo-cortical channel is disinhibited, leading to an amplification of the salience, fed back to the basal ganglia thanks to the cortical output $x^{\text{FC}}_{\text{ROE}}$ (this bonus is represented by the shaded area over the raw $S_{\text{ROE}}$ curve on Fig. 7). While the robot reloads, $S_{\text{ROE}}$ decreases with ($E_p \times (1 - E)$), but because of the $x^{\text{FC}}_{\text{ROE}}$ salience bonus, it follows the blue trajectory down to point C, where Wander is selected again. The deselection of ROE shuts off the $x^{\text{FC}}_{\text{ROE}}$ signal, causing an immediate decrease to point D. As soon as the robot activates Wander, Energy is consumed and $S_{\text{ROE}}$ increases again, along the raw $S_{\text{ROE}}$ curve. However, at point D, $S_{\text{ROE}} < S_W$, and as long as the robot manages to leave the resource before $S_{\text{ROE}}$ exceeds $S_W$ (points E and F, when the *OnEBlob* variable jumps from 1 to 0), no dithering occurs.

This observation is not trivial, as it has a direct consequence on the global $E_p$ storage of the ITE: both CBG and ITE keep high levels of $E_p$ (between 0.9 and 1) more than 50% of the time (Fig. 8, right), but for the rest of the time, the ITE level is very low (0–0.1) much more often (almost 20% of the time) than the CBG. Moreover, the CBG activates the Rest action often enough to extract, on average, less Potential Energy from the environment ($0.93 \times 10^{-2}\,\text{Ep}\,\text{s}^{-1}$, $\sigma = 0.30 \times 10^{-3}$) than the basic rate ($1 \times 10^{-2}\,\text{Ep}\,\text{s}^{-1}$). On the contrary, the dissipation of energy caused by the dithering of the ITE generates a much higher Potential Energy extraction rate ($1.17 \times 10^{-2}\,\text{Ep}\,\text{s}^{-1}$, $\sigma = 1.17 \times 10^{-3}$). The two-tailed Kolmogorov–Smirnov test reveals that the $E_p$ consumption rates measured for the CBG and the ITE (Fig. 9) are drawn from different distributions ($D_{KS} = 0.95$, $p < 0.001$). The ITE dithering thus generates so much dissipation that it has to extract extra Potential Energy from the environment, despite its use of the Sleep action to lower its consumption, while the CBG exploits as much as possible this possibility to limit Potential Energy extraction.

## 6. Discussion

We proposed a new action selection mechanism for an autonomous robot, using a multi-disciplinary approach combining computational neuroscience and dynamic system theory. This study proved fruitful in the three considered domains:

- We proposed an extension of the contraction theory to locally projected dynamical systems, which was necessary to study the stability of rate-coding neural networks.

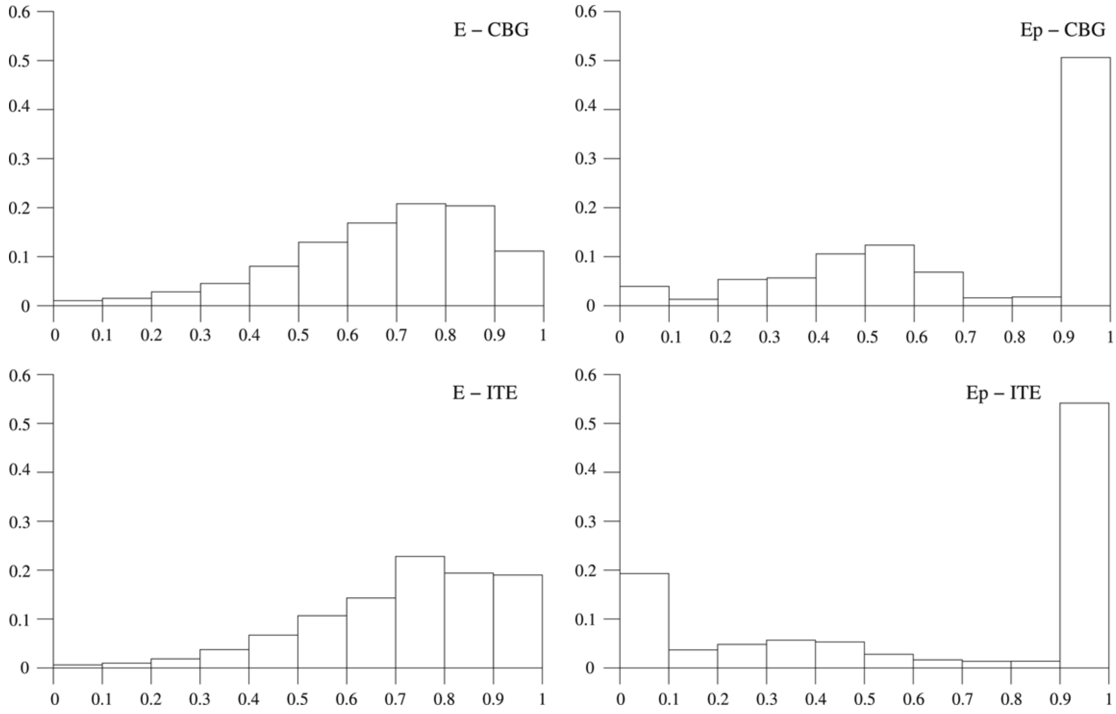

**Fig. 8.** Histograms of Energy (left) and Potential Energy (right) for the CBG (top) and the ITE (bottom), cumulated over all trials.

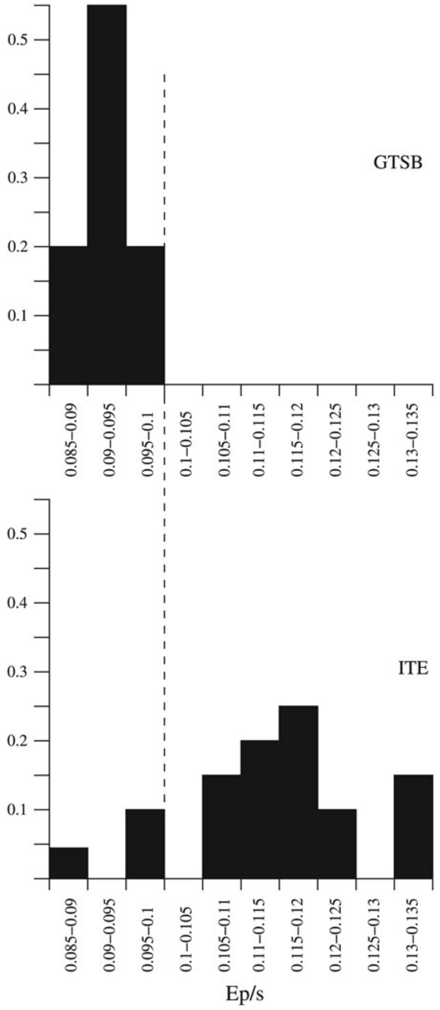

**Fig. 9.** Potential Energy consumption rate. These histograms represent the average $E_p$ consumption rate computed for each trial. Top: BG model; bottom: ITE; the dashed line shows the Energy consumption rate of all actions except Rest (0.001 E/s).

- As a consequence, we proposed a modified rate-coding artificial neuron model.
- Using these results, we designed a stable model of the cortico-baso-thalamo-cortical loops (CBG) using previously neglected anatomical data.
- After having tested this model offline, we integrated it in a simulated robot confronted to a standard survival task to assess its efficiency as an action selection mechanism.

### 6.1. Dynamic systems

In this paper, we have investigated the stability properties of locally projected dynamical systems (lPDS) using nonlinear contraction theory. In particular, we have given a sufficient condition for a general non-autonomous (i.e. with time-varying inputs) lPDS to be *globally exponentially stable*. By contrast, Zhang and Nagurney (1995) only studied the stability of a fixed equilibrium point in autonomous lPDS. Thus, the novelty of our theoretical result should be noticed.

Locally projected dynamical systems have attracted great interest since they were introduced in 1993 by Dupuis and Nagurney. Indeed, this theory is central to the study of oligopolistic markets, traffic networks, commodity production, etc (Dupuis & Nagurney, 1993). As we demonstrated in this article, this theory has also proved to be a valuable tool for establishing rigorous stability properties of neural networks. In this respect, further development of the theory as well as its application to numerous problems in theoretical neuroscience may represent exciting subjects of research.

### 6.2. Neuroscience

The CBG shares a number of similarities with the previously proposed GPR model (Gurney et al., 2001b), as its selection ability relies on two off-center on-surround subcircuits. However, it includes neglected connections from the GPe to the Striatum, which provide additional selectivity. It also considers the possible role of global projections of the GPe to the STN, GPi and SNr as a regulation of the activity in the whole basal ganglia.

We omitted two types of documented connections in the current CBG model. First, the STN projects not only to the GPe, GPi and SNr but also to the striatum (Parent et al., 2000). Intriguingly, the population of STN neurons projecting to the striatum does not project to the other targets, while the other STN neurons project to at least two of the other target nuclei (GPe, GPi or SNr). We could not decipher the role of this striatum-projecting population and did not include it in the current model. Its unique targeting specificity suggests it could be functionally distinct from the other STN neurons. To our knowledge, no modeling study has yet proposed a functional interpretation of this connection, a question that should be explored in future works. The other missing connections concern the fact that lateral inhibitions exist in GPe and SNr (Deniau, Kitai, Donoghue, & Grofova, 1982; Juraska, Wilson, & Groves, 1977; Park, Falls, & Kitai, 1982). These additional projections were added to a version of the GPR (Gurney, Humphries, Wood, Prescott, & Redgrave, 2004) and seemed to enhance its selectivity. We might add these connections and proceed to a similar test with the CBG.

The GPe to striatum connections have the previously evoked functional advantage of enhancing the quality of the selection, by silencing the unselected striatal neurons. Interestingly, the striatum is known for being a relatively silent nucleus (DeLong et al., 1984), a property supposed to be induced by the specific up/down state behavior of the striatal neurons. When using simple neuron models, like leaky integrators, it is usually difficult to reproduce this with a threshold in the transfer function only: when many channels have a strong salience input, all the corresponding striatal neurons tend to be activated. Our model suggests that in such a case, the GPe-striatum projections may contribute to silencing the striatum.

The proposed model includes the modulatory role of the dopamine (DA) in the BG selection process only, which corresponds to the tonic level of dopaminergic input from the ventral tegmental area and the substantia nigra pars compacta (VTA and SNc). The effects of the variation of this tonic DA level on the selection abilities of the BG has been examined in detail for the GPR (Gurney et al., 2001b), and compared with the symptoms of Parkinson's disease.

The role of the phasic dopamine activity in reinforcement learning, through the adaptation of the cortico-striatal synapses, is beyond the scope of our study. Nevertheless, such an extension of the CBG could allow the online adaptation of the saliences, which are here hand-tuned. The existing models of reinforcement learning in the BG are based on the temporal difference (TD) learning algorithm (Houk, Adams, & Barto, 1995; Joel, Niv, & Ruppin, 2002). These TD models are composed of two cooperating circuits: a *Critic* dedicated to learning to predict future reward given the current state, and an *Actor*, using the Critic's predictions to choose the most appropriate action. Our model can then be considered as an Actor circuit, more anatomically detailed than those usually used (simple winner-takes-all, without persistence properties). The first attempts at using detailed Actor models in TD architectures for tasks requiring a single motivation have been conducted (Frank, Santamaria, O'Reilly, & Willcutt, 2007; Khamassi, Girard, Berthoz, & Guillot, 2004; Khamassi, Lachèze, Girard, Berthoz, & Guillot, 2005). Note however that the use of the current TD-learning models would not necessarily be straightforward in our case: we had to use relatively complex salience computations (see Appendix B), in order to solve our relatively simple task. This is caused by its multi-motivational nature, quite common in action selection problems, but which has been given only little attention in RL-related works (Dayan, 2001; Konidaris & Barto, 2006).

### 6.3. Autonomous robotics

While early action selection mechanisms were based on a purely engineering approach (Pirjanian, 1999), progress in the understanding of the physiology of the brain regions involved in action selection now allows the investigation of biomimetic action selection mechanisms. Indeed, basal ganglia models – variations of the GPR – and reticular formation models have already been used as action selection mechanisms for autonomous robots (Girard et al., 2003, 2005; Humphries, Gurney, & Prescott, 2005; Montes-Gonzalez et al., 2000; Prescott et al., 2006).

We showed here that the CBG may exploit its cortical feedback to exhibit behavioral persistence and thus dithering avoidance, one of the fundamental properties of efficient ASMs (Tyrrell, 1993). In our experiment, this promotes energy storage and reduces energy consumption. These properties, which clearly provide a survival advantage, were also highlighted for the GPR when tested in a similar experiment (Girard et al., 2003). Thus, comparing the GPR and the CBG in exactly the same task could reveal some subtle differences which were not identified yet. Moreover, in the current version of the CBG, these cortico-striatal feedback connections are strictly channel to channel, the possible sequence generation effects that could result from cross channel connections probably deserves additional attention.

The contraction property of the CBG also provides a fundamental advantage for an autonomous robot. It provides a theoretical certainty regarding its stability of operation, whatever the sequences of input might be. For an autonomous agent confronted with a uncontrolled environment, where all possible sequences of inputs may happen, it seems to be essential. Of course, contraction analysis does not say anything about the pertinence of the resulting stable behavior, hence leading the necessity of verifying the CBG selection properties. However, the fact that stability issues have already been evoked for previous GPR versions (Girard et al., 2005; Prescott et al., 2006) confirms that such a rigorous proof is useful.

## Acknowledgment

B.G. and N.T. acknowledge the partial support of the European Community Neurobotics project, grant FP6-IST-001917.

## Appendix A. If-Then-Else decision rule

The If-Then-Else decision tree is the following:

```
if $E_p < 1$ and $onEpBlob = true$ then
  ReloadOnEp
else if $E < 1$ and $E_p > 0$ and $onEBlob = true$ then
  ReloadOnE
else if $E < 0.8$ and $E_p > 0$ and $seeEBlob = true$ then
  ApproachE
else if $E_p < 0.8$ and $seeEpBlob = true$ then
  ApproachEp
else if $E > 0.7$ and $E_p > 0.7$ then
  Rest
else if $SFL < 1$ or $SFR < 1$ or ($SFL < 1.5$ and $SFR < 1.5$) then
  AvoidObstacle
else
  Wander
end if
```

## Appendix B. Robot CBG saliences

Using the sigmoid transfer function

$$f(x) = \frac{2}{1 + \mathrm{e}^{-4x}} - 1$$

the saliences of each action (including the frontal cortex feedback) are:

$$S_{\mathrm{ROE}} = 950 \times f(4 \times onEBlob \times E_p \times (1 - E)) + 0.6 \times x^{\mathrm{FC}}_{\mathrm{ROE}}$$

$$S_{\mathrm{ROE}_p} = 750 \times f(4 \times \mathrm{onEpBlob} \times (1 - E_p)) + 0.2 \times x^{\mathrm{FC}}_{\mathrm{ROE}_p}$$

$$S_W = 380$$

$$S_{SI} = 550 \times f(2 \times \max(Ep \times E - 0.5, 0))$$

$$S_{AO} = 950 \times f(2 \times (\max(1.5 - SFL, 0) + \max(1.5 - \mathrm{SFR}, 0))) + 0.2 \times x^{\mathrm{FC}}_{AO}$$

$$S_{AE} = 750 \times f(\mathrm{seeEBlob} \times E_p \times (1 - E) \times (1 - onEBlob)) + 0.2 \times x^{\mathrm{FC}}_{AE}$$

$$S_{AE_p} = 750 \times f(seeEpBlob \times (1 - E_p) \times (1 - \mathrm{onEpBlob})) + 0.2 \times x^{\mathrm{FC}}_{AE_p}.$$

## References

Alexander, G. E., Crutcher, M. D., & DeLong, M. R. (1990). Basal ganglia-thalamocortical circuits: Parallel substrates for motor, oculomotor, "prefrontal" and "limbic" functions. *Progress in Brain Research*, *85*, 119–146.

Alexander, G. E., DeLong, M. R., & Strick, P. L. (1986). Parallel organization of functionally segregated circuits linking basal ganglia and cortex. *Annual Review of Neuroscience*, *9*, 357–381.

Bevan, M., Booth, P., Eaton, S., & Bolam, J. (1998). Selective innervation of neostriatal interneurons by a subclass of neurons in the globus pallidus of rats. *Journal of Neuroscience*, *18*(22), 9438–9452.

Chevalier, G., & Deniau, M. (1990). Disinhibition as a basic process of striatal functions. *Trends in Neurosciences*, *13*, 277–280.

Dayan, P. (2001). Motivated reinforcement learning. In T. Leen, T. Dietterich, & V. Tresp (Eds.), *Neural information processing systems*: *Vol. 13*. Cambridge, MA: The MIT Press.

Dayan, P., & Abbott, L. (2001). *Theoretical neuroscience: Computational and mathematical modeling of neural systems*. MIT Press.

DeLong, M., Georgopoulos, A., Crutcher, M., Mitchell, S., Richardson, R., & Alexander, G. (1984). Functional organization of the basal ganglia: Contributions of single-cell recording studies. *Ciba Foundation Symposium*, *107*, 64–82.

Deniau, J.-M., Kitai, S., Donoghue, J., & Grofova, I. (1982). Neuronal interactions in the substancia nigra pars reticulata through axon collateral of the projection neurons. *Experimental Brain Research*, *47*, 105–113.

Dupuis, P., & Nagurney, A. (1993). Dynamical systems and variational inequalities. *Annals of Operations Research*, *44*(1), 7–42.

Filippov, A. F. (1988). *Differential equations with discontinuous righthand sides*. Kluwer Academic Pub.

Frank, M., Santamaria, A., O'Reilly, R., & Willcutt, E. (2007). Testing computational models of dopamine and noradrenaline dysfunction in attention deficit/hyperactivity disorder. *Neuropsychopharmacology*, *32*, 1583–1599.

Gerkey, B., Vaughan, R., & Howard, A. (2003). The player/stage project: Tools for multi-robot and distributed sensor systems. In *11th International conference on advanced robotics* (pp. 317–323).

Gillies, A., & Arbruthnott, G. (2000). Computational models of the basal ganglia. *Movement Disorders*, *15*(5), 762–770.

Girard, B., Cuzin, V., Guillot, A., Gurney, K. N., & Prescott, T. J. (2003). A basal ganglia inspired model of action selection evaluated in a robotic survival task. *Journal of Integrative Neuroscience*, *2*(2), 179–200.

Girard, B., Filliat, D., Meyer, J.-A., Berthoz, A., & Guillot, A. (2005). Integration of navigation and action selection in a computational model of cortico-basal ganglia-thalamo-cortical loops. *Adaptive Behavior*, *13*(2), 115–130.

Girard, B., Tabareau, N., Berthoz, A., & Slotine, J.-J. (2006). Selective amplification using a contracting model of the basal ganglia. In F. Alexandre, Y. Boniface, L. Bougrain, B. Girau, & N. Rougier (Eds.), *NeuroComp* (pp. 30–33).

Girard, B., Tabareau, N., Slotine, J.-J., & Berthoz, A. (2005). Contracting model of the basal ganglia. In J. Bryson, T. Prescott, & A. Seth (Eds.), *Modelling natural action selection: Proceedings of an international workshop* (pp. 69–76). Brighton, UK: AISB Press.

Gurney, K., Humphries, M., Wood, R., Prescott, T., & Redgrave, P. (2004). Testing computational hypotheses of brain systems function: A case study with the basal ganglia. *Network: Computation in Neural Systems*, *15*, 263–290.

Gurney, K., Prescott, T., Wickens, J., & Redgrave, P. (2004). Computational models of the basal ganglia: From membranes to robots. *Trends in Neurosciences*, *27*, 453–459.

Gurney, K., Prescott, T. J., & Redgrave, P. (2001a). A computational model of action selection in the basal ganglia. I. A new functional anatomy. *Biological Cybernetics*, *84*, 401–410.

Gurney, K., Prescott, T. J., & Redgrave, P. (2001b). A computational model of action selection in the basal ganglia. II. Analysis and simulation of behaviour. *Biological Cybernetics*, *84*, 411–423.

Horn, R., & Johnson, C. (1985). *Matrix analysis*. Cambridge University Press.

Houk, J. C., Adams, J. L., & Barto, A. G. (1995). A model of how the basal ganglia generate and use neural signals that predict reinforcement. In J. C. Houk, J. L. Davis, & D. G. Beiser (Eds.), *Models of information processing in the basal ganglia* (pp. 249–271). Cambridge, MA: The MIT Press.

Humphries, M., Gurney, K., & Prescott, T. (2005). Is there an integrative center in the vertebrate brain-stem? A robotic evaluation of a model of the reticular formation viewed as an action selection device. *Adaptive Behavior*, *13*(2), 97–113.

Ioannou, P., & Sun, J. (1996). *Robust adaptive control*. Upper Saddle River, NJ, USA: Prentice Hall, Inc.

Joel, D., Niv, Y., & Ruppin, E. (2002). Actor-critic models of the basal ganglia: New anatomical and computational perspectives. *Neural Networks*, *15*(4–6).

Juraska, J., Wilson, C., & Groves, P. (1977). The substancia nigra of the rat: A golgi study. *Journal of Comparative Neurology*, *172*, 585–600.

Khamassi, M., Girard, B., Berthoz, A., & Guillot, A. (2004). Comparing three critic models of reinforcement learning in the basal ganglia connected to a detailed actor part in a s-r task. In F. Groen, N. Amato, A. Bonarini, E. Yoshida, & B. Krse (Eds.), *Proceedings of the eighth international conference on intelligent autonomous systems*, IAS8. (pp. 430–437). Amsterdam, The Netherlands: IOS Press.

Khamassi, M., Lachèze, L., Girard, B., Berthoz, A., & Guillot, A. (2005). Actor-critic models of reinforcement learning in the basal ganglia: From natural to artificial rats. *Adaptive Behavior*, *13*(2), 131–148.

Kimura, A., & Graybiel, A. (Eds.) (1995). *Functions of the cortico-basal ganglia loop*. Tokyo, New York: Springer.

Kita, H., Tokuno, H., & Nambu, A. (1999). Monkey globus pallidus external segment neurons projecting to the neostriatum. *Neuroreport*, *10*(7), 1476–1472.

Konidaris, G., & Barto, A. (2006). An adaptive robot motivational system. In S. Nolfi, G. Baldassarre, R. Calabretta, J. Hallam, D. Marocco, J.-A. Meyer, O. Miglino, & D. Parisi (Eds.), *LNAI*: *Vol. 4095. From animats to animats 9: Proceedings of the 9th international conference on the simulation of adaptive behavior* (pp. 346–356). Berlin, Germany: Springer.

Krotopov, J., & Etlinger, S. (1999). Selection of actions in the basal ganglia thalamocortical circuits: Review and model. *International Journal of Psychophysiology*, *31*, 197–217.

Lohmiller, W., & Slotine, J. (1998). Contraction analysis for nonlinear systems. *Automatica*, *34*(6), 683–696.

Lohmiller, W., & Slotine, J. (2000). Nonlinear process control using contraction analysis. *American Institute of Chemical Engineers Journal*, *46*(3), 588–596.

Middleton, F. A., & Strick, P. L. (1994). Anatomical evidence for cerebellar and basal ganglia involvement in higher cognitive function. *Science*, *266*, 458–461.

Mink, J. W. (1996). The basal ganglia: Focused selection and inhibition of competing motor programs. *Progress in Neurobiology*, *50*(4), 381–425.

Montes-Gonzalez, F., Prescott, T. J., Gurney, K. N., Humphries, M., & Redgrave, P. (2000). An embodied model of action selection mechanisms in the vertebrate brain. In J.-A. Meyer, A. Berthoz, D. Floreano, H. Roitblat, & S. W. Wilson (Eds.), *From animals to animats 6*: *Vol. 1* (pp. 157–166). Cambridge, MA: The MIT Press.

Parent, A., Sato, F., Wu, Y., Gauthier, J., Lévesque, M., & Parent, M. (2000). Organization of the basal ganglia: The importance of the axonal collateralization. *Trends in Neuroscience*, *23*(10), S20–S27.

Park, M., Falls, W., & Kitai, S. (1982). An intracellular HRP study of rat globus pallidus. I. responses and light microscopic analysis. *Journal of Comparative Neurology*, *211*, 284–294.

Pirjanian, P. (1999). *Behavior coordination mechanisms — state-of-the-art. Technical report IRIS-99-375*. Institute of Robotics and Intelligent Systems, School of Engineering, University of Southern California.

Prescott, T. J., Montes-Gonzalez, F., Gurney, K., Humphries, M. D., & Redgrave, P. (2006). A robot model of the basal ganglia: Behavior and intrinsic processing. *Neural Networks*, *19*, 31–61.

Redgrave, P., Prescott, T. J., & Gurney, K. (1999). The basal ganglia: A vertebrate solution to the selection problem? *Neuroscience*, *89*(4), 1009–1023.

Sato, F., Lavallee, P., Lévesque, M., & Parent, A. (2000). Single-axon tracing study of neurons of the external segment of the globus pallidus in primates. *Journal of Comparative Neurology*, *417*, 17–31.

Slotine, J., & Coetsee, J. (1986). Adaptive sliding controller synthesis for nonlinear systems. *International Journal of Control*, *43*(4), 1631–1651.

Slotine, J. J. E., & Lohmiller, W. (2001). Modularity, evolution, and the binding problem: A view from stability theory. *Neural networks*, *14*(2), 137–145.

Staines, W., Atmadja, S., & Fibiger, H. (1981). Demonstration of a pallidostriatal pathway by retrograde transport of HRP-labelled lectin. *Brain Research*, *206*, 446–450.

Tabareau, N., & Slotine, J. (2006). Notes on contraction theory. Arxiv preprint nlin.AO/0601011.

Tepper, J., & Bolam, J. (2004). Functional density and specificity of neostrital interneurons. *Current Opinion in Neurobiology*, *14*, 685–692.

Tepper, J., Koós, T., & Wilson, C. (2004). Gabaergic microcircuits in the neostriatum. *Trends in Neuroscience*, *11*, 662–669.

Tyrrell, T. (1993). The use of hierarchies for action selection. *Adaptive Behavior*, *1*(4), 387–420.

Wu, Y., Richard, S., & Parent, A. (2000). The organization of the striatal output system: A single-cell juxtacellular labeling study in the rat. *Neuroscience Research*, *38*, 49–62.

Zhang, D., & Nagurney, A. (1995). On the stability of projected dynamical systems. *Journal of Optimization Theory and Applications*, *85*(1), 97–124.

## B.2 A Contraction Theory Approach to Stochastic Incremental Stability

By Q.-C. Pham, N. Tabareau and J.-J. Slotine. Published in *IEEE Transactions on Automatic Control*, vol. 54, pp. 816-820, 2009.

# A Contraction Theory Approach to Stochastic Incremental Stability

Quang-Cuong Pham, Nicolas Tabareau, and Jean-Jacques Slotine

***Abstract*—We investigate the incremental stability properties of Itô stochastic dynamical systems. Specifically, we derive a stochastic version of nonlinear contraction theory that provides a bound on the mean square distance between any two trajectories of a stochastically contracting system. This bound can be expressed as a function of the noise intensity and the contraction rate of the noise-free system. We illustrate these results in the contexts of nonlinear observers design and stochastic synchronization.**

***Index Terms*—Incremental stability, nonlinear contraction theory, stochastic stability.**

## I. INTRODUCTION

Nonlinear stability properties are often considered with respect to an equilibrium point or to a nominal system trajectory (see e.g. [1]). By contrast, *incremental* stability is concerned with the behavior of system trajectories *with respect to each other*. From the triangle inequality, global exponential incremental stability (any two trajectories tend to each other exponentially) is a stronger property than global exponential convergence to a single trajectory.

Historically, work on deterministic incremental stability can be traced back to the 1950's [2]–[4] (see e.g. [5], [6] for a more extensive list and historical discussion of related references). More recently, and largely independently of these earlier studies, a number of works have put incremental stability on a broader theoretical basis and have clarified the relations with more traditional stability approaches [7]–[10]. Furthermore, it has been shown that incremental stability is especially relevant in the study of such problems as observer design or synchronization analysis.

While the above references are mostly concerned with *deterministic* stability notions, stability theory has also been extended to *stochastic* dynamical systems, see for instance [11], [12]. This includes important recent developments in Lyapunov-like approaches [13], [14], as well as applications to standard problems in systems and control [15]–[17]. However, stochastic versions of incremental stability have not yet been systematically investigated.

The goal of this technical note is to extend some concepts and results in incremental stability to stochastic dynamical systems. More specifically, we derive a stochastic version of contraction analysis in the specialized context of state-independent metrics.

We prove in Section II that the mean square distance between any two trajectories of a stochastically contracting system is upper-bounded by a constant after exponential transients. In contrast with previous works on incremental stochastic stability [18], we consider the case when the two trajectories are affected by *distinct* and independent noises, as detailed in Section II-B. This specificity enables our theory to have a number of new and practically important applications. However, the fact that the noise does not vanish as two trajectories get very close to each other will prevent us from obtaining asymptotic almost-sure stability results (see Section III-B). In Section III-D, we show that results on combinations of deterministic contracting systems have simple analogues in the stochastic case. Finally, as illustrations of our results, we study in Section IV the convergence of contracting observers with noisy measurements, and the synchronization of noisy FitzHugh-Nagumo oscillators.

## II. STOCHASTIC CONTRACTION THEOREM

### A. Background: Nonlinear Contraction Theory

Nonlinear contraction theory [8] provides a set of tools to analyze the incremental exponential stability of nonlinear systems, and has been applied notably to observer design [19], [20], synchronization analysis [21], [22] and systems neuroscience modelling [23]. Nonlinear contracting systems enjoy desirable aggregation properties, in that contraction is preserved under many types of system combinations given suitable simple conditions [8].

While we shall derive global properties of nonlinear systems, many of our results can be expressed in terms of eigenvalues of symmetric matrices [24]. Given a square matrix $\mathbf{A}$, the symmetric part of $\mathbf{A}$ is denoted by $\mathbf{A}_s$. The smallest and largest eigenvalues of $\mathbf{A}_s$ are denoted by $\lambda_{\min}(\mathbf{A})$ and $\lambda_{\max}(\mathbf{A})$. Given these notations, a matrix $\mathbf{A}$ is *positive definite* (denoted $\mathbf{A} > \mathbf{0}$) if $\lambda_{\min}(\mathbf{A}) > 0$. Finally, a time- and state-dependent matrix $\mathbf{A}(\mathbf{x}, t)$ is *uniformly* positive definite if

$$\exists \beta > 0 \quad \forall \mathbf{x}, t \quad \lambda_{\min}\left(\mathbf{A}(\mathbf{x}, t)\right) \geq \beta.$$

The basic theorem of contraction analysis, derived in [8], can be stated as follows

*Theorem 1 (Deterministic Contraction):* Consider, in $\mathbb{R}^n$, the deterministic system

$$\dot{\mathbf{x}} = \mathbf{f}(\mathbf{x}, t) \tag{1}$$

where $\mathbf{f}$ is a smooth nonlinear function satifying standard conditions for the global existence and uniqueness of solutions (for instance: for all $T \in [0, \infty)$, there are constants $M$ and $L$ such that $\forall t \in [0, T], \forall \mathbf{x} \in \mathbb{R}^n : \|\mathbf{f}(\mathbf{x}, t)\| \leq M + L\|\mathbf{x}\|$ [4]).

Denote the Jacobian matrix of $\mathbf{f}$ with respect to its first variable by $\partial \mathbf{f}/\partial \mathbf{x}$. If there exists a square matrix $\boldsymbol{\Theta}(\mathbf{x}, t)$ such that $\boldsymbol{M} = \boldsymbol{\Theta}^T\boldsymbol{\Theta}$ is uniformly positive definite and $\mathbf{F} = (\dot{\boldsymbol{\Theta}} + \boldsymbol{\Theta}(\partial \mathbf{f}/\partial \mathbf{x}))\boldsymbol{\Theta}^{-1}$ is uniformly negative definite, then all system trajectories converge exponentially to a single trajectory, with convergence rate $\sup_{\mathbf{x},t} |\lambda_{\max}(\mathbf{F})| = \lambda > 0$. The system is said to be *contracting*, $\mathbf{F}$ is called its *generalized Jacobian*, $\boldsymbol{M}$ its contraction *metric* and $\lambda$ its contraction *rate*.

### B. Settings

Consider a noisy system described by an Itô stochastic differential equation

$$\begin{cases} d\mathbf{a} = \mathbf{f}(\mathbf{a}, t)dt + \sigma(\mathbf{a}, t)dW^d \\ \mathbf{a}(0) = \xi \end{cases} \tag{2}$$

where $\mathbf{f}$ is a $\mathbb{R}^n \times \mathbb{R}^+ \to \mathbb{R}^n$ function, $\sigma$ is a $\mathbb{R}^n \times \mathbb{R}^+ \to \mathbb{R}^{nd}$ matrix-valued function, $W^d$ is a standard $d$-dimensional Wiener process and $\xi$ is a random variable independent of the noise $W^d$. To ensure existence and uniqueness of solutions to (2), we assume that for all $T \in [0, \infty)$

Manuscript received February 01, 2008; revised June 24, 2008 and October 03, 2008. Current version published April 08, 2009. This work was supported in part by the European Community Projects BACS (FP6-IST-027140) and Neurobotics (FP6-IST-001917). Recommended by Associate Editor D. Angeli.

Q.-C. Pham and N. Tabareau are with the Laboratoire de Physiologie de la Perception et de l'Action (LPPA), UMR 7152 Collège de France—CNRS, Paris, France (e-mail: cuong.pham@normalesup.org; tabareau.nicolas@gmail.com).

J.-J. Slotine is with the Nonlinear Systems Laboratory, Massachusetts Institute of Technology (MIT), Cambridge, MA 02139 USA (e-mail: jjs@mit.edu).

Digital Object Identifier 10.1109/TAC.2008.2009619

*(Lipschitz condition)* there exists a constant $K_1 > 0$ such that $\forall t \in [0,T], \forall \mathbf{a},\mathbf{b} \in \mathbb{R}^n$

$$\|\mathbf{f}(\mathbf{a},t) - \mathbf{f}(\mathbf{b},t)| + \|\sigma(\mathbf{a},t) - \sigma(\mathbf{b},t)\| \le K_1\|\mathbf{a}-\mathbf{b}\|.$$

*(restriction on growth)* there exists a constant $K_2 > 0$ such that $\forall t \in [0,T], \forall \mathbf{a} \in \mathbb{R}^n$

$$\|\mathbf{f}(\mathbf{a},t)\|^2 + \|\sigma(\mathbf{a},t)\|^2 \le K_2\left(1 + \|\mathbf{a}\|^2\right).$$

Under these conditions, one can show ([25, p. 105]) that equation (2) has on $[0,\infty)$ a unique $\mathbb{R}^n$-valued solution $\mathbf{a}(t)$, which is continuous with probability one.

In order to investigate the incremental stability properties of system (2), consider now two system trajectories $\mathbf{a}(t)$ and $\mathbf{b}(t)$. Our goal will consist of studying the trajectories $\mathbf{a}(t)$ and $\mathbf{b}(t)$ with respect to each other. For this, we consider the *augmented* system $\mathbf{x}(t) = (\mathbf{a}(t),\mathbf{b}(t))^T$, which follows the equation:

$$\begin{cases} d\mathbf{x} = \begin{pmatrix} \mathbf{f}(\mathbf{a},t) \\ \mathbf{f}(\mathbf{b},t) \end{pmatrix} dt + \begin{pmatrix} \sigma(\mathbf{a},t) & 0 \\ 0 & \sigma(\mathbf{b},t) \end{pmatrix} \begin{pmatrix} dW_1^d \\ dW_2^d \end{pmatrix} \\ \quad = \widehat{\mathbf{f}}(\mathbf{x},t)dt + \widehat{\sigma}(\mathbf{x},t)dW^{2d} \\ \mathbf{x}(0) = (\mathbf{a}(0),\mathbf{b}(0)) = (\xi_1,\xi_2) \end{cases}. \tag{3}$$

**Important remark** As stated in the introduction, the systems $\mathbf{a}$ and $\mathbf{b}$ are driven by *distinct* and independent Wiener processes $W_1^d$ and $W_2^d$. This makes our approach considerably different from [18], where the authors studied two trajectories driven by *the same* Wiener process.

Our approach enables us to study the stability of the system with respect to differences in initial conditions *and* to random perturbations: indeed, two trajectories of any real-life system are typically affected by *distinct realizations* of the noise. In the deterministic domain, incremental stability with respect to different initial conditions *and* different *deterministic inputs* (incremental Input-to-State Stability or $\delta$ISS) has been studied in [9], [10], [26]. Besides, it should be noted that our approach leads very naturally to nice results on the comparison of noisy and noise-free trajectories (cf. Section III-C), which are particularly useful in applications (cf. Section IV).

However, because of the very fact that the two trajectories are driven by distinct Wiener processes, one cannot expect the influence of the noise to vanish when the two trajectories get very close to each other. This constrasts with [18], and more generally, with standard stochastic stability approaches, where the noise is assumed to vanish near the origin. The consequences of this will be discussed in detail in Section III-B.

### C. Statement and Proof of the Theorem

We first recall a Gronwall-type lemma

*Lemma 1:* Let $g : [0,\infty) \to \mathbb{R}$ be a continuous function, $C$ a real number and $\lambda$ a *strictly positive* real number. Assume that

$$\forall u,t \quad 0 \le u \le t \quad g(t) - g(u) \le \int_u^t -\lambda g(s) + C ds. \tag{4}$$

Then

$$\forall t \ge 0 \quad g(t) \le \frac{C}{\lambda} + \left[g(0) - \frac{C}{\lambda}\right]^+ e^{-\lambda t} \tag{5}$$

where $[\cdot]^+ = \max(0,\cdot)$.

*Proof:* See [27] ☐

We now introduce two hypotheses

**(H1)** There exists a state-independent, uniformly positive definite metric $\boldsymbol{M}(t) = \boldsymbol{\Theta}(t)^T\boldsymbol{\Theta}(t)$, with the lower-bound $\beta > 0$ (i.e. $\forall \mathbf{x}, t \ \ \mathbf{x}^T\boldsymbol{M}(t)\mathbf{x} \ge \beta\|\mathbf{x}\|^2$) and $\mathbf{f}$ is contracting in that metric, with contraction rate $\lambda$, i.e. uniformly

$$\lambda_{\max}\left(\left(\frac{d}{dt}\boldsymbol{\Theta}(t) + \boldsymbol{\Theta}(t)\frac{\partial \mathbf{f}}{\partial \mathbf{a}}\right)\boldsymbol{\Theta}^{-1}(t)\right) \le -\lambda$$

or equivalently, uniformly

$$\mathbf{M}(t)\frac{\partial \mathbf{f}}{\partial \mathbf{a}} + \left(\frac{\partial \mathbf{f}}{\partial \mathbf{a}}\right)^T \mathbf{M}(t) + \frac{d}{dt}\mathbf{M}(t) \le -2\lambda\mathbf{M}(t).$$

**(H2)** $\mathrm{tr}(\sigma(\mathbf{a},t)^T\boldsymbol{M}(t)\sigma(\mathbf{a},t))$ is uniformly upper-bounded by a constant $C$

*Definition 1:* A system that verifies **(H1)** and **(H2)** is said to be *stochastically contracting* in the metric $\boldsymbol{M}(t)$, with rate $\lambda$ and bound $C$.

Consider the Lyapunov-like function $V(\mathbf{x},t) = (\mathbf{a}-\mathbf{b})^T\boldsymbol{M}(t)(\mathbf{a}-\mathbf{b})$. Using **(H1)** and **(H2)**, we derive below an inequality on $\mathcal{L}V(\mathbf{x},t)$ where $\mathcal{L}$ denotes the differential generator of the Itô process $\mathbf{x}(t)$ ([11], p. 15).

*Lemma 2:* Under **(H1)** and **(H2)**, one has

$$\forall \mathbf{x}, t \quad \mathcal{L}V(\mathbf{x},t) \le -2\lambda V(\mathbf{x},t) + 2C. \tag{6}$$

*Proof:* Let us compute first $\mathcal{L}V$

$$\begin{aligned} \mathcal{L}V(\mathbf{x},t) &= \frac{\partial V}{\partial t} + \frac{\partial V}{\partial \mathbf{x}}\widehat{\mathbf{f}}(\mathbf{x},t) + \frac{1}{2}\mathrm{tr}\left(\widehat{\sigma}(\mathbf{x},t)^T\frac{\partial^2 V}{\partial \mathbf{x}^2}\widehat{\sigma}(\mathbf{x},t)\right) \\ &= (\mathbf{a}-\mathbf{b})^T\left(\frac{d}{dt}\mathbf{M}(t)\right)(\mathbf{a}-\mathbf{b}) \\ &\quad + 2(\mathbf{a}-\mathbf{b})^T\mathbf{M}(t)\left(\mathbf{f}(\mathbf{a},t) - \mathbf{f}(\mathbf{b},t)\right) \\ &\quad + \mathrm{tr}\left(\sigma(\mathbf{a},t)^T\mathbf{M}(t)\sigma(\mathbf{a},t)\right) \\ &\quad + \mathrm{tr}\left(\sigma(\mathbf{b},t)^T\mathbf{M}(t)\sigma(\mathbf{b},t)\right). \end{aligned}$$

Fix $t > 0$, then, according to [28], there exists $\mathbf{c} \in [\mathbf{a},\mathbf{b}]$ such that

$$\begin{aligned} &(\mathbf{a}-\mathbf{b})^T\left(\frac{d}{dt}\mathbf{M}(t)\right)(\mathbf{a}-\mathbf{b}) \\ &\quad + 2(\mathbf{a}-\mathbf{b})^T\mathbf{M}(t)\left(\mathbf{f}(\mathbf{a}) - \mathbf{f}(\mathbf{b})\right) \\ &= (\mathbf{a}-\mathbf{b})^T\left(\frac{d}{dt}\mathbf{M}(t) + \mathbf{M}(t)\frac{\partial \mathbf{f}}{\partial \mathbf{a}}(\mathbf{c},t)\right. \\ &\qquad \left. + \frac{\partial \mathbf{f}}{\partial \mathbf{a}}(\mathbf{c},t)^T\mathbf{M}(t)\right)(\mathbf{a}-\mathbf{b}) \\ &\le -2\lambda(\mathbf{a}-\mathbf{b})^T\mathbf{M}(t)(\mathbf{a}-\mathbf{b}) = -2\lambda V(\mathbf{x}) \end{aligned} \tag{7}$$

where the inequality is obtained by using **(H1)**.

Finally, combining (7) with **(H2)** allows to obtain the desired result ☐

We can now state the stochastic contraction theorem

*Theorem 2 (Stochastic Contraction):* Assume that system (2) verifies **(H1)** and **(H2)**. Let $\mathbf{a}(t)$ and $\mathbf{b}(t)$ be two trajectories whose initial conditions are independent of the noise and given by a probability distribution $p(\xi_1,\xi_2)$. Then

$$\begin{aligned} \forall t \ge 0 \quad &\mathbb{E}\left((\mathbf{a}(t) - \mathbf{b}(t))^T\mathbf{M}(t)\left(\mathbf{a}(t) - \mathbf{b}(t)\right)\right) \\ &\le \frac{C}{\lambda} + e^{-2\lambda t}\int\left[(\mathbf{a}_0 - \mathbf{b}_0)^T\mathbf{M}(0)(\mathbf{a}_0 - \mathbf{b}_0) - \frac{C}{\lambda}\right]^+ \\ &\qquad \times dp(\mathbf{a}_0,\mathbf{b}_0). \end{aligned} \tag{8}$$

In particular, $\forall t \ge 0$

$$\begin{aligned} &\mathbb{E}\left(\|\mathbf{a}(t) - \mathbf{b}(t)\|^2\right) \\ &\quad \le \frac{1}{\beta}\left(\frac{C}{\lambda} + \mathbb{E}\left((\xi_1 - \xi_2)^T\mathbf{M}(0)(\xi_1 - \xi_2)\right)e^{-2\lambda t}\right). \end{aligned} \tag{9}$$

*Proof:* Let $\mathbf{x}_0 = (\mathbf{a}_0, \mathbf{b}_0) \in \mathbb{R}^{2n}$. By Dynkin's formula ([11, p. 10])

$$\mathbb{E}_{\mathbf{x}_0} V(\mathbf{x}(t), t) - V(\mathbf{x}_0, 0) = \mathbb{E}_{\mathbf{x}_0} \int_0^t \mathcal{L}V(\mathbf{x}(s), s)\, ds.$$

Thus one has $\forall u, t\ 0 \le u \le t < \infty$

$$\begin{aligned}
&\mathbb{E}_{\mathbf{x}_0} V(\mathbf{x}(t), t) - \mathbb{E}_{\mathbf{x}_0} V(\mathbf{x}(u), u) \\
&= \mathbb{E}_{\mathbf{x}_0} \int_u^t \mathcal{L}V(\mathbf{x}(s), s)\, ds \\
&\le \mathbb{E}_{\mathbf{x}_0} \int_u^t (-2\lambda V(\mathbf{x}(s), s) + 2C)\, ds \qquad (10)\\
&= \int_u^t (-2\lambda \mathbb{E}_{\mathbf{x}_0} V(\mathbf{x}(s), s) + 2C)\, ds \qquad (11)
\end{aligned}$$

where inequality (10) is obtained by using lemma 2 and equality (11) by using Fubini's theorem (since $s \mapsto \mathbb{E}_{\mathbf{x_0}} V(\mathbf{x}(s), s)$ is continuous on $[u, t]$, one has $\int_u^t |-2\lambda \mathbb{E}_{\mathbf{x_0}} V(\mathbf{x}(s), s) + 2C| ds < \infty$).

Denote by $g(t)$ the *deterministic* quantity $\mathbb{E}_{\mathbf{x_0}} V(\mathbf{x}(t))$. As remarked above, $g(t)$ is a continuous function of $t$. It then satisfies the conditions of the Gronwall-type lemma 1, and, as a consequence

$$\forall t \ge 0 \quad \mathbb{E}_{\mathbf{x}_0} V(\mathbf{x}(t), t) \le \frac{C}{\lambda} + \left[V(\mathbf{x}_0, 0) - \frac{C}{\lambda}\right]^+ e^{-2\lambda t}$$

which leads to (8) by integrating with respect to $(\mathbf{a}_0, \mathbf{b}_0)$. Next, (9) follows from (8) by observing that

$$\begin{aligned}
&\int \left[(\mathbf{a}_0 - \mathbf{b}_0)^T \mathbf{M}(0)(\mathbf{a}_0 - \mathbf{b}_0) - \frac{C}{\lambda}\right]^+ dp(\mathbf{a}_0, \mathbf{b}_0) \\
&\le \int (\mathbf{a}_0 - \mathbf{b}_0)^T \mathbf{M}(0)(\mathbf{a}_0 - \mathbf{b}_0) dp(\mathbf{a}_0, \mathbf{b}_0) \\
&= \mathbb{E}\left((\xi_1 - \xi_2)^T \mathbf{M}(0)(\xi_1 - \xi_2)\right)
\end{aligned}$$

and

$$\|\mathbf{a}(t) - \mathbf{b}(t)\|^2 \le \frac{1}{\beta} (\mathbf{a}(t) - \mathbf{b}(t))^T \mathbf{M}(t) (\mathbf{a}(t) - \mathbf{b}(t)).$$

□

## III. REMARKS

### A. "Optimality" of the Mean Square Bound

Consider the following linear dynamical system, known as the Ornstein-Uhlenbeck (colored noise) process

$$da = -\lambda a dt + \sigma dW. \qquad (12)$$

Clearly, the noise-free system is contracting with rate $\lambda$ and the trace of the noise matrix is upper-bounded by $\sigma^2$. Let $a(t)$ and $b(t)$ be two system trajectories starting respectively at $a_0$ and $b_0$ (deterministic initial conditions). Then by theorem 2, we have

$$\forall t \ge 0 \quad \mathbb{E}\left((a(t) - b(t))^2\right) \le \frac{\sigma^2}{\lambda} + \left[(a_0 - b_0)^2 - \frac{\sigma^2}{\lambda}\right]^+ e^{-2\lambda t}. \qquad (13)$$

Let us assess the quality of this bound by solving directly (12). The solution of (12) is ([25, p. 134])

$$a(t) = a_0 e^{-\lambda t} + \sigma \int_0^t e^{\lambda(s-t)} dW(s). \qquad (14)$$

Compute next the mean square distance between the two trajectories $a(t)$ and $b(t)$

$$\begin{aligned}
\mathbb{E}\left((a(t) - b(t))^2\right) &= (a_0 - b_0)^2 e^{-2\lambda t} \\
&\quad + \sigma^2 \mathbb{E}\left(\left(\int_0^t e^{\lambda(s-t)} dW_1(s)\right)^2\right) \\
&\quad + \sigma^2 \mathbb{E}\left(\left(\int_0^t e^{\lambda(u-t)} dW_2(u)\right)^2\right) \\
&= (a_0 - b_0)^2 e^{-2\lambda t} + \frac{\sigma^2}{\lambda}(1 - e^{-2\lambda t}) \\
&\le \frac{\sigma^2}{\lambda} + \left[(a_0 - b_0)^2 - \frac{\sigma^2}{\lambda}\right]^+ e^{-2\lambda t}.
\end{aligned}$$

The last inequality is in fact an equality when $(a_0 - b_0)^2 \ge (\sigma^2/\lambda)$. Thus, this calculation shows that the upper-bound (13) given by theorem 2 is optimal, in the sense that it can be attained.

### B. No Asymptotic Almost-Sure Stability

From the explicit form (14) of the solutions, one can deduce that the distributions of $a(t)$ and $b(t)$ converge to the normal distribution $\mathcal{N}(0, (\sigma^2/2\lambda))$ ([25, p. 135]). Since $a(t)$ and $b(t)$ are independent, the distribution of the difference $a(t) - b(t)$ will then converge to $\mathcal{N}(0, (\sigma^2/\lambda))$. The last observation shows that one cannot—in general—obtain *almost-sure* stability results.

Indeed, the main difference with the approaches in [16]–[18] lies in the term $2C$. This extra term comes from the fact that the influence of the noise does not vanish when two trajectories get very close to each other (cf. Section II-B). It prevents $\mathcal{L}V(\mathbf{x}(t))$ from being always non-positive, and as a result, $V(\mathbf{x}(t))$ is not always *non-increasing*. Thus, $V(\mathbf{x}(t))$ is not—in general—a supermartingale, and one cannot then use the supermartingale inequality (or its variations) to obtain asymptotic almost-sure bounds, as in ([11, pp. 47–48]) or in [16]–[18].

However, if one is interested in *finite time* bounds then the supermartingale inequality is still applicable, see ([11, p. 86]) for details.

### C. Noisy and Noise-Free Trajectories

Consider the following augmented system:

$$\begin{aligned}
d\mathbf{x} &= \begin{pmatrix} \mathbf{f}(\mathbf{a}, t) \\ \mathbf{f}(\mathbf{b}, t) \end{pmatrix} dt + \begin{pmatrix} 0 & 0 \\ 0 & \sigma(\mathbf{b}, t) \end{pmatrix} \begin{pmatrix} dW_d^1 \\ dW_d^2 \end{pmatrix} \\
&= \widehat{\mathbf{f}}(\mathbf{x}, t)dt + \widehat{\sigma}(\mathbf{x}, t)dW_{2d}. \qquad (15)
\end{aligned}$$

This equation is the same as (3) except that the $\mathbf{a}$-system is not perturbed by noise. Thus $V(\mathbf{x}) = \|\mathbf{a} - \mathbf{b}\|^2$ represents the distance between a noise-free trajectory and a noisy one. All the calculations are the same as in Section III-C, with $C$ being replaced by $C/2$. One can then derive the following corollary (for simplicity, we consider the case of identity metric; the general case can be easily adapted)

*Corollary 1:* Assume that system (2) verifies **(H1)** and **(H2)** with $\boldsymbol{M} = \mathbf{I}$. Let $\mathbf{a}(t)$ be a *noise-free* trajectory starting at $\mathbf{a}_0$ and $\mathbf{b}(t)$ a *noisy* trajectory whose initial condition is independent of the noise and given by a probability distribution $p(\xi_2)$. Then $\forall t \ge 0$

$$\mathbb{E}\left(\|\mathbf{a}(t) - \mathbf{b}(t)\|^2\right) \le \frac{C}{2\lambda} + \mathbb{E}\left(\|\mathbf{a}_0 - \xi_2\|^2\right) e^{-2\lambda t}. \qquad (16)$$

*Remarks:*

- One can note here that the derivation of corollary 1 is only permitted by our initial choice of considering *distinct* driving Wiener process for the $\mathbf{a}$- and $\mathbf{b}$-systems (cf. Section II-B).

- Corollary 1 provides a robustness result for contracting systems, in the sense that any contracting system is *automatically* protected against noise, as quantified by (16). This robustness could be related to the exponential nature of contraction stability.

### D. *Combination Properties*

Stochastic contraction inherits naturally from deterministic contraction [8] its convenient combination properties. Because contraction is a state-space concept, such properties can be expressed in more general forms than input-output analogues such as passivity-based combinations [29].

It should be noted that, in the deterministic domain, combination properties have been obtained for $\delta$ISS systems [10], [26] (for the definition of $\delta$ISS, see Section II-B).

Consider two connected systems

$$\begin{cases} d\mathbf{x}_1 = \mathbf{f}_1(\mathbf{x}_1, \mathbf{x}_2, t)dt + \sigma_1(\mathbf{x}_1, t)dW_1 \\ d\mathbf{x}_2 = \mathbf{f}_2(\mathbf{x}_1, \mathbf{x}_2, t)dt + \sigma_2(\mathbf{x}_2, t)dW_2 \end{cases}$$

where system $i$ $(i = 1, 2)$ is stochastically contracting with respect to $\boldsymbol{M}_i = \boldsymbol{\Theta}_i^T \boldsymbol{\Theta}_i$, with rate $\lambda_i$ and bound $C_i$ (here, $\boldsymbol{M}_i$ and $\boldsymbol{\Theta}_i$ are set to be constant matrices for simplicity; the case of time-varying metrics can be easily adapted).

Assume that these systems are connected by *negative feedback* [30], i.e. the Jacobian of their coupling matrices verify $\boldsymbol{\Theta}_1 \mathbf{J}_{12} \boldsymbol{\Theta}_2^{-1} = -k \boldsymbol{\Theta}_2 \mathbf{J}_{21}^T \boldsymbol{\Theta}_1^{-1}$, with $k$ a positive constant. The Jacobian matrix of the augmented noise-free system is given then by

$$\mathbf{J} = \begin{pmatrix} \mathbf{J}_1 & -k\boldsymbol{\Theta}_1^{-1}\boldsymbol{\Theta}_2\mathbf{J}_{21}^T\boldsymbol{\Theta}_1^{-1}\boldsymbol{\Theta}_2 \\ \mathbf{J}_{21} & \mathbf{J}_2 \end{pmatrix}.$$

Consider the coordinate transform $\boldsymbol{\Theta} = \begin{pmatrix} \boldsymbol{\Theta}_1 & \mathbf{0} \\ \mathbf{0} & \sqrt{k}\boldsymbol{\Theta}_2 \end{pmatrix}$ associated with the metric $\boldsymbol{M} = \boldsymbol{\Theta}^T \boldsymbol{\Theta} > \mathbf{0}$. After some calculations, one has

$$\begin{aligned} (\boldsymbol{\Theta}\mathbf{J}\boldsymbol{\Theta}^{-1})_s &= \begin{pmatrix} \left(\boldsymbol{\Theta}_1\mathbf{J}_1\boldsymbol{\Theta}_1^{-1}\right)_s & \mathbf{0} \\ \mathbf{0} & \left(\boldsymbol{\Theta}_2\mathbf{J}_2\boldsymbol{\Theta}_2^{-1}\right)_s \end{pmatrix} \\ &\leq \max(-\lambda_1, -\lambda_2)\mathbf{I} \quad \text{uniformly.} \end{aligned} \tag{17}$$

The augmented system is thus stochastically contracting in the metric $\boldsymbol{M}$, with rate $\min(\lambda_1, \lambda_2)$ and bound $C_1 + kC_2$.

Similarly, one can show that (with $\operatorname{sing}(\mathbf{A})$ denoting the largest singular value of $\mathbf{A}$)

- **Hierarchical combination:** If $\mathbf{J}_{12} = \mathbf{0}$ and $\operatorname{sing}^2(\boldsymbol{\Theta}_2\mathbf{J}_{21}\boldsymbol{\Theta}_1^{-1}) \leq K$, then the augmented system is stochastically contracting in the metric $\boldsymbol{M}_\epsilon$, with rate $(1/2)(\lambda_1 + \lambda_2 - \sqrt{\lambda_1^2 + \lambda_2^2})$ and bound $C_1 + (2C_2\lambda_1\lambda_2/K)$, where $\epsilon = \sqrt{2\lambda_1\lambda_2/K}$.
- **Small gains:** Define $\mathbf{B}_\gamma = (1/2)(\sqrt{\gamma}\boldsymbol{\Theta}_2\mathbf{J}_{21}\boldsymbol{\Theta}_1^{-1} + (1/\sqrt{\gamma})(\boldsymbol{\Theta}_1\mathbf{J}_{12}\boldsymbol{\Theta}_2^{-1})^T)$. If there exists $\gamma > 0$ such that $\operatorname{sing}^2(\mathbf{B}_\gamma) < \lambda_1\lambda_2$ then the augmented system is stochastically contracting in the metric $\boldsymbol{M}_\gamma$, with bound $C_1 + \gamma C_2$ and rate $\lambda$ verifying

$$\lambda \geq \frac{\lambda_1 + \lambda_2}{2} - \sqrt{\left(\frac{\lambda_1 - \lambda_2}{2}\right)^2 + \operatorname{sing}^2(\mathbf{B}_\gamma)}. \tag{18}$$

Taken together, the combination properties presented above allow one to build by recursion stochastically contracting systems of arbitrary size.

## IV. SOME EXAMPLES

### A. *Effect of Measurement Noise on Contracting Observers*

Consider a nonlinear dynamical system

$$\dot{\mathbf{x}} = \mathbf{f}(\mathbf{x}, t). \tag{19}$$

If a measurement $\mathbf{y} = \mathbf{y}(\mathbf{x})$ is available, then it may be possible to choose an output injection matrix $\mathbf{K}(t)$ such that the dynamics

$$\dot{\hat{\mathbf{x}}} = \mathbf{f}(\hat{\mathbf{x}}, t) + \mathbf{K}(t)(\hat{\mathbf{y}} - \mathbf{y}) \tag{20}$$

is contracting, with $\hat{\mathbf{y}} = \mathbf{y}(\hat{\mathbf{x}})$. Since the actual state $\mathbf{x}$ is a particular solution of (20), any solution $\hat{\mathbf{x}}$ of (20) will then converge towards $\mathbf{x}$ exponentially.

Assume now that the measurements are corrupted by additive “white noise”. In the case of *linear* measurement, the measurement equation becomes $\mathbf{y} = \mathbf{H}(t)\mathbf{x} + \Sigma(t)\eta(t)$ where $\eta(t)$ is a multidimensional “white noise” and $\Sigma(t)$ is the matrix of measurement noise intensities.

The observer equation is now given by the following Itô stochastic differential equation (using the formal rule $dW = \eta dt$)

$$d\hat{\mathbf{x}} = (\mathbf{f}(\hat{\mathbf{x}}, t) + \mathbf{K}(t)\left(\mathbf{H}(t)\mathbf{x} - \mathbf{H}(t)\hat{\mathbf{x}}\right))dt + \mathbf{K}(t)\Sigma(t)dW. \tag{21}$$

Next, remark that the solution $\mathbf{x}$ of system (19) is a also a solution of the noise-free version of system (21). By corollary 1, one then has, for any solution $\hat{\mathbf{x}}$ of system (21)

$$\forall t \geq 0 \quad \mathbb{E}\left(\|\hat{\mathbf{x}}(t) - \mathbf{x}(t)\|^2\right) \leq \frac{C}{2\lambda} + \|\hat{\mathbf{x}}_0 - \mathbf{x}_0\|^2 e^{-2\lambda t} \tag{22}$$

where

$$\begin{aligned} \lambda &= \inf_{\mathbf{x},t} \left| \lambda_{\max}\left(\frac{\partial \mathbf{f}(\mathbf{x}, t)}{\partial \mathbf{x}} - \mathbf{K}(t)\mathbf{H}(t)\right)\right| \\ C &= \sup_{t \geq 0} \operatorname{tr}\left(\Sigma(t)^T \mathbf{K}(t)^T \mathbf{K}(t) \Sigma(t)\right). \end{aligned}$$

*Remark:* The choice of the injection gain $\mathbf{K}(t)$ is governed by a trade-off between convergence speed $(\lambda)$ and noise sensitivity $(C/\lambda)$ as quantified by (22). More generally, the explicit computation of the bound on the expected quadratic estimation error given by (22) may open the possibility of *measurement selection* in a way similar to the linear case. If several possible measurements or sets of measurements can be performed, one may try at each instant (or at each step, in a discrete version) to select the most relevant, i.e., the measurement or set of measurements which will best contribute to improving the state estimate. Similarly to the Kalman filters used in [31] for linear systems, this can be achieved by computing, along with the state estimate itself, the corresponding bounds on the expected quadratic estimation error, and then selecting accordingly the measurement which will minimize it.

### B. *Synchronization of Noisy Fitzhugh-Nagumo Oscillators*

We analyze in this section the synchronization of two noisy FitzHugh-Nagumo oscillators (see [21] for the references). The interested reader is referred to [32] for a more complete study.

The dynamics of two diffusively-coupled noisy FitzHugh–Nagumo oscillators is given by

$$\begin{cases} dv_i = \left(c\left(v_i + w_i - \frac{1}{3}v_i^3 + I_i\right) + k(v_0 - v_i)\right)dt + \sigma dW_i \\ dw_i = -\frac{1}{c}(v_i - a + bw_i)dt \end{cases}$$

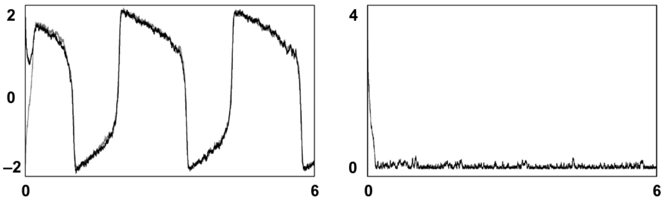

Fig. 1. Synchronization of two noisy FitzHugh–Nagumo oscillators. Left plot: membrane potentials of two coupled noisy FN oscillators. Right plot: absolute difference between the two membrane potentials.

where $i = 1,2$. Let $\mathbf{x} = (v_1, w_1, v_2, w_2)^T$ and $\mathbf{V} = 1/\sqrt{2}\begin{pmatrix} 1 & 0 & -1 & 0 \\ 0 & 1 & 0 & -1 \end{pmatrix}$. The Jacobian matrix of the projected noise-free system is then given by

$$\begin{pmatrix} c - \frac{c(v_1^2+v_2^2)}{2} - k & c \\ -1/c & -b/c \end{pmatrix}$$

Thus, if the coupling strength verifies $k > c$ then the projected system will be stochastically contracting in the diagonal metric $\boldsymbol{M} = \mathrm{diag}(1, c)$ with rate $\min(k-c, b/c)$ and bound $\sigma^2$. Hence, the average absolute difference between the two membrane potentials $|v_1 - v_2|$ will be upper-bounded by $\sigma/\sqrt{\min(1,c)\min(k-c, b/c)}$ after exponential transients (see Fig. 1 for a numerical simulation).

## ACKNOWLEDGMENT

The authors wish to thank Dr S. Darses, Dr. D. Bennequin, and Dr. M. Yor, for stimulating discussions, and the Editors and the Reviewers for their helpful comments.

## REFERENCES

[1] J.-J. Slotine and W. Li, *Applied Nonlinear Control*. Englewood Cliffs, NJ: Prentice-Hall, 1991.
[2] D. Lewis, "Metric properties of differential equations," *Amer. J. Math.*, vol. 71, pp. 294–312, 1949.
[3] B. Demidovich, "Dissipativity of a nonlinear system of differential equations," *Ser. Mat. Mekh.*, pp. 19–27, 1961.
[4] P. Hartmann, *Ordinary Differential Equations*. New York: Wiley, 1964.
[5] W. Lohmiller and J.-J. Slotine, "Contraction analysis of nonlinear distributed systems," *Int. J. Control*, vol. 78, pp. 678–688, 2005.
[6] J. Jouffroy, "Some ancestors of contraction analysis," in *Proc. IEEE Conf. Decision Control*, 2005, pp. 5450–5455.
[7] E. Sontag and Y. Wang, "Output-to-state stability and detectability of nonlinear systems," *Syst. Control Lett.*, vol. 29, pp. 279–290, 1997.
[8] W. Lohmiller and J.-J. Slotine, "On contraction analysis for nonlinear systems," *Automatica*, vol. 34, pp. 671–682, 1998.
[9] V. Fromion, G. Scorletti, and G. Ferreres, "Nonlinear performance of a PI controlled missile: An explanation," *Int. J. Robust Nonlin. Control*, vol. 9, pp. 485–518, 1999.
[10] D. Angeli, "A Lyapunov approach to incremental stability properties," *IEEE Trans. Automat. Control*, vol. 47, no. 3, pp. 410–421, Mar. 2002.
[11] H. Kushner, *Stochastic Stability and Control*. New York: Academic, 1967.
[12] R. Has'minskii, *Stochastic Stability of Differential Equations*. Rockville, MD: Sijthoff and Nordhoff, 1980.
[13] P. Florchinger, "Lyapunov-like techniques for stochastic stability," *SIAM J. Control Optim.*, vol. 33, pp. 1151–1169, 1995.
[14] X. Mao, *Stability of Stochastic Differential Equations With Respect to Semimartingales*. White Plains, NY: Longman, 1991.
[15] P. Florchinger, "Feedback stabilization of affine in the control stochastic differential systems by the control Lyapunov function method," *SIAM J. Control Optim.*, vol. 35, pp. 500–511, 1997.
[16] J. Tsinias, "The concept of "exponential ISS" for stochastic systems and applications to feedback stabilization," *Syst. Control Lett.*, vol. 36, pp. 221–229, 1999.
[17] H. Deng, M. Krstic, and R. Williams, "Stabilization of stochastic nonlinear systems driven by noise of unknown covariance," *IEEE Trans. Automat. Control*, vol. 46, no. 8, pp. 1237–1253, Aug. 2001.
[18] T. Caraballo, P. Kloeden, and B. Schmalfuss, "Exponentially stable stationary solutions for stochastic evolution equations and their pertubation," *Appl. Math. Optim.*, vol. 50, pp. 183–207, 2004.
[19] N. Aghannan and P. Rouchon, "An intrinsic observer for a class of Lagrangian systems," *IEEE Trans. Automat. Control*, vol. 48, no. 6, pp. 936–945, Jun. 2003.
[20] J. Jouffroy and T. Fossen, "On the combination of nonlinear contracting observers and UGES controllers for output feedback," in *Proc. IEEE Conf. Decision Control*, 2004, pp. 4933–4939.
[21] W. Wang and J.-J. E. Slotine, "On partial contraction analysis for coupled nonlinear oscillators," *Biol Cybern*, vol. 92, no. 1, pp. 38–53, Jan. 2005.
[22] Q.-C. Pham and J.-J. Slotine, "Stable concurrent synchronization in dynamic system networks," *Neural Networks*, vol. 20, no. 1, pp. 62–77, Jan. 2007.
[23] B. Girard, N. Tabareau, Q.-C. Pham, A. Berthoz, and J.-J. Slotine, "Where neuroscience and dynamic system theory meet autonomous robotics: A contracting basal ganglia model for action selection," *Neural Networks*, vol. 21, pp. 628–641, 2008.
[24] R. Horn and C. Johnson, *Matrix Analysis*. Cambridge, U.K.: Cambridge University Press, 1985.
[25] L. Arnold, *Stochastic Differential Equations: Theory and Applications*. New York: Wiley, 1974.
[26] A. Pavlov, N. van de Wouw, and H. Nijmeijer, *Uniform Output Regulation of Nonlinear Systems*. Boston, MA: Birkhauser, 2006.
[27] Q.-C. Pham, 2007, A Variation of Gronwall's Lemma [Online]. Available: http://arxiv.org/abs/0704.0922
[28] A. Pavlov, A. Pogromsky, N. van de Wouw, and H. Nijmeijer, "Convergent dynamics, a tribute to Boris Pavlovich Demidovich," *Syst. Control Lett.*, vol. 52, pp. 257–261, Jul. 2004.
[29] V. Popov, *Hyperstability of Control Systems*. New York: Springer-Verlag, 1973.
[30] N. Tabareau and J.-J. Slotine, Notes on Contraction Theory MIT, Cambridge, MA, NSL Rep., 2005.
[31] E. Dickmanns, *Dynamic Vision for Intelligent Vehicles*. Cambridge, MA: MIT, 1998.
[32] N. Tabareau, J.-J. Slotine, and Q.-C. Pham, How Synchronization Protects From Noise 2008 [Online]. Available: http://arxiv.org/abs/0801.0011

---

# Wavelet Amendment of Polynomial Models in Hammerstein Systems Identification

Przemysław Śliwiński, Jerzy Rozenblit, Michael W. Marcellin, and Ryszard Klempous

***Abstract*—A new wavelet algorithm for *on-line* improvement of an existing polynomial model of nonlinearity in a Hammerstein system is proposed and its properties are examined. The algorithm employs wavelet bases on interval. Convergence of the resulting assembly, comprising the parametric polynomial model and a nonparametric wavelet add-on, to the system nonlinearity is shown. Rates of convergence for uniformly smooth and piecewise smooth nonlinearities with discontinuities are both established.**

***Index Terms*—Hammerstein system, nonlinear system identification, order statistics, polynomial models, semiparametric approach, wavelet bypass, wavelet regression estimate.**

## I. INTRODUCTION

MANY existing models of nonlinear dynamic systems derived from a block-oriented methodology (where models are composed of interconnected static nonlinear and linear dynamic blocks; cf.

Manuscript received July 15, 2008; revised July 16, 2008, September 22, 2008, and October 06, 2008. Current version published April 08, 2009. Recommended by Associate Editor J.-F. Zhang.

P. Śliwiński and R. Klempous are with the The Institute of Computer Engineering, Control and Robotics, Wrocław University of Technology, Wrocław 50-370, Poland (e-mail: przemyslaw.sliwinski@pwr.wroc.pl; ryszard.klempous@pwr.wroc.pl).

J. Rozenblit and M. W. Marcellin are with the Department of Electrical and Computer Engineering, University of Arizona, Tucson, AZ 85721 USA (e-mail: jr@ece.arizona.edu; marcellin@ece.arizona.edu).

Color versions of one or more of the figures in this technical note are available online at http://ieeexplore.ieee.org.

Digital Object Identifier 10.1109/TAC.2008.2009620

## B.3 Analysis of Discrete and Hybrid Stochastic Systems by Nonlinear Contraction Theory

By Q.-C. Pham. Published in *Proceedings of the 10th International Conference on Control, Automation, Robotics and Vision (ICARCV)*, pp. 1054-1059, 2008.

2008 10th Intl. Conf. on Control, Automation, Robotics and Vision
Hanoi, Vietnam, 17–20 December 2008

# Analysis of Discrete and Hybrid Stochastic Systems by Nonlinear Contraction Theory

Quang-Cuong Pham
Laboratoire de Physiologie de la Perception et de l'Action
Collège de France – CNRS
Paris, France
cuong.pham@normalesup.org

***Abstract*—We investigate the stability properties of discrete and hybrid stochastic nonlinear dynamical systems. More precisely, we extend the stochastic contraction theorems (which were formulated for continuous systems) to the case of discrete and hybrid resetting systems. In particular, we show that the mean square distance between any two trajectories of a discrete (or hybrid resetting) contracting stochastic system is upper-bounded by a constant after exponential transients. Using these results, we study the synchronization of noisy nonlinear oscillators coupled by discrete noisy interactions.**

***Index Terms*—Discrete systems, hybrid resetting, stochastic systems, nonlinear contraction theory, incremental stability, oscillator synchronization**

## I. INTRODUCTION

Contraction theory is a set of relatively recent tools that provide a systematic approach to the stability analysis of a large class of nonlinear dynamical systems [1], [2], [3], [4]. A nonlinear nonautonomous system $\dot{\mathbf{x}} = \mathbf{f}(\mathbf{x}, t)$ is *contracting* if the symmetric part of the Jacobian matrix of $\mathbf{f}$ is uniformly negative definite in some metric. Using elementary fluid dynamics techniques, it can be shown that contracting systems are *incrementally stable*, that is, any two system trajectories exponentially converge to each other [1].

From a practical viewpoint, contraction theory has been successfully applied to a number of important problems, such as mechanical observers and controllers design [5], chemical processes control [6], synchronization analysis [2], [7] or biological systems modelling [8].

Recently, contraction analysis has been extended to the case of *stochastic* dynamical systems governed by Itô differential equations [4]. In parallel, hybrid versions of contraction theory have also been developped [3]. A hybrid system is characterized by a *continuous* evolution of the system's state, and intermittent *discrete* transitions. Such systems are pervasive in both artificial (e.g. analog physical processes controlled by digital devices) and natural (e.g. spiking neurons with subthreshold dynamics) environments.

The present paper benefits from these recent developments to provide an exponential stability result for discrete and hybrid systems governed by stochastic *difference* and *differential* equations. More precisely, we prove in section II and III that the mean square distance between any two trajectories of a discrete (respectively hybrid resetting) stochastic contracting system is upper-bounded by a constant after exponential transients. This bound can be expressed as function of the noise intensities and the contraction rates of the noise-free systems. In section IV, we briefly discuss a number of theoretical issues regarding our analysis. Finally, in section V, we study, using the previously developped tools, the synchronization of noisy nonlinear oscillators which interact by discrete noisy couplings.

**Notations** The symmetric part of a matrix $\mathbf{A}$ is defined as $\mathbf{A}_s = \frac{1}{2}\left(\mathbf{A} + \mathbf{A}^T\right)$. For a symmetric matrix $\mathbf{A}$, $\lambda_{\min}(\mathbf{A})$ and $\lambda_{\max}(\mathbf{A})$ denote respectively the smallest and the largest eigenvalue of $\mathbf{A}$. A set of symmetric matrices $(\mathbf{A}_i)_{i\in I}$ is uniformly positive definite if $\exists\alpha > 0,\ \forall i \in I,\ \lambda_{\min}(\mathbf{A}_i) \geq \alpha$. Finally, for a stochastic process $\mathbf{s}(t)$, we note $\mathbb{E}_{\mathbf{x}}(\cdot)$ the conditional expection $\mathbb{E}(\cdot \,|\, \mathbf{s}(0) = \mathbf{x})$.

## II. DISCRETE SYSTEMS

We first prove a lemma that makes explicit the initial "discrete contraction" proof (see section 5 of [1]). Note that a similar proof for continuous systems can be found in [9].

*Lemma 1 (and definition):* Consider two metrics $\mathbf{M}_i = \mathbf{\Theta}_i^T\mathbf{\Theta}_i$ defined over $\mathbb{R}^{n_i}$ $(i = 1, 2)$ and a smooth function $\mathbf{f} : \mathbb{R}^{n_1} \to \mathbb{R}^{n_2}$. The *generalized Jacobian* of $\mathbf{f}$ in the metrics $(\mathbf{M}_1, \mathbf{M}_2)$ is defined by

$$\mathbf{F} = \mathbf{\Theta}_2 \frac{\partial \mathbf{f}}{\partial \mathbf{x}} \mathbf{\Theta}_1^{-1}$$

Assume now that $\mathbf{f}$ is *contracting* in the metrics $(\mathbf{M}_1, \mathbf{M}_2)$ with rate $\beta$ $(0 < \beta < 1)$, i.e.

$$\forall \mathbf{x} \in \mathbb{R}^{n_1} \quad \lambda_{\max}(\mathbf{F}(\mathbf{x})^T\mathbf{F}(\mathbf{x})) \leq \beta$$

Then for all $\mathbf{u}, \mathbf{v} \in \mathbb{R}^n$, one has

$$d_{\mathbf{M}_2}(\mathbf{f}(\mathbf{u}), \mathbf{f}(\mathbf{v}))^2 \leq \beta d_{\mathbf{M}_1}(\mathbf{u}, \mathbf{v})^2$$

where $d_{\mathbf{M}}$ denotes the distance associated with the metric $\mathbf{M}$ (the distance between two points is defined by the infimum of the lengths in the metric $\mathbf{M}$ of all continuously differentiable curves connecting these points).

**Proof** Consider a $\mathrm{C}^1$ curve $\gamma : [0, 1] \to \mathbb{R}^{n_1}$ that connects $\mathbf{u}$ and $\mathbf{v}$ (i.e. $\gamma(0) = \mathbf{u}$ and $\gamma(1) = \mathbf{v}$). The $\mathbf{M}_1$-length of such a curve is given by

$$L_{\mathbf{M}_1}(\gamma) = \int_0^1 \sqrt{\left(\frac{\partial\gamma}{\partial u}(u)\right)^T \mathbf{M}_1 \left(\frac{\partial\gamma}{\partial u}(u)\right)} du$$

Since $\mathbf{f}$ is a smooth function, $\mathbf{f}(\gamma)$ is also a $\mathbf{C}^1$ curve, with

$$L_{\mathbf{M}_2}(\mathbf{f}(\gamma)) = \int_0^1 \sqrt{\left(\frac{\partial \mathbf{f}(\gamma)}{\partial u}(u)\right)^T \mathbf{M}_2 \left(\frac{\partial \mathbf{f}(\gamma)}{\partial u}(u)\right)} du$$

The chain rule next implies that

$$\frac{\partial \mathbf{f}(\gamma)}{\partial u}(u) = \frac{\partial \mathbf{f}}{\partial \mathbf{x}} \frac{\partial \gamma}{\partial u}(u)$$

which leads to

$$\begin{array}{rcl} L_{\mathbf{M}_2}(\mathbf{f}(\gamma)) & = & \int_0^1 \sqrt{\left(\frac{\partial \gamma}{\partial u}^T \frac{\partial \mathbf{f}}{\partial \mathbf{x}}^T \mathbf{\Theta}_2^T \mathbf{\Theta}_2 \frac{\partial \mathbf{f}}{\partial \mathbf{x}} \frac{\partial \gamma}{\partial u}\right)} du \\ & = & \int_0^1 \sqrt{\left(\frac{\partial \gamma}{\partial u}^T \mathbf{\Theta}_1^T\right) \mathbf{F}^T \mathbf{F} \left(\mathbf{\Theta}_1 \frac{\partial \gamma}{\partial u}\right)} du \\ & \leq & \int_0^1 \sqrt{\beta \left(\frac{\partial \gamma}{\partial u}^T \mathbf{\Theta}_1^T \mathbf{\Theta}_1 \frac{\partial \gamma}{\partial u}\right)} du \\ & = & \sqrt{\beta} L_{\mathbf{M}_1}(\gamma) \end{array} \quad (1)$$

Choose now a sequence of curves $(\gamma_n)_{n \in \mathbb{N}}$ such that $\lim_{n \to \infty} L_{\mathbf{M}_1}(\gamma_n) = d_{\mathbf{M}_1}(u, v)$. From (1), one has $\forall n \in \mathbb{N},\ L_{\mathbf{M}_2}(\mathbf{f}(\gamma_n)) \leq \sqrt{\beta} L_{\mathbf{M}_1}(\gamma_n)$. By definition of distance, one then has $\forall n \in \mathbb{N},\ d_{\mathbf{M}_2}(\mathbf{f}(u), \mathbf{f}(v)) \leq \sqrt{\beta} L_{\mathbf{M}_1}(\gamma_n)$. Finally, by letting $n$ go to infinity in the last inequality, one obtains the desired result. □

*Theorem 1 (Discrete stochastic contraction):* Consider the stochastic difference equation

$$\left\{ \begin{array}{l} \mathbf{a}_{k+1} = \mathbf{f}(\mathbf{a}_k, k) + \sigma(\mathbf{a}_k, k) w_{k+1} \\ \mathbf{a}_0 = \xi \end{array} \right. \quad (2)$$

where $\mathbf{f}$ is a $\mathbb{R}^n \times \mathbb{N} \to \mathbb{R}^n$ function, $\sigma$ is a $\mathbb{R}^n \times \mathbb{N} \to \mathbb{R}^{nd}$ matrix-valued function, $\{w_k, k = 1, 2, \ldots\}$ is a sequence of independent $d$-dimensional Gaussian noise vectors, with $w_k \sim \mathscr{N}(\mathbf{0}, \mathbf{Q}_k)$ and $\xi$ is a $n$-dimensional random variable independent of the $w_k$.

Assume that the system verifies the following two hypotheses

**(H1)** the dynamics $\mathbf{f}(\mathbf{a}, k)$ is contracting in the metrics $(\mathbf{M}_k, \mathbf{M}_{k+1})$, with contraction rate $\beta$ $(0 < \beta < 1)$, and the metrics $(\mathbf{M}_k)_{k \in \mathbb{N}}$ are uniformly positive definite.

**(H2)** the impact of noise is uniformly upper-bounded by a constant $\sqrt{C}$ in the metrics $\mathbf{M}_k$

$$\forall \mathbf{a}, k \quad d_{\mathbf{M}_k}(\mathbf{f}(\mathbf{a}, k), \mathbf{f}(\mathbf{a}, k) + \sigma(\mathbf{a}, k) w_k) \leq \sqrt{C}$$

Let $\mathbf{a}_k$ and $\mathbf{b}_k$ be two trajectories whose initial conditions are given by a probability distribution $p(\xi, \xi')$. Then for all $k \geq 0$

$$\mathbb{E}\left(d_{\mathbf{M}_k}(\mathbf{a}_k, \mathbf{b}_k)\right) \leq \frac{2\sqrt{C}}{1 - \sqrt{\beta}} + \sqrt{\beta}^k \int \left[d_{\mathbf{M}_0}(\mathbf{a}, \mathbf{b}) - \frac{2\sqrt{C}}{1 - \sqrt{\beta}}\right]^+ dp(\mathbf{a}, \mathbf{b}) \quad (3)$$

where $[\cdot]^+ = \max(0, \cdot)$.

This implies in particular that for all $k \geq 0$

$$\mathbb{E}\left(d_{\mathbf{M}_k}(\mathbf{a}_k, \mathbf{b}_k)\right) \leq \frac{2\sqrt{C}}{1 - \sqrt{\beta}} + \sqrt{\beta}^k \mathbb{E}\left(d_{\mathbf{M}_0}(\xi, \xi')\right) \quad (4)$$

**Proof** Let $\mathbf{x} = (\mathbf{a}, \mathbf{b})^T \in \mathbb{R}^{2n}$. We have by the triangle inequality (to avoid long formulas, we drop the second argument of $\mathbf{f}$ and $\sigma$ in the following calculations)

$$\begin{array}{rcl} d_{\mathbf{M}_{k+1}}(\mathbf{a}_{k+1}, \mathbf{b}_{k+1}) & \leq & d_{\mathbf{M}_{k+1}}(\mathbf{f}(\mathbf{a}_k), \mathbf{f}(\mathbf{b}_k)) \\ & + & d_{\mathbf{M}_{k+1}}(\mathbf{f}(\mathbf{a}_k), \mathbf{f}(\mathbf{a}_k) + \sigma(\mathbf{a}_k) w_{k+1}) \\ & + & d_{\mathbf{M}_{k+1}}(\mathbf{f}(\mathbf{b}_k), \mathbf{f}(\mathbf{b}_k) + \sigma(\mathbf{b}_k) w'_{k+1}) \end{array}$$

Let us examine the conditional expectations of the three terms of the right hand side

- From **(H1)** and lemma 1 one has

$$\mathbb{E}_{\mathbf{x}}(d_{\mathbf{M}_{k+1}}(\mathbf{f}(\mathbf{a}_k), \mathbf{f}(\mathbf{b}_k))) \leq \sqrt{\beta} \mathbb{E}_{\mathbf{x}}(d_{\mathbf{M}_k}(\mathbf{a}_k, \mathbf{b}_k))$$

- Next, from **(H2)**

$$\mathbb{E}_{\mathbf{x}}(d_{\mathbf{M}_{k+1}}(\mathbf{f}(\mathbf{a}_k), \mathbf{f}(\mathbf{a}_k) + \sigma(\mathbf{a}_k) w_{k+1})) \leq \sqrt{C}$$

  and similarly for $d_{\mathbf{M}_{k+1}}(\mathbf{f}(\mathbf{b}_k), \mathbf{f}(\mathbf{b}_k) + \sigma(\mathbf{b}_k) w'_{k+1})$.

If we now set $u_k = \mathbb{E}_{\mathbf{x}}(d_{\mathbf{M}_k}(\mathbf{a}_k, \mathbf{b}_k))$ then the above implies

$$u_{k+1} \leq \sqrt{\beta} u_k + 2\sqrt{C} \quad (5)$$

Define next $v_k = u_k - 2\sqrt{C}/(1 - \sqrt{\beta})$. Then replacing $u_k$ by $v_k + 2\sqrt{C}/(1 - \sqrt{\beta})$ in (5) yields

$$v_{k+1} \leq \sqrt{\beta} v_k$$

This implies that $\forall k \geq 0,\ v_k \leq v_0 \sqrt{\beta}^k \leq [v_0]^+ \sqrt{\beta}^k$. Replacing $v_k$ by its expression in terms of $u_k$ then yields

$$\forall k \geq 0 \quad u_k \leq \frac{2\sqrt{C}}{1 - \sqrt{\beta}} + \sqrt{\beta}^k \left[u_0 - \frac{2\sqrt{C}}{1 - \sqrt{\beta}}\right]^+$$

which is the desired result.

Next, integrating the last inequality with respect to $\mathbf{x}$ leads to (3). Finally, (4) follows from (3) by remarking that

$$\int \left[d_{\mathbf{M}_0}(\mathbf{a}, \mathbf{b}) - \frac{\sqrt{C}}{1 - \sqrt{\beta}}\right]^+ dp(\mathbf{a}, \mathbf{b}) \leq \int d_{\mathbf{M}_0}(\mathbf{a}, \mathbf{b}) dp(\mathbf{a}, \mathbf{b}) = \mathbb{E}\left(d_{\mathbf{M}_0}(\xi, \xi')\right) \quad \square$$

**Remark** In the particular context of state-independent metrics, hypothesis **(H2)** is equivalent to the following simpler condition

$$\forall \mathbf{a}, k \quad \mathrm{tr}\left(\sigma(\mathbf{a}, k)^T \mathbf{M}_{k+1} \sigma(\mathbf{a}, k) \mathbf{Q}_k\right) \leq C$$

Also, for state-independent metrics, one has

$$d_{\mathbf{M}_k}(\mathbf{a}_k, \mathbf{b}_k)^2 = (\mathbf{a}_k - \mathbf{b}_k)^T \mathbf{M}_k (\mathbf{a}_k - \mathbf{b}_k) = \|\mathbf{a}_k - \mathbf{b}_k\|^2_{\mathbf{M}_k}$$

which leads to the following stronger result instead of (4)

$$\mathbb{E}\left(\|\mathbf{a}_k - \mathbf{b}_k\|^2_{\mathbf{M}_k}\right) \leq \frac{2C}{1 - \beta} + \beta^k \mathbb{E}\left(\|\xi - \xi'\|^2_{\mathbf{M}_0}\right)$$

## III. HYBRID SYSTEMS

We have derived above the discrete stochastic contraction theorem for *time- and state-dependent* metrics, contrary to the context of continuous systems, where the state-dependent-metrics version of the contraction theorem is still unproved [4]. We now address the case of hybrid systems, but due to the present limitations of continuous stochastic contraction, only state-independent metrics will be considered.

For clarity, we assume in this paper *constant dwell-times*, although more elaborate conditions regarding dwell-times can be adapted from [3].

Consider the hybrid resetting stochastic dynamical system

$$\begin{cases} \forall k \geq 1 \quad \mathbf{a}(k\tau^+) = \mathbf{f}_d(\mathbf{a}(k\tau^-),k) + \sigma_d(\mathbf{a}(k\tau^-),k)w_k \\ \forall k \geq 0 \ \forall t \in ]k\tau,(k+1)\tau[ \quad d\mathbf{a} = \mathbf{f}_c(\mathbf{a},t)dt + \sigma_c(\mathbf{a},t)dW \\ \mathbf{a}(0^+) = \xi \end{cases} \tag{6}$$

where $\mathbf{f}_d$, $\sigma_d$, $\mathbf{f}_c$, $\sigma_c$ are four functions of appropriate dimensions and $\xi$ is a random variable independent of the $w_k$ and of the process $W$. Furthermore, $\mathbf{f}_c$ and $\sigma_c$ verify suitable conditions for the existence and uniqueness of the solutions of the continuous parts (cf e.g. [4]).

All the contraction properties below will be stated with respect to a uniformly positive definite time-varying metric $\mathbf{M}(t) = \mathbf{\Theta}(t)^T\mathbf{\Theta}(t)$. Furthermore, it will be assumed that for all $k \geq 0$, $\mathbf{M}$ is continuously differentiable in $]k\tau,(k+1)\tau[$. Finally, $\mathbf{M}(k\tau^-)$ and $\mathbf{M}(k\tau^+)$ will respectively denote the left and right limits of $\mathbf{M}(t)$ at $t = k\tau$ (and similarly for $\mathbf{\Theta}$).

### A. The discrete and continuous parts are both contracting

*Theorem 2 (Hybrid stochastic contraction, case $\lambda > 0$):* Assume the following conditions

(i) For all $k$, the discrete part is stochastically contracting at $k\tau$ with rate $\beta < 1$ and bound $C_d$, i.e.

$$\forall \mathbf{a} \in \mathbb{R}^n \quad \lambda_{\max}\left(\mathbf{F}(k\tau)^T\mathbf{F}(k\tau)\right) \leq \beta$$

where $\mathbf{F}(k\tau) = \mathbf{\Theta}(k\tau^+)\frac{\partial \mathbf{f}_d}{\partial \mathbf{a}}(\mathbf{a},k)\mathbf{\Theta}(k\tau^-)$, and

$$\forall \mathbf{a} \in \mathbb{R}^n \quad \mathrm{tr}\left(\sigma_d(\mathbf{a},k)^T\mathbf{M}(k\tau^+)\sigma_d(\mathbf{a},k)\mathbf{Q}_k\right) \leq C_d$$

(ii) For all $k$, the continuous part is stochastically contracting in $]k\tau,(k+1)\tau[$ with rate $\lambda > 0$ and bound $C_c$, i.e. $\forall \mathbf{a} \in \mathbb{R}^n$, $\forall t \in ]k\tau,(k+1)\tau[$,

$$\begin{gathered} \lambda_{\max}\left(\left(\frac{d}{dt}\mathbf{\Theta}(t) + \mathbf{\Theta}(t)\frac{\partial \mathbf{f}}{\partial \mathbf{a}}\right)\mathbf{\Theta}^{-1}(t)\right)_s \leq -\lambda \\ \mathrm{tr}\left(\sigma_c(\mathbf{a},t)^T\mathbf{M}(t)\sigma_c(\mathbf{a},t)\right) \leq C_c \end{gathered} \tag{7}$$

Let $\mathbf{a}(t)$ and $\mathbf{b}(t)$ be two trajectories whose initial conditions are given by a probability distribution $p(\xi,\xi')$. Then for all $t \geq 0$

$$\begin{gathered} \mathbb{E}\left(\|\mathbf{a}(t) - \mathbf{b}(t)\|^2_{\mathbf{M}(t)}\right) \leq \\ C_1 + \mathbb{E}\left(\|\xi - \xi'\|^2_{\mathbf{M}(0)}\right)\beta^{\lfloor t/\tau \rfloor}e^{-2\lambda t} \end{gathered}$$

where $C_1 = \frac{2\lambda C_d + (1-\beta)(1+\beta-r_1)C_c}{\lambda(1-\beta)(1-r_1)}$ and $r_1 = \beta e^{-2\lambda\tau}$.

**Proof** For all $t \geq 0$, let $u(t) = \mathbb{E}\left(\|\mathbf{a}(t) - \mathbf{b}(t)\|^2_{\mathbf{M}(t)}\right)$ and let us study the evolution of $u(t)$ between $k\tau^+$ and $(k+1)\tau^+$.

Condition (ii) and theorem 2 of [4] yield

$$u((k+1)\tau^-) \leq \tfrac{C_c}{\lambda} + u(k\tau^+)e^{-2\lambda\tau} \tag{8}$$

Next, condition (i) and theorem 1 above yield

$$u((k+1)\tau^+) \leq \tfrac{2C_d}{1-\beta} + \beta u((k+1)\tau^-) \tag{9}$$

Substituting (8) into (9) leads to

$$\begin{aligned} u((k+1)\tau^+) &\leq \tfrac{2C_d}{1-\beta} + \beta\left(\tfrac{C_c}{\lambda} + \beta u(k\tau^+)e^{-2\lambda\tau}\right) \\ &= \tfrac{2C_d}{1-\beta} + \tfrac{\beta C_c}{\lambda} + \beta e^{-2\lambda\tau}u(k\tau^+) \end{aligned}$$

Define $D_1 = \frac{2C_d}{1-\beta} + \frac{\beta C_c}{\lambda}$ and $v_k = u(k\tau^+) - D_1/(1-r_1)$. Then, similarly to the proof of theorem 1, we have $v_{k+1} \leq r_1 v_k$, and then $v_k \leq r_1^k[v_0]^+$, which implies

$$\begin{aligned} u(k\tau^+) &\leq \frac{D_1}{1-r_1} + \left[u(0^+) - \frac{D_1}{1-r_1}\right]^+ r_1^k \\ &\leq \frac{D_1}{1-r_1} + u(0^+)r_1^k \end{aligned}$$

Now, for any $t \geq 0$, choose $k = \lfloor t/\tau \rfloor$. Then

$$\begin{aligned} u(t) &\leq \frac{C_c}{\lambda} + u(k\tau^+)e^{-2\lambda(t-k\tau)} \\ &\leq \frac{C_c}{\lambda} + \frac{D_1 e^{-2\lambda(t-k\tau)}}{1-r_1} + u(0^+)\beta^k e^{-2\lambda t} \\ &\leq \frac{C_c}{\lambda} + \frac{D_1}{1-r_1} + u(0^+)\beta^k e^{-2\lambda t} \end{aligned}$$

which leads to the desired result after some algebraic manipulations. □

### B. Only the discrete part is contracting

Let us examine now the more interesting case when the continuous part is not contracting, more precisely when $\lambda \leq 0$ in (7). For this, we shall need to revisit the proof of theorem 2 in [4].

*Theorem 3 (Case $\lambda = 0$):* Assume all the hypotheses of theorem 2 except that $\lambda = 0$ in (7). Then for all $t \geq 0$

$$\begin{gathered} \mathbb{E}\left(\|\mathbf{a}(t) - \mathbf{b}(t)\|^2_{\mathbf{M}(t)}\right) \leq \\ C_2 + \mathbb{E}\left(\|\xi - \xi'\|^2_{\mathbf{M}(0)}\right)\beta^{\lfloor t/\tau \rfloor} \end{gathered}$$

where $C_2 = \frac{2C_d + 2\beta(1-\beta)C_c\tau}{(1-\beta)^2}$.

**Proof** As in the proof of theorem 2 in [4], let

$$V(\mathbf{x},t) = V((\mathbf{a},\mathbf{b})^T,t) = (\mathbf{a}-\mathbf{b})^T\mathbf{M}(t)(\mathbf{a}-\mathbf{b})$$

Lemma 1 of [4] is unchanged, yielding (see [4] for more details)

$$\forall t \in ]k\tau,(k+1)\tau[ \quad \widetilde{A}V(\mathbf{x}(t),t) \leq 2C_c$$

where $\widetilde{A}$ is the infinitesimal operator associated with the process $\mathbf{x}(t)$ (see section 2.1.2 of [4] or p. 15 of [10] for more details).

By Dynkin's formula [10], one then obtains for all $\mathbf{x} \in \mathbb{R}^{2n}$

$$\begin{array}{rcl} \mathbb{E}_{\mathbf{x}} V(\mathbf{x}(t),t) - V(\mathbf{x},k\tau^+) & = & \mathbb{E}_{\mathbf{x}} \int_{k\tau}^t \widetilde{A}V(\mathbf{x}(s),s)ds \\ & \leq & \mathbb{E}_{\mathbf{x}} \int_{k\tau}^t 2C_c ds \\ & = & 2C_c(t-k\tau) \end{array}$$

Integrating the above inequality with respect to $\mathbf{x}$ then yields

$$\forall t \in ]k\tau,(k+1)\tau[ \quad u(t) \leq 2C_c(t-k\tau) + u(k\tau^+)$$

In particular, (8) becomes

$$u((k+1)\tau^-) \leq 2C_c\tau + u(k\tau^+)$$

which leads to, after substitution into (9),

$$u((k+1)\tau^+) \leq \frac{2C_d}{1-\beta} + 2\beta C_c\tau + \beta u(k\tau^+)$$

This finally implies

$$u(k\tau^+) \leq \frac{\frac{2C_d}{1-\beta} + 2\beta C_c \tau}{1-\beta} + u(0^+)\beta^k$$

The remainder of the proof can be adapted from that of theorem 2. □

*Theorem 4 (Case $\lambda < 0$):* Assume all the hypotheses of theorem 2 except that $\lambda < 0$ in (7). Let $k = \lfloor t/\tau \rfloor$. There are two cases:

- If $\beta < e^{-2|\lambda|\tau}$, then let $r_2 = \beta e^{2|\lambda|\tau} < 1$. For all $t \geq 0$
$$\begin{array}{c} \mathbb{E}\left(\|\mathbf{a}(t)-\mathbf{b}(t)\|^2_{\mathbf{M}(t)}\right) \leq \\ C_3 + \mathbb{E}\left(\|\xi-\xi'\|^2_{\mathbf{M}(0)}\right) e^{2|\lambda|\tau} r_2^k \end{array}$$
where $C_3 = \frac{2|\lambda|C_d + (1-\beta)(1+\beta-r_2)e^{2|\lambda|\tau}C_c}{|\lambda|(1-\beta)(1-r_2)}$.
- If $\beta \geq e^{-2|\lambda|\tau}$, then there is – in general – no finite bound on $\mathbb{E}\left(\|\mathbf{a}(t)-\mathbf{b}(t)\|^2_{\mathbf{M}(t)}\right)$ as $t \rightarrow +\infty$.

**Proof** One has now for all $t \in ]k\tau,(k+1)\tau[$,

$$\widetilde{A}V(\mathbf{x}(t),t) \leq 2|\lambda|V(\mathbf{x}(t),t) + 2C_c$$

with $|\lambda| > 0$. By Dynkin's formula, one has, for all $\mathbf{x} \in \mathbb{R}^{2n}$

$$\mathbb{E}_{\mathbf{x}} V(\mathbf{x}(t),t) - V(\mathbf{x},k\tau^+) \leq \mathbb{E}_{\mathbf{x}} \int_{k\tau}^t (2|\lambda|V(\mathbf{x}(s),s) + 2C_c)ds$$

Let now $g(t) = \mathbb{E}_{\mathbf{x}} V(\mathbf{x}(t),t)$. The above equation then yields

$$g(t) = V(\mathbf{x},k\tau^+) + 2C_c(t-k\tau) + 2|\lambda| \int_{k\tau}^t g(s)ds$$

Applying the classical Gronwall's lemma [11] to $g(t)$ leads to

$$\begin{array}{rcl} g(t) & \leq & V(\mathbf{x},k\tau^+) + 2C_c(t-k\tau) + \\ & & 2|\lambda| \int_{k\tau}^t (V(\mathbf{x},k\tau^+) + 2C_c s) \exp\left(\int_s^t 2|\lambda|du\right) ds \\ & = & \frac{C_c}{|\lambda|}\left(e^{2|\lambda|(t-k\tau)} - 1\right) + V(\mathbf{x},k\tau^+)e^{2|\lambda|(t-k\tau)} \end{array}$$

Integrating the above inequality with respect to $\mathbf{x}$ then yields $\forall t \in ]k\tau,(k+1)\tau[$,

$$u(t) \leq \frac{C_c}{|\lambda|}\left(e^{2|\lambda|(t-k\tau)} - 1\right) + u(k\tau^+)e^{2|\lambda|(t-k\tau)}$$

which implies

$$u((k+1)\tau^+) \leq D_2 + \beta e^{2|\lambda|\tau} u(k\tau^+) \qquad (10)$$

where $D_2 = \frac{2C_d}{1-\beta} + \frac{\beta C_c}{|\lambda|}\left(e^{2|\lambda|\tau} - 1\right)$.

There are three cases:

- If $\beta < e^{-2|\lambda|\tau}$, then $r_2 = \beta e^{2|\lambda|\tau} < 1$. By the same reasoning as in theorem 1, one obtains
$$u(k\tau^+) \leq \frac{D_2}{1-r_2} + u(0^+)r_2^k$$
The remainder of the proof can be adapted from that of theorem 2
- If $\beta = e^{-2|\lambda|\tau}$, then (10) reads
$$u((k+1)\tau^+) \leq D_2 + u(k\tau^+)$$
which implies $\forall k \geq 0,\ u(k\tau^+) \leq kD_2 + u(0^+)$. From this, it is clear that there is – in general – no finite bound for $u(k\tau^+)$.
- If $\beta > e^{-2|\lambda|\tau}$, then $r_2 = \beta e^{2|\lambda|\tau} > 1$. By the same reasoning as in theorem 1, one obtains
$$u(k\tau^+) \leq \left(u(0^+) + \frac{D_2}{r_2 - 1}\right) r_2^k - \frac{D_2}{r_2-1}$$
Since $r_2 > 1$ in this case, it is clear that there is – in general – no finite bound for $u(k\tau^+)$. □

**Remarks** Theorems 3 and 4 show that it is possible to stabilize an unstable system by discrete resettings. If the continuous system is *indifferent* ($\lambda = 0$), then *any* sequence of uniformly contracting resettings is stabilizing. However, it should be noted that the asymptotic bound $C_2 \rightarrow \infty$ when $\beta \rightarrow 1$. In contrast, if the continuous system is *strictly unstable* ($\lambda < 0$), then specific contraction rates (depending on the dwell-time and the "expansion" rate of the continuous system) of the resettings are required. Finally, note that in both cases, the asymptotic bounds $C_2$ and $C_3$ are increasing functions of the dwell-time $\tau$.

## IV. COMMENTS

### A. Modelling issue: distinct driving noise

In the same spirit as [4], and contrary to previous works on the stability of stochastic systems (see the references in [4]), the $\mathbf{a}$ and $\mathbf{b}$ systems considered in sections II and III are driven by *distinct* and independent noise processes. This approach enables us to study the stability of the system with respect to variations in initial conditions *and* to random perturbations: indeed, two trajectories of any real-life system are typically affected by distinct *realizations* of the noise. In addition, this approach leads very naturally to nice results regarding the comparison of noisy and noise-free trajectories (see section IV-B), which are particularly useful in applications (see e.g. section V).

However, because of the very fact that the two trajectories are driven by distinct noise processes, we cannot expect the influence of noise to vanish when the two trajectories get very close to each other. As a consequence, the asymptotic bounds $2C/(1-\beta)$ (for discrete systems) and $C_1$, $C_2$, $C_3$ (for hybrid systems) are strictly positive. These bounds are nevertheless *optimal*, in the sense that they can be attained (adapt the Ornstein-Uhlenbeck example in section 2.3.1 of [4]).

### *B. Noisy and noise-free trajectories*

Instead of considering two noisy trajectories $\mathbf{a}$ and $\mathbf{b}$ as in theorem 1, we assume now that $\mathbf{a}$ is noisy, while $\mathbf{b}$ is noise-free. More precisely, for all $k \in \mathbb{N}$

$$\mathbf{a}_{k+1} = \mathbf{f}(\mathbf{a}_k, k) + \sigma(\mathbf{a}_k, k) w_{k+1}$$

$$\mathbf{b}_{k+1} = \mathbf{f}(\mathbf{b}_k, k)$$

To show the exponential convergence of $\mathbf{a}$ and $\mathbf{b}$ to each other, one can follow the same reasoning as in the proof of theorem 1, with $C$ being replaced by $C/2$. This leads to the following result

*Corollary 1:* Assume all the hypothesis of theorem 1 and consider a noise-free trajectory $\mathbf{b}_k$ and a noisy trajectory $\mathbf{a}_k$ whose initial conditions are given by a probability distribution $p(\mathbf{a}_0)$. Then, for all $k \in \mathbb{N}$

$$\mathbb{E}\left(\|\mathbf{a}_k - \mathbf{b}_k\|^2_{\mathbf{M}_k}\right) \leq \frac{C}{1-\beta} + \beta^k \int \left[\|\mathbf{a} - \mathbf{b}_0\|^2_{\mathbf{M}_0} - \frac{C}{1-\beta}\right]^+ dp(\mathbf{a}) \qquad (11)$$

**Remarks**

- The above derivation of corollary 1 is only permitted by our choice of considering distinct driving noise processes for systems $\mathbf{a}$ and $\mathbf{b}$ (see section IV-A).
- Based on theorems 2, 3 and 4, similar corollaries can be obtained for hybrid systems.
- These corollaries provide a robustness result for contracting discrete and hybrid systems, in the sense that any contracting system is *automatically* protected against noise, as quantified by (11). This robustness could be related to the exponential nature of contraction stability.

## V. APPLICATION: OSCILLATOR SYNCHRONIZATION BY DISCRETE COUPLINGS

Using the above developped tools, we study in this section the synchronization of nonlinear oscillators in presence of random perturbations. The novelty here is that the interactions between the oscillators occur at *discrete* time instants, contrary to many previous works devoted to synchronization in the *state-space*[1] (see [7] and references therein).

Specifically, consider the Central Pattern Generator (CPG) delivering $2\pi/3$-phase-locked signals of section 5.3 in [7]. This CPG consists of a network of three Andronov-Hopf oscillators $\mathbf{x}_i = (x_i, y_i)^T,\ i = 1, 2, 3$. We construct below a discrete-couplings version of this CPG.

At instants $t = k\tau,\ k \in \mathbb{N}$, the three oscillators are coupled in the following way (assuming noisy measurements)

$$\begin{aligned}\mathbf{x}_i(k\tau^+) &= \mathbf{x}_i(k\tau^-) \\ &+ \gamma\left(\mathbf{R}\left(\mathbf{x}_{i+1}(k\tau^-) + \tfrac{\sigma_d}{\sqrt{2}} w_k\right) - \mathbf{x}_i(k\tau^-)\right)\end{aligned}$$

with $\mathbf{x}_4 \equiv \mathbf{x}_1$ and

$$\mathbf{R} = \begin{pmatrix} -\frac{1}{2} & -\frac{\sqrt{3}}{2} \\ \frac{\sqrt{3}}{2} & -\frac{1}{2} \end{pmatrix}$$

Between two interaction instants, the oscillators follow the uncoupled, noisy, dynamics

$$d\mathbf{x}_i = \mathbf{f}(\mathbf{x}_i)dt + \frac{\sigma_c}{\sqrt{2}} dW$$

where

$$\mathbf{f}(\mathbf{x}_i) = \mathbf{f}\begin{pmatrix} x_i \\ y_i \end{pmatrix} = \begin{pmatrix} x_i - y_i - x_i^3 - x_i y_i^2 \\ x_i + y_i - y_i^3 - y_i x_i^2 \end{pmatrix}$$

We apply now the projection technique developped in [7], [4]. We recommend the reader to refer to these papers for more details about the following calculations.

Consider first the (linear) subspace $\mathcal{M}$ of the global state space (the global state is defined by $\widehat{\mathbf{x}} = (\mathbf{x}_1, \mathbf{x}_2, \mathbf{x}_3)^T$) where the oscillators are $2\pi/3$-phase-locked

$$\mathcal{M} = \left\{\left(\mathbf{R}^2(\mathbf{x}), \mathbf{R}(\mathbf{x}), \mathbf{x}\right)^T : \mathbf{x} \in \mathbb{R}^2\right\}$$

Let $\mathbf{V}$ and $\mathbf{U}$ be two orthonormal projections on $\mathcal{M}^\perp$ and $\mathcal{M}$ respectively and consider $\widehat{\mathbf{y}} = \mathbf{V}\widehat{\mathbf{x}}$. Since the mapping is linear, using Itô differentiation rule yields the following dynamics for $\widehat{\mathbf{y}}$

$$\forall k \in \mathbb{N} \quad \widehat{\mathbf{y}}(k\tau^+) = \mathbf{g}_d(\widehat{\mathbf{y}}(k\tau^-)) + \gamma\frac{\sigma_d}{\sqrt{2}} w_k \qquad (12)$$

$$\forall t \in ]k\tau, (k+1)\tau[ \quad d\widehat{\mathbf{y}} = \mathbf{g}_c(\widehat{\mathbf{y}})dt + \frac{\sigma_c}{\sqrt{2}} dW \qquad (13)$$

with

$$\mathbf{g}_d(\widehat{\mathbf{y}}) = \mathbf{VL}\widehat{\mathbf{x}} = \mathbf{VL}(\mathbf{V}^T\widehat{\mathbf{y}} + \mathbf{U}^T\mathbf{U}\widehat{\mathbf{x}}) = \mathbf{VLV}^T\widehat{\mathbf{y}}$$

$$\mathbf{g}_c(\widehat{\mathbf{y}}) = \mathbf{V}\widehat{\mathbf{f}}(\mathbf{V}^T\widehat{\mathbf{y}} + \mathbf{U}^T\mathbf{U}\widehat{\mathbf{x}})$$

where

$$\mathbf{L} = \begin{pmatrix} (1-\gamma)\mathbf{I}_2 & \gamma\mathbf{R} & \mathbf{0} \\ \mathbf{0} & (1-\gamma)\mathbf{I}_2 & \gamma\mathbf{R} \\ \gamma\mathbf{R} & \mathbf{0} & (1-\gamma)\mathbf{I}_2 \end{pmatrix}$$

$$\widehat{\mathbf{f}}(\widehat{\mathbf{x}}) = (\mathbf{f}(\mathbf{x}_1), \mathbf{f}(\mathbf{x}_2), \mathbf{f}(\mathbf{x}_3))^T$$

Remark that $\mathbf{g}_d(\mathbf{0}) = \mathbf{0}$ and $\mathbf{g}_c(\mathbf{0}) = \mathbf{0}$ (the last equality holds because of the symmetry of $\mathbf{f}$: $\forall \mathbf{x},\ \mathbf{f}(\mathbf{Rx}) = \mathbf{R}(\mathbf{f}(\mathbf{x}))$). Thus, $\mathbf{0}$ is a particular solution to the noise-free version of the hybrid stochastic system (12,13).

Let us now examine the contraction properties of equations (12) and (13).

We have first

$$\frac{\partial \mathbf{g}_d}{\partial \widehat{\mathbf{y}}}^T \frac{\partial \mathbf{g}_d}{\partial \widehat{\mathbf{y}}} = \mathbf{VL}^T\mathbf{V}^T\mathbf{VLV}^T = (3\gamma^2 - 3\gamma + 1)\mathbf{I}_4$$

---

[1] Discrete couplings are more frequent in the literature devoted to *phase oscillators* synchronization, where *phase reduction* techniques are used (see e.g. [12]). However, contrary to our approach, these techniques are only applicable in the case of weak coupling strenghs and small noise intensities.

so that $\lambda_{\max}\left(\frac{\partial \mathbf{g}_d}{\partial \widehat{\mathbf{y}}}^T \frac{\partial \mathbf{g}_d}{\partial \widehat{\mathbf{y}}}\right) = 3\gamma^2 - 3\gamma + 1 < 1$ (for $0 < \gamma < 1$).

Second,

$$\frac{\partial \mathbf{g}_c}{\partial \widehat{\mathbf{y}}} = \mathbf{V}\frac{\widehat{\partial \mathbf{f}}}{\partial \widehat{\mathbf{x}}}\mathbf{V}^T = \mathbf{V}\begin{pmatrix} \frac{\partial \mathbf{f}}{\partial \mathbf{x}}(\mathbf{x}_1) & \mathbf{0} & \mathbf{0} \\ \mathbf{0} & \frac{\partial \mathbf{f}}{\partial \mathbf{x}}(\mathbf{x}_2) & \mathbf{0} \\ \mathbf{0} & \mathbf{0} & \frac{\partial \mathbf{f}}{\partial \mathbf{x}}(\mathbf{x}_3) \end{pmatrix}\mathbf{V}^T$$

Now observe that $\lambda_{\max}\left(\frac{\partial \mathbf{f}}{\partial \mathbf{x}}\right)_s = 1 - x^2 - y^2 \leq 1$. Since $\mathbf{V}$ is an orthonormal projection, one then has $\lambda_{\max}\left(\frac{\partial \mathbf{g}_c}{\partial \widehat{\mathbf{y}}}\right)_s \leq 1$.

Therefore, if

$$3\gamma^2 - 3\gamma + 1 < e^{-2\tau} \tag{14}$$

then theorem 4 together with the corollaries of section IV-B imply that, after exponential transients,

$$\mathbb{E}\left(\|\widehat{\mathbf{y}}\|^2\right) \leq \frac{2\gamma^2\sigma_d^2 + (1-\beta)(1+\beta-\beta e^{2\tau})e^{2\tau}\sigma_c^2}{2(1-\beta)(1-\beta e^{2\tau})}$$

where $\beta = 3\gamma^2 - 3\gamma + 1$.

To conclude, observe that

$$\|\widehat{\mathbf{y}}\|^2 = \|\mathbf{V}\widehat{\mathbf{x}}\|^2 = \frac{1}{3}\sum_{i=1}^{3}\|\mathbf{R}\mathbf{x}_{i+1} - \mathbf{x}_i\|^2$$

Define the *phase-locking quality* $\delta$ by

$$\delta = \sum_{i=1}^{3}\|\mathbf{R}\mathbf{x}_{i+1} - \mathbf{x}_i\|^2$$

then one finally obtains

$$\mathbb{E}(\delta) \leq \frac{6\gamma^2\sigma_d^2 + 3(1-\beta)(1+\beta-\beta e^{2\tau})e^{2\tau}\sigma_c^2}{2(1-\beta)(1-\beta e^{2\tau})} \tag{15}$$

after exponential transients.

A numerical simulation is provided in Fig. 1.

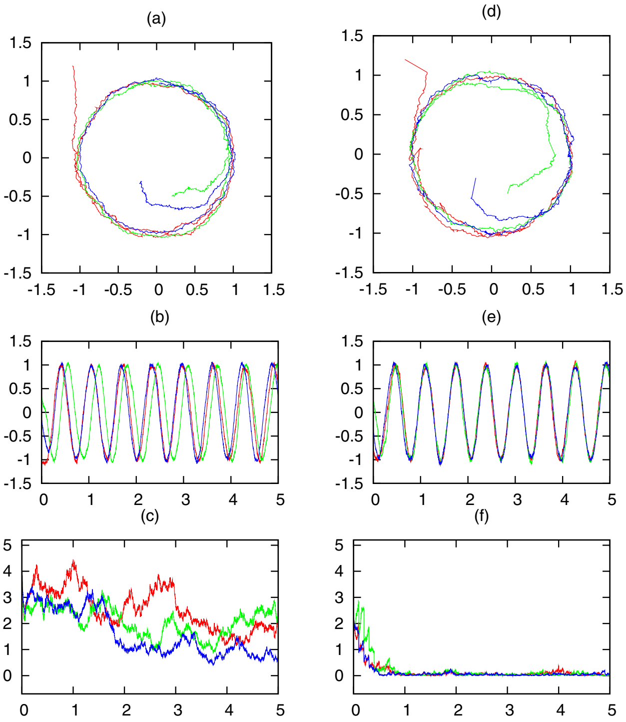

Fig. 1. Numerical simulation using the Euler-Maruyama algorithm [13]. The following set of parameters was used: $\sigma_c = 0.1$, $\sigma_d = 0.05$, $\tau = 0.1$. Two coupling strengths were tested: $\gamma_{\text{weak}} = 0.01$ for plots (a), (b), (c), and $\gamma_{\text{strong}} = 0.2$ for plots (d), (e), (f). Note that $\gamma_{\text{weak}}$ does not satisfy condition (14), while $\gamma_{\text{strong}}$ does, and yields the theoretical bound $\simeq 0.446$ (as provided by (15)) on the phase-locking quality $\delta$. Plots (a) and (d) show the 2d trace of sample trajectories of the three oscillators for $t \in [0, 1]$. Plots (b) and (e) show sample trajectories of the first coordinates of $\mathbf{x}_1$, $\mathbf{R}(\mathbf{x}_2)$ and $\mathbf{R}^2(\mathbf{x}_3)$ as functions of time. Plot (c) and (f) show three sample trajectories of the phase-locking quality $\delta$.

## ACKNOWLEDGMENT

The author is grateful to Prof J.-J. Slotine and N. Tabareau for stimulating discussions, and to Dr H. Hicheur for the careful reading of the manuscript. This work has been supported by the BACS project (EC – contract number FP6-IST-027140, action line : Cognitive Systems). This publication reflects only the author's views. The European Community is not liable for any use that may be made of the information contained therein.

## REFERENCES

[1] W. Lohmiller and J.-J. Slotine, "On contraction analysis for nonlinear systems," *Automatica*, vol. 34, pp. 671–682, 1998.

[2] W. Wang and J.-J. E. Slotine, "On partial contraction analysis for coupled nonlinear oscillators." *Biol Cybern*, vol. 92, no. 1, pp. 38–53, Jan. 2005.

[3] K. El Rifai and J.-J. Slotine, "Compositional contraction analysis of resetting hybrid systems," *IEEE Transactions on Automatic Control*, vol. 51, no. 9, pp. 1536–1541, 2006.

[4] Q.-C. Pham, N. Tabareau, and J.-J. Slotine. (2007) A contraction theory approach to stochastic incremental stability. [Online]. Available: http://arxiv.org/abs/0704.0926

[5] W. Lohmiller and J. Slotine, "Control system design for mechanical systems using contraction theory," *IEEE Transactions on Automatic Control*, vol. 45, no. 5, pp. 984–989, 2000.

[6] W. Lohmiller and J.-J. Slotine, "Nonlinear process control using contraction theory," *A.I.Ch.E. Journal*, 2000.

[7] Q.-C. Pham and J.-J. Slotine, "Stable concurrent synchronization in dynamic system networks." *Neural Netw*, vol. 20, no. 1, pp. 62–77, Jan. 2007.

[8] B. Girard, N. Tabareau, Q.-C. Pham, A. Berthoz, and J.-J. Slotine, "Where neuroscience and dynamic system theory meet autonomous robotics: a contracting basal ganglia model for action selection," *Neural Networks*, vol. 21, pp. 628–641, 2008.

[9] N. Aghannan and P. Rouchon, "An intrinsic observer for a class of lagrangian systems," *IEEE Transactions on Automatic Control*, vol. 48, 2003.

[10] H. Kushner, *Stochastic Stability and Control*. Academic Press, 1967.

[11] J. Robbin. (2006) Gronwall's inequality. [Online]. Available: www.math.wisc.edu/∼robbin/angelic/gronwall.pdf

[12] E. Izhikevich, "Weakly pulse-coupled oscillators, FM interactions, synchronization, and oscillatory associative memory," *Neural Networks, IEEE Transactions on*, vol. 10, no. 3, pp. 508–526, 1999.

[13] D. Higham, "An algorithmic introduction to numerical simulation of stochastic differential equations," *SIAM Review*, vol. 43, pp. 525–546, 2001.